AHTD TRC TRANSPORTATION RESEARCH COMMITTEE

TRC0203

Permeability and Drainage of Superpave

Kevin D. Hall, Norman D. Dennis, Adnan Qazi, Xuhui Chang

Final Report

2014

FINAL REPORT

TRC-0203

Permeability and Drainage of Superpave

by

Kevin D. Hall, Norman D. Dennis, Adnan Qazi, and Xuhui Chang

Conducted by

Department of Civil Engineering
University of Arkansas

In cooperation with

Arkansas State Highway and Transportation Department

U.S. Department of Transportation
Federal Highway Administration

University of Arkansas
Fayetteville, Arkansas 72701

AUGUST 2013

TRC-0203

Permeability and Drainage of Superpave

EXECUTIVE SUMMARY

With the implementation of the Superpave volumetric mixture design system starting in late 1996, concerns arose regarding the permeability of the relatively open-graded nature of resulting ACHM mixes. TRC-9901 was funded to investigate ACHM permeability and its effects on pavement performance. The primary product arising from that study was a laboratory standard test for measuring ACHM permeability, published by ASTM as PS-129. However, still lacking in the permeability discussion was a relationship between lab and field permeability and an understanding of the exact nature of moisture infiltration into pavement structures.

TRC-0203 was conducted in two phases, corresponding to the two primary emphases for the project: (Phase One) establish the relationship between lab and field permeability; and (Phase Two) investigate the mechanism(s) of moisture infiltration through base and subgrade materials beneath pavement structures. It is noted that Phase Two also was extended to include an assessment of the Enhanced Integrated Climatic Model (EICM) incorporated into the AASHTO Mechanistic-Empirical Pavement Design Guide (MEPDG) for modeling and predicting moisture contents throughout a pavement structure and subgrade.

This Project Final Report consists of two stand-alone documents, which report the results from each phase of the study. For clarity and convenience, the major findings of each project phase are reproduced in this Executive Summary.

PRIMARY FINDINGS: PHASE ONE

Field and laboratory permeability was compared for variety of mix designs, using both field-compacted and laboratory-compacted specimens. The results of the comparisons generally agreed with previous/subsequent research conducted in other regions of the U.S. However, no single, robust relationship (regression model) was identified between laboratory and field permeability values; thus no model is presented which would allow the estimation of field permeability based on laboratory permeability tests conducted on laboratory-compacted specimens. Pertinent conclusions for Phase One follow.

Field Permeability Testing

- Field permeability or equivalent field percolation was dependent on testing time of the year or/and testing time after the pavement construction.
- Field permeability is not affected by the wheel path.
- Field permeability was dependent upon both longitudinal and cross slope of the pavement; there appeared to be more laterally interconnected void pathways than vertically connected void pathways on steep longitudinal slopes.
- The UAF field permeameter, which features a low initial hydraulic head, large test surface area, and a constant-head testing approach, provides estimates of in-place permeability that are different than those estimates provided by the NCAT permeameter, which uses a falling-head testing approach, high initial hydraulic head, and small test surface area. It is suggested that the differences in initial hydraulic head and test surface area are significant factors in the difference in test results.

- The UAF field permeameter generally provided lower permeability values than the NCAT permeameter – but could only measure up to $179x10^{-5}$ cm/s of field permeability.
- Although not quantified, observed replicate test variability appears to be similar for both the NCAT and the UAF field test methods.
- Field permeability was generally below $50x10^{-5}$ cm/s at 5.5 percent in-place air voids.

Laboratory Permeability Testing

- All samples exhibited laminar flow, so the primary *assumption* of laminar flow was valid; therefore the laboratory permeameter could be used to measure the permeability of highly permeable cores.
- Field cores with in-place air voids of 6 percent or less were almost impermeable for all field sites when tested in the laboratory.
- Field cores with in-place air voids between 7 percent and 9 percent generally exhibited laboratory permeability values of less than $100x10^{-5}$ cm/s.
- Field cores having greater than 9 percent air voids were highly permeable.

Recommendations

Results from Phase One clearly indicate the desirability for proper field compaction of asphalt mixtures. Demarcation between highly permeable, somewhat permeable, and impermeable – while site and mixture specific – is typically characterized by only a few percentage points of in-place air voids (e.g. 'compaction'). Certainly, current AHTD specifications regarding compaction, e.g. 92-96 percent of maximum density (Gmm), are appropriate, as long as the minimum compaction of 92 percent is achieved.

The UAF field permeameter proved to be a reliable and repeatable test device when used in accordance with proposed testing procedures. Laboratory permeability test methods and equipment are generally not as reliable and repeatable. It is recommended that measurements of permeability for asphalt pavements be conducted in the field, rather than by using cores taken to the laboratory.

PRIMARY FINDINGS: PHASE TWO

Moisture infiltration through pavement structures was evaluated by modeling and by field observations at a pavement test pad constructed at the University of Arkansas and at a field test site in Fort Smith. A comprehensive laboratory testing program was performed to obtain engineering properties of the pavement materials and underlying soils at the ERC and Fort Smith test sites. A comprehensive monitoring and measuring program was also conducted at the ERC and Fort Smith sites to investigate the responses of the pavement systems to various environmental factors. Based on measured data, a water migration pattern through the pavement systems was developed; this pattern was partially validated with a transient FEM seepage model. Additionally, the EICM was evaluated by comparing predicted data with the measured data. Pertinent conclusions for Phase Two follow.

Material Properties of Pavements

- The hydraulic conductivity of the asphalt concrete hot mix (ACHM) measured with a specific device may vary widely with sample location. Field and laboratory test results from the UAF test pad showed a variation from near 0 to about 1×10^{-3} cm/s when the test location changed.

- When comparing the results of field hydraulic conductivity tests and laboratory tests, it appears that the results of long-term (at least 2 or 3 days) field testing were in closer agreement to laboratory measured results than the results obtained from short-term (less than 1 hour) field testing. In general, the short term field tests reported hydraulic conductivities that were at least an order of magnitude higher than the long term field and laboratory tests.
- As implemented in the MEPDG, soil-water characteristic curves (SWCCs) created using Fredlund and Xing equations might have good agreement with laboratory-measured SWCCs. However, the results of the FEM analyses suggest that in-situ SWCCs might be far different from the SWCCs developed using Fredlund and Xing equations. This is likely due to micro- or macro- structures in soils creating anisotropy, which cannot be accounted for in laboratory and Fredlund and Xing equations.

Moisture Content Changes in Pavements

- Changes in groundwater levels appear to follow seasonal trends. Groundwater levels and moisture contents at the UAF test location, for example, had high peak values in summers and low peak values in winters.
- Based on measured responses of moisture to precipitation events in the Class 7 base materials, moisture migrated much faster in the horizontal direction than in the vertical direction. The moisture migration pattern appeared to include only the extreme upper region of the Class 7 base.
- Only moisture contents of base materials at the shallowest depth (2 inches below the base surface) responded significantly to precipitation events. Moisture content

changes in the base materials at deeper depths (deeper than 2 inches) changed according to season – not in response to individual precipitation events.

- Precipitation events at both sites had almost no effect on the moisture content in subgrade soils, except for those areas in close proximity to the edge drains. The moisture content in subgrade soils changed seasonally, and independently of precipitation events.
- After a precipitation event, some portion of water that migrated into pavement systems would remain in pavement systems for a relatively long period because the Class 7 base materials were not free-draining materials.
- Frost depths in the Northwest Arkansas area and River Valley area were less than one foot measured from pavement surfaces during the period of this study.
- Degrees of saturation in the base and subbase materials at the UAF and Ft. Smith test sites generally increased with depth from approximately 55 percent to near 100 percent. Degrees of saturation in the subgrade soils at the UAF and the Ft. Smith test sites changed with seasons and can be predicted using the predicative models developed in this study. A single prediction model could be used for both sites.
- Resilient modulus of the A-6 subgrade soils encountered at the UAF and the Ft. Smith test siteS changed with seasons and could be described with periodic functions developed in this study. Predicted values ranged from 18 ksi during winters and values of 3 to 6 ksi during summers. A single model could not be used to predict modulus for both sites.

Evaluation of the EICM and FEM Analyses

- Air temperature obtained from nearby NOAA weather stations in this study (less than 5 miles from the sites) can be used in the EICM with adequate accuracy (less than 11 percent effect on predicted asphalt modulus).
- Air temperatures from a weather station located 50 miles from the test site could not be used reliably in the EICM to predict asphalt temperatures. The asphalt modulus could be off by as much as 30 percent by using the distant weather station data.
- The EICM predicted temperatures in the pavement adequately during the winter, spring and fall at the test site in Fort Smith, Arkansas. However, a relatively large discrepancy between measured and predicted soil temperature was observed in the summer.
- The EICM did not predict moisture content well in the base and subbase materials at either site. The EICM generally under-predicted moisture content in the base and subbase materials by as much as 100 percent.
- The EICM did not predict seasonal changes in moisture content in the subgrade soils at either site. Based on field measurements the EICM under-predicted moisture contents in the summer by as much as 50 percent. While, in the winter, the EICM over-predicted moisture contents by as much as 50 percent. It appears that the EICM prediction on moisture content is better with depth.
- The finite element method appears to be able to predict general trends of moisture migration through the pavement system with reasonable accuracy when well calibrated.

Recommendations

In general, moisture movements through a pavement structure and subgrade – while complex – can be modeled, particularly when field data is available for calibrating the model. The EICM implemented in the MEPDG performed reasonably well in modeling subsurface temperature. However, the EICM did not model moisture contents in base, subbase, and subgrade materials accurately for all seasons of the year. Specific recommendations for further consideration follow.

- More test sites and monitoring and measuring programs should be conducted in other areas of Arkansas to either verify the observations and conclusions obtained in this study.
- Additional environmental factors, such as wind speed, percent sunshine and humidity that are included in the EICM should be measured at test sites for a better evaluation of the EICM in Arkansas.
- Asphalt temperature should be measured because temperature is more critical to asphalt engineering properties than those of unbound base and subgrade materials.
- A better flow measurement device that is suitable for uncontrolled field conditions should be developed and used for future measurements of runoff and subsurface drainage.
- Consideration should be given to conduct tests on two identical test sites except that one test site has an edge drain and the other one does not. This would result in a better understanding of effectiveness of edge drains.
- Additional study of the EICM across regions of Arkansas is warranted.

PHASE ONE

A COMPARISON OF FIELD AND LABORATORY PERMEABILITY OF HOT-MIX ASPHALT CONCRETE

Table of Contents

List of Tables

List of Figures

PROBLEM STATEMENT

For approximately sixty years, Arkansas and other states used the Marshall method for designing hot-mix asphalt concrete (HMA) mixtures for pavements. Bruce Marshall first developed the Marshall method in 1939; the method was subsequently adopted and improved by the U.S. Army Corps of Engineers. HMA mixes designed using the Marshall method tended to be dense graded and relatively impermeable, but could suffer durability and permanent deformation (rutting) problems. The Strategic Highway Research Program (SHRP), conducted from 1987 to 1993, included a research effort to improve existing HMA mixture design procedures to produce mixtures exhibiting increased durability and rutting resistance. The mixture design procedure developed under SHRP was termed "Superpave" (SUperior PERforming asphalt PAVEment).

Starting in 1995 the Arkansas State Highway and Transportation Department (AHTD) implemented Superpave methods, replacing the Marshall mix design system. Unlike the Marshall method, Superpave gradation specifications tend to produce coarse and/or open-graded HMA. The open graded characteristic of the HMA allows moisture to percolate through the mix – to move either laterally or through to the underlying layers, or to be trapped inside the pavement structure. In order to resolve premature moisture-related pavement problems, AHTD initiated the research project TRC-9901 in July 1998. The project was intended to develop an accurate method to measure the permeability of HMA and to correlate permeability with pavement performance, so that limiting values of permeability for HMA could be recommended. According to Cruz (2000), the TRC-9901 researchers concluded that laboratory-compacted samples and field cores showed inconsistent permeability results. Based on this inconsistency, laboratory permeability could not be

related directly to in-service performance. From these findings, the need arose to correlate laboratory permeability with a measure of field permeability determined directly on constructed pavements.

The overall objective of this study is to develop design criteria and construction specifications related to the permeability of HMA in flexible pavements. In order to account for the effect of HMA permeability on flexible pavement performance during mixture design, a logical first step is to correlate field permeability to laboratory permeability for a variety of mix designs. It is proposed to accomplish this first step by measuring and comparing the permeability of laboratory compacted specimens to field permeability values measured both in-place and in the laboratory using cores taken from in-place pavements. The outcome of this study will enable designers to consider permeability effects in the design and construction of flexible pavements in order to avoid premature failures due to moisture-related problems.

LITERATURE REVIEW

Permeability of asphalt pavements is not a new subject. Hall (2001) provides a review of pertinent permeability-related research efforts, a summary of which follows.

"McLaughlin and Goetz correlated the permeability and air void content of asphalt paving mixtures to mixture durability. They used an air permeameter and concluded that permeability depends upon the gradation, compaction effort and asphalt content. Hein and Schmidt also utilized air as the flow medium and concentrated on effects of construction technology on permeability measured on in-situ pavements. Their fieldwork was in agreement with the conclusions made by McLaughlin and Goetz in the laboratory. However, McWilliams concluded that air and water were not quantifiably identical. His studies indicated that asphalt mixtures were 150 times more permeable to air than to water. McWilliams also showed that air and water permeability were greatly reduced by inducing higher quantity of mineral filler (minus #200 sieve material) in the gradation of any mix design. His studies also indicated that permeability is directly affected by aggregate gradation and compaction effort. Shikarsky and Kimchi studied permeability of sand asphalt mixtures using water as the flow medium to prove that Darcy's law is valid for bituminous mixtures. Unfortunately no single standard exists to consistently measure the permeability of asphalt concrete specimens. Kumar and Goetz developed an "improved" method for measuring permeability on asphalt specimens. Their equipment was the forerunner of the device specified in a "standardized test" for measuring asphalt concrete permeability detailed in ASTM D3637-84. However few researchers and designers used the equipments and methods contained in ASTM D3637, and subsequently the standard was discontinued. The Florida Department of Transportation (FDOT) performed the first comprehensive studies of

permeability on superpave-designed HMA which was presented near the end of 1997. The FDOT developed a rigid-wall permeameter to test 2-in. (50mm) field cores, that uses epoxy coating as a sealant for the edges. Based on their initial findings, the allowable permeability was specified to be $100x10^{-5}$ cm/s, which related to 6 percent air voids. The FDOT studies further recommended a minimum thickness of coarse paving mixtures equal to 3 times the maximum aggregate size."

Cooley (1999) conducted a study to evaluate four field permeameters (FP1, FP2, FP3 and FP4). He compared their results to a laboratory testing permeameter. All of the field permeameters were based on falling head principle and used some kind of sealant underneath the base plate. He recommended FP3, which was developed by NCAT, to be the standard field permeameter because it was relatively easy to use, had better repeatable data and could be used to measure relatively impermeable pavements due to different sizes of tiers.

Ng (2000) concluded that void pathways were largely interconnected in the field than the SGC samples and Cruz (2000) has shown that SGC samples greater than 75mm thickness had surface air voids connected internally to the side of the specimens.

Izzo and Button (1997) have shown that permeability of coarse matrix-high binder (CMHB) mixes – similar to superpave mixtures – increased proportionally with air void levels up to about 8 to 10 percent. Above 10 percent voids no significant change in the permeability was noted. They also reported that new pavements are more permeable, while a year old pavement exhibited two orders of magnitude lower permeability – suggesting that after one year of exposure to traffic permeability should be of no concern.

Choubane, Page, and Musselman (1998) reported findings from ongoing studies conducted by the Florida Dept. of Transportation. Their results indicated that, in order to

attain an impermeable coarse graded Superpave pavement, one has to design it with 6 percent or less air voids. They also concluded that samples compacted using the superpave gyratory compactor (SGC) had low permeability relative to field cores – indicating the air void pathway was not similar among the specimens, even at the same air void level. Primary factors resulting in lower in-place air voids and permeability were found to be increased lift thickness, compactive effort, mat temperature and running at the lower end of acceptable air voids at the plant during production.

Kanitpong, Benson and Bahia (2000) indicated that the permeability of HMA was mainly controlled by the air void content, but was also dependent upon gradation and specimen thickness. They stated that hydraulic gradient exhibited little effect on the permeability of HMA. They devised a new apparatus for laboratory permeability testing, which produced steady and repeatable data based on backpressure saturation procedure. They found that finer blends tend to be less permeable while S-shaped gradations tend to be more permeable.

Maupin (June, 2000) concluded that sealant is necessary to prevent water flow along the sides in the falling head test for laboratory compacted specimens and field cores. He found that one side sawing affected the permeability by 50percent and recommended to seek an alternative method for separating layers during core testing. Later Maupin (2000), in contrast to an earlier effort he reported (June, 2000), concluded that the sawing did not affect permeability if the saw blade was kept in good condition and the pressure between the saw blade and the specimen was properly managed. He also found that the limited repeat tests by different operators were not the same.

Maupin (June, 2000) also stated that fine mixtures (small NMAS) had lower permeability than coarse mixtures, which was in agreement with the statement made by Kanitpong, Benson and Bahia (2000). He also indicated that the laboratory permeability test of laboratory compacted specimens were similar to field cores in 5 of his 6 cases. He used four 12.50mm NMAS and one 9.50mm NMAS Superpave mixes for his laboratory and field correlation studies. The 9.50mm did not show any correlation. His average test data included five field cores and ten laboratory compacted specimens for each mix design case. The mixture for laboratory samples was sampled during the construction of the pavement. He did a significant amount of testing to find the magnitude of permeability for the mixtures in place and concluded that the field cores had excessive permeability than the maximum allowable of $125x10^{-5}$ cm/s, later set by FDOT. He also found that the constant head equipment normally used for soils testing was not appropriate to test asphalt specimens that were more permeable. It did not permit the low-pressure differentials required to measure water flow in semi porous mixtures. The falling head device was more convenient in handling than the constant head device.

According to Mallick, Cooley and Teto (1999), the permeability of dense graded hot mix asphalt (HMA) increased extensively at levels of voids in total mix (VTM) greater than a "threshold" VTM, whereas the threshold VTM depends on the mix type. They also stated that gradation affected the permeability characteristics. The permeability was significant for fine mix at higher VTM, while it was significant for coarse mix at lower VTM. They proposed a critical value of $100x10^{-5}$ cm/s for the dense graded HMA. They concluded that increase in lift thickness reduced permeability but the rate of change of permeability with the corresponding change in thickness was dependent on NMAS. They ran total of 50 tests in the

field and 49 tests in the laboratory on the field cores and analyzed that field and lab permeability results were similar for 9.50 mm and 12.50 mm NMAS but significantly differed for higher NMAS, i.e. 19.0 mm and 25.0mm. They used a falling head permeameter to record three readings for each location with a time lapse of 60 seconds. They developed their own field permeameter based on NCAT field permeameter. It had three tiers, a flexible closed-cell sponge rubber base and two donut-shaped weights. Initially they had problem with leakage through the base but they stopped the leakage by using three more weights (total of 47 kg) to seal off the permeameter without use of caulking sealant. The diameters of the tiers from top to bottom were 3.8cm, 8.9cm, 14cm and 8.9cm, respectfully. They used Karol-Warner laboratory permeameter for laboratory permeability testing according to Florida DOT specification (FM 5-565). Their explanation of no correlation for higher NMAS was the high horizontal permeability in the field.

Cooley, Brown and Maghsoodloo (2001) reported a solid relationship between field permeability and in-place air void contents for Superpave pavements. They also concluded that permeability characteristics varied with a change in NMAS, in agreement with many other researchers. They indicated that 12.50mm and 9.50mm NMAS have same permeability characteristics. These pavements were substantially permeable at approximately 92.3 percent density. They proposed $100x10^{-5}$ cm/s as the critical field permeability for 9.50mm and 12.50mm NMAS, while this same value was proposed by FDOT for all NMAS (but FDOT later changed it to $125x10^{-5}$ cm/s). They proposed critical field permeability of $120x10^{-5}$ cm/s for 19.0mm NMAS and $150x10^{-5}$ cm/s for 25.0mm NMAS mixes. They also found that 19.0mm NMAS and 25.0mm NMAS were extremely permeable at 94.5 and 95.6 percent density, respectively.

Cooley, Prowell and Brown (2002) concluded that both field and laboratory permeability relates to the density of Superpave mixes. They also concluded that the nominal maximum aggregate size (NMAS) of the mix played an important role in the permeability characteristics of a pavement. The NMAS of 12.50mm and 9.50mm showed the same permeability characteristics but usually permeability increased with the increase in NMAS. In contrast to Mallick, Cooley and Teto (1999), their large testing effort showed that the field and lab permeability results were approximately similar at permeability values up to $500x10^{-5}$ cm/s for a pavement. They used a field permeameter, based on a falling head principle, which was devised by the National Center for Asphalt Technology. Their laboratory permeameter, based on the same principle, was developed by the Florida DOT. They also developed a relationship between in-place density, lift thickness and permeability – i.e. permeability reduced with the increase in lift thickness and in-place density. They established, in addition to above, a relationship between water absorption using AASHTO T-166 and permeability (both field and lab). According to same limited studies, except for 9.50mm NMAS, field cores and field mix (representative of the cores) compacted using Superpave gyratory compactor (SGC) had similar laboratory permeability results. This limited data was based on approximately 50 field cores and 50 SGC samples of 9.50mm, 12.50mm and 19.0mm NMAS.

It is expected that continued efforts expended on this project will utilize the experiences of previous researchers and agencies to develop an integration of permeability with other key factors for hot-mix designs. Table 1 summarizes some of the key points from previous research efforts related to HMA permeability.

Table 1. Summary of permeability research effects.

Reference (Year)	Major Findings
Choubane, Page, and Musselman (1998)	• To attain an impermeable coarse graded Superpave pavement, one has to design it with 6 percent or less air voids. • Samples compacted using the superpave gyratory compactor (SGC) had low permeability relative to field cores.
Cooley (1999)	• Recommended FP3, which was developed by NCAT, to be the standard field permeameter.
Cooley, Maghsoodloo, Brown (2001)	• Found sturdy relationship between field permeability and in-place air void contents. • 12.50mm and 9.50mm NMAS have same permeability characteristics.
Cooley, Prowell, and Brown (2002)	• The field and lab permeability results were approximately similar at permeability values up to $500x10^{-5}$ cm/s for a pavement. • According to their limited data studies, except 9.50mm NMAS, field cores and field mix (representative of the cores), compacted using Superpave gyratory compactor (SGC), had similar laboratory permeability results.
Cruz (2000)	• SGC samples greater than 75mm thickness had surface air voids connected internally to the side of the specimens.
Hall (2001)	• Permeability depends upon the gradation, compaction effort and asphalt content. • Permeability was greatly reduced by inducing higher quantity of mineral filler. • No single standard exists to consistently measure the permeability.
Izzo and Buttonn (1997)	• Increased proportionally with air void levels up to about 8 to 10 percent. • New pavements are more permeable.
Kanitpong , Benson and Bahia (2000)	• Hydraulic gradient has not much effect on the permeability of HMA. • They found that finer blends tend to be less permeable while S-shaped gradations tend to be more permeable.
Mallick, Cooley, and Teto (1999)	• Increase in lift thickness reduced permeability but the rate of change of permeability with the corresponding change in thickness was dependent on NMAS. • Field and lab permeability results were similar for 9.50 mm and 12.50 mm NMAS but significantly differed for higher NMAS i.e. 19.0 mm and 25.0mm. • No correlation for higher NMAS, was the high horizontal permeability in the field.
Maupin (2000)	• The sawing did not affect permeability if the saw blade was kept in good condition. • Permeability results vary due to different operators.
Maupin (June 2000)	• The sealant is necessary to prevent water flow along the sides in the falling head lab. test. • One side sawing affected the permeability by 50percent. • The laboratory permeability test of laboratory compacted specimens were similar to field cores in 5 of his 6 cases.
Ng (2000)	• Void pathways were largely interconnected in the field than the SGC samples.

TESTING METHODS

Laboratory and in-place permeability measurements were based on different methods and are discussed in the sections that follow.

Field permeability testing devices

There were two devices used for the field permeability testing:

1. Kuss field permeameter
2. National Center for Asphalt Technology (NCAT) permeameter

It should be noted that results from the field permeability testing devices do not represent a true measure of permeability, but rather an indicator of permeability. Water flows in horizontal and/or vertical directions after percolating into a pavement (three dimensional flow), but to relate this field percolation with laboratory permeability, it is assumed that flow is only vertical in the field and is termed "field permeability" in this report.

Kuss field permeameter

The Kuss permeameter estimates the permeability of a porous material by confining water over its surface at a given constant pressure, and measuring the amount of air needed to replace (percolating) water to maintain the constant pressure head. The volume of air necessary to replace percolating water is measured through the use of a patented gas-measurement system. Figure 1(a) shows the Kuss field permeameter while Figure 1(c) is a schematic diagram of the system. The permeameter data-logging interface measures and records the data simultaneously. An advantage of the system relates to the ability to measure the permeability of a relatively large surface area under hydraulic gradients similar to those found in "real world" conditions.

The system includes software to plot flow rate (mm/minute) versus time (minutes). If there was zero permeability for 15 minutes the test was terminated; otherwise the test was run to a point of "constant" flow (only minor fluctuations between consecutive flow rate measurements) or for a maximum of 30 minutes. Figure 1(b) illustrates the plot of flow rate against time measured by Kuss permeameter that also exhibits the typical fluctuation of discharge with respect to time. Flow rates recorded for the last five minutes were averaged and used to calculate the coefficient of permeability as follows.

$$k = \frac{Q}{60 * \left(\frac{2.54 + L}{L} \right) * A}$$

Where :

k = coefficient of water permeability, cm/s,

Q = flow rate, cm^3/min

A = area (35.56cm x 35.56cm) of base plate, cm^2,

L = pavement thickness for Superpave mix design only.

The above formula was derived from Darcy's law with following assumptions.

1. When the testing layer has 25.0mm of water head above its surface then the pressure head at the bottom of testing layer would be negligible.
2. Water was assumed to flow vertically (perpendicular to the testing layer). Horizontal flow was neglected.
3. In case of overlay, as existing pavement was based on Marshall mix design that is usually impermeable so it was assumed that water would not flow through existing pavement.

Figure 1(a) – Kuss Field Permeability Testing Apparatus

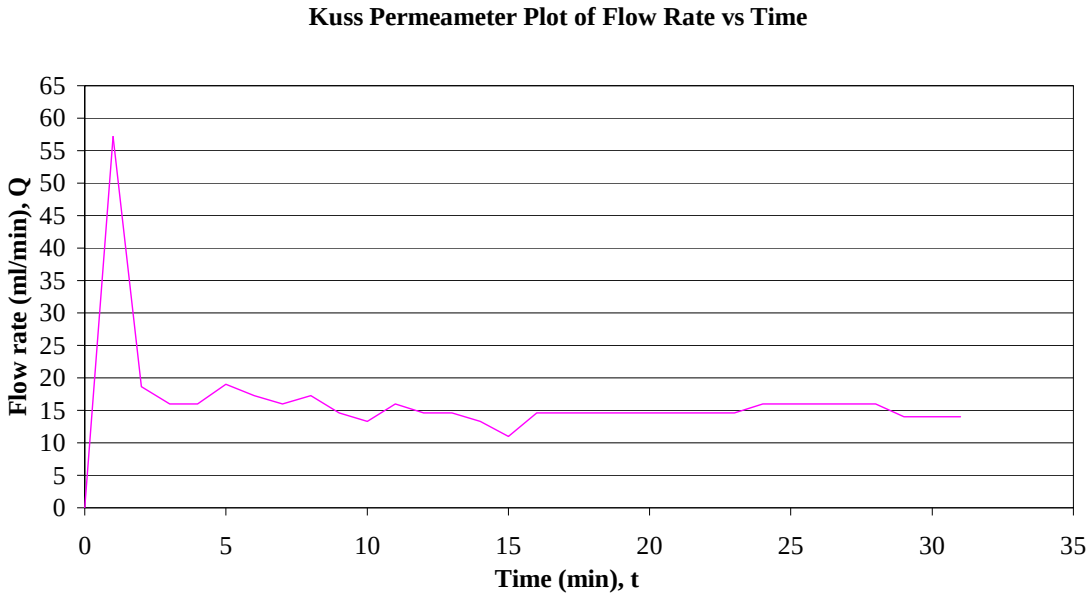

Figure 1(b) – Kuss Permeameter Plot Shown By The Computer

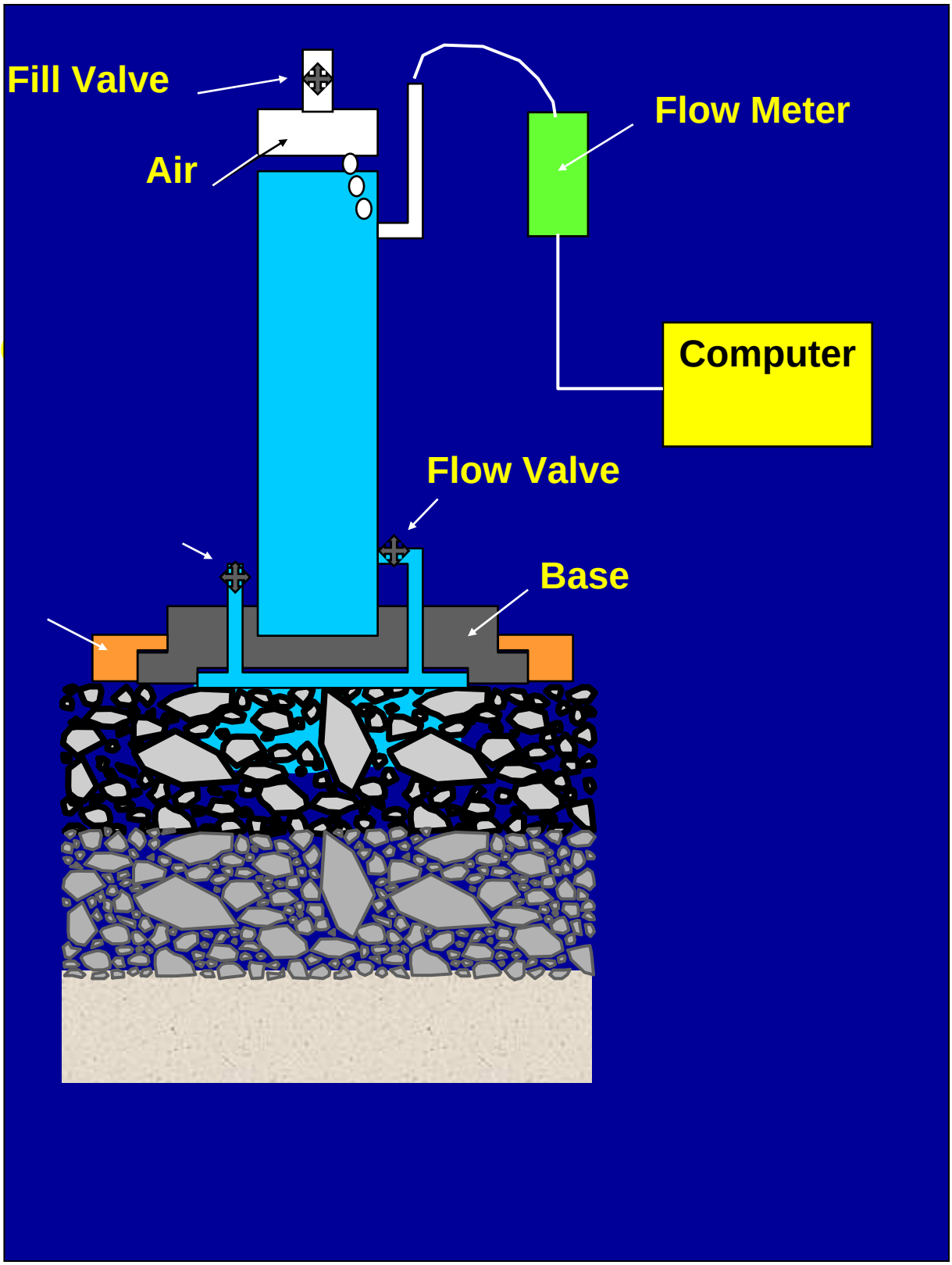

Figure 1(c) – Kuss Field Permeability Testing schematic diagram

NCAT field permeameter

The NCAT field permeameter operates using a “falling head” procedure. The device is a series of stacked tubes, which are placed on the pavement surface. The tubes are graduated to allow estimation of water height within the device (and thus, knowing the inside diameter of the tube, the volume of water may be calculated). Water is added and allowed to flow freely. The water level “drop” within the tubes is timed. The permeameter is sealed by putty at the base, followed by placing weights at the top of base plate; however, even then it is hard to seal the permeameter on the same spot. Consequently, each test was repeated twice on the same spot without displacing the permeameter. Figure 2 shows the NCAT permeameter on a pavement section.

Figure 2. NCAT Permeameter

Cooley (1999) recommended this permeameter for field permeability testing because it correlated to laboratory test results better than other field permeameters, was easy to use and

produced repeatable data. The coefficient of permeability is calculated using the following relationship.

$$k = \frac{a * l}{A * t} \ln\left(\frac{h_1}{h_2}\right)$$

Where :

k = coefficient of water permeability, cm/s,

a = inside cross-sectional area of inlet standpipe, cm^2,

l = thickness of test pavement, cm,

A = cross-sectional area of test pavement, cm^2,

t = average elapsed time of water flow between timing marks, s,

h_1= hydraulic head on pavement at time t_1, cm, and

h_2= hydraulic head on pavement at time t_2, cm.

Laboratory permeability testing device

Figure 3 shows the water permeability laboratory testing apparatus and Figure 4 shows its testing schematic. The test is based on the principle of a falling-head constant-tail permeability test. The apparatus and testing procedure are detailed in ASTM PS 129-01 (contained in appendix III).

The initial mark, the final mark and the time were recorded to calculate the coefficient of permeability. If the water level did not fall to the zero mark then a reading of water level in the graduated cylinder was taken after 30 minutes had elapsed and the test was re-run for another 30 minutes to obtain the average reading, which was considered for calculation purposes. If the water level fell to the zero mark then the specimen was considered sufficiently saturated if four consecutive permeability results were within ten percent of the mean result and the fourth permeability result was considered as final.

In this test, the coefficient of water permeability through the specimen is calculated as follows (ASTM PS 129-01), similar to NCAT permeameter calculations:

$$k = \frac{a * l}{A * t} \ln\left(\frac{h_1}{h_2}\right)$$

Where :

k = coefficient of water permeability, cm/s,

a = inside cross-sectional area of inlet standpipe, cm^2,

l = thickness of test specimen, cm,

A = cross-sectional area of test specimen, cm^2,

t = average elapsed time of water flow between timing marks, s,

h_1= hydraulic head on specimen at time t_1, cm, and

h_2= hydraulic head on specimen at time t_2, cm.

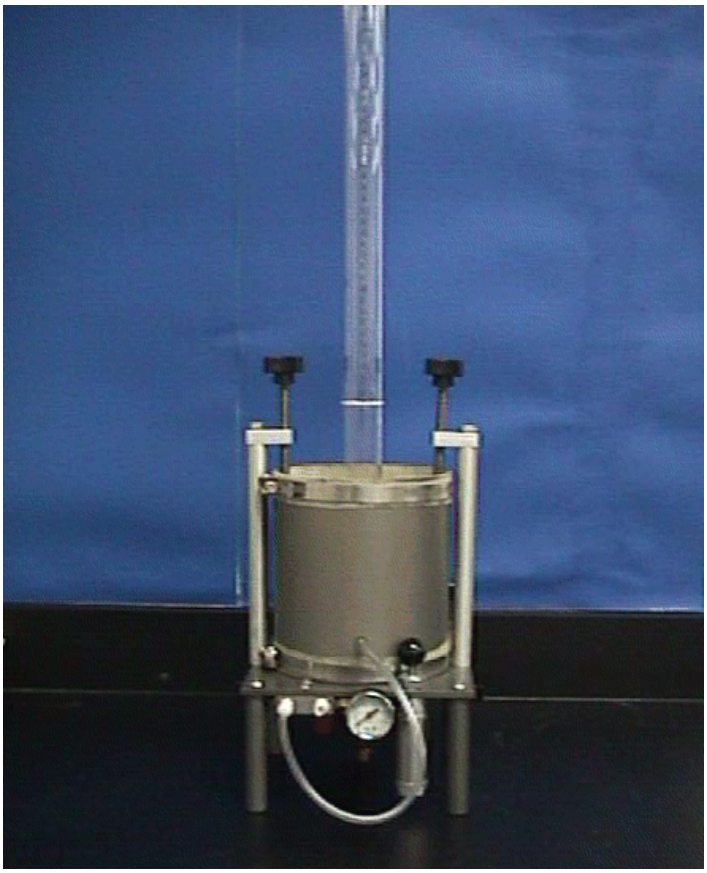

Figure 3– Water Permeability Laboratory Testing Apparatus

Some key assumptions regarding this calculation of permeability are as following.

1. Flow of water is laminar,
2. Permeability is unaffected by hydraulic gradient
3. Darcy's law is valid.

As seen in the literature review, there has been some debate concerning the validity of the assumptions necessary to use a falling-head type permeability test for HMA. However, one objective of this research is to validate the current, relatively simple, HMA laboratory test (ASTM PS129) by showing a relationship to field permeability results.

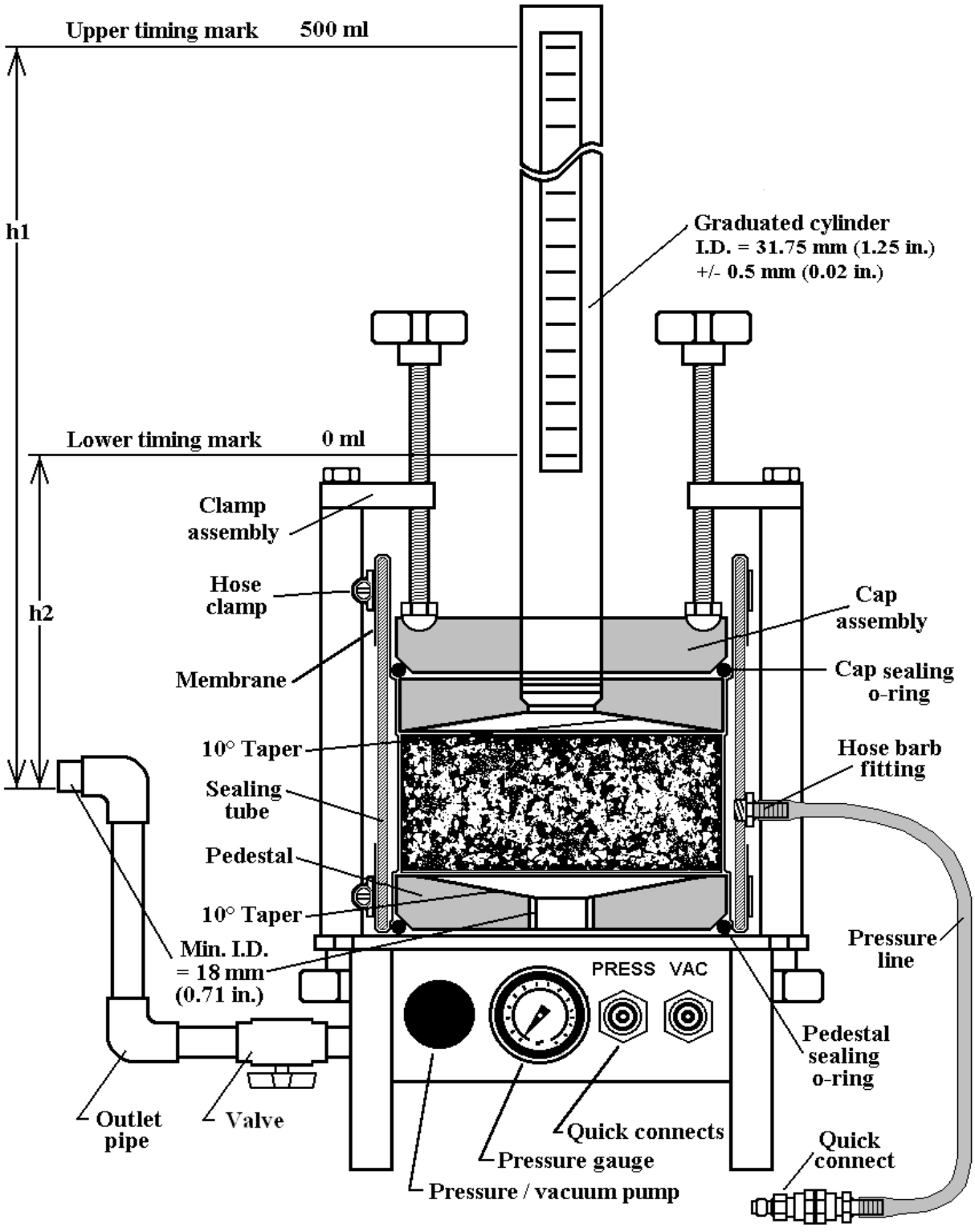

Figure 4– Water Permeability Laboratory Testing schematic (ASTM PS 129-01).

Corelok Testing device

Bulk specific gravity (G_{mb}) and effective air voids (η) of all SGC samples and cores were determined using the Corelok vacuum sealing method as detailed in ASTM D6752 and ASTM D6857. A specimen and plastic bag are weighed separately; the sample is then placed inside the bag and sealed using the Corelok device. The sealed bag is submerged into water and weighed. The submerged bag is cut (allowing water to saturate the specimen) and another weight is recorded. Based on these weights, bulk specific gravity and effective air voids are calculated. Bulk specific gravity and maximum specific gravity (Gmm) are used to calculate air voids. Maximum specific gravity is computed based on AASHTO T209. Figure 5 shows the Corelok device ready to seal a specimen of compacted hot-mix asphalt.

Figure 5. Corelok Vacuum Sealing Device

PROJECT SCOPE AND OBJECTIVES

Objective:

The overall objective of the project is to relate in-place and laboratory measures of permeability in order to establish permeability specifications for HMA. Several tasks were completed in order to progress toward this objective.

Task 1: Field Permeability Testing

Construction of test pads

Two testing pads were constructed at the Engineering Research Center (ERC) of the University of Arkansas. One of the pads had approximately 75mm thick, 12.50mm ACHM surface/wearing course over approximately 100mm thick, 25.0mm ACHM binder course. The other test pad had only the 25.0mm binder course, constructed to determine the moisture effects when a binder course would be exposed to traffic during one or more seasons. Both of the testing pads were constructed over approximately 175mm thick dense graded class 7 base material and approximately 300mm thick sub-base material. In order to get some permeability results, neither tack coat nor prime coat was used during construction of the pads. Normal size compaction and paving equipment was used so actual construction conditions could be replicated. For both of the pads asphalt cold-mix was used along the shoulders.

Field permeability testing of test pads

Each pad at ERC was subdivided into several grid sections. The Kuss field permeameter was used to measure the field permeability in all of the inner grid sections of both testing pads. The permeameter was not used in outer grid sections because the pads were without shoulders during that time, otherwise water would quickly permeate through sideways and

would result in erroneous data. The NCAT permeameter was also used for measuring the field permeability of different sections in the testing pads.

Permeability tests were performed during different times of the day and the test results are compared to the laboratory measurements of the mixes, prepared in a gyratory compactor, and to laboratory measurements of the cores taken from the pads.

Field permeability testing of different sites in Arkansas

A total of 17 sites were identified by AHTD for potential inclusion in the study. Field permeability measurements were conducted in the summer and fall of 2002. Each site was divided into three sections according to the severity of distresses i.e. good, average and poor section. For each section at least one field permeability test was performed using the Kuss permeameter and the NCAT permeameter. All of these recently constructed HMA highway/interstate sites were located within state of Arkansas as shown in Figure 6.

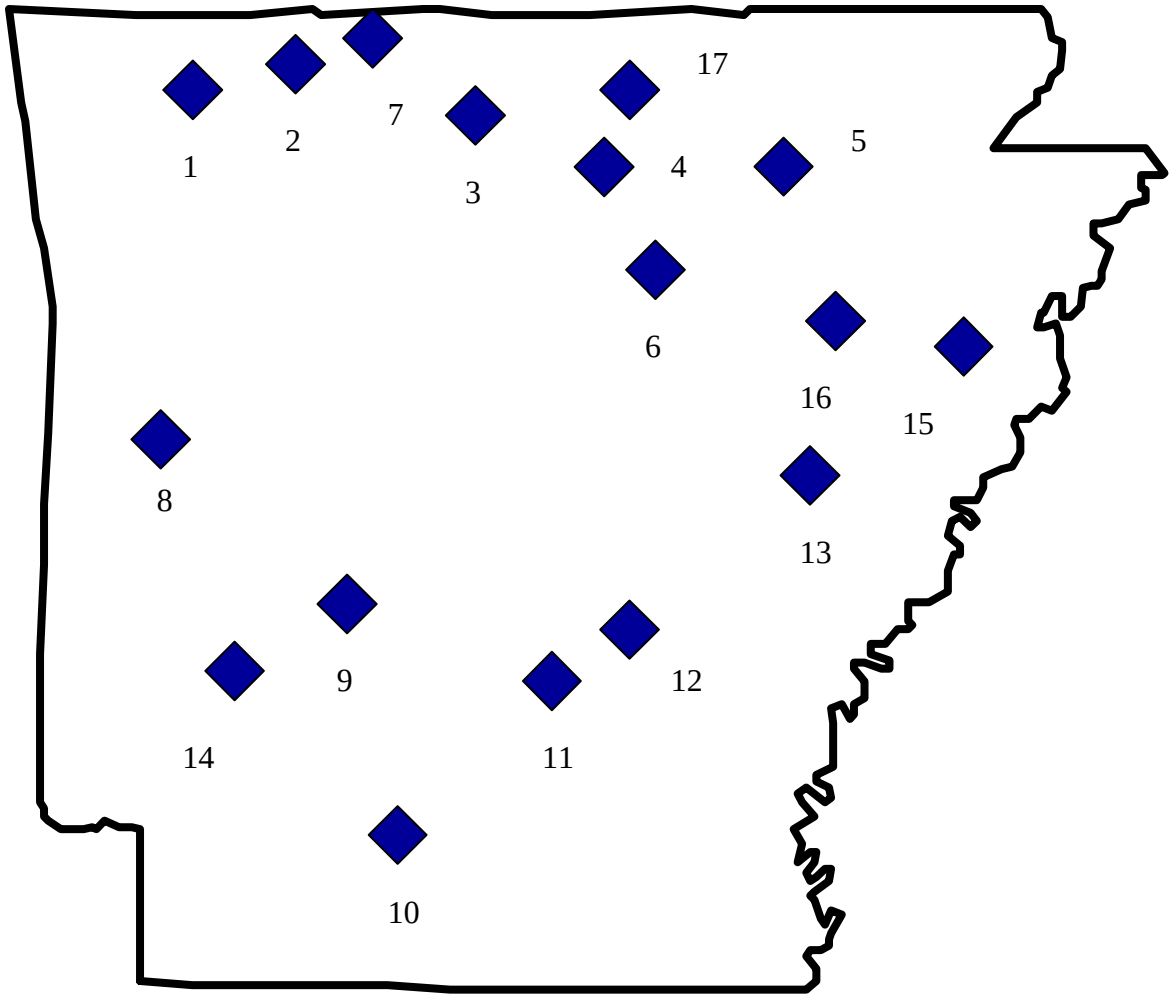

Figure 6– Arkansas map showing location of seventeen sites for field permeability testing.

1. Huntsville
2. Carrollton
3. Leslie
4. Melbourne
5. Newark
6. Pleasant Plain
7. Stateline
8. Y-city
9. Arkadelphia
10. Camden
11. Kingsland
12. Pine Bluff
13. Brinkley
14. Murfreesboro
15. Marked Tree
16. Wynne
17. Salem

Table 2 shows the design information for 16 out of 17 sites tested during this research work. Site no. 17 could not be tested in the laboratory because cores taken from the surface course were thinner than 75mm thickness required for the laboratory testing. The thickness requirement is explained later under the topic “Sampling”. Design compactive effort for these sites ranged from 114 to 195 gyrations. Binder contents ranged from 3.9 percent to 7.1 percent using performance grades of PG64-22 and PG76-22. These sites included overlay and full-depth HMA projects following Superpave protocols but only the top 70mm to 80mm of field cores were tested in the laboratory. Design lift thickness varied from site to site and nominal maximum aggregate size (NMAS) also ranged from 12.50mm to 37.50 mm depending on each site. Voids in mineral aggregate (VMA) ranged from 11.5 to 16.1 percent and design air voids were either 4.0 or 4.5 percent. Voids filled with asphalt ranged from 64 to 75 percent.

Results from the field permeability measurements are used for two purposes: (1) comparison to laboratory permeability measurements; (2) comparison of two different field permeability measurement methods.

Task 2: Laboratory Permeability Testing

Laboratory permeability testing was performed on three classes of HMA specimens:

1. field cores obtained from 16 AHTD in-service pavements
2. field cores obtained from the University of Arkansas test pavement
3. laboratory-compacted specimens
    a. specimens created using loose mix sampled during construction of the University of Arkansas test pavement
    b. specimens created using aggregates from local hot-mix asphalt plants

Table 2. Summary of the design information for 16 sites

Job No.	MIX TYPE	No. of Gyrations	PG Binder Content, %	PG Binder	Design Air Voids	VMA, %	VFA, %
1	12.5 mm	129	5.7	64	4.0	14.5	72
	25 mm	129	4.5	64	4.0	13.2	66
2	12.5 mm	169	7.1	64	4.0	15.7	75
	25 mm	129	5.6	64	4.0	12.9	69
	37.5 mm	169	4.1	64	4.0	11.9	66
3	12.5 mm	129	5.8	64	4.0	15.8	75
4	12.5 mm	169	5.2	64	4.0	15.4	74
	25 mm	169	3.9	64	4.0	12.8	69
	37.5 mm	160	3.9	64	4.0	13.1	69
5	12.5 mm	129	5.3	64	4.0	15.4	74
	25 mm	129	4.3	64	4.0	13.9	71
	37.5 mm	169	4.3	64	4.0	14	71
6	12.5 mm	160	5.9	64	4.0	14.9	73
	25 mm	160	4.9	64	4.5	12.9	65
7	12.5 mm	160	6.2	64	4.5	16.1	72
	25 mm	169	4.9	64	4.0	12.5	68
	37.5 mm	169	4.3	64	4.0	11.5	65
8	12.5 mm	160	4.5	64	4.5	15.1	70
9	12.5 mm	195	5.7	76	4.0	15	73
	37.5 mm	195	4.3	76	4.0	12.3	68
10	25 mm	115	4.9	64	4.0	13.8	71
11	12.5 mm	169	5.2	64	4.0	14.7	73
	25 mm	169	4.8	64	4.0	14.1	72
	37.5 mm	169	4.3	64	4.0	12.7	69
12	12.5 mm	160	5.3	64	4.5	14.7	69
	37.5 mm	169	4.8	76	4.0	12.9	69
13	12.5 mm	195	5.4	76	4.0	14.9	74
	25 mm	195	5.5	76	4.0	14.4	72
14	25 mm	129	4.8	64	4.0	13.3	70
	37.5 mm	129	4.8	64	4.0	13.1	70
15	12.5 mm	195	5.3	64	4.0	14.8	73
16	12.5 mm	115	5.4	64	4.5	15.3	71

Task 3: Analysis of results and recommendations

Results of both the laboratory and the field were analyzed statistically using an analysis of variance (ANOVA) or rank method, considering the data as a full factorial design with

permeability as the response variable. Effective air voids was considered instead of total air voids as a factor because it is already known from previous research that total air voids is a significant factor. Effective air voids are those internal voids which are accessible by water from the outer face of a specimen. Effective air voids are not necessarily interconnected from any face of a specimen to another opposite face. A set of three factors considered, along with different treatment levels, is shown below:

Factor	Type of Permeameter	Construction	Effective Air voids
Level 1	Laboratory	Full	Low (<5%)
Level 2	Kuss	Overlay	High(>=5%)
Level 3	NCAT	-	-

In addition to the ANOVA and rank analysis, a regression analysis was used to develop a relationship between significant factors. Further recommendations for considering permeability criteria in the mix design are suggested based on the analysis.

SAMPLING

Total number of Superpave Gyratory Compacted (SGC) samples and field cores used in this study are shown in Tables 3,4 and 5. SGC samples were compacted to a target of 7.0 percent air voids while field cores were as constructed. SGC samples were saw cut to a thickness of 75.0 mm with maximum deviation of 3.0mm while field cores were saw cut to a thickness of 75.0 mm with maximum deviation of 5.0mm. Field cores could not be cut with same allowable deviation as laboratory because of core faces being non-parallel. In some cases, where the difference between two edges was more than 5mm, then both sides of the core were saw cut, else the core was voided as the SGC cores were saw cut only on bottom side. According to previous researchers, samples thicker than 75mm are usually impermeable while permeability result varies with different thicknesses less than 75mm so a standard thickness was chosen, otherwise it would be difficult to compare field cores with SGC samples from the same mix-design.

The Gmm of field cores was determined, from the first core of each site tested for laboratory permeability, after removing the exposed aggregates from the surface of core, as per AASHTO T209.

Table 3. Summary of SGC samples and field cores from ERC test pad

Type	NMAS	Samples drilled or compacted	Laboratory test	Field NCAT test	Field Kuss test
SGC samples	12.50 mm	13	6	-	-
SGC samples	25.00 mm	20	7	-	-
Field cores	12.50 mm	17	17	17	17
Field cores	25.00 mm	17	17	17	17

Table 4. Summary of SGC samples using aggregate from local asphalt plant

Source	NMAS	Samples drilled or compacted	Laboratory test
McClinton Anchor @ Sharps	12.50 mm	21	10
McClinton Anchor @ Sharps	25.00 mm	23	10
Arkhola @ JennyLind	12.50 mm	22	15
Arkhola @ JennyLind	25.00 mm	12	6

Table 5. Summary of field cores from 17 sites

Site No.	AHTD Job No.	Samples drilled	Laboratory test	Field NCAT test	Field Kuss test
1	009948	15	3	-	6
2	009918	15	4	-	4
3	R90116	15	4	-	5
4	R50067	15	5	6	5
5	R50017	15	4	5	6
6	R50084	15	6	6	6
7	090001	15	5	-	5
8	R40107	17	7	5	4
9	070018	15	5	6	6
10	070079	15	4	6	6
11	070138	15	5	5	5
12	R20149	15	4	6	6
13	R10055	15	4	-	5
14	R30112	15	4	6	6
15	R00152	15	6	-	7
16	110413	15	9	6	6
17	50073	15	-	-	6

RESULTS AND DISCUSSIONS

A discussion follows which includes the results of analyses performed to address the project objectives. The statistical procedures used in the analyses are explained, followed by specific discussion of objectives.

Statistical Analysis

Balanced data was used for statistical analysis because the data was not collected uniformly for all factors. The factor having the least results after all combinations formed the basis for choosing the maximum number of replicates.

The balanced data of sixty observations based on five replicates for each combination of three factors is shown in Appendix I. It was analyzed using an analysis of variance (ANOVA), considering the data as a full factorial design with permeability as the response variable. After running ANOVA, the Normal probability plot showed that data was not normal as shown in Figure (f) of Appendix I. This violated the assumption of normality NID $(0,\sigma^2)$. The plot should have resembled a straight line and more emphasis was placed on the central values than the extreme values. The plot of residuals versus fitted values also exhibited obvious patterns like an outward-opening funnel or megaphone in Figure (g) of Appendix I. So, it confirmed that the plot illustrated non-constant variance.

Rank transformation was used to resolve the normality issue. Programming code is presented in the beginning of Appendix I. After rank transformation, the p-value of Shapiro-wilk and most of other tests of normality became greater than the significance level of 0.05 and the normal probability plot became a straight line as illustrated in Figure (a). The plot of residuals versus fitted values as exhibited in Figure (b), and plots of residuals versus other variables such as type of permeameter, air voids or effective air voids and type of

construction did not explain any patterns in Figures (c), (d) and (e) so assumptions of independence and constant variance were also justified.

Significant factors two main effects i.e. type of permeameter and effective air voids, and also the interaction of effective air voids and type of construction at a significance level of 0.05. These observations are summarized in Tables 6.

Table 6. Significant factors at significance level of 0.05

Significance level	Significant factors
0.05	Effective air voids, Type of permeameters and Interaction of Effective air voids and Type of construction

It was considered to take into account all of the aggregate sources corresponding to field mixes, but the main data was so unbalanced that results might be misleading.

Regression model was also written in the programming code to check the R-square value that explained the variability of the data. A low R-square value indicates the model does not adequately describe the variability exhibited by the data. The R-square value obtained was less than 20 percent so the regression model not reliable.

It is recommended to plot graphs of only total air void versus permeability for each type of permeameter.

Assessment of Validity of Permeability Tests

One primary assumption for calculation of permeability was that flow was laminar. If the Reynolds number was greater than 2000 then the flow would not be laminar and that assumption would be invalid. Table 7 shows the calculation of Reynolds number for samples having very high permeability. F25 was an SGC sample supplied by FDOT for round robin

studies. It was 50mm thick and exhibited a effective air voids of 10.3 percent. Its coefficient of permeability was $319x10^{-5}$ cm/s. It had only one dimensional flow in the laboratory permeameter. Sample no. 18 was obtained from site no. 6 (Pleasant Plain, AR) and it had co-efficient of permeability of $703x10^{-5}$ cm/s. It was 75mm thick and its effective air voids was 8.1 percent. The other highly permeable sample (no. 64) represented an approximate location in site no. 9 (Arkadelphia, AR), which was tested using NCAT permeameter. It was 150mm thick and its effective air voids was approximately 9.6 percent based on 81mm field core. It had probably either two or three dimensional flow in the field.

In order to calculate Reynolds no., two assumptions were made. Firstly, it was assumed that all the voids are interconnected and secondly, they are distributed linearly along the thickness of a sample just like a circular pipe. If first assumption of considering interconnected voids was wrong then these samples could still have laminar flow till the effective flow area would be at least 1 percent of the total voids area. The minimum effective area required for each sample is shown in Table 7. If the other assumption of considering a void pathway like a circular pipe was also wrong then Reynolds no. was most likely underestimated but the question would be that how much was it underestimated?. After analyzing the Reynolds no. for a single void pathway in Table 7, it can be concluded that replacing a single void pathway with several pathways would not jump the Reynolds no. shown in Table 7 above 2000. Finally, it can be concluded that all samples had laminar flow passing through them and there effective area will be certainly more than the corresponding minimum effective area shown in the table. So, primary assumption seems to be valid for most of the cases and these permeameters could be used to determine highly permeable pavements or cores.

Table 7. Check of a laminar flow for samples having high permeability

Sample No.	F25	18	64
Source	FDOT SGC sample	Pleasant plain (site no.6)	Arkadelphia (site no.9)
Type of test	Laboratory	Laboratory	NCAT
Air voids (%)	10.3	11	9.6
Effective air voids (%) (η)	10.3	8.1	9.6
Permeability (cm/s) (k)	0.00319	0.00703	0.03135
Head loss (cm) (H)	63.5	63.5	10
Discharge (cm^3/s) (Q)	5.46	8.02	9.59
Volume of voids (cm^3) Vv= (η/100) x sample vol.	92.53	111.10	241.24
Voids Area (cm^2) A=(Vv/sample thickness)	18.24	14.73	16.08
Voids diameter (cm) D=sqrt(4xA/π)	4.82	4.33	4.52
Voids Velocity (cm/s) (V=Q/A)	0.30	0.54	0.60
Reynolds no. (R=DV/ν) where ν=kinematic viscosity	162	264	302
Laminar flow (R<2000)	**Yes**	**Yes**	**Yes**
Minimum effective area for laminar flow	**0.65%**	**0.38%**	**0.26%**

Relationship Between Laboratory Permeability and Air Voids

One of the objectives of this study was to evaluate the relationship between laboratory permeability and air voids. Figures 7 through 10 explain the relationship between laboratory permeability and air voids of SGC samples using aggregate blends from McClinton Anchor and Arkhola. The binder contents of 25.0 mm and 12.50 NMAS mixes from McClinton Anchor were 5.2 and 6.0 percent, respectively. The binder contents of 25.0 mm and 12.50 NMAS mixes from Arkhola were 5.0 and 6.1 percent, respectively.

Graphs of McClinton Anchor illustrated relatively low R^2 values for both NMAS mixes, which suggests that the source of aggregate also may affect permeability. The relatively few data points contained in Figures 7 through 10 reduces the usefulness of the regression models shown, but it does illustrate that air voids of SGC samples had a relationship with permeability. The 25.00 mm NMAS plots for both sources have lower R^2 value than the 12.50 mm NMAS; suggesting that larger aggregates did not generate consistent interconnected air void paths in the gyratory compactor. It is generally accepted that SGC specimens having low air void levels are impermeable; adding data points of zero permeability at low air voids (as shown in Figure 11 for the 'blend 1' originally plotted in Figure 10) effectively reduces the R^2 value by 22 percent. This suggests a need for zoning permeability levels in the plots. Permeability zones should be divided into impermeable, low permeable and high permeable regions. After zoning better relationships might be established; this would better measure the water percolation of same SGC mixes in the field.

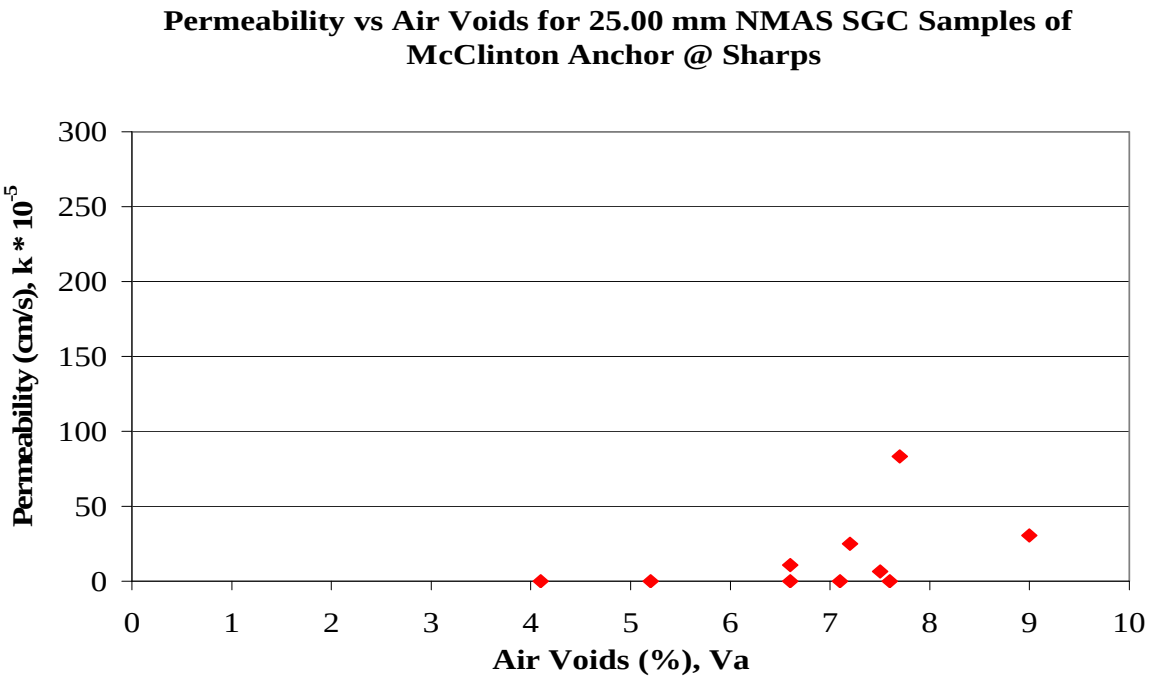

Figure 7. 25.00 mm NMAS SGC Samples of McClinton Anchor

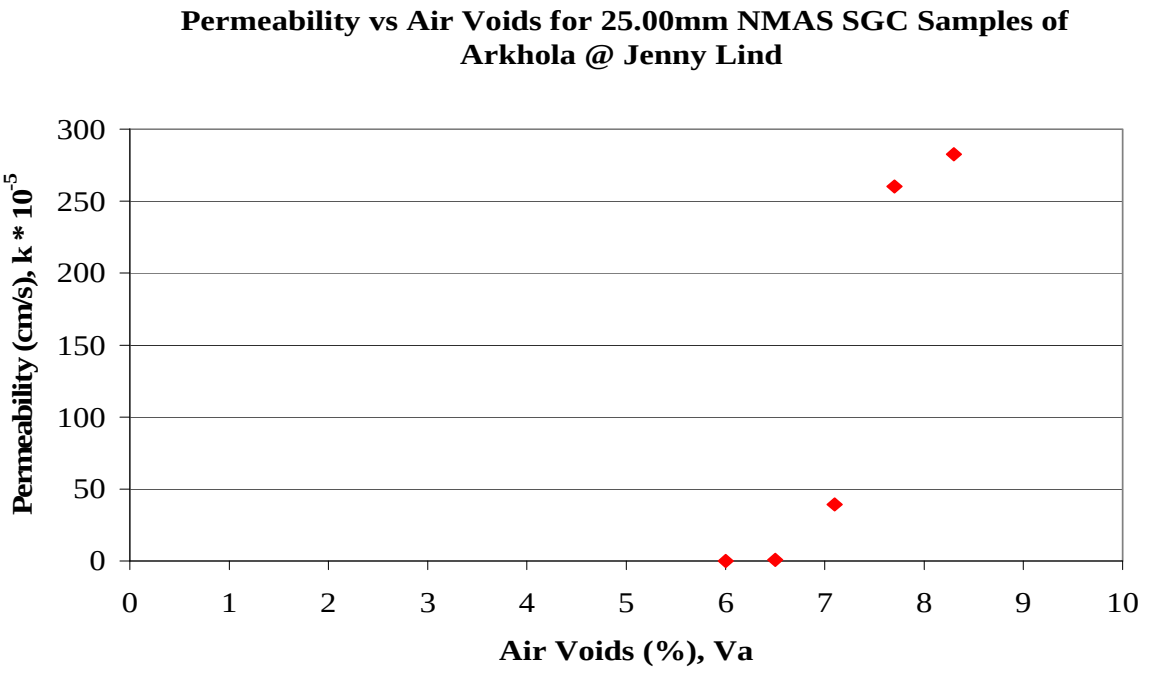

Figure 8. 25.00 mm NMAS SGC Samples of Arkhola

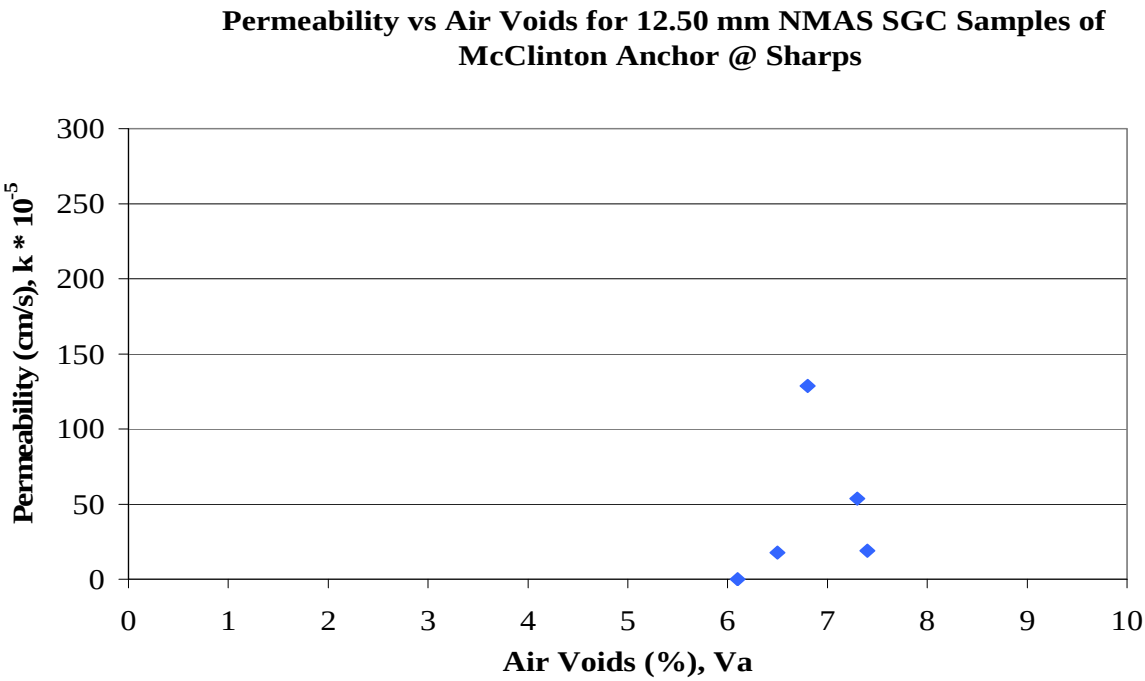

Figure 9. 12.50 mm NMAS SGC Samples of McClinton Anchor

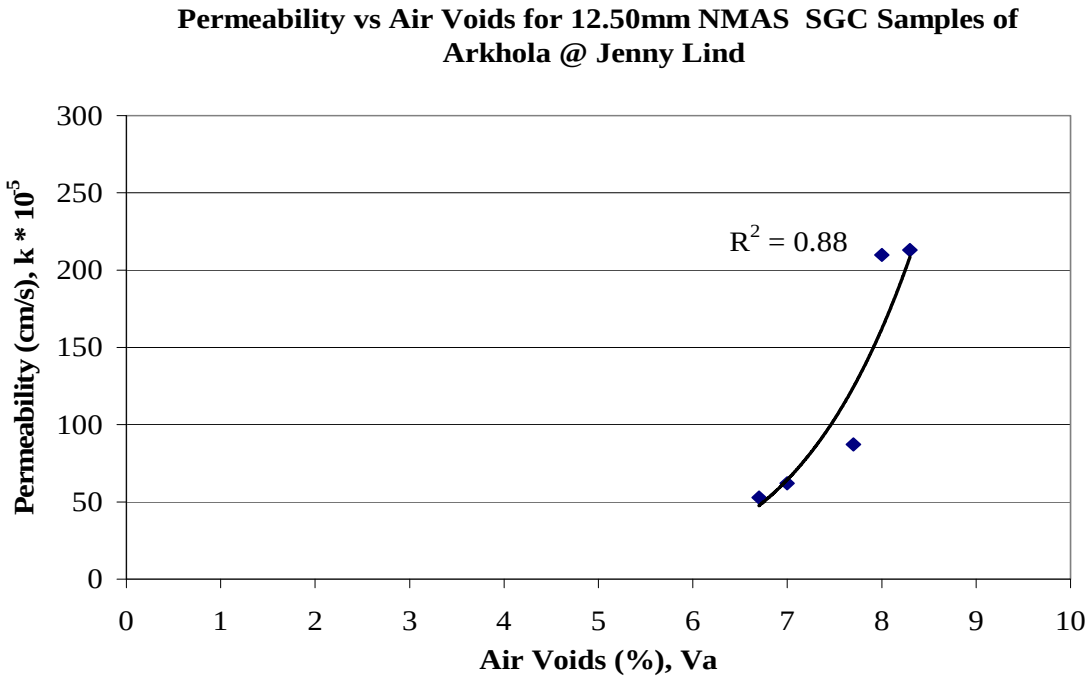

Figure 10. 12.50 mm NMAS SGC Samples of Arkhola (power relationship)

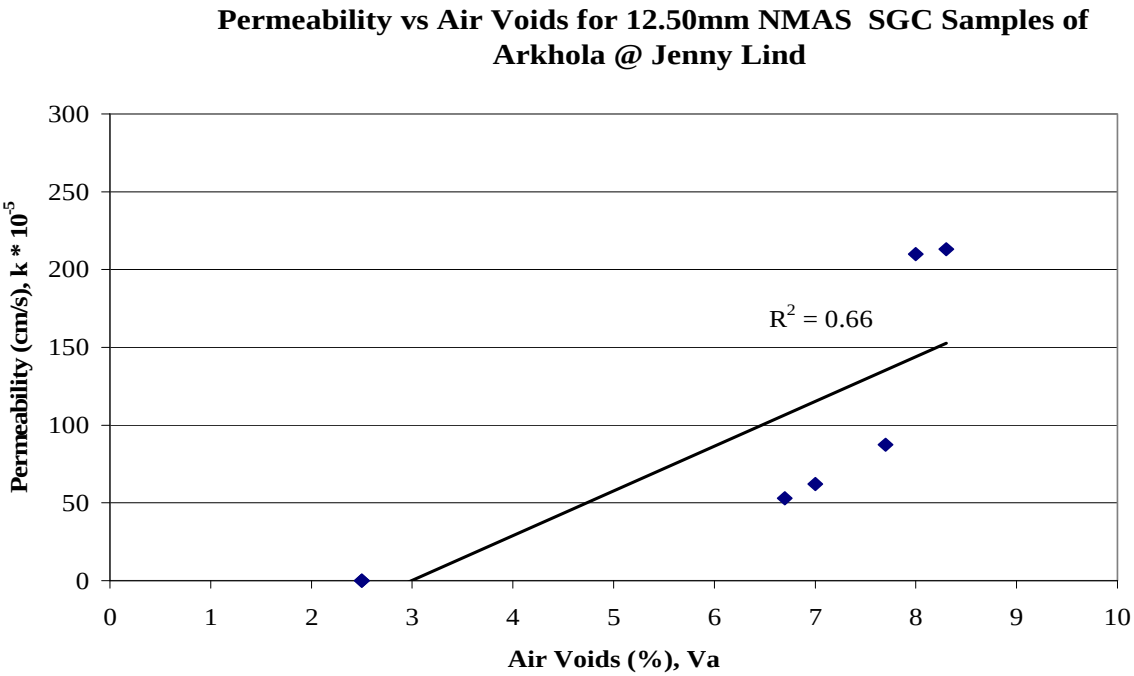

Figure 11. 12.50 mm NMAS SGC Samples of Arkhola (linear relationship)

Figure 12 shows that field cores having air voids of 6 percent or less were impermeable at all sites, while field cores having air voids between 7 percent and 9 percent show laboratory permeability of less than $100x10^{-5}$ cm/s. All field cores having greater than 9 percent air voids were highly permeable. It was concluded that laboratory permeability results showed a good relationship to in-place air voids, even though there were many variable factors such as binder content, source of aggregate and volumetric properties.

All sites were analyzed individually by plotting their laboratory permeability against the in-place air voids as shown in Figures 13 to 27. Laboratory permeability for cores having air void levels between 6 percent and 8 percent varied from site to site; all the field cores exhibited either high or very high permeability above 8 percent air voids. Mixes with 25mm NMAS size seemed to be less permeable than 12.5mm NMAS – although the data set for this is limited. Specific observations related to this analysis follow.

- Field cores obtained from Carrollton, Leslie, Melbourne, Murfreesboro, Marked Tree and Wynne were all impermeable. All had in-place voids of less than 7 percent, with the exception of one core from Melbourne (7.4 percent).
- Field cores obtained from Sulphur Rock, State Line, Arkadelphia exhibited some permeability at relatively low air voids (i.e. 6 percent), and exhibited relatively high permeability at higher air voids.
- Field cores acquired from Y-City, Kingsland, Brinkley and Pine Bluff were either impermeable or showed low permeability at air void levels up to 7 percent, but showed moderate laboratory permeability at higher air voids.
- Field cores from Camden exhibited low permeability even at 8 percent air voids.
- Field cores obtained from Pleasant Plain had higher air voids, and correspondingly higher permeability.

Relationship of Field Permeability with Air Voids Level

As stated earlier, field permeability was used as a term to represent "equivalent field percolation", which in reality just indicated a measure of flow, not a true permeability. For its calculation it was assumed that surface course was placed over a free draining material and water permeated through the full thickness of a surface course. When calculated co-efficient of permeability was compared with the testing time so it was noticed that water could not have permeated all the way through the thickness of a surface course in the field. If thickness was reduced in next trial calculation then it substantially decreased the co-efficient of permeability due to increase in the gradient and consequently another iteration would be required. This never ending iteration process proved that the flow was three dimensional and the formula used to calculate field permeability provided just an approximate value.

Arkansas Field Sites

Field permeability data was available for both field permeameters for only ten sites. This data was plotted against air voids and, as noted in Figure 12, R^2 values were 0.50 and 0.55 for NCAT and Kuss permeameters, respectively. A number of external factors may help to explain this observation:

- The pavements represented in Figure 12 had different volumetric properties, (shown in table 2).
- The pavements had different sources of aggregates and different types of binder.
- Two operators performed the field testing potentially introducing an operator or testing error into the results.
- The field density might be different in those spots where the Kuss and NCAT devices were setup. Both permeameters could not be setup on the same spot because the sealant would not seal properly on a wet spot.
- There were many impermeable spots reported by Kuss permeameter whereas the NCAT device indicated permeability next to these spots. However, it was more difficult to seal the NCAT permeameter at the base than the Kuss permeameter using same sealant (plumber's putty); it was likely that the NCAT measurement was misleading due to little leakage.

All of the field data from different sites was plotted individually to compare the field permeability of each site with the in-place air voids. Observations related to the analysis follow.

- Figure 13 shows that the field permeability recorded by Kuss permeameter in Carrollton (over a 12.5 mm surface course) was almost zero, even for air voids between 6 percent and 7 percent.
- Figure 14 shows the Leslie site (also having a 12.5mm surface course) to be almost impermeable.
- The NCAT permeameter recorded permeability at the Melbourne site (shown in Figure 15) even at low air voids – in direct contrast to the Kuss permeameter.
- Similar to Melbourne, the NCAT permeameter recorded Sulphur Rock site as permeable while Kuss permeameter recorded it as impermeable even at high in-place air voids (Figure 16).
- Both permeameters recorded a similar trend of field permeability in the Pleasant Plain site – increasing permeability with higher air voids as illustrated in Figure 17.
- Usually Kuss permeameter determined the pavements having low in-place air voids as less permeable except in Figure 18 where Kuss permeameter was used near State line that illustrated very high permeability even at intermediate air voids. Field testing spots, on highway 65 near State line, were on steep longitudinal grade which verified that field permeability was affected by steep slope.
- NCAT permeameters recorded high permeability at low air voids and low permeability at intermediate air voids in Y-City so Figure 19 illustrated that Kuss permeameter was more consistent than NCAT permeameter in that particular site.
- Figure 20 explained that Arkadelphia site had some sections extremely permeable which were recorded by both field permeameters. Kuss permeameters could not

record higher values because the discharge was higher than 158 ml/min (equivalent permeability of $179x10^{-5}$ cm/s) while it was only designed to measure up to 158 ml/min. Kuss permeameter had the same problem on Highway 65 near state line where almost all the sections were extremely permeable but it could not measure the discharge of more than 158 ml/min ($179x10^{-5}$ cm/s).

- Camden site illustrated good relationship in Figure 21, between field permeability and in-place air voids but NCAT measured more permeability than Kuss permeameters at intermediate and high in-place air voids.
- Where as, Figure 23 of PineBluff site except one data point shows that both permeameters had similar permeability trends and also relatively closer field permeability values recorded at intermediate air voids.
- Kingsland site was impermeable even at high air voids as depicted in Figure 22 while Figure 24 shows that field permeability of Brinkley site slightly changed with the change in air voids even at low permeability values.
- In Murfreesboro both permeameters depicted in Figure 25 that 25mm NMAS surface course was almost impermeable at low air voids.
- In Marked Tree only Kuss permeameters was used and Figure 26 presents that it had low in-place air voids and pavement was impermeable.
- In Wynne, three spots were chosen in between wheel paths for field permeability measurements while two spots were selected in inner and outer wheel paths. Kuss permeameter recorded “between wheel paths” as permeable while inner and outer wheel path as impermeable. NCAT permeameter verified “between wheel paths” as

permeable with higher permeability values and illustrated relatively very low permeability value for “inner and outer wheel paths” in Figure 27. Field permeability results of Kuss and NCAT permeameter for each site were averaged according to “wheel path” and “between wheel path” as shown in the Tables 8 and 9. It was noticed that in general field permeability was not affected by wheel path.

Table 8. Average field permeability of “Wheel path” and “Between wheel path” using Kuss permeameter

SITE	Outside/Inside Wheel Path $k*10^5$ (cm/s)	Between Wheel Path $k*10^5$ (cm/s)
Arkadelphia	210	170
Brinkley	9	31
Camden	5	2
Carrollton	1	0
Huntsville	2	-
Kingsland	30	1
Leslie	0	0
Marked Tree	0	0
Melbourne	1	0
Murfreesboro	0	2
PineBluff	20	19
Pleasant plain	130	315
Stateline	140	20
Sulphur rock	30	105
Wynne	1	0
Y-city	40	1

Table 9. Average field permeability of "Wheel path" and "Between wheel path" using NCAT Permeameter

SITE*	Outside/Inside Wheel Path $k*10^5$ (cm/s)	Between Wheel Path $k*10^5$ (cm/s)
Arkadelphia	212	30
Camden	10	0
Kingsland	1	1
Melbourne	47	20
Murfreesboro	0	2
PineBluff	6	20
Pleasant plain	200	330
Y-city	195	4
Sulphur rock	6	10
Wynne	7.5	110

*NCAT permeameter was not available for sites not shown in the above table.

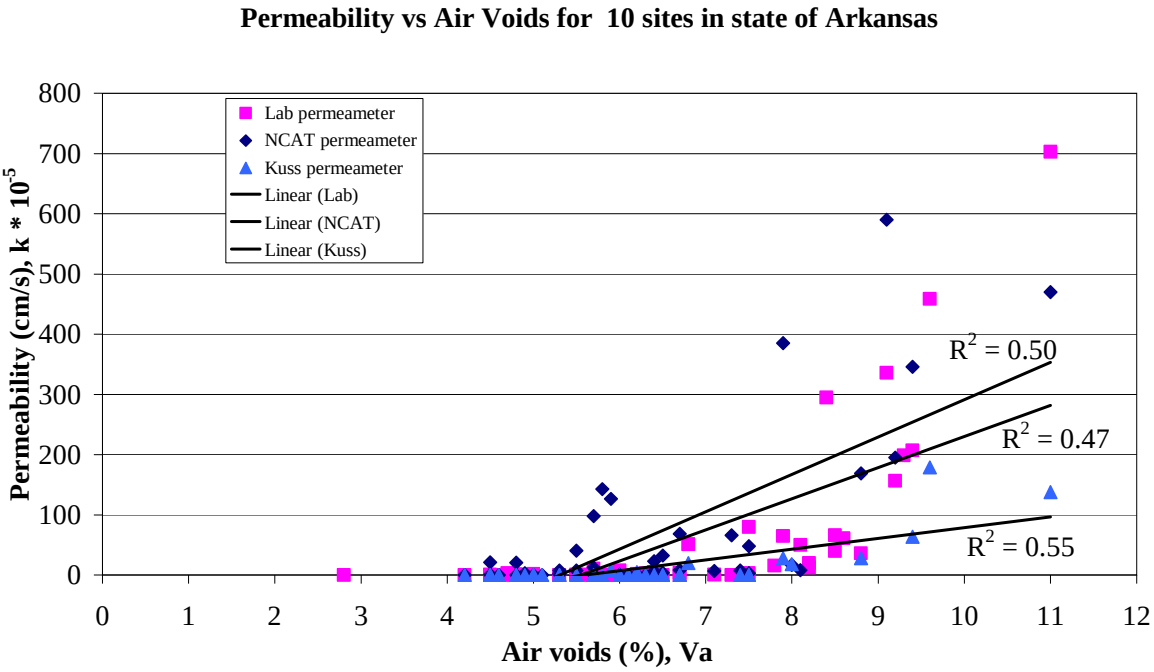

Figure 12. Permeability vs Air Voids for field cores of 10 selected sites

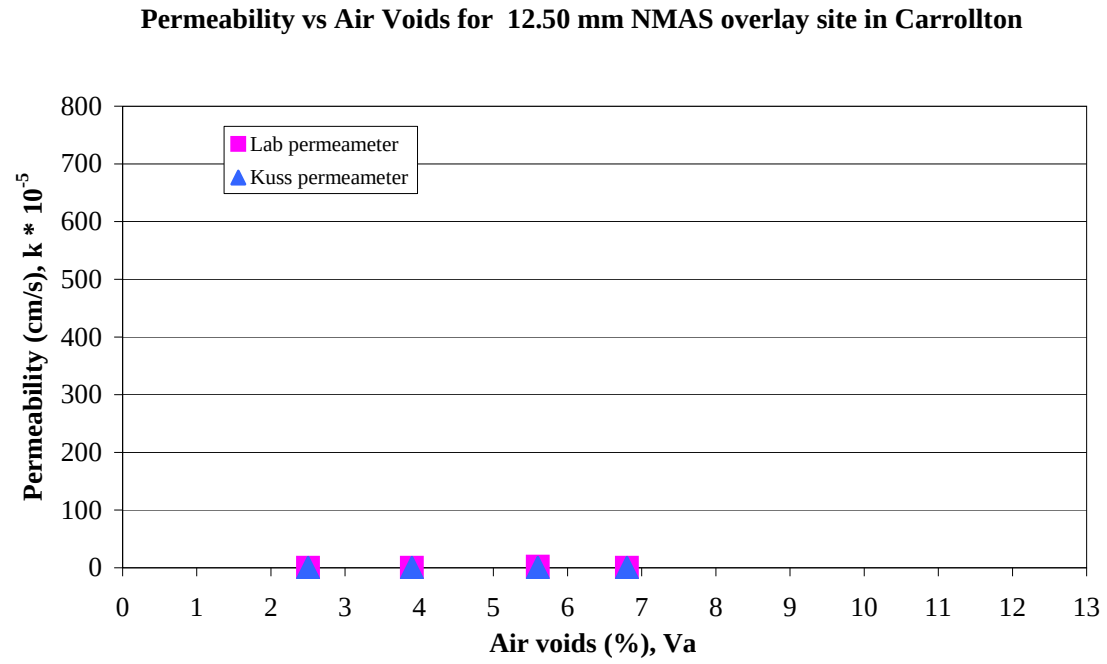

Figure 13. Permeability vs Air Voids for the site in Carrollton

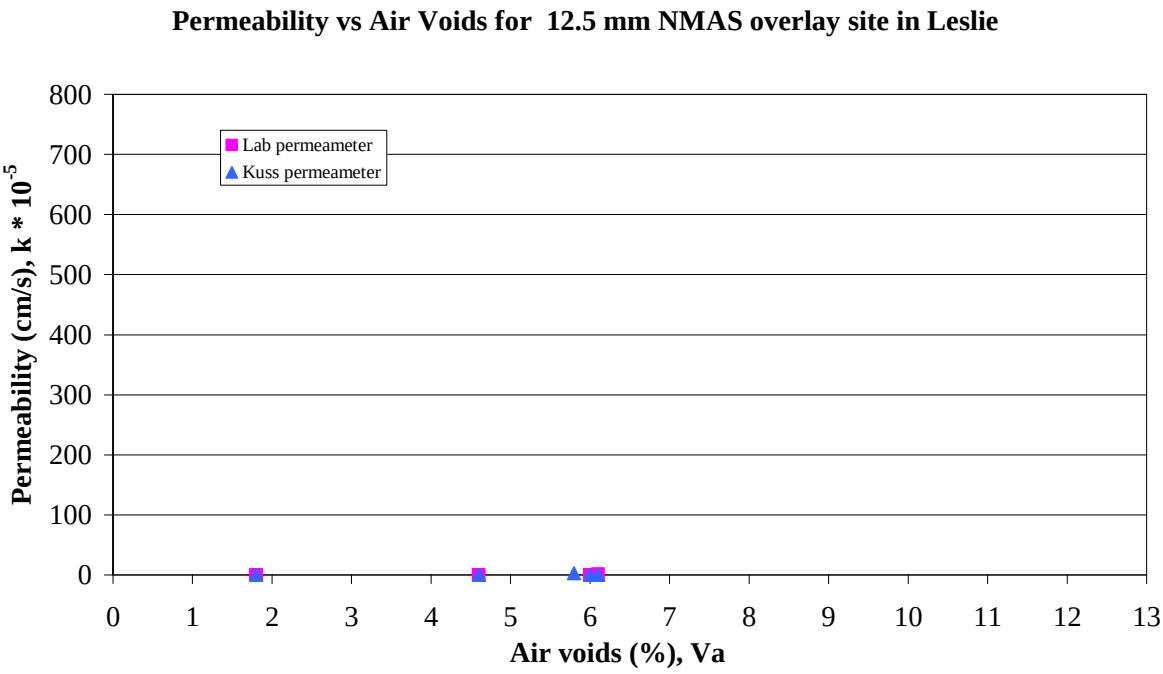

Figure 14. Permeability vs Air Voids for the site in Leslie

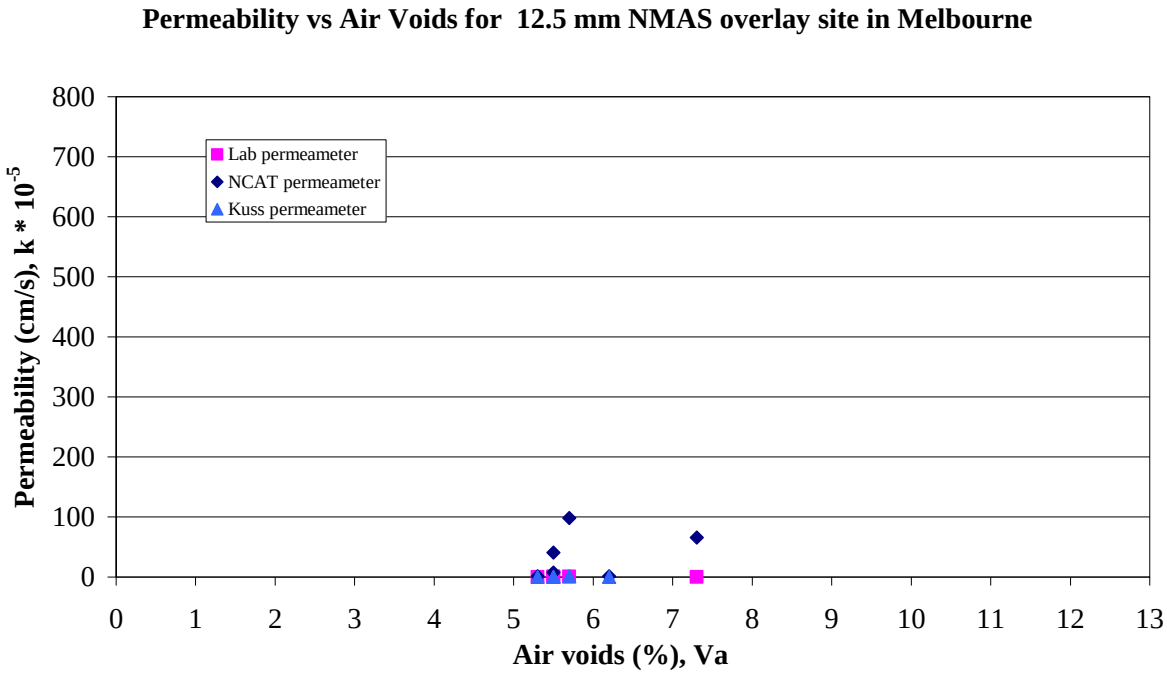

Figure 15. Permeability vs Air Voids for the site in Melbourne

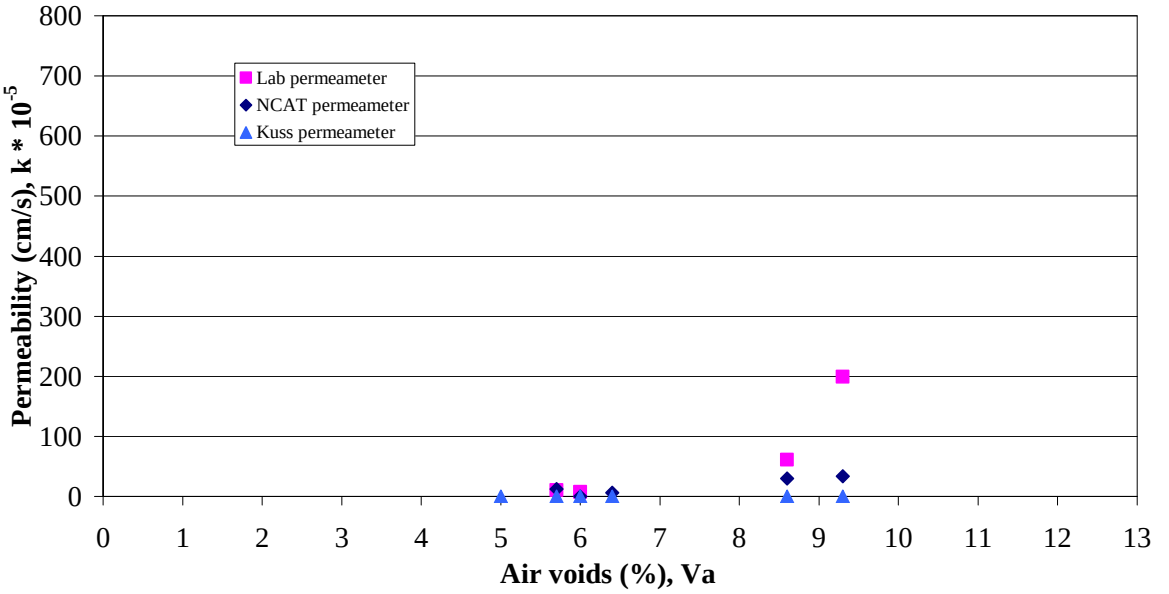

Figure 16. Permeability vs Air Voids for the site in Sulphur Rock

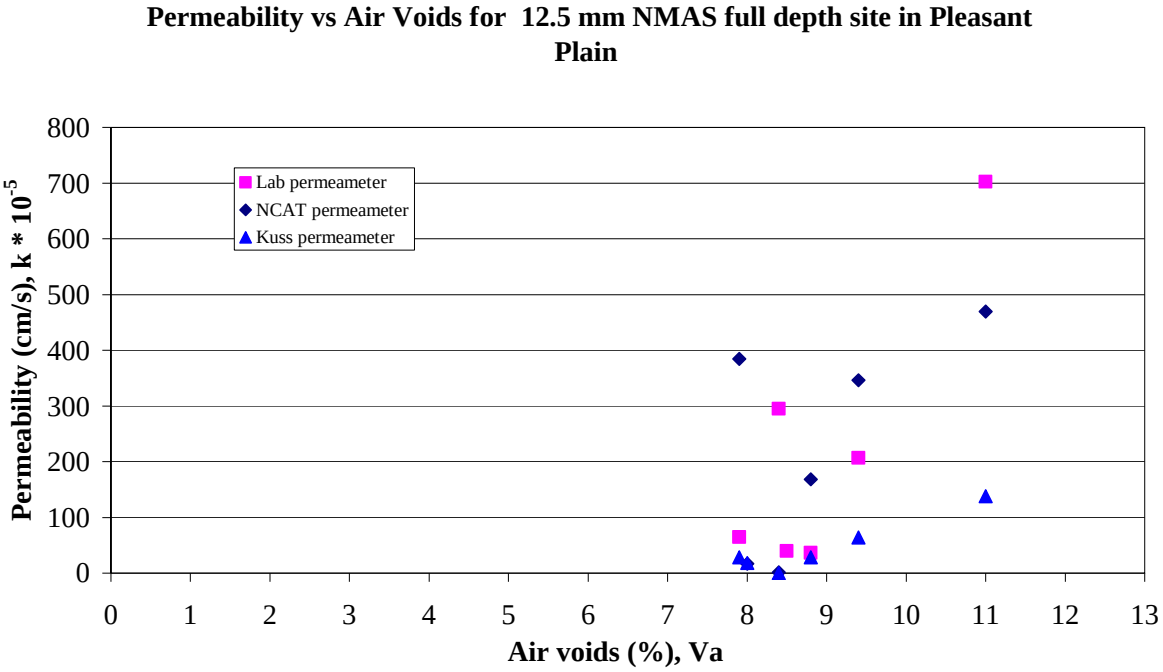

Figure 17. Permeability vs Air Voids for the site in Pleasant Plain

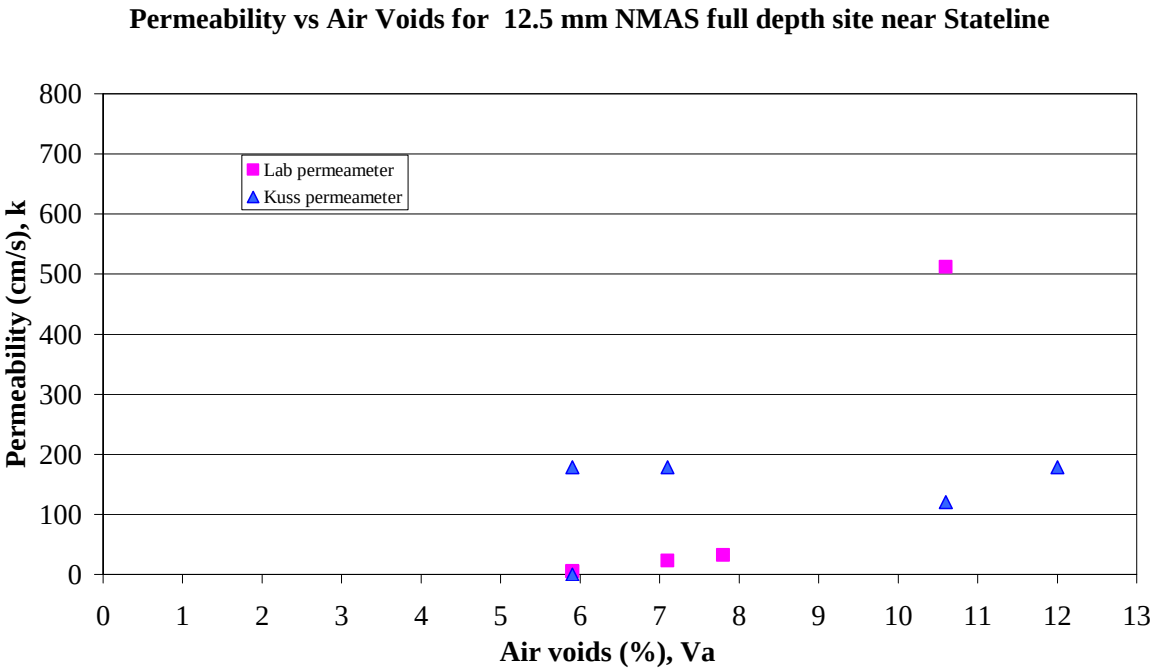

Figure 18. Permeability vs Air Voids for the site near State Line

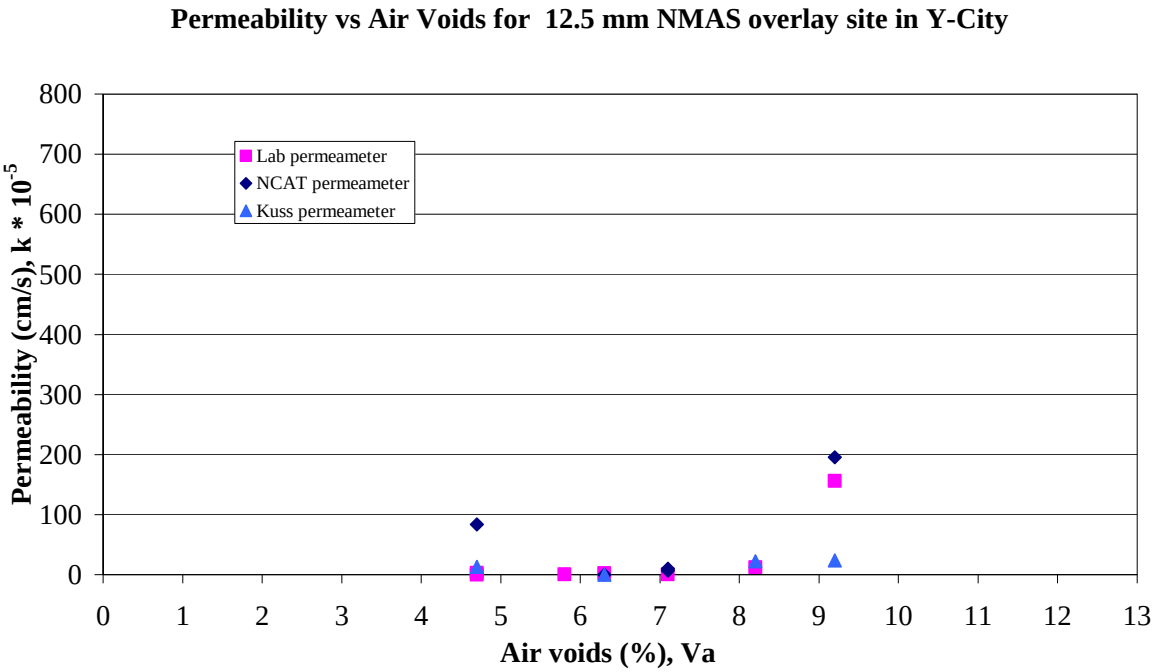

Figure 19. Permeability vs Air Voids for the site in Y-City

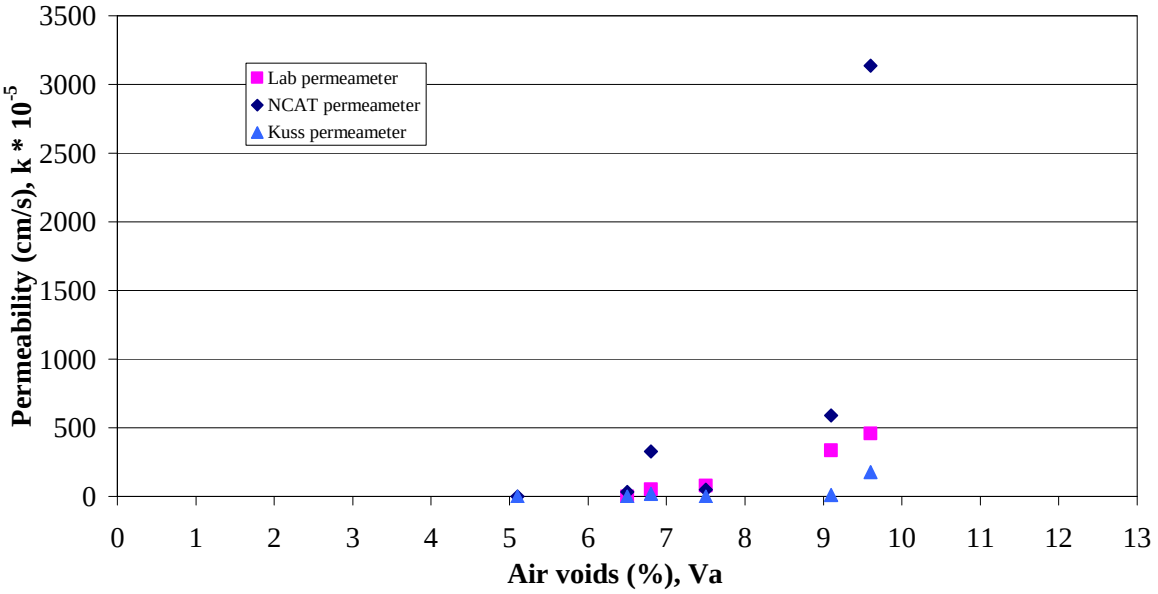

Figure 20. Permeability vs Air Voids for the site in Arkadelphia

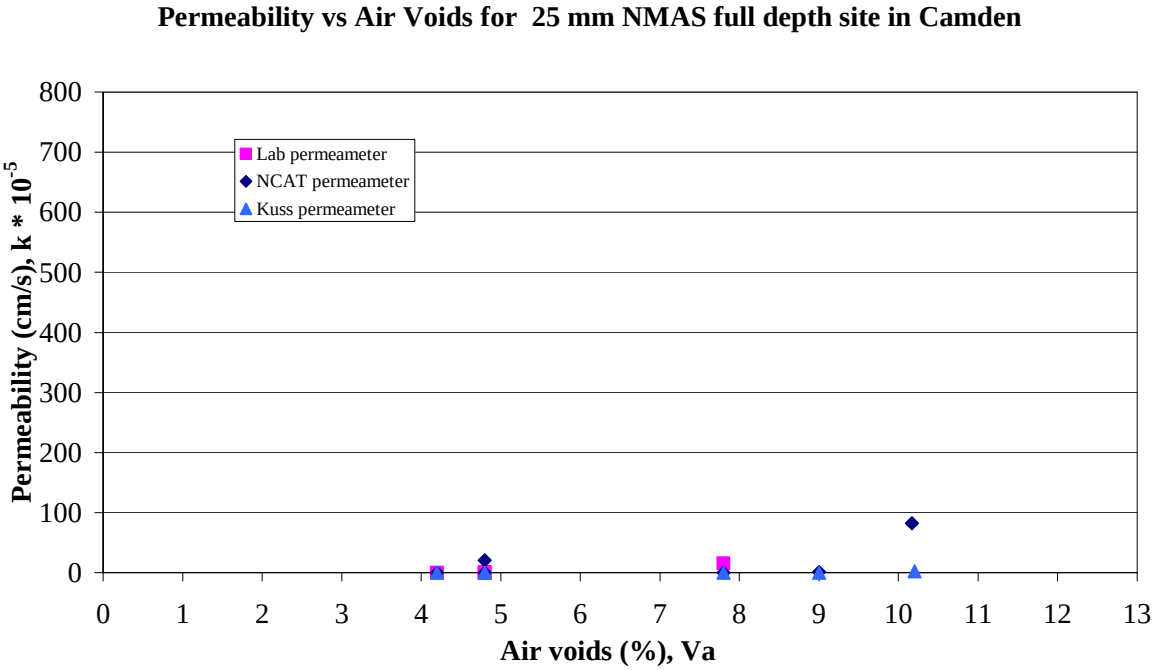

Figure 21. Permeability vs Air Voids for the site in Camden

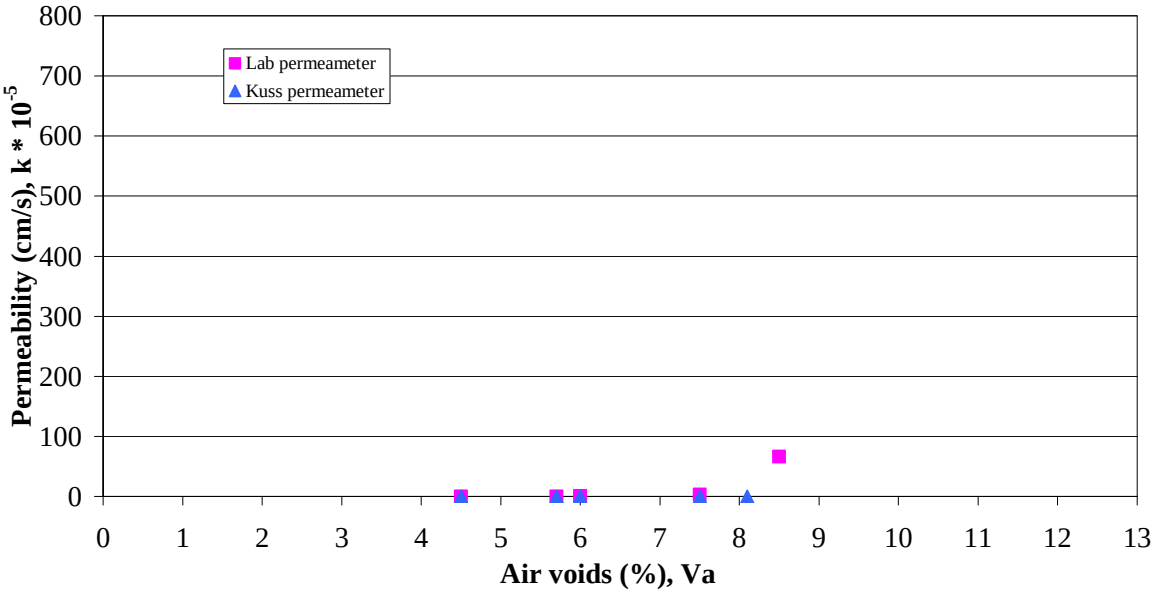

Figure 22. Permeability vs Air Voids for the site in Kingsland

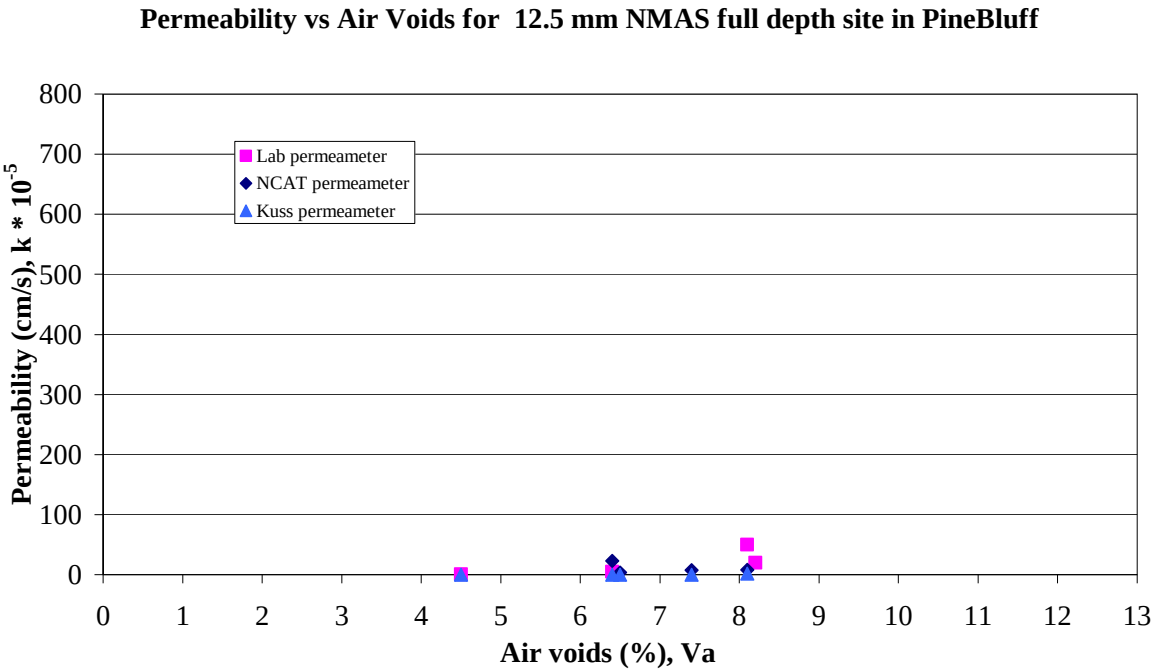

Figure 23. Permeability vs Air Voids for the site in PineBluff

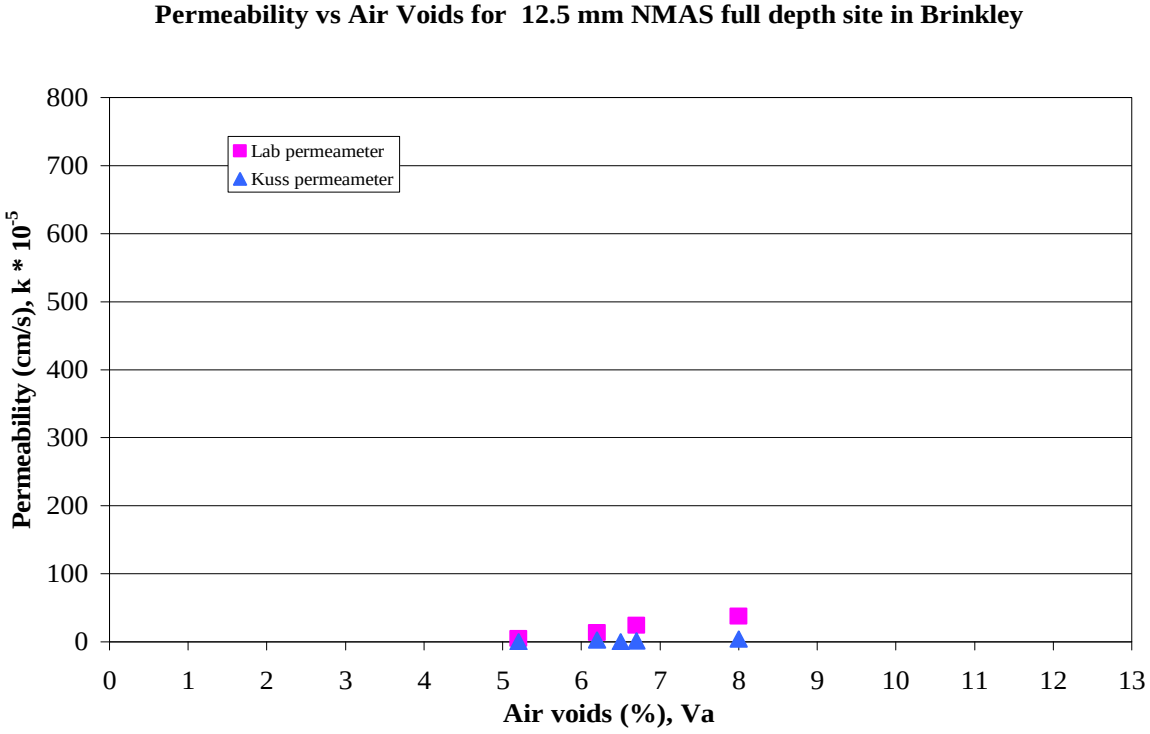

Figure 24. Permeability vs Air Voids for the site in Brinkley

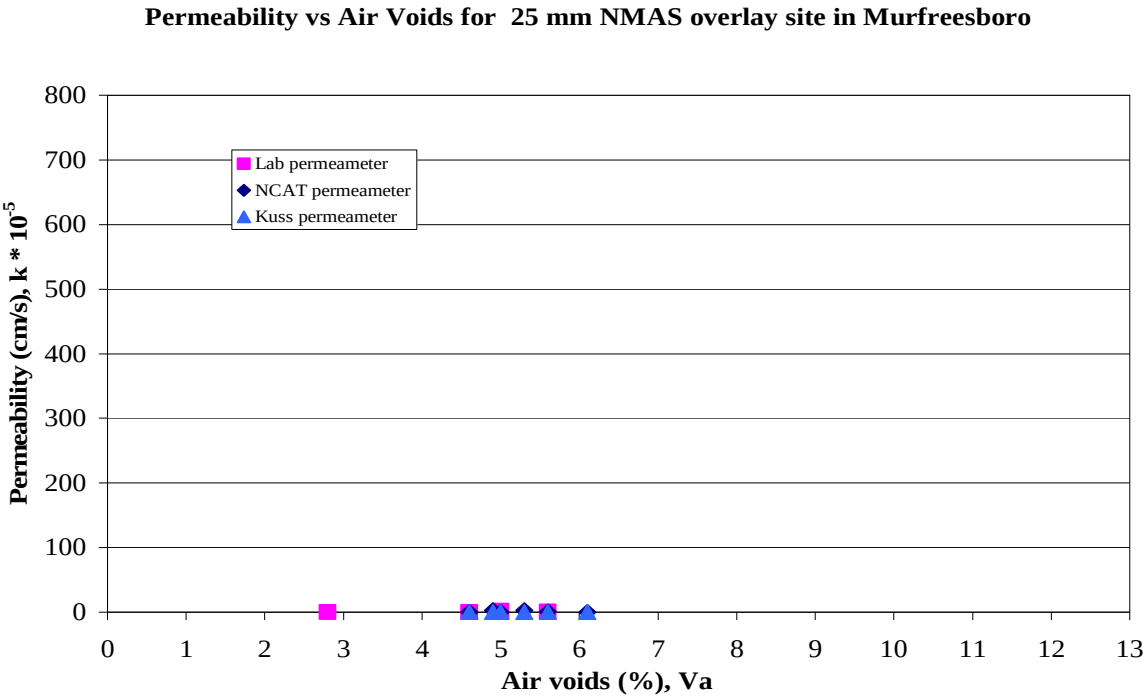

Figure 25. Permeability vs Air Voids for the site in Murfreesboro

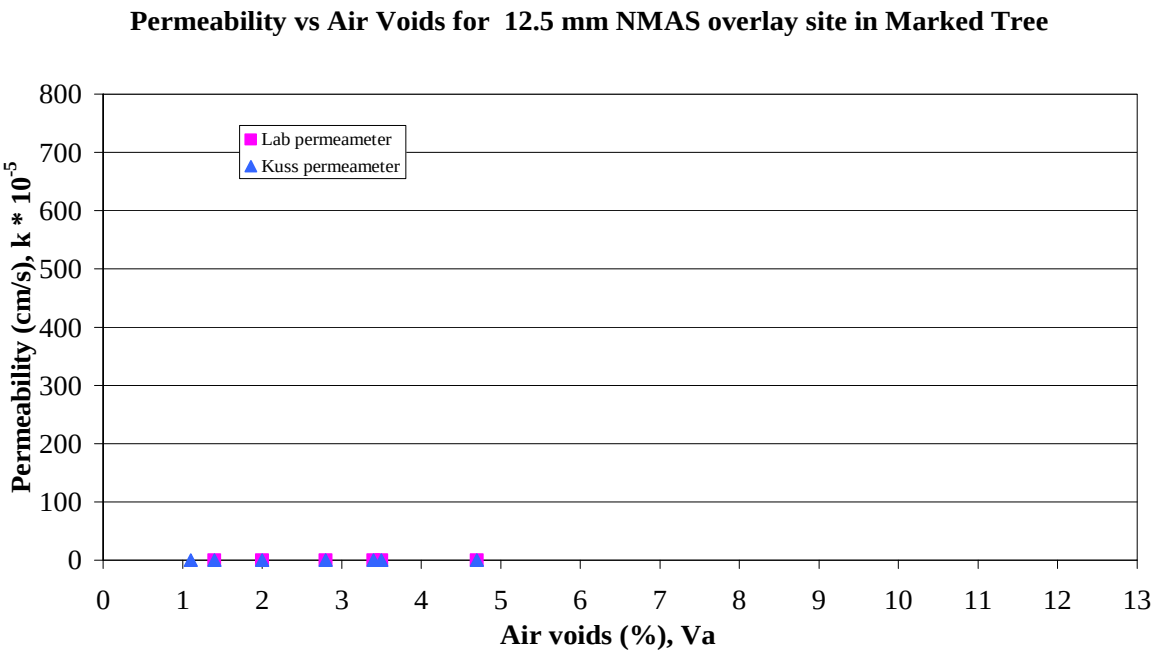

Figure 26. Permeability vs Air Voids for the site in Marked Tree

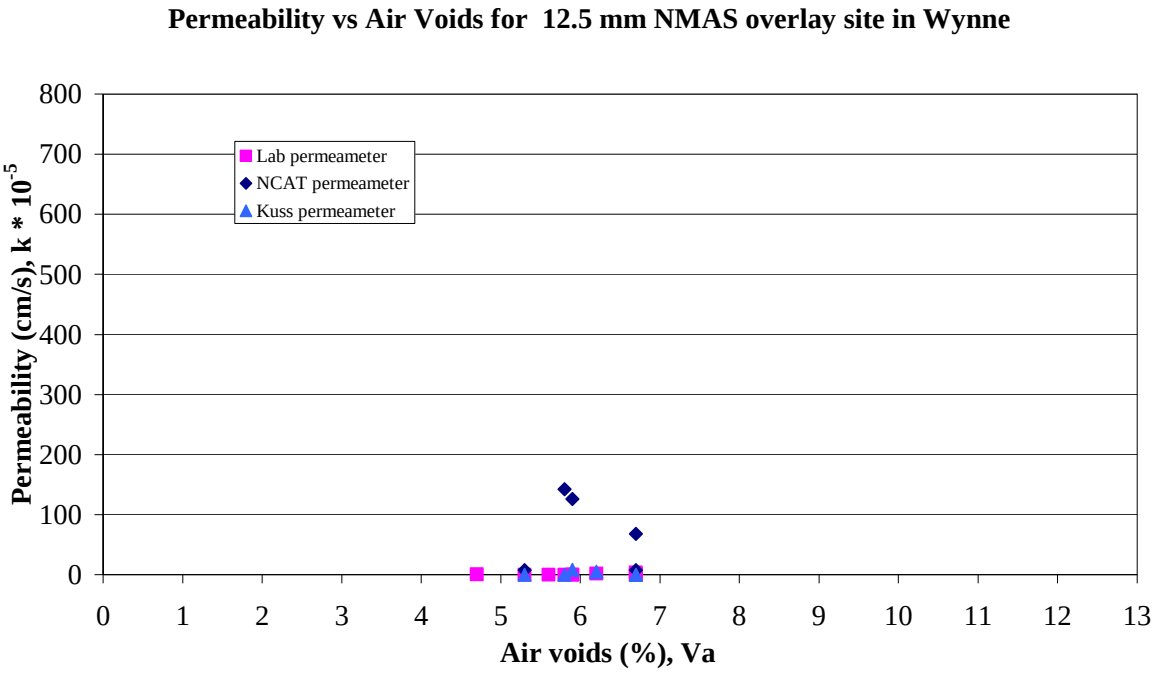

Figure 27. Permeability vs Air Voids for the site in Wynne

Some field sites contained different NMAS surface courses so similar NMAS surface courses were grouped together to analyze their permeability results against in-place air voids. Data from all field permeameters i.e. Kuss permeameter and NCAT permeameter were used for this analysis. 25.0 mm surface courses were based on only two sites data while 12.50mm surface courses were based on the other 14 sites. When data was plotted for 12.50mm and 25.0mm surface courses, as shown in Figures 28 and 29, it was noticed that NCAT permeameters yielded higher permeability than the Kuss permeameter in both cases. After analyzing the data 12.50mm surface course was found 8 times more permeable than the 25.0mm surface course according to the NCAT permeameter while it was 50 times more permeable according to Kuss permeameter. Overall, both figures illustrate that field permeability increased significantly at higher in-place air voids according to both field permeameters.

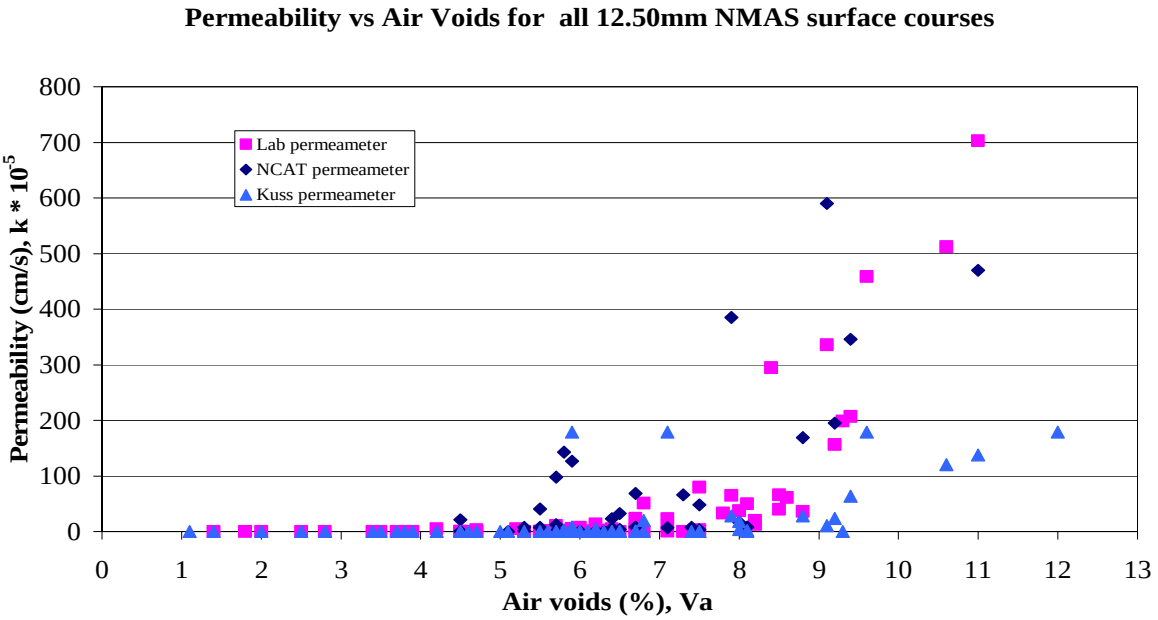

Figure 28. Permeability vs Air Voids for all 12.50mm NMAS surface courses in the State of Arkansas

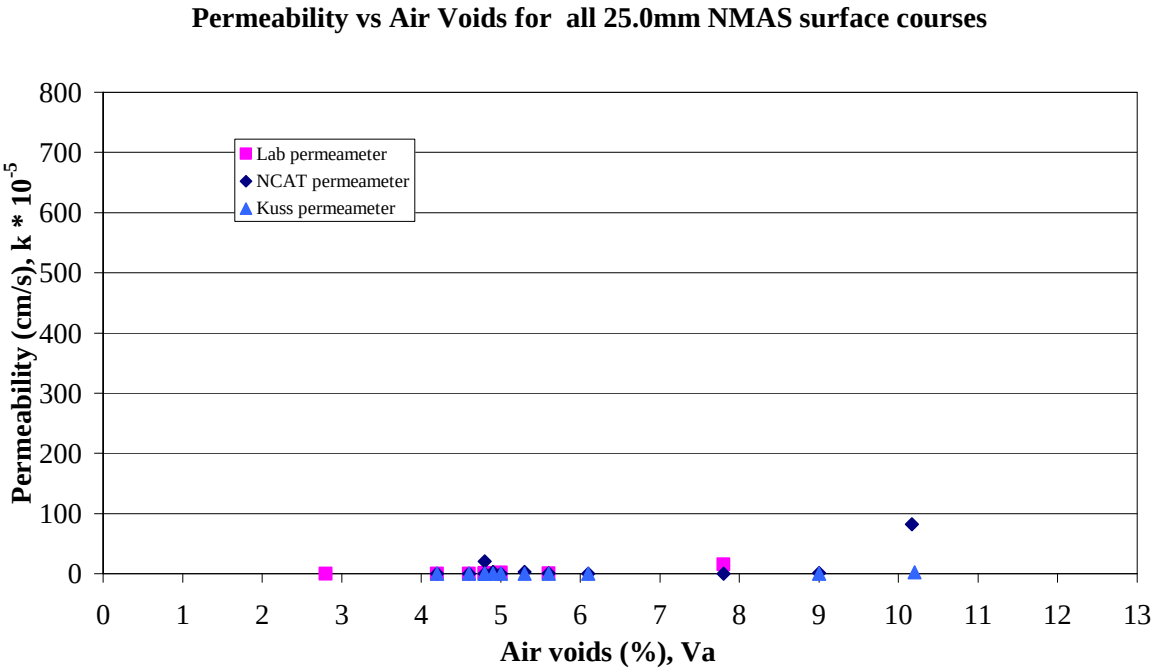

Figure 29. Permeability vs Air Voids for all 25mm NMAS surface courses in the State of Arkansas

ERC Test Pad

Field permeability for the two permeameters was compared to in-place air voids for the ERC test pad that was constructed in June 2002. The width of the pad was approximately 12 feet and its length was 49 feet. This test pad consisted of two sections, one having both surface and binder courses while the other having only binder course. The first Kuss permeameter field testing was performed in July 2002; the second round of testing was performed in April 2003. Permeability values exhibited a significant drop between the two testing efforts. Figure 30 is a plot of field permeability versus in-place voids for the ERC test pavement; the Kuss results shown in Figure 30 represent the first round of testing (performed soon after construction). This observation confirms those made by Cooley, et al, (2002) among others – that is, that initial permeability exhibited by pavement surfaces tends to reduce over time. This pavement was not subjected to traffic; field permeability or equivalent field percolation may be dependent on testing time of the year or/and testing time after the pavement construction. NCAT permeameter testing was performed only once in April, 2003.

After studying Figures 30, 31 and 32 it was noticed that slope of the pavement affected field permeability even at low in-place air voids. One of the ends of surface course pavement had a varying steep slope so the field permeability values were very high in those grid sections. When that data was plotted in Figure 30 along with other data of constant longitudinal slope for the surface course then the relationship found between field permeability and in-place air voids was not satisfactory. Afterwards only those testing spots were considered which were fairly at the same slope and consequently relationship became stronger as shown in Figure 31.

Figure 32 also exhibits a strong relationship between field permeability and in-place air voids for binder course because all of the data presented same longitudinal and cross slope. Figures 31 and 32 illustrate that the field permeability was dependent upon longitudinal and cross slope of the pavement and there might be more laterally interconnected void pathways then the vertically connected void pathways on steep slopes. Figures 31 and 32 also show that Kuss permeameter is far more consistent than the NCAT permeameter.

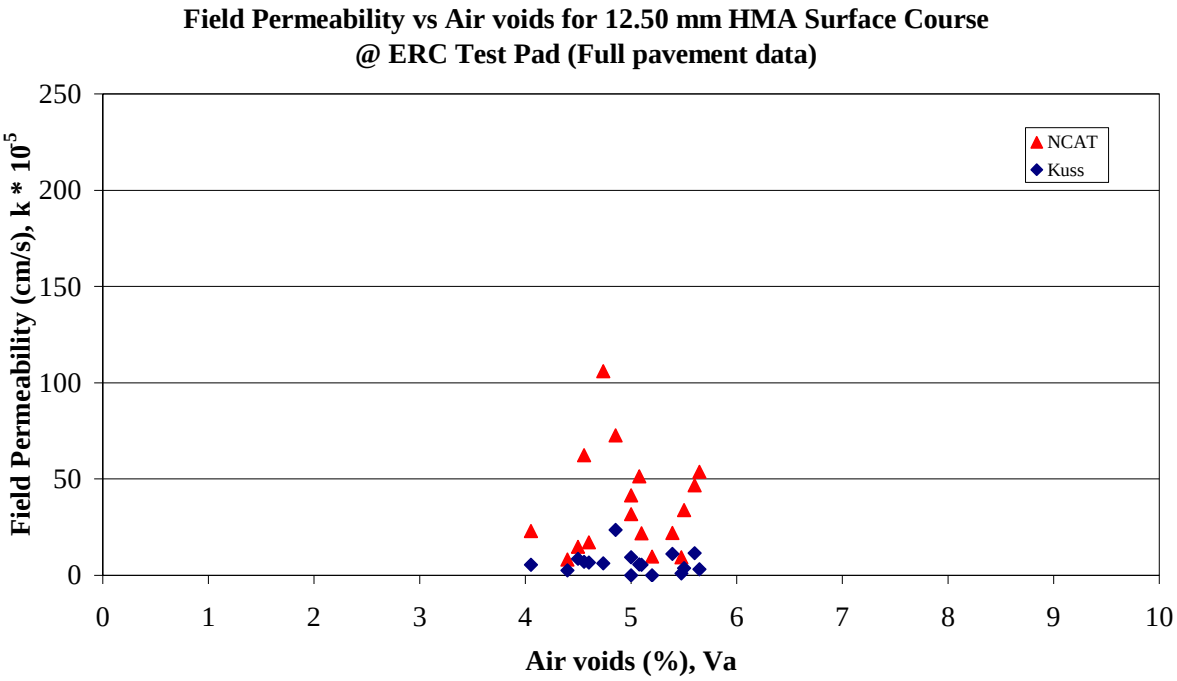

Figure 30. Field Permeability vs Air Voids for surface course at ERC test pad

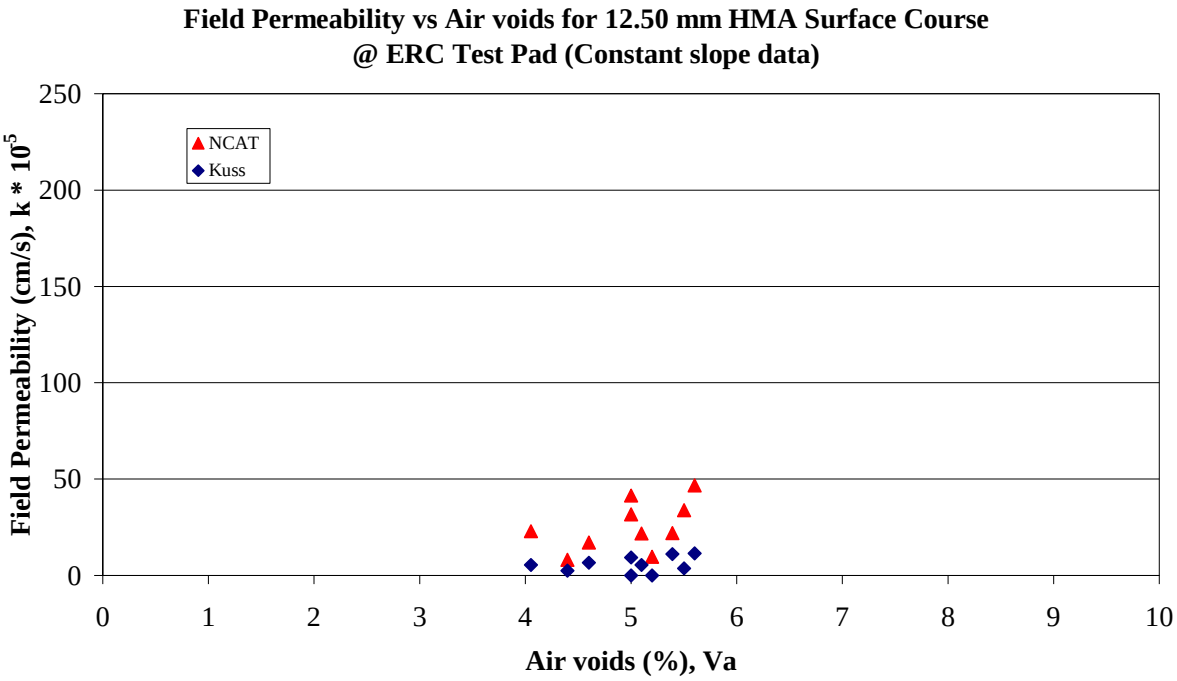

Figure 31. Field Permeability vs. Air Voids for surface course (only constant slope section) at ERC test pad

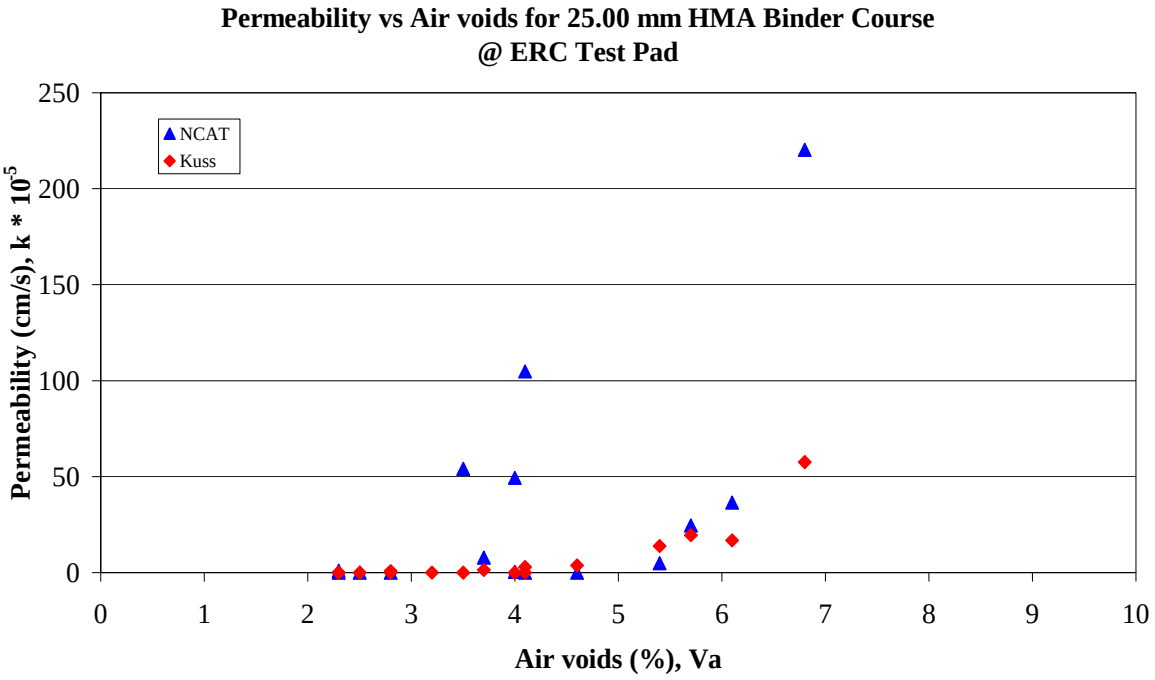

Figure 32. Field Permeability vs Air voids for binder course at ERC test pad

Comparison of Field and Laboratory Permeability

Figure 33 is a plot of field permeability results (NCAT permeameter) versus laboratory permeability results, using the same air voids content and corresponding locations. For example, the laboratory permeability result of a core taken from the inner wheel path of a "good" section was plotted against the NCAT field permeability of a spot nearby on the inner wheel path in the same section of a particular site. Figure 33 shows high field permeability at low laboratory permeability values, while field permeability values tend to decrease when the laboratory permeability values increased. This trend in the data is most likely related to the three-dimensional nature of water flow through an in-service pavement.

The R^2 value of the permeability relationship shown in Figure 33 was 0.63, which is reasonable because the field permeability results included different pavement temperatures and various unsaturated pavement thicknesses. In addition, laboratory results of 75.0mm +/- 5mm thick cores were corrected by viscosity correction factor to get the results at 20°C. The obtained regression model $y=0.8653x+0.0004$ was compared with another model, $y=5.7074x^{0.7037}$, developed by Cooley, Prowell and Brown (2002) that was based on data from four states. Table 10 shows that each model predicts field permeability results from laboratory permeability values with acceptable difference up to $800x10^{-5}$ cm/s. Beyond this value, the difference becomes large because model values obtained from this research were based on permeability values less than $800x10^{-5}$ cm/s whereas Cooley's model was based on values as high as $2800x10^{-5}$ cm/s. It is also noted that the current model includes different NMAS combinations while the previous researcher's model analyzed single NMAS cores.

Table 10. Comparison of obtained model with previous researcher's model

Laboratory permeability values ($k \times 10^5$ cm/s)	Field permeability (Previous researchers) ($k \times 10^5$ cm/s)	Field permeability Current model ($k \times 10^5$ cm/s)	Difference
10	29	9	20
50	90	43	46
100	146	87	59
150	194	130	64
250	278	216	62
400	387	346	41
700	573	606	-32
800	630	692	-62
1000	737	865	-128

Figures 34 and 35 show the relationship between field permeability (both Kuss and NCAT permeameters) and laboratory permeability, for surface and binder courses at the ERC test pad. The regression model obtained from Figures 34 and 35 did not match the model obtained from Figure 33 leading to the speculation that regression models for individual sites would be different from regression models based on group of sites. In both Figures 34 and 35, the Kuss permeameter tended to be closer to line of equality; the R^2 value for binder course was almost 80 percent.

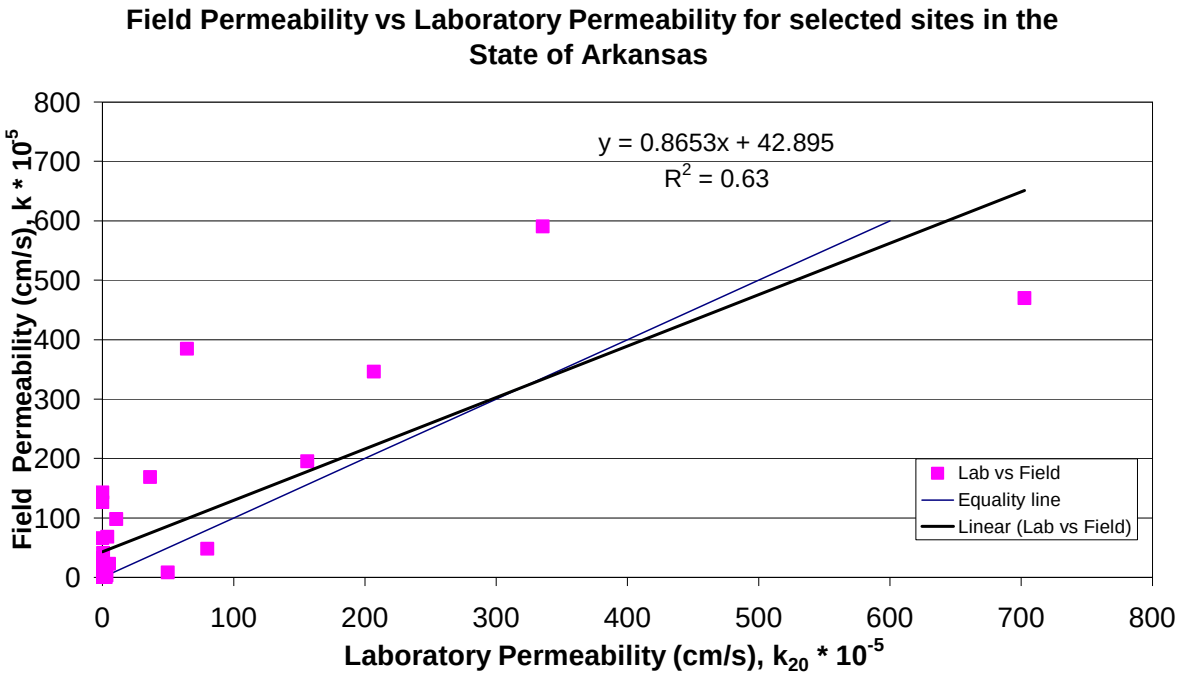

Figure 33. Field Permeability vs Laboratory Permeability for 10 selected sites

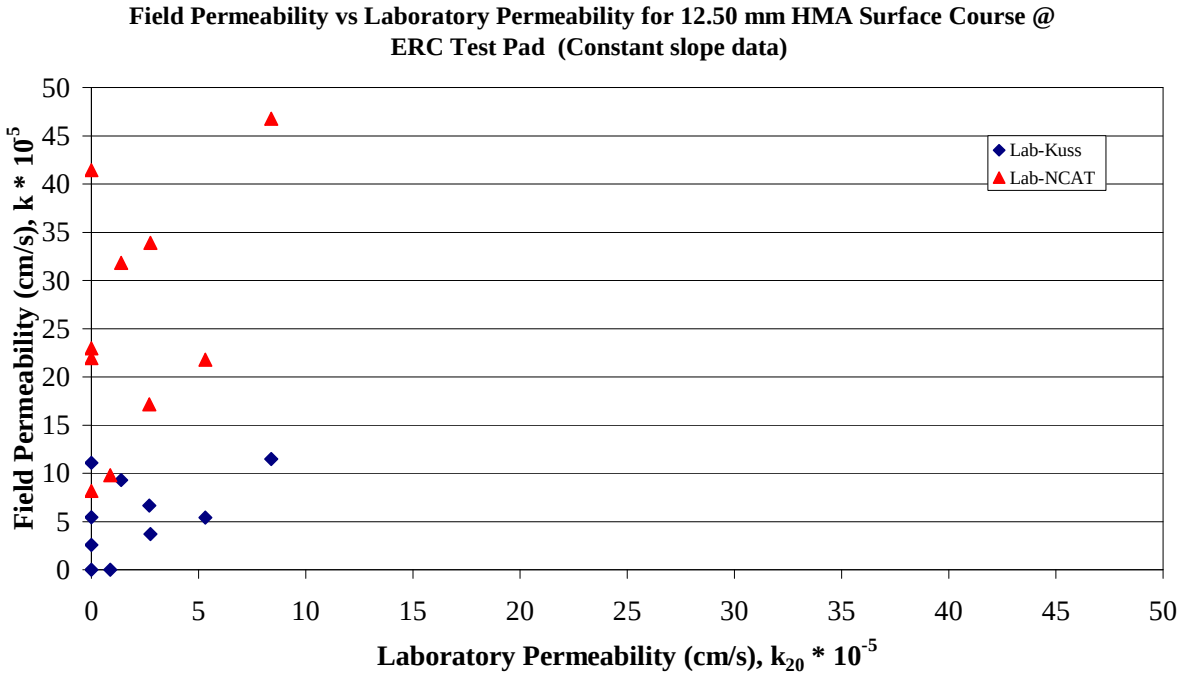

Figure 34. Field Permeability vs Laboratory Permeability for surface course (constant slope section) at ERC test pad

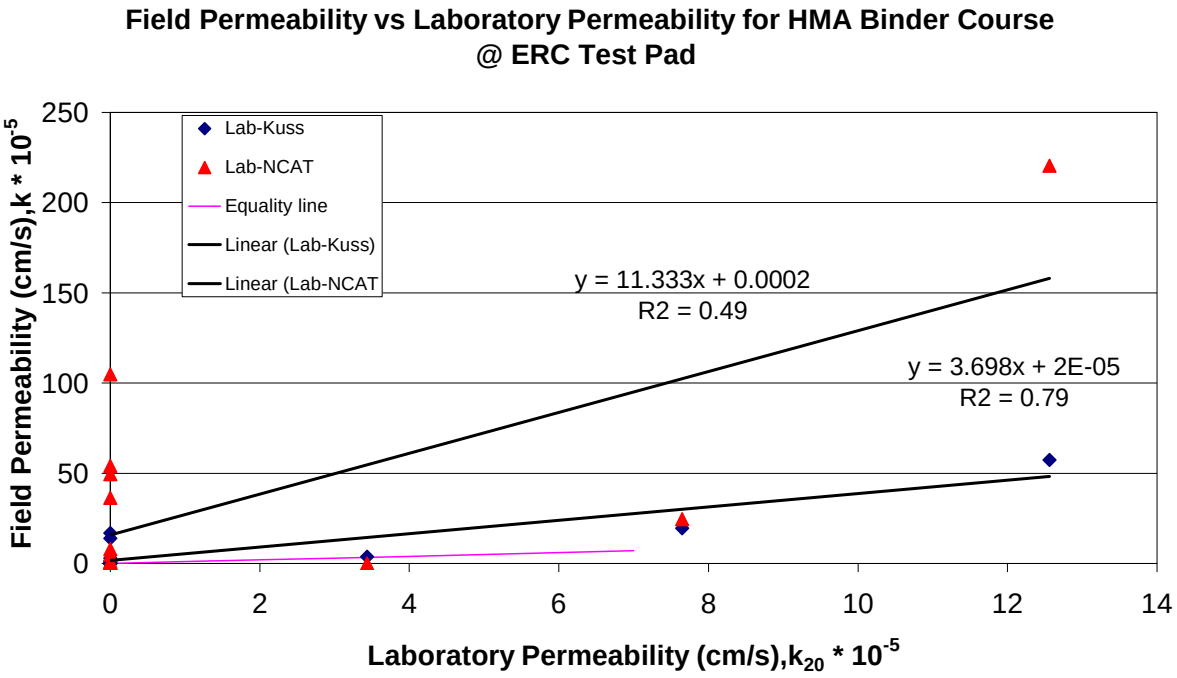

Figure 35. Field Permeability vs Laboratory Permeability for binder course at ERC test pad

Comparison between permeability of field cores and SGC samples

Laboratory permeability data of field cores and SGC samples obtained from ERC surface and binder courses were plotted in Figures 36 and 37. It was already known that SGC samples were impermeable at lower air voids, so they were compacted with fewer gyrations. Unfortunately, the SGC samples ended up ranging from 6.5 to 7.5 percent air voids for the surface course while the field cores only exhibited a range from 4.0 to 6.0 percent air voids. As such, it would be difficult to build a regression model mathematically by extrapolating this limited data. Figures 36 and 37 show only a weak relationship in permeability values for field cores and SGC specimens.

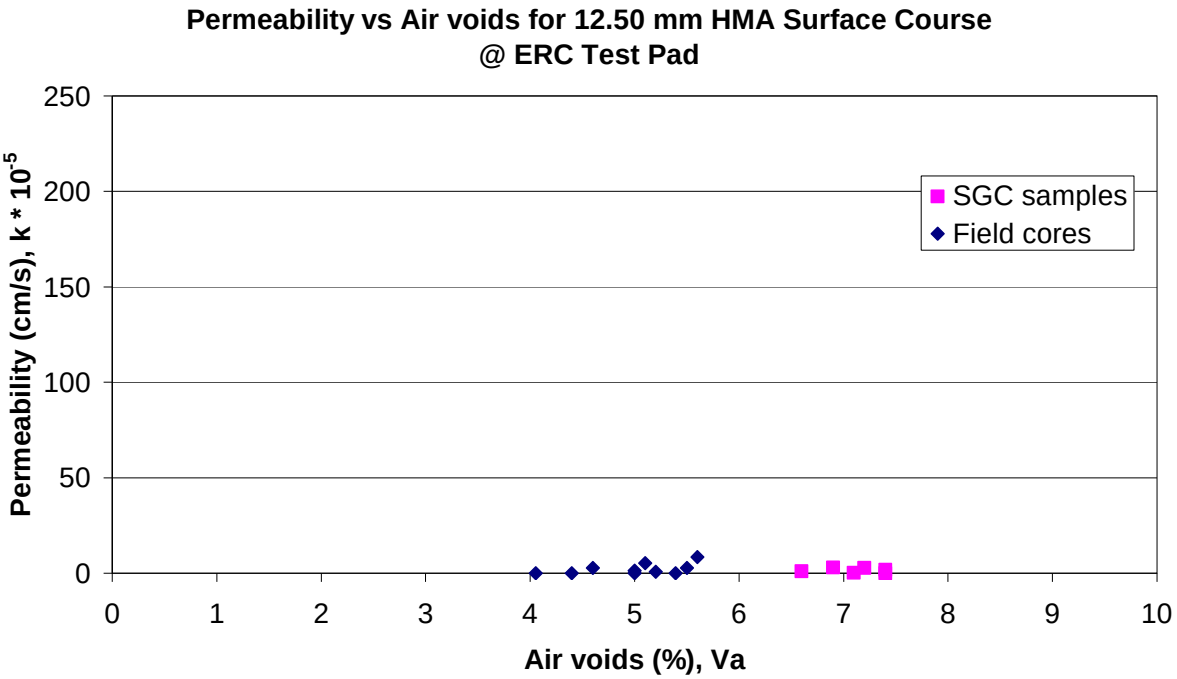

Figure 36. Laboratory Permeability vs Air voids for surface course at ERC test pad

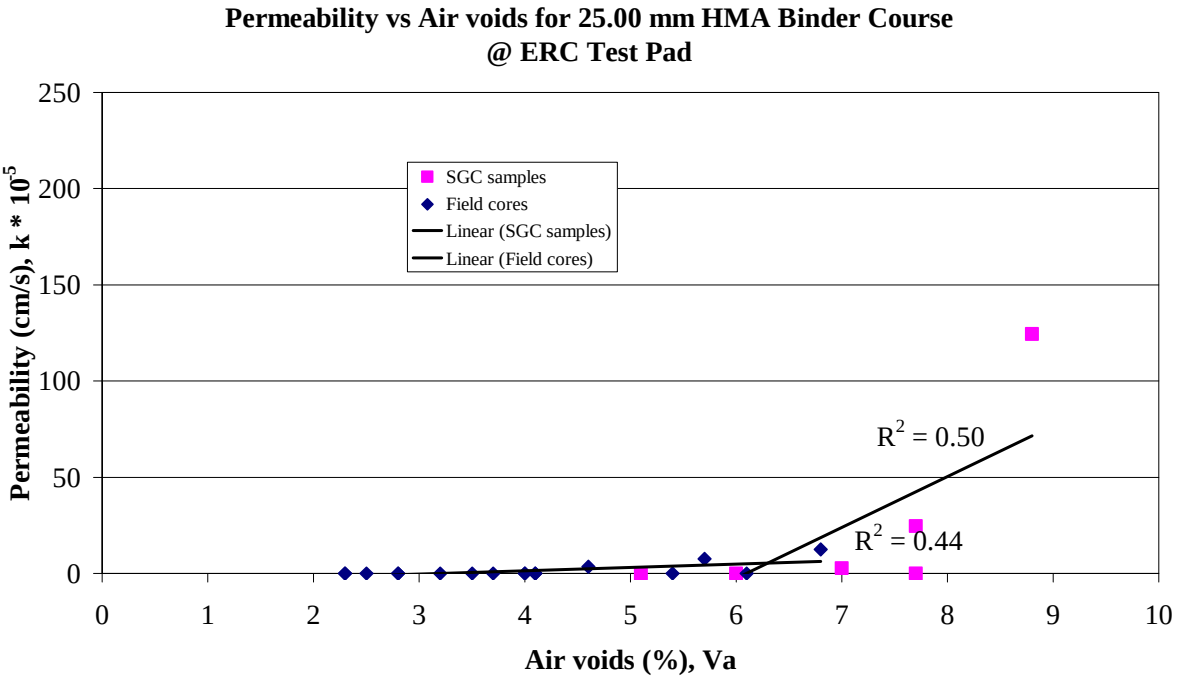

Figure 37. Laboratory Permeability vs Air voids for binder course at ERC test pad

CONCLUSIONS

The overall objective of this study was to develop design criteria and construction specification related to the permeability of HMA in flexible pavements. In order to account for the effect of HMA permeability on flexible pavement performance, field and laboratory permeability was compared for variety of mix designs. Though no regression model with a very high R-square value could be obtained through this study that could determine the field permeability of a future pavement from running laboratory permeability test on its Superpave Gyratory Compacted samples but the results obtained were in agreement with the other researchers, working on the same objective, in different states. After analyzing all the graphs it was noticed that the field permeability was below $50x10^{-5}$ cm/s at 5.5 percent in-place air voids. If the road had a flatter longitudinal slope then the field permeability was low between 5.5 percent and 8 percent air voids else it would be higher and it substantially increased above 8 percent. Whereas, laboratory permeability results illustrated that in-place air voids of 6 percent or less were almost impermeable in all sites of State of Arkansas, while in-place air voids between 7 percent and 9 percent exhibited laboratory permeability of less than $100x10^{-5}$ cm/s. All field cores having greater than 9 percent air voids were highly permeable.

Conclusions based on the analysis of the data accumulated during the two year study period are summarized as following.

- All samples exhibited laminar flow, so the primary *assumption* of laminar flow was valid; therefore the laboratory permeameter could be used to measure the permeability of highly permeable cores.
- According to the statistical analysis effective air voids did not appeare to have a good relationship with permeability.

- The Kuss permeameter exhibited greater consistency than the NCAT permeameter for determining the field permeability of an individual site.
- Field permeability or equivalent field percolation was dependent on testing time of the year or/and testing time after the pavement construction.
- Field permeability is not affected by the wheel path.
- Field permeability was dependent upon both longitudinal and cross slope of the pavement; there appeared to be more laterally interconnected void pathways then the vertically connected void pathways on steep longitudinal slopes.
- Field permeability of a 12.50mm surface course is typically higher than a 25.0mm binder course.
- Field permeability was typically high at low laboratory permeability values, and field permeability values tend to decrease when the laboratory permeability values increased.
- The regression model ($y=0.8653x+0.0004$) obtained for field permeability vs laboratory permeability (using the NCAT field permeameter and field cores) generally agreed with models created by previous researchers.
- The Kuss permeameter generally provided lower permeability values than the NCAT permeameter and could only measure up to $179x10^{-5}$ cm/s of field permeability.

RECOMMENDATIONS

As no relationship could be determined between permeability of field cores and SGC samples so its recommended to compact the pavement in such a way that high air voids field cores could be obtained. Also, more field testing should be performed with better sealant so leakage through the base plate of NCAT equipment could be avoided. More research is needed to find out the real depth of flow in to the asphalt pavement so the field permeability calculation could be made more precise for field permeameters. It is recommended to perform testing on newly constructed sites where sampling for laboratory samples could be also performed. This would provide SGC samples permeability data for each site that would further help in comparing field permeability with laboratory permeability.

REFERENCES

- ASTM "Annual book of ASTM standards, Construction:Road and Paving Materials; Vehicle-Pavement Systems" Vol. 04.03, American society for Testing and Materials, 2001.

- Choubane, B; Page, GC and Musselman, JA; "Investigation of Water Permeability of Coarse Graded Superpave Pavements", Journal of the Association of Asphalt Paving Technologists, Vol. 67, 1998.

- Cooley, Jr., L. A.; " Permeability of Superpave mixtures: Evaluation of Field Permeameters", NCAT Report No. 99-1, February 1999.

- Cooley, Jr., L. A.; Maghsoodloo, S.; Brown, E. R.; " Development of Critical Field Permeability and Pavement Density Values for Coarse-Graded Superpave Pavements", NCAT Report No. 01-03, September 2001.

- Cooley, Jr., L. A.; Prowell, B. D. and Brown, E. R.; "Issues Pertaining to the Permeability Characteristics of Coarse-graded Superpave Mixes", NCAT Report No. 2002-06, July 2002.

- Cruz, J.S; "Permeability of Hot-Mix Asphalt Concrete", MS Thesis, University of Arkansas, Fayetteville, AR, August 2000.

- Hall, K.D.; "Superpave Permeability TRC 0203 Proposal", Research Project Proposal, University of Arkansas, Fayetteville, AR, May 2001.

- Izzo, R. P. and Button, J. W.; "Permeability of Coarse Matrix-High Binder Mixtures and its Effects on Performance", Texas Transportation Institute, April 1997.

- Kanitpong K., Benson C.H. and Bahia H.U.; "Hydraulic Conductivity (Permeability) of Laboratory-Compacted Asphalt Mixtures", Transportation Research Record No. 1767, 2000.

- Mallick, R.; Cooley, L. A.and Teto, M.; " Evaluation of Permeability of Superpave Mixes in Maine", Worcester Polytechnic Institute, November 1999.

- Maupin, G.W., Jr.; "Asphalt Permeability Testing: Specimen Preparation and Testing Variability", Transportation Research Record No. 1767, 2000.

- Maupin, G.W., Jr.; "Investigation of Test Methods, Pavements, and Laboratory Design Related to Asphalt Permeability", Virginia Transportation Research Council, June 2000.

- Ng, H.G.; "Void Pathway Test", MS Thesis, University of Arkansas, Fayetteville, AR, August 2000.

APPENDIX I

```
/* Permeability project thesis based on full factorial design BY A.R. QAZI
*/
/* Factor A = Type of Permeameter, 3 types  */
/* Factor B = Effective air voids (Low < 5% and High >=5%), 2 levels  */
/* Factor C = Construction (Overlay or Full Depth Superpave),2 types */
/* Response Variable - Permeability (cm/s) */

OPTIONS NOCENTER LINESIZE=85 ;

DATA SAMPLE23 ;
  DO A =  1 TO 3 BY 1;
  DO B = -1 TO 1 BY 2;
  DO C = -1 TO 1 BY 2;
      DO REP= 1 TO 5;
      INPUT RESP @@;
      LIST ;
      OUTPUT ;
      END;
  END;
  END;
  END;

  DATALINES ;
0.00000 0.00000 0.00002 0.00000 0.00000
0.00000 0.00000 0.00000 0.00000 0.00000
0.00002 0.00002 0.00006 0.00097 0.00160
0.00000 0.00001 0.00002 0.00029 0.00073
0.00000 0.00020 0.00021 0.00032 0.00000
0.00001 0.00003 0.00001 0.00068 0.00100
0.00004 0.00020 0.00380 0.00346 0.00590
0.00006 0.00000 0.00070 0.00030 0.00195
0.00000 0.00000 0.00000 0.00000 0.00000
0.00000 0.00013 0.00000 0.00000 0.00002
0.00000 0.00003 0.00179 0.00138 0.00011
0.00000 0.00000 0.00003 0.00000 0.00024
;

PROC PRINT DATA=SAMPLE23 ;
  TITLE1 'GENERAL FORM OF A 2^3 FACTORIAL DESIGN' ;

PROC RANK DATA=SAMPLE23 OUT=RANKDATA ;
RANKS RRESP ;
VAR RESP ;
PROC PRINT DATA=RANKDATA ;
TITLE1 'RANKED DATA FOR RANK TRANSFORMATION PROCEDURE' ;
PROC GLM DATA=RANKDATA ;
CLASS A B C ;
MODEL RRESP = A|B|C ;
LSMEANS A B C / PDIFF ;
OUTPUT OUT = SUMMARY P=YHAT R=RESIDUAL ;
TITLE2 'THE ANALYSIS OF RANKED DATA' ;
PROC PRINT DATA = SUMMARY ;
  TITLE2 'DATA SET CREATED CONTAINING THE PREDICTED AND RESIDUAL VALUES' ;
```

```
PROC UNIVARIATE DATA=SUMMARY NORMAL PLOT ;
  VAR RESIDUAL ;
  TITLE2 'MODEL ADEQUACY CHECKS' ;

PROC PLOT DATA=SUMMARY ;
  PLOT RESIDUAL*YHAT='*' ;
  TITLE2 'PLOT OF THE RESIDUALS VS PREDICTED VALUES' ;
  PLOT RESIDUAL*A='*' ;
  TITLE2 'PLOT OF THE RESIDUALS VS A';
  PLOT RESIDUAL*B='*' ;
  TITLE2 'PLOT OF THE RESIDUALS VS B';
  PLOT RESIDUAL*C='*' ;
  TITLE2 'PLOT OF THE REDIDUALS VS C';
RUN ;
PROC GLM DATA=SAMPLE23 ;
  CLASS A B C ;
  MODEL RESP = A|B|C ;
  OUTPUT OUT = SUMMARY P=YHAT R=RESIDUAL ;
  TITLE2 'THE ANALYSIS' ;

PROC PRINT DATA = SUMMARY ;
  TITLE2 'DATA SET CREATED CONTAINING THE PREDICTED AND RESIDUAL VALUES' ;

PROC UNIVARIATE DATA=SUMMARY NORMAL PLOT ;
  VAR RESIDUAL ;
  TITLE2 'MODEL ADEQUACY CHECKS' ;

PROC PLOT DATA=SUMMARY ;
  PLOT RESIDUAL*YHAT='*' ;
  TITLE2 'PLOT OF THE RESIDUALS VS PREDICTED VALUES' ;
  PLOT RESIDUAL*A='*' ;
  TITLE2 'PLOT OF THE RESIDUALS VS A';
  PLOT RESIDUAL*B='*' ;
  TITLE2 'PLOT OF THE RESIDUALS VS B';
  PLOT RESIDUAL*C='*' ;
  TITLE2 'PLOT OF THE REDIDUALS VS C';
RUN ;

PROC SUMMARY ;
CLASS A B C;
VAR RESP ;
OUTPUT OUT= INTERACT MEAN=MEAN ;
PROC PRINT DATA=INTERACT;
TITLE2 'DATA SET CREATED BY PROC SUMMARY CONTAINING MEANS' ;
DATA BXC;
SET INTERACT ;
IF _TYPE_=3 THEN OUTPUT BXC ;
PROC PRINT DATA=BXC ;
TITLE2 'DATA SET FOR THE INTERACTION PLOT OF B AND C' ;
PROC PLOT DATA=BXC;
PLOT MEAN*C=B ;
TITLE2 'INTERACTION PLOT FOR B AND C';
DATA A ;
SET INTERACT ;
IF _TYPE_=4 THEN OUTPUT A ;
PROC PRINT DATA=A ;
TITLE2 'DATA SET FOR FACTOR A' ;
```

```
PROC PLOT DATA=A ;
PLOT MEAN*A='*' ;
DATA B ;
SET INTERACT ;
IF _TYPE_=2 THEN OUTPUT B ;
PROC PRINT DATA=B ;
TITLE2 'DATA SET FOR FACTOR B' ;
PROC PLOT DATA=B ;
PLOT MEAN*B='*' ;
DATA REGRESS ;
SET SAMPLE23 ;
BC = B*C ;
PROC REG DATA=REGRESS ;
MODEL RESP = A B BC / R ;
TITLE2 'REGRESSION ANALYSIS INCLUDING ONLY POTENTIALLY SIGNIFICANT
FACTORS' ;
RUN ;
QUIT ;
```

GENERAL FORM OF A FULL FACTORIAL DESIGN

Obs	A	B	C	REP	RESP
1	1	-1	-1	1	.00000
2	1	-1	-1	2	.00000
3	1	-1	-1	3	.00002
4	1	-1	-1	4	.00000
5	1	-1	-1	5	.00000
6	1	-1	1	1	.00000
7	1	-1	1	2	.00000
8	1	-1	1	3	.00000
9	1	-1	1	4	.00000
10	1	-1	1	5	.00000
11	1	1	-1	1	.00002
12	1	1	-1	2	.00002
13	1	1	-1	3	.00006
14	1	1	-1	4	.00097
15	1	1	-1	5	.00160
16	1	1	1	1	.00000
17	1	1	1	2	.00001
18	1	1	1	3	.00002
19	1	1	1	4	.00029
20	1	1	1	5	.00073
21	2	-1	-1	1	.00000
22	2	-1	-1	2	.00020
23	2	-1	-1	3	.00021
24	2	-1	-1	4	.00032
25	2	-1	-1	5	.00000
26	2	-1	1	1	.00001
27	2	-1	1	2	.00003
28	2	-1	1	3	.00001
29	2	-1	1	4	.00068
30	2	-1	1	5	.00100
31	2	1	-1	1	.00004
32	2	1	-1	2	.00020
33	2	1	-1	3	.00380
34	2	1	-1	4	.00346
35	2	1	-1	5	.00590
36	2	1	1	1	.00006
37	2	1	1	2	.00000
38	2	1	1	3	.00070
39	2	1	1	4	.00030
40	2	1	1	5	.00195
41	3	-1	-1	1	.00000
42	3	-1	-1	2	.00000
43	3	-1	-1	3	.00000
44	3	-1	-1	4	.00000
45	3	-1	-1	5	.00000
46	3	-1	1	1	.00000
47	3	-1	1	2	.00013
48	3	-1	1	3	.00000
49	3	-1	1	4	.00000
50	3	-1	1	5	.00002
51	3	1	-1	1	.00000
52	3	1	-1	2	.00003
53	3	1	-1	3	.00179
54	3	1	-1	4	.00138
55	3	1	-1	5	.00011
56	3	1	1	1	.00000
57	3	1	1	2	.00000
58	3	1	1	3	.00003
59	3	1	1	4	.00000
60	3	1	1	5	.00024

The GLM Procedure

Class Level Information

Class	Levels	Values
A	3	1 2 3
B	2	-1 1
C	2	-1 1

Number of observations 60

Dependent Variable: RRESP Rank for Variable RESP

Source	DF	Sum of Squares	Mean Square	F Value	Pr > F
Model	11	8698.80000	790.80000	4.76	<.0001
Error	48	7981.20000	166.27500		
Corrected Total	59	16680.00000			

R-Square	Coeff Var	Root MSE	RRESP Mean
0.521511	42.27792	12.89477	30.50000

Source	DF	Type I SS	Mean Square	F Value	Pr > F
A	2	3129.175000	1564.587500	9.41	0.0004*
B	1	3824.016667	3824.016667	23.00	<.0001*
A*B	2	368.358333	184.179167	1.11	0.3386
C	1	205.350000	205.350000	1.24	0.2720
A*C	2	35.425000	17.712500	0.11	0.8992
B*C	1	866.400000	866.400000	5.21	0.0269*
A*B*C	2	270.075000	135.037500	0.81	0.4499

***Interactions B and C are significant while main effect A and B are significant at a significance level of 0.05.**

Source	DF	Type III SS	Mean Square	F Value	Pr > F
A	2	3129.175000	1564.587500	9.41	0.0004
B	1	3824.016667	3824.016667	23.00	<.0001
A*B	2	368.358333	184.179167	1.11	0.3386
C	1	205.350000	205.350000	1.24	0.2720
A*C	2	35.425000	17.712500	0.11	0.8992
B*C	1	866.400000	866.400000	5.21	0.0269
A*B*C	2	270.075000	135.037500	0.81	0.4499

Tests for Normality

Test	--Statistic---		-----p Value------		
Shapiro-Wilk	W	0.967765	Pr < W	0.1133	
Kolmogorov-Smirnov	D	0.119616	Pr > D	0.0319	**Though less than 0.05 but**
Cramer-von Mises	W-Sq	0.115023	Pr > W-Sq	0.0728	**others are more than 0.05**
Anderson-Darling	A-Sq	0.674215	Pr > A-Sq	0.0785	

Figure (a) Normal Probability Plot

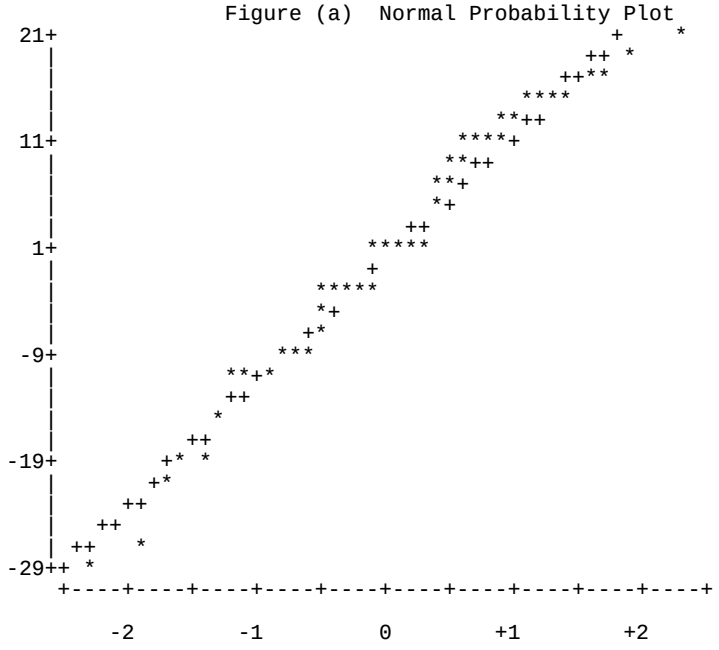

No problem with Normality after rank transformation.

Figure (b) Plot of RESIDUAL*YHAT. Symbol used is '*'.

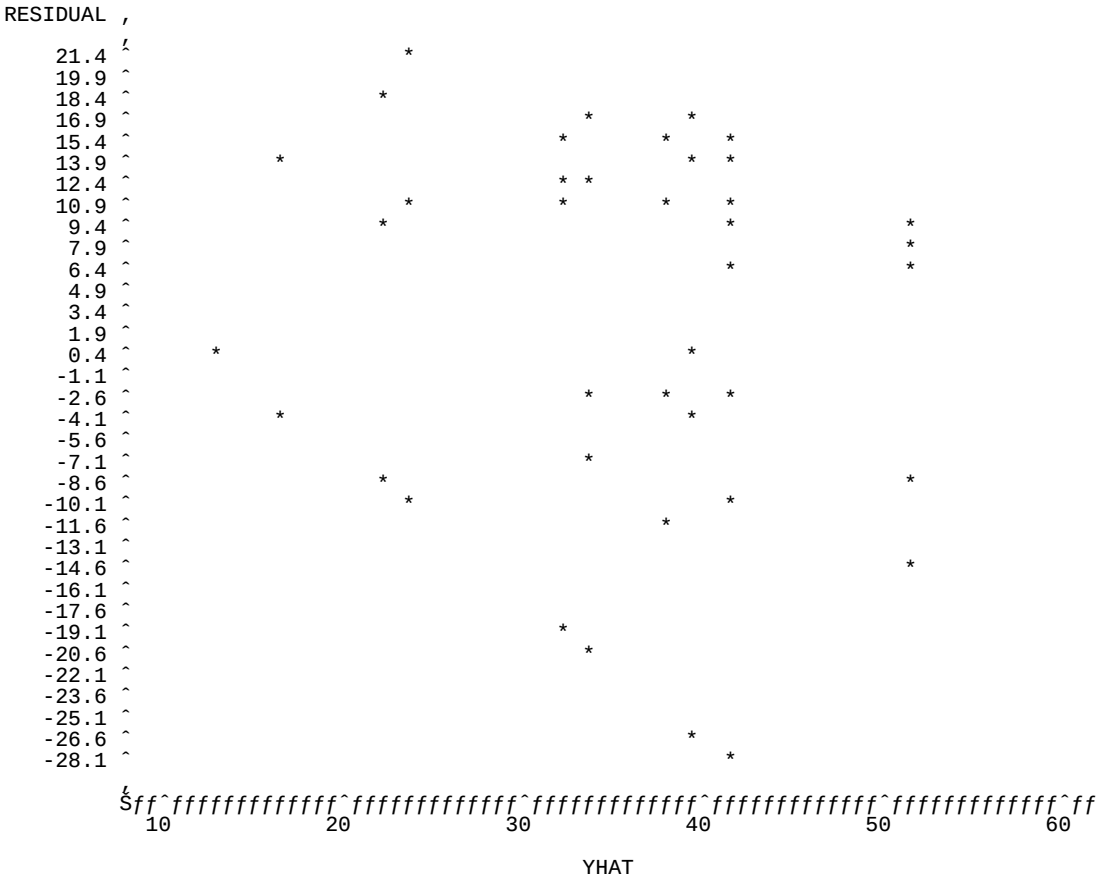

NOTE: 20 obs hidden.

Independence assumption justified after rank transformation.

Figure (c) Plot of RESIDUAL*A. Symbol used is '*'.

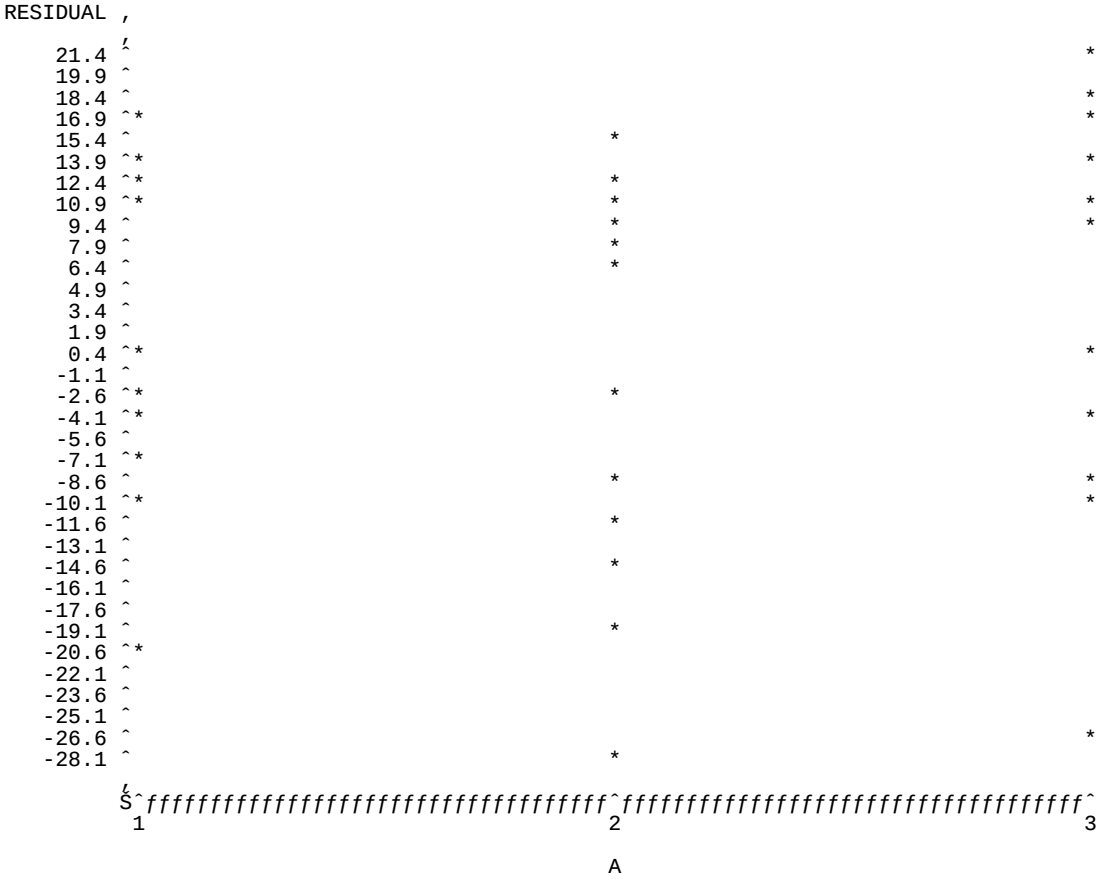

NOTE: 27 obs hidden.

Constant variance assumption justified after rank transformation.

Figure (d) Plot of RESIDUAL*B. Symbol used is '*'.

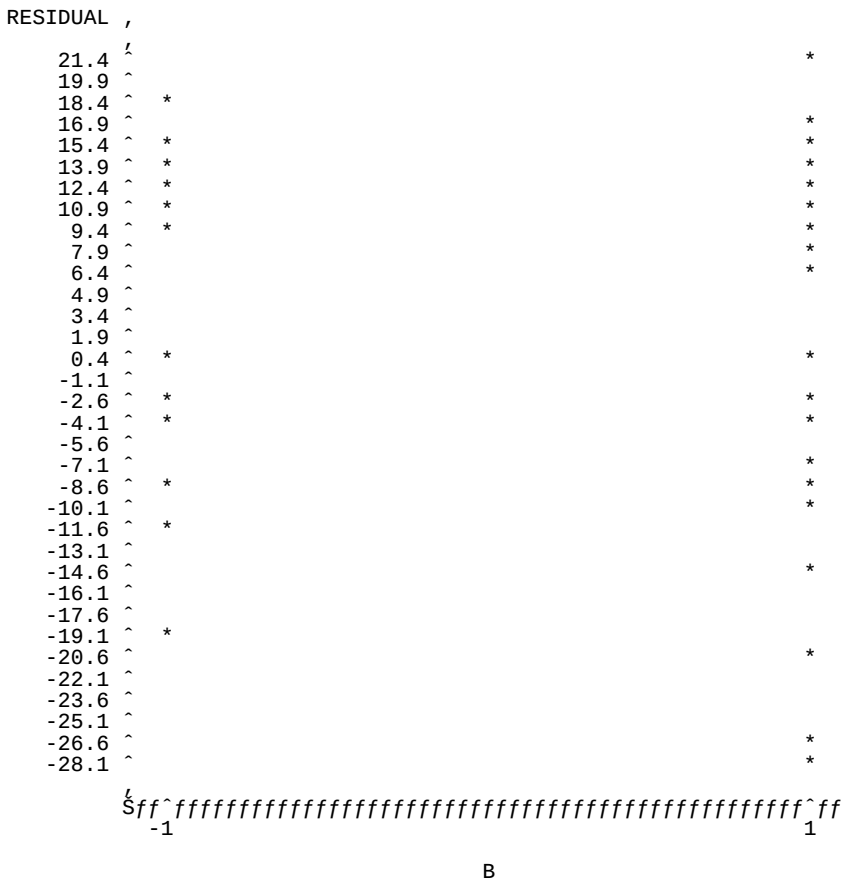

NOTE: 29 obs hidden.

Constant variance assumption justified after rank transformation.

Figure (e) Plot of RESIDUAL*C. Symbol used is '*'.

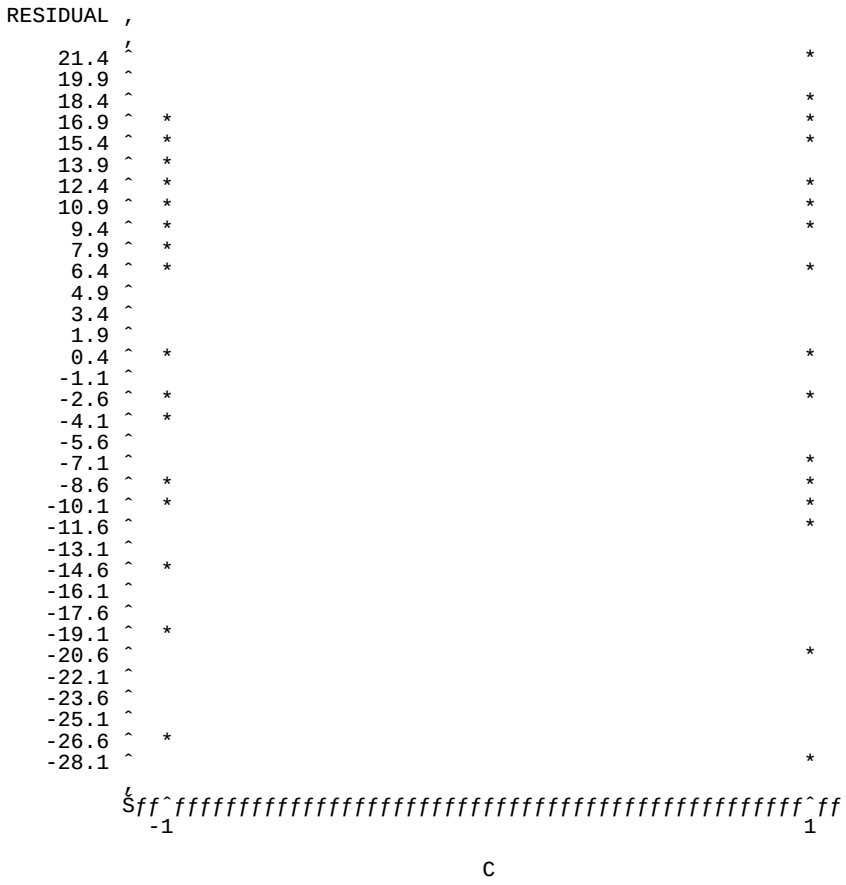

NOTE: 28 obs hidden.

Constant variance assumption justified after rank transformation.

The GLM Procedure

Class Level Information

Class	Levels	Values
A	3	1 2 3
B	2	-1 1
C	2	-1 1

Number of observations 60

The GLM Procedure

Dependent Variable: RESP

Source	DF	Sum of Squares	Mean Square	F Value	Pr > F
Model	11	0.00003072	0.00000279	3.90	0.0005
Error	48	0.00003433	0.00000072		
Corrected Total	59	0.00006506			

R-Square	Coeff Var	Root MSE	RESP Mean
0.472244	192.6535	0.000846	0.000439

Source	DF	Type I SS	Mean Square	F Value	Pr > F
A	2	7.63561E-6	3.817805E-6	5.34	0.0081
B	1	7.4061067E-6	7.4061067E-6	10.35	0.0023
A*B	2	3.5967633E-6	1.7983817E-6	2.51	0.0915
C	1	3.22944E-6	3.22944E-6	4.51	0.0388
A*C	2	1.73125E-6	8.65625E-7	1.21	0.3071
B*C	1	4.3632067E-6	4.3632067E-6	6.10	0.0171
A*B*C	2	2.7602033E-6	1.3801017E-6	1.93	0.1563

Source	DF	Type III SS	Mean Square	F Value	Pr > F
A	2	7.63561E-6	3.817805E-6	5.34	0.0081
B	1	7.4061067E-6	7.4061067E-6	10.35	0.0023
A*B	2	3.5967633E-6	1.7983817E-6	2.51	0.0915
C	1	3.22944E-6	3.22944E-6	4.51	0.0388
A*C	2	1.73125E-6	8.65625E-7	1.21	0.3071
B*C	1	4.3632067E-6	4.3632067E-6	6.10	0.0171
A*B*C	2	2.7602033E-6	1.3801017E-6	1.93	0.1563

Tests for Normality

Test	--Statistic---		-----p Value------	
Shapiro-Wilk	W	0.773922	Pr < W	<0.0001
Kolmogorov-Smirnov	D	0.231186	Pr > D	<0.0100
Cramer-von Mises	W-Sq	0.901669	Pr > W-Sq	<0.0050
Anderson-Darling	A-Sq	4.689557	Pr > A-Sq	<0.0050

All p values less than 0.05 So data after rank transformation will be considered.

The UNIVARIATE Procedure
Variable: RESIDUAL

Figure (f) Normal Probability Plot

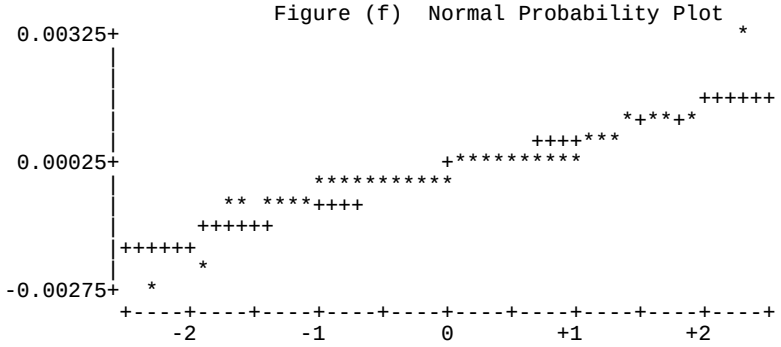

Normality problem is evident prior to rank transformation.

Figure (g) Plot of RESIDUAL*YHAT. Symbol used is '*'.

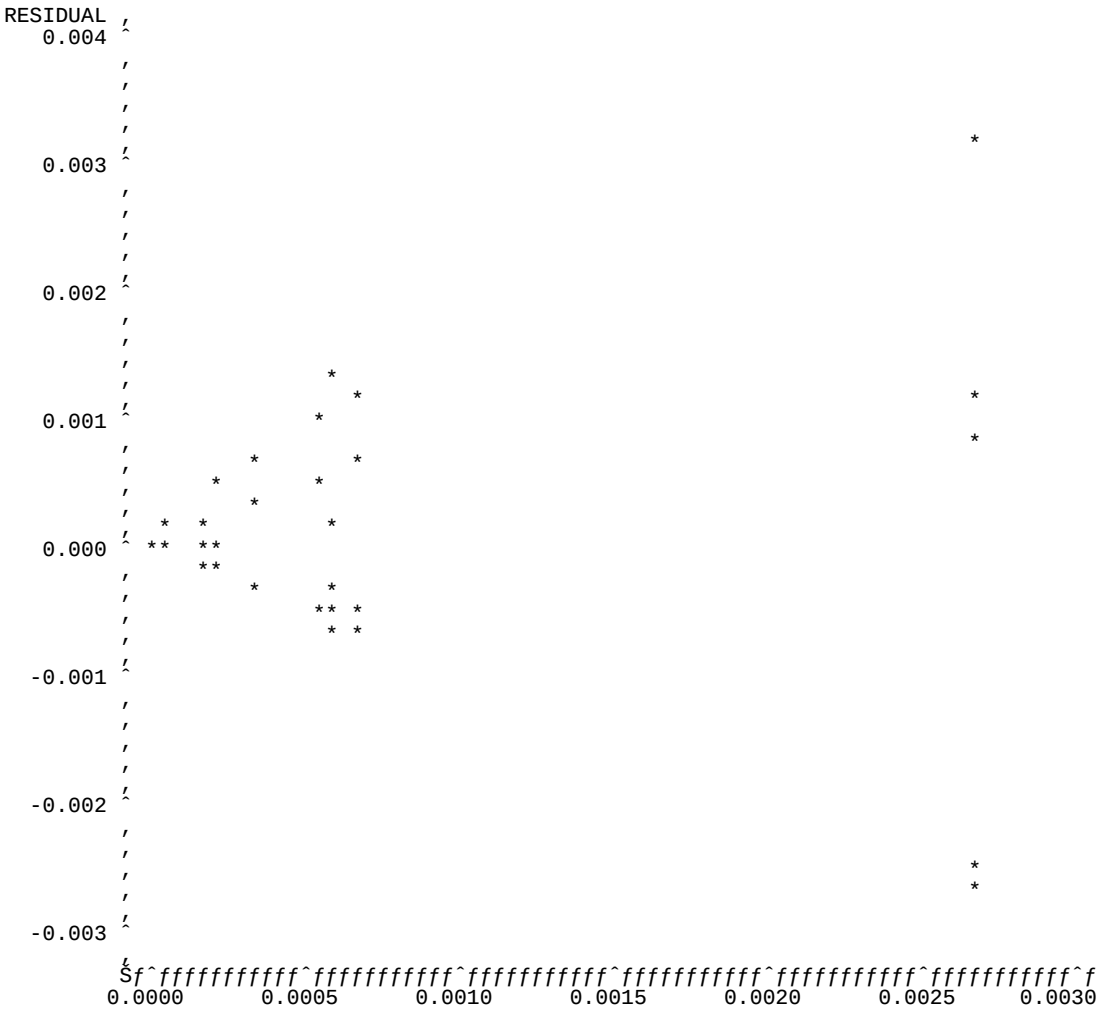

NOTE: 31 obs hidden.

Independence assumption NOT justified prior to rank transformation.

Figure (h) Plot of RESIDUAL*A. Symbol used is '*'.

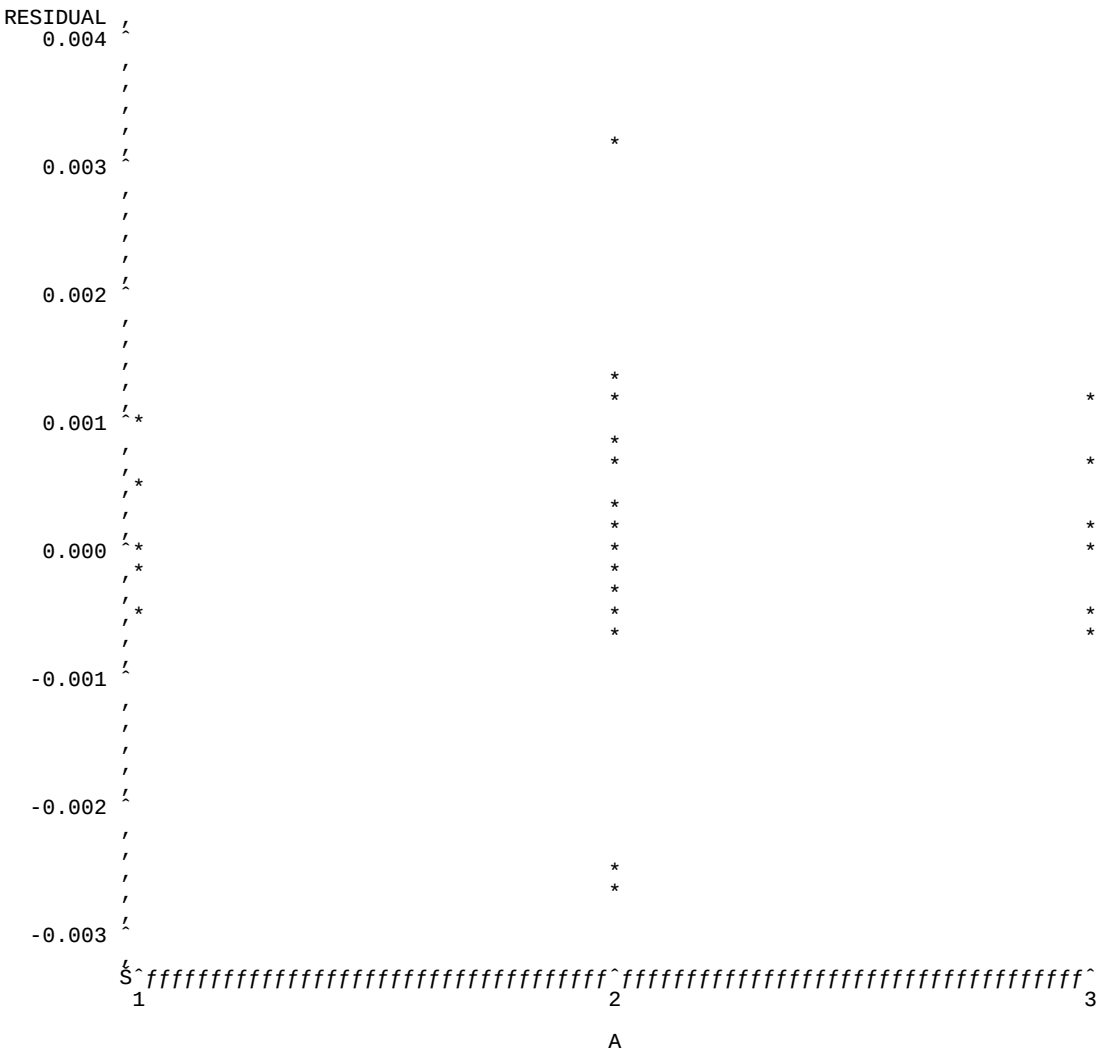

NOTE: 35 obs hidden.

No problems evident here so constant variance assumption justified.

Figure (i) Plot of RESIDUAL*B. Symbol used is '*'.

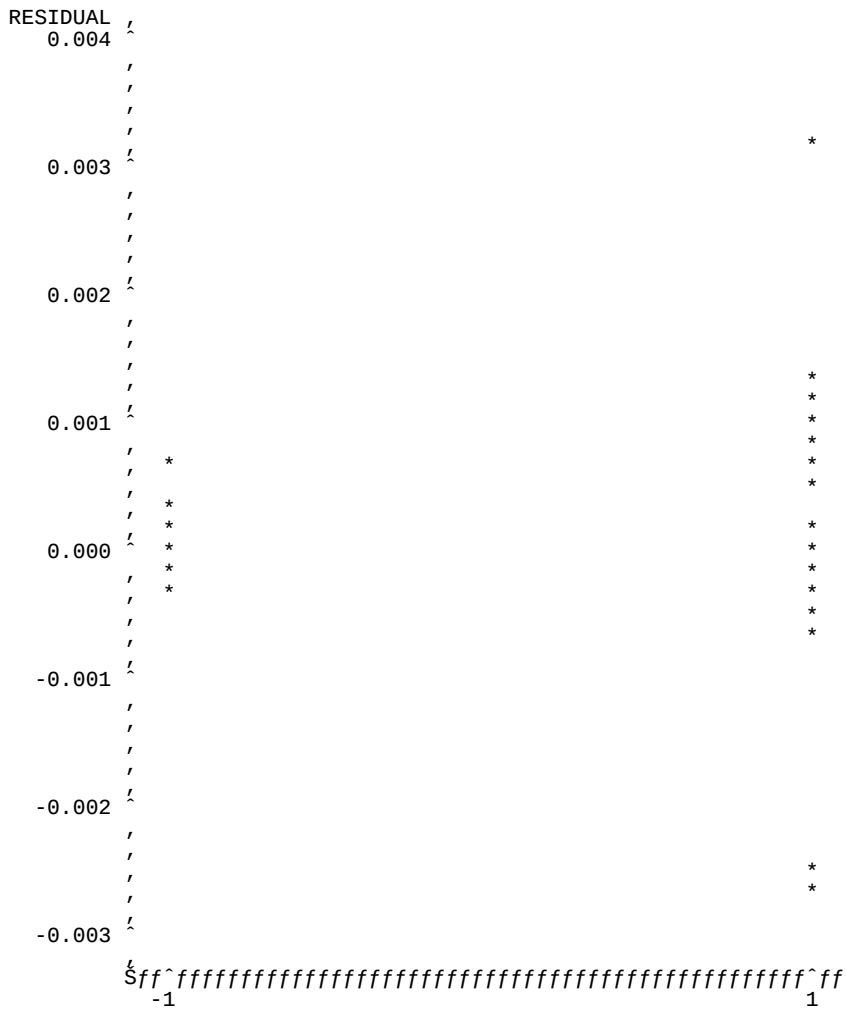

NOTE: 39 obs hidden.

As it shows pattern so constant variance assumption NOT justified.

Figure (j) Plot of RESIDUAL*C. Symbol used is '*'.

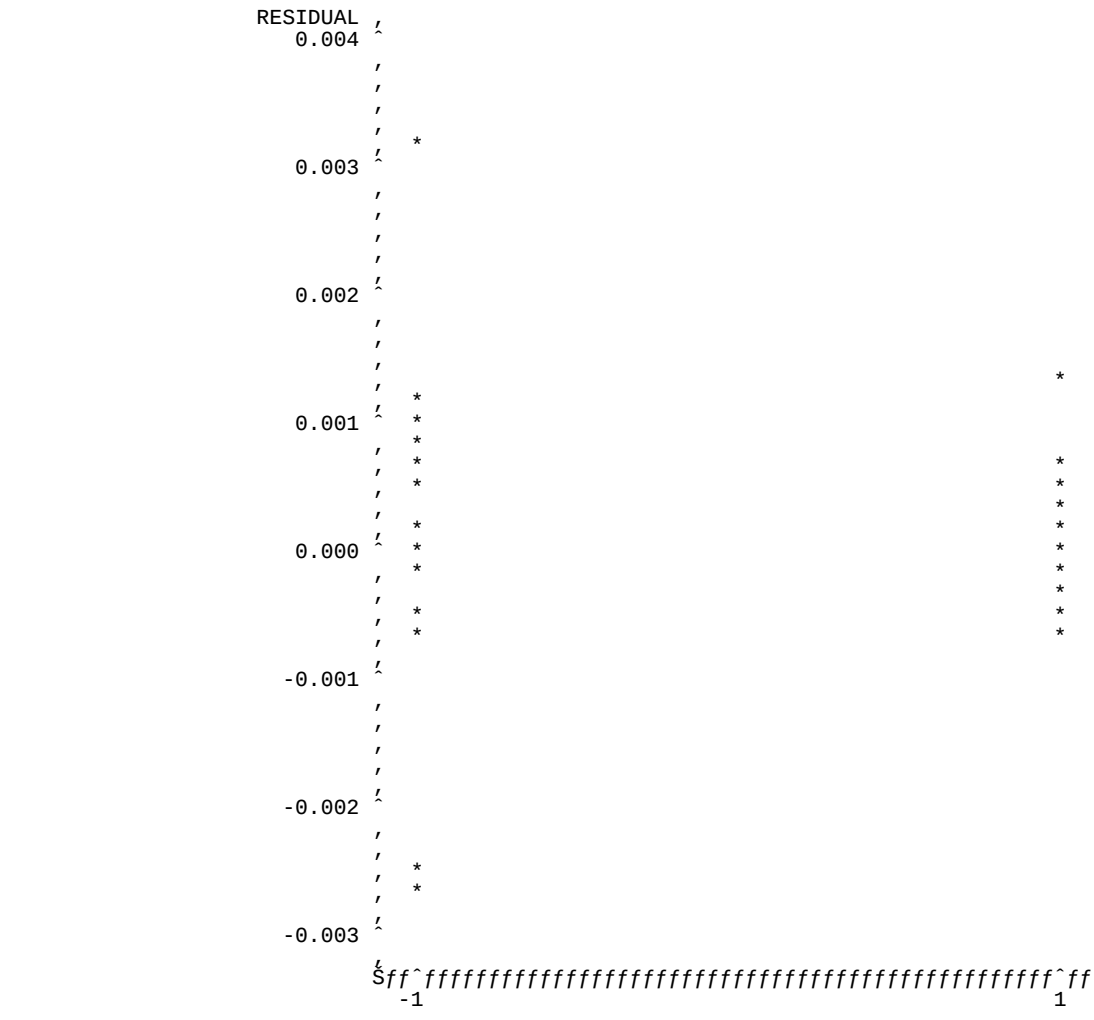

NOTE: 37 obs hidden.

As it does not show any pattern so constant variance assumption justified.

Obs	A	B	C	_TYPE_	_FREQ_	MEAN
1	.	.	.	0	60	.000439000
2	.	.	-1	1	30	.000671000
3	.	.	1	1	30	.000207000
4	.	-1	.	2	30	.000087667
5	.	1	.	2	30	.000790333
6	.	-1	-1	3	15	.000050000
7	.	-1	1	3	15	.000125333
8	.	1	-1	3	15	.001292000
9	.	1	1	3	15	.000288667
10	1	.	.	4	20	.000187000
11	2	.	.	4	20	.000943500
12	3	.	.	4	20	.000186500
13	1	.	-1	5	10	.000269000
14	1	.	1	5	10	.000105000
15	2	.	-1	5	10	.001413000
16	2	.	1	5	10	.000474000
17	3	.	-1	5	10	.000331000
18	3	.	1	5	10	.000042000
19	1	-1	.	6	10	.000002000
20	1	1	.	6	10	.000372000
21	2	-1	.	6	10	.000246000
22	2	1	.	6	10	.001641000
23	3	-1	.	6	10	.000015000
24	3	1	.	6	10	.000358000
25	1	-1	-1	7	5	.000004000
26	1	-1	1	7	5	0
27	1	1	-1	7	5	.000534000
28	1	1	1	7	5	.000210000
29	2	-1	-1	7	5	.000146000
30	2	-1	1	7	5	.000346000
31	2	1	-1	7	5	.002680000
32	2	1	1	7	5	.000602000
33	3	-1	-1	7	5	0
34	3	-1	1	7	5	.000030000
35	3	1	-1	7	5	.000662000
36	3	1	1	7	5	.000054000

Figure (k) Plot of MEAN*C. Symbol is value of B.

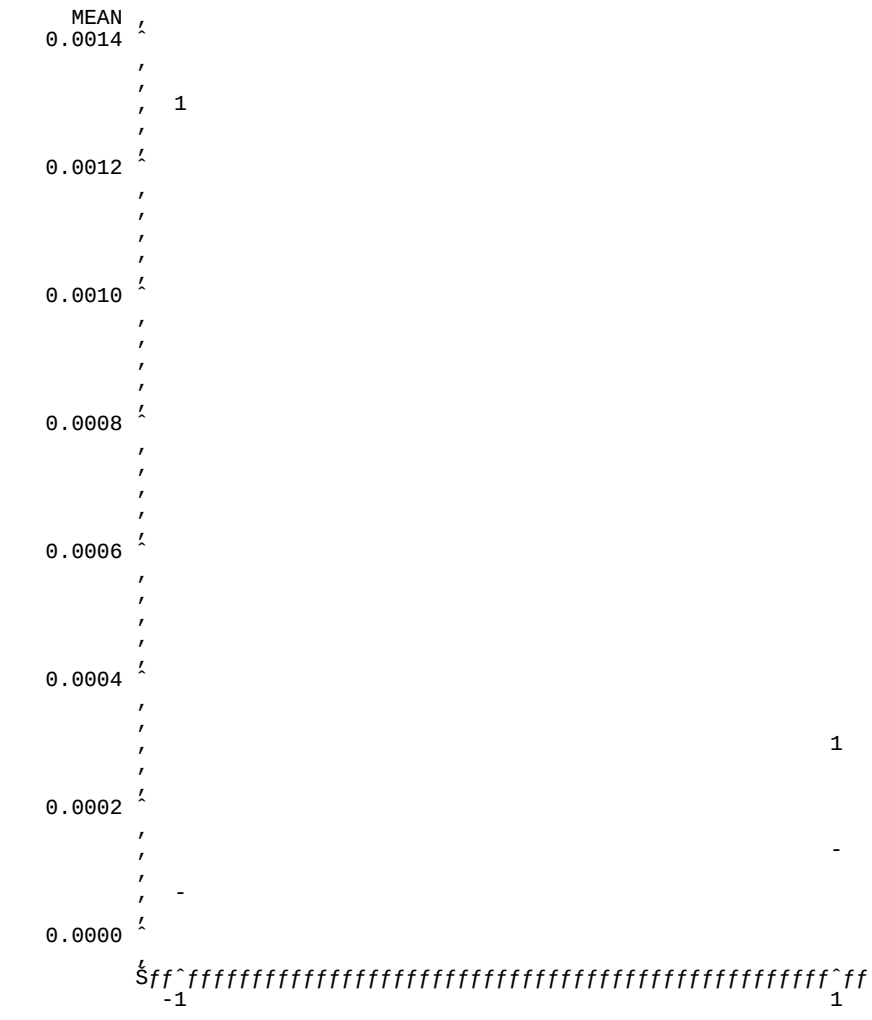

If lines would be drawn through the same pair of values then it would not be parallel and that would prove factor C as insignificant.

Figure (l) Plot of MEAN*A. Symbol used is '*'.

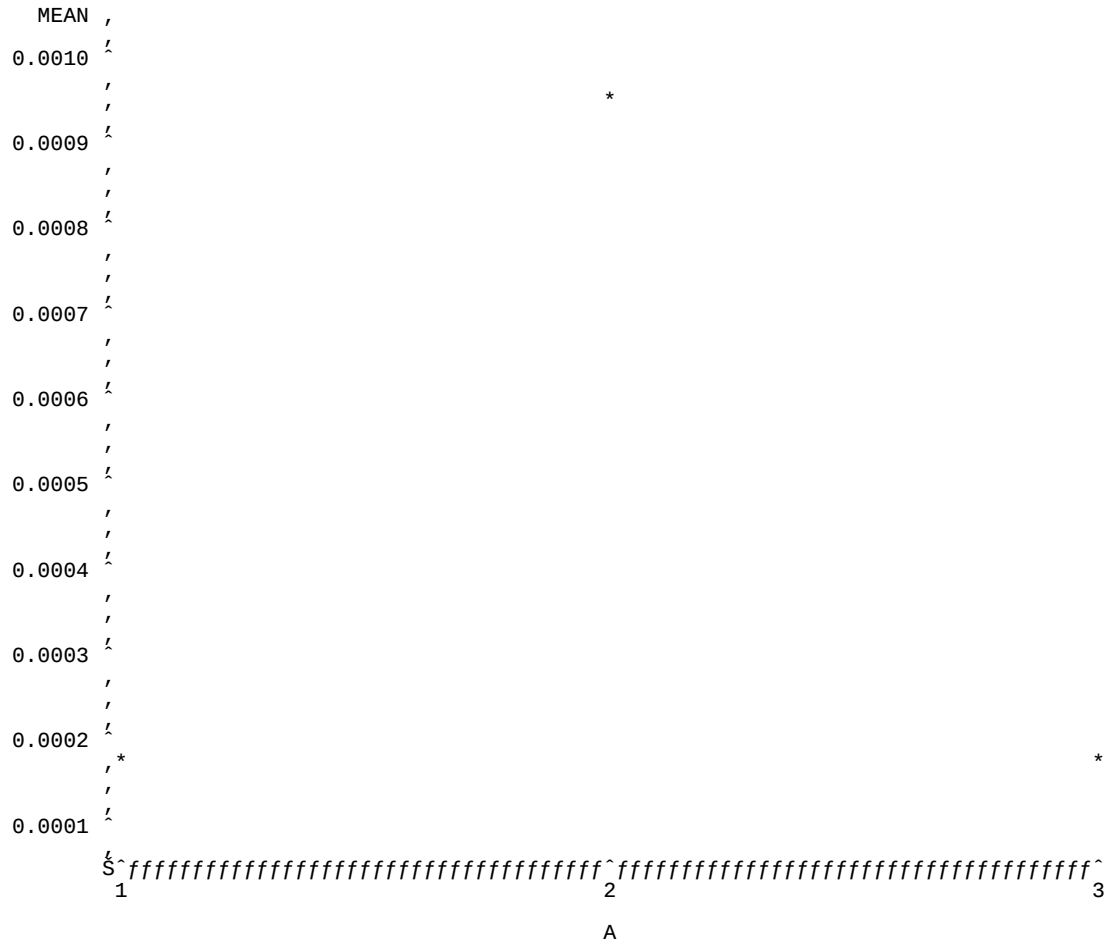

This graph shows that mean response variable is lower at level 1 (laboratory permeameter) and level 3 (Kuss permeameter) of factor A while its high at level 2 (NCAT permeameter).

Figure (m) Plot of MEAN*B. Symbol used is '*'.

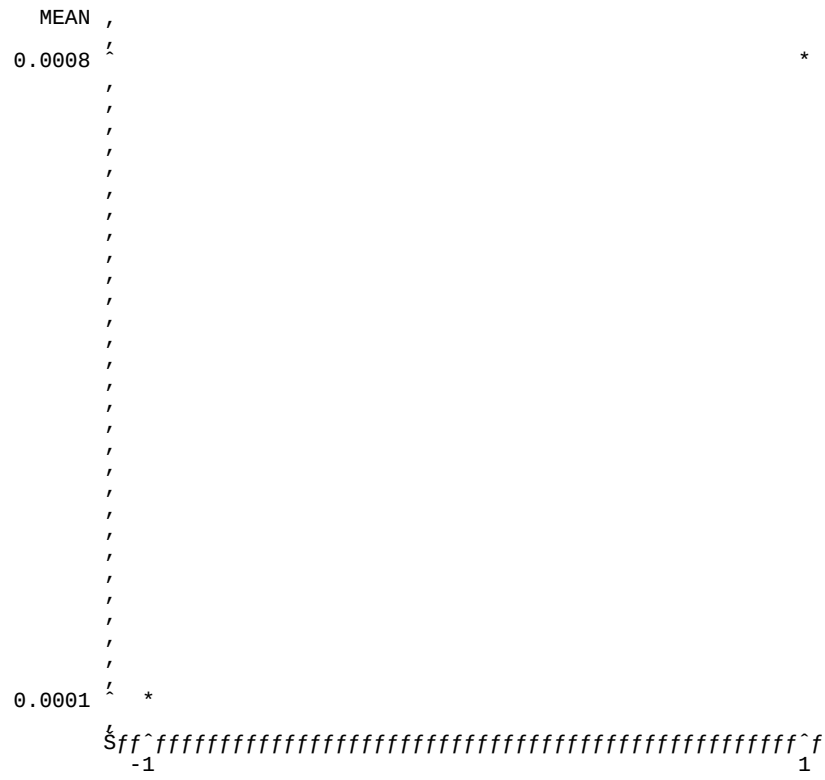

At low effective air voids (factor B),the response variable (permeability) is low and it increases when the air voids become higher.

The REG Procedure
Model: MODEL1
Dependent Variable: RESP

Analysis of Variance

Source	DF	Sum of Squares	Mean Square	F Value	Pr > F
Model	3	0.00001177	0.00000392	4.12	0.0103
Error	56	0.00005329	9.515576E-7		
Corrected Total	59	0.00006506			

Root MSE	0.00097548	R-Square	0.1809
Dependent Mean	0.00043900	Adj R-Sq	0.1370
Coeff Var	222.20458		

Parameter Estimates

Variable	DF	Parameter Estimate	Standard Error	t Value	Pr > |t|
Intercept	1	0.00043950	0.00033319	1.32	0.1925
A	1	-2.5E-7	0.00015424	-0.00	0.9987
B	1	0.00035133	0.00012593	2.79	0.0072
BC	1	-0.00026967	0.00012593	-2.14	0.0366

The REG Procedure
Model: MODEL1
Dependent Variable: RESP

Output Statistics

Obs	Dep Var RESP	Predicted Value	Std Error Mean Predict	Residual	Std Error Residual	Student Residual
1	0	-0.000182	0.000267	0.000182	0.00094	0.194
2	0	-0.000182	0.000267	0.000182	0.00094	0.194
3	0.0000200	-0.000182	0.000267	0.000202	0.00094	0.215
4	0	-0.000182	0.000267	0.000182	0.00094	0.194
5	0	-0.000182	0.000267	0.000182	0.00094	0.194
6	0	0.000358	0.000267	-0.000358	0.00094	-0.381
7	0	0.000358	0.000267	-0.000358	0.00094	-0.381
8	0	0.000358	0.000267	-0.000358	0.00094	-0.381
9	0	0.000358	0.000267	-0.000358	0.00094	-0.381
10	0	0.000358	0.000267	-0.000358	0.00094	-0.381
11	0.0000200	0.001060	0.000267	-0.001040	0.00094	-1.109
12	0.0000200	0.001060	0.000267	-0.001040	0.00094	-1.109
13	0.0000600	0.001060	0.000267	-0.001000	0.00094	-1.066
14	0.000970	0.001060	0.000267	-0.000090	0.00094	-0.0962
15	0.001600	0.001060	0.000267	0.000540	0.00094	0.575
16	0	0.000521	0.000267	-0.000521	0.00094	-0.555
17	0.0000100	0.000521	0.000267	-0.000511	0.00094	-0.545
18	0.0000200	0.000521	0.000267	-0.000501	0.00094	-0.534
19	0.000290	0.000521	0.000267	-0.000231	0.00094	-0.246
20	0.000730	0.000521	0.000267	0.000209	0.00094	0.223
21	0	-0.000182	0.000218	0.000182	0.00095	0.191
22	0.000200	-0.000182	0.000218	0.000382	0.00095	0.402
23	0.000210	-0.000182	0.000218	0.000392	0.00095	0.412
24	0.000320	-0.000182	0.000218	0.000502	0.00095	0.528
25	0	-0.000182	0.000218	0.000182	0.00095	0.191
26	0.0000100	0.000357	0.000218	-0.000347	0.00095	-0.365
27	0.0000300	0.000357	0.000218	-0.000327	0.00095	-0.344
28	0.0000100	0.000357	0.000218	-0.000347	0.00095	-0.365
29	0.000680	0.000357	0.000218	0.000323	0.00095	0.339
30	0.001000	0.000357	0.000218	0.000643	0.00095	0.676
31	0.0000400	0.001060	0.000218	-0.001020	0.00095	-1.073
32	0.000200	0.001060	0.000218	-0.000860	0.00095	-0.905
33	0.003800	0.001060	0.000218	0.002740	0.00095	2.882
34	0.003460	0.001060	0.000218	0.002400	0.00095	2.524
35	0.005900	0.001060	0.000218	0.004840	0.00095	5.091
36	0.0000600	0.000521	0.000218	-0.000461	0.00095	-0.485
37	0	0.000521	0.000218	-0.000521	0.00095	-0.548
38	0.000700	0.000521	0.000218	0.000179	0.00095	0.189
39	0.000300	0.000521	0.000218	-0.000221	0.00095	-0.232
40	0.001950	0.000521	0.000218	0.001429	0.00095	1.503
41	0	-0.000182	0.000267	0.000182	0.00094	0.194
42	0	-0.000182	0.000267	0.000182	0.00094	0.194
43	0	-0.000182	0.000267	0.000182	0.00094	0.194
44	0	-0.000182	0.000267	0.000182	0.00094	0.194
45	0	-0.000182	0.000267	0.000182	0.00094	0.194
46	0	0.000357	0.000267	-0.000357	0.00094	-0.381
47	0.000130	0.000357	0.000267	-0.000227	0.00094	-0.242
48	0	0.000357	0.000267	-0.000357	0.00094	-0.381
49	0	0.000357	0.000267	-0.000357	0.00094	-0.381
50	0.0000200	0.000357	0.000267	-0.000337	0.00094	-0.359
51	0	0.001060	0.000267	-0.001060	0.00094	-1.130
52	0.0000300	0.001060	0.000267	-0.001030	0.00094	-1.098
53	0.001790	0.001060	0.000267	0.000730	0.00094	0.778
54	0.001380	0.001060	0.000267	0.000320	0.00094	0.341
55	0.000110	0.001060	0.000267	-0.000950	0.00094	-1.012
56	0	0.000520	0.000267	-0.000520	0.00094	-0.555
57	0	0.000520	0.000267	-0.000520	0.00094	-0.555
58	0.0000300	0.000520	0.000267	-0.000490	0.00094	-0.523
59	0	0.000520	0.000267	-0.000520	0.00094	-0.555
60	0.000240	0.000520	0.000267	-0.000280	0.00094	-0.299

Sum of Residuals	0
Sum of Squared Residuals	0.00005329
Predicted Residual SS (PRESS)	0.00005969

APPENDIX II

ASTM Subcommittee Draft 5

(December 5, 2000)

Standard Provisional Test Method for

Measurement of Permeability of Bituminous Paving Mixtures Using a Flexible Wall Permeameter

1. Scope

1.1 This test method covers procedures for determining the relative permeability (also referred to as *coefficient of permeability*) of either water saturated laboratory compacted HMA specimens or field cores of compacted bituminous paving mixtures using a flexible wall permeameter. The measurement provides an indication of water permeability of a particular compacted mixture specimen relative to other hot mix asphalt mixtures compacted and tested in the same manner.

1.2 The values stated in SI units are to be regarded as the standard. The values given in parentheses are for information only.

1.3 *This standard does not purport to address all of the safety concerns, if any, associated with its use. It is the responsibility of the user of this standard to establish appropriate safety and health practices and determine the applicability of regulatory limitations prior to use.*

2. Referenced Documents

2.1 *ASTM Standards:*

D 8 Standard Terminology Relating to Materials for Roads and Pavements

D 1188 Bulk Specific Gravity and Density of Compacted Bituminous Mixtures Using Parafilm-Coated Specimens

D 2041 Theoretical Maximum Specific Gravity and Density of Bituminous Paving Mixtures

D 2726 Bulk Specific Gravity and Density of Non-Absorptive Compacted Bituminous Mixtures

D 4867 Effect of Moisture on Asphalt Concrete Paving Mixtures

2.2 *AASHTO Standards:*

TP 4 Preparing and Determining the Density of Hot-Mix Asphalt (HMA) Specimens by Means of the Superpave Gyratory Compactor

T 283 Resistance of Compacted Bituminous Mixture to Moisture Induced Damage

3. Terminology

3.1 *Definitions*

3.1.1 Refer to D 8 for definitions of terms used in this method.

4. Summary of Test Method

4.1 A falling head permeability test is used to determine the rate of flow of water through a saturated specimen. Water from a graduated standpipe is allowed to flow through the saturated bituminous paving mixture specimen and the time interval to reach a known change in head is recorded. The coefficient of water permeability of the compacted paving mixture is then determined based on Darcy's Law.

5. Significance and Use

5.1 This test method provides a means for determining the water permeability of water-saturated samples. It applies to one-dimensional, laminar flow of water.

5.2 It is assumed that Darcy's Law is valid and that the permeability is essentially unaffected by hydraulic gradient. The validity of Darcy's Law may be evaluated by measuring the hydraulic conductivity of the specimen at three hydraulic gradients. If all measured values are similar (i.e. within approximately 25%), then Darcy's Law may be taken as valid.

6. Apparatus

6.1 *Permeameter* – See Figure 4. The device shall meet the following requirements:

6.1.1 A graduated cylinder, having an inner diameter of 31.75 ± 0.5 mm (1.25 ± 0.02 in.), graduated in millimeters and capable of dispensing 500 ml of water.

6.1.2 A specimen cylinder using a flexible latex membrane 0.635 mm (0.025 in.) thick and capable of confining asphalt concrete specimens up to 152.4 mm (6.0 in.) in diameter and 80 mm (3.15 in.) in height.

6.1.3 An upper cap assembly for supporting the graduated cylinder and expanding an o-ring against the sealing tube. The opening in the upper cap shall have the same diameter as the outer diameter of the calibrated cylinder mentioned previously in 5.1.1. The underside of the upper cap assembly should be tapered at an angle of 10 ± 1° (see Figure 1.)

6.1.4 A lower pedestal plate for supporting the asphalt concrete specimen and expanding an o-ring against the sealing tube. The opening in the plate should have a minimum diameter of 18 mm (0.71 in.). The top side of the lower cap should be tapered at an angle of 10 ± 1° (see Figure 1).

6.1.5 O-rings of sufficient diameter and thickness for maintaining a seal against the sealing tube.

6.1.6 A frame and clamp assembly for supplying a compressive force to the upper cap assembly and lower pedestal necessary to expand the o-rings.
6.1.7 An air pump capable of applying 103.42 kPa (15 psi) pressure and capable of applying vacuum to evacuate the air from the sealing tube/membrane cavity.
6.1.8 A pressure gauge with range 0 to 103.42 kPa (15 psi) with ± 2% accuracy.
6.1.9 Quick connects and pressure line for inflating and evacuating the sealing tube/membrane cavity.
6.1.10 An outlet pipe with an inside diameter of 18 mm (0.71 in.).
6.1.11 Flow control valve positioned upstream of the outlet pipe.

NOTE 1: A device manufactured by Karol-Warner Soil Testing Systems has been found to meet the above specifications.

6.2 *Vacuum container, Type E,* described in D 2041.
6.3 *Vacuum pump,* specified in D 2041.
6.4 *Manometer,* specified in D 2041.
6.5 *Spacer,* described in AASHTO T 283.
6.6 *Balance,* meeting the requirements specified in D 2726.
6.7 *Water bath,* meeting the requirements specified in D 2726.
6.8 *Stopwatch,* or other timing device capable of measurements to at least the nearest 0.1 s and accurate to within 0.05% when tested over intervals of not less than 15 min.
6.9 *Meterstick,* capable of measuring to the nearest 0.5 mm.
6.10 *Caliper,* capable of measuring to the nearest 0.01 mm for measuring specimen thicknesses.
6.11 *Thermometer,* calibrated liquid-in-glass type capable of measuring the temperature of water to the nearest $0.1^{o}C$ ($0.2^{o}F$).
6.12 *Graduated Cylinder,* 100 ml minimum capacity with 1 ml or smaller graduations.
6.13 *Saw,* with diamond impregnated blade for wet cutting of specimens to the desired thickness. Dry cut type saws are not to be used.
6.14 *Sealing Agent (petroleum jelly),* to produce a watertight seal between the specimen and the flexible wall membrane of the permeameter.
6.15 *Spatula,* for applying the petroleum jelly sealant to the sides of the specimen.
6.16 *Electric fan,* for drying the wet cut specimens.

7. Reagents

7.1 Supply of clean, non-aerated tap water.

8. Preparation of Test Specimens

8.1 *Laboratory prepared specimens:*
8.1.1 Specimens shall be compacted in accordance with AASHTO TP 4.
8.1.2 After compaction, specimens shall be allowed to cool to room temperature.
8.1.3 Specimens shall then be sawed on one side to the desired test sample thickness (e.g. the anticipated in-place lift thickness).

8.1.4 The air void level of the specimen is user defined; however, it is recommended that the air void level represent the anticipated in-place density of the bituminous paving mixture.

8.2 *Roadway cores*:

8.2.1 Layers of compacted bituminous paving mixture field cores shall be separated by sawing. Sawing shall also be required to remove any tack coat that would otherwise affect the test results.

8.3 Wash the test specimen thoroughly with water to remove any loose, fine material produced by the sawing and then dry the specimen to a constant mass by means of the electric fan.

8.4 Determine the bulk specific gravity of the specimen in accordance with D 2726 or D1188 as appropriate.

8.5 Measure and record the height and diameter of the specimen to the nearest 0.5 mm (0.02 in.) or better. Individual height and diameter measurements shall be taken at three different locations. The three individual measurements shall not vary by more than 5 mm (0.2 in.). The diameter of the specimen shall not be less than 150 mm (5.91 in.) nor greater than 152.4 mm (6.0 in.).

9. Saturation of Test Specimens

9.1 Place the specimen in a horizontal position in the vacuum container supported above the container bottom by the spacer. Fill the container with water at room temperature so that the specimens have at least 25 mm of water above their surface.

9.2 Remove trapped air and saturate the specimen by applying increased vacuum gradually until the residual pressure manometer reads 525 ± 2 mm of Hg. Maintain this residual pressure for 5 ± 1 minutes.

9.3 At the end of the vacuum period, release the vacuum by slowly increasing the pressure.

9.4 Allow the specimen to stand undisturbed for 5 to 10 minutes or leave specimen submerged until ready for testing.

10. Permeameter Setup

10.1 With the permeameter completely assembled (with a specimen of the size to be tested), use the meterstick to measure a distance of 10 cm from the top plate of permeameter and place a mark onto the standpipe. This mark will be designated as the lower timing mark.

NOTE 3: Complete assembly is important since the springs of the top plate must be fully compressed in order to insure an accurate distance measurement.

10.2 Using the meterstick, establish a mark on the graduated tube at a distance of 63.1 cm from the lower timing mark. This shall be designated as the upper timing mark. Additional 'upper' timing marks may be established (e.g. at 10 cm intervals) in order to facilitate the testing of mixtures having a wide range of permeability values.

NOTE 4: If the permeameter's graduated cylinder has manufacturer established timing marks, then steps 10.1 – 10.2 should be done to verify that the timing marks have been properly positioned.

NOTE 5: The permeameter setup described will produce a hydraulic gradient of approximately 8 to 12 (depending on specimen thickness). Tests using other hydraulic gradients may be conducted to verify the validity of Darcy's Law.

11. Testing Procedure

11.1 Disassemble the permeameter specimen cylinder from the permeameter base.

11.2 Connect the pressure line of the permeameter to the vacuum side of the pump. Using the pump, apply a vacuum to the flexible wall to remove entrapped air and collapse the membrane to the inside diameter of the cylinder. This will facilitate loading of the specimen.

11.3 With the flow control valve open, fill the outlet pipe with water until the taper in the base plate pedestal overflows.

11.4 For laboratory compacted specimens, it is necessary to apply a thin layer of petroleum jelly to the sides of the specimen to achieve a satisfactory seal between the membrane and the specimen. This shall be accomplished using a spatula or similar instrument. Sealant shall be applied ONLY to the sides of the specimen. Remove the specimen from the vacuum container filled with water, dry to SSD, apply the petroleum jelly sealant to the sides, and then quickly place the specimen on the pedestal of the permeameter. For core specimens, remove the specimen from the vacuum container filled with water, dry to SSD, and then quickly place the specimen on the pedestal of the permeameter.

11.5 Expeditiously reassemble the permeameter making sure that all connections and clamps are tightened.

11.6 Disconnect the pressure line from the vacuum side of the pump and connect it to the pressure side.

11.7 Apply a confining pressure of 96.5 ± 7 kPa(14 ± 1 psi).

NOTE 6: Observe for fluctuations in confining pressure. Variations may be the result of insufficient seal or a hole in the flexible membrane. Care should be exercised to ensure that the confining pressure remains constant throughout the test.

11.8 Fill the permeameter graduated cylinder until water begins to flow from the outlet tube. Exercise care when filling to minimize the incorporation of air bubbles.

11.9 Close the flow control valve.

11.10 Carefully lean the permeameter from side to side to allow the escape of any entrapped air. Continue this operation until all entrapped air has been removed.

11.11 Fill the graduated cylinder above the upper timing mark (h1).

11.12 Refill the outlet pipe until it overflows.

11.13 Commence the water flow by opening the flow control valve of the permeameter. Start the timing device when the bottom of the meniscus of the water reaches the upper timing mark. Allow water to flow until the water level reaches the lower timing mark (h2). Once the water level reaches the lower timing mark, stop the timing device and close the valve. Record the elapsed time to the nearest second.

11.14 Saturation of the specimen may require many test runs. Therefore, steps 11.11 – 11.13 must be repeated. The specimen is considered sufficiently saturated when four consecutive measurements do not differ by more than ten percent (10%) of the mean of the four consecutive test results. Once saturation has been verified, the final time measured shall be recorded as the test time and subsequently used in the calculations.

NOTE 7: If the test time is approaching thirty minutes during the first test run without the water reaching the lower timing mark, then the test may be terminated at the thirty minute mark and the water level at this time recorded. In this case, the test shall be conducted one additional time by allowing water to flow for thirty minutes and recording the water mark at this time with the average of the two elapsed time measurements being recorded for use in calculating the permeability.

11.15 Measure and record the temperature of the permeate water in the system to the nearest 0.5°C.

11.16 After saturation has been achieved and verified and the final time and/or mark recorded, release the pressure from the permeameter, remove the clamp assemblies, upper platen and specimen. Wipe clean any excess sealant off of the latex membrane.

12. Calculation

12.1 The coefficient of water permeability, *k*, is determined using the following equation:

$$k = \frac{al}{At} \ln\left(\frac{h_1}{h_2}\right)$$

Where,

k = coefficient of water permeability, cm/s
a = inside cross-sectional area of inlet standpipe, cm^2
l = thickness of test specimen, cm
A = cross-sectional area of test specimen, cm^2
t = average elapsed time of water flow between timing marks, s
h_1 = hydraulic head on specimen at time t_1, cm
h_2 = hydraulic head on specimen at time t_2, cm

12.2 Correct the calculated permeability to that for 20°C (68 °F) , k_{20}, by multiplying k by the ratio of the viscosity of water at the test temperature to the temperature of water at 20°C (68 °F), R_T, from Table 1, as follows:

$$k_{20} = R_T k$$

13. Report

13.1 Report the following information:

13.1.1 Specimen identification,

13.1.2 Mixture type/description,

13.1.3 Specimen type (i.e. lab prepared or roadway core),

13.1.4 Specimen air voids,

13.1.5 Water temperature,

13.1.6 Coefficient of water permeability is reported to the nearest whole unit x 10^{-5} cm/s.

14. Precision and Bias

14.1 *Precision* - Work is underway to develop a precision statement for this provisional test method. This method should not be used to accept or reject materials until the precision statement is available.

14.2 *Bias* – No information can be presented on the bias of the procedure in this provisional test method because no material having an accepted reference value is available.

15. Keywords

15.1 bituminous paving mixture, permeability, coefficient of permeability

TABLE 1 Correction Factor, R_T, for Viscosity of Water at Various Temperatures

Temperature, °C	R_T	Temperature, °C	R_T
15.0	1.135	25.0	0.889
15.5	1.121	25.5	0.879
16.0	1.106	26.0	0.869
16.5	1.092	26.5	0.860
17.0	1.077	27.0	0.850
17.5	1.064	27.5	0.841
18.0	1.051	28.0	0.832
18.5	1.038	28.5	0.823
19.0	1.025	29.0	0.814
19.5	1.013	29.5	0.805
20.0	1.000	30.0	0.797
20.5	0.988	30.5	0.789
21.0	0.976	31.0	0.780
21.5	0.965	31.5	0.772
22.0	0.953	32.0	0.764
22.5	0.942	32.5	0.757
23.0	0.931	33.0	0.749
23.5	0.921	33.5	0.741
24.0	0.910	34.0	0.733
24.5	0.900	34.5	0.725

PHASE TWO

Prediction of Moisture Migration in Flexible Pavement Systems: an Evaluation of the Enhanced Integrated Climatic Model

Table of Contents

List of Figures

List of Tables

Chapter 1 Introduction

1.1 Problem Statement

Superior Performing Asphalt Pavement (Superpave) was introduced by the Strategic Highway Research Program (SHRP) in 1992 after five years of extensive study. Superpave was developed primarily to address two pavement distresses: permanent deformation and low temperature cracking. Since 1995, the Arkansas State Highway and Transportation Department (AHTD) began to adopt Superpave for flexible pavement projects. Compared with the conventional Marshall mix design, the Superpave designs typically use more coarse-graded aggregate blends which normally make them more permeable than mixes developed using the Marshall design criteria. This fact was reported by Westerman (1998) based on permeability test results on asphalt cores obtained from 16 projects in Arkansas. Because of the relatively high permeability, Superpave allows more water to migrate into the underlying base course and subgrade soil than the Marshall mix design. This increase in moisture in the underlying pavement structure can result in a variety of water-related problems. These water-related problems cannot be well understood until we have a mature understanding of the exact nature of moisture migration through pavement surface and into underlying layers. Unfortunately, this mature understanding of moisture migration through pavement systems does not currently exist.

Moisture content has an important yet indirect effect on the current empirical pavement design. The current empirical flexible pavement design procedure - AASHTO Guide for Design of Pavement Structures (AASHTO 1993) uses resilient modulus of the subgrade soil as a primary input for determining the required structural number of the

pavement system. Many studies (Thompson, et al. 1985; Elliot et al. 1988; Monismith 1992, Ksaibati, et al 2000, Tian, et al 1998) have already established that an increase in moisture content results in a decrease in the resilient modulus of base materials and underlying subgrade soils, which, in turn, will result in a reduced pavement life. The AASHTO design guide (1993) recommends establishing a relationship between resilient modulus and moisture content for a soil. The resilient modulus of the soil can then be obtained by first developing a relationship between moisture content and modulus and then estimating moisture content for each season. It is obvious that both, a better understanding how moisture migrates through pavement systems, and the development of methods to appropriately estimate the moisture content in pavement systems based on precipitation and other seasonal events are vitally important if the correct resilient modulus for pavement material and underlying subgrade soils is to be determined. An understanding of moisture migration and its affect on modulus is even more important with the implementation of Superpave and the new Mechanistic-Empirical Design Guide. Not only are the older methods for estimating moisture content in pavement systems that were suitable for the dense-graded Marshall mix designs not be suitable for the open-graded Superpave designs, the new M-E design procedures make the accurate determination of modulus even more important.

In order to better predict moisture conditions in pavement systems, an Enhanced Integrated Climatic Model (EICM) was proposed for the new AASHTO design guide (MEPDG). The EICM has the ability to predict moisture content and soil temperature profiles in pavement systems using available climatic information from national weather stations. The EICM has been incorporated into The Mechanistic-Empirical Pavement

Design Guide Software program (MEPDG) in an attempt to better predict changes in subgrade modulus due to environmental conditions. However, Ahmed and his coworkers (2005) evaluated the EICM using measured data from two LTPP test sites in New Jersey and a wide discrepancy was observed between predicted and measured temperatures and moisture contents. Therefore, they concluded that the EICM was not suitable for New Jersey. So far, the EICM has not been evaluated in Arkansas.

1.2 Purpose and Scope

The major objectives of this study are:

1. Experimentally and analytically determine the pattern of moisture migration through pavement systems;
2. Develop a relationship between environmental factors and moisture content in pavement systems;
3. Develop a suitable model to predict moisture content in pavement system;
4. Evaluate the accuracy of the EICM in Arkansas. Develop and calibrate a Finite Element Model (FEM) which predicts moisture migration and compare it to the measured data.

1.3 Research Strategy

A comprehensive literature review was conducted and used to demonstrate the importance of a mature understanding of water migration through pavement systems and underlying layers. The comprehensive literature review was also used to identify factors that could possibly affect moisture content in pavement systems. In addition the

literature review was used to identify the appropriate instrumentation equipment required to measure moisture content and temperature in pavement systems, surface and subsurface water flow, ground water levels, and environmental factors.

Two test pads were built and instrumented at the Engineering Research Center (ERC) of the University of Arkansas to measure moisture migration through two different pavement systems. Also, a 100-foot long field pavement section located on Highway 253 in Ft. Smith, Arkansas was instrumented to achieve the goals discussed previously for a pavement system subject to traffic.. For the test pads at the ERC and the field test site, climatic information comprised of air temperature and precipitation, surface water and subsurface water during precipitation events, moisture content and soil temperature in the pavement systems, and ground water levels were measured for a relatively long period. The basic idea is to measure how much water fell on the surface of the pavements (precipitation multiplied by the area of the pavements), how much water ran off from the surface of the pavements, how much water was collected in the edge drains, and how much and how fast the water content of base and subgrade soils changed in response to precipitation events and to seasonal changes.

A comprehensive laboratory testing program was also performed to obtain the engineering properties of pavement materials and underlying soils. Laboratory tests consisted of classification tests, standard and modified Proctor compaction tests, permeability tests and resilient modulus tests.

Using laboratory-measured values for material properties of the pavement material and underlying soils along with measured temporal values of precipitation, air temperature, surface and subsurface water flow, ground water levels, moisture content

and soil temperature in the pavement system, statistical analyses were performed to obtain predictive models for air temperature, moisture content and soil temperature in the pavement systems, surface subsurface water flow, and resilient modulus of subgrade soils. A water balance analysis was also performed to better understand water migration through pavement systems.

With measured climatic information supplemented by climatic data obtained from nearby national weather stations and laboratory-measured material properties, the EICM was evaluated for the test pads at the ERC and the field test site on Highway 253 in Ft. Smith. Before the evaluation of the EICM, sensitivity analyses were performed on climatic factors that were not measured on site and had to be supplemented with data from nearby national weather stations.

Lastly, a commercially-available finite element analysis software, called PlaxFlow, was employed to develop a Finite Element Model (FEM) to simulate water migration in pavement systems and underlying soils during several precipitation events. The FEM was then calibrated based on measured data.

Chapter 2 Literature Review

2.1 Introduction

Many pavement system problems, such as stripping, freeze-thaw damage, oxidation, and base and subgrade deterioration, are due to water intruding into the pavement system. With the implementation of Superpave, which stands for Superior Performing Asphalt Pavements, these problems become even more serious, because the aggregate blends used in hot-mix asphalt concrete for Superpave are typically more coarse-graded than mixes of the Marshall design era. So in designing and constructing Superpave, much more attention must be paid to the potential damages that can be caused by water. Unfortunately, until now we do not have a mature understanding of the exact nature of moisture migration through pavement structures and into underlying layers.

Moisture can infiltrate into pavement systems through cracks, joints, porous pavement surfaces and shoulders. In addition, a high ground water table can be an important source of moisture in pavements. The detrimental impact of moisture on the performance of pavement systems can be summarized as follows (Huang 1993):

- Moisture affects the durability and strength characteristics of soils, and consequently, the ability of the subgrade to support the pavement,
- In cold weather, freeze-thaw can occur, which results in the dramatic reduction of load-carrying capacity during the frost melting period,
- Moisture can cause differential heaving over swelling soils,
- With the pore pressure generated by moving traffic, pumping of fines into the base course may occur with resulting loss of support,
- Stripping of asphalt mixtures can occur due to continuous contact with water.

The AASHTO Guide for Design of Pavement Structures (AASHTO 93) considers the effect of the moisture content in pavement design by relating the moisture content to the resilient modulus of base and subgrade materials, which is a primary input parameter to evaluate the properties of base and subgrade materials. The following section includes literature regarding how moisture content affects the resilient modulus, how the current AASHTO Design Guide (1993) and the proposed future design Guide (2002) take the effects of the moisture content into consideration in pavement designs, and why an understanding of the nature of moisture content migration through pavement systems is critical to the current empirical and mechanistic-empirical flexible pavement design procedures.

2.2 Effects of moisture on properties of base and subgrade materials

There are a number of testing procedures available to evaluate pavement base and subgrade materials, including: modulus of subgrade reaction (k-value), California Bearing Ratio (CBR), R-value, triaxial coefficients c and ϕ, elastic coefficients Elastic Modulus (E) and Poisson's Ratio (υ), soil support value S, and resilient modulus M_R. While design procedures can be found that use of each of these material properties, the most commonly employed empirical design procedure for flexible pavement design is that which appears in the AASHTO Guide for Design of Pavement Structures (AASHTO 1993). This procedure uses resilient modulus as the primary input parameter to evaluate the properties of subgrade materials.

Resilient modulus is defined by AASHTO as "a measure of the elastic property of soil recognizing certain non-linear characteristics" (AASHTO, 93). Deformation of

highway pavement layers under traffic loading can be divided into two parts: the recoverable resilient part (elastic strain) and irrecoverable non-resilient part (plastic strain) as shown in Figure 2.1. The value of elastic modulus based on the recoverable strain under repeated loading is called the resilient modulus M_R, and is defined by Equation 2.1.

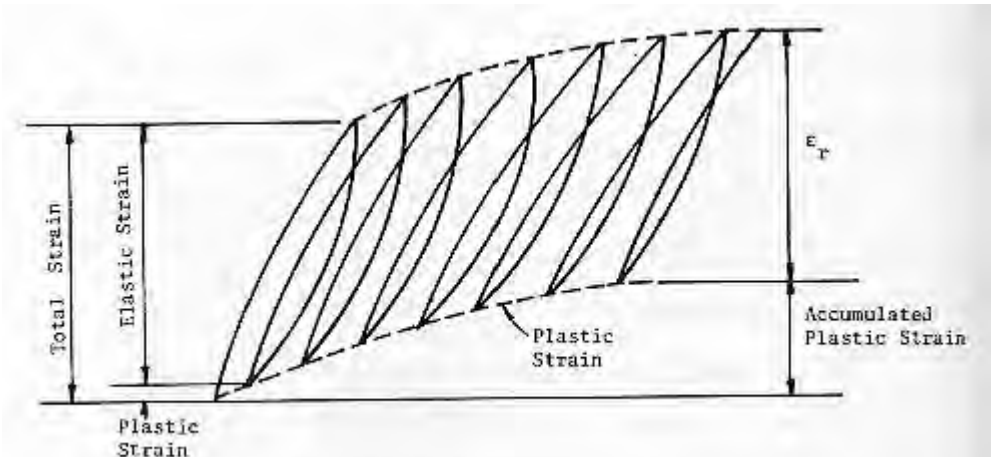

Figure 2.1 Strain under repeated load (after Huang, 1993).

$$M_R = \frac{\sigma_d}{\varepsilon_r} \qquad 2.1$$

Where:

σ_d = deviator stress;

ε_r = resilient strain.

Several standard test methods for resilient modulus have been developed by AASHTO over the years and all involve repeated-load triaxial testing. The AASHTO Guide for Design of Pavement Structures (AASHTO 1986) recommended that the laboratory resilient modulus test procedures prescribed in AASHTO T 274-82, be used to determine the engineering properties of subgrade soils. Since the introduction of AASHTO T 274-82, many studies have been carried out to improve the testing

procedures, such as the National Cooperative Highway Research Program (NCHRP) I-28 project (Barksdale et al. 1997). As a result, several resilient modulus test procedures were proposed, including AASHTO T 292-91I, AASHTO T 294-92 (the Strategic Highway Research Program's Protocol P46), and the current version, AASHTO T-307. Unfortunately, all of these test methods for resilient modulus are time-consuming and procedurally complex, which makes it difficult for them to be widely adopted by highway design agencies. As a result, highway design agencies often measure other material properties, such as CBR and R-value, and relate them to resilient modulus, instead of measuring the value of resilient modulus directly. For example, the Arkansas State Highway and Transportation Department uses resilient modulus values for pavement design that are derived from correlations with the R-value test.

Even if true values for resilient modulus were used in design, a complicating factor is that the value of resilient modulus does not remain constant for a specific soil and will change with loading and seasonal environmental factors. A procedure recommended by the 1993 AASHTO Guide to determine the seasonal variation of the resilient modulus in subgrade soils is to obtain a laboratory relationship between resilient modulus and the moisture content of a soil. Then with an estimate of the in-situ moisture content of the soil during various seasons, a value for resilient modulus for each season may be estimated. It is obvious that an accurate prediction of the seasonal variation of moisture content is the key to correctly estimating the seasonal variations in resilient modulus according to AASHTO Guide 93.

Elliott, et al (1988) investigated the resilient modulus behavior of 15 Arkansas soils and found moisture content, freeze-thaw, and deviator stress to have a significant

impact on the soils' resilient modulus. Among all the environmental parameters investigated, moisture content was found to be the most critical variable for Arkansas subgrades. Other studies (Thompson, et al. 1985; Elliot et al. 1988; Monismith 1992, Ksaibati, et al 2000) had concluded that an increase in water content, for most fine-grained soils used as subgrade material, results in a decrease in resilient modulus, leading to increased deflections in the pavement system and reduced pavement life. The same principle applies for the aggregate bases. Tian and his co-workers (1998) found that an increase in moisture content of unbound aggregate base leads to a decrease in resilient modulus.

Knowing the adverse effect of moisture content on the resilient modulus of base course and subgrade materials, many studies have been performed to investigate the relationship between moisture content and resilient modulus (Jones et al. 1977, Rada et al. 1981, Elliot et al. 1988, Jin et al. 1994, Santha 1994, Drumm et al. 1997 and Muhanna et al. 1998). The intent of these studies was to develop equations to predict resilient modulus with which required only knowledge of the moisture content and other simple material properties. During the last two decades, many prediction models of the resilient modulus have been proposed for different soil types and are summarized below.

2.2.1 Li & Selig Model for Fine-grained Subgrade Soils

Li and Selig (1994) reviewed the available resilient modulus test results from the literature and proposed two models. For the first model, twenty-seven repeated load triaxial test results on 11 fine-grained soils were included to obtain a relationship of resilient modulus with moisture content at values of the same dry density. For the second

model, twenty-six repeated load triaxial test results on 10 fine-grained subgrade soils were included to obtain a relationship of resilient modulus to moisture content with the same compactive effort. These two models are given by Equations 2.2 and 2.3.

$$M_R = R_{m1} M_{R(opt)} = \left(0.98 - 0.28(w - w_{opt}) + 0.029(w - w_{opt})^2\right) M_{R(opt)} \qquad 2.2$$

Where:

M_R = resilient modulus at any given moisture content, w(%), and the same dry density as M_R(opt);

M_R(opt) = resilient modulus at maximum dry density and optimum moisture content

w_{opt}(%) for any compactive effort.

$$M_R = R_{m2} M_{R(opt)} = \left(0.96 - 0.18(w - w_{opt}) + 0.067(w - w_{opt})^2\right) M_{R(opt)} \qquad 2.3$$

Where:

M_R = resilient modulus at moisture content w(%) and the same compactive effort as

M_R(opt);

M_R(opt) = resilient modulus at maximum dry density and optimum moisture content

w_{opt}(%) for any compactive effort.

Theoretically, if the resilient modulus at maximum dry density and optimum moisture content at a compactive effort is known for a soil, resilient modulus at any soil physical conditions for the same soil can be determined using Li & Selig models. For example, in Figure 2.2, each of the three curves stands for a certain compaction effort. Suppose that resilient modulus at point O (maximum dry density and optimum moisture

content at this compaction effort) is known. Using Equation 2.2, resilient modulus at point A can be obtained. Then resilient modulus at points P and Q can be determined using Equation 2.3.

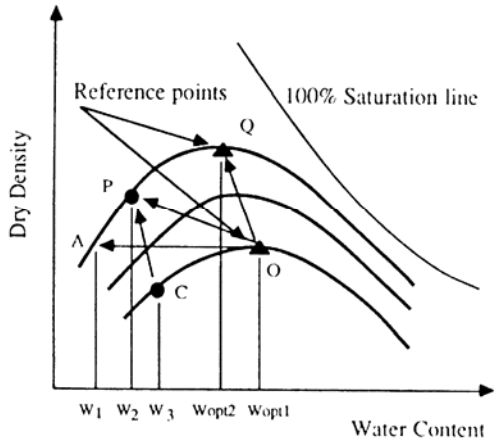

Figure 2.2 Paths for determining resilient modulus at any soil physical states (Li & Selig, 1994).

2.2.2 Drumm et al. Model for Fine-grained Subgrade Soils

Drumm et al. (1997) conducted laboratory resilient modulus tests in general accordance with the Strategic Highway Research Program Protocol P-46 (SHRP Proctor P-46) on 11 fine-grained subgrade soils representing a range of subgrade soils used throughout Tennessee. For each soil, three specimens were prepared and tested. These specimens were compacted to target values of optimum water content and maximum dry density with "Standard Proctor", AASHTO T-99 energy. One specimen was tested at optimum moisture content while the other two were tested at higher degrees of saturation. It was concluded that a nearly linear relationship exists between the degree of saturation and the soil's resilient modulus. On this basis, the model represented in Equation 2.4 was proposed by Drumm et al (1997).

$$M_{R(wet)} = M_{R(opt)} + \frac{dM_R}{dS}\Delta S \qquad 2.4$$

Where:

$M_{R(wet)}$ = resilient modulus at increased post compaction saturation, (MPa);

$M_{R(opt)}$ = resilient modulus at optimum moisture content and maximum dry density, (MPa);

ΔS = change in post compaction degree of saturation (expressed as a decimal);

dM_R/dS = gradient of resilient modulus with respect to saturation, or the slope of the M_R versus degree of saturation curve (MPa)

Two methods were developed by Drumm et al (1997) to obtain the change in M_R versus the change in degree of saturation. The first was derived based on a linear regression analysis and is shown in Equation 2.5.

$$\frac{dM_R}{dS} = 1{,}690 - 194(CLASS) - 11.2\left[M_{R(opt)}\right] \qquad 2.5$$

Where:

CLASS = AASHTO classification (e.g. for A-4, CLASS = 4.0)

$M_{R(opt)}$ = resilient modulus (MPa) at optimum moisture content and maximum dry density tested at, σ_c = 41 kPa (6 psi) and σ_d =28 kPa (4psi)

The gradient of the resilient modulus with respect to the degree of saturation can also be obtained using Table 2.1 if the AASHTO or USCS soil classification is known.

Table 2.1 Gradient of Resilient Modulus with Respect to Saturation Degree (after Drumm et al 1997).

Soil Classification		Resilient Modulus Gradient (Dm_R/Ds)
AASHTO	USCS	(Measured)
A-4	CL	-390
A-4	CL	-280
A-4	ML	-260
A-6	CL	-390
A-6	CL	-330
A-6	CL	-470
A-7-5	CH	-810
A-7-5	MH	-1540
A-7-6	CH	-1780
A-7-6	CL	-2390
A-7-6	CH	-1560

This model provides a simple way to predict resilient modulus with knowing the resilient modulus at maximum dry density and optimum moisture content. However, unlike Li & Selig model, Drumm et al. model can only predict resilient modulus at various moisture contents for the same compaction effort as that to obtain maximum dry density and optimum moisture content.

2.2.3 Jones and Witczak Model for Fine-Grained Subgrade Soils

Resilient modulus tests on both laboratory-molded and undisturbed subgrade soils from 35 different road test sections in San Diego, California were performed using repeated-load, triaxial compression tests. The subgrade soil for all test sections was an A-7-6 soil. Moisture content and dry densities were measured for all the samples. Degrees of saturation were calculated and used in a multiple linear regression analysis. Based on the test results and the multiple linear regression analysis, Jones and Witczak (1977)

proposed two models to predict resilient modulus. One is for the laboratory-molded samples and the other is for undisturbed field subgrade soils. It should be noted that all the values of resilient modulus used in the analysis corresponded to a deviator stress of 6 psi and a confining pressure of 2 psi.

For laboratory-molded samples

$$\log M_R = 2.31909 - 0.13282(w\%) + 0.013405 * S \quad 2.6$$

For undisturbed samples:

$$\log M_R = 1.17869 - 0.111109(w\%) + 0.021699 * S \quad 2.7$$

Where:

M_R = resilient modulus (ksi) at 6 psi deviator stress and 2 psi confining stress;

w% = percent water content (%);

S = degree of saturation (%).

Since Jones and Witczak model was derived based on the laboratory test results of resilient modulus on the A-7-6 subgrade soil obtained in California, it seems this model is only applicable to this specific subgrade soil.

2.2.4 Muhanna et al. model Fine-grained Subgrade Soils

Muhanna et al (1998) tested fifteen A-6 soil specimens obtained form North Carolina. Each specimen were prepared at three different water contents, 2.5 percent dry of optimum moisture content, optimum moisture content, and 2.5 percent wet of optimum moisture content and were compacted at standard Proctor energy according to AASHTO T-99. A deviator stress as a percentage of the deviator stress at failure (σ_{df}) was applied

for 10,000 load applications for each specimen. Based on a regression analysis on test results, the following model was proposed to predict resilient strain as a function of moisture content and deviator stress.

$$\sum \varepsilon_p^{*} = SL^{\frac{7}{4}} e^{3} 10^{1.3+2.476\frac{w-w_0}{w_0}} \quad 2.8$$

$$\varepsilon_r^{*} = \left(0.0132 + 0.27 \times \sum \varepsilon_p^{*}\right)\left[1 - \frac{w - w_0}{w_0}\right] \quad 2.9$$

$$M_R = \frac{\sigma_d}{\varepsilon_r^{*}} \quad 2.10$$

Where:

$\sum \varepsilon_p^{*}$ = accumulated plastic deformation at the state of "apparent shakedown" (%);

Apparent Shakedown State = after a large number of repetitions, during which significant permanent deformation accumulates, the plastic strain is no longer significant for an individual cycle of load.

SL = stress level $= \frac{\sigma_d}{\sigma_{df}}$;

σ_d = deviator stress (kPa);

σ_{df} = deviator stress at failure or at 5.0% axial strain (kPa);

e = void ratio (decimal);

w = molding water content (%);

w_0 = optimum moisture content (%);

ε_r^{*} = resilient strain at the state of "apparent shakedown" (%).

It appears that this study tried to develop a predictive model for resilient modulus based on test results obtained from a test method more complicated than the resilient test methods recommended by AASHTO using a different number of load cycles recommended by AASHTO. It is believed that these deviations of the test method used in this study away from the AASHTO recommended test methods make this model less promising.

2.2.5 Jin et al. Model for Coarse-grained Subgrade Soils

Jin and his co-worker (1994) carried out field measurements for in-situ moisture contents and temperatures at two selected sites in Rhode Island. The two sites were selected considering the typical physiography and glacial geology in Rhode Island: an upland till plain and an outwash deposit. Then laboratory resilient modulus tests at simulated field conditions on these two typical soils were performed. The AASHTO test method T274-82 was modified to make test procedures feasible for these two soils in this study. Modifications to AASHTO T-274-82 included specimen preparation procedure, soil-stress analysis, sample conditioning procedure and data-collection procedure. Based on the laboratory data and multiple linear regression analyses, two regression equations with R^2 of 0.82 and 0.72 were proposed for these two typical soils in Rhode Island.

$$\log M_R = 0.8956 + 0.278(\log\theta) - 0.0202(w\%) - 0.0091(T) + 0.0038(\gamma_d) \qquad 2.11$$

$$\log M_R = -3.1895 + 0.535(\log\theta) - 0.00862(w\%) - 0.0084(T) + 0.0021(\gamma_d) \qquad 2.12$$

Where:

M_R = resilient modulus (MPa);

θ = bulk stress (kPa);

w% = percent water content (%);

T = temperature (^{0}C);

γ_d = dry density (kg/m^3).

2.2.6 Rada and Witczak Model for Base/Subbase Materials

Based on 271 test results on granular materials obtained from 10 different research agencies, Rada and Witczak (1981) proposed a predictive model for resilient modulus for granular materials. The model takes into account the effect of the state of stress and percent compaction of a variety of granular materials used as subbase and base courses in the state of Maryland.

$$\log M_R = c_1 + c_2(S) + c_3 PC + c_4 \log(\theta) \qquad 2.13$$

Where:

M_R = resilient modulus (psi);

θ = bulk stress (psi);

S = degree of saturation (%);

PC = percentage compaction relative to modified density (%).

c_i = regression constants are given in the following table.

Table 2.2 Regression Constants (after Rada et al 1981).

Aggregate	c1	c2	c3	c4	R^2
DGA-limestone-1	3.406	-0.005289	0.01194	0.4843	0.79
DGA-limestone-2	-0.3017	-0.005851	0.05054	0.4445	0.6
CR-6-crushed stone	1.0666	-0.003106	0.03556	0.6469	0.81
CR-6-slag	3.2698	-0.003999	0.01663	0.384	0.59
Sand-aggregate blend	4.1888	-0.003312	0.02138	0.6785	0.83
Bank-run gravel	0.9529	-0.01207	0.04117	0.6035	0.84
All data	4.022	-0.006832	0.007055	0.5516	0.61

2.2.7 Santha's Models for Coarse-grained and Fine-grained Subgrade Soils

Resilient modulus tests (AASHTO T 274-82) were performed by Santha (1994) on fourteen cohesive and fifteen granular soils collected from different locations in Georgia. Sieve analysis, Atterberg limits, percent swell and shrinkage, standard Proctor, and California Bearing Ratio tests were also performed for each sample. Multiple-variable linear regression analyses were performed and the following models were proposed.

For Granular Materials:

$$\log(M_R) = \log(k_1 p_a) + k_2 \log\left(\frac{\theta}{p_a}\right) + k_3 \log\left(\frac{\sigma_d}{p_a}\right) \qquad 2.14$$

Where:

$$\log k_1 = 3.479 - 0.07 * MC + 0.24 * MCR + 3.681 * COMP + 0.011 * SLT + 0.006 * CLY - 0.025 * SW - 0.039 * DEN + 0.004 * \frac{SW^2}{CLY} + 0.003 * \frac{DEN^2}{S40}$$

$$k_2 = 6.044 - 0.053 * MOIST - 2.076 * COMP + 0.0053 * SATU - 0.0056 * CLY + 0.0088 * SW - 0.0069 * SH - 0.027 * DEN + 0.012 * CBR + 0.003 * \frac{SW^2}{CLY} - 0.31 * \frac{SW + SH}{CLY}$$

$$k_3 = 3.752 - 0.068 * MC + 0.309 * MCR - 0.006 * SLT + 0.0053 * CLY + 0.026 * SH - 0.033 * DEB - 0.0009 * \frac{SW^2}{CLY} + 0.00004 * \frac{SATU^2}{SH} - 0.0026 * (CBR * SH)$$

For Cohesive Materials:

$$\log(M_R) = \log(k_1 P_a) + k_3 \log\left(\frac{\sigma_d}{P_a}\right) \qquad 2.15$$

Where:

$$\log k_1 = 19.813 - 0.045 * MOIST - 0.131 * MC - 9.171 * COMP + 0.037 * SLT + 0.015\ LL - 0.016\ PI - 0.021 * SW - 0.052 DEN + 0.00001 * (S40 \bullet SATU)$$

$$k_3 = 10.274 - 0.097 * MOIST - 1.06 * MCR - 3.471 * COMP + 0.0088 * S40 - 0.0087 * PI + 0.014 * SH - 0.046 * DEN$$

MC = moisture content (%);

SATU = percent saturation (%);

COMP = percent compaction (%);

MOIST = optimum moisture content (%);

MCR = the ratio of MC and MOIST;

S40 = percent passing U.S. No.40 sieve (%);

CLY = percentage of clay (%);

SLT = percentage of silt (%);

SW = percent swell (%);

SH = percent shrinkage (%);

DEN = maximum dry unit weight (pcf);

CBR = California Bearing Ratio;

LL = liquid limit;

PI = plasticity index.

These two models included too many variables. To predict resilient modulus using these models, all these variables included in the models have to be determined. Laboratory tests to obtain these variables are more time-consuming and complicated than resilient modulus tests, which makes these models less promising.

2.2.8 CRREL Model for Frozen Coarse-Grained and Fine-Grained Materials

Berg and his coworkers (1996) conducted resilient modulus tests on two samples of clay subgrade soils from beneath the Mn/ROAD test site and on different types of base materials under frozen conditions. Specimens of the materials were molded at optimum moisture/density conditions and then saturated. Once saturated, the materials were frozen at three temperatures below freezing with an open drainage system, allowing movement of any additional water required to the freezing front. Based on the test results and regression techniques, a power model including three forms was proposed for frozen materials as the following;

$$M_R = K_1\left(\frac{w_{u-g}}{w_t}\right)^{K_2} \quad 2.16$$

$$M_R = K_1\left(\frac{w_{u-g}}{w_o}\right)^{K_2} \quad 2.17$$

$$M_R = K_1\left(\frac{w_{u-v}}{w_o}\right)^{K_2} \quad 2.18$$

Where:

M_R = resilient modulus,

w_t = total gravimetric water content in samples, including water both in frozen and unfrozen conditions,

w_o = unit unfrozen water content (1.0),

$w_{u\text{-}g}$ = gravimetric unfrozen moisture content only including water in the unfrozen condition, in decimal form,

$w_{u\text{-}v}$ = volumetric unfrozen moisture content, in decimal form,

K_1 and K_2 = regression coefficients.

The regression coefficients in the model for Minnesota clay subgrade soils and base materials are presented in the following table:

Table 2.3 Regression Coefficients of K_1 and K_2 (after Berg et al 1996).

Material	Equation	n	R^2
Clay subgrade 1206	$M_R = 1{,}087\left(w_{u-g} / w_t\right)^{-5.259}$	207	0.319
	$M_R = 1{,}049\left(w_{u-g} / w_o\right)^{-2.344}$	207	0.275
	$M_R = 1{,}052\left(w_{u-v} / w_o\right)^{-2.929}$	207	0.262
Clay subgrade 1232	$M_R = 905\left(w_{u-g} / w_t\right)^{-4.821}$	244	0.378
	$M_R = 846\left(w_{u-g} / w_o\right)^{-2.161}$	244	0.423
	$M_R = 848\left(w_{u-v} / w_o\right)^{-2.633}$	244	0.394
Class 3	$M_R = 5{,}824\left(w_{u-g} / w_t\right)^{-2.026}$	186	0.491
	$M_R = 5{,}488\left(w_{u-g} / w_o\right)^{-1.076}$	210	0.507
	$M_R = 5{,}542\left(w_{u-v} / w_o\right)^{-1.249}$	186	0.467
Class 4	$M_R = 2{,}826\left(w_{u-g} / w_t\right)^{-5.220}$	69	0.835
	$M_R = 1{,}813\left(w_{u-g} / w_o\right)^{-1.733}$	85	0.885
	$M_R = 1{,}652\left(w_{u-v} / w_o\right)^{-2.813}$	69	0.916
Class 5	$M_R = 11{,}320\left(w_{u-g} / w_t\right)^{-2.036}$	28	0.404
	$M_R = 8{,}695\left(w_{u-g} / w_o\right)^{-1.2814}$	28	0.511
	$M_R = 9{,}245\left(w_{u-v} / w_o\right)^{-1.489}$	28	0.432
Class 6	$M_R = 19{,}924\left(w_{u-g} / w_t\right)^{-1.243}$	260	0.372
	$M_R = 19{,}427\left(w_{u-g} / w_o\right)^{-0.795}$	260	0.338
	$M_R = 19{,}505\left(w_{u-v} / w_o\right)^{-0.897}$	260	0.341

2.2.9 Model Proposed to Be Adopted in Future AASHTO Design Guide

Using the published models from the literature (Li and Selig model, Drumm et al model, Jones and Witczak model, Muhanna et al model, Jin et al model, Rada and Witczak model, and Santha model), resilient modulus M_R at a moisture content w (%) or a degree of saturation S (%) can be calculated. Plots of log (M_R/M_{Ropt}) versus differences between the moisture content/saturation and optimum moisture content/degree of saturation at optimum moisture content for all the models show a linear relationship (Witczak, Anderei and Houston, 2002). On this basis, a model was proposed using linear regression analyses shown as the following equations 2.19 and 2.20.

$$\log \frac{M_R}{M_{Ropt}} = k_w \bullet \left(w - w_{opt}\right) \qquad 2.19$$

$$\log \frac{M_R}{M_{Ropt}} = k_s \bullet \left(S - S_{opt}\right) \qquad 2.20$$

Where,

M_R = resilient modulus at moisture content w (%) or degree of saturation S (%);

M_{Ropt} = resilient modulus at maximum dry density and optimum moisture content;

w_{opt} (%) = optimum moisture content;

S_{opt} (%) = degree of saturation at optimum moisture content and maximum dry density;

k_w = gradient of log resilient modulus ratio (log(M_R/M_{Ropt})) with respect to variation in percent moisture content ($w-w_{opt}$); k_w can be obtained by linear regression in semi-log space;

k_s = gradient of log resilient modulus ratio ($\log(M_R/M_{Ropt})$) with respect to variation in degree of saturation ($S\text{-}S_{opt}$) expressed in percentage; k_s can be obtained by linear regression in semi-log space.

However, all the data available in the literature (Li and Selig 1994, Drumm et al 1997, Jones and Witczak 1977, Muhanna et al 1998, Jin et al 1994, Rada and Witczak 1981, and Santha 1994) consisted of only laboratory test results within above and below 30 percent of degree of saturation at maximum dry density and optimum moisture content S_{opr}. Witczak, Anderei and Houston (2002) thought that the linear relationship illustrated in Equations 2-19 and 2-20 was not valid any more when degree of saturation is 30 percent lower than the optimum and the further decrease in moisture content would produce less increase in resilient modulus. To account this in the model, a revised sigmoid model was proposed to be adopted in the further AASHTO Design Guide as shown in Equation 2.21 (Witczak, Anderei and Houston, 2002).

$$\log \frac{M_R}{M_{Ropt}} = a + \frac{b-a}{1+EXP\left(\ln\frac{-b}{a} + k_m \bullet \left(S - S_{opt}\right)\right)} \qquad 2.21$$

where,

M_{Ropt} = resilient modulus at maximum dry density and optimum moisture content;

a = Minimum of $\log(M_R/M_{Ropt})$, regression parameter;

b = Maximum of $\log(M_R/M_{Ropt})$, regression parameter;

k_m = Regression parameter,

$(S\text{-}S_{opt})$ = Variation in degree of saturation expressed in decimal.

Maximum resilient modulus ratios (M_R/M_{Ropt}) of 2.5 and 2 were assumed for fine-grained and coarse-grained materials, respectively (Witczak, Anderei and Houston, 2002). A regression analysis was performed using the available literature data and regression parameters a and k_m were obtained shown in Table 2.4.

Table 2.4 Coefficients obtained from regression analysis (200X design guide).

Parameter	Coarse-Grained Materials	Fine-Grained Materials	Comments
a	-0.3123	-0.5934	Regression parameter
b	0.3	0.4	Conservatively assumed, corresponding to modulus ratios of 2 and 2.5, respectively
k_m	6.8157	6.1324	Regression parameter

To use any of the proposed models that predict resilient modulus, based at least in part, on moisture content, the moisture content of the soil has to be known. To predict the variation of the moisture content with time, an Enhanced Integrated Climatic Model (EICM) was proposed to be adopted by the further AASHTO Design Guide. The EICM is a one-dimensional coupled heat and moisture flow program developed for the Federal Highway Administration (FHWA). The EICM has three major components (200x AASHTO Design Guide):

1. The infiltration and Drainage Model (ID Model) developed at the Texas A&M University;
2. The climatic-Materials-Structural Model (CMS Model) developed at the University of Illinois; and

3. The CRREL Frost Heave and Thaw Settlement Model (CRREL Model) developed at the United States Army Cold Regions Research and Engineering Laboratory (CRREL).

Inputs for the EICM consist of climatic information, material properties and initial moisture content and temperature. Practically, climatic information obtained from a nearby national weather station could be used as input to this model, which makes the prediction of the moisture content in a pavement system very easy and convenient. However, climatic patterns vary from region to region, which makes it difficult to develop standard models that are equally applicable for all regions. Ahmed and his coworkers (2005) evaluated the EICM using data from the two LTPP test sites (Sites 5E and 9C) in New Jersey. The field measurements of temperatures and moisture contents in pavement systems of the two sites and EICM predicted temperatures and moisture contents are shown in Table 2.5 and 2.6 (Ahmed et al 2005). From Tables 2.5 and 2.6, a wide discrepancy was observed between predicted and measured temperatures and moisture contents. They therefore concluded that the EICM was not suitable and site-specific models needed to be developed for New Jersey.

Table 2.5 Comparison of measured and predicted temperature data (Ahmed, 2005).

		LTPP Site 5E				LTPP Site 9C			
		2002				2002			
		April	July	Sept.	Dec.	April	July	Sept.	Dec.
AC	Field Data	17.5	30.2	27.9	0.9	17.8	29.3	27.1	-2
	EICM	20.8	33.5	30.1	-1.3	20.9	33.9	30	1.1
Base	Field Data	14.6	28.8	26.6	3.3	14.6	28.7	26.4	3.3
	EICM	18.4	32	27.4	-1	18.4	31.8	27.1	-1.1
Subbase	Field Data	14.1	28.8	26.5	5	13.3	28.1	26	5.8
	EICM	18.5	32.4	27.7	-1	18.6	32.1	27.8	-1
Subgrade	Field Data	12.2	26.4	25.4	8.8	11.6	25.4	24.8	9.5
	EICM	19.4	31.7	28.2	-1	20.5	31.8	29	-2.1
		2003				2003			
AC	Field Data	8.9	24.8	23.9	5.5	18.9	25	23.7	1.3
	EICM	11.6	31.4	25.7	4.8	24.4	31.2	25.9	0.7
Base	Field Data	6.9	27.8	24.2	5.4	15.6	27.8	24.1	4.3
	EICM	8.9	30.5	23.9	1.9	22.2	30	24	0
Subbase	Field Data	7.6	27.8	24.7	6.3	14.5	26.9	24.4	6.9
	EICM	9.6	30	24.5	2.4	23.4	28.8	24.9	0.4
Subgrade	Field Data	9.2	24.6	24.2	9.7	12.5	23.4	23.5	10.8
	EICM	10.5	25.4	24.5	4.4	24.3	24.2	25	-0.2

Table 2.6 Comparison of measured and predicted moisture contents (Ahmed, 2005).

		LTPP Site 5E				LTPP Site 9C			
		2002				2002			
		April	July	Sept.	Dec.	April	July	Sept.	Dec.
Base	Field Data	41	41	34.8	-	18	22.9	18	34.8
	EICM	18.3	15.9	16.2	3.1	18.7	16	18.1	9.6
Subbase	Field Data	24.2	33.7	20.4	29.4	38	34.8	35.9	34.8
	EICM	21.5	18.8	19.1	26.1	24.9	21.6	24.1	12.6
Subgrade	Field Data	40	39.1	38	38.3	48	48.7	49.5	48.7
	EICM	33.3	30.2	30.8	12.5	35.6	31.9	34.8	18.3
		2003				2003			
Base	Field Data	45.5	43.8	43.8	45.5	29	31.4	31.4	22.9
	EICM	19.5	19.6	16.4	19.2	18.5	19.6	18.7	18.9
Subbase	Field Data	29	31.4	29	43.8	46.4	42.1	42.9	38
	EICM	22.8	22.9	19.4	22.5	24.7	25.9	24.8	25.1
Subgrade	Field Data	54.8	50	53.3	29	48.7	49.5	50.3	48
	EICM	34.7	34.8	31	34.3	35.4	36.6	35.6	35.9

All the models proposed to predict the resilient modulus under various loading and environmental conditions require moisture content as a primary input parameter. Although the introduction of the EICM makes moisture content predictions easy and

convenient, the EICM may not be suitable for all regions across the United State (Ahmed et al 2005). It is very clear that a sound understanding of moisture migration through pavement systems as well as better predictions of the variation of the moisture content with seasonal and environmental factors are the important factors in correctly predicting material strength properties and in implementing the current mechanistic-empirical flexible pavement design method.

To get an understanding of moisture migration through pavement systems and to develop a model that might predict moisture migration in pavement systems, it is critical to actually measure the moisture content in pavement systems and the surrounding environmental factors continuously for a relatively long period. The traditional method of measuring soil moisture content is oven-dry gravimetric method described in AASHTO T-265 “Laboratory Determination of Moisture Content of Soils”. This method is considered to be the reference standard and any other measurement technique must be calibrated to this reference standard. The problems associated with utilizing this method are: it can only be done in laboratory, it requires a sample, and it takes at least 12 hours for a soil sample to dry in an oven. These factors make the “oven-dry” method unsuitable for long term in-situ measurements. Currently, the Time Domain Reflectometry (TDR) technique is widely used for long-term pavement moisture measurements. Since the TDR technique is relatively new for this application, it is addressed in detail in the following section.

2.3 Time Domain Reflectometry Technology

2.3.1 Introduction

Time Domain Reflectometry (TDR) is a remote sensing electrical measurement technique that has been used for many years to determine the spatial location and nature of various objects (Andrews, 1994). An early form of TDR is radar. Radar equipment sends out electromagnetic waves in all directions. The waves are reflected back if they meet any object. By measuring (i) the time interval between launching the electromagnetic waves and detection of the reflections, (ii) the amplitude of the reflections and (iii) the direction of the reflections and combining this information with knowledge of the velocity of the waves in air, it is possible to determine position and size of the subject that created the reflections (Nissen et al. 1994).

During the last two decades, researchers applied this technology to the measurement of moisture content. A waveguide or probe can be embedded in soil. The signal propagation velocity in the waveguide or probe depends on the dielectric constant of the soil surrounding the waveguide or probe. Generally a soil comprises of soil particles, air and water. The dielectric constant of soil particles ranges from 4 to 7, the dielectric constants of air and water are about 1 and 81, respectively (Richard et al, 1998). The dielectric constant of the soil is mainly dependent on moisture content. The high dependency of dielectric constant of the soils on moisture content makes TDR a good method to measure moisture content in soils. Some commercially available TDR moisture probes are shown in Figures 2.3 and 2.4:

Figure 2.3 CS 616 moisture probe (Campbell Scientific, Inc.).

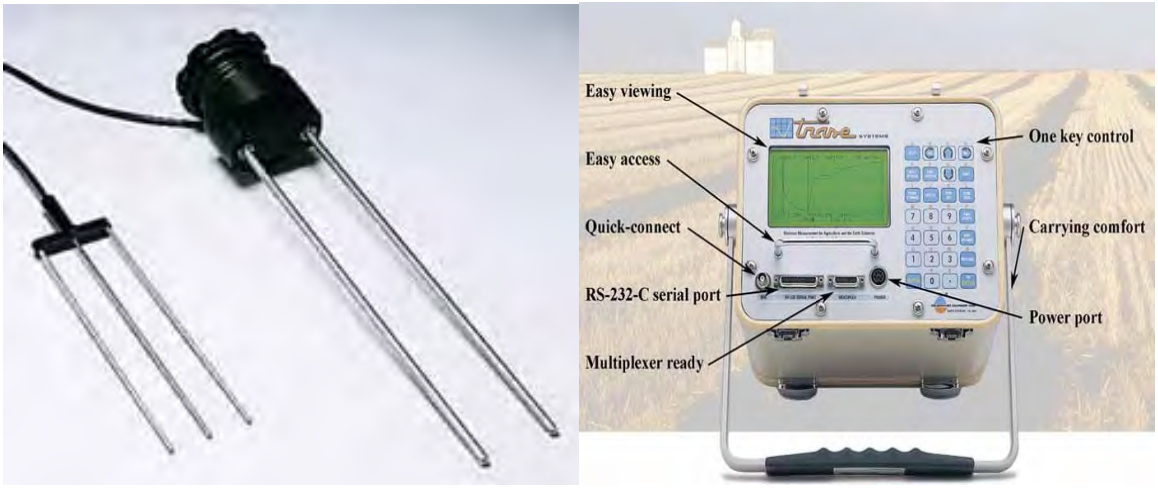

Figure 2.4 TDR moisture probes (ICT International, Trase System 1).

Compared with other methods of determining moisture in soils, the TDR method has many superior features for measuring water contents in field.

1. Accuracy to within 1 or 2 % volumetric water content;
2. Probes are simple and easy to install in field;
3. Calibration requirements are minimal. In many cases a soil-specific calibration is not needed;
4. Measurements can be easily made remotely and the process can be automated;

5. There is no radiation hazard.
6. There is no requirement for a soil sample.

Because of these advantages, TDR technology has recently been widely used in measuring moisture contents of pavement systems. The Department of Transportation, Federal Highway Administration (1994) developed a TDR equipment and guideline used for measuring water content in pavement systems in the Long Term Pavement Performance program (LTPP). Many researchers (Hossam et al. 1997; Vincent et al. 2000, Andrew 2003; Watson et al. 2000; Brian et al. 2000) have successfully used the TDR technology in measuring moisture contents for long-term pavement monitoring.

2.3.2 History of application of TDR on measuring moisture content

The measurement of soil moisture content using coaxial transmission lines and TDR principles was initiated by Topp et al in 1980. Topp et al designed a coaxial soil container of 5 cm inside diameter as shown in Figure 2.5. Lengths of the soil in the coaxial container were either 1.0 m or 0.33 m, depending on the electrical conductivity of the soil under test. Water was added or removed from the soil through 1 cm diameter porous ceramic disks spaced 5 cm apart on the sides of the coaxial sample holder.

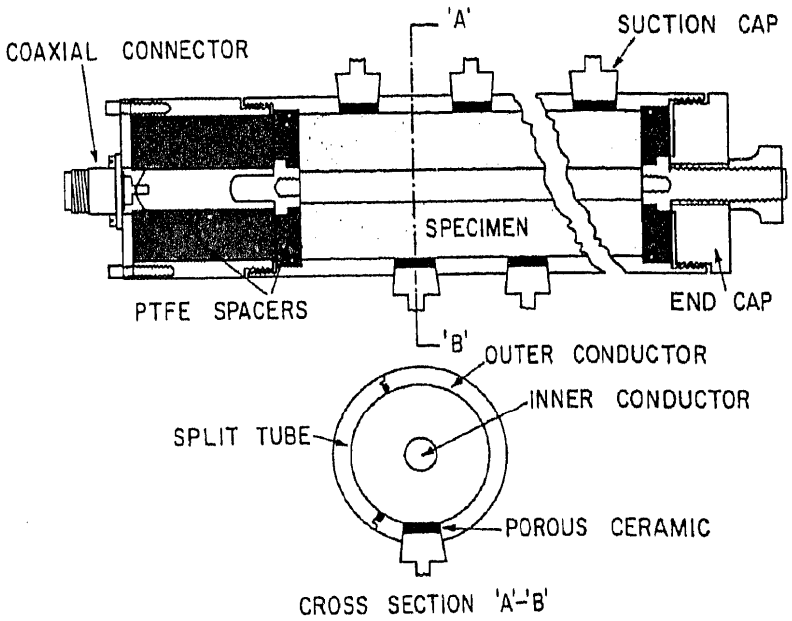

Figure 2.5 Coaxial soil container (after Topp et al., 1980).

Using this coaxial container, eighteen different experiments were performed to investigate the influence of texture, bulk density, temperature, salinity, and hysteresis on the relationship between the dielectric constant and the water content. Finally, Topp et al (1980) proposed a "universal" third-order polynomial equation to predict volumetric moisture content as shown in Equation 2.22.

$$\theta_v = -5.3\times10^{-2} + 2.92\times10^{-2} K_a - 5.5\times10^{-4} K_a^{\,2} + 4.3\times10^{-6} K_a^{\,3} \qquad 2.22$$

Where:

θ_v = the volumetric water content,

K_a = the apparent dielectric constant, generally measured from a cable tester.

Topp's equation was thought to be universal for all soil types for several years after it was first proposed. Many researchers (Patterson, et al. 1981; Dalton, et al. 1986; Drungil et al. 1989; Topp et al. 1984; Topp et al. 1985; Zegelin 1989) applied this equation successfully and verified that Topp equation was quite broadly applicable.

Patterson et al. (1981) applied the equation to measure the unfrozen water content of partially frozen soils. Topp et al. (1984, 1985) verified the equation in clay and sandy loam soils. Drungil et al. (1989) verified that the equation was valid and yielded accurate results in coarse textured soils. However, recent studies (Roth et al. 1990; Dirksen et al. 1993; Zegelin et al. 1992; Topp et al. 1994; Baran et al. 1994) have all shown that this equation does not provide sufficient accuracy for highly plastic clays, organic soils or soils having very low or very high densities.

2.3.3 Empirical and dielectric mixing models

Two basic approaches have been used to establish the relationship between the apparent dielectric constant and the volumetric water constant (or gravimetric water content). One is the empirical model and the other one is the dielectric mixing model. The empirical model simply fits the measured data using regression analysese The dielectric mixing model uses dielectric constants and volume fractions for each of the soil components (soil particles, water, and air) to derive a relationship describing the composite dielectric constant.

2.3.3.1 Empirical models

Since Topp et al (1980) initiated the application of TDR on moisture content measurements and proposed the regression equation, many studies have been carried out to investigate relationships between the combined dialectic constant and moisture content on different soil types using the regression technique. Table 2.7 lists some of the empirical models found in the literature.

Table 2.7 Lists of calibration equations.

Author	Calibration Equation
Ledieu et al. 1986	$\theta = 0.1138\sqrt{K_a} - 0.1758$ $\theta = 0.1138\sqrt{K_a} - 0.0338\rho_d - 0.153$
Dasberg and Hopmans 1992	$\theta = \left(-751 + 424K_a - 18.5K_a^{\,2} + 0.38K_a^{\,3}\right)\times 10^{-4}$ *For the sandy loam* $\theta = \left(-1090 + 581K_a - 22.7K_a^{\,2} + 0.32K_a^{\,3}\right)\times 10^{-4}$ *For the clay loam*
Roth et al. 1992	$\theta = \left(-728 + 448K_a - 19.5K_a^{\,2} + 0.36K_a^{\,3}\right)\times 10^{-4}$ *For the* min *eral soils* $\theta = \left(-233 + 285K_a - 4.3K_a^{\,2} + 0.03K_a^{\,3}\right)\times 10^{-4}$ *For the organic soils*
Siddiqui and Drnevich 1995	$w = \frac{1}{b}\left[\frac{\rho_w}{\rho_d}\sqrt{K_a} - a\right]$ $a \cong 1, b \cong 8 to 9$

Where:

θ = the volumetric water content;

K_a = the apparent dielectric constant (measured combined dielectric constant);

w = the gravimetric water content;

ρ_d = dry density of soil;

ρ_w = density of water;

a, b = soil dependent calibration constants, a is near 1 and b is near 8 to 9.

2.3.3.2 Mixing models

Instead of simple regression analyses, a great deal of effort has been devoted to developing more theoretical relationships between the dielectric constants of individual soil components and the moisture content. These models are called mixing models (De Loor, 1990; Dirksen et al. 1993; Dobson et al. 1985; Roth et al. 1992). In the mixing

model, the soil is considered a mixture of three or four phases: water (free water and bound water), soil and air. Two main approaches were developed. The one is called the semi-empirical mixing model. While the other one is called the theoretical model and uses Maxwell's equation for electromagnetic wave propagation to determine individual dielectric constants.

The semi-empirical mixing model derives the dielectric constant of soil mixture based on the volume fraction of water, air and soil particles in the mixture. The model is expressed in Equation 2.23 (Birchak 1974; Roth et al. 1990):

$$K^{\alpha} = (1-\phi)K_s{}^{\alpha} + \theta K_w{}^{\alpha} + (\phi-\theta)K_g{}^{\alpha} \qquad 2.23$$

Where:

K = dielectric constant of soil mixtures;

K_s = dielectric constant of soil particles;

K_w = dielectric constant of water;

K_g = dielectric constant of air;

ϕ = porosity of soil;

θ = volumetric water content;

α = geometric factor that depends upon the spatial arrangement of the mixture and its orientation in the electric field (depending on soil types and excitation frequencies used,)in most case $\alpha = 0.5$,.

The theoretical relationship, based on Maxwell's equation, was first proposed by Birchak et al. (1974). This model took the bound water into consideration. It described a homogeneous mixture of one or more substances randomly distributed in a medium with different dielectric constants using Equation 2.24.

$$K = \frac{3K_s + 2(\theta - \theta_{bw})(K_{fw} - K_s) + 2\theta_{bw}(K_{bw} - K_s) + 2(\phi - \theta)(K_g - K_s)}{3 + (\theta - \theta_{bw})(K_s / K_{fw} - 1) + \theta_{bw}(K - s / K_{bw} - 1) + (\phi - \theta)(K_s / K_g - 1)} \quad 2.24$$

Where:

K_{bw}, θ_{bw} = dielectric constant and volume fraction of bound water;

K_{fw}, θ_{fw} = dielectric constant and volume fraction of free water;

and the other constants are as defined previously.

Bohl et al. (1994) found that the theoretical model yielded the most accurate predictions of water contents for both mineral soils and organic soils. The optimal value for the volume fraction of the bound water is 0.03 in mineral soils and 0.06 in organic soils, respectively. In all cases, the dielectric constant is 3.2 for the bound water and 80.36 for the free water. The dielectric constant of soil particles was assumed as 3.9 in mineral soils and as 5 in organic soils.

2.3.4 Theory and Instrumentation of TDR

A typical TDR instrument to measure moisture includes a pulse generator, a probe and an oscilloscope and is shown in Figure 2.6

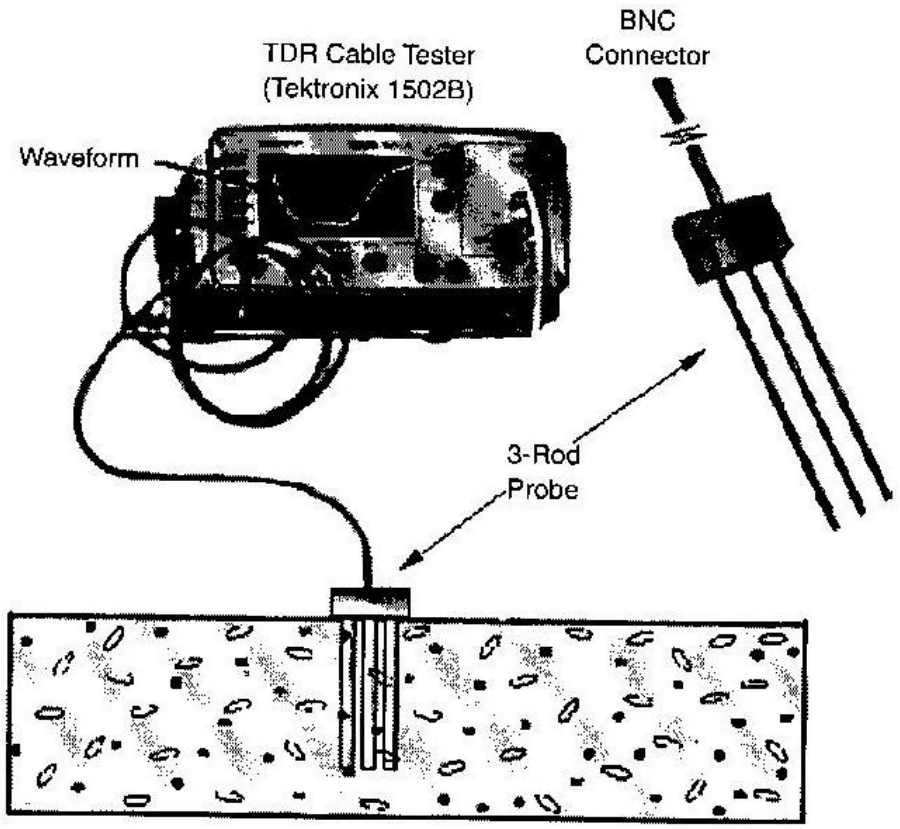

Figure 2.6 A typical TDR moisture content measuring setup. (after Jones et al 2001).

As shown in Figure 2.6, a Tektronix 1502B cable tester generates and sends a step pulse through a transmission line to a three-rod moisture probe. When the signal reaches the moisture probe, a portion of the signal is reflected back to the cable tester due to a rapid change in dielectric properties of the transmission cable and the probe. The remaining signal keeps going along the probe until it meets the end of the probe. When it meets the end of the probe, another reflection of the signal occurs. These two reflections cause two voltage changes on the cable tester screen (TDR waveform). A typical TDR waveform is shown in Figure 2.7.

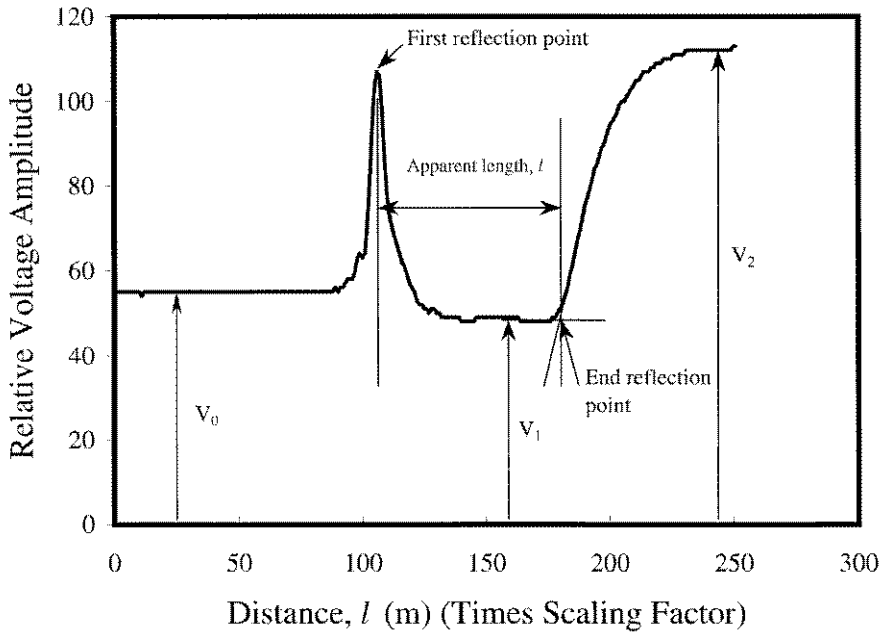

Figure 2.7 A typical TDR waveform (after Siddiqui et al 2000).

The time between "first reflection point" and "end reflection point" as shown in Figure 2.7, is the time (t) required for the signal to travel twice length (L) of the probe embedded in a soil. The velocity (v) of signal traveling along the probe embedded in soil can be calculated using Equation 2.25.

$$v = \frac{2L}{t} \qquad 2.25$$

Where:

v = velocity of the signal travel through the probe embedded in soil;

L = physical length of the probe;

t = time different between the two voltage reflections.

The velocity at which an electromagnetic wave can travel through a media depends on the dielectric constant of the media as indicated in Equation 2.26.

$$v = \frac{c}{\sqrt{K_a}} \qquad 2.26$$

Where:

c = velocity of an electromagnetic wave in vacuum (3×10^8 m/s);

K_α = apparent dielectric constant of the media.

Rearranging Equation 2.26, Equation 2.27 can be obtained.

$$K_a = \left(\frac{c}{v}\right)^2 \qquad 2.27$$

The apparent dielectric constants of some materials are listed in the table 2.8

Table 2.8 Apparent Dielectric constant of some materials (after Richard et al. 1998).

Material	**Dielectric Constant**
Vacuum/Air	1
Water	81
Sand (dry)	4-6
Sand (wet)	30
Silt (wet)	10
Clay (wet)	8-12
Ice (fresh)	4
Granite (dry)	5
Limestone (dry)	7-9
Portland Cement Concrete	6-11
Roller-Compacted Concrete	5-7
Asphaltic Concrete	5-7

2.3.5 Factors effecting the TDR measurement

2.3.5.1 Bound water

Water in soils exists in two forms. One is free water and the other one is bound water. The free water is not rotationally hindered by forces acting on it from soil particle surfaces and can move freely in soils. However, the bound water, which exists on and within the near vicinity of soil particle surfaces, is bound to soil particle surfaces due to interfacial forces. The binding constrains movement of the bound water and hinders its rotation. Consequently, bound water's ability to follow the alternating electric field is

also hindered, and its dielectric property is more closely related to that of soil particles rather than water. High surface-area porous media (e.g. clays, peat, some forest soils) bind a substantial fraction of the water phase, which results in reduced bulk dielectric constant measurements relative to low surface-area materials (e.g. sandy soils) when compared at similar water contents (Jones et al 2001).

2.3.5.2 Temperature

Temperature can effect the TDR measurements in two ways. As temperature increases, the thickness of the layer of the bound water decreases, which results in an increased TDR-measured water content. This effect will be relatively substantial for soils with large surface area (e.g. clays, peat, some forest soils). Wraith (1999) developed a model for the temperature-dependent thickness of the bound water phase. On the other hand, as temperature increases, the dielectric constant of the pure water decreases which results in the decreased TDR-measured water content. The dielectric constant of pure water changes with temperature as shown in Table 2.9. Many researchers (Topp et al. 1980, Halbertsma et al. 1995, Verstricht et al. 1994, Alvenas et al. 1995, Van Loon et al. 1995) had investigated the effect of temperature on TDR measurements. But there has not been a consensus. It seems to be a function of the soil type and water content itself.

Table 2.9 Dielectric constant of water at different temperature.

Temperature (^{o}C)	**Dielectric constant of water**
0	88
20	80
25	78.5
60	66

For soils with a large specific surface area (fine-grained), both of the above-mentioned effects can be substantial in opposite directions and so the composite effects can be neglected. For soils with small specific surface area (coarse-grained), the effect of bound water can be neglected and the effect of temperature dependence of dielectric constant of water will be significant and governs. This conclusion has been verified by some researchers (Pepin et al. 1995, Halbertsma et al. 1995). Tests conducted by these researchers showed that the dielectric constant of fine-grained soils varies very little within the range of temperatures encountered in geotechnical problems (5-55 ^{0}C) and thus no temperature correction is required. However, for coarse-grained soils the sensitivity to temperature is more significant and a temperature correction is required. The data obtained from tests performed by Pepin et al. (1995) suggest that a correction factor ranging between 0.0015 $^{0}C^{-1}$ and 0.0025 $^{0}C^{-1}$ is adequate.

2.3.5.3 Effect of air gap

Often the use of a coaxial or a multiple-rod probe requires inserting rods into the soil. During insertion, a rod can sway laterally in the soil, producing an air gap around the rod. Because the dielectric constant of air and soil are significantly different, the air gap can result in substantial reductions in the TDR-measured water content. Siddiqui et al. (2000) proved that the presence of a very thin air gap could reduce the measured dielectric constant significantly.

2.3.5.4 Effect of density

Many researchers (Malicki et al. 1994, Logsdon 1994, Siddiqui et al 1996), to mention a few, have investigated the effect of density on TDR moisture content measurements. Malicki et al. (1994) studied 894 quadruplets of K_a, θ_v, ρ_b, and ρ_d and developed a empirical relationship between the dielectric constant and moisture content including the bulk density of the soil as a parameter as shown in Equation 2.28.

$$\theta_v = [K_a - 0.819 - 0.168\rho_b^{\,2}]/[7.17 + 1.18\rho_b] \qquad 2.28$$

Siddiqui and Drnevich (1996) found that for the two soil samples with the same moisture content, the square root of the dielectric constant has a linear relationship with the density of the soil as shown in Equation 2.29.

$$\frac{\sqrt{K_{a1}}}{\sqrt{K_{a2}}} = \frac{\rho_{d1}}{\rho_{d2}} \qquad 2.29$$

2.3.5.5 Signal attenuation

In electrically conductive soils such as dense compacted clays, sand-bentonite mixtures, and mine rock, the signal attenuation can be so serious that the signal strength reduces to zero before it reaches the end of the probe rods and the second reflection cannot occur. This makes the TDR analysis for water content impossible. In such a case, if no action is taken to reduce attenuation, the physical length of the rods will have to be relatively short in order to get the second reflection, which will however reduce the accuracy of travel time measurement.

Some studies (Ferre et al. 1996; Baran 1994; van Loon et al. 1997, Suwansawat 1997) have been carried out specifically to investigate signal attenuation. It was found

that a non-conductive coating is a good way to prevent electrical loss to the medium. Baran (1994) used a three-rod TDR probe in Winton Sandstone, a highly conductive fine grained material. Initially he found that the second reflected signal could not be detected due to the high conductivity of the surrounding soil. A coating of 1 mm thick epoxy resin was then used on the center probe, which successfully overcome the signal attenuation. Coatings that have been used successfully include vinyl insulation, acrylic paint, and epoxy. Among them the epoxy coating is the most effective and durable (Suwansawat 1997). In addition, Suwansawat (1997) showed that the calibration curves for a wide variety of compacted clays fell on a single curve when coated probes were used, whereas a unique curve existed for each clay when uncoated probes were used.

2.3.5.6 TDR probe *configurations*

TDR probe configurations include the number of rods, the length of rods, the diameter of rods, and the spacing of rods.

2.3.5.6.1 Number of rods

The TDR technology was first developed in coaxial cables. The parallel-rod probes developed later are intended to approximate coaxial cables in that the inner rod acts as the inner conductor of coaxial cables and the outer rods act as the outer conductor. So the more outer rods present, the better the simulation of coaxial cables. However, more rods results in more installation difficulty and more soil disturbance.

When an AC signal travels along a coaxial transmission line, the center conductor carries the signal, and the shield serves as ground. A signal propagating through a line

with this configuration is typically referred to as “unbalanced” with respect to ground. If a transmission line consists of two parallel conductors carrying signals equal in magnitude but opposite in sign, this configuration is referred to as “balanced” with respect to ground (Suwaansawat, 1997). For two-rod probes, to reduce unwanted noise and signal loss, impedance-matching transformer (balun) is generally required between the coaxial transmission line and parallel rods to convert an electrical field from unbalanced to balanced, which tends to distort the shape of the signal. The three-rod probe closely approximates a coaxial condition, eliminates the use of impedance-matching transformer, and also provides a minimum of ground disturbance when inserted. (Zegelin et al 1989). These advantages make the three-rod probe most widely used. However, recent studies (Suwansawat and Benson 1998), have illustrated that the two-rod probe produces a waveform with more distinct changes in slope than probes with a larger number of rods, which makes the computerized automation of results analysis easier. For a practical perspective, both two-rod and three-rod probes are equally acceptable when calibrated properly (Benson and Bosscher, 1999).

2.3.5.6.2 Length of rods

Basically, the length of rods should be such that a detectable reflection from the end of the probe occurs (Siddiqui et al 1996). The accuracy of the time measurement sets a lower limit on the rod length. If the probes are too short, the travel time determination is less accurate. The length of the rods must be greater than 10 cm for optimum results (Hilhorst, et al. 1994). The maximum length of the rods is set by the maximum allowable attenuation of the reflected signal. If the probes are too long, the signal attenuation will

be a problem and the signal will lose all of its strength before it reaches the end of the rods. Experimental results (Siddiqui et al. 2000) showed that a maximum length of about 40 in could be used for relatively less conductive soils (e.g., sands), and 8 in could be used for more conductive soils (e.g. bentonite with high water content).

2.3.5.6.3 Spacing of rods

The spacing of rods may not be an influencing parameter if the rod spacing to rod diameter ratio remains constant. Two different probes having the same ratio of rod diameter to rod spacing have been shown to produce the same signal as far as the shape of the waveform is concerned. (Siddiqui et al. 1996) Topp and David (1985) stated that parallel transmission lines having rods with a center-to-center spacing of about 5 cm could be used to obtain reasonable resolution. However, the spacing of rods can affect the sampled volume of a soil. Bake and Lascano (1989) did investigation about sampling volume and found that soil moisture measured by the two-rod TDR is largely confined to a quasi-rectangular area of approximately 1000 mm^2 surrounding the probe.

2.3.5.6.4 Diameter of rods

The diameter of rods should match the spacing between rods. The ratio between the rod diameter and the rod spacing should be not less than 0.1 (Knight, 1992). The diameter of rods should not be too large comparing with the spacing. Otherwise, the probe will compact the soil between the rods significantly when inserted into soils. In addition, for a soil with large particles, the diameter of rods should be large enough to provide good contact between probe and soil.

2.4 Hydraulic Conductivity of Pavement

2.4.1 Introduction

Hydraulic conductivity is a measure of the capability of a medium to transmit water and is often used interchangeable with the coefficient of permeability. The hydraulic conductivity of pavement materials is a very important material property needed to investigate migration of water in pavement systems. The hydraulic conductivity can be measured either by laboratory tests or field tests. Both laboratory and field hydraulic conductivity tests are based on the Darcy's law described in Equation 2.30.

$$q = kiA \tag{2.30}$$

where:

q = rate of discharge

k = hydraulic conductivity (normally called permeability)

i = hydraulic gradient

A = cross-section area

Currently there are two widely used approaches to measure the hydraulic conductivity of a material using Darcy's law: a constant head test and a falling head test.

Constant head hydraulic conductivity tests are illustrated in Figure 2.8. As shown in Figure 2.8, the hydraulic gradient i is constant.

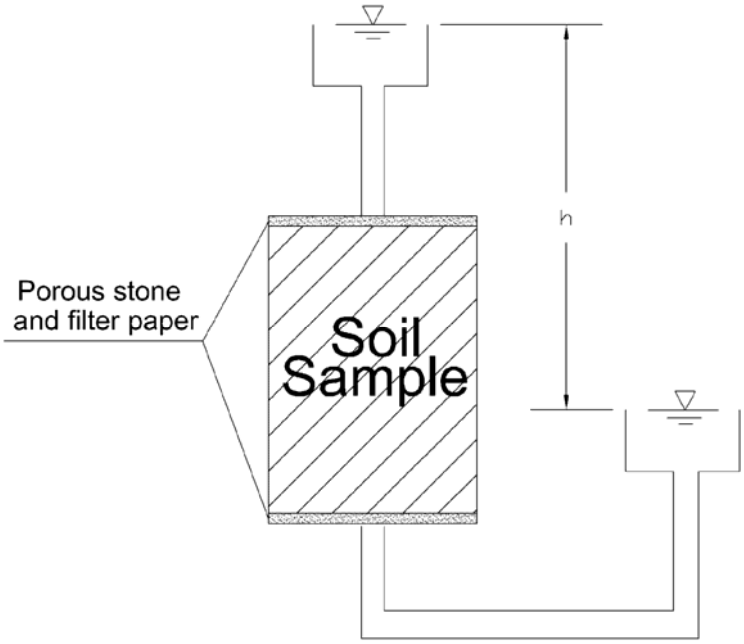

Figure 2.8 Constant-head hydraulic conductivity test.

For constant head hydraulic conductivity tests, hydraulic conductivity can be calculated using equation 2.31:

$$k = \frac{Q}{iA} = \frac{QL}{hAt} \qquad 2.31$$

where:

Q = total discharge volume

L = length of specimen

h = constant water head on specimen

A = cross-sectional area of specimen

t = time during which the total discharge is collected.

Falling head hydraulic conductivity tests are illustrated in Figure2.9. As shown in Figure 2.9, the gradient changes with time.

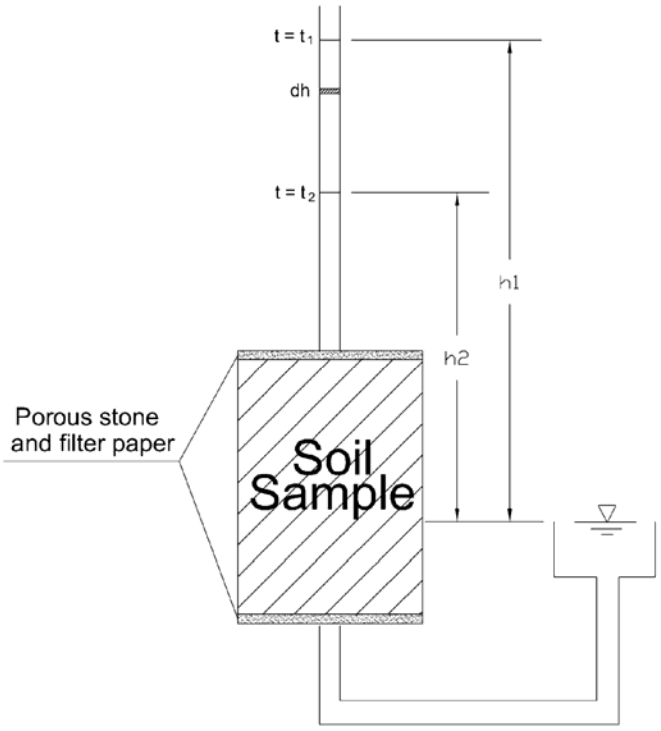

Figure 2.9 Falling-head hydraulic conductivity tests.

For falling-head hydraulic conductivity tests, the hydraulic conductivity can be calculated using Equation 2.32:

$$k = \frac{aL}{At} Ln\left(\frac{h_1}{h_2}\right) \qquad 2.32$$

where:

a = area of stand pipe

L = length of sample

A = cross-sectional area of sample

t = time over which head is allowed to fall

h_1 = water head at beginning of test

h_2 = water head at end of test

2.4.2 Lab testing of hydraulic conductivity

Hydraulic conductivity of pavement is an important parameter to investigate water migration through pavement systems. With the increase of hydraulic conductivity, more water can infiltrate into pavement systems, which could result in many water-related problems such as reduced subgrade strength, asphalt stripping, or pumping of fines, all of which reduce the life of a pavement. From 1987 through 1993, the Strategic Highway Research Program (SHRP) developed a new way to design asphalt concrete called Superpave. With the implementation of Superpave, the aggregate blends used in hot-mix asphalt concrete are typically more coarse-graded than mixes of the Marshall design era. There is a possibility that the hydraulic conductivity of these coarse-graded mixes will increase, which will allow more water or air to infiltrate into pavement systems and could result in many problems associated with water.

Since the implementation of Superpave, many efforts have been devoted to the investigation of hydraulic conductivity of Superpave (Maupin, 2000; Prowell, et al. 2002; Mallick, et al. 2001; Cooley, et al. 2000). Due to a number of problems associated with Superpave designed mixtures in Florida, the Florida Department of Transportation (FDOT) developed a laboratory hydraulic conductivity device and a standard test method for the determination of asphalt hydraulic conductivity (FDOT, 2000). The Florida permeameter is considered to be a falling head hydraulic conductivity test apparatus, as shown in Figure 2.10. The water contained in a graduated cylinder is allowed to flow through a saturated asphalt specimen and the interval of time taken to reach a defined change in head is recorded. The hydraulic conductivity is then determined based on Darcy's law. This device and test method has been widely adopted by many researchers

(Maupin, 2000; Prowell, et al. 2002; Mallick, et al. 2001; Cooley, et al. 2000). American Society for Testing and Materials (ASTM) also adopted this device and test method as a standard test method as ASTM PS 129-01 “Standard Provisional Test Method for Measurement of Permeability of Bituminous Paving Mixtures Using a Flexible Wall Permeameter”.

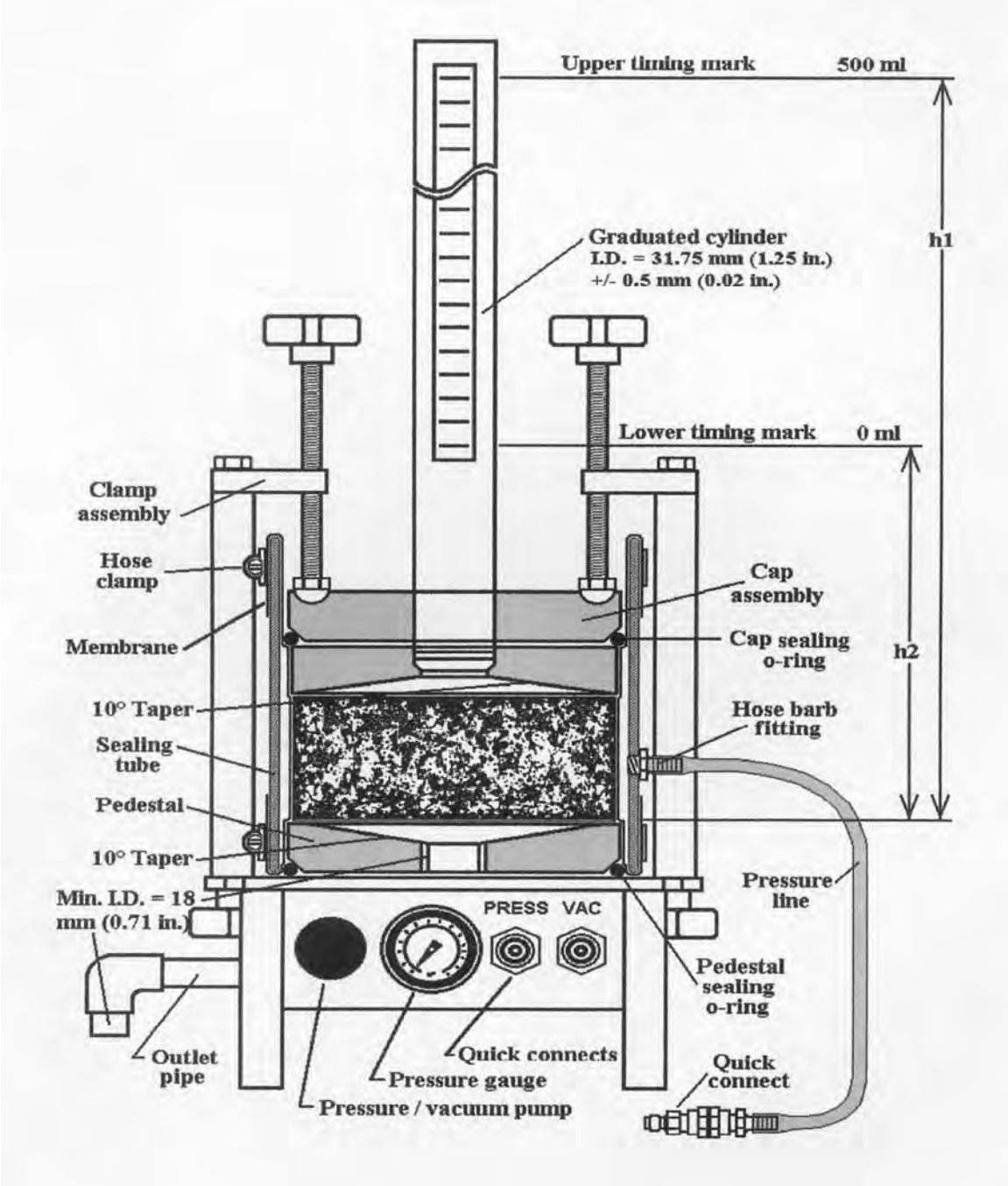

Figure 2.10 Laboratory permeameter (after FDOT, 2000, ASTM PS 129-01).

It is believed that the water flow is forced to be one dimensional in this test, which makes Darcy's law applicable. However, a study conducted by Hall et al. (2001) showed that the void pathway is convoluted rather than straight and vertical as originally believed. In this study, dry air was blown into one cross-sectional face of a cylindrical

specimen. A concentrated soap solution was brushed on the surface of the specimen, forming bubbles at openings through which air was expelled. It was found there were far more void openings in perimeter surfaces of the specimen than in cross-sectional surfaces. Hall's study indicates that horizontal hydraulic conductivity of asphalt concrete may be much greater than vertical hydraulic conductivity and water may migrate through asphalt concrete faster horizontally than vertically.

2.4.3 Field hydraulic conductivity testing

Because laboratory tests are essentially destructive tests and cores must be cut from the roadway, field hydraulic conductivity tests are often necessary to get the in-situ hydraulic conductivity without cutting cores from the roadway. In addition, field hydraulic conductivity tests better account for macro structures in the pavement than laboratory tests.

However, all the filed hydraulic conductivity tests essentially measure the infiltration rate instead of hydraulic conductivity of a soil. The main reason is that it is almost impossible to control water flow only in the vertical direction in field tests. Water will actually travel both vertically and horizontally. However, the term "hydraulic conductivity" is widely used instead of "infiltration rate" by researchers.

Sealed, double-ring infiltrometers (SDRI), described in ASTM D 5093 Test Method for Field Measurement of Infiltration Rate Using a Double-Ring Infiltrometer with a Sealed-Inner Ring, can be used in the field to measure the infiltration rate for natural soil deposits, recompacted soil layers, and amended soils such as soil bentonite and soil lime mixtures. Neupane et al. (2003) employed a SDRI to measure the hydraulic

conductivity for hydraulic asphalt concrete. A new flow volume measurement device called a constant head board (CHB) was developed and employed to replace the commonly used flexible bag to accomplish measurement of very small flow increments. This improvement enabled field hydraulic conductivity measurements as low as 10^{-11} m/s to be accurately estimated in a matter of a day or two. It should be noted that SDRIs are intended to measure infiltration rates in the range of 1×10^{-7} to 1×10^{-10} m/s. For materials with infiltration rates greater than 1×10^{-7} m/s, ASTM D 3385, Standard Test Method for Infiltration Rate of Soils in the Field Using Double-Ring Infiltrometer, DRI, can be used. This test is intended to measure infiltration rates in the range of 1×10^{-4} to 1×10^{-8} m/s.

Although the two methods mentioned above can be used to measure the hydraulic conductivity of asphalt concrete in field, they are time-consuming and relatively complicated to operate, which prevent them being widely accepted. Recently, studies (Maupin, 2000; Colley, et al. 2000 and 2002; Prowell, et al. 2002) have been performed to find an appropriate field permeameter, which can perform hydraulic conductivity testing quickly and easily without the need for cutting cores. Most proposed field permeameters are based on the falling-head test. The biggest problem associated with falling head field permeameters lies in the difficulty of sealing the device to the pavement surface. The combination of the rough surface texture of the pavement and the relatively high water head applied through the device can create leaks at the pavement surface which results in unaccounted for flow.

Colley (1999) evaluated the four field hydraulic conductivity devices, shown in Figure 2.11. Two of the devices, labeled as Field Permeameter 1 and Field Permeameter 2, were developed by a commercial supplier while the other two, labeled as Field

Permeameter 3 and Field Permeameter 4, were designed by National Center for Asphalt Technology (NCAT). A standardized procedure for each permeameter was developed. All four pemeameters are based on the falling head test.

Field Permeameter 1

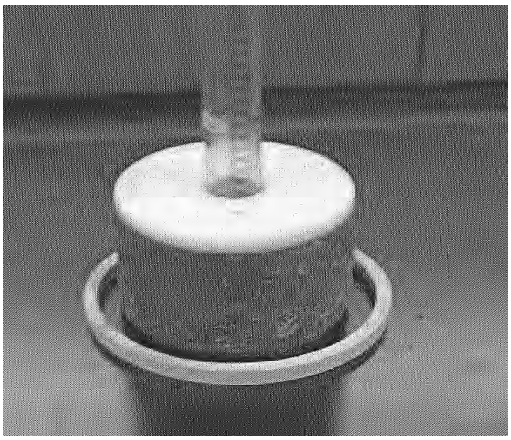

Field Permeameter 2

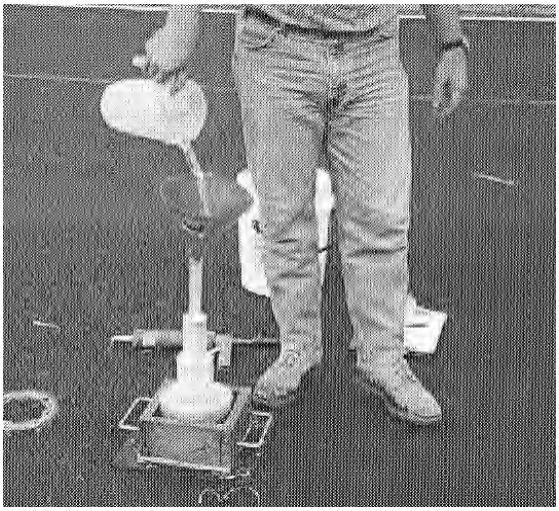

Field Permeameter 3

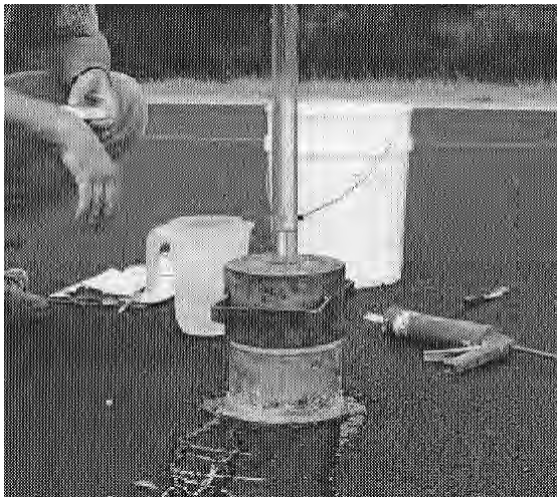

Field Permeameter 4

Figure2.11 Four field permeameters (after Cooley, 1999).

Based on three criteria: correlation with measurements from the laboratory permeameter, repeatability of hydraulic conductivity measurements, and ease of use, Colley (1999) concluded that field permeameter 3 was the best.

2.4.4 Factors influencing the hydraulic conductivity

2.4.4.1 Viscosity of the permeant

Viscosity is the measurement of resistance or drag of a fluid when in motion. It describes a fluid's internal resistance to flow. A fluid with lower viscosity will have a higher flow rate though the same porous media than a fluid with higher viscosity. For any fluid, viscosity is a function of temperature. As the temperature increases, the viscosity of the fluid decreases. The fluid used in hydraulic conductivity testing is normally water. The viscosity of water at different temperatures is listed in Table 2.10. Because of the temperature dependency of viscosity, the hydraulic conductivity of a medium is normally expressed as the hydraulic conductivity at a temperature of 20 ^{o}C. If the hydraulic conductivity is not measured at 20 ^{o}C, it can be converted to the hydraulic conductivity at 20 ^{o}C using Equation 2.33.

$$k_{20} = k_t \frac{\mu_t}{\mu_{20}} \qquad 2.33$$

where,

k_{20} = hydraulic conductivity at 20 ^{o}C;

k_t = hydraulic conductivity at t ^{o}C;

μ_t = viscosity of a fluid at t ^{o}C;

μ_{20} = viscosity of a fluid at 20 ^{o}C.

Table2.10 Viscosity of water at different temperatures.

Temp	Absolute Viscosity
°F	Centipoises

32	1.79
50	1.31
60	1.12
70	0.98
80	0.86
85	0.81
100	0.68
120	0.56
140	0.47
160	0.4
180	0.35
212	0.28

2.4.4.2 Air void contents

Many researchers (Mohammad et al. 2003; Gogula et al. 2003; Prowell et al. 2002; Mallick et al. 2001; Cooley et al. 2002) have determined that high air void contents result in more interconnected voids in asphalt mixes, which can result in higher hydraulic conductivity. According to Cooley (1999), for dense-graded mixtures, numerous studies have shown that the initial in-place air void content should not below approximately 3 percent or above approximately 8 percent. Low air voids have been shown to lead to rutting and shoving while high void contents are believed to allow water and air to penetrate into the pavement resulting in an increased potential for water damage, oxidation, raveling, and cracking. For Superpave mixtures, it was concluded that the coarse-graded superpave mixtures tended to be permeable at air void contents significantly below 8 percent (Cooley et al. 2000; Mohammad et al. 2003). Coarse-graded Superpave mixes seem to be more permeable than conventional dense-graded mixes at similar air void contents (Hainin and Cooley, 2003).

2.4.4.3 Gradation and nominal maximum aggregate sizes

Many researchers (Mohammad et al. 2003; Kanitpong et al. 2001) have investigated the effects of gradation and the nominal maximum aggregate sizes on the hydraulic conductivity of asphalt mixtures. Gradations that pass below the maximum density line (MDL) are normally called coarse-graded. Gradations that pass above MDL are called dense-graded. Coarse-graded mixtures have less fine aggregate to fill the void spaces between the larger aggregate particles than dense-graded mixtures do. This results in larger individual air voids and a higher potential for interconnected air voids. Thus, all other factors being equal, coarse-graded mixtures are usually more permeable than dense-graded mixtures.

2.4.4.4 Sample thickness

The larger the specimen height, the lower the specimen's hydraulic conductivity tends to be (Mohammad et al. 2003; Kanitpong et al. 2001). This can be attributed to the fact that as thickness increases, the probability of some of the void paths becoming blocked increases and the overall permeability is reduced (Mohammad et al. 2003). There is also a possibility that thin specimens will have a different aggregate structure and thus a different distribution of air voids than will be present in thicker specimens (Kanitpong et al. 2001).

2.5 Current Studies Regarding Water Migration in Pavement

There are two main sources of water in base courses and subgrade soils. One is from precipitation and infiltration from above and the other one is through suction of water from the groundwater table.

2.5.1 Precipitation

Precipitation is an important source of water that may migrate into pavement systems. Rainwater et al. (1999) recorded precipitation events and the corresponding changes of moisture contents of base and subgrade soils at three test sites in Tennessee. The three test sites were Blount County Test Site, McNairy County Test Site and Sumner County Test Site. The cross sections of the test sites generally consisted of surface layers, binder layers, asphaltic concrete, asphalt stabilized base, stone base and subgrade soil. Exceptions occurred at Sumner County Test Site and McNairy County Test Site. Sumner County Test Site had a layer of prime coat between asphalt stabilized base and stone base and McNairy County Test Site did not have surface and binder layers. It was determined in this study that moisture content in asphalt-stabilized base and stone base could be related very closely with precipitation. However, moisture content in subgrade soils had no significant change during or after precipitation. The change of moisture content of subgrade soil is likely seasonal.

Based on data from seasonal monitoring program (SMP) testing in a test site in Ohio, Heydinger (2003) concluded that the seasonal variations in moisture content and temperature are similar following sinusoidal curves and the seasonal variation of subgrade soil moisture can be predicted independent of precipitation.

2.5.2 Ground Water Table

Ground water is another source of water in subgrade soils (Ksaibati, et al. 2000). When the ground water is relatively close to the surface of the subgrade soil, the moisture content of subgrade soil will be affected due to the capillary effect. AI-Samahiji et al. (2000) investigated this capillary rise and concluded that soils wetted above the groundwater table through capillary rise remain at a degree of saturation averaging about 60 percent. Heydinger (2003) analyzed the data obtained from the seasonal monitoring program (SMP) instrumentation in the State of Ohio. The subgrade soil at the site was classified as an A6 (low plasticity clay) soil by the AASHTO Soil System or CL (lean clay) by the Unified Soil Classification System. The base was an asphalt-treated base without edge drain The groundwater table was very shallow, ranging from 0.5 ft below the top of the subgrade soil in summer to 4.0 ft in late fall and early winter. Heydinger found that the curves describing the moisture content of both the base and subgrade soils with time appeared to be sinusoidal curves with the maximum moisture content in summer and the minimum moisture content in late fall and early winter. Correspondingly, the groundwater table was shallowest in summer and deepest in late fall and early winter.

2.6 Conclusions

From the extensive literature review presented previously in this chapter, it is learned that moisture content has an adverse effect on resilient modulus, which is the primary input parameter to evaluate the properties of base and subgrade materials in the current AASHTO Design Guide. The 200X Design Guide proposed a predictive model for resilient modulus at least partially based on moisture content of base and subgrade materials. These indicate that it is important to investigate nature of moisture content

migration through pavement systems and then obtain a predictive model for moisture content variations with seasons and environmental factors, which are the main goals of this project. To achieve these goals, moisture content in pavement systems in two test pads at the ERC and a field test site in Fort Smith was measured and environmental factors, including precipitation, temperature, groundwater water table, surface water and subsurface water collected during and after precipitation events, were also measured at these test sites.

From the literature review, it is also learned that TDR is a widely accepted method for long-term measurements of moisture content and has many advantages over the conventional method. TDR probes were therefore used in the research to measure moisture content of pavement system.

Chapter 3 Methodology and Equipment

3.1 Introduction

Based on information derived from an extensive literature review, a research methodology was established to monitor the migration of water through pavement systems and to obtain the variation of moisture content over time. The necessary monitoring and measurement equipment was selected and purchased. Test pads were built and all sensors were installed. Continuous and periodic monitoring of the field installation was performed.

3.2 Methodology

The goals of this project were: to develop a migration pattern of water through pavement systems, to obtain a predictive model to predict the variation of moisture content with seasons and environmental factors, to evaluate suitability of the Enhanced Integrated Climatic Model (EICM) in Arkansas and then to provide some guidelines for the current empirical and mechanistic- empirical flexible pavement design procedures.

To achieve these goals, extensive measurements and monitoring were performed on two test pads built at the Engineering Research Center (ERC) of the University of Arkansas and at a field site consisting of a 100-foot long pavement section on Highway 253 in Fort Smith, Arkansas. The measurements and monitoring included:

- Material properties.
- Amounts and intensities of precipitation for a relatively long period,

- Air temperatures, along with base and subgrade soil temperatures,
- Time rate of surface water runoff from the pavement surface during and after precipitation events,
- Time rate of subsurface water that is collected from edge drains during and after precipitation events,
- Moisture content at various levels in the pavement system,
- Ground water levels.

The goals of this study were to measure how much water fell on the surface of the pavement sections, how much water ran off from the surface of the pavement sections, how much water was collected from the edge drains, how much and how fast water content in base and subgrade materials changed, and how groundwater level changed with time.

Based on these measurements, statistical analyses were performed on data obtained from the two test pads and the field test site to create predictive models for moisture content in the pavement systems, air and soil temperatures, surface water and subsurface water; a water balance during precipitation events was achieved; a water migration pattern through pavement systems was developed and a predictive model of moisture content in pavement systems over time was proposed; measured moisture content and soil temperatures in the pavement systems were compared with predicted moisture content and soil temperatures using the EICM to evaluate the suitability of the EICM in Arkansas. Finally, a finite element software program, called PlaxFlow, was employed to simulate water migration through pavement systems based solely on material and geometric properties of the sections. The results obtained from finite

element simulations were compared to measured data to calibrate the finite element model.

The measurements of material properties, equipment selection and calibration, test pad construction and installation of instrumentation at the field test site are described in their respective sections in this chapter.

3.3 Material Properties

3.3.1 Soil Sampling

Bulk samples were obtained from base courses and subgrade soils at the ERC and the field test site. Relatively undisturbed subgrade soil samples were also obtained using 3-inch diameter thin-wall Shelby tubes pushed into subgrade soils.

3.3.2 Classification Tests

Classification tests, consisting of Atterberg limits tests (AASHTO T-89 and 90) and sieve analysis tests (AASHTO T-88), were performed on bulk samples obtained from base and subgrade soils at the ERC and the field test site. Atterberg limits test results are tabulated in Tables 3.2 and 3.3, and sieve analysis test results are presented as grain-size distribution curves in Figures 3.1 through 3.5. Based on the laboratory classification test results, the subgrade soil at the ERC was classified as an AASHTO A-6 soil based on the AASHTO classification system and as sandy lean clay (CL) based on the Unified Soils Classification System (USCS). The subgrade soil at the field test site was classified as an AASHTO A-6 soil based on the AASHTO classification system and as clayey gravel

with sand (GC) based on the USCS. Base aggregate material at the ERC satisfied the requirements to be Class 7 base course according to the 2003 Arkansas Standard Specifications for Highway Construction. According to those specifications, Class 7 aggregate is defined as "any mechanically crushed natural rock or stone of igneous, sedimentary, and/or metamorphic origin produced from a solid geological formation by quarrying methods". In addition, Class 7 base must also meet the gradation requirements presented in Table 3.1. Base course aggregate material at the field test site did not satisfy the gradation requirements of Class 7 because the percentages passing U.S. No. 40 sieve and No. 200 sieve exceeded the upper limits of Class 7 criteria. Since the pavement section at the field test site did not have a subbase layer as a separator layer between the base course and subgrade, it is believed that fine material had already migrated into base material from the underlying subgrade soil.

Table 3.1 Gradation requirements for Class 7.

Sieve (mm)	Percent Passing (%)
1.5" (37.5)	100
1" (25.0	60 – 100
¾" (19.0)	50 – 90
No.4 (4.75)	25 – 55
N0.40 (0.425)	10 – 30
No. 200 (0.075)	3 – 10

Table 3.2 Atterberg limits test results for materials at the ERC.

Material	Liquid Limit (LL)	Plasticity Limit (PL)	Plasticity Index (PI)	AASHTO Classification	USCS Classification
Subgrade	37	22	15	A-6	Sandy Lean Clay, CL
Base	16	16	0	A-1-a	Gravel with Silt and Sand, GP-GM
Subbase	17	17	0	A-1-a	Gravel with Silt and Sand, GP-GM

Table 3.3 Atterberg limit test results for materials at the field test site in Fort Smith.

Material	Liquid Limit (LL)	Plasticity Limit (PL)	Plasticity Index (PI)	AASHTO Classification	USCS Classification
Subgrade	36	23	13	A-6	Clayey Gravel with Sand, GC
Base	16	16	0	A-1-b	Silty Gravel with Sand, GM

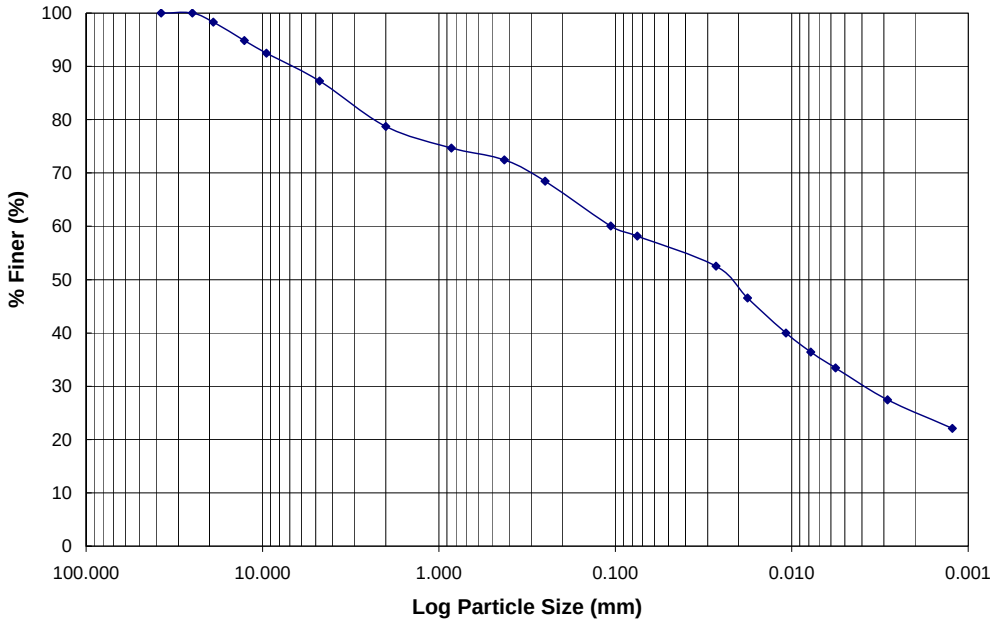

Figure 3.1 Grain-size distribution curve for the subgrade soil at the ERC.

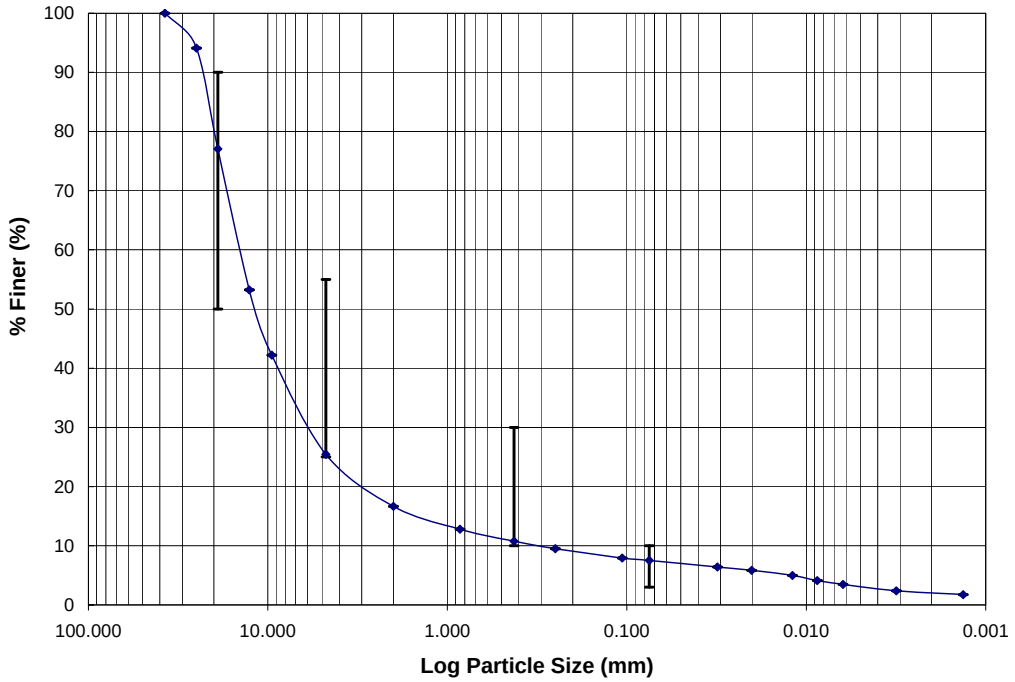

Figure 3.2 Grain-size distribution curve for base course at the ERC. The range bars at selected particle sizes represent the upper and lower limits required for a Class 7 material classification, as established by Arkansas Highway and Transportation Department.

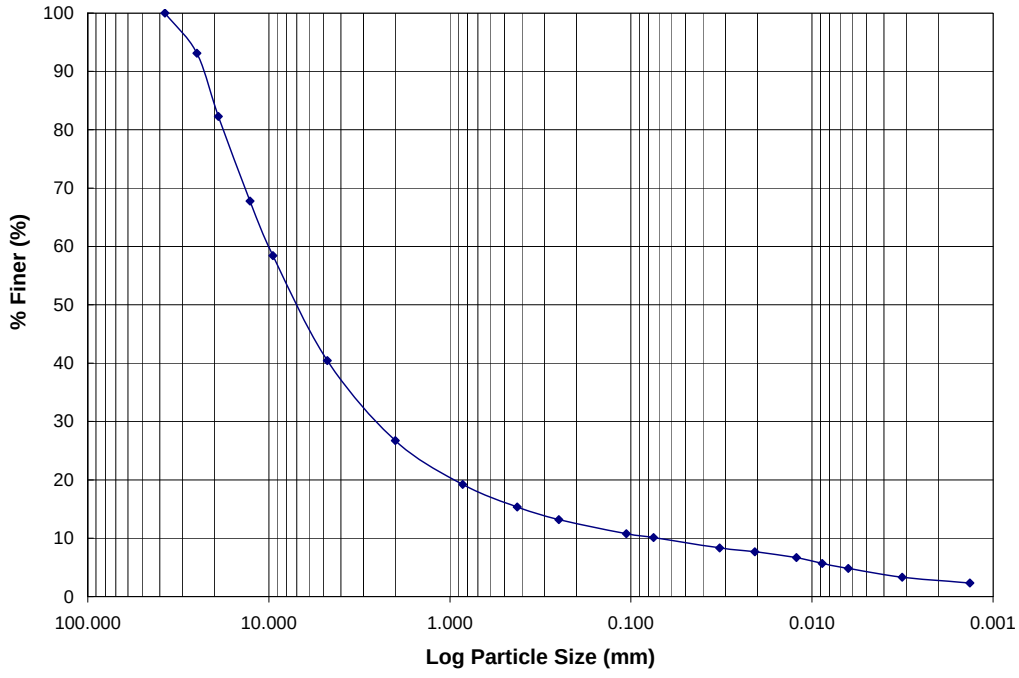

Figure 3.3 Grain-size distribution curve for subbase material at the ERC.

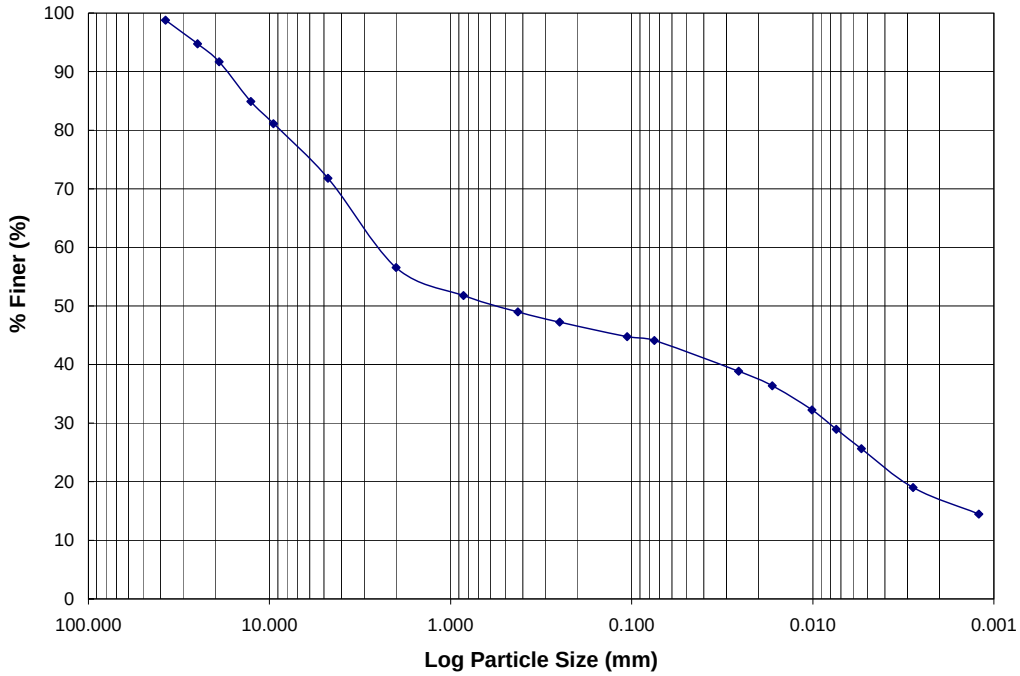

Figure 3.4 Grain-size distribution curve for the subgrade soil at the field test site on Highway 253 in Fort Smith.

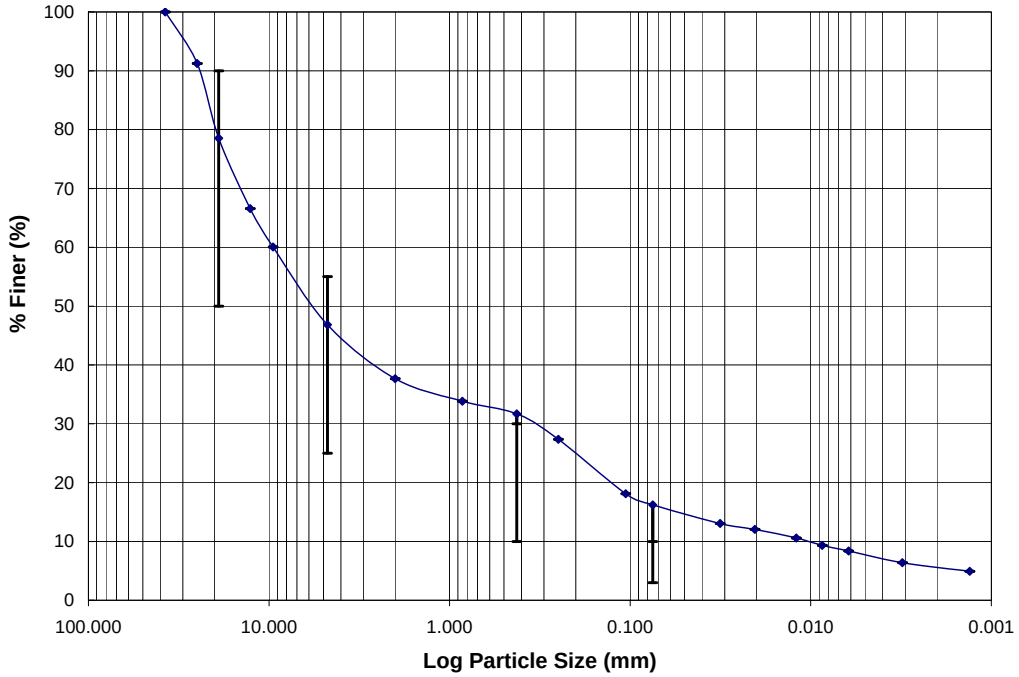

Figure 3.5 Grain-size distribution curve for base course material at the field test site in Fort Smith. Range bars on selected particle sizes represent upper and lower limits for Class 7 material established by Arkansas Highway and Transportation Department.

3.3.3 Proctor Tests

Standard Proctor tests (AASHTO T 99, Method A) were performed on bulk samples of the subgrade soils at both locations while modified Proctor tests (AASHTO T 180, Method D) were performed on bulk samples obtained from base and subbase courses at both sites. The test results are presented in Table 3.4.

Table 3.4 Proctor test results.

Location	Layer	Maximum Dry Density (pcf)	Optimum Moisture Content (%)
ERC	Base	144.7	6.3
	Subbase	138.6	6.8
	Subgrade	111.8	16.4
Fort Smith	Base	135.2	6.2
	Subgrade	112.8	16.4

3.3.4 Hydraulic Conductivity Tests on Base and Subgrade Materials

Hydraulic conductivity tests were performed on remolded samples for base and subbase courses and on relatively undisturbed thin-wall Shelby tube samples for subgrade soils. Remolded base and subbase samples were fabricated using a 6-inch diameter split mold and modified Proctor energy (AASHTO T-180). A constant gradient of 1 was used to conduct hydraulic conductivity tests on the remolded base and subbase samples.

Since the hydraulic conductivity of subgrade soils was relatively low, falling head test procedures were adopted for good accuracy. To reduce the time required to perform tests, gradients of 10 to 25 were used. Hydraulic conductivity tests were performed on

relatively undisturbed subgrade soils from the ERC and the field test location in Fort Smith. Hydraulic conductivity test results are presented in Table 3.5.

Table 3.5 Hydraulic conductivity test results.

Location	Material	Hydraulic conductivity (cm/s)
ERC	Base	$3.3X10^{-3}$
	Subbase	$3.1X10^{-3}$
	Subgrade	$3X10^{-8}$
Fort Smith	Base	$6.0X10^{-4}$
	Subgrade	$1X10^{-7}$

3.3.5 Hydraulic Conductivity Tests on Hot Mix Asphalt Concrete

As discussed in the literature review, the laboratory hydraulic conductivity test is an essentially destructive test and requires core samples. In order to maintain the integrity of the asphalt surfaces at the test sites it was necessary to find an appropriate non-destructive test method for field hydraulic conductivity tests, which could be correlated to laboratory tests. Currently, several field permeameters are available to conduct Non-Destructive Testing (NDT) of asphalt pavement surfaces (Maupin, 2000; Colley, et al. 2000 and 2002; Prowell, et al. 2002, Kuss 2004, Qazi, 2004). All these field permeameters actually measure infiltration rates of water through asphalt mixes. However, to compare field data obtained using field permeameters with laboratory hydraulic conductivity data on asphalt cores and then to establish correlations between field and laboratory tests, the following assumptions were made by researchers ((Maupin, 2000; Colley, et al. 2000 and 2002; Prowell, et al. 2002, Kuss 2004, Qazi, 2004).

- Water flow through the entire thickness of asphalt concrete
- At the bottom of asphalt concrete, water head decreases to zero;
- Water flow through asphalt concrete is vertical and no horizontal flow.
- Darcy's law is valid

To evaluate selected field permeameters and to get the relatively accurate field hydraulic conductivity measurements of asphalt concrete, which could be correlated well with laboratory test results, both field and laboratory hydraulic conductivity tests were performed on Hot Mix Asphalt Concrete (HMAC) at selected spots shown in Figures 3.6 and 3.7 on the test pads at the ERC by Qazi (2004) as a part of this project. Qazi (2004) used the Kuss field permeameter and the National Center for Asphalt Technology (NCAT) field permeameter for field hydraulic conductivity tests. Each test was generally performed for about 30 minutes to 1 hour. The Kuss field permeameter operates using a constant water head as shown in Figure 3.8 while the NCAT field permeameter operates using a "falling head" procedure as shown in Figure 3.9. Detailed descriptions of these two field permeameters can be found in Qazi's thesis (2004). Once field testing was completed the HMAC was cored at each location where field testing was done and laboratory tests were performed on asphalt concrete cores by Qazi (2004). The core locations were then filled with the HMAC, which was compacted using hand tools.

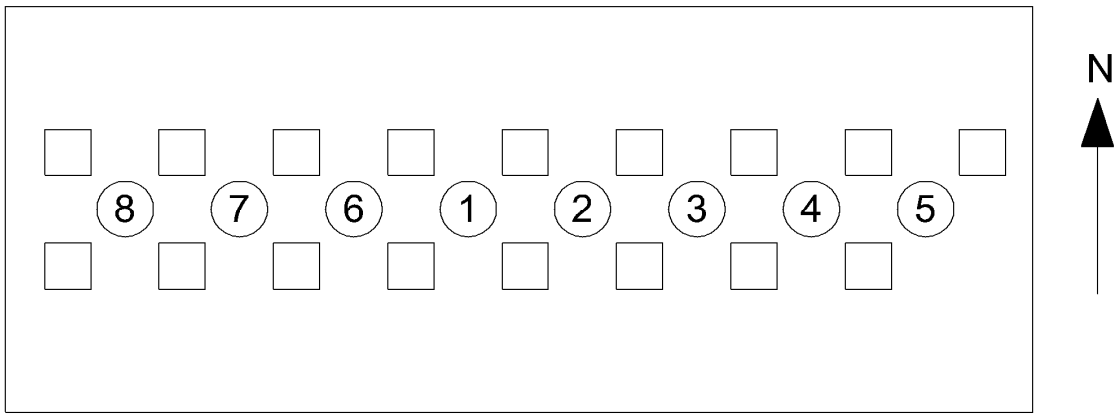

Figure 3.6 Configuration of hydraulic conductivity test locations of Pad A at the ERC. Square areas are Qazi's test locations and circular areas are Chang's test locations.

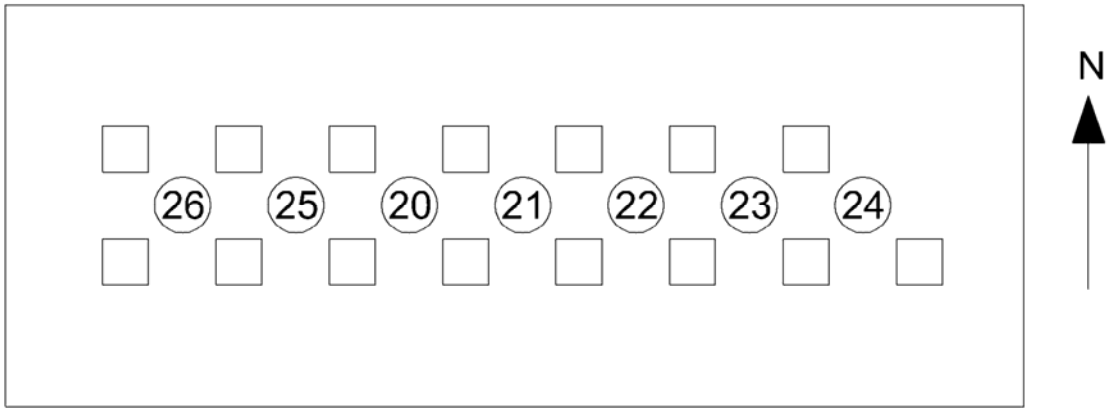

Figure 3.7 Configuration of hydraulic conductivity test locations of Pad B at the ERC. Square areas are Qazi's test locations and circular areas are Chang's test locations.

Figure 3.8 Kuss Field Hydraulic Conductivity Testing Apparatus (Qazi, 2004).

Figure 3.9 NCAT Permeameter (Qazi, 2004).

To further evaluate the field permeameters and to determine the possible radial and vertical variation of moisture content in the pavement system during field hydraulic conductivity tests, a constant head permeameter as shown in Figure 3.10, using the Marriott Bottle principle, was employed to perform long-term (4-7 days per test) field hydraulic conductivity tests with a 1-inch water head on the surface of the test pads. A detailed description about this permeameter was included in the "Equipment Selection and Calibration" section of this chapter. Since the HMAC had already been cored at Qazi's test locations, long-term field hydraulic conductivity tests were conducted near the middles of Qazi's test locations as shown in Figures 3.6 and 3.7.

Figure 3.10 Constant head Marriott Bottle permeameter.

To compare long-term hydraulic conductivity results with short-term hydraulic conductivity results and laboratory results performed by Qazi, test results obtained at three or four locations around a location where the long-term hydraulic conductivity test was conducted were averaged, which was used in comparison. The results of hydraulic conductivity, obtained from field and laboratory tests, were compared and presented in semi-log spaces as shown in Figures 3.11 and 3.12. It should be noted that data are missing at some locations in Figure 3.11 and 3.12 because the hydraulic conductivity results are zero at these locations.

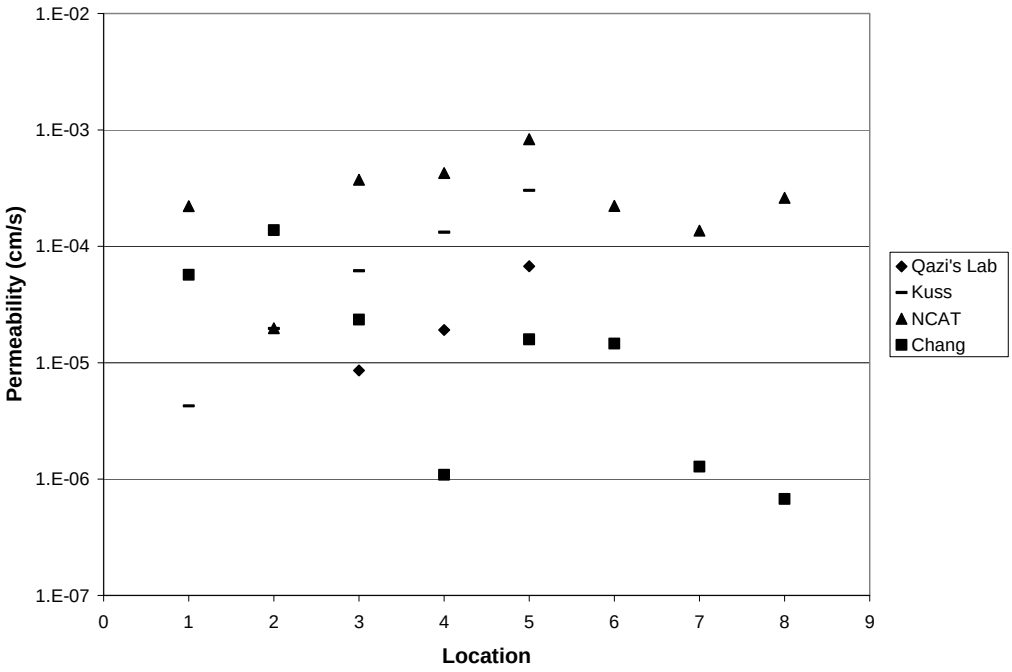

Figure 3.11 Comparison of results of field hydraulic conductivity tests and laboratory tests on binder course (25 mm aggregate).

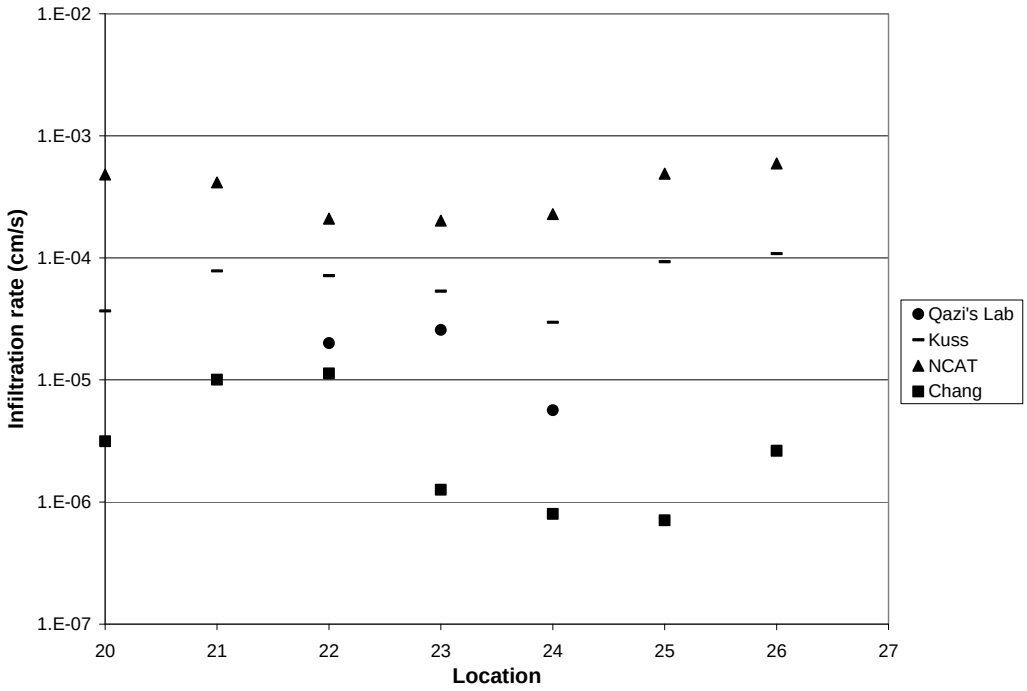

Figure 3.12 Comparison of results of field hydraulic conductivity tests and laboratory tests on surface course (12.5 mm aggregate).

3.3.6 Resilient Modulus of the Subgrade Soils

According to the Arkansas Standard Specifications for Highway Construction, subgrade soils need to be compacted to at least 95 percent of the material's standard Proctor dry unit weight at near optimum moisture content (OMC) (AASHTO T-99). Upon completion of construction of pavements, moisture contents in fine-grained subgrade soils generally increase with time due to capillary effects or migration of surface water into the subgrade soils. TDR-measured moisture content data at the ERC and Ft Smith test sites indicates that maximum moisture contents are approximately 120 percent of the OMC in summers, and minimum moisture contents are approximately 95 percent of the OMC in winters. Elliott (1988) stated that for Arkansas, a moisture content of 120 percent of optimum has been identified as a reasonable estimate of in-service

moisture content. Therefore, laboratory specimens were prepared at a target dry unit weight of 95 percent of the material's standard Proctor dry unit weight (AASHTO T-99). The specimens were fabricated at a 5 different moisture contents; at OMC and then at 105, 110, 120, 140 percent of the OMC.

Samples were prepared using the same method as described by Zhao (2007) and are repeated here for reference. The soil sample was air dried. The moisture content of the air-dried sample was determined in accordance with AASHTO T-87. Then a split mold 2.8 inches in diameter and 5.6 inches in height was used to fabricate specimen. The amount of the air-dried sample required to fill the split mold to the target dry unit weight was calculated. Then a certain amount of water was added and thoroughly mixed with the soil sample to obtain the target moisture content. An extra 0.4 percent of water was added to account for the moisture loss during preparation of soil specimens. The soil sample was then compacted in the split mold in three exactly equal layers. During compaction of each layer, a tamp foot with marks on its rod was constantly inserted in the mold to check the thickness of the layer being compacted. After a layer was compacted to the target thickness, groves were made on the surface of the layer in order to increase bondage between layers. Figure 3.13 is the equipment used for specimen fabrication. After the last layer was finished, the split mold was removed and the specimen was warped in a plastic film and further protected by a wrap of aluminum foil. The wrapped specimen was then marked and stored in the refrigerator for 72 hours for further testing (Zhao, 2007). Because the sample was too wet at the target moisture content of 140 percent of the OMC, the specimen at this moisture content were not able to be compacted to 95 percent

of the material's standard Proctor dry unit weight. However, every effort was put to compact the specimen as close to the target dry unit weight as possible.

Figure 3.13 Equipment used for specimen preparation (Zhao, 2007).

The testing was performed using a PC controlled Material Testing System (MTS) servo-hydraulic test frame as shown in Figure 3.14. Air pressure was used in the triaxial chamber to provide confining stress (σ_3) and repeated vertical loads were used to provide deviator stress (σ_d). A load pulse of 0.1 second with 0.02 second of ramp-up, 0.06 second of hold and 0.02 second of ramp-down, and rest period of 0.9 second were used for the deviator stress. During testing, the deviator stress was measured by a load cell, confining pressure was monitored by a digital pressure gauge, and deformation was measured using two LVTDs. Each specimen was subjected to 200 repetitions of cyclic loading in accordance with AASHTO T-307. The loading and deformation were automatically collected by the MTS data acquisition system. Per AASHTO T-307, the resilient modulus

tests were performed at three confining pressures (2, 4 and 6 psi) and five deviator stresses (2, 4, 6, 8, and 10 psi) for each specimen. The test results are presented in Figures 3.15 through 3.24. Note that the specimens at the moisture content of 140 percent of the OMC failed at lower deviator stresses than 10 psi. Therefore, the tests were performed up to applicable maximum deviator stresses for these specimens.

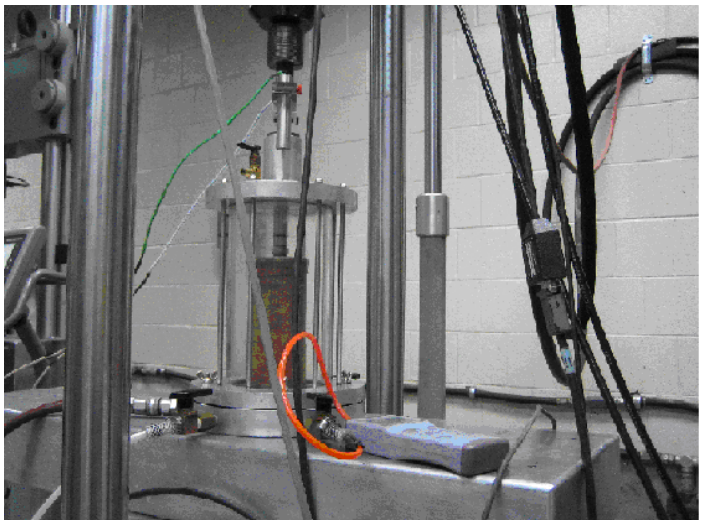

Figure 3.14 Test setup for repeated load triaxial testing (Zhao, 2007).

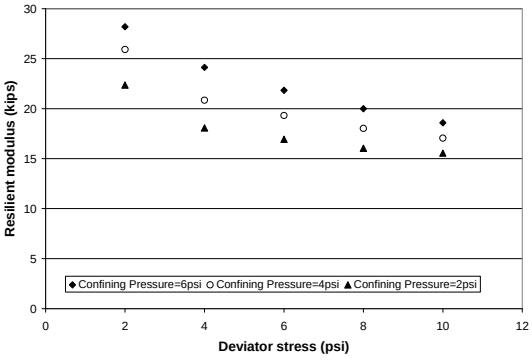

Figure 3.15 Results of resilient modulus tests on the subgrade soil at the ERC at 100 percent of OMC.

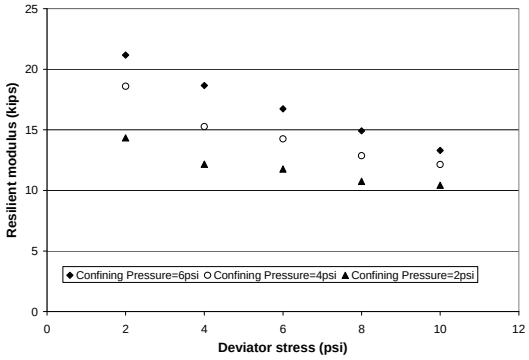

Figure 3.16 Results of resilient modulus tests on the subgrade soil at the ERC at 105 percent of OMC.

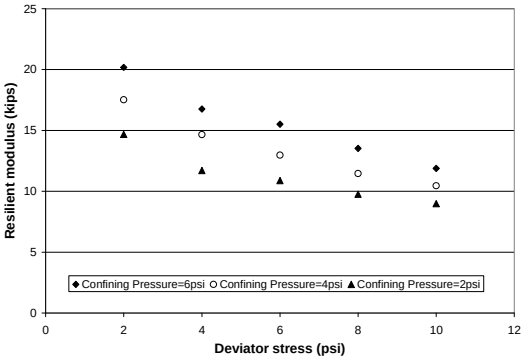

Figure 3.17 Results of resilient modulus tests on the subgrade soil at the ERC at 110 percent of OMC.

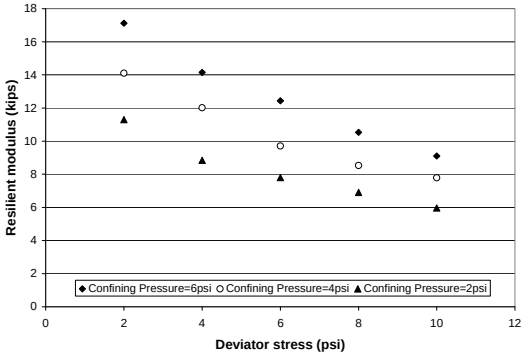

Figure 3.18 Results of resilient modulus tests on the subgrade soil at the ERC at 120 percent of OMC.

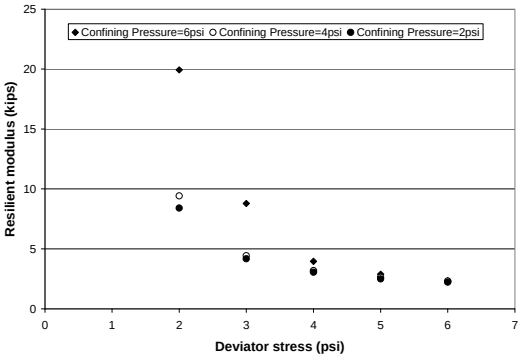

Figure 3.19 Results of resilient modulus tests on the subgrade soil at the ERC at 140 percent of OMC.

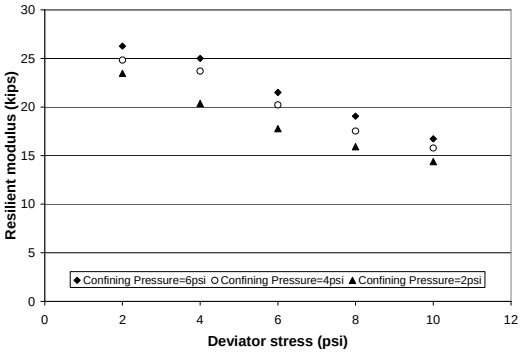

Figure 3.20 Results of resilient modulus tests on the subgrade soil at the Ft. Smith site at 100 percent of OMC.

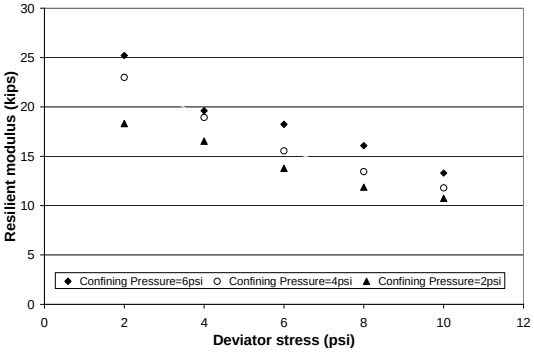

Figure 3.21 Results of resilient modulus tests on the subgrade soil at the Ft. Smith site at 105 percent of OMC.

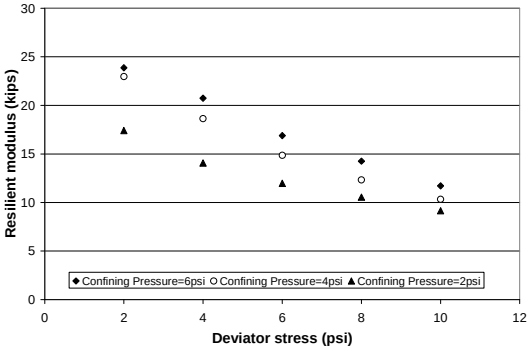

Figure 3.22 Results of resilient modulus tests on the subgrade soil at the Ft. Smith site at 110 percent of OMC.

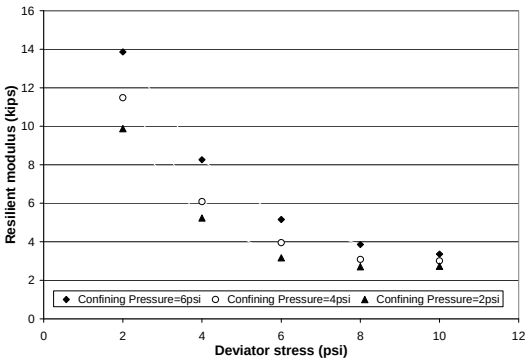

Figure 3.23 Results of resilient modulus tests on the subgrade soil at the Ft. Smith site at 120 percent of OMC.

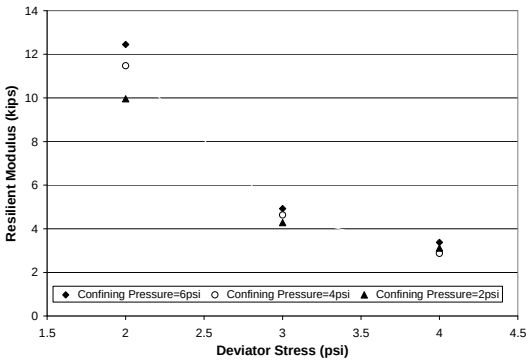

Figure 3.24 Results of resilient modulus tests on the subgrade soil at the Ft. Smith site at 140 percent of OMC.

3.4 Equipment Selection and Calibration

3.4.1 Data Acquisition System

The data acquisition system selected for this study consisted of a Campbell Scientific CR10X datalogger with two megabytes memory, a Campbell Scientific AM16/32 multiplexter, a telecommunication system, a power system and an equipment enclosure. Figure 3.25 illustrates how the data acquisition system works. Detailed introductions to these components are presented in there respective sections in the followings.

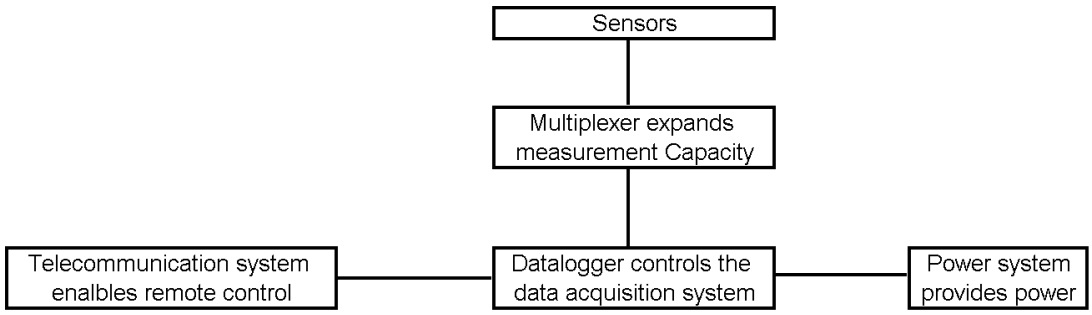

Figure 3.25 Sketch of the data acquisition system.

3.4.1.1 Datalogger and Multiplexer

The CR10X datalogger shown in Figure 3.26 consists of a wiring panel and an internal computer which controls the manner and timing of the acquisition and storage of data received from a wide variety of sensors. The wiring panel provides terminals for connecting sensors, controlling external electrical devices, and providing DC 5 and 12V power to sensors and other external devices. The datalogger communicates with external sources (computers, modems, etc) through a 9-pin I/O port using proprietary Campbell Scientific I/O logic. Special cable or converter must be used to convert this logic to RS232 logic when communicating with RS232 devices such as laptop computers. A control program can be entered into the datalogger via a computer or a compatible portable keyboard display sold by Campbell Scientific, Inc. The program can tell the datalogger how often to scan the sensors, how often to take readings from the sensors, and how to reduce the readings and save them.

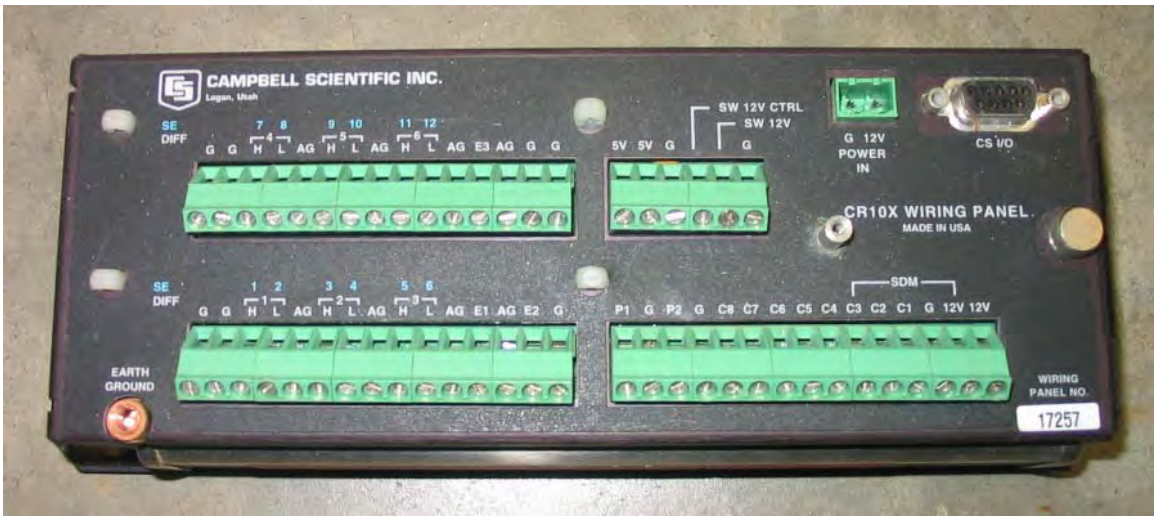

Figure 3.26 Campbell Scientific, Inc, model CR10X datalogger.

The software used to create control program and communicate with the data logger is called PC208W and is a windows-based software program that is sold by Campbell Scientific, Inc. This program facilities the programming and communication

with the datalogger and provides a reliable exchange of data between a computer and the datalogger.

The AM16/32 multiplexer shown in Figure 3.27 is used to increase the number of sensors that may be scanned by the datalogger. The multiplexer is positioned between the sensors and one channel of the datalogger. Based on a control program stored in the datalogger, which addresses specific sensors, mechanical relays in the AM16/32 are energized to switch power to the desired sensor and allow the datalogger to receive a signal from that sensor. The AM16/32 multiplexer can multiplex up to 32 single-ended two-wire sensors or 16 differential four-wire sensors at a time. It supports various types of sensors, such as moisture probes, temperature probes, strain gages, and so on.

Figure 3.27 Campbell Scientific, Inc, model AM16/32 Multiplexer.

3.4.1.2 Telecommunication system

The telecommunication system consists of a Motorola M600 cellular transceiver, a RJ-11C interface, an ASP 962 Yagi antenna and a Campbell Scientific, Inc. Com 210 modem as shown in Figures 3.28 and 3.29.

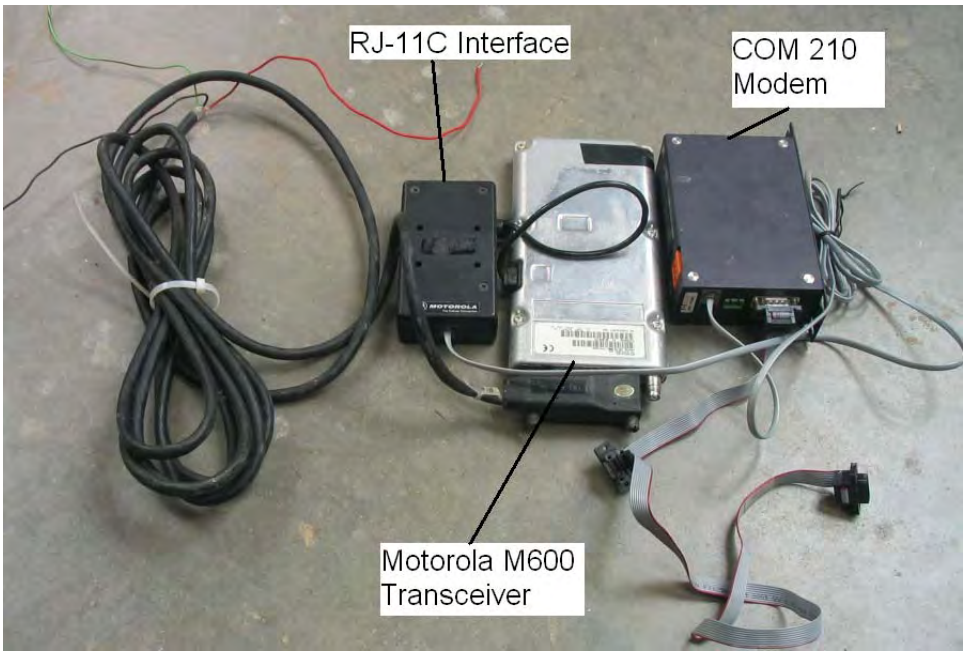

Figure 3.28 Motorola M600 Transceiver, RJ-11C Interface and Com 210 Modem.

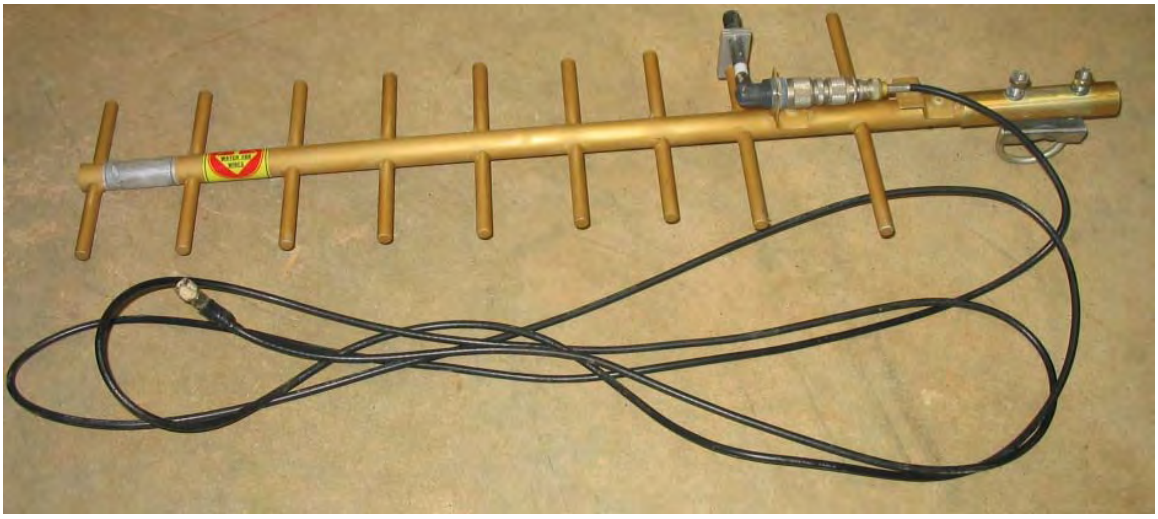

Figure 3.29 Campbell Scientific, Inc, ASP962 Yagi Antenna.

The transceiver was connected to the modem through the RJ11C interface. There are two ways to control power to the transceiver. One way is by manually pushing the red power indicator/switch on the RJ11C interface. Another way is through the control line included in the transceiver, which is the green line shown in Figure 3.16 and is connected to the datalogger. The datalogger can be programmed to switch power to the transceiver

through the control line at predetermined time periods. Since the transceiver has a high demand of power, the control line included in the transceiver is very important for the datalogger to control the power on just when needed.

Using the features of the software program PC208W and this telecommunication system the data acquisition system can be remotely monitored and controlled over a standard telephone line using a computer and modem. The PC208W software, residing on an office computer, can be set up to autonomously call the cell phone to either give it instructions and/or download the data regularly to the computer. The datalogger can be programmed so that it can initiate a call to a remote polling computer if a specific piece of data is recorded in the field that prompts an alarm,

3.4.1.3 Power system

Since all of the equipment and sensors used in these installations have a relatively high and sometimes continuous demand of power, a battery alone would not be able to continuously provide the power to the system for long periods of time. For this study a combination of a 12-volt deep cycle marine battery and a solar panel was used to provide continuous uninterrupted power to the system. The solar panel was a model US-21, manufactured by Uni-Solar as shown in Figure 3.30. A charge controller shown in Figure 3.31 above the battery was used to prevent the solar panel from overcharging the battery during the day and to prevent the solar panel from dis-charging the battery at the night.

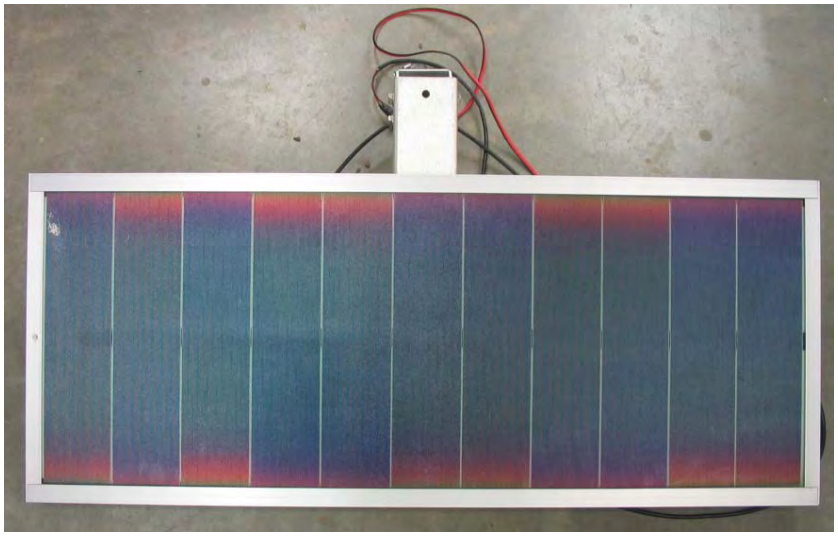

Figure 3.30 Uni-Solar US-21 solar panel.

Figure 3.31 Marine battery and controller.

3.4.1.4 Equipment enclosure

The equipment enclosure as shown in Figure 3.32 is manufactured by Vynckier Enclosure Systems, Inc. Houston, Texas. The enclosure consists of a SP3030da

enclosure, a SP335 backplate, and a cylinder lock. The enclosure is made from self-extinguishing, hot molded halogen-free fiberglass reinforced polyester and is maintenance-free and corrosion-resistant. The enclosure is well sealed, which provides outstanding protection against atmospheric and weather corrosion in outdoor settings. The cylinder lock provides security of installed equipment.

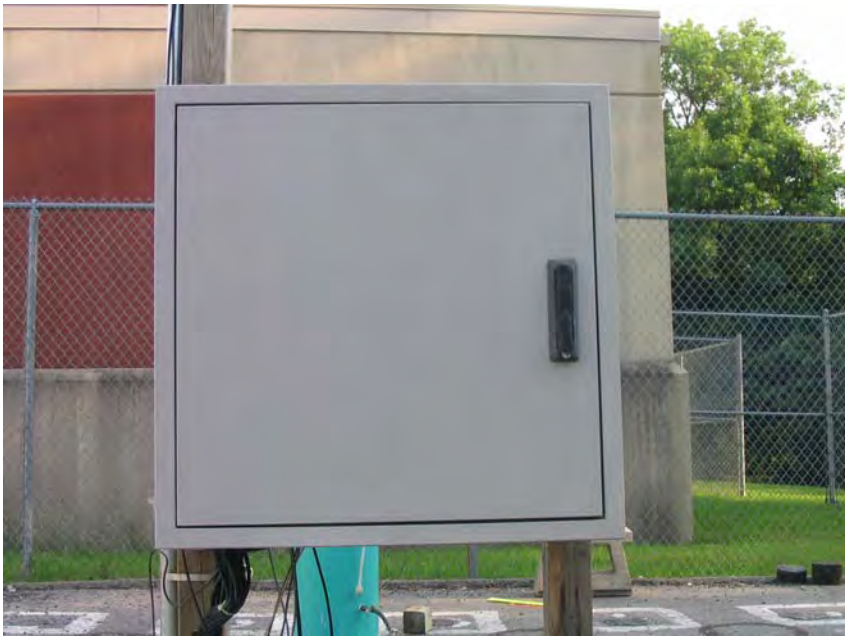

Figure 3.32 Equipment enclosure.

3.4.2 CS615 moisture probe

Since TDR moisture probes have many advantages over other methods as discussed in the literature review, the CS615 moisture probe, utilizing TDR technique, was chosen to measure moisture content in pavement systems. The CS615 moisture probe is manufactured by Campbell Scientific, Inc., Logan, Utah. The CS615 moisture probe, illustrated in Figure 3.33, consists of two parallel stainless steel rods 300mm long and 3.2mm in diameter. The spacing between two rods is 32mm. On one end of the rods there is a printed circuit board, which is encapsulated, along with a short section of the

two rods, in an epoxy housing. A shielded four-conductor cable is connected to the circuit board to supply power, enable the probe, and monitor the pulse output.

Figure 3.33 CS616 moisture probe.

High speed electronic components on the circuit board are configured as a bistable multivibrator. The output of the multivibrator is connected to the probe rods which act as a wave guide. The oscillation frequency of the multivibrator is dependent on the dielectric constant of the media being measured. The dielectric constant is predominantly dependent on the water content. Digital circuitry scales the multivibrator output to an appropriate frequency for measurement with a datalogger. The CS615 output is essentially a square wave with an amplitude swing of ±2.5 VDC. The period of the square wave output ranges from 0.7 to 1.6 milliseconds and is used for the calibration to water content. (CS615 water content reflectometer instruction manual, Campbell Scientific, Inc. 1996)

Table 3.6 presents the calibration equations, provided by Campbell Scientific, to convert probe output, at room temperature (20^{o}C), to volumetric moisture content for soils having ranges of electrical conductivities

Table 3.6 Calibration equations provided by manufacture (Campbell scientific).

Electrical conductivity (dS m^{-1})	Calibration
≤1.0	$\theta_v(\tau)=-0.187+0.037*\tau+0.335*\tau^2$
1.8	$\theta_v(\tau)=-0.207+0.097*\tau+0.288*\tau^2$
3	$\theta_v(\tau)=-0.298+0.361*\tau+0.096*\tau^2$

Since the output of the CS615 is affected by temperature, a temperature correction procedure depicted in Equations 3.1 and 3.2 was also provided by manufacture.

$$Coef_{temperature} = -3.46\times10^{-4} + 0.0199\theta_v - 0.045\theta_v^{\,2} \quad 3.1$$

$$\theta_{vcorrected} = \theta_{vuncorrected} - (T-20)\times Coef_{temperature} \quad 3.2$$

Where:

τ = output from moisture probe;

θ_v = volumetric water content;

$\theta_{vcorrected}$ = temperature corrected volumetric water content;

$\theta_{vuncorrected}$ = uncorrected volumetric water content;

$Coef_{temperature}$ = temperature correction coefficient.

Although calibration equations have already been provided, it is not easy to apply calibration equations without knowing the electrical conductivity of a soil. In addition, a soil-specific calibration can provide a more accurate relationship between the dielectric constant of the soil and its moisture content. Therefore, soil-specific calibrations were performed for this project. Because gravimetric moisture content is more useful than

volumetric moisture content from a geotechnical engineering standpoint, the output of the moisture probe was correlated to gravimetric moisture content.

For a specific soil, most factors are fixed, such as soil constitution, organic content and conductivity, only two factors, which are variable and can affect the relationship between the dielectric constant and moisture content, are density and temperature at which measurements are performed. Arkansas 2003 Standard Specifications for Highway Construction requires that subgrade and base materials be compacted at least to 95 percent of standard Proctor maximum dry density or 98 percent of modified Proctor maximum dry density at optimum moisture content. So for this study, calibrations were performed at 95 percent of standard Proctor maximum dry density or 98 percent of modified Proctor maximum dry density at room temperature. The effect of temperature on calibrations will be discussed later in this section.

Calibrations for base and subgrade material at the ERC and the field test site in Fort Smith were performed in the laboratory using a 6 inch by 12 inch concrete cylinder mold. Calibrations were performed in accordance with the following procedures:

1. Take bulk samples from the site where probes will be imbedded.
2. Air-dry samples.
3. Calculate the quantity of the dry sample needed to fill the concrete mold provided when the dry density is equal to 95 percent of standard Proctor maximum dry density (subgrade) or 98 percent of modified Proctor maximum dry density (base).
4. Add some water into the sample and mix them until water is evenly distributed.

5. Compact the sample in the concrete mold in 5 layers of equal weight.
6. Insert the moisture probe into the compacted sample and take a reading from the probe.
7. Take moisture content samples from different locations of the concrete mold, normally top, middle and bottom to measure actual gravimetric moisture content using the oven-dry method (AASHTO T-265).
8. Repeat steps 4-7 while increasing the moisture content of the sample.
9. Obtain calibration curves using the linear regression analysis.

Calibration curves for base and subgrade soils are presented in Figures 3.34 through 3.38.

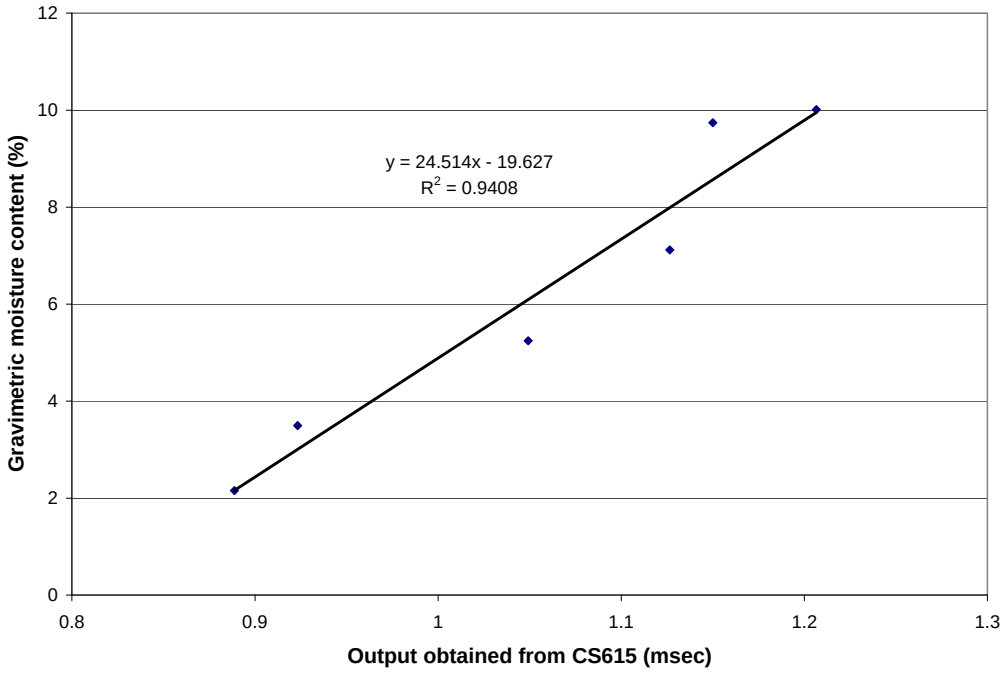

Figure 3.34 Calibration curve for base material at the ERC.

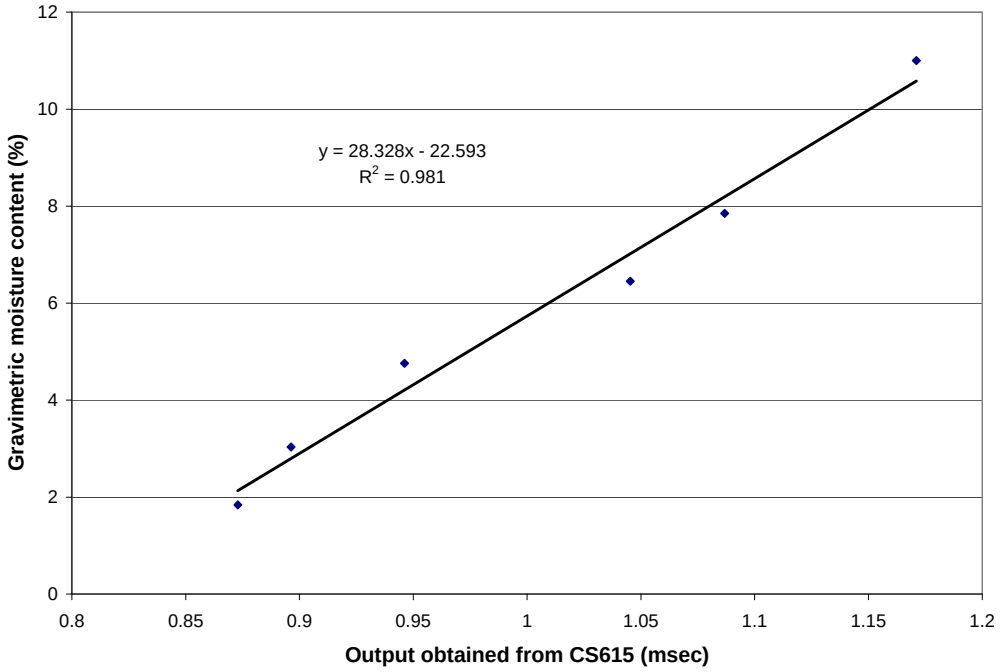

Figure 3.35 Calibration curve for subbase material at the ERC.

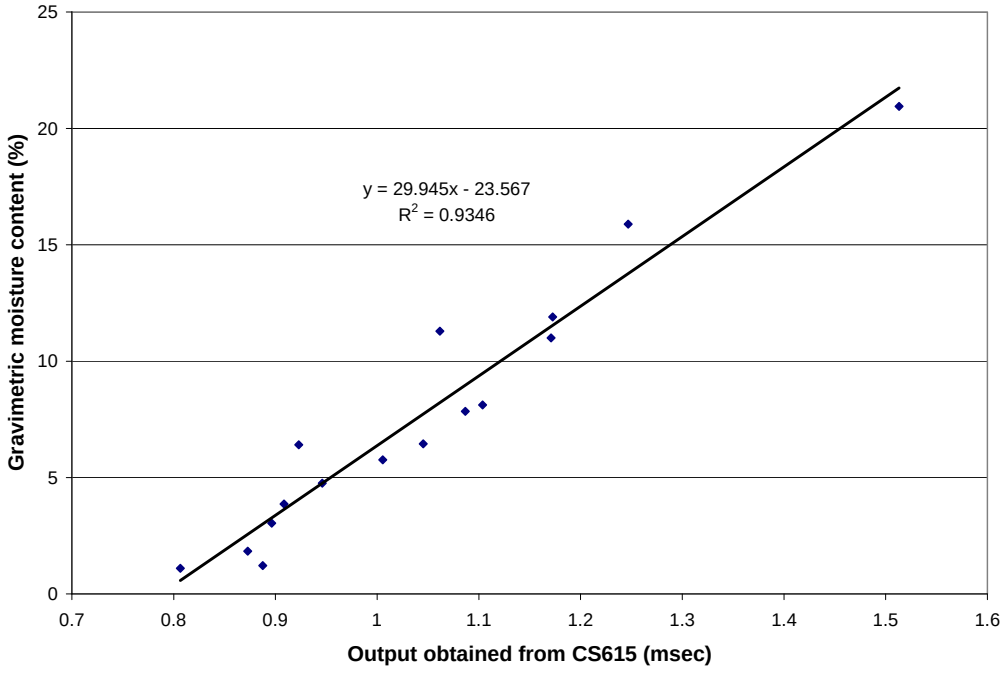

Figure 3.36 Calibration curve for subgrade soil at the ERC.

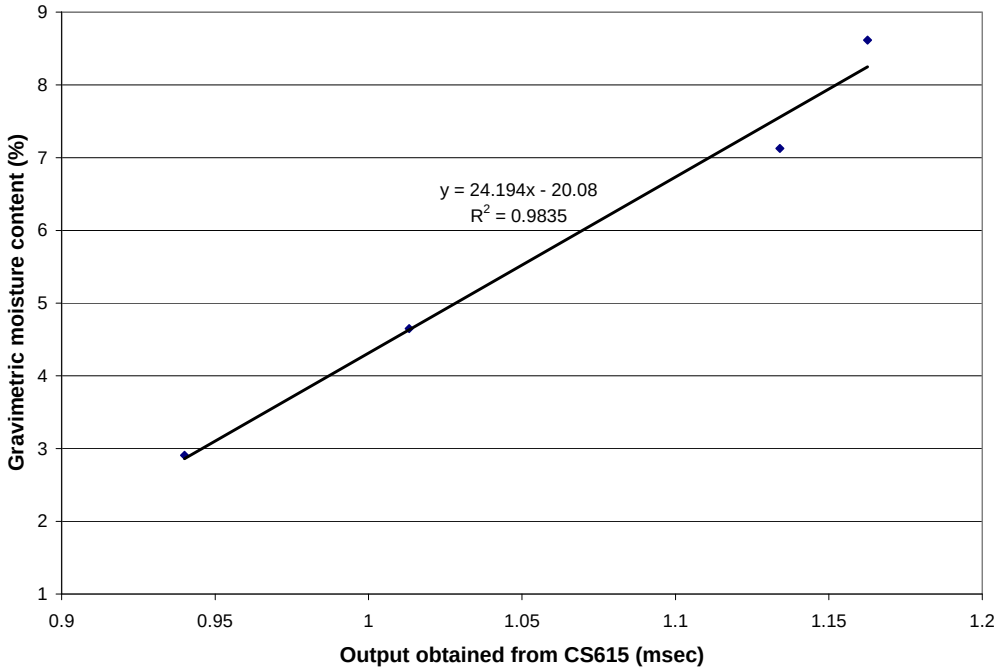

Figure 3.37 Calibration curve for base material at the field test site in Ft. Smith.

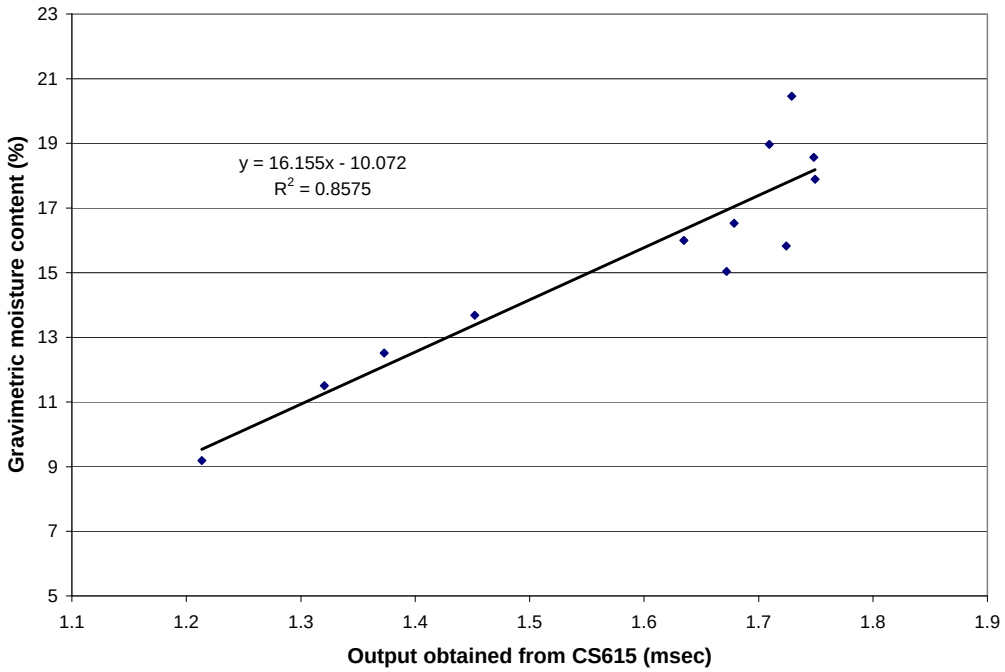

Figure 3.38 Calibration curve for subgrade soil at the field test site in Ft. Smith.

To investigate the effect of temperature on the output of the CS615 moisture probe, a concrete mold, which is the same as used in calibrations, was filled with the subgrade soil at certain water content and was compacted to 95 percent of standard Proctor maximum dry density. A CS615 moisture probe and a temperature sensor, which were connected to a datalogger, were inserted into the soil. The top of the concrete mold was then sealed using plastic wrap and tape to avoid the loss of moisture. The moisture content, obtained using calibration curves obtained previously, and temperature were recorded. The concrete mold with the soil and sensors remained at room temperature for one day to establish a baseline moisture content-probe output profile. The assembly was then placed in a refrigerator for a day then removed and monitored for another day. The temperature and moisture content of the soil were measured at 10 minutes intervals for the whole process. The results of this procedure are presented in Figure 3.39. It can be seen that moisture content increased a little bit at the beginning of the test which was probably the result of moisture redistribution to an equilibrium condition. Following this the moisture content appeared to change at the same trend as temperature. However, the apparent gravimetric moisture content of the soil changed by only 0.5 percent as the temperature decreased from 21 to 2.5 ^{o}C, which indicates the effect of temperature is relatively small. Therefore, temperature was not included in calibration curves for this project. It should be noted that moisture content dropped relatively significantly at time about 3800 minutes, which indicates that moisture was partially frozen at this time.

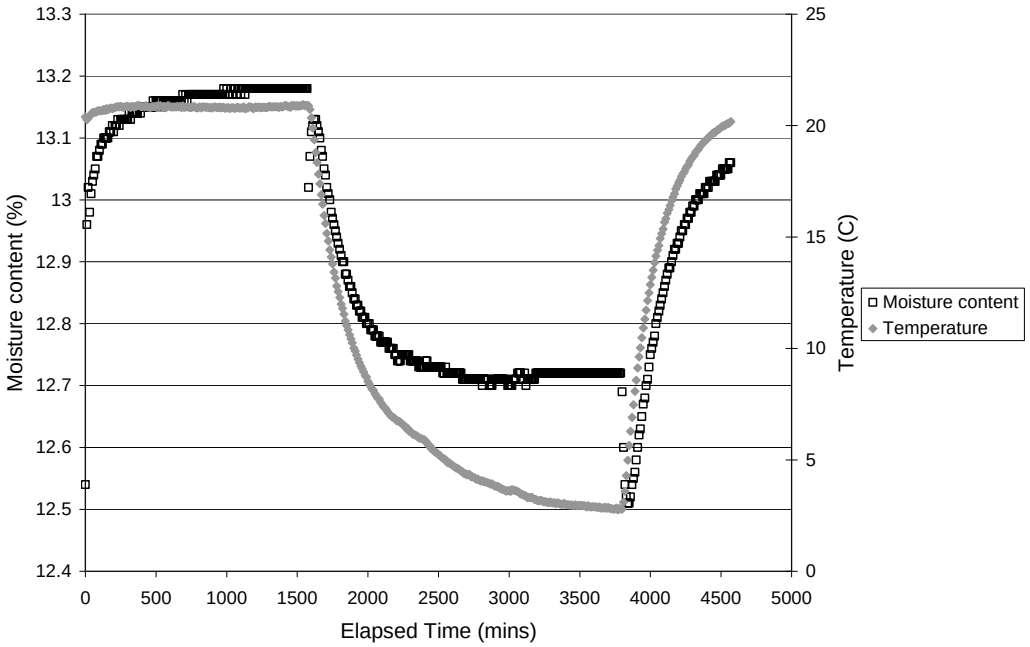

Figure 3.39 Effect of temperature on moisture content measurement.

3.4.3 Temperature probe

National Weather Service reports that the maximum and minimum air temperatures in Fayetteville are 43 degree C and -26 degree C, respectively, during 1971 to 2000. To measure air temperatures over this range, a model 107 temperature probe shown in Figure 3.40, manufactured by Campbell Scientific, Inc. was chosen. This probe uses a thermistor to measure temperature changes ranging from –35 to 50 degree C. The overall accuracy of this probe is ±0.4 ^{o}C over the range -24 ^{o}C to 48 ^{o}C and ±0.9 ^{o}C over the range -38 ^{o}C to 53 ^{o}C. It can be used for measuring air, soil and water temperatures. When used outdoors for air temperature measurement, the temperature probe was housed and protected by a radiation shield to prevent the effect of the radiation of the sunshine. The reported resolution is <±0.5 ^{o}C over the measurement range.

Figure 3.40 107 temperature probe.

3.4.4 TR-525USW Rainfall Sensor

TR-525USW Rainfall Sensor is manufactured by Texas Electronics, Inc. The rain gage consists of an open top 8 inches in diameter called collector, a funnel and a tipping bucket mechanism. The collector allows rainfall to fall into the rain gage. Collected water is then funneled to a tipping bucket, which tips when filled to a specific volume. A magnet attached to the tipping mechanism actuates a switch as the bucket tips and sends a pulse of energy to a data collector which records the pulse as a function of time. For TR-525USW rain gage, a tip was calibrated in the factory to be equal to 0.01 inch of precipitation falling over the area of the collector. The total precipitation can be obtained easily by multiplying the number of tips by 0.01 in inch. The rate of precipitation can be determined by associating the number of tips with time.

Figure 3.41 TR-525USW rainfall sensor.

3.4.5 Flow Measuring Devices

Before selection of an appropriate flow measuring device for surface runoff measurements, the maximum flow rate that may occur at the surface of test pads was estimated. Based on the 100-year maximum 5-minute precipitation density and surface areas of the test pads at the ERC, the maximum flow rate was estimated to be about 32 gallon per minute (GPM). A single flow measuring device cannot accurately measure water flows ranging from 0 to 32 GPM. Therefore, a combination of an H-flume and a tipping bucket rain gauge were selected to create the flow meter. The H-flume is designed to measure a rather large range of water flows. It has V shaped design, which allows a wide flow range to be measured. Good accuracy is obtained at low flow rates due to the small opening at the bottom of the V. The large open area at the top of the V results in a high capacity. The 0.4' HS-flume selected for this study can measure a water flow ranging from 0.07 to 36 GPM. For the water flows less than 0.07 GPM, a tipping bucket meter (TR-525USW Rainfall Sensor) was chosen, which can accurately measure water flows up to about 0.1 GPM.

Two 0.4’ HS flumes were fabricated by Mark Kuss, the Master Scientific Research Technician, in the Civil Engineering Department at the University of Arkansas. These devices are illustrated in Figure 3.42. The dimensions of the flume are illustrated in Figure 3.44. At the midpoint of the tapered cross-section, a stilling well is connected to the side wall of the flume. The stilling well receives water from the flume through a small hole drilled through the sidewall of the flume at the same elevation as the flume floor. A pressure transducer, manufactured by Honeywell International, Inc and shown in Figure 3.43, was used to measure the water level in the stilling well, The pressure transducer was housed inside of an electrical project box, which is glued on the flume as illustrated in Figure 3.42. A small vinyl tube was connected to the pressure transducer at one end and was inserted into the stilling well at the other end. When water enters into the stilling well, air in the vinyl tube will be compressed, which can be sensed by the pressure transducer. The recorded pressure can be then converted to a flow rate using a calibration equation.

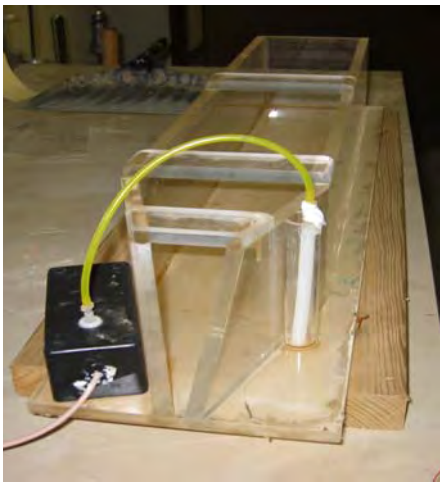

Figure 3.42 0.4’HS Flume.

Figure 3.43 Pressure transducer.

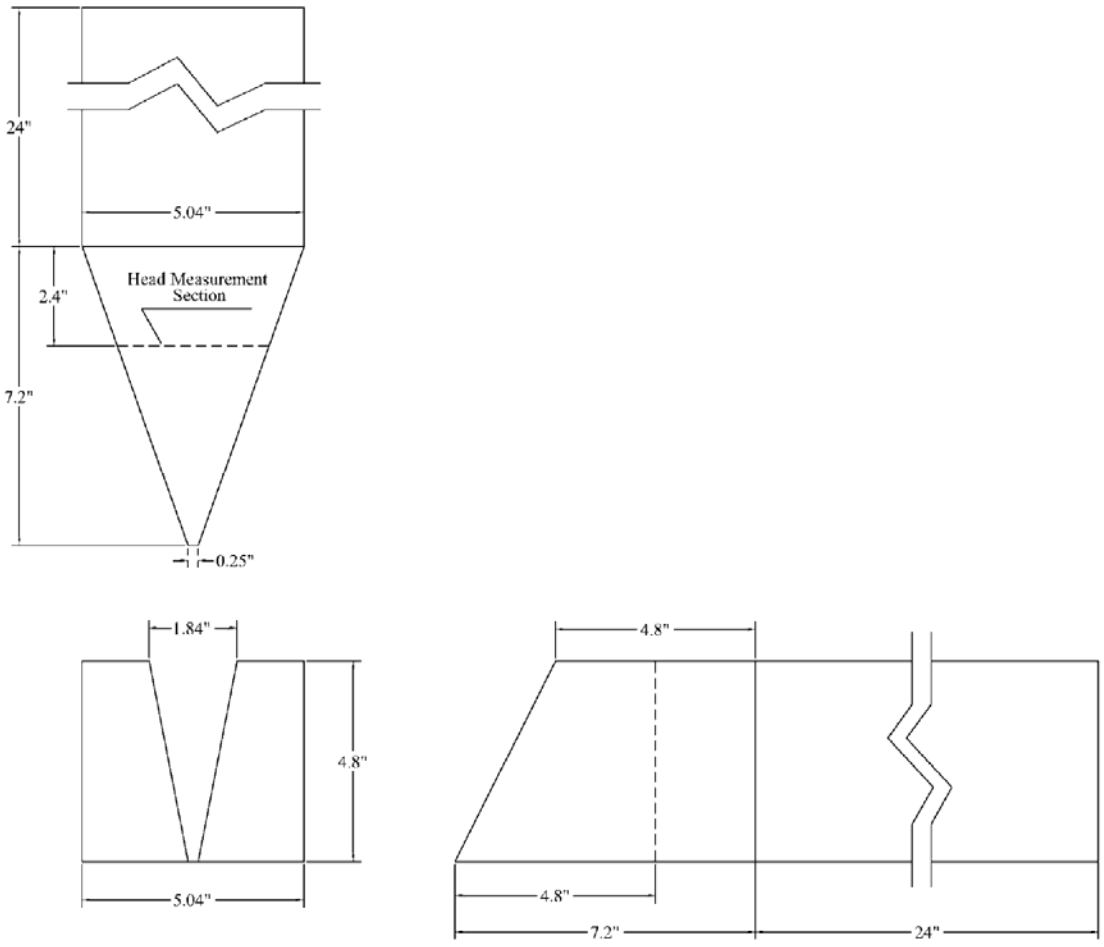

Figure 3.44 Dimensions of the 0.4’ HS-flume.

Both flumes and the tipping bucket flow meters were calibrated in laboratory. Calibrations were performed according to the following procedures:

1. Set the flume or tipping bucket flow meter on a flat surface;
2. Open a controllable water source, fix the water flow starting at a relatively small value as shown in Figure 3.45 and 3.46;
3. Obtain the water flow rate. A graduate cylinder or a five gallon bucket, depending on how large water flow is, is filled full with water and the time required for

filling is recorded. The water flow rate is obtained by dividing the volume of water by the time.

4. For the flume, record the reading of the pressure transducer when water surface within the flume is relatively constant at the established flow rate. For the tipping bucket flow meter, record tips in 5 minutes.
5. Increase the water flow and repeat steps 3-4.
6. Obtain calibration curves using the linear regression analysis.

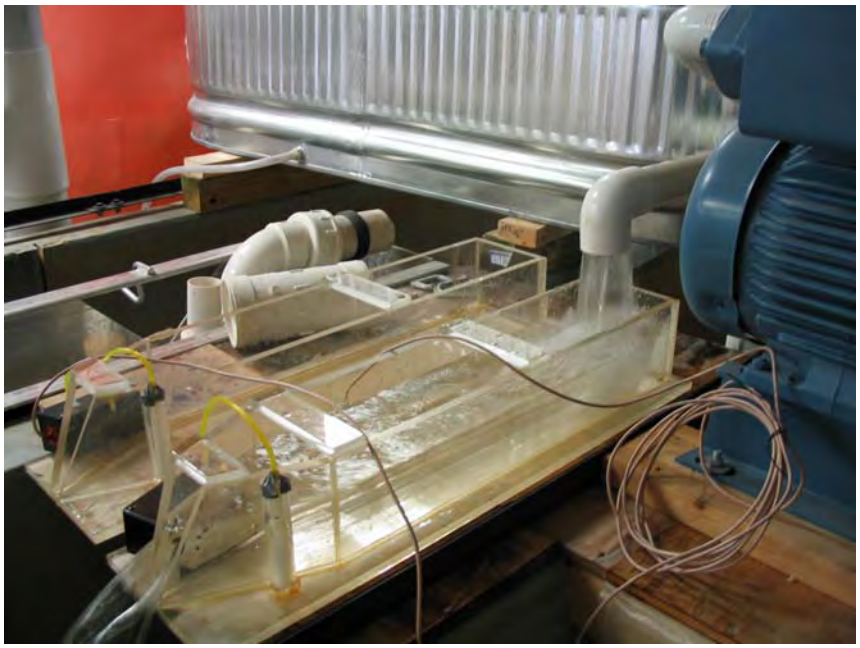

Figure 3.45 calibrating flumes with a big pump.

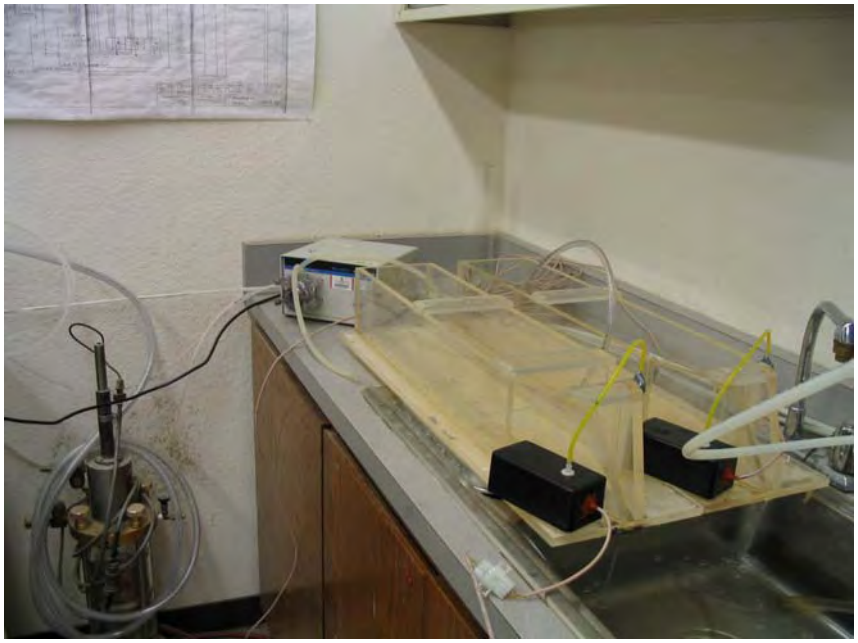

Figure 3.46 Calibrating flumes with a small pump.

Calibration curves for two flumes, referred as Flume A and Flume B, are shown in Figures 3.47 through 3.49. In the figures, voltage readings obtained from the pressure transducers are directly related to flow rates actually measured in the flumes. Flume A was used to measure surface water and was calibrated for both relatively small water flows and relatively large water flows. The reason to use two calibration curves for small water flows and large water flows is to get relatively good regression equations for both small water flows and large water flows, especially for small water flows, which occur much more often than large water flows. Flume B was used to measure subsurface water flows, which are relatively small. Flume B was therefore calibrated only for relatively small water flows up to about 2 GPM. The calibration curve for the tipping bucket flow meter is shown in Figure 3.50.

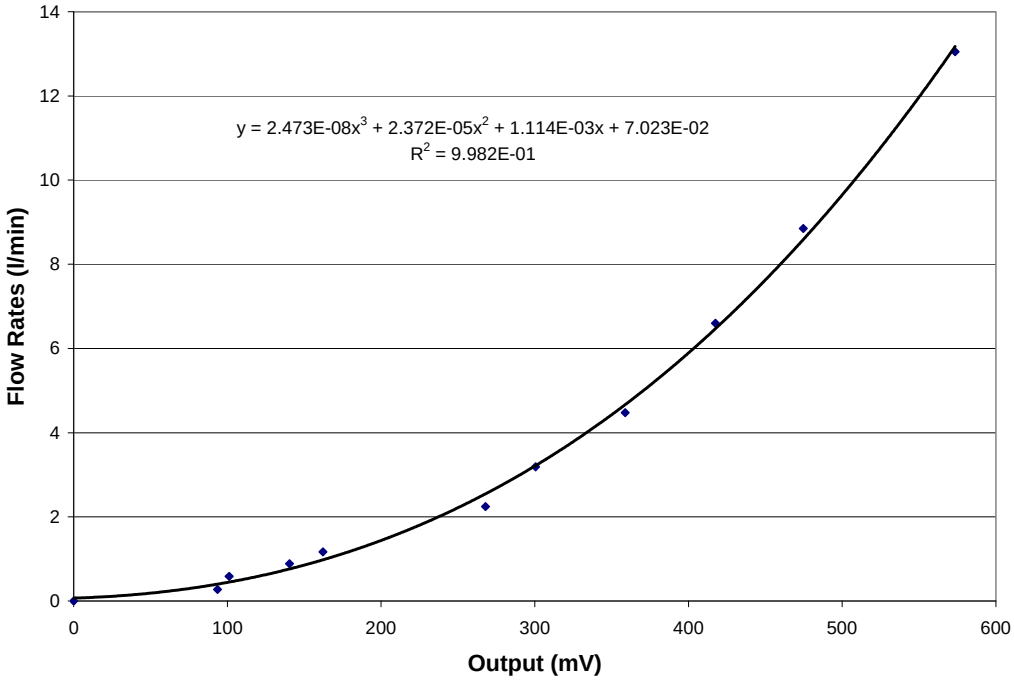

Figure 3.47 Calibration curve of the flume A (small flow part).

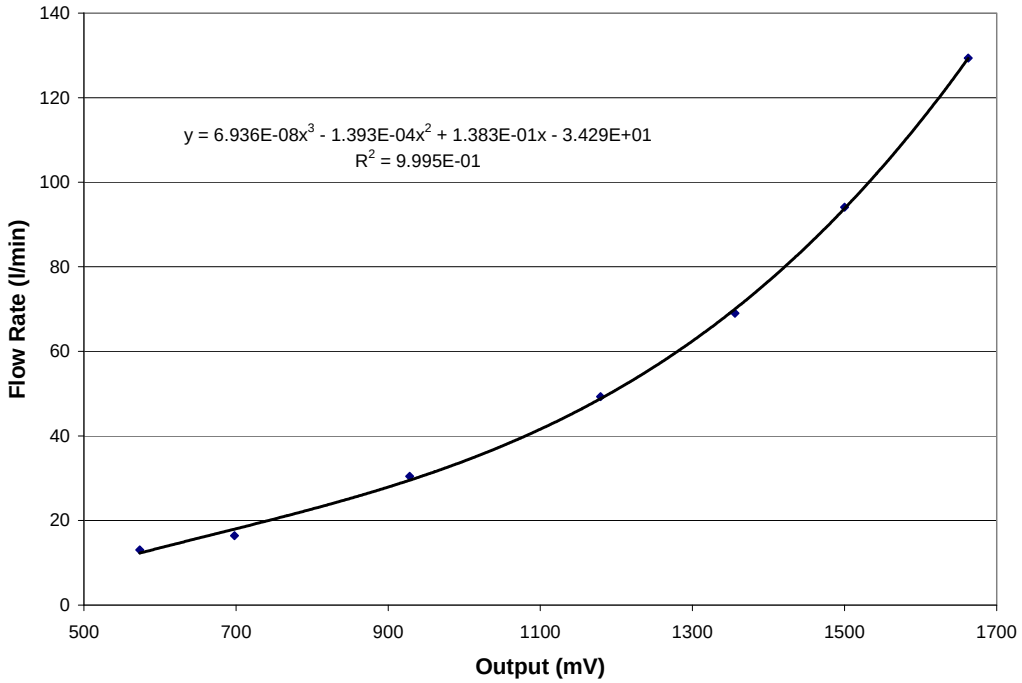

Figure 3.48 Calibration curve of the flume A (large flow part).

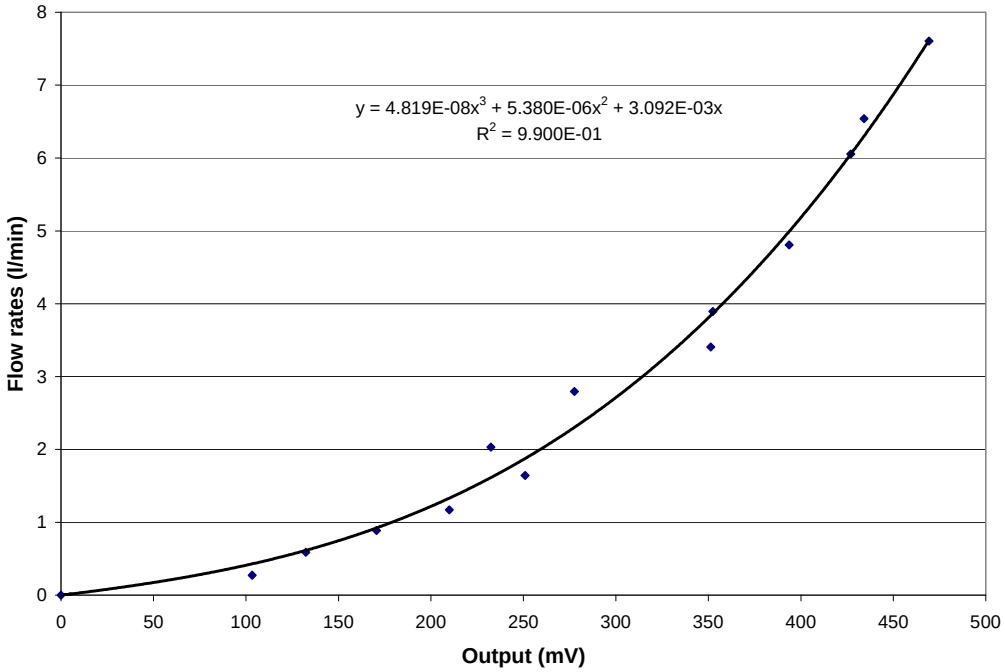

Figure 4.49 Calibration curve of the flume B for low flows.

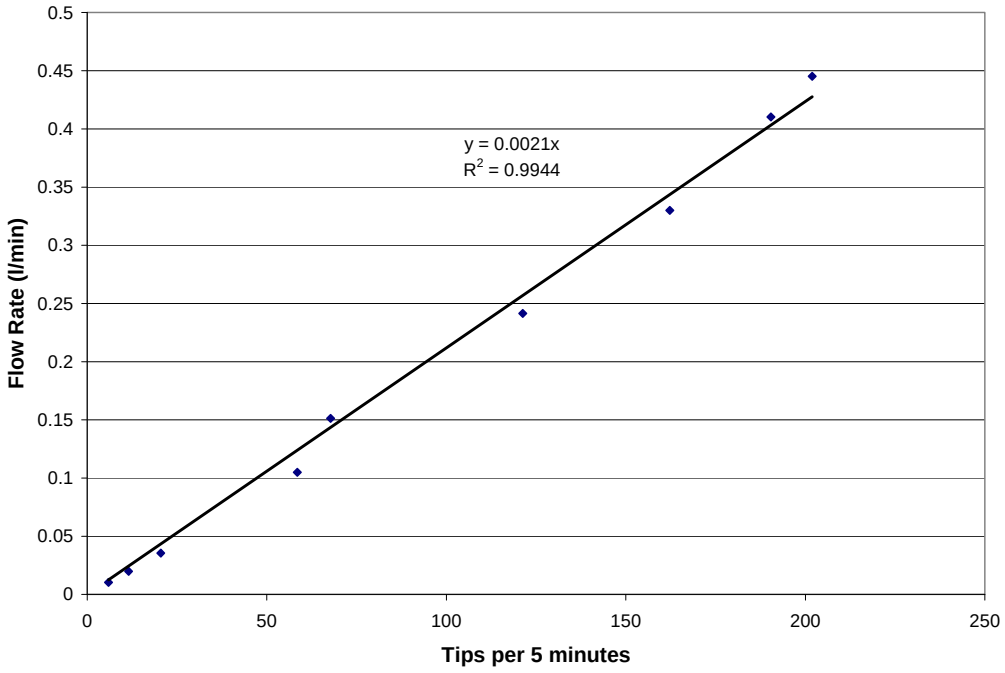

Figure 3.50 Calibration curve for the tipping bucket flow meter.

Since the maximum height of water in the flume is only about 5 inches, water head measurements in flumes require relatively high accuracy. The reported maximum pressure ranges that the pressure transducer can measure are from -10 to +10 inches of water. The reported accuracy is ± 0.5 percent span. Although the manual of the pressure transducer says that the pressure transducer is temperature compensated, it was checked to make sure that the possible effect of temperature can be ignored.

Figure 3.51 shows temperature changes over the course of a day and output of the pressure transducer for the same period. It can be seen that the output of the pressure transducer fluctuated between 2270 and 2275 mV as temperature changed by about 12^0C during the day. From the calibration equations obtained previously, a change of 5 mV in pressure transducer output is equal to a change of about 1 liter per minute in flow rates at the steepest curve location of calibration curves, which occur at the high flow rate end shown in Figure 3.36 from flow rates of 94 to 129 liters per minute. A change in temperatures from about 15^0C to 27^0C during the day only resulted in a change of maximum 1 percent in flow rates, which is relatively small and indicates that the effect of temperature can be ignored.

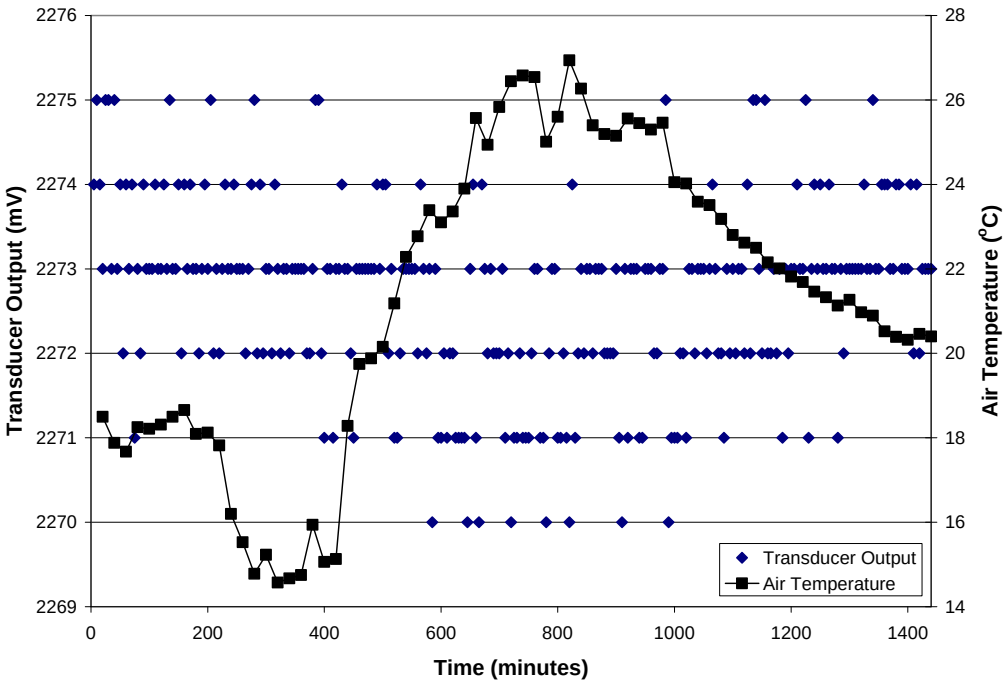

Figure 3.51 Output of Honeywell Model XCX pressure transducer and air temperature during a 24 hour period when not subjected to pressure.

3.4.6 Single Ring Infiltrometer

A single ring infiltrometer, using the principle of the Mariotte bottle to provide a reservoir of fluid at a constant head, was employed to measure the permeability of asphalt concrete. The principle of the infiltrometer is illustrated in Figure 3.52. The infiltrometer must first be sealed to the surface over which a measurement is to be made. In this study plumbers putty was used to seal the base of the infiltrometer to the pavement surface. To fill the infiltrometer, the vent tube is sealed and a vacuum is applied from an external source to the vacuum tube. Water is allowed to flow, under vacuum, into the infiltrometer through the inlet tube. For this study a 20 gallon tub was served as the water supply. Once the water level in the infiltrometer reaches a predetermined height,

the inlet and vacuum tubes are sealed. At this point the column of water inside the infiltrometer is being supported by the vacuum above it and no water can escape from the bottom of the infiltrometer and infiltrate into the pavement. To start an infiltration test, the bottom vent, or bubble, tube is adjusted to a specified level above the surface of the material being tested, the water level in the calibrated sight glass is recorded and the vent tube is unsealed. Once the vent tube is unsealed water can infiltrate the material below the infiltrometer. As water infiltrates into the material, air bubbles will enter the infiltrometer through the vent tube to reduce vacuum above the water column so the water head remains constant at the height established at the lower end of the vent tube, as illustrated in Figure 3.52. The volume of water infiltrating into the material below the infiltrometer can be determined by observing the change of the water level in the sight glass of the infiltrometer. The infiltration rate can be determined by plotting water volume change in the infiltrometer with time. The infiltrometer shown in Figure 3.53 was fabricated by Jeff Knox, a machinist at the ERC of the University of Arkansas.

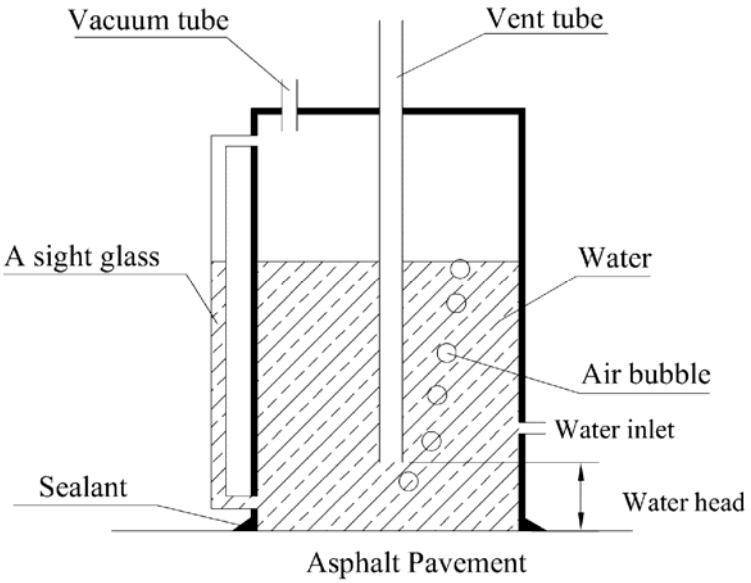

Figure 3.52 Schematic of the Mariotte bottle.

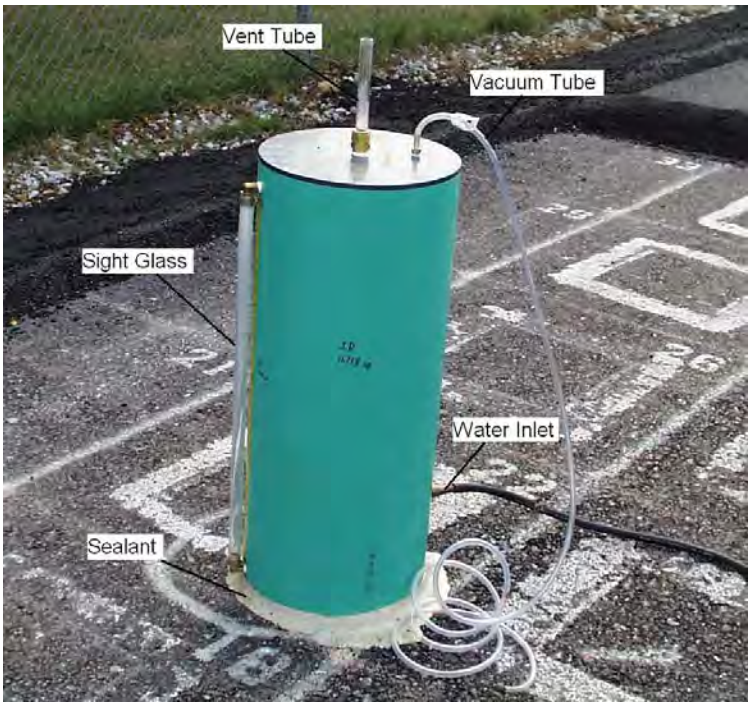

Figure 3.53 Mariotte bottle used for infiltration testing.

3.4.7 Piezometer

As discussed in the literature review, the ground water level may have an important impact on the moisture content of pavement systems. Piezometers are commonly used to measure the level of the ground water. A simple piezometer typically consists of a PVC pipe, with perforated slots at the bottom, inserted into a borehole as shown in Figure 3.54. The annulus between the PVC pipe and the borehole wall is filed with pea gravel or sand for a specified height above the perforations, while the space above the aggregate is sealed with a bentonite-cement grout to prevent any surface water from infiltrating into the borehole. As the ground water level fluctuates, the level of water inside the PVC pipe mirrors the movement. This water level can be monitored manually using a weighted porous line or dip stick or it can be monitored in an automated fashion using a pressure transducer. For the installations in this study a pressure

transducer was placed in the base of the piezometer tube to measure the water pressure, which was related to the position of the ground water table.

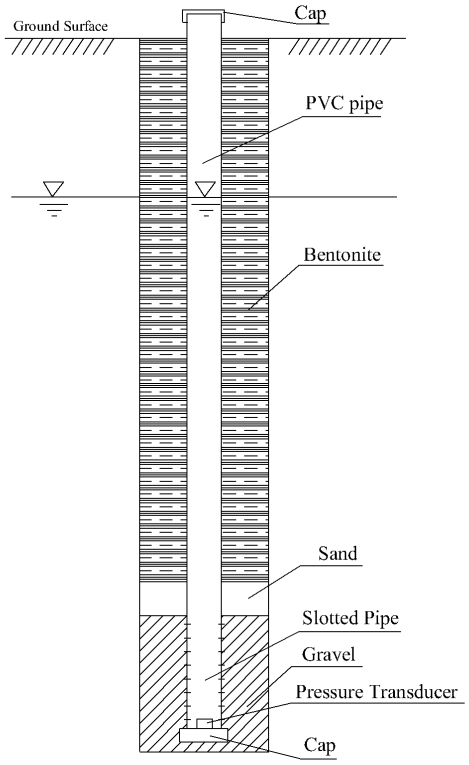

Figure 3.54 Schematic diagram of a typical piezometer.

An old pressure transducer, originally used for a big size H-flume, was borrowed in this study to measure the ground water level in the piezometer. There was no calibration equation for the pressure transducer. Therefore, the calibration was performed according to the following procedures.

1. Put the pressure transducer into a PVC pipe sealed at the bottom vertically;
2. Pour some water into the PVC pipe;
3. Record the height of water inside the PVC pipe;
4. Obtain several pressure transducer readings and average the readings;

5. Pour more water into the PVC pipe, and repeat steps 3 and 4;
6. Plot the output from the pressure transducer vs. water heads in the PVC pipe.

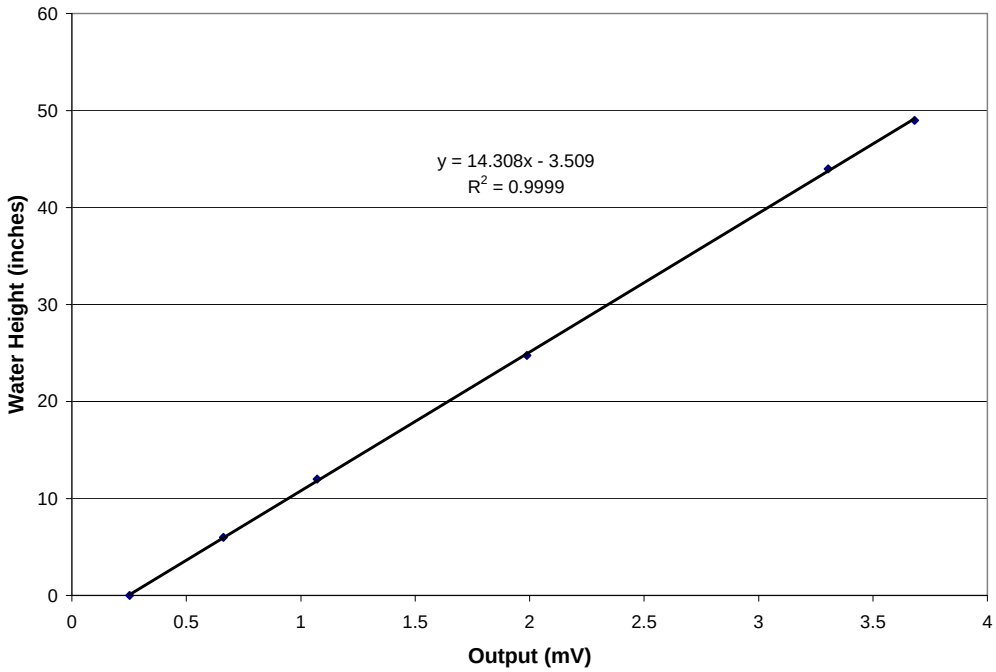

Figure 3.55 Calibration curve of the pressure transducer used in the piezometer.

3.5 Construction of test pads

To comprehensively measure responses of pavement systems to environmental factors, especially to precipitation, and to develop a migration pattern of water through pavement systems, two test pads, referred to as Pad A and Pad B, were built at the Engineering Research Center at the University of Arkansas during the summer of 2002. Each test pad is about 25 ft long and 12 ft wide. The cross-sectional structures of both test pads were essentially the same. The only difference was that the surface of test pad A consist of only a 75 mm binder course (25.0 mm aggregate) while test pad B has both the

75 mm layer of binder course (25.0 mm aggregate) and a 100mm layer of surface course (12.5 mm aggregate). The cross section of the test pad was shown in Figure 3.56.

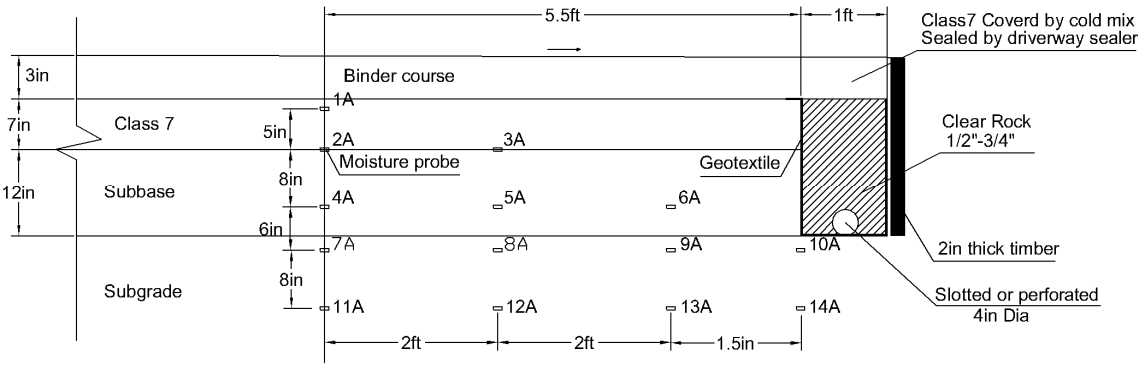

Figure 3.56 Pavement cross section at the ERC.

Before the construction of the test pads, a retaining wall that extended at least 250 mm above the pavement surface was built on the downhill side of the test pads as shown in Figure 3.57. There were two main reasons to build the retaining wall. One was to retain the pavement structure. Another reason was to facilitate the surface water measurement by forcing all the water to the designated locations coupled with berms. As illustrated in Figure 3.57, a geomembrane was placed against the retaining wall on the side of the pavement to make it waterproof.

Figure 3.57 Waterproof retaining wall.

In preparation for construction of the test pads the top 12 inches of subgrade soils were compacted to at least 95 percent of standard maximum Proctor dry density (AASHTO T-99, Method A). A trench was dug transversely to a depth of about 10 inches below the finished subgrade elevation in the middle of each test pad. Four moisture probes were then placed at the bottom of each trench. Sand was placed around the end of each probe at the location of the circuit board to void potential damage to the circuit board when the native soil was compacted around the sensor. Excavated soil was then spread back into the trench in loose lifts less than 8 inches and compacted to at least 95 percent of maximum Proctor dry density (AASHTO T-99, Method A) as illustrated in

Figure 3.58. The second layer of sensors was installed in the same way at a depth of about 2 inches below the finished subgrade elevation. Then approximately 12 inches of subbase course comprised of crushed limestone aggregate and about 7 inches of Class 7 aggregate base course were placed and compacted to at least 98 percent of maximum modified Proctor dry density (AASHTO T-180, Method D). The material properties of the subgrade soil, subbase and base courses, and the definition of Class 7 aggregate base were discussed previously in the “Material Properties” section of this chapter. Three layers of moisture probes were installed during the placement of subbase and base courses. In total, 14 moisture probes were installed in five layers for each test pad. The configuration of moisture probes in each test pad is essential the same and is illustrated in Figure 3.56.

Figure 3.58 Installing moisture probes in subgrade soils.

All the cables of moisture probes for each test pad were then gathered and routed through a PVC pipe which penetrated the waterproofed retaining wall to the multiplexer in an equipment enclosure as shown in Figures 3.59 To prevent the leakage of surface or subsurface water through the contact between the PVC pipe and the retaining wall, the PVC pipe was sealed around the contact using expanding polyurethane foam and silicone sealant. Also to prevent the possible migration of water through pavement systems from one test pad to another test pad, two test pads were separated by a piece of geomembrane, which extended from about 2 inches below the subgrade elevation to the bottom of asphalt concrete, as shown in Figure 3.60

Figure 3.59 Cables of moisture probes went through a PVC pipe, which penetrated through the waterproof retaining wall.

Figure 3.60 Surface of subbase course, a geomembrane separated the two test pads.

An edge drain was built right above the subgrade at the side of the retaining wall. The edge drain consisted of a 4-inch diameter rugged perforated pipe surrounded by about one foot wide clear rock, which was wrapped by geotextile to prevent fine materials from entering into the clean rock and clogging the edge drain. An elbow PVC pipe was connected to the edge drain through the retaining wall to a tipping bucket flow meter for measuring subsurface water as illustrated in Figure 3.61. The contact between the elbow PVC pipe and the retaining wall was sealed using expanding polyurethane foam and silicone sealant to prevent the leakage. Figure 3.62 shows the finished base course surface and edge drain before paving.

Figure 3.61 One end of a white PVC pipe was connected to the edge drain on the other side of the retaining wall (not shown in this picture), and the other end runs to a wooden box, where a tipping bucket rain gage would be installed.

Figure 3.62 Finished base course surface before paving, edge drain wrapped in a geotextile can be seen in the left upper corner.

Asphalt binder was then paved for both test pads and asphalt surface course was paved only for test pad B. Because of the presence of the retaining wall when paving, the asphalt concrete was paved up to about 12 inches away from the retain wall to avoid the potential damage to the retaining wall. Cold asphalt mixes were then placed and compacted manually between hot asphalt mixes and the retaining wall above the edge drain. A layer of driveway sealer was then applied over the cold asphalt mixes to prevent water from infiltrating into the edge drain directly from the surface of cold asphalt mixes.

To collect surface runoff during precipitation events, the surface of each test pad was constructed so that it sloped toward the northwest corner of the pad, where the surface water was channeled into through a PVC pipe which penetrated the waterproof retaining wall shown in Figure 3.63 and routed the runoff to a flume and a tipping bucket rain gauge at its outfall as shown in Figure 3.64. To avoid the influence of direct sunlight and direct rainfall on the accuracy of the measurements, the flume and tipping bucket rain gauge were housed under a steel sheet roof. As illustrated in Figure 3.65, the waterproof retaining wall extending at least 600 mm above the pavement surface on the downhill side of each pad and asphalt berms extending 100 mm above the pavement surface channel all of the water falling on each test pad during precipitation events to the flume and rain gauge.

Figure 3.63 A PVC pipe penetrated the waterproof retaining wall and sealed around the contact between the PVC pipe and the retaining wall to channel surface water to flow measuring devices in the other side of the retaining wall, shown in the next figure.

Figure 3.64 Combination of a HS flume and a tipping bucket flow meter.

Figure 3.65 Retaining wall and asphalt berms constructed to channel surface water to water flow measuring equipment.

A simple weather station, shown in Figure 3.66 including a temperature sensor and a tipping bucket rain gage, was built beside test pads to measure temperature and precipitation. A piezometer was also built beside the test pads to measure the groundwater level, which can significantly affect the moisture content of subgrade soils when it is relatively low (Ksaibati, et al. 2000, AI-Samahiji, et al. 2000 and Heydinger 2003).

Figure 3.66 A 107 temperature probe (left), housed in a radiation shield, and a TR-525USW rainfall sensor (right).

The data acquisition system described in the "Equipment Selection and Calibration" section of this chapter was installed and housed in a weather resistant enclosure. All the sensors were connected to the data acquisition system. A program was made to control the data acquisition system scanning, collecting and saving data from sensors at a predetermined time interval. The programs used at the ERC and the field test site in Fort Smith are presented in Appendix A.

3.6 Installation of field testing station

A field testing station was installed on Highway 253 near the intersection of Interstate 540 and Highway 253 in Fort Smith, Arkansas during March, 2005. Figure 3.67 shows the approximate location of the field test site. At the section of the field test site,

the pavement was about 74 feet wide and sloped transversely about 9 degrees downhill toward the east. Longitudinally, the pavement sloped downhill from the north to south. Figure 3.68 shows a picture taken from the south at the site.

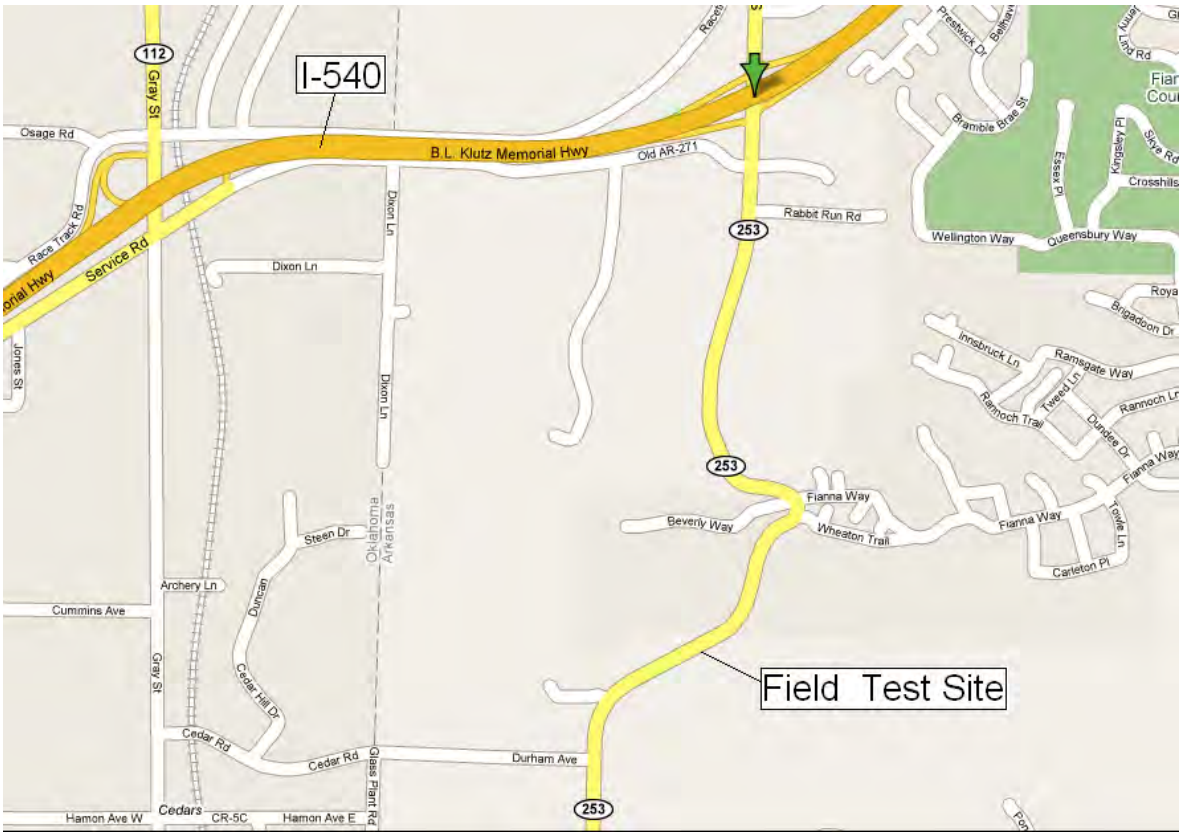

Figure 3.67 Vicinity map of the field test site in Fort Smith, Arkansas.

Figure 3.68 A site picture taken from the south to north.

The field test site was intended to replicate the test pads at the ERC. Almost the same equipment used for test pads at the ERC was employed for the field testing site including a simple weather station, a piezometer, moisture probes, temperature probes, flumes, tipping bucket flow meters and a data acquisition system.

The pavement section at the field test site consisted of about 8 to 10 inches of asphalt concrete over 3 to 5 inches of crushed stones base course. A trench was excavated transversely to a depth of 37 inches below the existing pavement surface as shown in Figure 3.70. Moisture probes and temperature probes were imbedded in the base and subgrade and the trench was then backfilled with excavated materials and compacted to at least 95 percent of maximum standard Proctor dry density for the subgrade soil and to at least 98 percent of maximum modified Proctor density for the base material. The

configuration of moisture probes and temperature probes in the base course and the subgrade soil is shown in Figure 3.69. The pavement section at the field test site did not have an edge drain installed when it was built originally. A 100-foot long edge drain was constructed along the inner edge of the shoulder to intercept subsurface flow. In an attempt to channel surface runoff to the flume and tipping bucket flow meter, 4 inch high asphalt berms on the outside edge of the shoulder and on the lower end of the 100-foot long pavement section was constructed to capture the water and direct it to a concrete channel which carried all the surface flow from the test area to the flow measuring devices as illustrated in Figure 3.71. A combination of a flume and tipping bucket rain gauge was used as a flow meter to measure both surface and subsurface water. Two sets of flumes and tipping bucket rain gauges were housed in a fiber-glass box with a cover as shown in Figure 3.72. A weather station, a data acquisition system and a piezometer were also built the same way as those at the ERC.

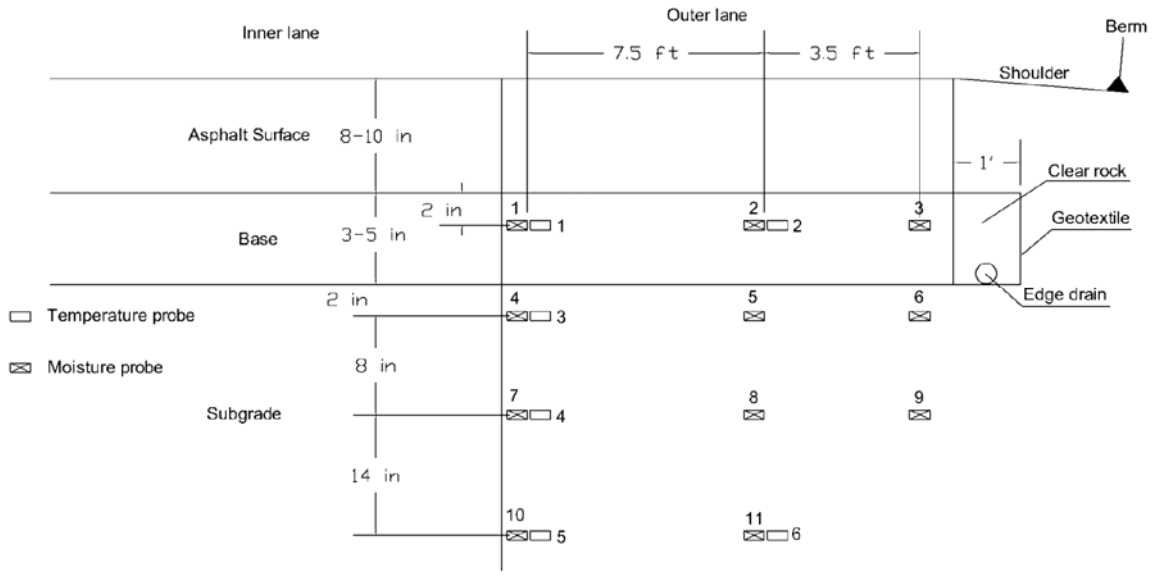

Figure 3.69 Configuration of moisture and temperature sensors at the field test site on Highway 253 in Fort Smith Arkansas.

Figure 3.70 Trench excavation for installing moisture and temperature probes at the field test site on Highway 253 in Fort Smith Arkansas.

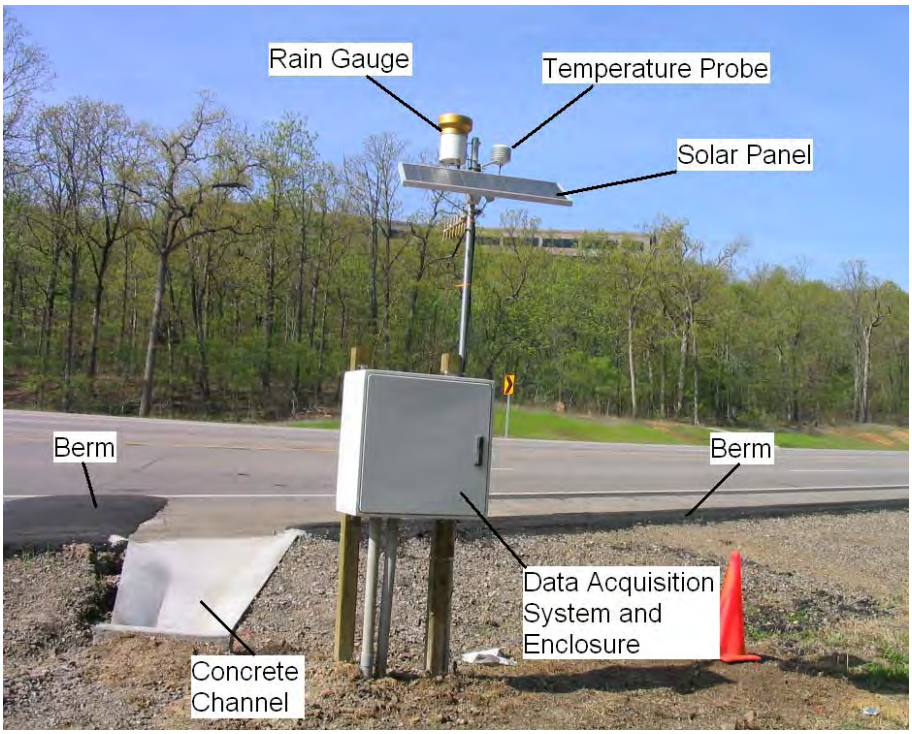

Figure 3.71 Asphalt berms and concrete channel, data acquisition system, solar panel and weather station.

Figure 3.72 Flumes and tipping bucket flowing meters housed in a fiber glass box.

Chapter 4 Results and Analyses

4.1 Introduction

All monitoring and physical measurements were performed at the test pads at the ERC of the University of Arkansas and at the 100-foot long field test site on Highway 253 in Fort Smith, Arkansas. The measurements primarily related to environmental factors, which include air temperatures, precipitation and groundwater levels, and the responses of the pavement systems, which include surface runoff, subsurface runoff, soil temperatures and moisture contents in the pavement systems. In this chapter, raw data are presented, statistical analyses are performed to obtain predictive models, and some conclusions are drawn.

4.2 Air Temperatures

4.2.1 Raw data

Obviously, air temperature is an important environmental factor that affects the temperature profile of pavement systems. Temperature in the pavement systems can then affect the pavement performance. For example, high temperatures in asphaltic concrete can decrease its stiffness resulting in more rutting and cracking. Temperatures below-freezing in the base aggregate and subgrade soils can create ice lenses in the base and subgrade soils, which may result in heaving of the pavements and potholes during thawing. As discussed more completely in the next chapter, air temperature is a required input for the Enhanced Integrated Climatic Model (EICM). For the above reasons air temperatures were measured at both the ERC and the Ft. Smith test sites.

Air temperatures at the ERC were recorded for more than 2 years from August, 2002 to December, 2004 using a Campbell Scientific Model 107 temperature probe. From August 21, 2002 to May 26, 2003, temperatures were recorded every 2 hours. From May 27, 2003 to August 20, 2003, temperatures were recorded every hour, and beginning on August 21, 2003, temperatures were recorded at 20 minute intervals. The frequency of measurements was adjusted mainly because of an addition of memory to the data logger. Daily average temperatures at the ERC were calculated and are plotted in Figure 4.1. In an effort to evaluate the variability of air temperatures between nearby NOAA weather stations and the ERC, daily average temperatures from the Drake Field Airport and Fayetteville/Springdale (Northwest Arkansas Regional Airport) weather stations are also plotted along with daily average temperatures obtained from the ERC in Figure 4.1.

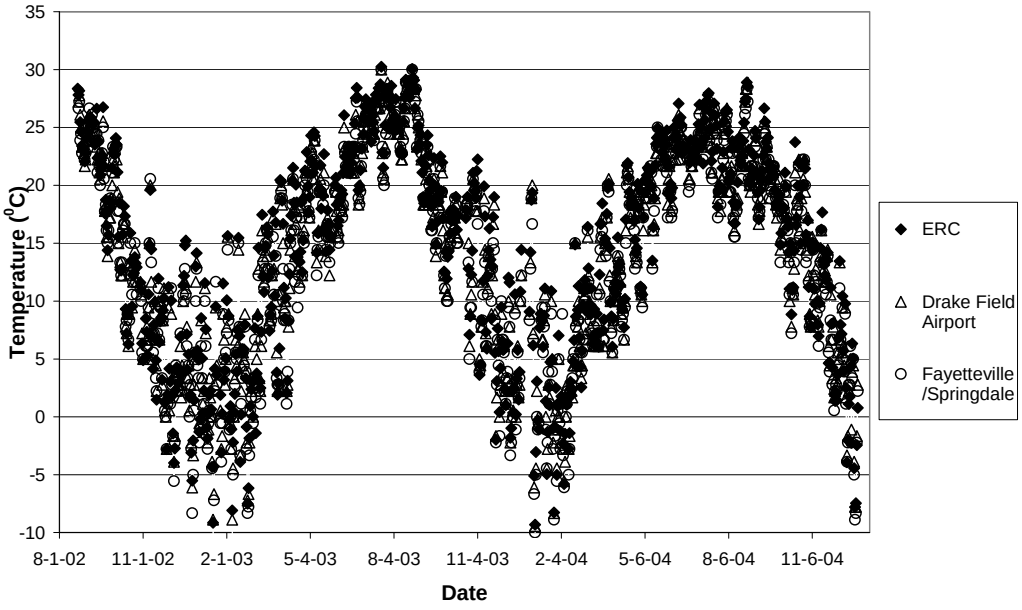

Figure 4.1 Daily average air temperatures at the ERC and obtained from two NOAA weather Stations.

Air temperatures at the Ft. Smith test site were recorded for approximately 15 months from March 2005 to June 2006 using the same model temperature probe as that used at the ERC. Temperatures were recorded every 20 minutes for the entire period. However, temperatures could not be collected from July 2005 to December 2005. The actual reason that the data logger would not record or store data from the temperature sensors is really unknown. While it is hypothesized that the connections between temperature probes and multiplexer became loose with time, the problem was not solved until the multiplexer was removed from the system and the sensor connections were made directly to the data logger. The missing air temperatures were supplemented by air temperatures obtained from the Fort Smith Municipal Airport NOAA Weather Station, which is located about 5 miles northeast of the Ft. Smith site. Because of the missing temperature data an effort was made to evaluate the consistency of air temperatures between the Fort Smith Municipal Airport weather station and the Ft. Smith test site. Therefore the daily average temperatures at the Ft. Smith test site are plotted along with daily average temperatures obtained from the Ft. Smith weather station for the entire reporting period in Figure 4.2.

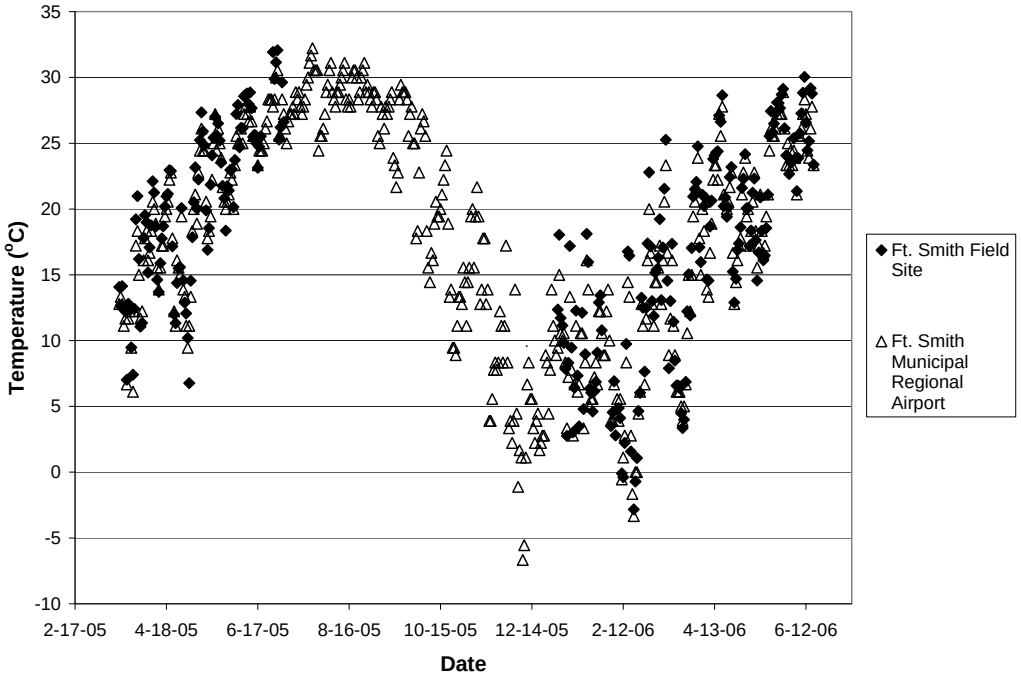

Figure 4.2 Daily average air temperatures measured at the Ft. Smith field site and obtained from the Fort Smith Municipal Airport NOAA Weather Station.

From Figure 4.1, it can be seen that daily average temperatures at the ERC ranged from about -10 ^{0}C in February to about 30 ^{0}C in July. From Figure 4.2, it can be seen that air temperatures at the Ft. Smith test site ranged from about -5 ^{0}C in January to about 33 ^{0}C in July. From Figures 4.1 and 4.2, it can also be visually concluded that air temperatures obtained from the two test sites and the nearby NOAA weather stations follow the same trends. However there appears to be scatter in the data. To substantiate whether or not the data sets are of the same population, t-tests were performed on the mean of differences between measured air temperatures at the two test sites and air temperatures obtained from the nearby NOAA weather stations. The results of the t-tests are presented in Table 4.1.

From the results of the t-tests, it can be concluded that measured air temperatures at the two test sites and air temperatures obtained from the nearby NOAA weather stations are from different populations at a significance level of 0.05. However, one can be 95 percent sure that the maximum difference between the measured air temperatures at the ERC and air temperatures obtained from Drake Field is only 2.5 degree Celsius, the maximum difference in temperature between the ERC and Northwest Arkansas Regional Airport is 3.0 degree Celsius, and the maximum difference in temperature between the Ft. Smith test site and Ft. Smith Regional Airport is 2.6 degree Celsius. Therefore, one can be 95 percent sure that differences between the measured air temperatures and air temperatures obtained from the nearby NOAA weather stations are within 3^0C. As will be discussed in the next chapter, a maximum 3.0^0C change in air temperature would result in an approximately 11 percent change in asphalt modulus. From a practical standpoint, a difference in air temperature of less than 3.0^0C is acceptable. On this basis, it is reasonable to conclude that air temperatures from the nearby NOAA weather stations can be used in the EICM with adequate accuracy.

To determine the temperature variability between the Northwest Arkansas and Ft. Smith areas, a t-test was performed on the mean of differences of daily average air temperatures between the northwest Arkansas area and the Ft. Smith area. Because measured air temperatures at the ERC and Ft. Smith test sites were for different time periods, the t-test was performed on the mean of differences of daily average air temperatures between the Drake Field Airport and Ft. Smith Regional Airport weather stations. The results of the t test are presented in Table 4.1.From the results of the t test, one can be 95 percent sure that the maximum difference in temperature between the

Drake Field Airport and Ft. Smith Regional Airport is 5.3 degree Celsius. As will be discussed in the next chapter, a difference of up to 5.3 degrees Celsius would cause an approximately 30 percent change in asphalt modulus. On this basis, it can be reasonable to say that air temperatures from weather stations located about 75 miles away from a site can not be used in the EICM with adequate accuracy. More specifically, air temperature from the Northwest Arkansas area should not be used in the EICM for a site in the River Valley area or vice versa.

Table 4.1 Results of t-tests on daily average temperatures.

	ERC-Drake	ERC-XNA	Field-FSM	Drake-FSM
Null hypothesis H_0	$\mu_d=0$	$\mu_d=0$	$\mu_d=0$	$\mu_d=0$
Level of significance	0.05	0.05	0.05	0.05
Sample Size	815	815	264	357
Sample mean (mean of sample difference)	0.49	0.73	0.50	2.57
Sample standard deviation	1.008	1.170	1.081	1.393
t test statistic	13.86	17.88	7.59	34.85
$t_{0.025,n-1}$	1.96	1.96	1.97	1.97
95% Confidence Interval	0.49±0.07	0.73±0.08	0.50±0.13	2.57±0.15

Where:

ERC-Drake = t-test on the mean of differences between measured air temperatures at the ERC and air temperatures obtained from the Drake Field Airport weather station;

ERC-XNA = t-test on the mean of differences between measured air temperatures at the ERC and air temperatures obtained from the Northwest Arkansas Regional Airport weather station;

Field-FSM = t-test between on the mean of differences between measured air temperatures at the field site and air temperatures obtained from the Ft. Smith Regional Airport weather station;

Drake-FSM = t-test on the mean of differences between air temperatures obtained from the Drake Field Airport weather station and the Ft. Smith Regional Airport weather station;

μ_d = temperature differences between two t-test populations at the same day;

Level of significance = the maximum acceptable probability of rejecting a true null hypothesis. The significance level is usually chosen to be 0.05;

t test statistic = this value is used to decide whether or not the null hypothesis should be rejected in the t test. If this value is less than the value at a select level of significance, the null hypothesis could not be rejected at the selected level of significance. Otherwise, the null hypothesis should be rejected;

$t_{0.025,n-1}$ = a critical value for the t test to which the value of the test statistic is compared to determine whether or not the null hypothesis is rejected;

Confidence interval = a confidence interval is to identify the range for an interval estimate of a parameter at a selected level of confidence. The level of confidence is usually chosen to be 95 percent.

4.2.2 Air Temperature Predictive Models

From the plots of daily average temperature data at both the ERC and the Ft. Smith test sites, it can be seen that daily average temperatures change with season following a periodic function. In an effort to model the periodic nature of temperature changes and to catch extreme daily average temperatures, a Fourier series shown in Equation 4.1 was used to model the measured temperature data. Considering a leap year

every four years, a model year was assumed to have an average of 365.25 days, as shown in Equation 4.1.

$$T = a_0 + \sum_{n=1}^{N} (a_n \cos(\frac{n\pi t}{365.25}) + b_n \sin(\frac{n\pi t}{365.25})) \qquad 4.1$$

Where

T = daily average temperatures (^{0}C);

t = serial date in MS-Excel date-time code;

a_0, a_n, b_n = fitting parameters to be obtained from a regression analysis of the data.

The first few terms of a Fourier series often are a pretty good approximation to the whole function. Therefore, to simplify the model used to predict air temperatures, only the first two terms of the Fourier series were used. As a result, the model can be written as Equation 4.2.

$$T = a_0 + a_1 \cos(\frac{\pi t}{365.25}) + b_1 \sin(\frac{\pi t}{365.25}) + a_2 \cos(\frac{2\pi t}{365.25}) + b_2 \sin(\frac{2\pi t}{365.25}) \qquad 4.2$$

The goal of the regression analysis is to find appropriate parameters of a_0, a_1, b_1, a_2, b_2, that satisfy the criterion of least squares. Because extreme daily average temperatures have a significant effect on asphalt modulus, it was important not to eliminate the extremes in any model that was created to predict temperature. In an effort to catch extreme temperatures in the model, weights were assigned to each of the measured temperatures so that extreme temperatures were assigned higher weights and median temperatures received lower weights. The weighting factors used in the analyses were the cubes of the absolute values of measured daily average temperatures minus the average of the measured daily average temperatures. The regression analysis process is illustrated in Equations 4.3 and 4.4.

$$W = (abs(T_m - Mean(T_m))^3 \quad 4.3$$

$$Min_{a_0,a_n,b_n} \left\| T_m - a_0 - \sum_{n=1}^{2} (a_n \cos(\frac{n\pi t}{365.25}) + b_n \sin(\frac{n\pi t}{365.25})) \right\|^2 \times W \quad 4.4$$

Where,

W = weight;

T_m = measured daily average air temperature.

Equation 4.3 illustrates the method to calculate the weights. Then the fitting parameters a_0, a_1, b_1, a_2, b_2 can be determined by minimizing Equation 4.4. Matlab® software was employed to perform the analyses.

The coefficients resulting from regression analyses on the daily average temperatures collected from the ERC and Ft. Smith test sites are presented in Table 4.2. Figures 4.3 and 4.4 present the measured daily average temperature data and predicted temperatures using the predictive models.

Table 2: Summary of Regression Coefficients from the Analyses of Daily Average Air Temperatures for the ERC and Ft. Smith test sites.

Site	a_0	a_1	b_1	a_2	b_2
ERC	12.53	0.55	0.23	-14.88	-5.38
Ft. Smith	14.74	1.35	0.65	-15.92	-4.08

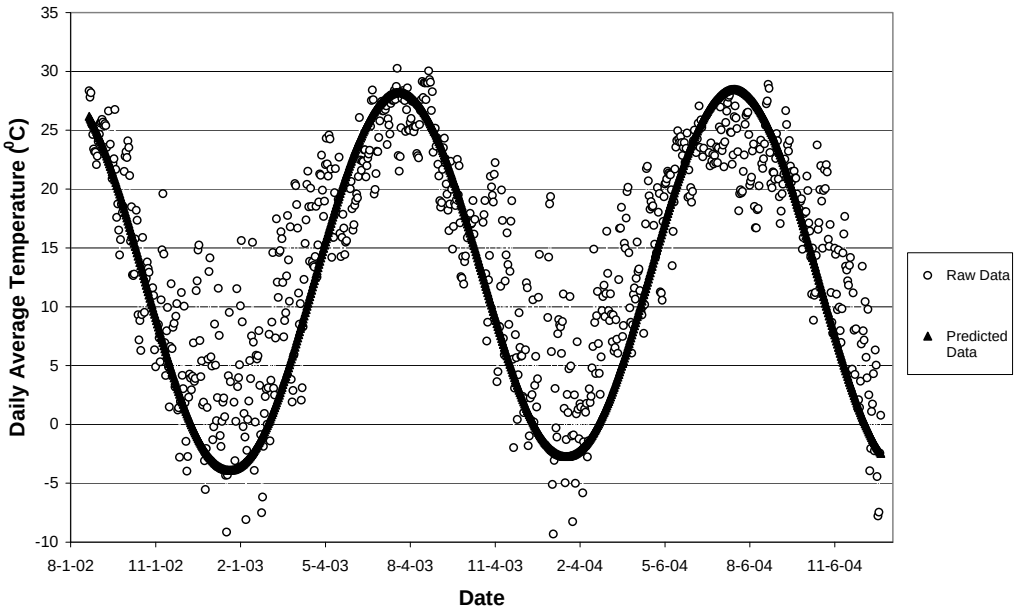

Figure 4.3 Comparison of predicted daily average air temperatures to measured average daily air temperatures at the ERC, using the proposed prediction model.

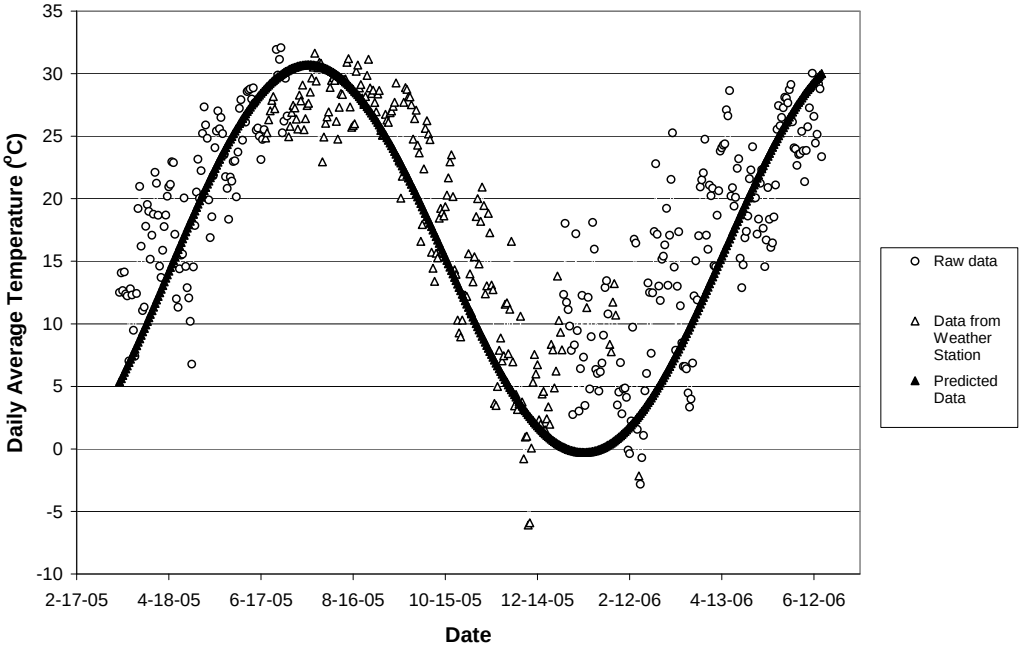

Figure 4.4 Comparison of predicted daily average air temperatures to measured average daily air temperatures at the Ft. Smith site, using the proposed prediction model.

4.3 Temperatures in Pavement System

As discussed in the previous section, the temperature profile in pavement systems has an important effect on pavement performance. In addition, one of the outputs of the EICM is the temperature profile through the pavement system. To evaluate the accuracy of the EICM in Arkansas, soil temperatures in a pavement system must be measured and compared with values predicted using the EICM.

Pavement temperatures were not measured at the ERC because there was originally no intention of investigating the applicability of the EICM in Arkansas during this study. However, during the data collection efforts at the ERC it was discovered that a portion of the base material was partially or fully frozen based on sudden drops in the moisture content indicated by the TDR probes. Unfortunately, there was no independent measure of temperature in the base material to verify this assumption from the TDR measurements. As a result it was decided that the temperatures in the pavement system at the Ft. Smith test site would be measured with temperature probes to verify the results of the TDR probes and to possibly identify the depth of frost penetration. Temperatures in the base and subgrade materials were measured with a Model 108 temperature probe from Campbell Scientific, but temperatures in the asphalt were not measured. Even though the temperature of the asphalt layer is far more important for its material properties than it is for unbound materials, the intent of temperature measurements was only to determine the depth of frost penetration. Additionally, the maximum survival temperature for the temperature probes used in this study was only 100 ^{0}C, which is lower than the placement temperature of the hot-mix asphalt concrete. In retrospect it

would have been better to select a temperature probe with a higher survival temperature so that one or more could have been embedded in the asphalt layer.

Soil temperatures at different depths were measured and recorded at the Ft. Smith test site using the Model 108 temperature probes. Two temperature probes were installed in the base material approximately 2 inches below the surface of the base material. Three layers of temperature probes were installed in the underlying subgrade soil at depths of approximately 2 inches, 10 inches and 24 inches below the subgrade surface. The detailed layout of temperature probes can be found in Figure 3.52 in Chapter 3.

The data in Figures 4.5 to 4.8 reveal that the same periodic nature as the air temperature. So the same regression analyses that were performed on air temperatures were also carried out for soil temperatures to produce the predictive equations. The results of the analyses are presented in Table 4.3. A comparison of the measured data and values developed using the proposed predictive models are also plotted in Figures 4.5 through 4.8.

From Figure 4.5, it can be seen that the maximum predicted temperature in the base material is about 43 degrees Celsius, while the minimum predicted temperature in the base material is about 9 degrees Celsius. From Figure 4.6, it can be seen the maximum predicted temperature in the subgrade soils at a depth of about 2 inches below the subgrade surface is about 42 degrees Celsius, while the minimum predicted temperature is about 9.5 degrees Celsius. From Figure 4.7, it can be seen the maximum predicted temperature in the subgrade soils at a depth of about 10 inches below the subgrade surface is about 39 degrees Celsius, while the minimum predicted temperature is about 11 degrees Celsius. From Figure 4.8, it can be seen the maximum predicted

temperature in the subgrade soils at a depth of about 24 inches below the subgrade surface is about 37 degrees Celsius, while the minimum predicted temperature is about 12.5 degrees Celsius. The maximum temperatures in the pavement system may seem high. However, the same temperature probes were used for soil temperature measurements as for air temperature measurements, and measured air temperatures have a pretty good agreement with those obtained from the nearby NOAA weather stations as discussed previously in this chapter.

Table 4.3 Summary of Regression Coefficients from the Analyses on soil temperatures at the field test site in Fort Smith.

Location	a_0	a_1	b_1	a_2	b_2
Base Layer	27.92	-2.23	1.69	-13.47	-11.15
Subgrade -2”	27.60	-1.87	1.80	-12.94	-10.63
Subgrade-10”	25.88	-0.51	1.11	-11.39	-8.77
Subgrade-24”	25.22	-0.37	0.72	-9.92	-7.75

.

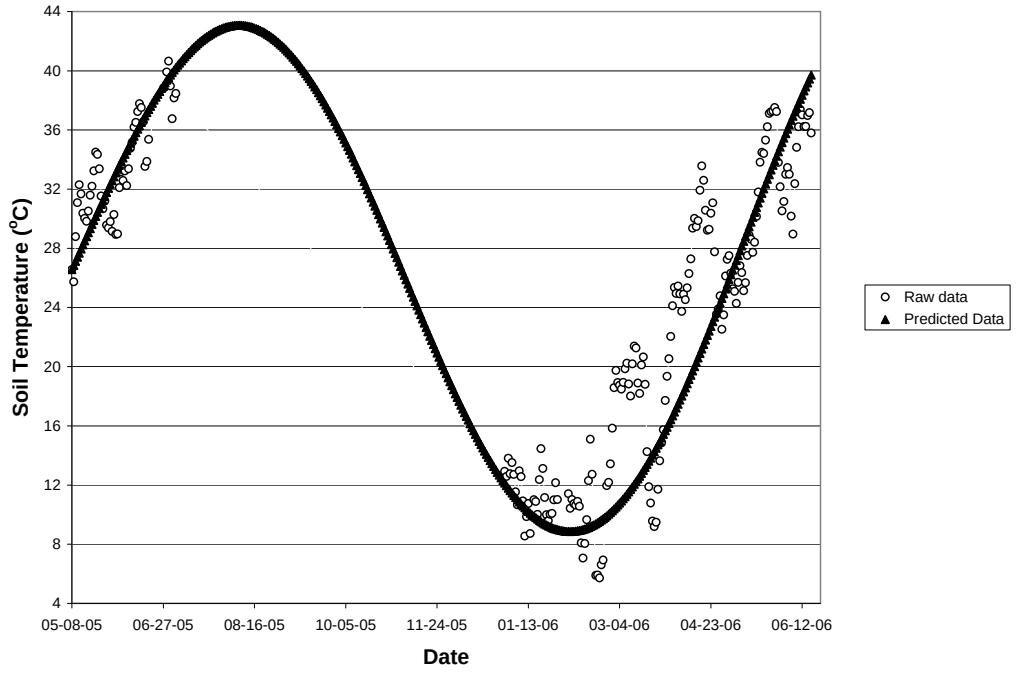

Figure 4.5 Temperature variations in the base material at the Ft. Smith site for a depth of 2 inches below the base surface.

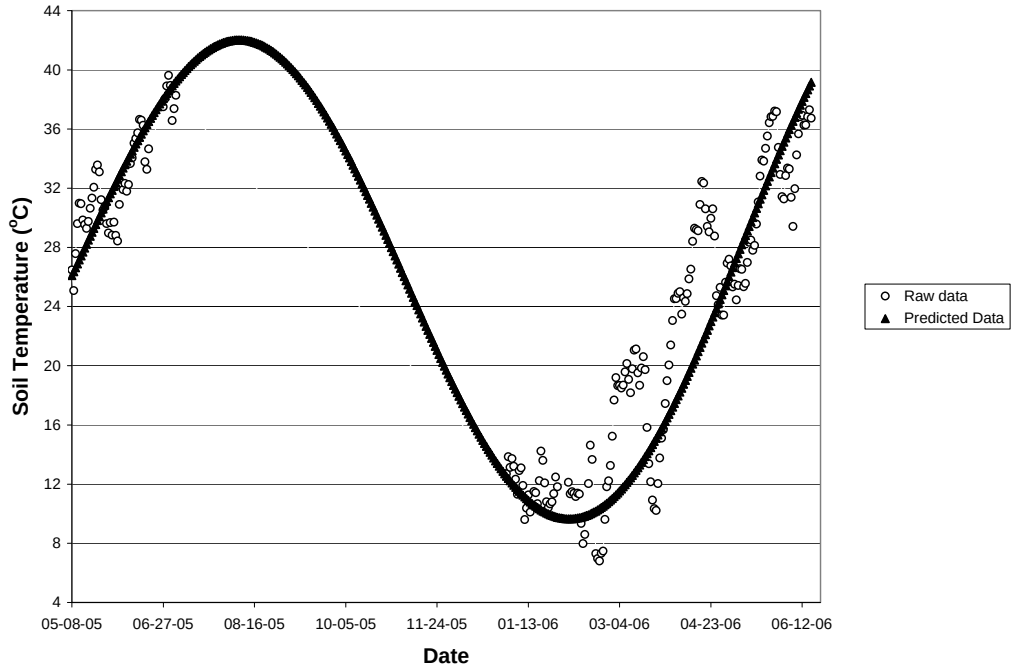

Figure 4.6 Temperature variations in the subgrade soil at the Ft. Smith site for a depth of 2 inches below the subgrade surface.

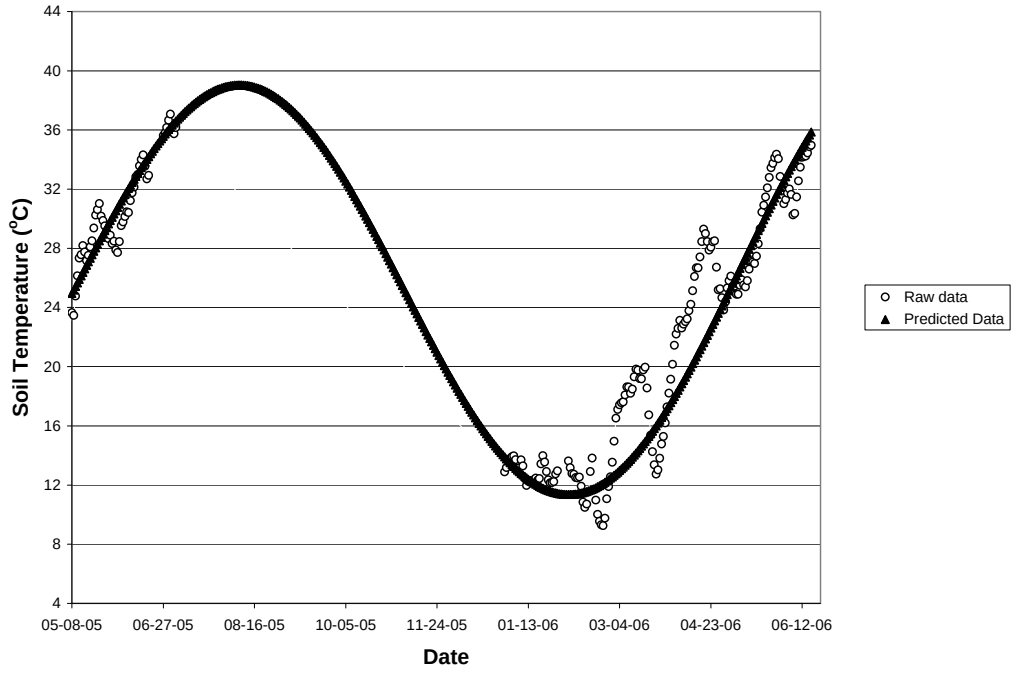

Figure 4.7 Temperature variations in the subgrade soil at the Ft. Smith site for a depth of 10 inches below the subgrade surface.

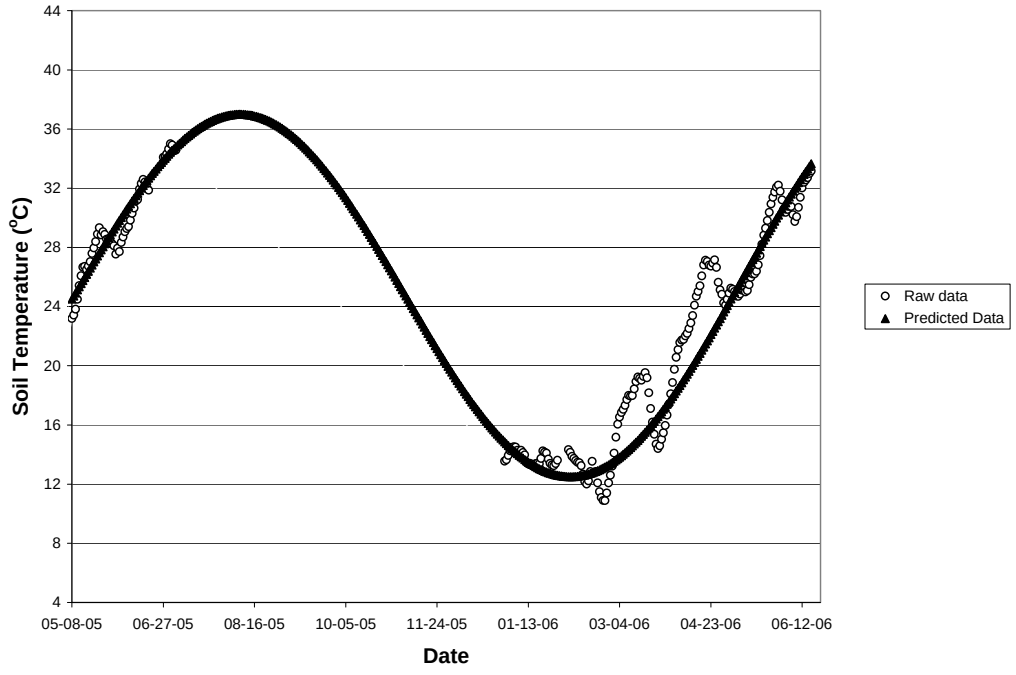

Figure 4.8 Temperature variations in the subgrade soil at the Ft. Smith site for a depth of 24 inches below the subgrade surface.

To visually investigate temperature changes with depths in the pavement at the Ft. Smith test site, two temperature profiles are plotted in Figures 4.9 and 4.10. Figure 4.9 was plotted for a relatively high air temperature on June 30, 2005, while Figure 4.10 was plotted for a relatively low air temperature on February 19, 2006. In both figures, the X-axis represents the temperature in degrees Celsius and the Y-axis represents the depth from the surface of the pavement. Because asphalt temperature was not measured at the Ft. Smith test site, predicted asphalt surface temperatures using the EICM were used in Figure 4.9 and 4.10. Air temperature was 35.8 ^{o}C on June 30, 2005 and was -2.2 ^{o}C on February 19, 2006. From Figure 4.9, it can be concluded that temperatures in the pavement system decrease with depth in the summer and predicted asphalt surface temperature is as much as 17.8 ^{o}C higher than air temperature. From Figure 4.10 it can be seen that temperatures increase with depth in the pavement system during the winter months and predicted asphalt surface temperature is about 4.5 ^{o}C higher than air temperature. It is believed that these conclusions are reasonable. Temperatures at shallower depths in pavement systems are more affected by air temperature, while temperatures at deeper depths are less affected by air temperature.

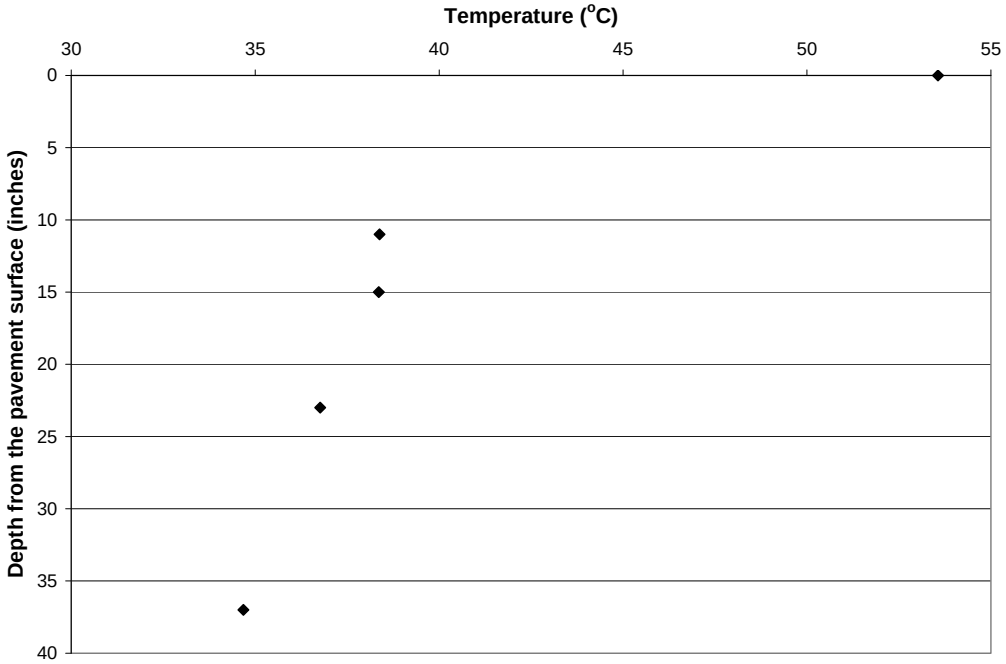

Figure 4.9 Temperature profile of the pavement system at the Ft. Smith test site at June 30, 2005.

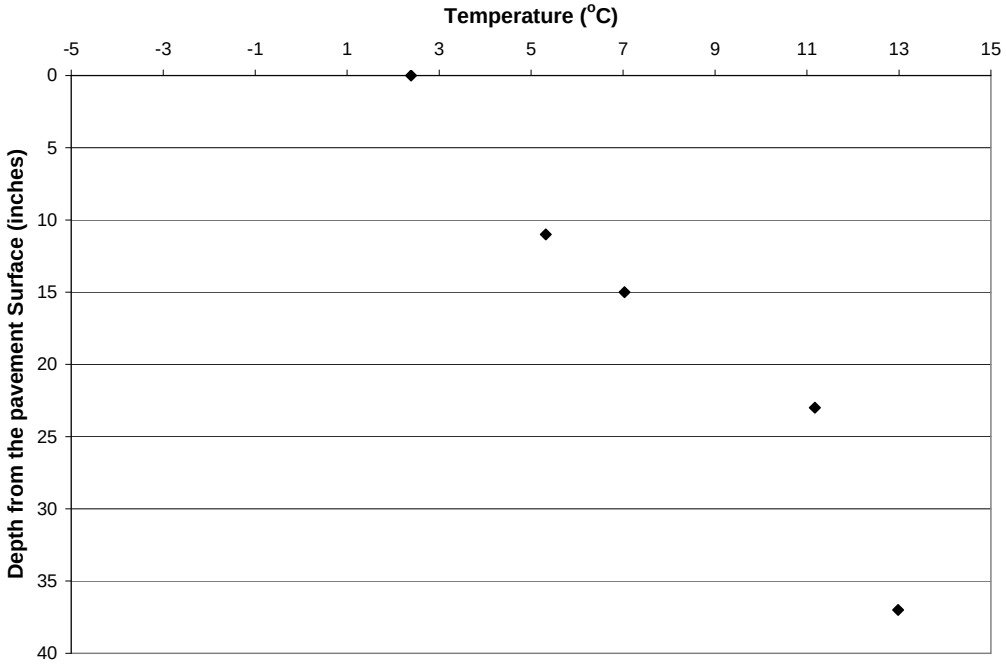

Figure 4.10 Temperature profile of the pavement system at the Ft. Smith test site at February 19, 2006.

4.4 Precipitation Events

4.4.1 Introduction

Hall and Rao (1999) stated that "the effect of precipitation on measured or observed subgrade moisture content is not well defined. While some studies (Low 1959, Bandyopadhyay 1983, and Field Moisture Content Investigation, U.S Army Corps of Engineers, 1955) have suggested that precipitation has a considerable influence on subgrade moisture, others (Marks 1969, Kubler 1963, and Cumberledge 1974) could not establish a firm relationship". Rainwater, et al (1999) and Heydinger (2003) investigated the effect of precipitation on the moisture content of pavement systems. Neither investigator found a common response to precipitation for base materials primarily because the base materials were different in the two studies. However, for moisture contents in the subgrade soils they both concluded that the change in moisture content was seasonal and could be predicted independently from precipitation events. To investigate the effect of precipitation on the moisture content of the pavement systems, precipitation events must be measured coupled with moisture content measurements in the pavement systems.

4.4.2 Measurements of Precipitation Events

Precipitation events were recorded at the ERC site for 19 months from June of 2003 to January of 2005 and at the Fort Smith site for approximately 15 months, starting in March 2005. Precipitation at both sites was measured using a TE525WS tipping bucket rain gage. Due to limitations of the tipping bucket rain gage used, snow events could not be recorded accurately. The lack of snowfall data does not have a significant

impact on this study, since there were only two or three snow events during the entire recording period and they were small events.

All of the precipitation data for the ERC and the Ft. Smith field site are shown in Figures 4.11 and 4.12. Each vertical bar in the figures represents the total precipitation during a 24 hour period from mid-night to mid-night. In an effort to evaluate the variability of precipitation between the two sites and the nearby NOAA weather stations, t-tests were performed on the means of the absolute differences between measured precipitation events at the two sites and corresponding precipitation data obtained from nearby weather stations. Because precipitation events less than 0.03 inches would be trapped in depressions as will be discussed later in the section on "Water Balance Analysis" of this chapter, no surface water, subsurface water or moisture content change would occur for a precipitation event of 0.03 inch or less. Therefore, when comparing weather station data using the t-test, precipitation events were removed from the data set for all the days with a precipitation event less than 0.03 inches at both sites. The results of the t-tests are presented in Table 4.4. From the results of the t-tests, it can be seen that null hypotheses have to be rejected at a confidence level of 95 percent and one can be 95 percent sure that a maximum difference between measured precipitation and precipitation obtained from the nearby weather stations could be as much as 1 inch.

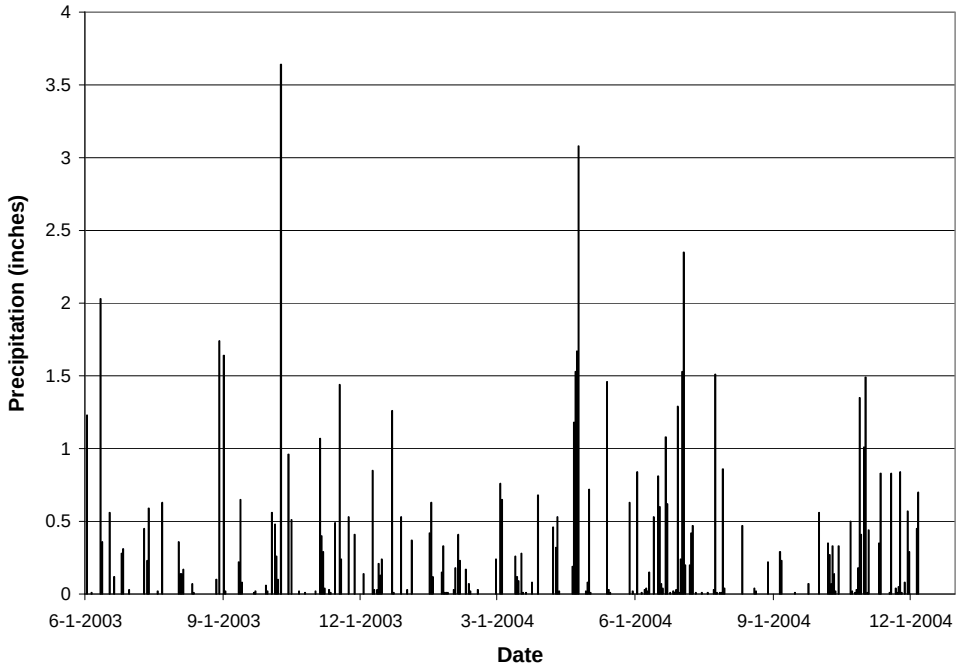

Figure 4.11 Precipitation events at the ERC.

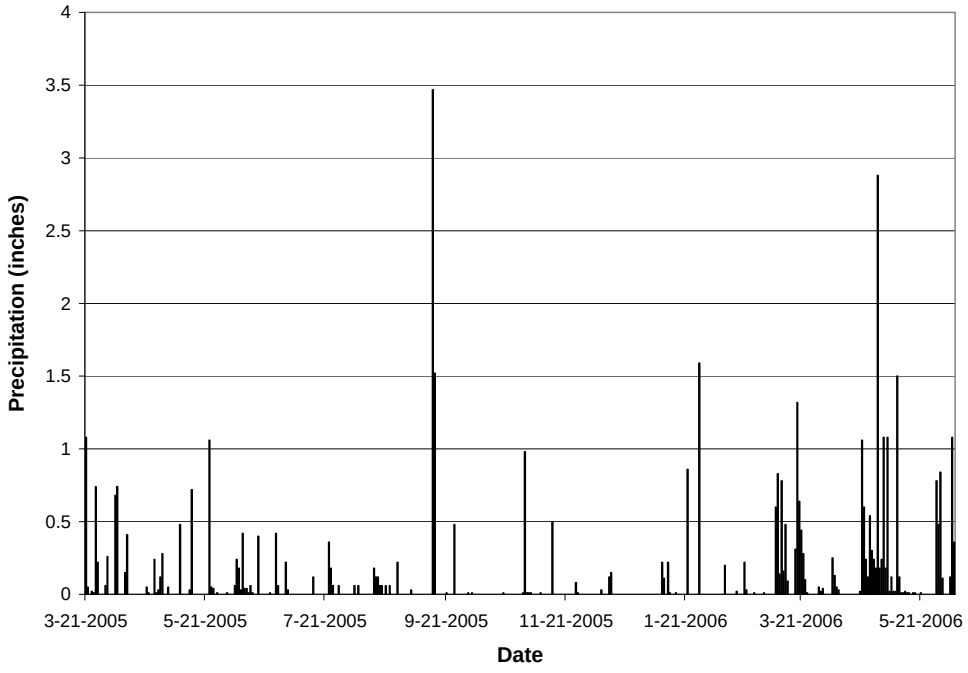

Figure 4.12 Precipitation events at the Ft. Smith test site.

To determine the precipitation variability between the Northwest Arkansas and Ft. Smith areas and to determine how far the weather station can be from the area in which

rainfall data is needed, the absolute differences between precipitation data from the Drake Field Airport and Ft. Smith Regional Airport were analyzed using a t-test. The differenced between precipitation events for these weather stations is plotted in Figure 4.13. The results from the t-test are presented in Table 4.4. Because the precipitation data obtained from the ERC and the Ft. Smith test site were from different periods, the measured data from the two sites are not comparable. Therefore, precipitation data from the weather stations were used here. From the results of the t test, it can be seen that the null hypothesis has to be rejected and one can be 95 percent sure that a maximum difference between precipitation data obtained from the Ft. Smith Regional Airport and Drake Field Airport weather stations could be as much as 1.3 inches.

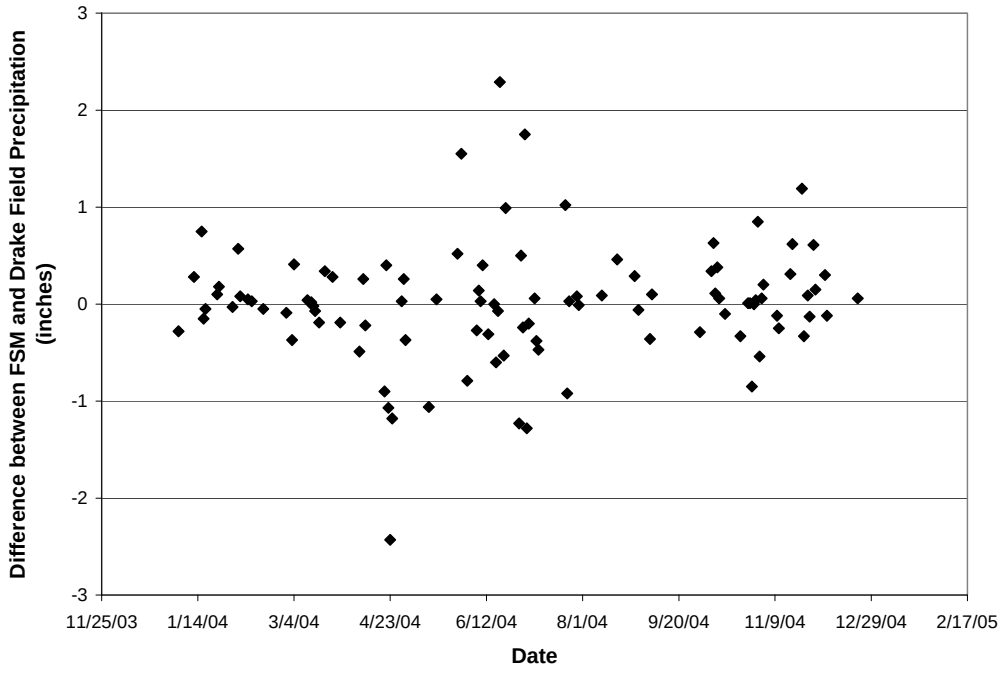

Figure 4.13 Comparison of precipitation data between the Drake Field Airport and Ft. Smith Regional Airport weather stations.

Table 4.4 Results of t-tests on precipitation data excluding precipitation of 0.03 inch or less for both sites under investigation.

	ERC-Drake	ERC-XNA	Field-FSM	Drake-FSM
Null hypothesis H_0	$\mu_d=0$	$\mu_d=0$	$\mu_d=0$	$\mu_d=0$
Level of significance	0.05	0.05	0.05	0.05
Sample Size	212	141	116	101
Sample mean	0.18	0.29	0.18	0.40
Sample standard deviation	0.25	0.39	0.19	0.47
t test statistic	8.10	8.78	10.01	8.64
$t_{0.025,n-1}$	1.98	1.98	1.98	1.98

Where:

ERC-Drake = t-test on the mean of absolute differences between measured precipitation at the ERC and precipitation data obtained from the Drake Field Airport weather station;

ERC-XNA = t-test on the mean of absolute differences between measured precipitation at the ERC and precipitation obtained from the Northwest Arkansas Regional Airport weather station;

Field-FSM = t-test on the mean of absolute differences between measured precipitation at the field site and precipitation data obtained from the Ft. Smith Regional Airport weather station;

Drake-FSM = t-test on the mean of absolute differences between precipitation data obtained from the Drake Field airport and Ft. Smith Regional Airport weather stations;

μ_d = precipitation differences between two populations at the same day;

4.5 Ground Water Levels

From the literature review, it was learned that groundwater levels have a significant effect on the moisture content of pavement systems. This is due to the capillary effect when the location of the free water surface is relatively shallow (Ksaibati, et al. 2000, Heydinger 2003). In addition, the groundwater level is an input variable for the EICM. It is necessary to measure groundwater levels in order to evaluate the EICM in Arkansas.

The groundwater level at the ERC was measured for approximately one half of a year from June 2004 to December 2004. The ground water level measurements were stopped around December 2004 because some of the equipment required to take the readings had to be taken to the Ft. Smith site and complete measurements could not be obtained. The groundwater level at the Ft. Smith site was measured for approximately 15 months from April 2005 to June 2006. The results of the monitoring are illustrated in Figures 4.14 and 4.15. In these two figures, the Y-axis represents the depth to the ground water table referenced from the elevation of the edge of the pavement surface at a point closest to the piezometers. In an effort to identify the possible effect of precipitation on groundwater levels at the two test sites, daily precipitation events during the same periods are also plotted as the secondary Y-axis in Figures 4.14 and 4.15.

In Figures 4.14 and 4.15, it can be seen that the groundwater level generally responded well to precipitation events. At the ERC, the groundwater level increased from June 2004 to August 2004 because of relatively significant precipitation events from June

to August of 2004. Then the groundwater level decreased because of a relatively dry period between August and October of 2004. Because of the relatively significant and frequent precipitation events between October and November of 2004, the groundwater level increased. Then with no appreciable precipitation in December the ground water table dropped.

At the Ft. Smith site, the groundwater level increased by about 4.5 feet during March to May of 2005. The major reason for this increase is believed to be the fact that the observation well was not initially operating in a steady state condition. The groundwater began to infiltrate the initially empty piezometer to reach an equilibrium state upon its installation. Because of the relatively low permeability of the subgrade soils (1×10^{-7}cm/s), it took about 2 months to reach equilibrium. In addition, some of the increase was probably due to the relatively frequent precipitation events which occurred before and during this period. To investigate the relatively high groundwater level at the beginning of the measurements after the equilibrium state was established in May of 2005, annual precipitation data were compared between 2004 and 2005. The annual precipitation obtained from the Ft. Smith Regional Airport weather station for 2004 and 2005 was about 49 inches and 26 inches, respectively. The 100-year average annual precipitation from 1901 to 2000 was 40.4 inches. Based on these facts, it is believed that the relatively high ground water level at the beginning of the measurements was the result of above-average annual precipitation during 2004. Then, even through some precipitation events occurred during 2005, the ground water generally decreased constantly through the year because of the much lower-than-average annual precipitation.

From March of 2006 to the end of the recording period, the ground water level began to increase due to the frequent precipitation events between March and May.

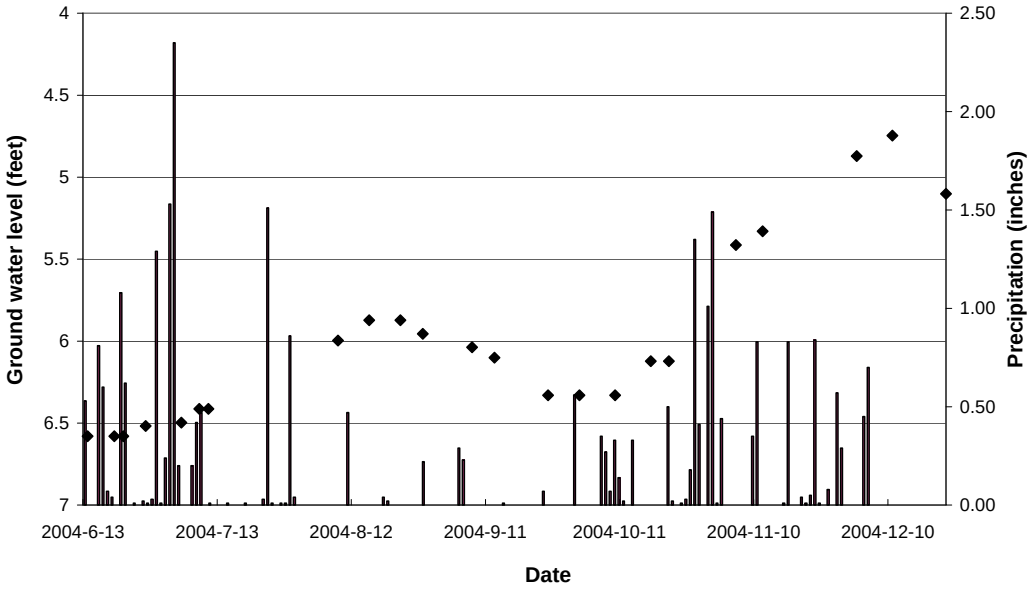

Figure 4.14 Comparison of groundwater levels and precipitation events at the ERC test site.

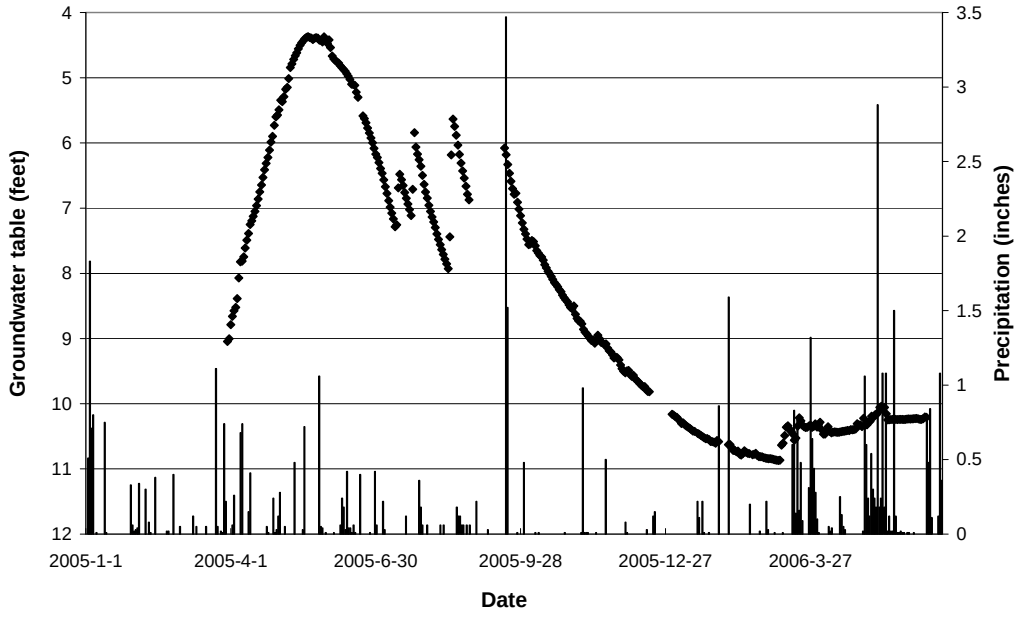

Figure 4.15 Comparison of groundwater levels and precipitation events at the Ft. Smith test site.

4.6 Surface and Subsurface Runoff

To develop an insight into the nature of water migration through a pavement system during precipitation events, it is important to know how much water runs off the pavement surface and how much water is collected in edge drains during precipitation events. This information coupled with changes in moisture content in the unbound materials of the pavement system allows one to conduct a water balance analysis. The surface and subsurface runoff data are presented in this section. The moisture content data in the pavement systems and water balance analysis are presented later in this chapter.

For a given precipitation event, the total precipitation volume was calculated by multiplying the cumulative depth of precipitation, measured using a rain gage, by the contributing pavement surface area. For the test sites at the ERC, the pavements were surrounded by berms on three sides and a retaining wall on the remaining side. Therefore, the contributing surface areas could be easily defined by the areas within the berms and retaining wall (12.5 feet wide by 24.5 feet long). It was not practical to build berms on all sides at the Ft. Smith test site because of traffic. As discussed in Chapter 3, in an attempt to channel surface runoff to the flume and tipping bucket flow meter, a 100-foot long by 4-inch high longitudinal asphalt berm was constructed on the outside edge of the shoulder and a 10-foot long transverse berm was constructed on the shoulder at the lower end of the 100-foot long berm. For the purpose of calculating total precipitation, the contributing surface area was assumed to be the product of the length of the longitudinal berm and the width of the pavement (64 feet wide by 100 feet long). At both sites, surface runoff and subsurface runoff collected in the edge drains were channeled into flumes and tipping

bucket rain gages as discussed in Chapter 3. Figure 4.16 is presented to illustrate how the total precipitation and runoff volumes were calculated. Basically the total volume of precipitation or runoff is equal to the area under the line which connects all of the data points for a given rainfall event.

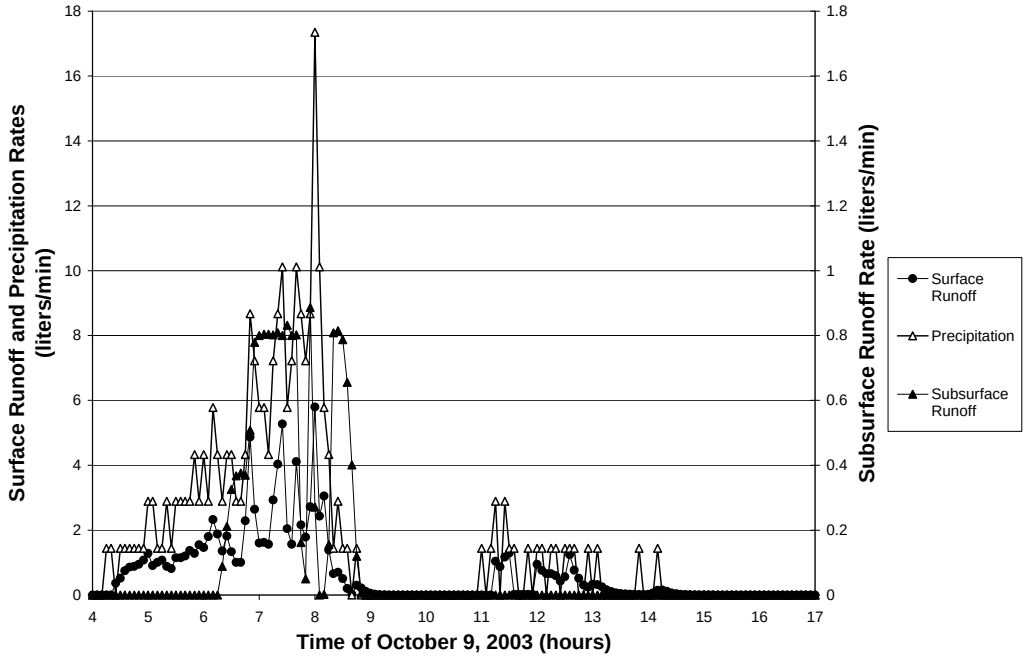

Figure 4.16 Illustration of calculation of precipitation and runoff volumes.

Since the surface of test pad B at the ERC was not built to slope toward a single point, where all of the surface runoff could be collected, surface runoff was not able to be collected. Therefore, only the moisture content in the pavement system for test pad B was measured. Surface and subsurface runoff collected at the ERC in this chapter refer to those collected from test pad A.

Calculated total precipitation volumes were plotted along with collected surface and subsurface runoff for all precipitation events during the monitoring period. This data is illustrated in Figures 4.17 through 4.20. Linear regression analyses, with the regression

line forced through the origin, were then performed to obtain relationships between total precipitation volumes and surface and subsurface runoff for the two sites. This mathematical relationship is an important first step for conducting a water balance analyses.

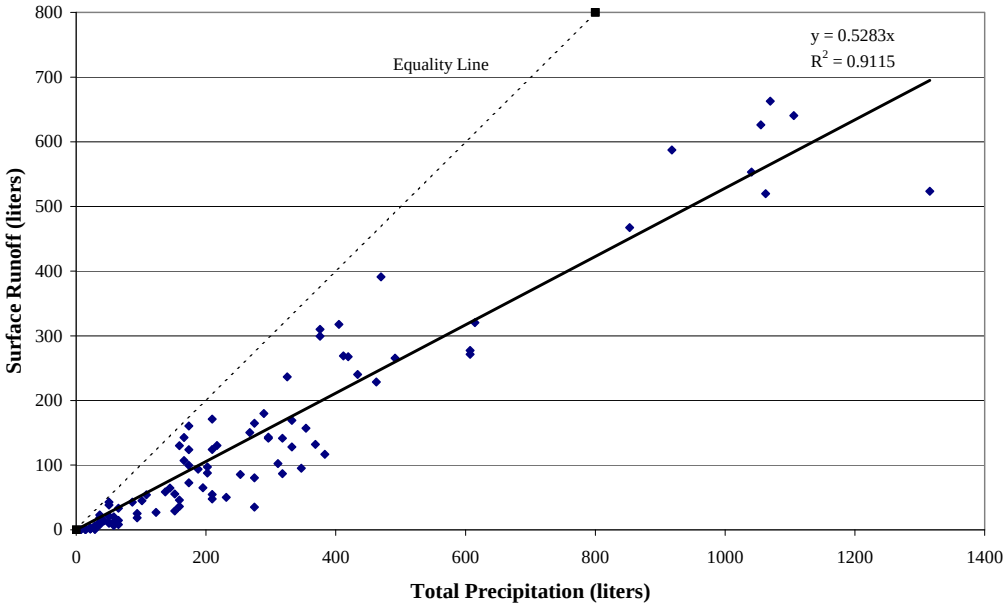

Figure 4.17 Relationship between precipitation volume and surface water runoff for test pad A at the ERC.

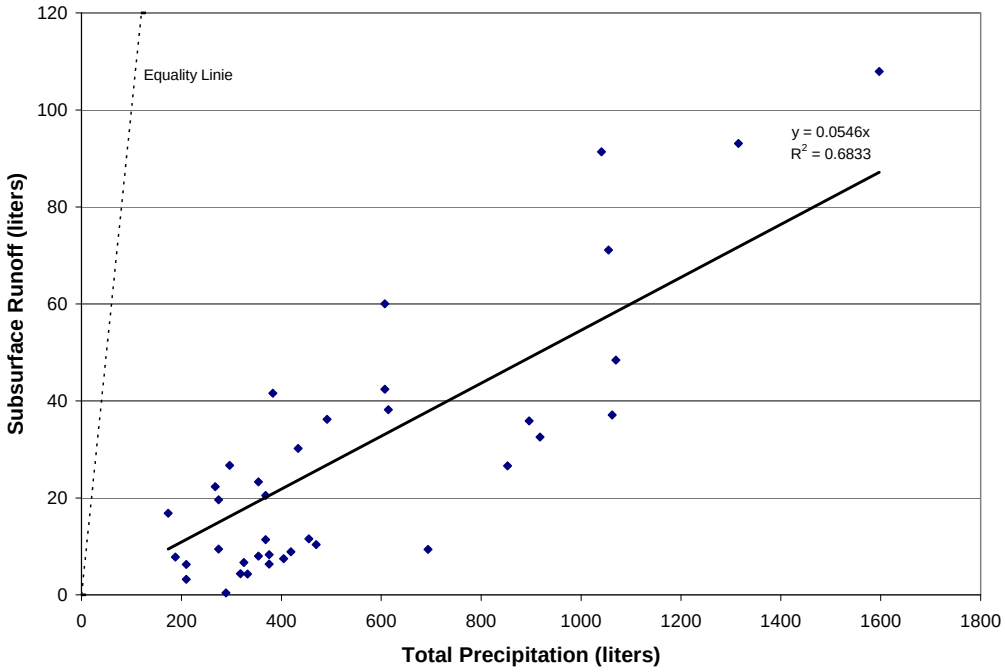

Figure 4.18 Relationship between precipitation volume and subsurface water runoff for test pad A at the ERC.

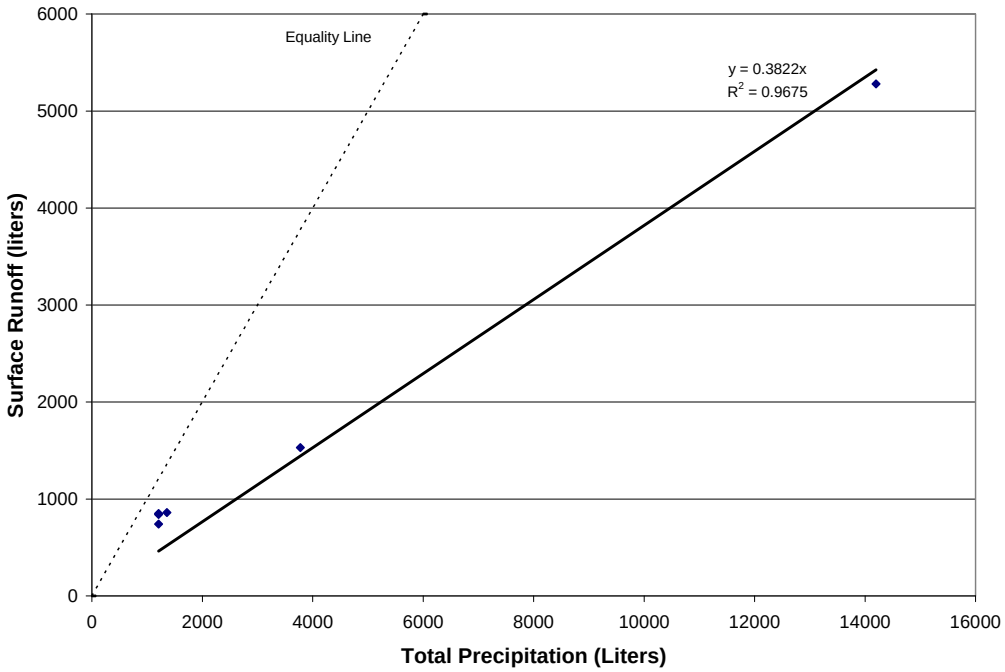

Figure 4.19 Relationship between precipitation volume and surface water runoff for the Ft. Smith test site.

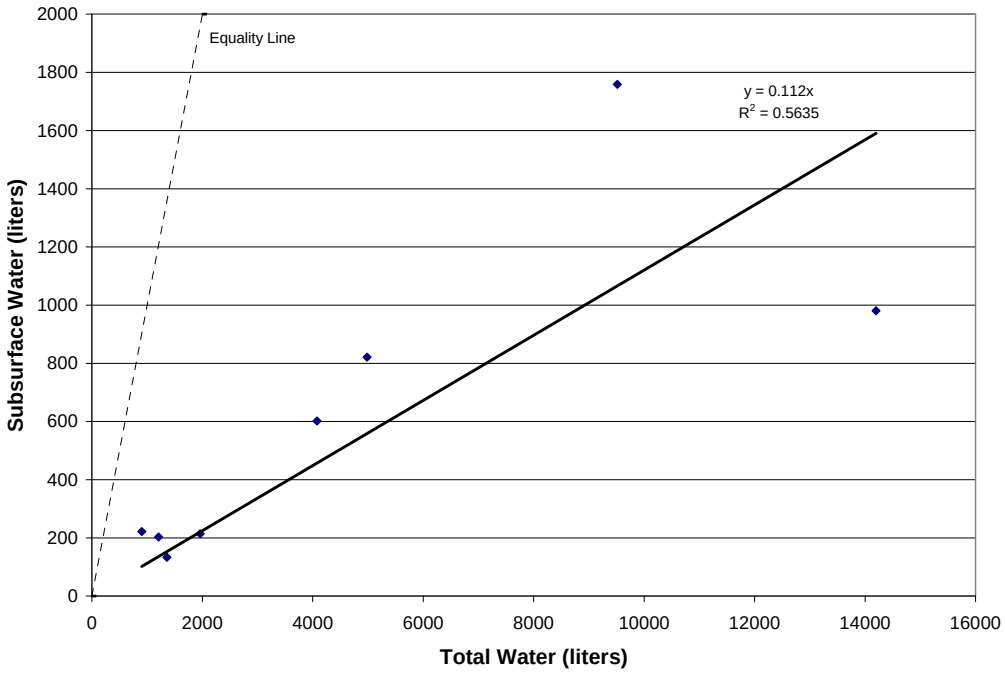

Figure 4.20 Relationship between precipitation volume and subsurface water runoff for the Ft. Smith test site.

From Figures 4.15 and 4.16, it can be seen that only five surface runoff and eight subsurface runoff events are plotted. However, far more than eight precipitation events occurred during the 15 months of measurement. The reason for this discrepancy in the data is that the flume used in this project was found not to be suitable for flow measurements in an uncontrolled field environment. During regular site visits, it was observed that dirt and debris from the pavement surface was washed into the flume despite the use of filtering screens. This debris settled on the bottom of the flume channel and clogged the relatively small discharge opening at the end of the flume. This in turn caused the water to back up and remain in the flume which resulted in grossly over predicted flows. Alternatively, the debris blocked the small hole in the sidewall of the flume leading to the stilling well where the water head was measured. This condition

caused either a very low, or excessively high water head to be measured in the stilling well with a corresponding erroneous flow prediction. This phenomenon was often reflected by an almost constant water head measurement for a relatively long period both during and after a precipitation event. The same problem with less severity also occurred in the flume that was used to measure the subsurface flow even though subsurface flow had been filtered by the drain material. Because of this problem, surface and subsurface runoff could not be collected for most of the precipitation events.

From Figures 4.13 through 4.16, it can be seen that linear relationships generally exist between total precipitation volumes and surface and subsurface runoff. Approximately 53 percent of the total precipitation volume ran off from the surfaces of test pad A at the ERC while only 38 percent ran off from the Ft. Smith test site. Approximately 5.5 percent of the total precipitation volume was collected from the edge drains at test pad A at the ERC while 11 percent was collected from the Ft. Smith test site.

It should be noted that too few surface and subsurface runoff data were collected at the Ft. Smith test site to obtain a reliable regression analysis, especially for surface runoff. Even though the data are limited, it seems reasonable to conclude that more subsurface runoff was collected in the edge drain at the Ft. Smith site than at the ERC site for the following reasons.

- The asphalt wear in course at the Ft. Smith site may have more interconnected cracking than its counterpart at the ERC because the pavement at Ft Smith had experienced significant traffic loading and subsequent distress, while the pavement at the ERC had not had any traffic or distress.

- The Ft. Smith site has a significant slope both in the longitudinal and transverse directions. The 100 foot edge drain that was installed as a part of this study likely collected water which migrated into the pavement from areas outside of the test section because of the significant slopes present at the site. However, the total volume of precipitation was calculated based on an assumption that the contributing area only consisted of the 100-foot long section.

4.7 Water Balance Analysis

This section couples the rainfall data presented earlier to runoff and moisture content data collected during the same period in an attempt to determine a pattern of moisture movement through pavement systems under varying environmental conditions. As a first step in the analysis of this data a basic water balance must be satisfied to insure that all of the precipitation is being properly accounted for. Once patterns of moisture migration through the pavement system can be established physical, properties for the unbound materials in the pavement system can be predicted.

4.7.1 Theoretical Water Balance

During a precipitation event over a broad multi-use area not all of the rainfall will actually reach the ground. Some rainfall may be intercepted by vegetation before it can reach the ground. The water that does reach the ground can either form puddles, infiltrate into the soil, or flow as a thin sheet of water across the land surface. Because soil has a finite and variable capacity to absorb water, infiltration capacity varies not only from soil to soil, but also is different for dry versus moist conditions in the same soil. Hydrologists

refer to the water trapped in puddles as depression storage. It ultimately evaporates or infiltrates, but it does not run off. The overland flow process, sometimes called Horton overland flow occurs only when the precipitation rate exceeds depression storage and the infiltration capacity of the underlying soil. (Fetter, C.W., 2001).

The asphalt pavement surfaces investigated in this study do not have surface vegetation, so it is reasonable to say that 100 percent of the rainfall in any precipitation event reaches the pavement surface. After depression storage and infiltration capacity are satisfied, surface runoff occurs. A rational runoff coefficient is often used by hydrologists to predict the amount of runoff that will occur from a given storm. The rational runoff coefficient is a volumetric based coefficient ranging from 0 to 1 that indicates the fraction of runoff that will result from a given volume of rainfall (Malcom, 1989). Cristina and Sansalone (2003) measured surface runoff on a 15-m by 20-m pavement section for eleven precipitation events and reported runoff coefficients ranging from 0.19 to 0.92. Rainfall that does not runoff is either trapped by depressions of the pavement surfaces, or infiltrates into the pavement system. The water that infiltrates into the pavement system (pavement storage) either remains in the pavement system or migrates to edge drains or to the underlying subgrade soils.

To perform the water balance analysis, depression storage, surface runoff and pavement storage have to be determined. Theoretically, the total volume of precipitation should be equal to the sum of depression storage, surface runoff and pavement storage. The total precipitation volume for each precipitation event was discussed earlier in the section of “Surface and Subsurface Runoff” of this chapter. Depression storage, surface runoff and pavement storage are discussed in the following sections.

4.7.2 Depression Storage and Surface Runoff

Some portion of precipitation will become trapped in depressions of the pavement surfaces. This is commonly referred to as depression storage. Based on the measured data, there was generally no surface runoff collected for precipitation events less than 0.03 inch. This indicates that the first 0.03 inch of precipitation was trapped in depressions. Shackel (2003) stated that the depression storage for paved roads is typically 0.04 inch or less. While some portion of the depression storage infiltrates into the pavement and some evaporates, the distribution of infiltration and evaporation is unknown. The amount of the depression storage that evaporates will depend on air temperature, wind speed, humidity and so on. The portion that infiltrates into the pavement should be included as storage in the water balance analysis. Because the depression storage is relatively small for asphalt pavements (Cristina, 2003) and its ultimate fate is unclear, it was assumed that all the depression storage finally infiltrates into the pavements and the depression storage will be included as the pavement storage in the water balance analysis.

As discussed previously, surface runoff was measured using a combination of an instrumented flume and a tipping bucket rain gauge. In the section of "Surface and Subsurface Runoff" of this chapter, collected surface runoff was plotted along with total precipitation volumes for all precipitation events during the monitoring period. A linear regression analysis was preformed between total precipitation volumes and surface runoff. The results of the linear regression analysis indicate that approximately 53 percent of total precipitation at the ERC was collocated for test pad A as surface runoff with a R^2 value of 0.91. At the Ft. Smith test site, only approximately 38 percent of the total

precipitation was collected as surface runoff with a R^2 value of 0.97. It should be noted, however, that surface runoff was only collected for five precipitation events at the Ft. Smith site and there were too few surface runoff data to produce a reliable regression analysis.

4.7.3 Pavement Storage

To illustrate how to calculate the pavement storage during precipitation events, three typical precipitation events at the ERC were chosen. The three precipitation events, presented in Table 4.5, include a relatively small, a medium and a large event. While, one might not consider a precipitation event of 0.45 inch to be small, it was determined during the course of this study that precipitation events less than 0.3 inch did not produce subsurface runoff. As a result, a precipitation event of 0.45 inch is considered to be small for the purposes of quantifying all of the elements of the water balance.

Table 4.5 Three typical precipitation events at the ERC.

Date	Beginning time	Ending time	Precipitation (inches)	Event Size
4/30/2004	9:15	23:20	0.45	Small
6/2/2004	12:15	18:40	0.84	Medium
10/9/2003	4:10	14:10	1.82	Large

Pavement storage is manifested by changes in moisture content of various layers in the pavement system. In an effort to quantify the amount of water stored in the pavement system during and after precipitation events, moisture content as a function of time was plotted at various locations in the pavement system during and after the three typical precipitation events for the test pads at the ERC. This data is illustrated in Figures 4.22 through 4.33. The moisture probe configuration for test pad A at the ERC was presented in Chapter 3 and is repeated here in Figure 4.21 for reference. The moisture

probe configuration for test pad B at the ERC was the same except that the numbers of the probes end with “B” instead of “A”. In Figures 4.22 through 4.33, the X-axis represents the time of the precipitation events starting from the beginning of the precipitation events. The primary Y-axis represents the gravimetric moisture content and the secondary Y-axis represents the precipitation rate in liters per minute. As mentioned in the “Precipitation Events” section of this chapter, the total precipitation during a day was treated as a single precipitation event. However, in some cases in Figures 4.22 through 4.33, the X-axis spans more than 24 hours because moisture content changes occurred for more than 24 hours after the start of a precipitation event.

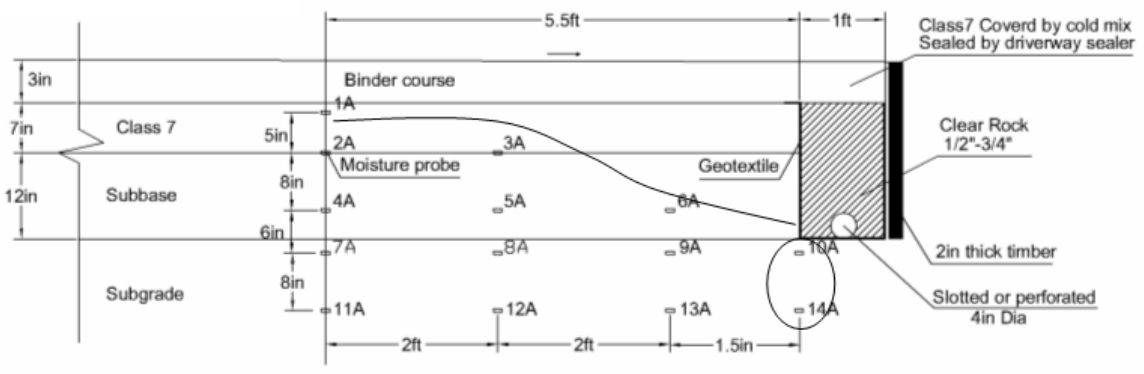

Figure 4.21 Pavement cross section and moisture probe configuration for test pad A at the ERC.

From Figures 4.22 and 4.23 one can see that only the moisture contents from Probes 1A, 10A and 14A increased by an easily measurable amount (~0.3%) while the moisture contents from the remaining probes in the base and subbase materials remained relatively constant. This indicates that moisture migrated much faster in the horizontal direction than in the vertical direction. Water migrated horizontally to the edge drain as illustrated by the curved line in Figure 4.21, some water drained out of the pavement system and migrated to the underlying subgrade soils via the edge drain as evidenced by

moisture increase at probes 10A and 14A, shown in the ellipse in Figure 4.21. By contrast, Figures 4.23 and 4.24 show that moisture contents in the base and subbase materials remained relatively constant under test pad B. There was a minor increase in moisture contents at the locations of Probes 3B and 4B which was about equivalent to the increases at probes 2A, 6A and 7A under pad A. Inspection of these figures indicates a significantly different response for each pad to the same precipitation event. The reason for this difference is believed to be that test pad B had both a surface course and a binder course, for a total of 6 inches of asphalt, while test pad A only had a binder course of approximately 3 inches. The difference in asphalt thickness and texture allowed more water to infiltrate into test pad A than into test pad B. During this precipitation event, about 9.5 liters of water were collected from the edge drain of test pad A, while, no water was collected from the edge drain of test pad B. This indicates that more water infiltrated in test pad A than in test pad B.

From Figures 4.22 and 4.24, it can be seen that moisture contents in the subgrade soils of both test pads generally remained constant except for locations in the vicinity the edge drains (probes 11 and 14). Also, it can be seen that moisture contents at locations of probes 11A and 14A increased more than those at locations of probes 11B and 14B. The reason for this is that pad B allowed less water to infiltrate.

Also, from Figures 4.22 through 4.24, one can see that this precipitation event actually consisted of two precipitation peaks separated by approximately 14 hours. The first peak was 0.07 inch and the second was 0.38 inch. During the first peak of precipitation, no subsurface runoff was collected for either test pad. Also, there was not any moisture response in either of the test pads. However, approximately 43 liters of

surface runoff was collected during the first peak of precipitation from test pad A. Only from this precipitation, it might be able to say that a minimum 0.07 inch of precipitation is necessary before any moisture content change occurs in the pavement. However, during the entire measuring period, noticeable moisture content changes were observed for other precipitation events of 0.07 inch. Because changes in moisture content depend on both magnitude of precipitation events and pre-moisture contents in the pavement before precipitation events, it is hard to establish a threshold precipitation event before there is a change in moisture.

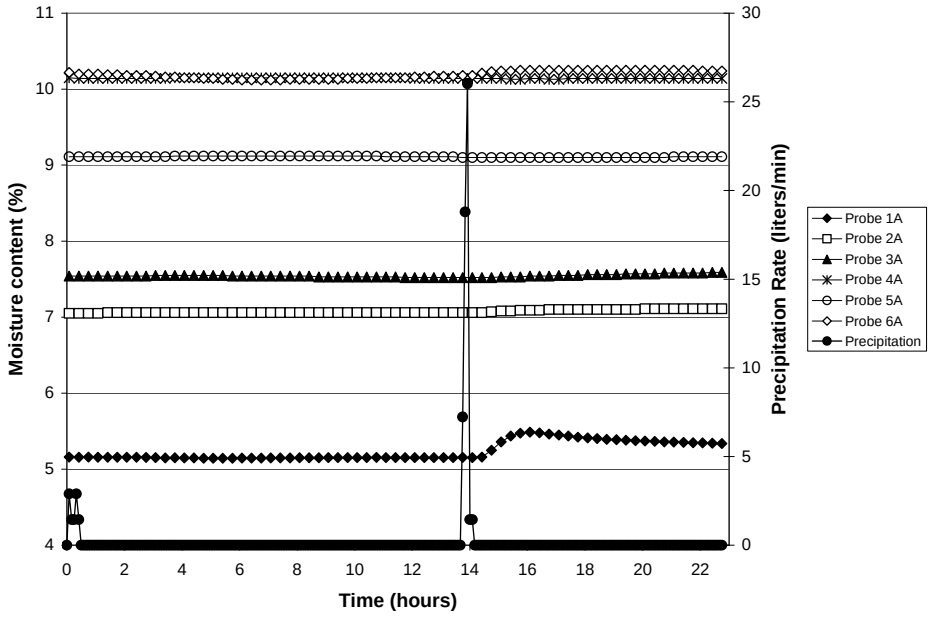

Figure 4.22 Moisture contents in the base material of test pad A at the ERC during the small precipitation event.

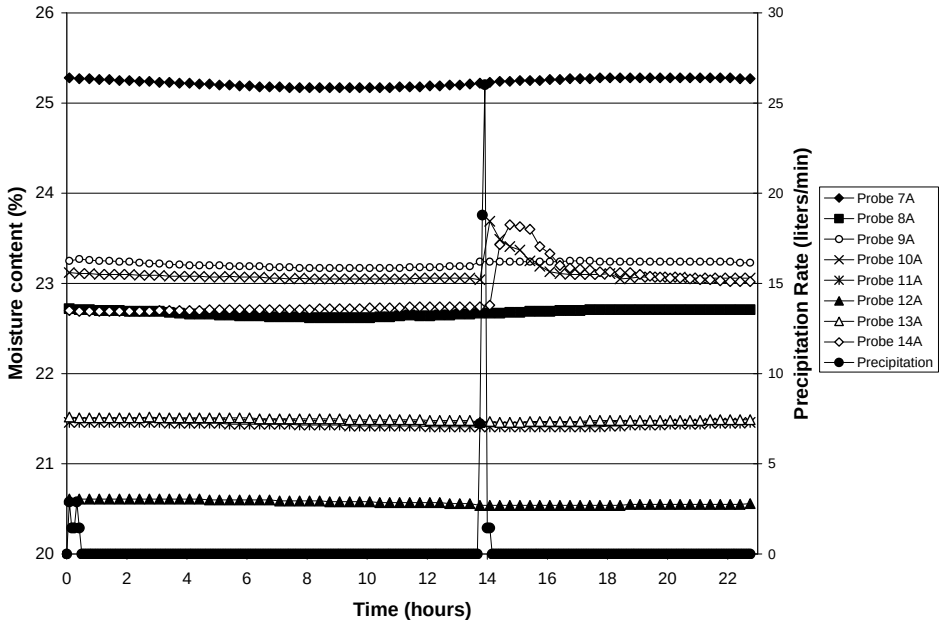

Figure 4.23 Moisture contents in the subgrade soil of test pad A at the ERC during the small precipitation event.

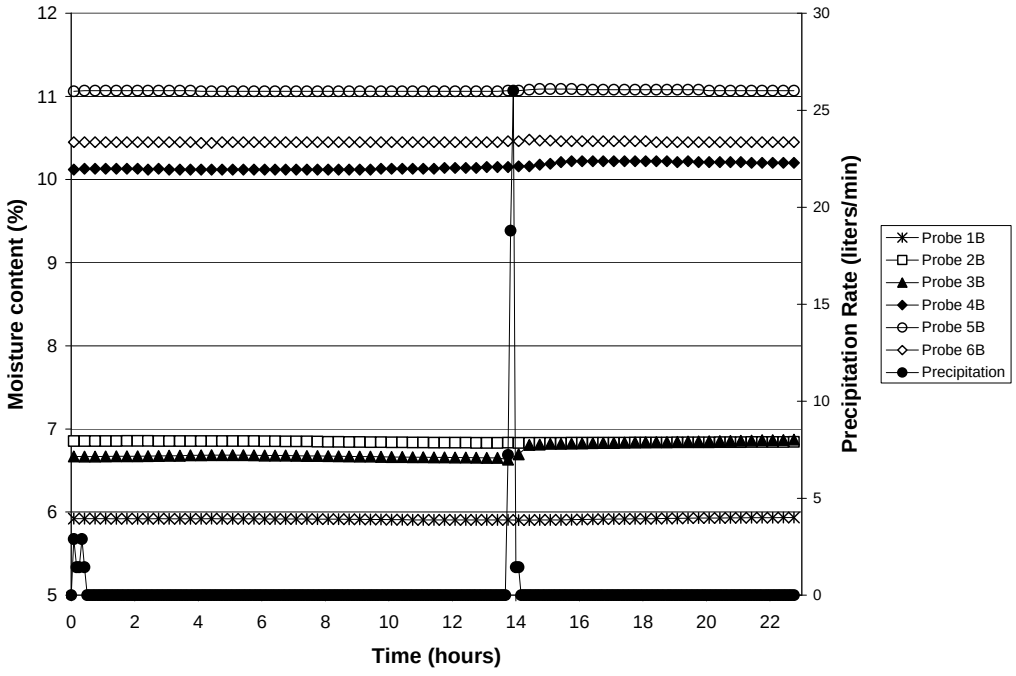

Figure 4.24 Moisture contents in the base material of test pad B at the ERC during the small precipitation event.

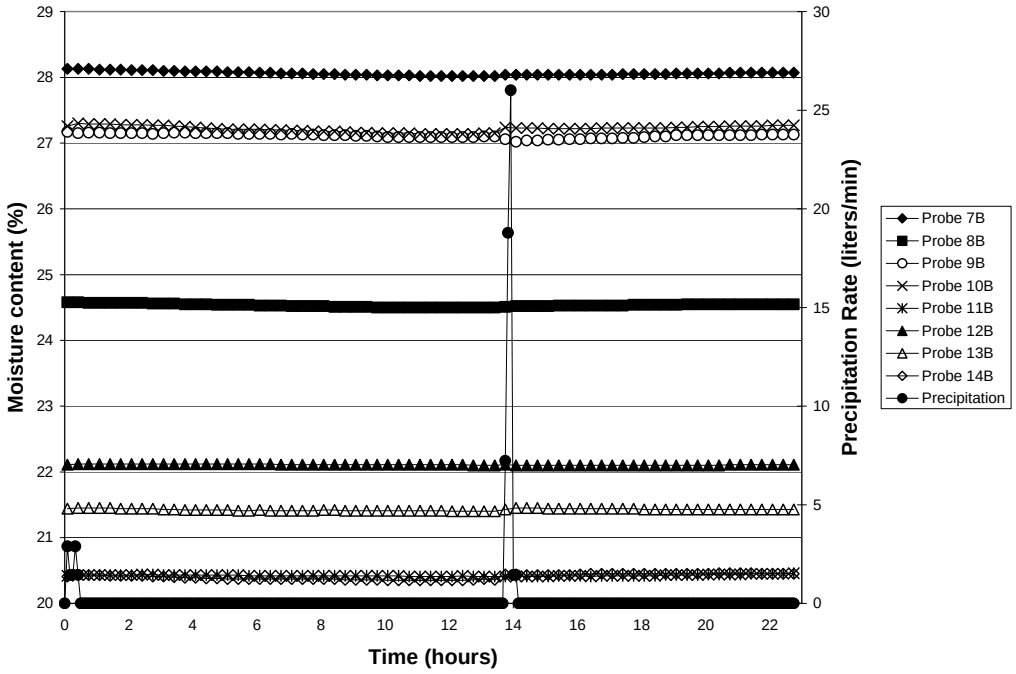

Figure 4.25 Moisture contents in the subgrade soil of test pad B at the ERC during the small precipitation event.

From Figures 4.26 through 4.29, the same phenomena can be observed as that seen in Figures 4.22 through 4.25. However, moisture contents generally increased more significantly at the same locations during the medium precipitation event than those during the small event. In addition to Probes 1, 10 and 14 which had significant responses to the small precipitation event, probes 3 and 6 had also significant responses during the medium event. This substantiates the migration pattern as shown in Figure 4.21. In addition, it was noticed that the moisture contents at a depth of approximately 10 inches below the subgrade surface (Probes 11, 12 and 13) had slight but noticeable increases during the medium event. While, the moisture contents at the depth of approximately 2 inches below the subgrade surface (Probes 7, 8 and 9) did not have a noticeable increase. This indicates that the moisture content increase from Probes 11, 12 and 13 might be the

result of water migration from the sides of the test pads instead of directly from the pavement surfaces.

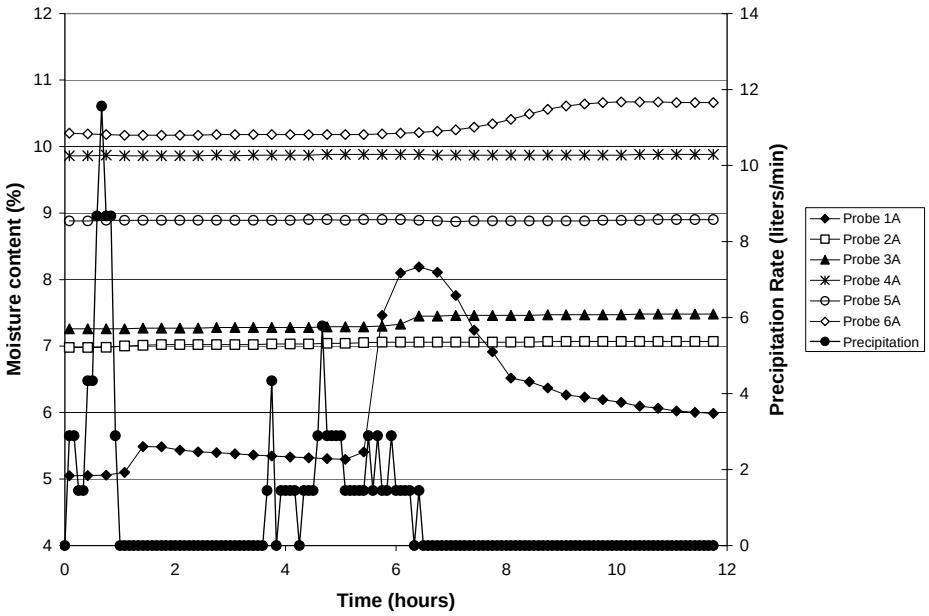

Figure 4.26 Moisture contents in the base material of test pad A at the ERC during the medium precipitation event.

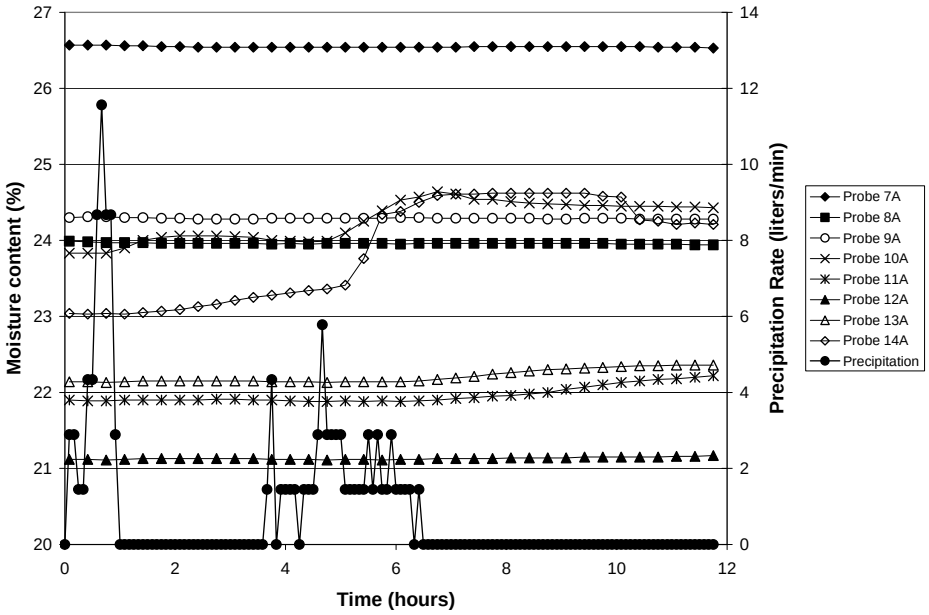

Figure 4.27 Moisture contents in the subgrade soil of test pad A at the ERC during the medium precipitation event.

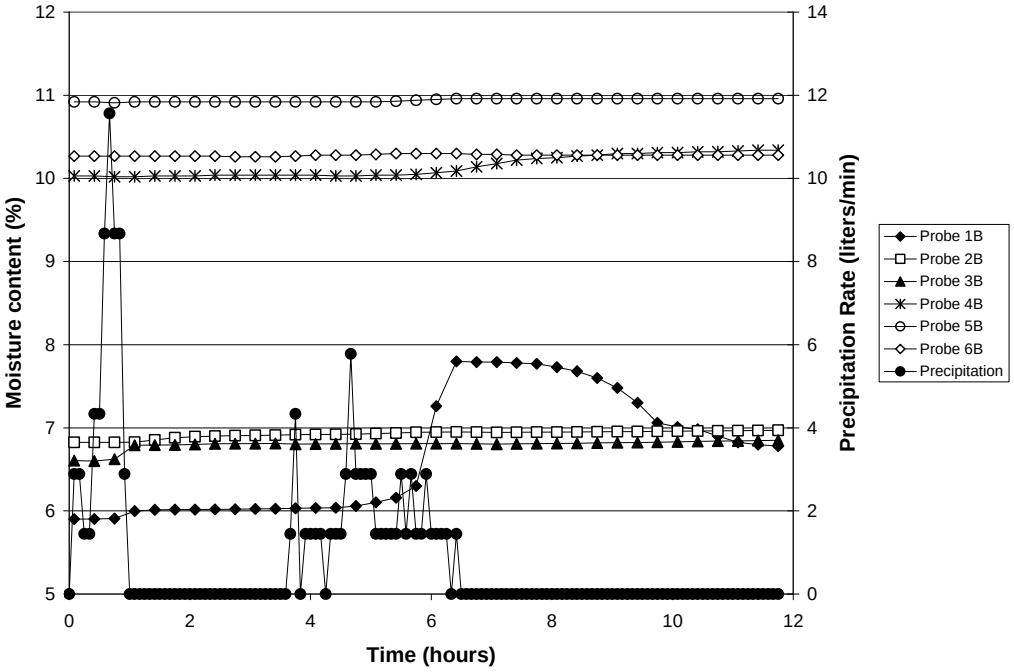

Figure 4.28 Moisture contents in the base material of test pad B at the ERC during the medium precipitation event.

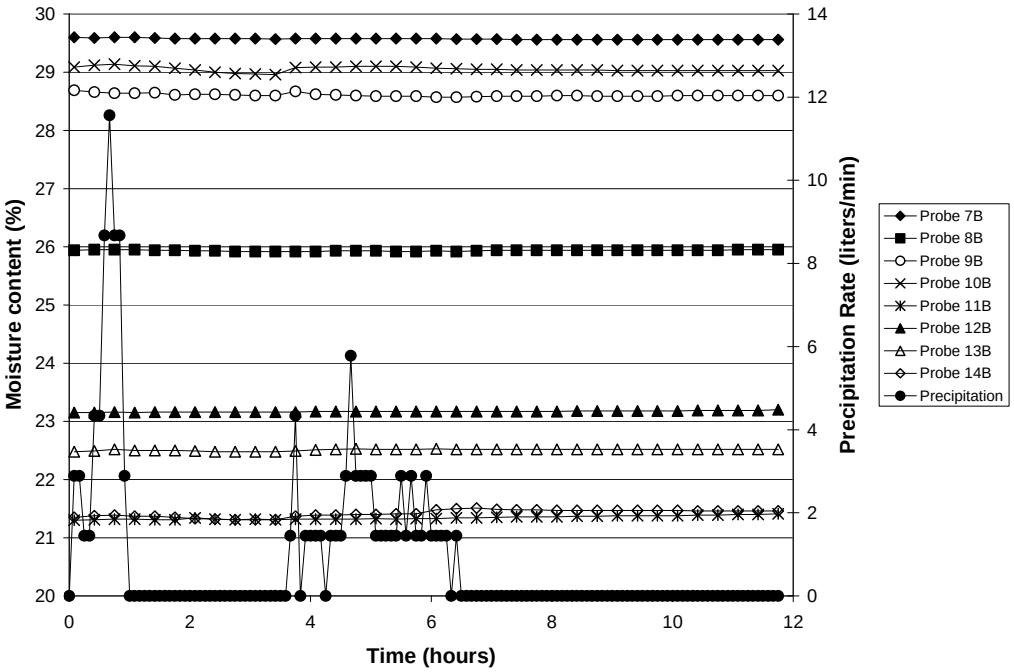

Figure 4.29 Moisture contents in the subgrade soil of test pad B at the ERC during the medium precipitation event.

From Figures 4.30 through 4.33, it can be seen that moisture contents at more locations began to response to the large precipitation event because this event was much larger than the small and medium events. To visually investigate the moisture content changes and therefore understand the water migration pattern through the pavement system during this precipitation event, maximum changes of moisture contents at each of the moisture probe locations and the times required to achieve the changes are illustrated in Figures 4.34 and 4.35 for large precipitation event. The reason that this precipitation event was chosen for illustration of moisture migration was because of the large changes in moisture contents at many locations in the pavement system resulting from this event. These large changes in moisture content in turn, more clearly illustrate the water migration patterns in the pavement system.

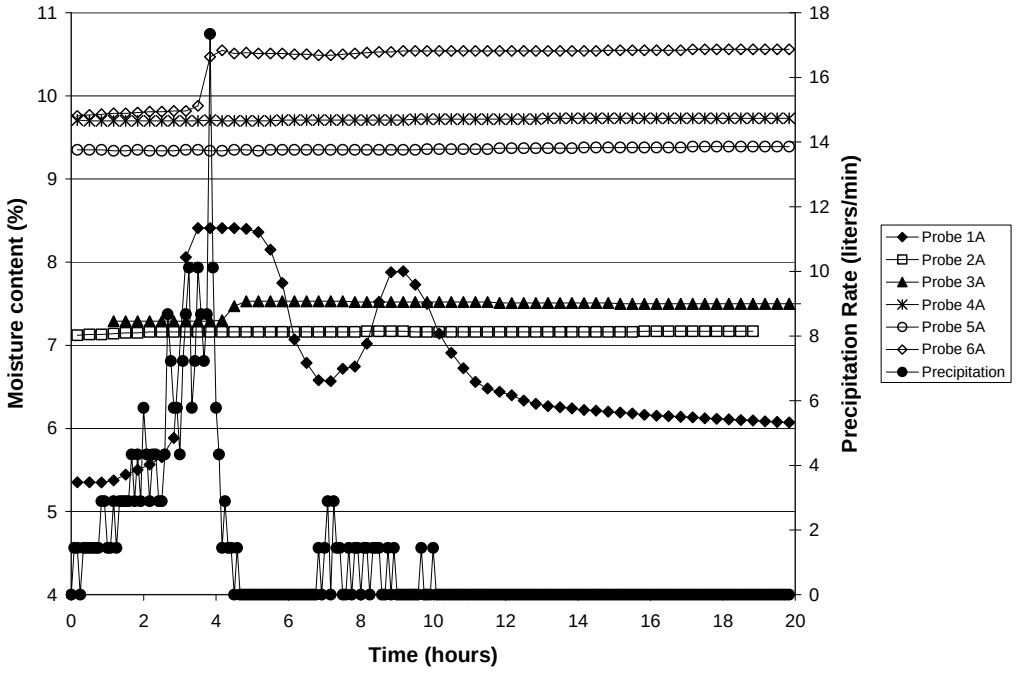

Figure 4.30 Moisture contents in the base material of test pad A at the ERC during the large precipitation event.

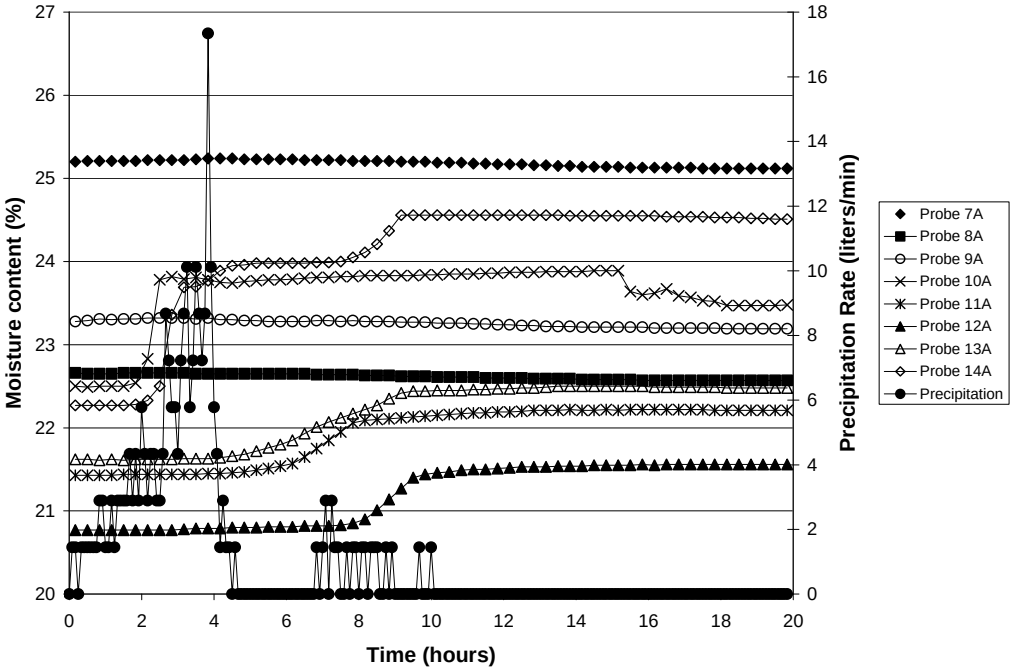

Figure 4.31 Moisture contents in the subgrade soil of test pad A at the ERC during the large precipitation event.

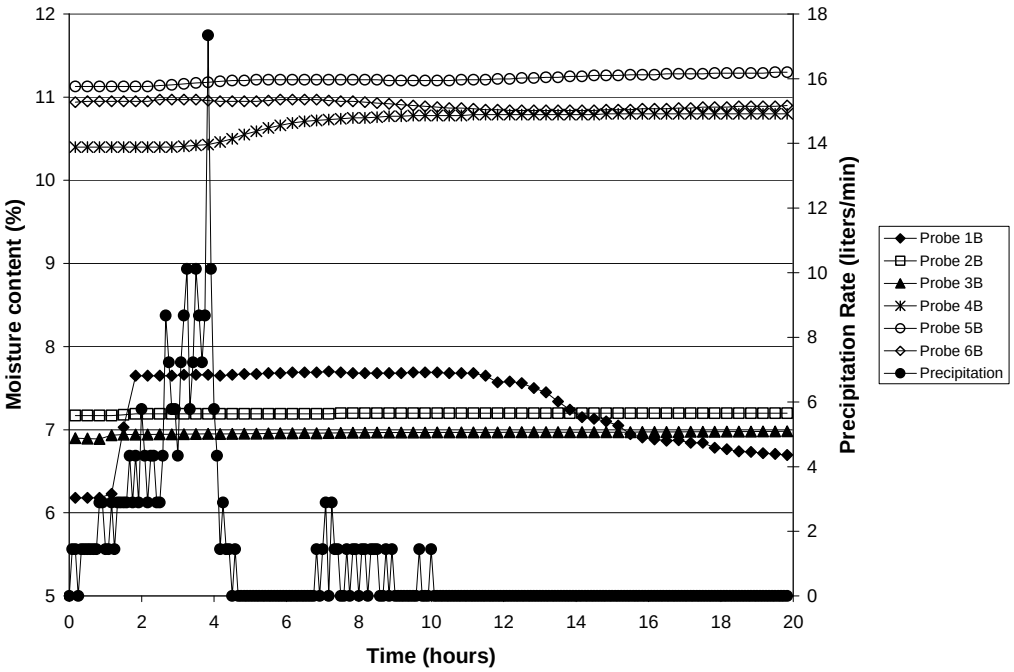

Figure 4.32 Moisture contents in the base material of test pad B at the ERC during the large precipitation event.

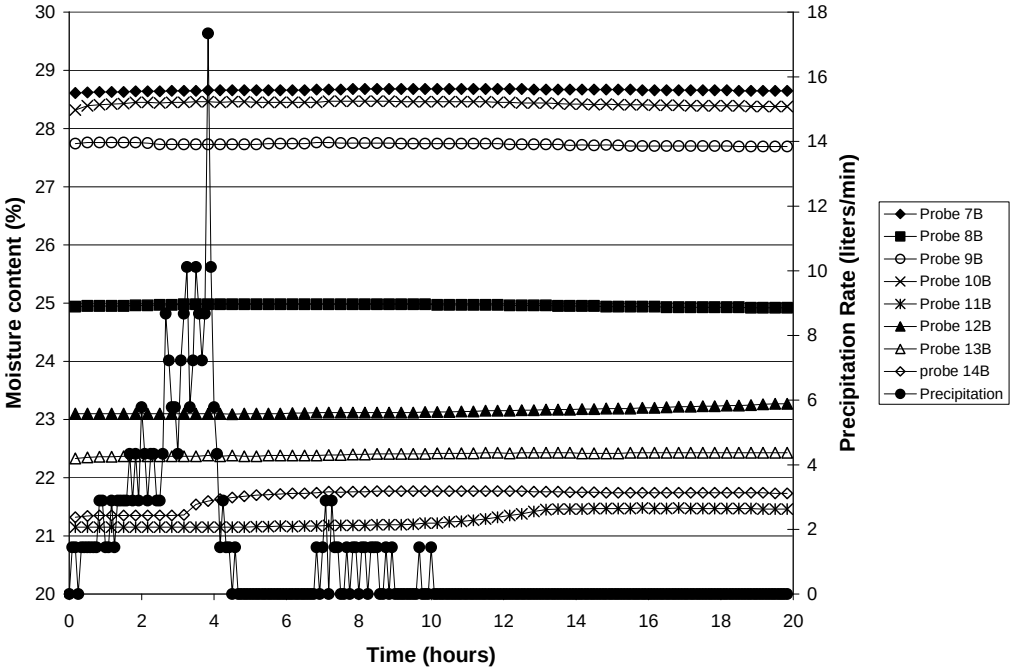

Figure 4.33 Moisture contents in the subgrade soil of test pad B at the ERC during the large precipitation event.

In Figures 4.34 and 4.35, the first number on the right side of each moisture probe stands for the maximum change of the moisture content at this location, the second number on the right of each moisture probe represents the lag time between the start of precipitation and start of moisture contents change, while the third number represents the time required to achieve the maximum change in moisture content.

From Figure 4.34, it can be seen that the changes of the moisture contents were relatively significant for moisture probes 1A, 3A, 6A, 10A and 14A. While the moisture contents at the locations of moisture probes 2A, 4A and 5A increased only slightly or had no change. This substantiates the conclusion that water moved much faster in the horizontal direction than in the vertical direction in the base and the water migration

pattern can be best illustrated by the flow line starting from 1A to 3A and 6A as shown in Figure 4.34.

Moisture contents at 2 inches below the subgrade surface (probes 7A, 8A and 9A) increased by 0.17 to 0.22 percent about 75 hours after the beginning of the precipitation event, which might be the result of perched water remaining in the subbase material above the subgrade surface after the precipitation event. However, moisture contents at 10 inches below the subgrade surface (probes 11A through 13A) increased by about 0.63 to 0.8 percent about 7.8 to 9.8 hours after the beginning of the precipitation event. This substantiates the conclusion that moisture content changes at 10 inches below the subgrade surface were not the result of the direct water migration from the pavement surface. The moisture content changes were more likely from the result of water migration via microstructures in soils from an area between the test pads and a building on the south of the test pads. This is illustrated by the flow line starting from the left side to the subgrade soils at 10 inches below the subgrade surface as shown in Figure 4.34.

A similar phenomenon was observed for Figure 4.35 for test pad B during the same precipitation event. However, relatively significant moisture content increases were observed at locations of probes 4B and 5B. Considering no moisture content increase was observed for probe 2B, it is reasonable to conclude that moisture content increases of probes 4B and 5B might be the result of water migration from the side of the test pad.

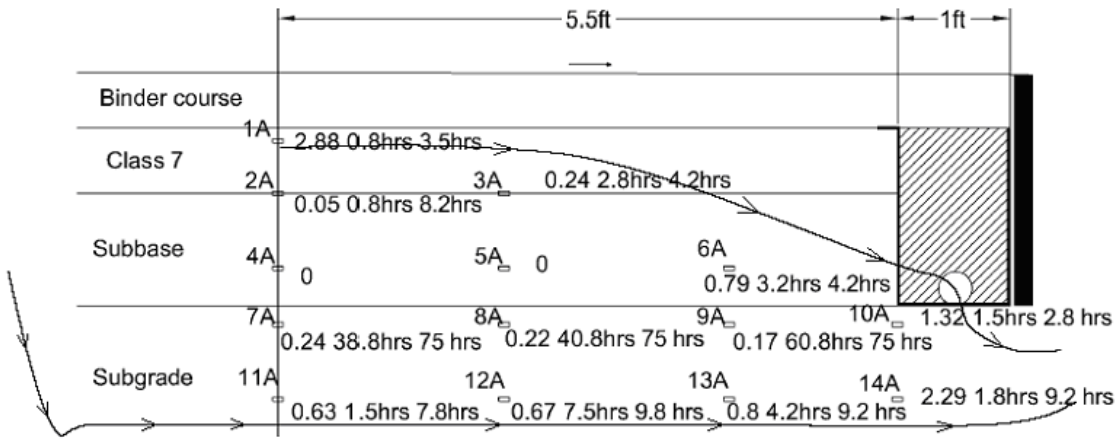

Figure 4.34 Changes of moisture contents and times to achieve the changes at the moisture probe locations for test pad A at the ERC during the large precipitation event.

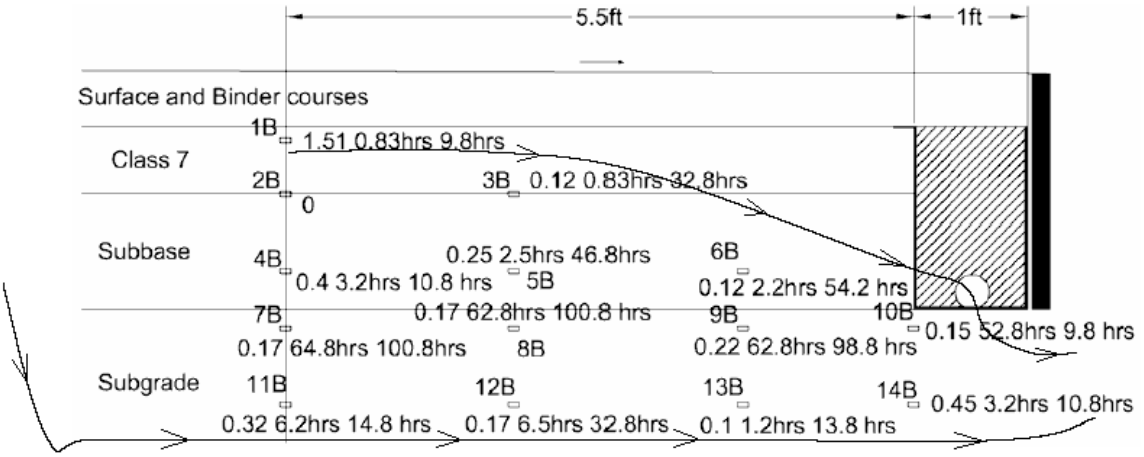

Figure 4.35 Changes of moisture contents and times to achieve the changes at the moisture probe locations for test pad B at the ERC during the large precipitation event.

In an effort to determine if some probes responded to the precipitation event at later times and to determine how long it took to return to pre-rainfall moisture levels, moisture content as a function of time was plotted during the large precipitation event for about 100 hours after the precipitation event. The reason that it was plotted only for 100

hours after the precipitation is that another precipitation event occurred about 100 hours after the October 9, 2003 event. This data is illustrated in Figure 4.36 through 4.39.

From Figures 4.36 and 4.39, it can be seen that most moisture probes that had an increase in moisture content had not returned to their pre-rainfall moisture levels at the end of 100 hours. This indicates that some water remained in the pavement after the precipitation event for a relatively long period. This clearly indicates that the base and subbase materials are not free-draining materials.

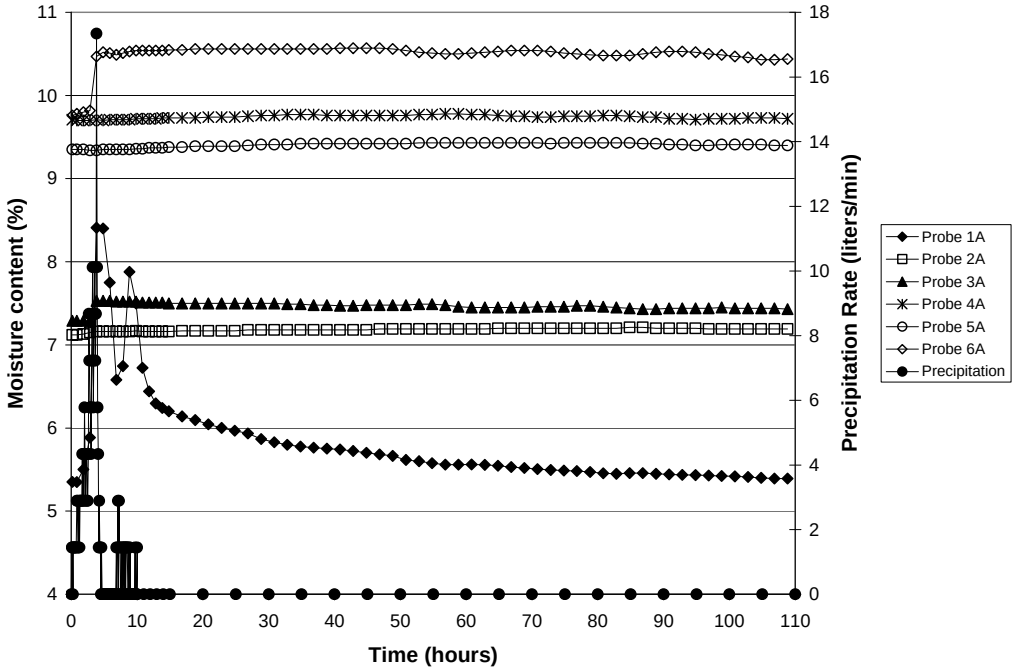

Figure 4.36 Moisture contents in the base material of test pad A at the ERC during and 100 hours after the large precipitation event.

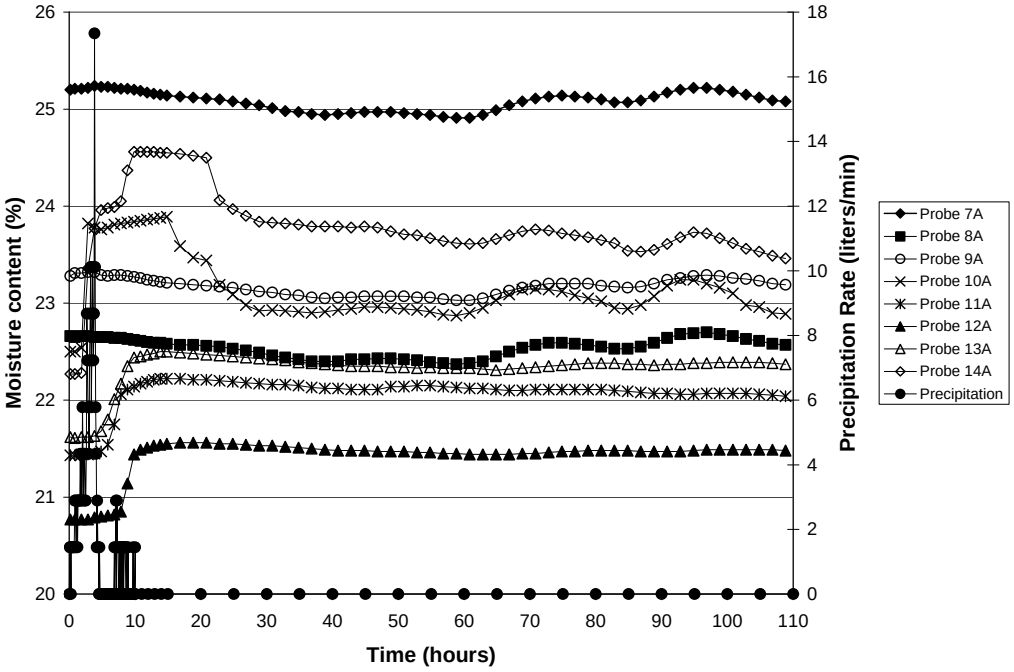

Figure 4.37 Moisture contents in the subgrade soil of test pad A at the ERC during and 100 hours after the large precipitation event.

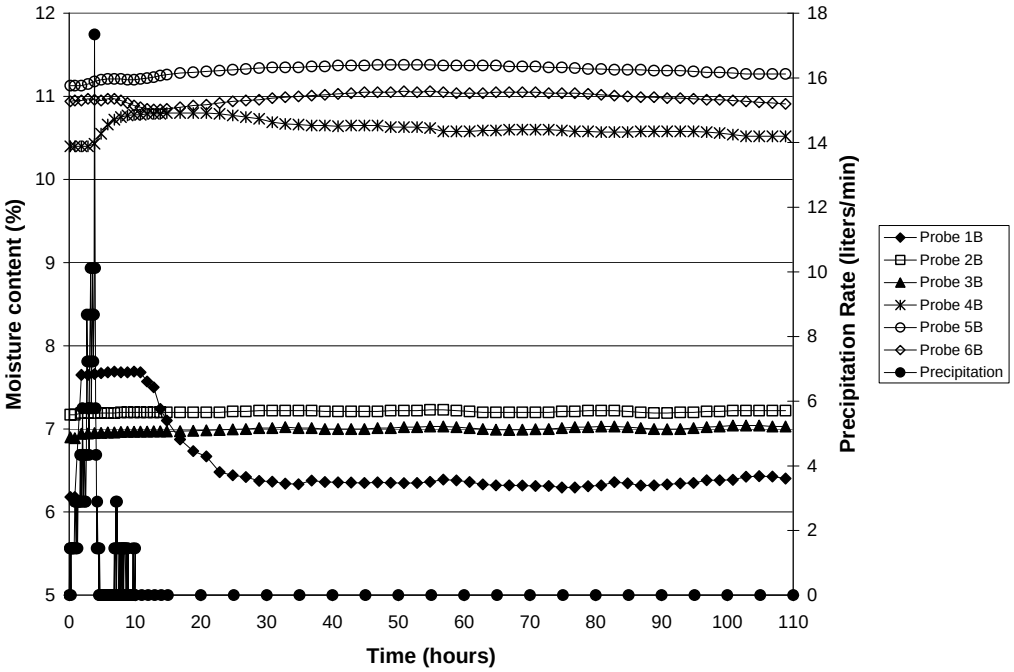

Figure 4.38 Moisture contents in the base material of test pad B at the ERC during and 100 hours after the large precipitation event.

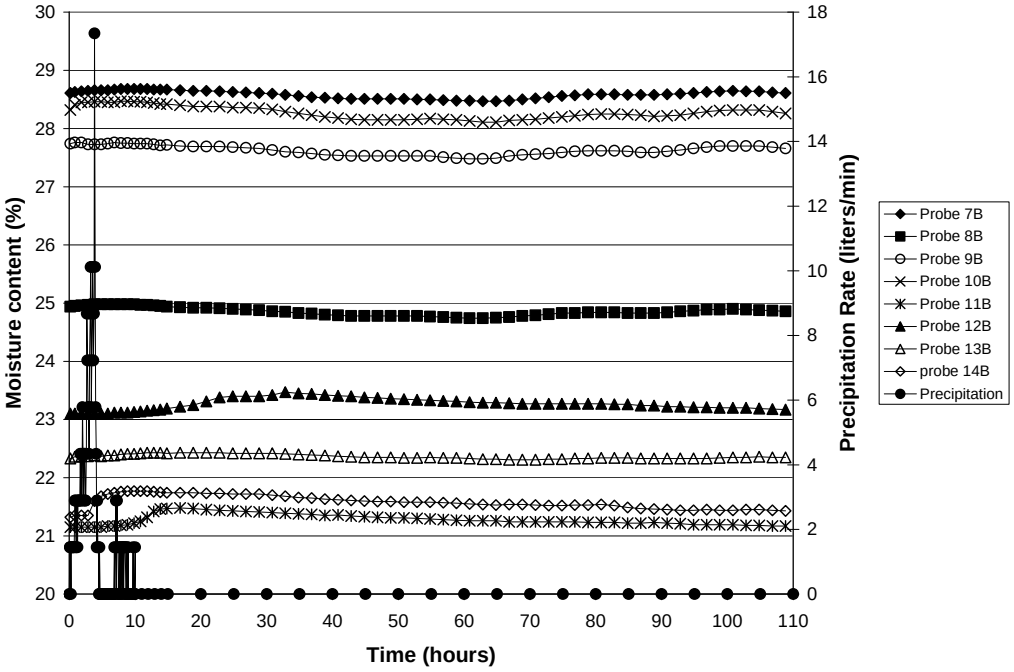

Figure 4.39 Moisture contents in the subgrade soil of test pad B at the ERC during and 100 hours after the large precipitation event.

From Figure 4.30 presented earlier for moisture contents during the large precipitation event, it can be seen that there were two peaks in the moisture contents at the location of probe 1A corresponding to two precipitation peaks. The first peak occurred about 3.5 hours after the precipitation event and the second peak occurred about 9.2 hours after the precipitation event. Shortly after the first peak in moisture content at probe 1A occurred the moisture contents at probes 3A and 6A also increased to peak values. This indicates that water moved horizontal very quickly. After the first peak in moisture content change at probe 1A, a drop in moisture content was observed until the second peak in precipitation. This drop in moisture content indicates that some of the pavement storage was transferred to the edge drain or underlying subgrade soils between the individual precipitation peaks. When the second precipitation peak occurred, the moisture content at probe 1A reached its second peak. This indicates that second peak of

the moisture content at probe 1A was the result of the second peak of the precipitation. Therefore, the pavement storage can be calculated based on moisture content changes during two peaks corresponding to two precipitation peaks.

4.7.4 Pavement Storage Model

As mentioned earlier, the pavement storage during precipitation events is manifested by the moisture content changes in the pavement system. To calculate the pavement storage in the test pads at the ERC, the following assumptions were made.

- The moisture content changes at the same depth in the pavement systems are assumed to be the same across the entire cross section. In reality, the moisture content changes from left to right across the section with the downhill or edge drain side having lager changes than locations at the opposite side. However, no moisture probes were installed in the far half of the pavement cross section so the variation is unknown. Therefore, moisture content changes with depths in the middle of the pavement (Probes 1, 2 and 4) were plotted as solid diamonds in Figures 4.40 and 4.41 and were used to calculate the pavement storage. For comparison, moisture content changes with depths in the next column of probes (Probes 3 and 5) were also plotted as circles in Figures 4.40 and 4.41.
- The pavement storage in the asphalt layer was negligible. This assumption is believed to be valid for several reasons. First, the porosity of the asphalt layer was small. The porosities of the asphalt layers at the ERC were measured by Qazi (2004). The average porosity was approximately 2.75 percent for the binder course and approximately 4.5 percent for the surface course. While the porosity of

the base material was approximately 23 percent and the porosity of the subgrade soil was approximately 62 percent. Second, the measured permeability of the asphalt layer was between 1×10^{-3} and 1×10^{-6} cm/s and the measured permeability of the base material was approximately 3.3×10^{-3} cm/s. Because the permeability of the asphalt layers is much lower than that of the underlying aggregate base materials, the asphalt layer would not become saturated during the precipitation events. Finally, the moisture content in the asphalt layers was not measured during the field experiments.

The changes of moisture contents with depths were plotted for the large precipitation event in Figures 4.40 and 4.41 for the two peaks. Regression analyses were performed on the moisture content changes using power equations to develop a curve that fit the data. The power equations were then used to integrate the area under the regression lines for calculating the pavement storage.

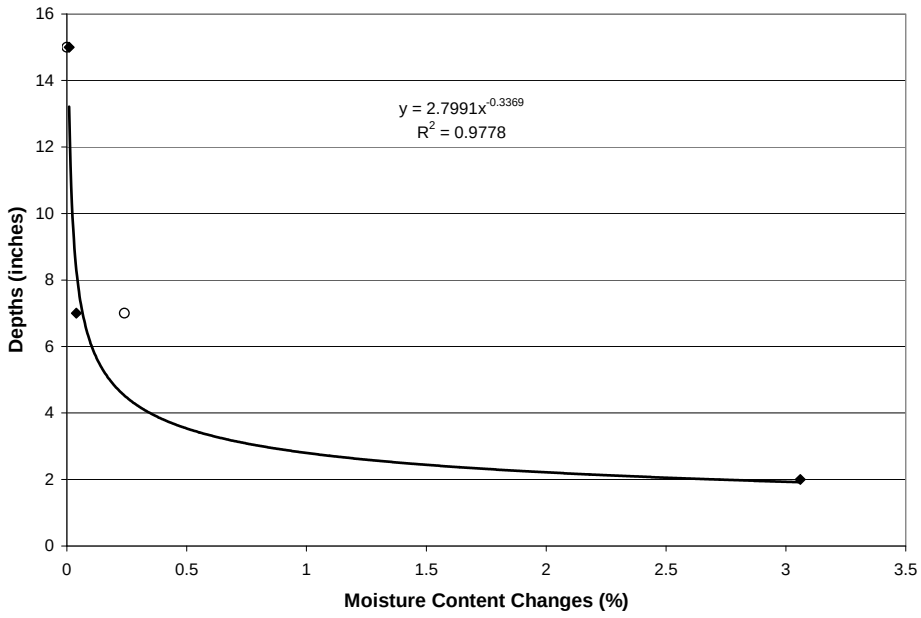

Figure 4.40 Changes of moisture contents versus depths referenced from the bottom of the asphalt layer for the first peak.

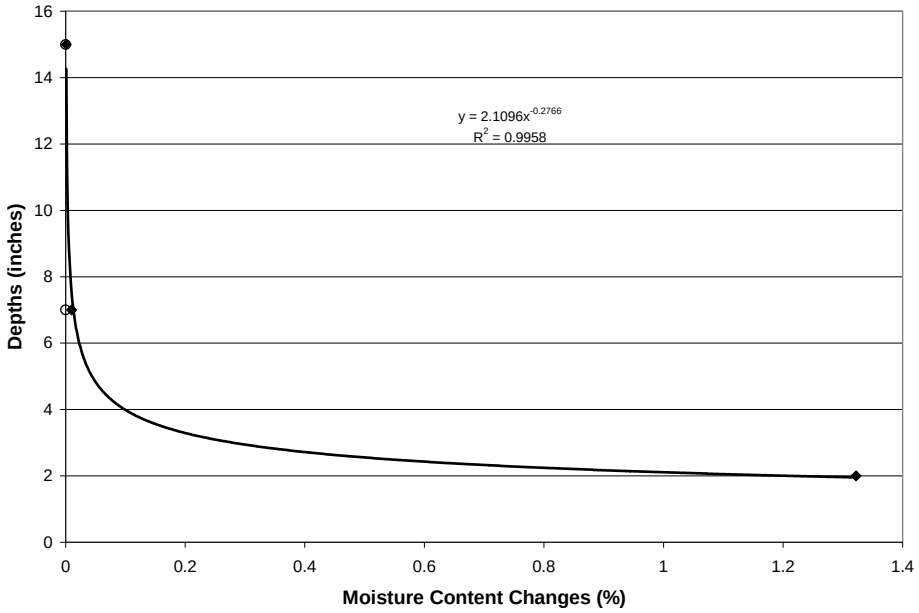

Figure 4.41 Changes of moisture contents versus depths referenced from the bottom of the asphalt layer for the second peak.

Water stored in the pavement systems of the test pads at the ERC during precipitation events can then be calculated using Equation 4.5:

V_w = Contributing Area × Measured Dry Density of Base Materials ÷ 1200×

Areas under Power Regression Lines in Figures 4.40 and 4.41 ÷2.19 4.5

Where:

V_w - stored water in the pavement (liters)

Contributing area - defined by the area surrounded by the berms and retaining wall for test pad A as discussed previously (ft^2);

Measured Dry Density - dry densities of base materials were measured using a nuclear density gauge at eight locations, an average value of 142.5 pcf was used;

Area under power regression lines in Figures 4.40 and 4.41 – the area can be

obtained by integrating the regression equations.

Using Equation 4.5, the pavement storage during the larger precipitation event was determined to be 421.7 liters for test pad A and 132.3 liters for test pad B.

Using the pavement storage model as described in Equation 4.5, the pavement storage during each precipitation event was calculated for both test pads. In Figure 4.42 and 4.43, total precipitation volume was plotted with the pavement storage for test pads A and B. From Figures 4.42 and 4.43, it can be seen that, in general, a higher percentage of precipitation migrated into the pavement system for smaller precipitation events. Therefore, logarithmic regression analyses were performed between the total precipitation volume and pavement storage. The logarithmic regression lines and equations, along with the line of equality are shown in Figures 4.42 and 4.43. From Figures 4.42 and 4.43, it can be seen that statistically more than twice the quantity of water migrated into the base material in test pad A when compared to pad B for the same precipitation event. This can be explained by the fact that test pad A had only a 3-inch thick layer of the binder course while test pad B had a combined 6-inch thick layer of the surface and binder courses.

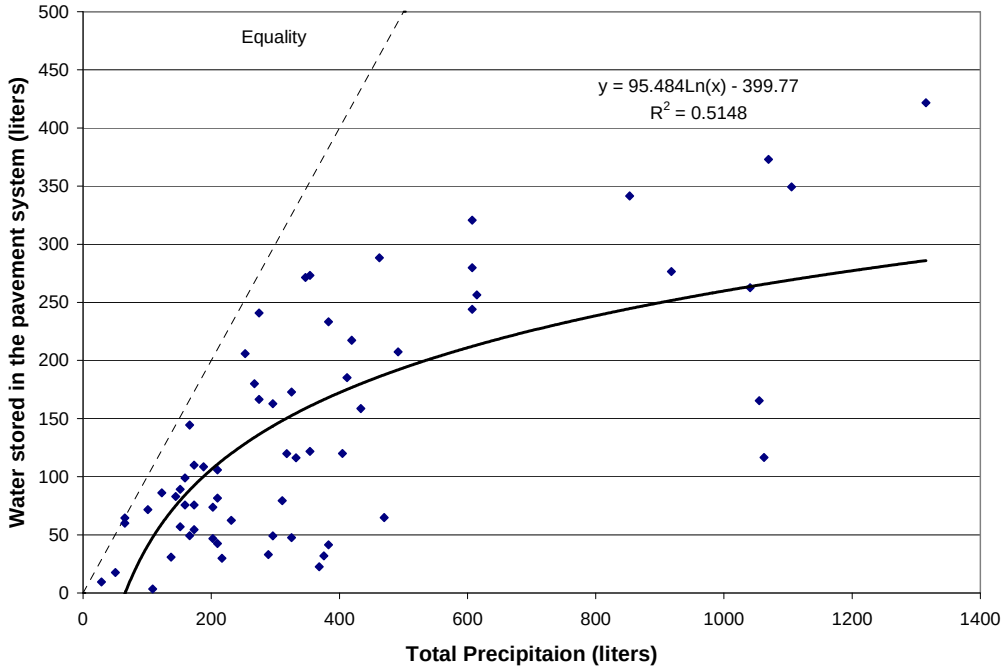

Figure 4.42 Total precipitation versus water stored in test pad A at the ERC.

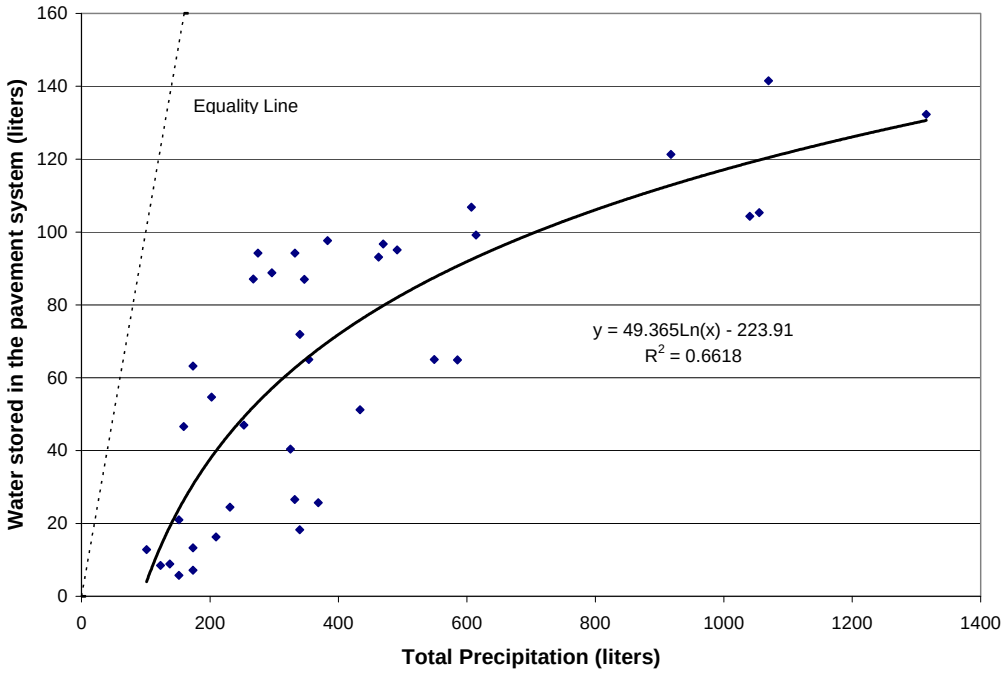

Figure 4.43 Total precipitation versus water stored in test pad B at the ERC.

Only one layer of moisture probes was installed in the base material at the Ft. Smith site because the base course layer only had an average thickness of approximately 4 inches. For the purpose of calculating the pavement storage, the moisture content changes in the base material were assumed to be the same across the entire cross section as those from Probe 1, which was installed in the middle of the base layer. Based on this assumption, the calculated pavement storage would generally be smaller than collected subsurface runoff. For example, during a measured 0.63-inch precipitation event on April 21, 2006, the moisture content from Probe 1 increased by 0.12 percent and the calculated pavement storage was only 150 liters. However, collected subsurface water during this precipitation event was 1759 liters. This indicates that most of water that migrated into the pavement at the Ft. Smith site moved horizontally to the edge drain through either the relatively thick asphalt layer (approximately 9 inches) or via the interface between the asphalt and base layers. This phenomenon may also be explained by the fact that the laboratory-measured hydraulic conductivity of the base materials at the Ft. Smith site is 6×10^{-4} cm/s, which is about one fifth of the laboratory-measured hydraulic conductivity of the base materials at the ERC. The lower hydraulic conductivity of the base materials at the Ft. Smith test site would require more time for water to migrate through the base materials and therefore more water would be held above the base material for the same period and move horizontally through either the relatively thick asphalt layer or via the interface between the asphalt and base layers.

4.7.5 Water Balance Analysis

Theoretically, the total precipitation volume should be equal to the sum of surface runoff and the pavement storage. In Figure 4.44, total precipitation volume was plotted against the sums of the pavement storage and surface runoff for test pad A at the ERC. A linear regression analysis was then performed between the total precipitation volume and the sum of the pavement storage and surface runoff. The regression line and equation along with the line of equality are shown in Figure 4.44.

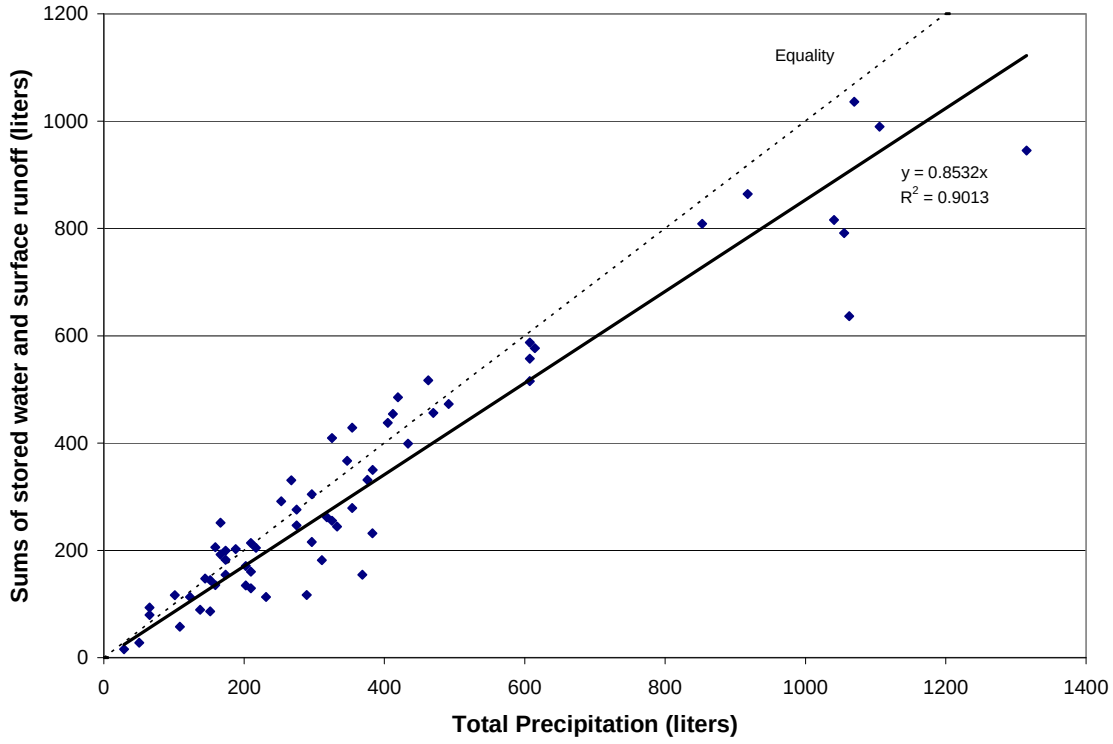

Figure 4.44 Total precipitation versus the sum of surface runoff and stored water for all events recorded for test pad A at the ERC.

The results of the regression analysis indicate that about 85 percent of the total precipitation volume either ran off from the pavement surface or infiltrated into the pavement. On average, less than 100 percent of total precipitation was accounted for.

However, for some events slightly more than 100 percent of the precipitation volume was accounted for by runoff and storage. The variations might be explained by the following:

- As described in Chapter 3, test pad A at the ERC was surrounded by an approximately 2-foot high retaining wall on the downhill side and approximately 4-inch high berms on the other three sides. Due to the difference in heights between the retaining wall and berms, the contributing area may be bigger or smaller than the area of the pavement surface depending on the direction of the wind in a rainfall event, as illustrated in Figure 4.45. In Figure 4.45, For calculation purposes, w stands for the width of the pavement that is used in Equation 4.5. While w' stands for the actual width of pavement that receives precipitation. In scenario 1, more precipitation than assumed was actually collected on the pavement surface. In scenario 2, less precipitation was collected. For example, if the precipitation is off vertical by 30 degrees, the precipitation actually collected is different from the theoretical calculation by about 10 percent. This could explain why the precipitation which was accounted for with the model could both exceed and be less than 100 percent of the total precipitation volume.

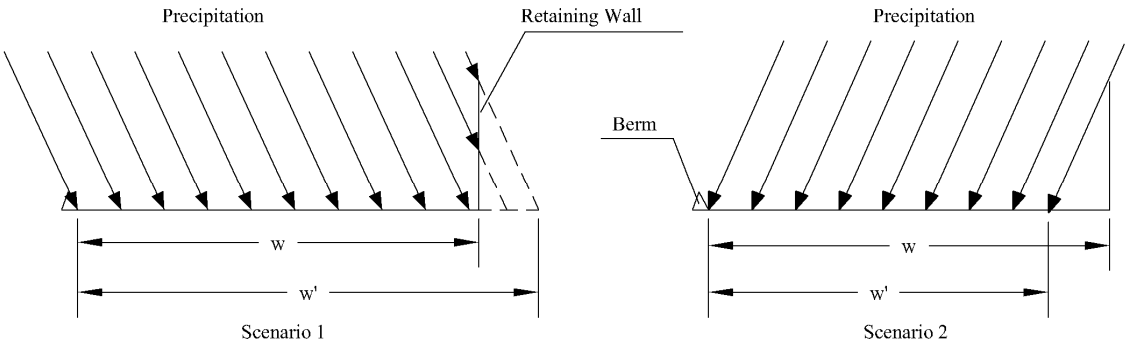

Figure 4.45 Effects of wind on collected precipitation on the pavement.

- A portion of the depression storage evaporated and was not included in the water balance analysis.
- Some portion of water was stored in the asphalt layers and was not included in the water balance analysis.

4.8 Moisture Content in Pavement Systems

The moisture content in the base and subgrade of the pavement systems at the ERC was monitored from July 2002 to December of 2004 using Campbell Scientific Model CS615 moisture probes. From August 21, 2002 to May 26, 2003, the moisture content was measured every 2 hours. From May 27, 2003 to August 20, 2003, the moisture content was measured every hour. After August 21 2003, the moisture content was measured at 20 minute intervals. As discussed previously, the change of measurement frequency was due to an addition of memory to the data logger. The moisture content at the Ft. Smith test site was recorded every 20 minutes for approximately 15 months from March 2005 to June 2006. As discussed in the previous chapter, the output of TDR moisture probes was calibrated to gravimetric water content. To take both unit weight and moisture content into consideration, moisture contents were converted to degrees of saturation using Equation 4.6.

$$S = \frac{\gamma_d w G_s}{62.4 G_s - \gamma_d} \times 100 \qquad 4.6$$

Where,

S = degree of saturation (%);

γ_d = dry unit weight (pcf);

w = gravimetric water content (decimal);

G_s = specific gravity.

Specific gravities of the base and subgrade soils at the ERC and the Ft. Smith test site were measured in the laboratory in accordance with ASHTO T-84. Gravimetric moisture contents of the base and subgrade soils were measured using TDR moisture probes installed in the pavement systems. Dry densities of the base and subgrade soils at the ERC were measured using a nuclear densitometer. Dry densities of the base and subgrade soils at the Ft. Smith test site were not measured, however, Arkansas 2003 Standard Specifications for Highway Construction requires that subgrade soils need to be compacted to 95 percent of standard Proctor maximum dry density (AASHTO T-99) and base materials need to be compacted to 98 percent of modified Proctor maximum dry density (AATHTO T-180). It was assumed that these requirements were satisfied during the original pavement construction and after the sensor installation. Therefore, the dry densities were assumed to be 95 percent of standard Proctor maximum dry density (AASHTO T-99) for the subgrade soil and 98 percent of modified Proctor maximum dry density (AATHTO T-180) for the base material. Using these values, the daily average degrees of saturation in the pavement system were calculated.

Daily average degrees of saturation for base and subbase materials at the ERC were plotted in Figures 4.46 through 4.48 for test pad A and in Figures 4.49 through 4.51 for test pad B. From Figure 4.46, it can be seen that degrees of saturation in the base material at a depth of 2 inches below the bottom of the asphalt in test pad A at the ERC (probe 1A) were generally between 55 and 65 percent. As discussed in the section on "Water Balance Analysis", the moisture content at this level had relatively significant

changes during and immediately after precipitation events. This is reflected by the significant fluctuations in the saturation levels above 65 percent in Figure 4.46. To visually observe the effect of precipitation events on degrees of saturation in this layer, precipitation data were superimposed on the saturation data in Figure 4.46. In addition, it can be seen that TDR measured degrees of saturation during January of 2003 and December of 2004 decreased significantly. This sudden decrease in moisture content indicates that the ground at this depth was partially or completely frozen.

From Figure 4.47, it can be seen that degrees of saturation in the base material at a depth of about 7 inches below the asphalt bottom in test pad A at the ERC were generally between 65 and 80 percent. Comparing Figures 4.47 with 4.46, it can be seen that moisture contents at the depth of 7 inches below the asphalt bottom fluctuated much less than those at the depth of 2 inches below the asphalt bottom. This indicates that precipitation events have much less effect on the moisture contents at the depth of 7 inches than those at the depth of 2 inches below the asphalt bottom. Significant drops in degrees of saturation were also observed at this depth during Jan 2003 and Dec 2004 indicating the ground was frozen to at least 10 inched below the pavement surface during these periods.

Probes 4A, 5A and 6A were installed in the subbase material at a depth of approximately 15 inches below the bottom of the asphalt and 2 inches above the surface of the subgrade soil in test pad A at the ERC. When converting moisture contents for probes 4A, 5A and 6A to degrees of saturation, more than 100 percent degrees of saturation were obtained for some data points. To prevent having degrees of saturation above 100% the dry unit weight of the subbase material, which was measured in the field,

was decreased slightly (less than 1%). As a result of this minor change the degrees of saturation for these probes were all equal to or below 100 percent. From Figure 4.48, it can be seen that changes in the degree of saturation for probes 4A and 5A appear to follow a pattern that is independent of precipitation events and more likely seasonal. This may be explained by the fact that these probes were about 2 inches above the subgrade soil. The subbase material at this depth might be contaminated by fines migrating into the subbase layer due to water seepage from the soil on the left side of the test pad as illustrated in Figure 4.21. Therefore, hydraulic conductivity at this depth could be lower than that of the base and subbase materials at shallower depths. Moisture probe 6A was installed near the edge drain and the degree of saturation at this location was likely more affected by precipitation events and did not follow the same seasonal pattern as probes 4A and 5A. Also, it can be seen that there is no abrupt drop in the degree of saturation for any of the probes at this level, which indicates that the ground was never frozen at this depth during the period of the study.

From Figures 4.46 through 4.48, it can be concluded that degree of saturation generally increased with depth from about 55 percent to near 100 percent in the base and subbase materials. The frost depth in test pad A at the ERC is about the depth of probe locations 2A and 3A, which are about 10 inches from the top of the asphalt surface.

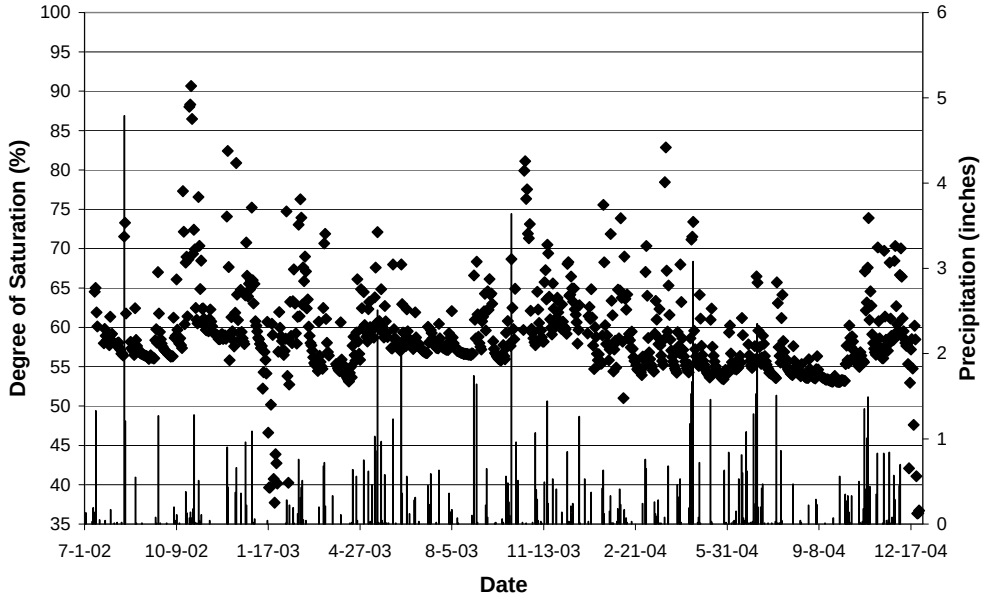

Figure 4.46 Degree of saturation vs. time for a depth of approximately 2 inches below the bottom of asphalt in the base material (probe 1A) in test pad A at the ERC.

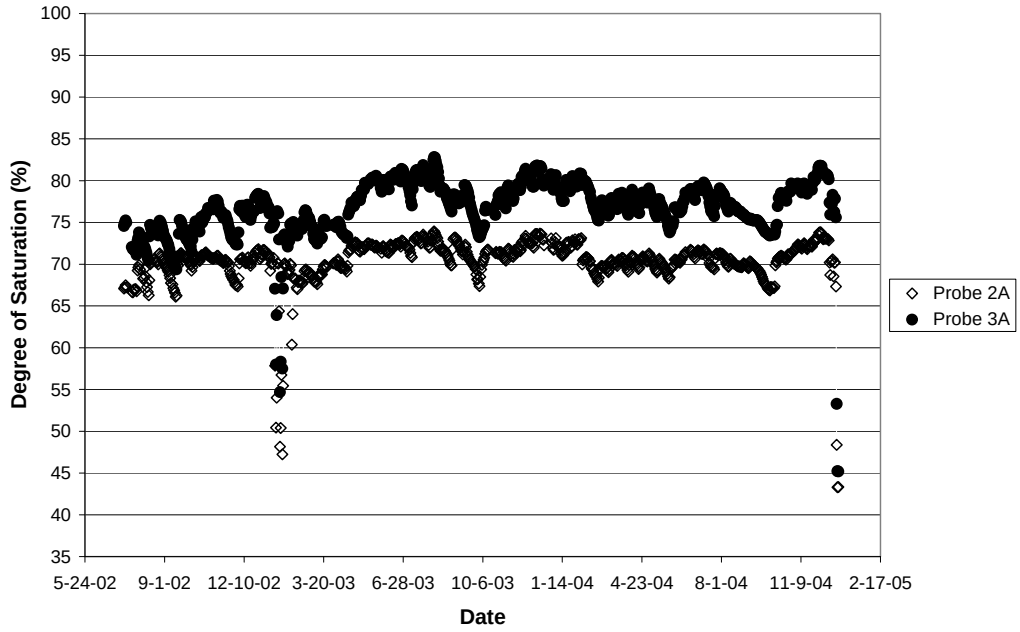

Figure 4.47 Degree of saturation vs. time for a depth of approximately 7 inches below the bottom of asphalt (probes 2A and 3A) at the interface between base and subbase materials in test pad A at the ERC.

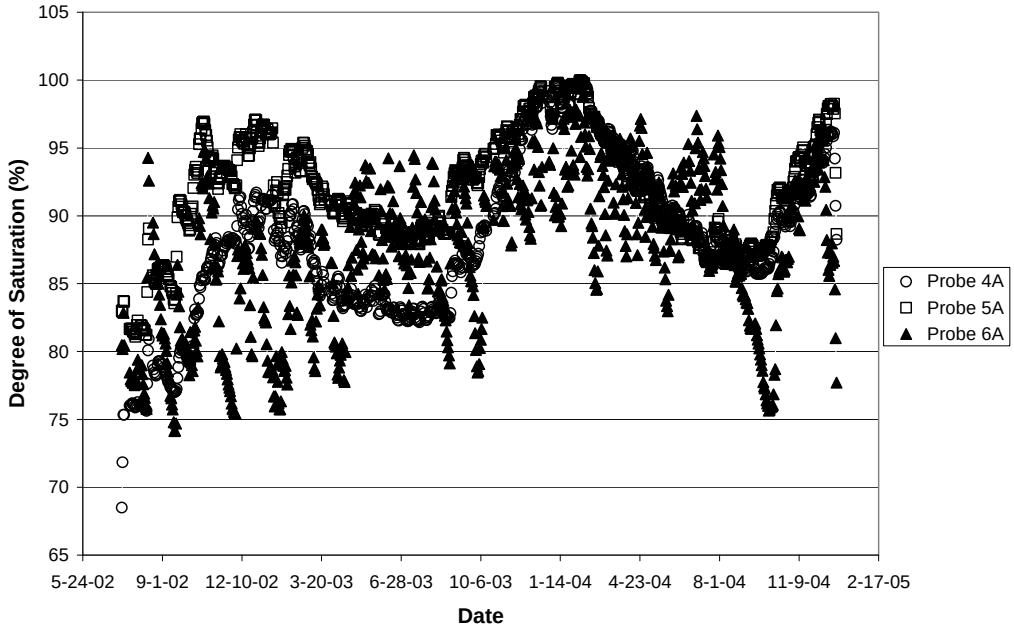

Figure 4.48 Degree of saturation vs. time for a depth of approximately 15 inches below the bottom of asphalt and 2 inches above the subgrade soil in the subbase material in test pad A at the ERC.

Figure 4.49 illustrates the variation in saturation for probe 1B in test pad B. Its behavior is similar to that of probe 1A in test pad A, which indicates that the moisture in the upper reaches of both test pads responded to precipitation events. However, from Figures 4.50 and 4.51, it can be seen that moisture content changes in the base and subbase materials at depths of 7 inches or deeper below the asphalt bottom appear to be more likely affected by season rather than by precipitation. This may be explained by the difference in asphalt thickness between the two test pads. Also, it can be seen that a significant drop in degrees of saturation is only observed at the depth of about 2 inches below the asphalt bottom during Jan 2003 indicating the ground was frozen to only 8 inches below the pavement surface during this period compared to 10 inches for test pad A. This can be explained by the thicker asphalt layer for test pad B than for test pad A.

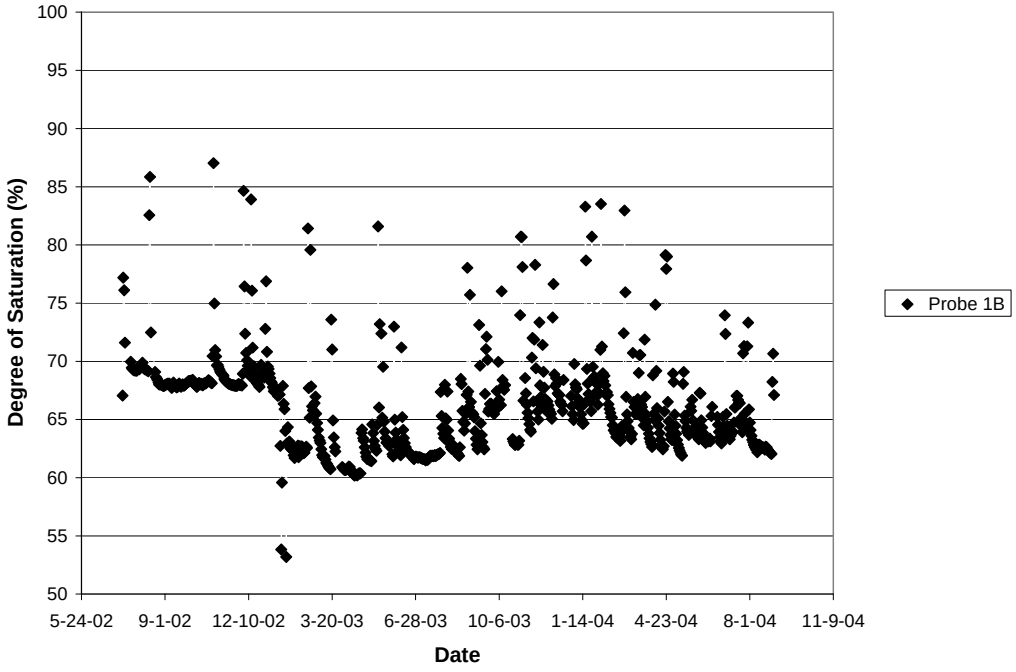

Figure 4.49 Degree of saturation vs. time for a depth of approximately 2 inches below the bottom of asphalt in the base material (probe 1B) in test pad B at the ERC.

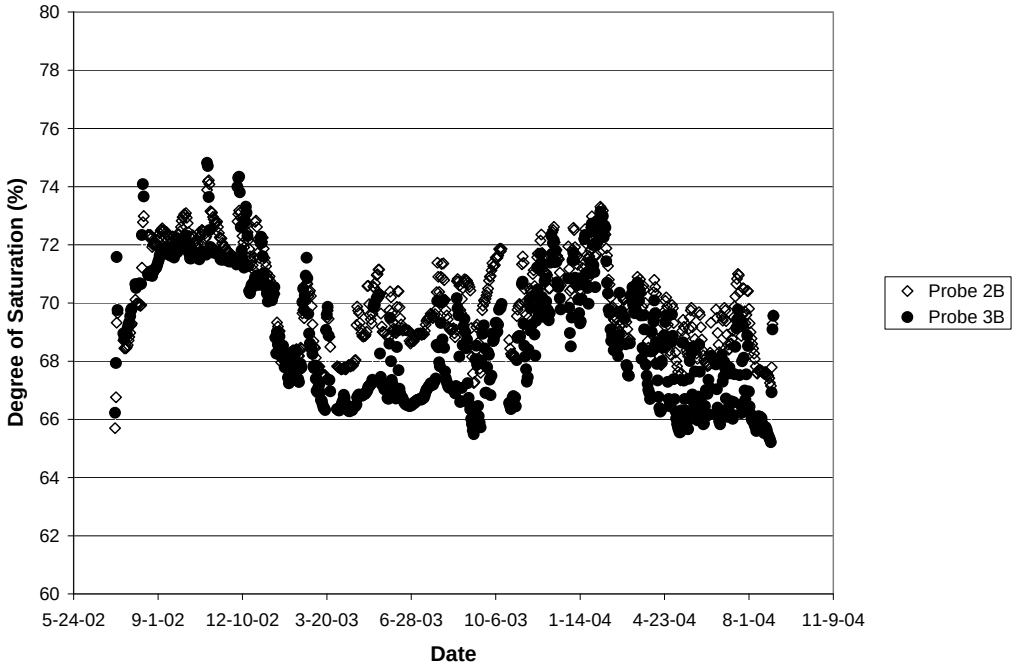

Figure 4.50 Degree of saturation vs. time for a depth of approximately 7 inches below the bottom of asphalt (probes 2B and 3B) at the interface between base and subbase materials in test pad B at the ERC.

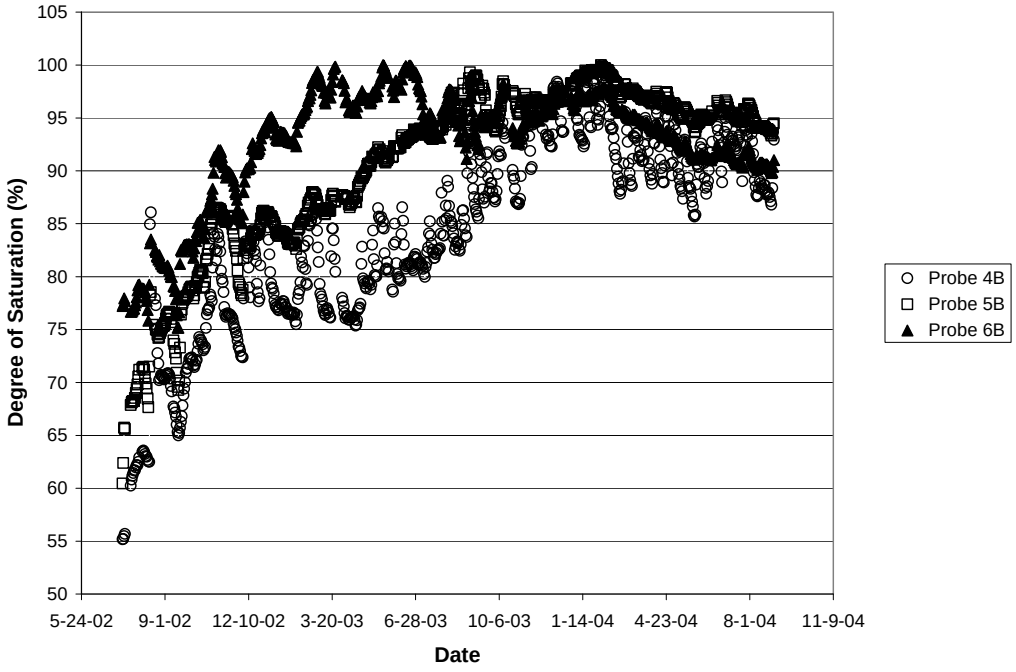

Figure 4.51 Degree of saturation vs. time for a depth of approximately 15 inches below the bottom of asphalt and 2 inches above the subgrade soil in the subbase material in test pad B at the ERC.

Daily average degrees of saturation for the subgrade soil at the ERC are plotted in Figures 4.52 and 4.53 for test pad A and in Figures 4.54 and 4.55 for test pad B. At the ERC, four moisture probes were installed for each layer in the subgrade soils. In Figures 4.52 through 4.55, an average of the four probe's reported degrees of saturation was used for each depth.

From Figures 4.52 and 4.53, it can be seen that degrees of saturation in the subgrade soil for test pad A at the ERC changed with seasons following a periodic function. Therefore, the same regression analyses as used for air temperature were performed on degrees of saturation in the subgrade soil for test pad A at the ERC. The regression coefficients are presented in Table 4.46. Predicted degrees of saturation are also plotted in Figures 4.52 and 4.53. Extremes for high degrees of saturation occurred in

summers while extremes for low degrees of saturation occurred in winters. Degrees of saturation in the subgrade soil for test pad A generally changed from 64 percent in winters to 84 percent in summers. From Figures 4.52 and 4.53, it can also be seen that extremes for degrees of saturation changed from year to year. This may be the result of changes in frequencies and quantities of precipitation from year to year. While efforts have been made to incorporate precipitation data into predicative models, no obvious relationship was found between precipitation and degrees of saturation in the pavement systems. To visually observe the effect of precipitation on degrees of saturation in subgrade soils, precipitation data were superimposed on the saturation data in Figure 4.52. Inspection of Figure 4.52 indicates no obvious relationship between precipitation and degrees of saturation. It is possible that changes in extreme degrees of saturation from year to year could be the result of long-term environmental factors. A much longer monitoring period for moisture contents and environmental factors would be required to determine why and how extreme degrees of saturation change from year to year.

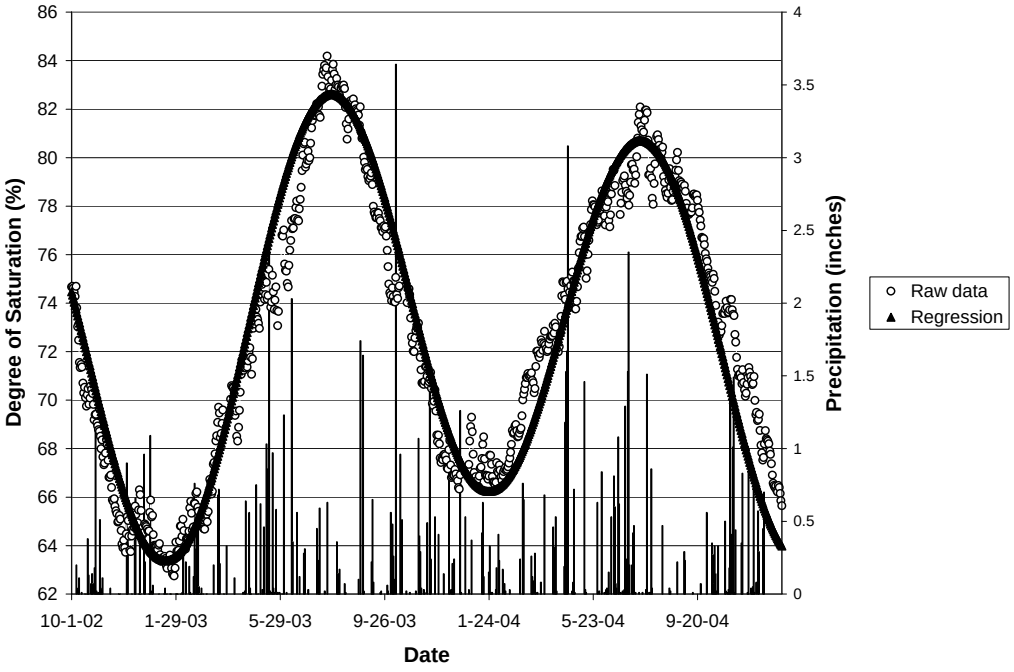

Figure 4.52 Average degree of saturation v.s. time in the subgrade soil at a depth of 2 inches below the subgrade surface for test pad A at the ERC.

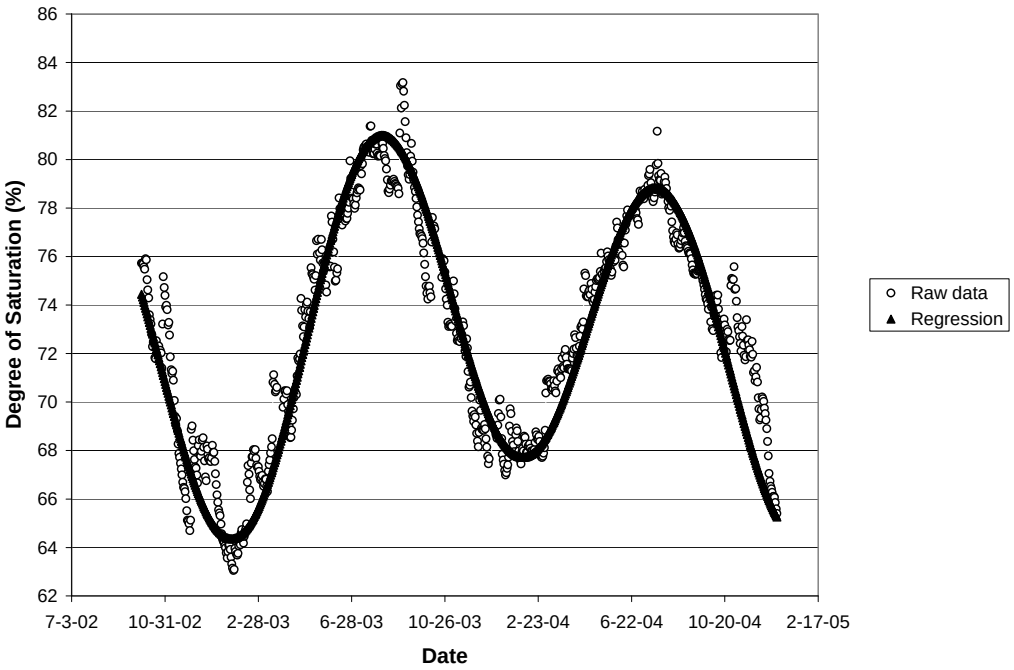

Figure 4.53 Average degree of saturation v.s. time in the subgrade soil at a depth of 10 inches below the subgrade surface in test pad A at the ERC.

Figures 4.54 and 4.55 illustrate degree of saturation versus time for test pad B. Changes in degree of saturation in test pad B are similar to those observed for test pad A. The same type of regression analysis was performed on degrees of saturation in the subgrade soil for test pad B at the ERC. Regression coefficients are presented in Table 4.6.

When comparing degrees of saturation in the subgrade soil for test pad A with those for test pad B, it is obvious that extreme degrees of saturation for both pads occurred at almost the same times. However, it appears that degrees of saturation for test pad A fluctuated more significantly with season than those for test pad B. This may be explained by the difference in asphalt thickness between two test pads.

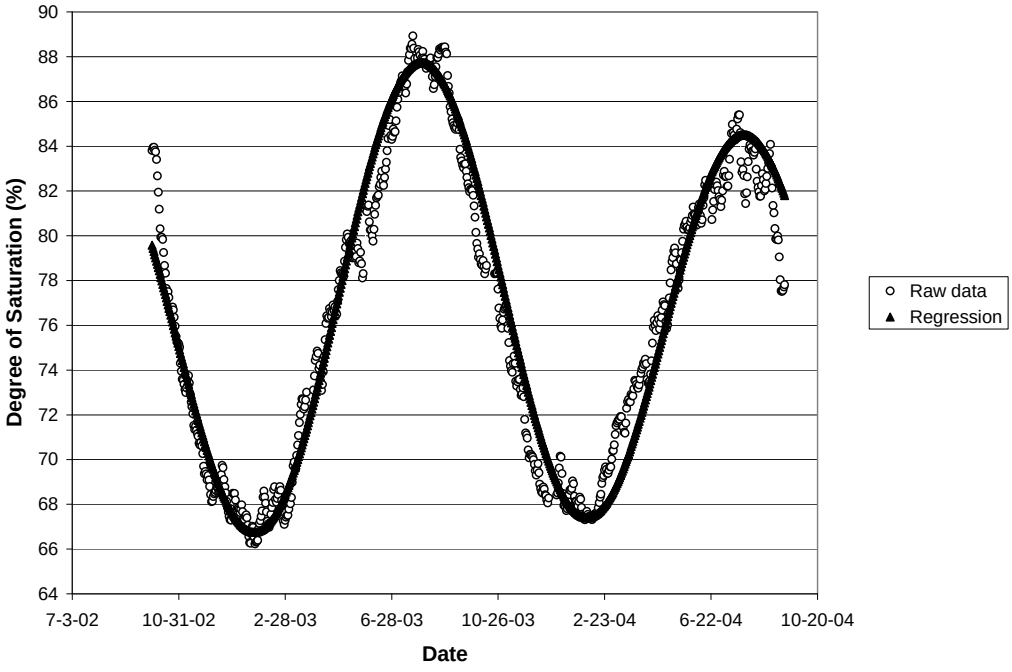

Figure 4.54 Degree of saturation vs. time in the subgrade soil at a depth of 2 inches below the subgrade surface in test pad B at the ERC.

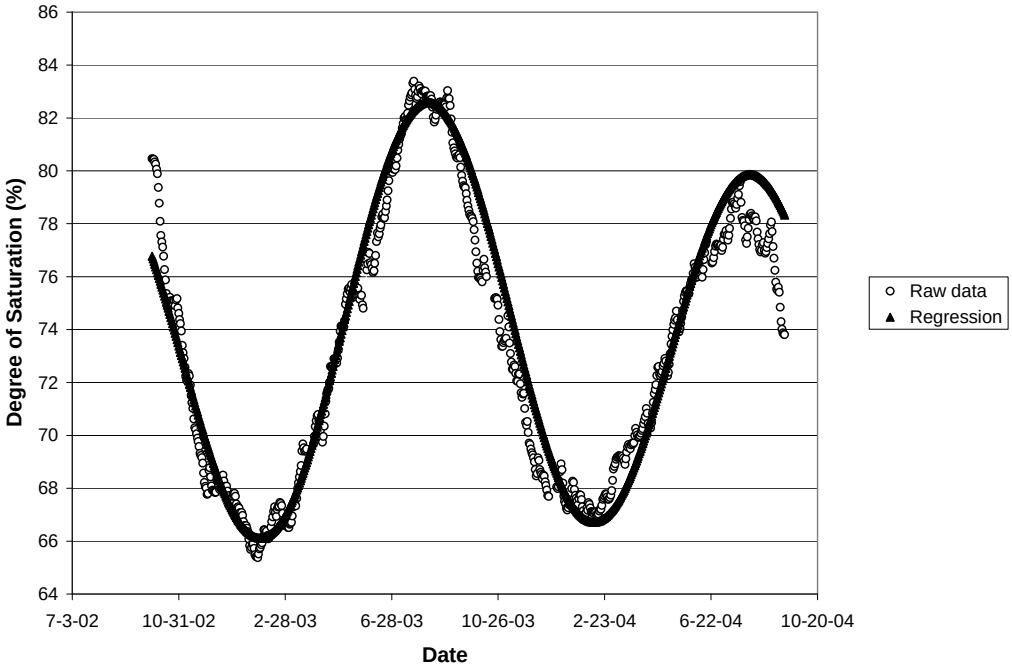

Figure 4.55 Degree of saturation vs. time in the subgrade soil at a depth of 10 inches below the subgrade surface in test pad B at the ERC.

Table 4.6 Results of the Analyses on degrees of saturation in the pavement systems at the ERC.

		a_0	a_1	b_1	a_2	b_2
Test pad A	1st layer	73.23	1.58	-0.69	-7.88	-2.92
	2nd layer	72.97	1.90	-0.63	-6.05	-3.33
Test pad B	1st layer	76.62	0.71	-1.48	-8.33	-4.59
	2nd layer	73.84	0.71	-1.20	-5.98	-4.35

Daily average degrees of saturation are plotted in Figure 4.56 for the base material and in Figures 4.57 through 4.59 for the subgrade soil at the Ft. Smith site. From Figure 4.56, it can be seen that degrees of saturation in the base material at the Ft. Smith test site seems to change with seasons following a periodic function. This may be explained by the fact that the base material had been partially mixed with the subgrade soil during the

probe installation. This may also be the result of significant slopes in both the longitudinal and the transverse direction at the Ft Smith site. Fines in the subgrade soils at the uphill side might have been migrating into the base material at the downhill side along with water seepage in the pavement system. This is indicated by the fact that the percentage of fine materials (material passing a U.S. No. 200 sieve) in the base material at the Ft. Smith site was 16.2 percent and is much higher than that allowed by the AHTD for Class 7 base and is certainly higher that the fines content at the ERC, which was 7.5 percent. The measured hydraulic conductivity of the base material at the Ft. Smith site was about one fifth of that of the base material at the ERC. It is possible that the lower hydraulic conductivity and a thicker asphalt layer caused the base material to behave hydraulically more like subgrade material, which resulted in seasonal variations in moisture as opposed to responses to precipitation events.

From Figures 4.57 through 4.59 one can see a similar pattern of moisture variation at the Ft. Smith site as was observed at the ERC. The same regression analysis procedures that were used for air temperatures were used to develop a periodic function for degrees of saturation versus time in the subgrade materials. The results of those analyses are presented in Table 4.7. The predicted degrees of saturation using the predicative models are also plotted in Figure 4.56 through 4.59 along with the measured values.

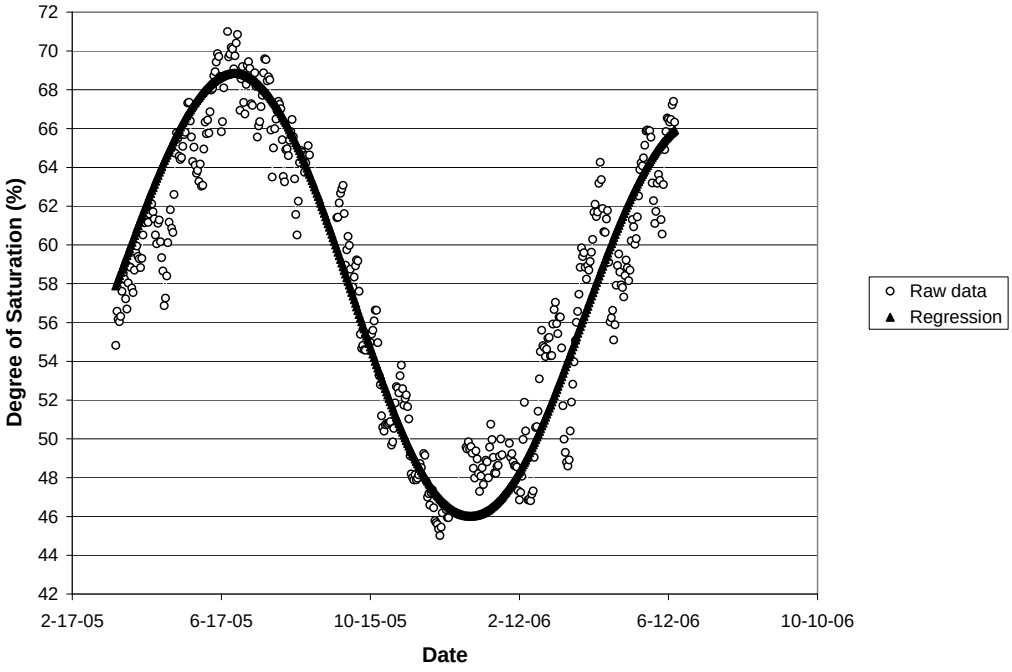

Figure 4.56 Degree of saturation vs. time in the base material at a depth of 2 inches below the base surface at the Ft. Smith test site.

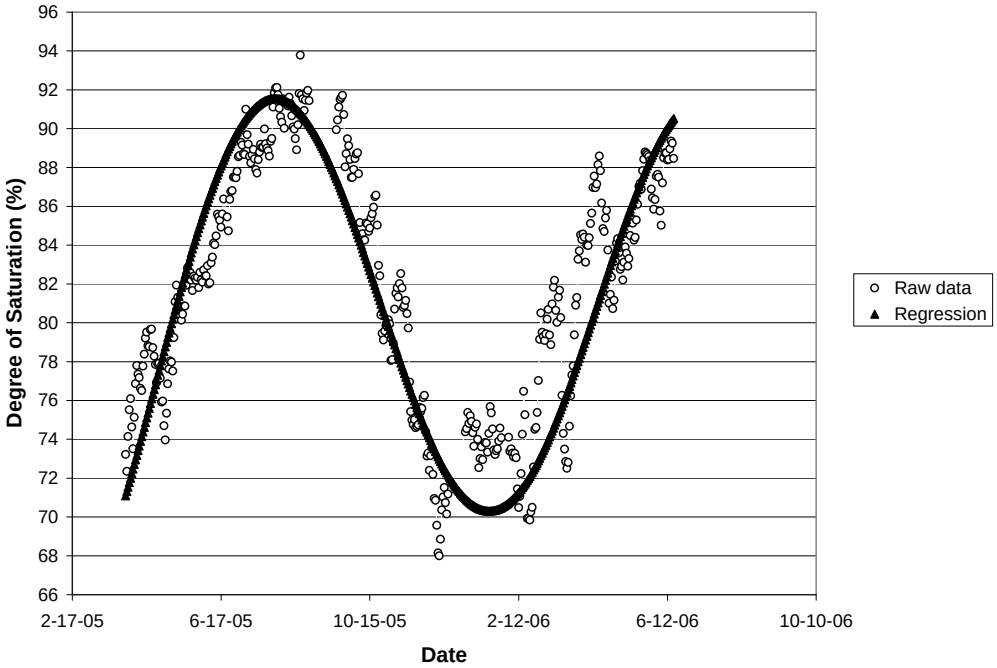

Figure 4.57 Degree of saturation vs. time in the subgrade soil at a depth of 2 inches below the subgrade surface at the Ft. Smith test site.

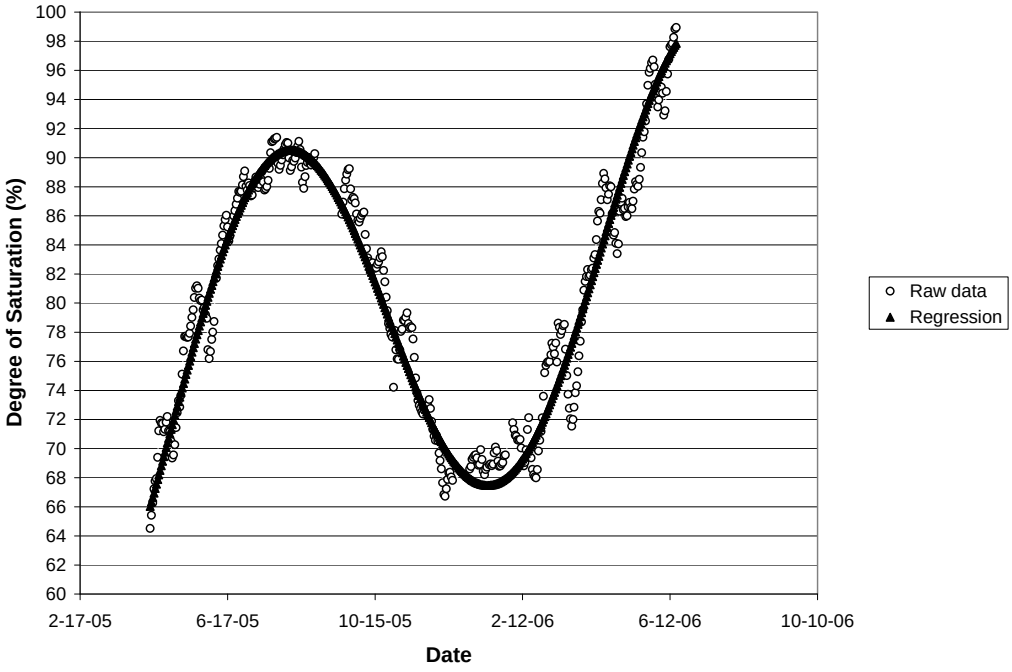

Figure 4.58 Degree of saturation vs. time in the subgrade soil at a depth of 10 inches below the subgrade surface at the Ft. Smith test site.

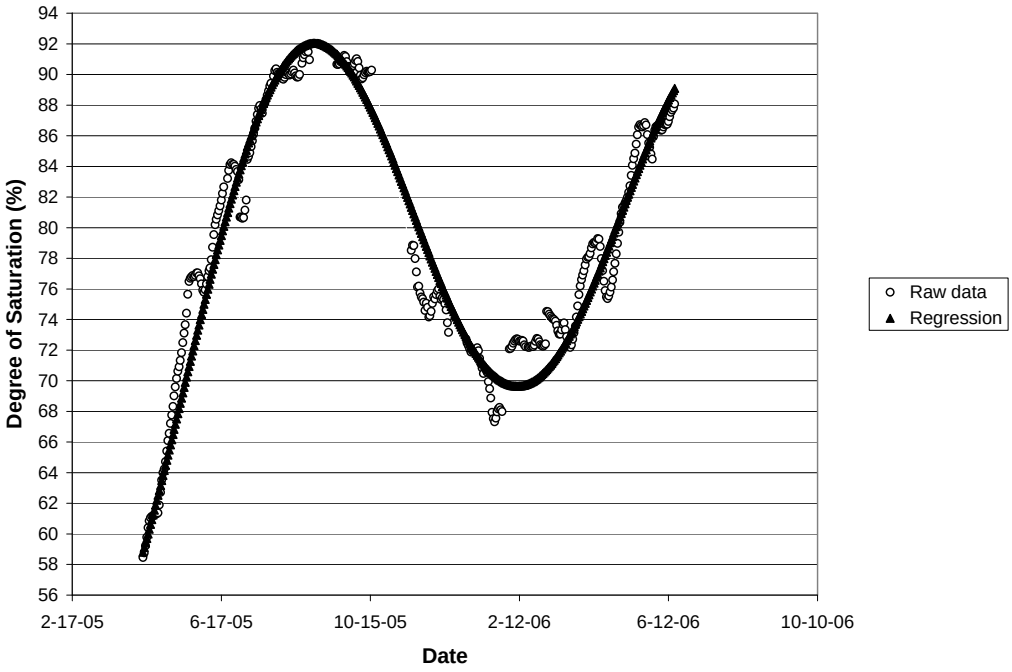

Figure 4.59 Degree of saturation vs. time in the subgrade soil at a depth of 24 inches below the subgrade surface at the Ft. Smith test site.

Table 4.7 Results of the Analyses on degrees of saturation in the pavement system at the Ft. Smith test site.

	a_0	a_1	b_1	a_2	b_2
Layer in Base Course	57.50	-1.33	-1.22	-10.12	-0.10
First Layer in Subgrade Soil	78.72	4.20	0.74	-11.94	-4.25
Second Layer in Subgrade Soil	77.45	6.34	6.00	-15.80	-6.88
Third Layer in Subgrade Soil	75.07	9.96	3.67	-12.07	-10.55

From Table 4.7, it can be seen that coefficients for the base course are significantly different from those for the subgrade soils, especially for coefficient a_0, which is the most important coefficient for determining magnitude of predicted degrees of saturation. However, the coefficients for three layers of subgrade soils are relatively close to each other. Comparing the coefficients for the subgrade soils at the Ft. Smith site shown in Table 4.7 and those for the subgrade soils at the ERC shown in Table 4.6, one can see that those coefficients are also relatively close to each other. In addition, the subgrade soils at both sites had similar plastic indexes (15 vs. 13) and were both AASHTO A-6 soils. In an effort to investigate if one prediction model could be used for the similar subgrade soils for both sites, a single predictive model was developed using the combined data from both sites. The coefficients of the regression analysis are presented in Table 4.8. Predicted values of degrees of saturation using the single model for both sites along with measured degrees of saturation are plotted against time in Figure 4.60. From Figure 4.60, one can see that maximum differences between predicted and measured degrees of saturation occurred in July of 2004. At this time, the single model over-predicted peak degrees of saturation by approximately 10 percent, which is about 12

percent of measured peak degrees of saturation at this time. Therefore, it can be reasonable to say that one single equation could be used for the similar subgrade soils at both sites.

Table 4.8 Results of the Analysis on degrees of saturation of the subgrade soils for both sites.

	a_0	a_1	b_1	a_2	b_2
Subgrade Soils	79.22	3.61	3.94	-11.49	-6.53

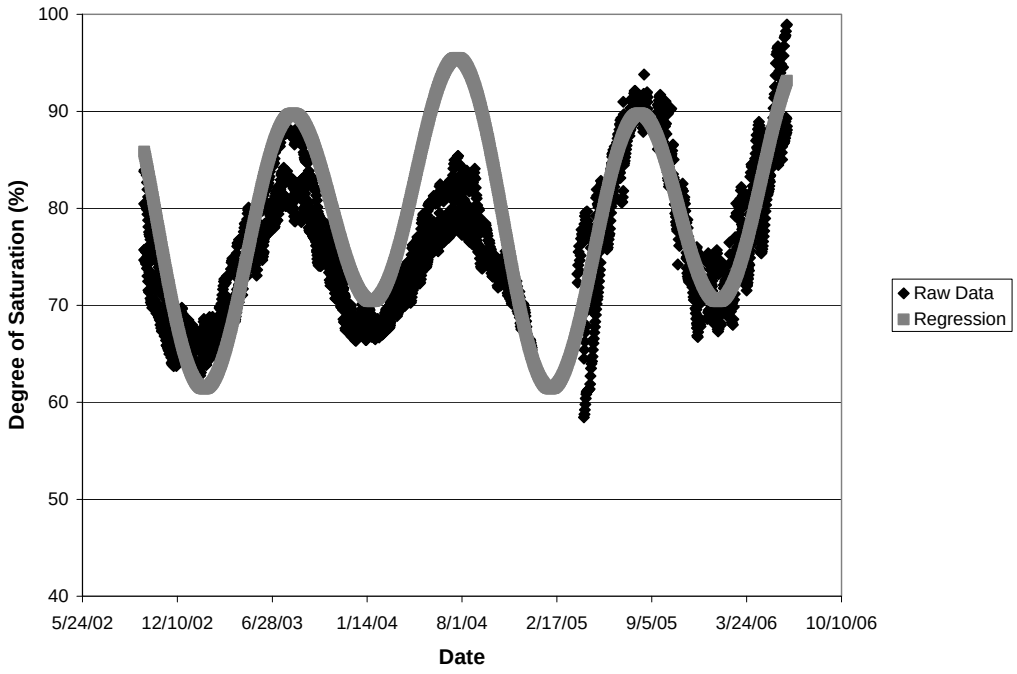

Figure 4.60 Comparison of predicted and measured degree of saturation in the subgrade soils vs. time for the Fayetteville and Ft Smith sites.

4.9 Effects of Moisture Content on Resilient Modulus

Resilient modulus of subgrade soils is one of the primary material properties required in the current empirical and mechanistic-empirical flexible pavement design procedures described in the AASHTO Design Guide 2004. As such the impact of changes

in moisture content on modulus values is extremely important in the design of pavement systems. As described in Chapter 3 (pages 76-80), repeated load triaxial tests were performed in accordance with AASHTO T-307 on the compacted specimens of the subgrade soils obtained from the ERC and the Ft. Smith test sites.

As shown in Figures 3.15 through 3.24 (page 79-80) the AASHTO test procedure produces a set of resilient modulus values for a soil corresponding to combinations of three confining pressures and five deviator stresses. However, the current pavement design procedure requires a single input value for the resilient modulus. AASHTO T-307 does not provide recommendations regarding how to reduce the test results to a single value of resilient modulus for design purposes. In fact AASHTO T-307 does not even consider the affects of variations in moisture content. As a result the designer is often unaware of the affect moisture contents can have on the value of resilient modulus selected for design. In the mechanistic-empirical flexible pavement design, the designer would know the stress conditions and therefore would choose values of resilient modulus at these stress conditions. However, changes in resilient modulus with moisture contents are still unresolved. To investigate the effect of moisture content on resilient modulus of subgrade soils, a single modulus value for each specimen has to be chosen using a combination of a single confining pressure and a single deviator stress.

SHRP Proctor P-46 (1989) recommended reporting resilient modulus values at a deviator stress of 4 psi and a confining pressure of 6 psi. Elliott (1988) recommended that the resilient modulus testing of cohesive soils can be simplified by using a single confining pressure of 3 psi and a single deviator stress of 8 psi. Elliott (1988) also concluded that unconfined testing (0 psi confining pressure) might also be considered,

which would produce conservative results. Recommendations from SHRP Proctor P-46 and Elliott are significantly different. Recommendations from Elliott would give a more conservative value of resilient modulus than those from SHRP Proctor P-46. Also, Elliott's recommendations were developed based on three typical Arkansas subgrade soils. So the Elliott's recommendations were adopted. However, a confining pressure of 3 psi was not included in the AASHTO T-307. For the purpose of describing the effects of moisture contents on resilient modulus, values of resilient modulus were taken at a deviator stress of 8 psi and a confining pressure of 2 psi. It should be noted that some samples at 140% of OMC failed before a deviator stress of 8 psi could be achieved. For these specimens a straight line projection was used to obtain a value for resilient modulus at a deviator stress of 8 psi.

Resilient modulus is plotted against the degree of saturation and percent of the OMC of subgrade soils at the ERC and the Ft. Smith site in Figures 4.61 and 4.62. Linear regression analyses were performed to obtain the relationship between degrees of saturation and resilient modulus values.

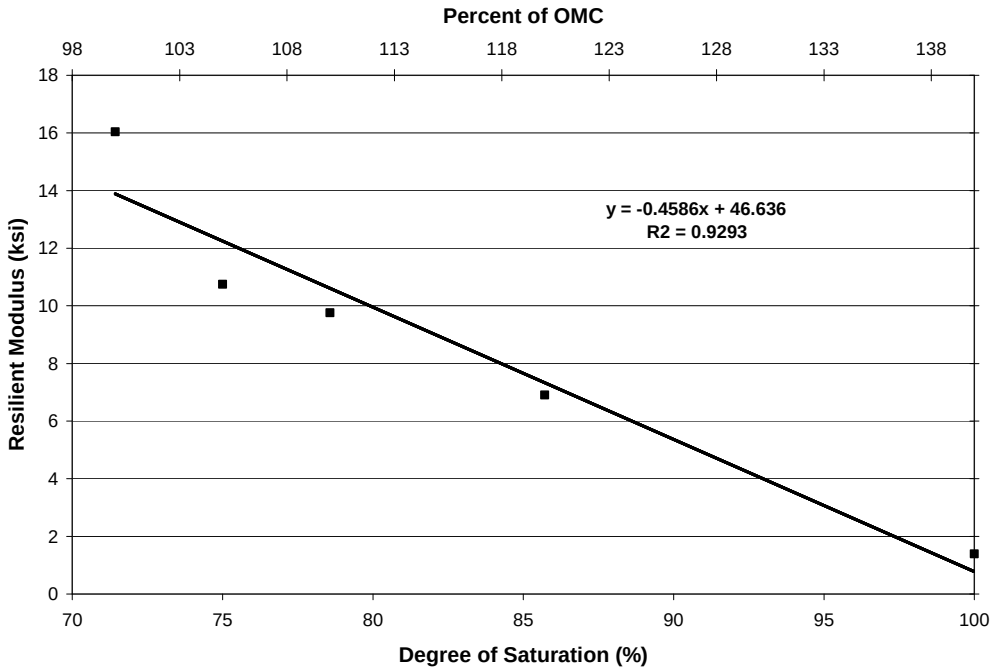

Figure 4.61 Degree of saturation versus resilient modulus of the subgrade soil at a deviator stress of 8 psi and a confining pressure of 2 psi at the ERC.

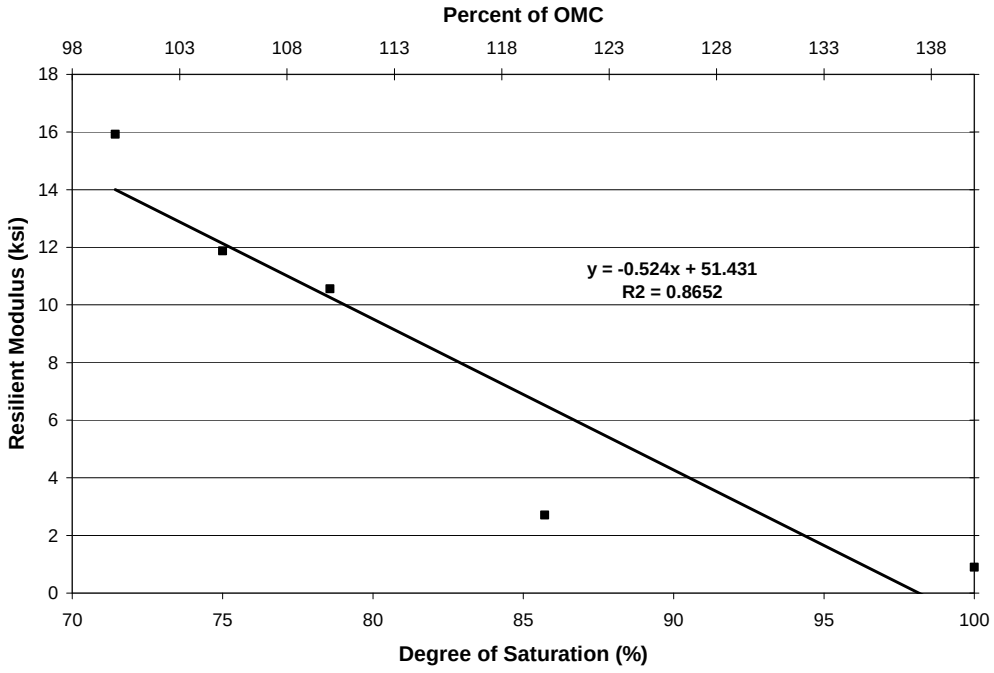

Figure 4.62 Degree of saturation versus resilient modulus of the subgrade soil at a deviator stress of 8 psi and a confining pressure of 2 psi at the Ft. Smith test site.

Using the linear regression relationship between degrees of saturation and resilient modulus, values of resilient modulus of subgrade soils were calculated based on measured degrees of saturation in subgrade soils at both the ERC and the Ft. Smith sites. Seasonal changes of resilient modulus are presented in Figures 4.63 through 4.69 for subgrade soils at the ERC and the Ft. Smith test site. Using the regression analysis procedures that were used previously to fit a periodic function to the temperature data, a model was developed to predict resilient modulus as a function of the seasonal moisture content change. The regression coefficients of the analyses are tabulated in Table 4.9 for the ERC soil and Table 4.10 for the Ft. Smith soil.

Because linear regression equations were used to relate moisture contents to resilient modulus of subgrade soils, the trend of the data in figures 4.63 through 4.69 are inversely related to the moisture content data presented in Figures 4.52 through 4.55 and 4.57 through 4.59. Therefore, the same trend but in an inverse manner was observed in Figures 4.63 through 4.69. From Figures 4.63 through 4.66, it can be seen that extremes for high resilient modulus of the subgrade soil at the ERC occurred in the winters and were approximately 18 ksi. While extremes for low resilient modulus occurred in summers and were approximately 6 ksi. From Figures 4.67 through 4.69, it can be seen that extremes for high resilient modulus for the subgrade soil at the Ft. Smith site were approximately 18 ksi in winters and extremes for low resilient modulus were approximately 3 ksi in summers.

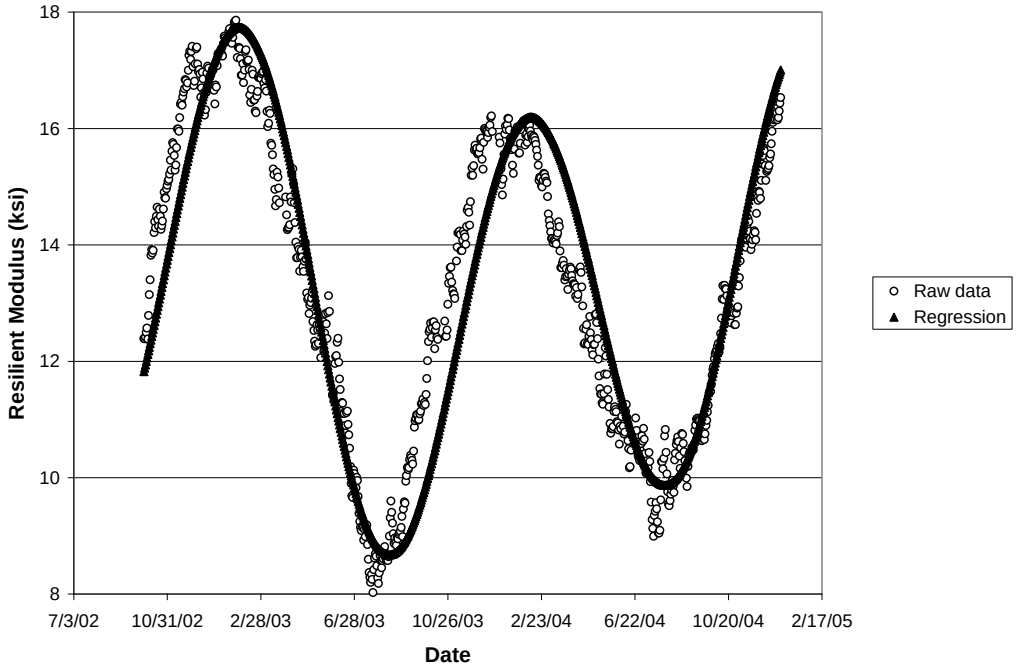

Figure 4.63 Soil resilient modulus vs. time at a depth of 2 inches below the subgrade surface in test pad A at the ERC.

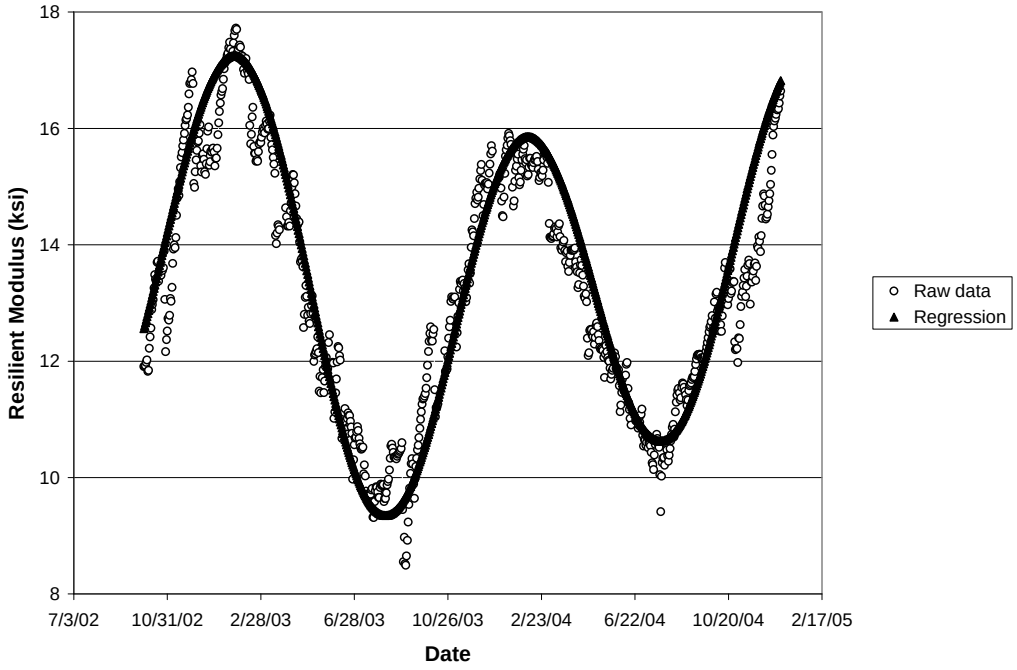

Figure 4.64 Soil resilient modulus vs. time at a depth of 10 inches below the subgrade surface in test pad A at the ERC.

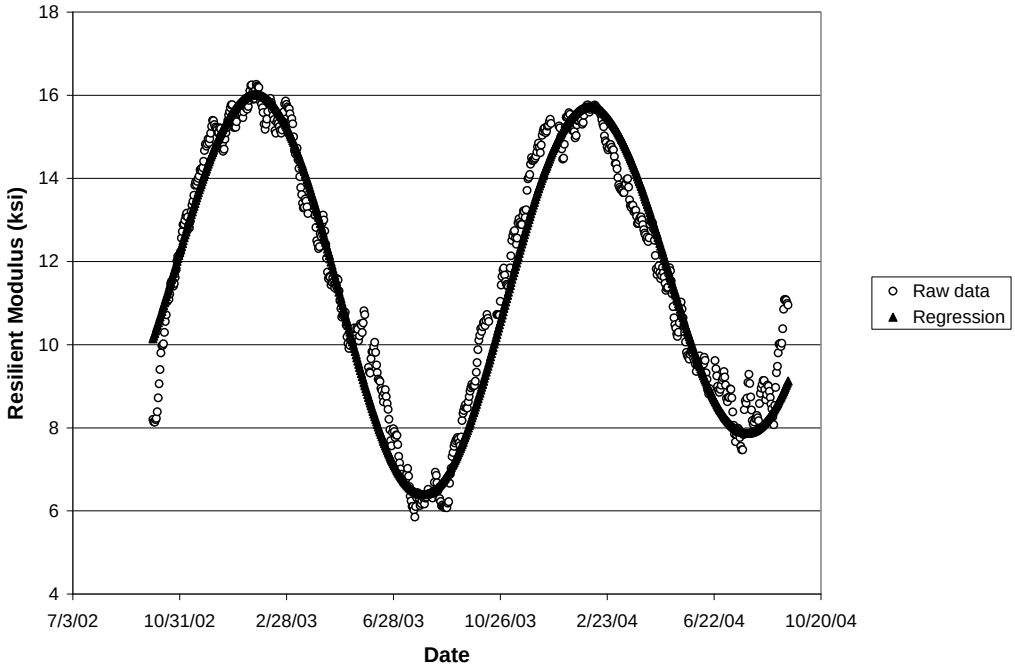

Figure 4.65 Soil resilient modulus vs. time at a depth of 2 inches below the subgrade surface in test pad B at the ERC.

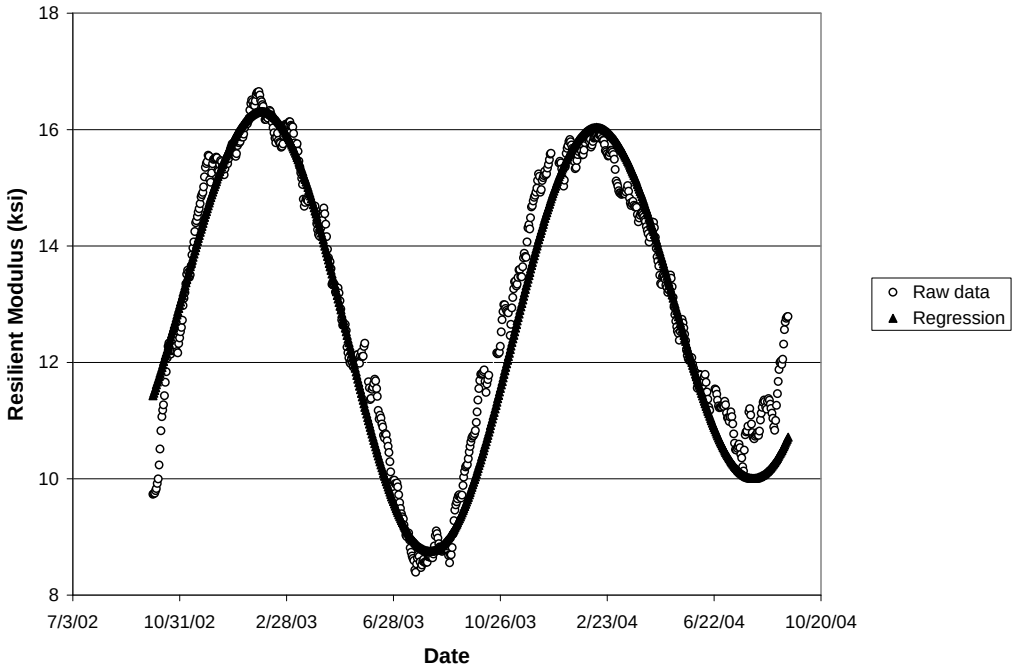

Figure 4.66 Soil resilient modulus vs. time at a depth of 10 inches below the subgrade surface in test pad B at the ERC.

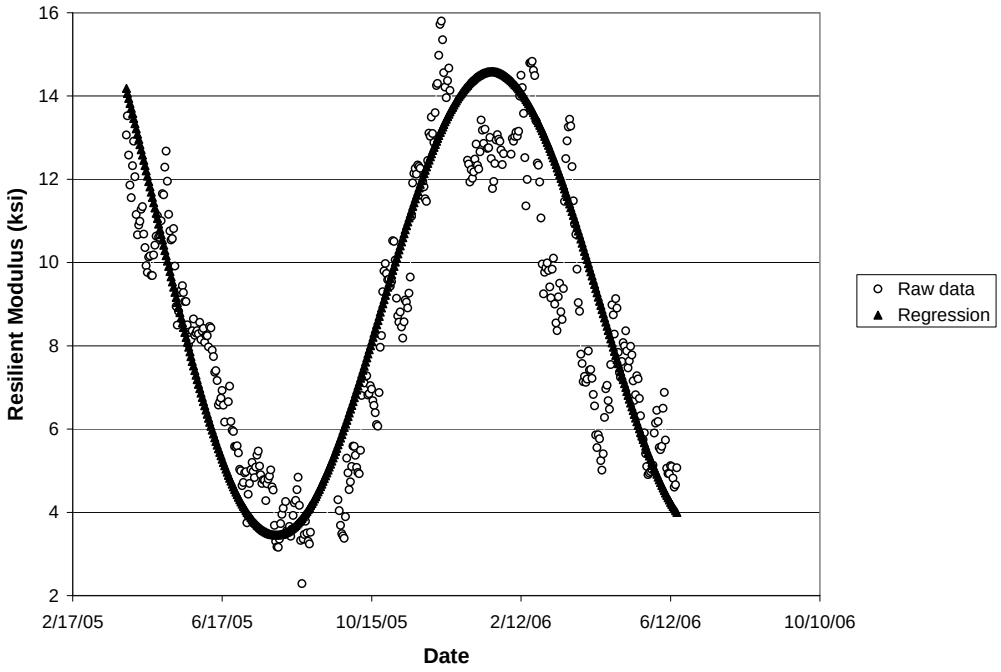

Figure 4.67 Soil resilient modulus vs. time at a depth of 2 inches below the subgrade surface at the Ft. Smith test site.

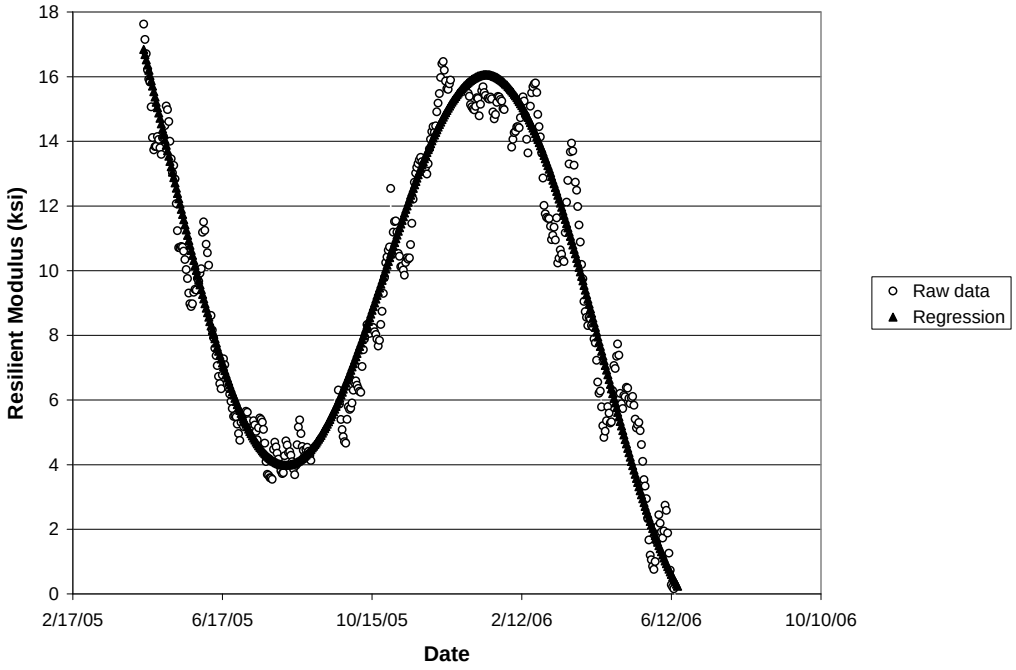

Figure 4.68 Soil resilient modulus vs. time at a depth of 10 inches below the subgrade surface at the Ft. Smith test site.

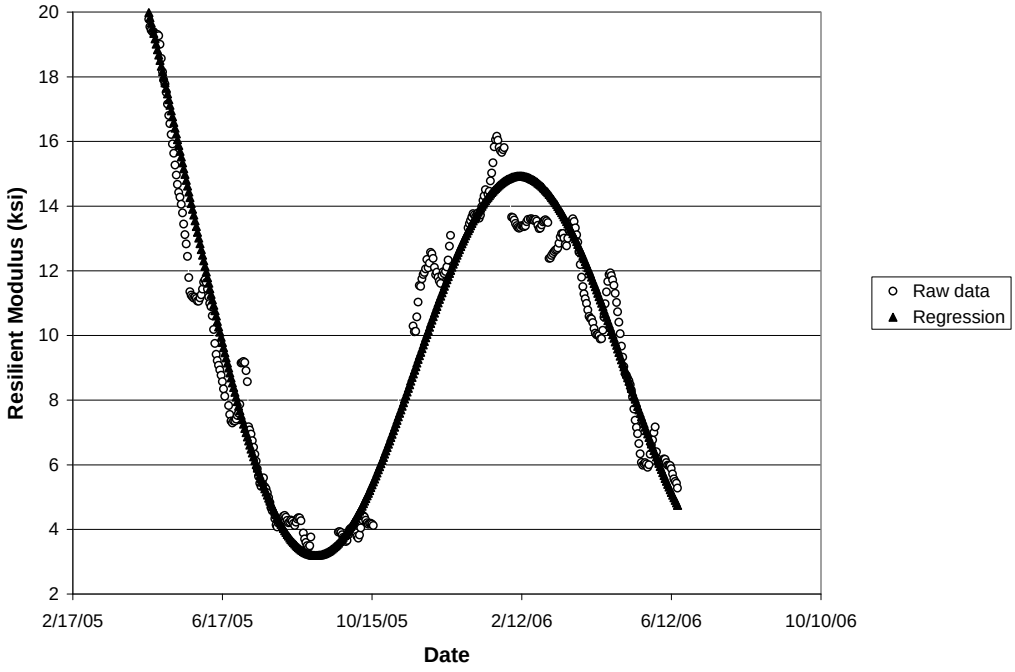

Figure 4.69 Soil resilient modulus vs. time at a depth of 24 inches below the subgrade surface at the Ft. Smith test site.

Table 4.9 Results of the Analyses on resilient modulus of the subgrade soil at the ERC.

		a_0	a_1	b_1	a_2	b_2
Test pad A	1st layer	13.12	-0.92	0.34	3.12	2.22
	2nd layer	13.27	-0.84	0.44	2.82	1.65
Test pad B	1st layer	11.50	-0.33	0.68	3.82	2.10
	2nd layer	12.77	-0.32	0.55	2.74	1.99

Table 4.10 Results of the Analyses on resilient modulus of the subgrade soil at the Ft. Smith test site.

	a_0	a_1	b_1	a_2	b_2
First Layer in Subgrade Soil	10.18	-2.20	-0.39	6.26	2.23
Second Layer in Subgrade Soil	10.94	-3.45	-3.07	8.32	3.53
Third Layer in Subgrade Soil	12.09	-5.22	-1.92	6.33	5.53

In an effort to investigate if one prediction model could be used for both sites, a single predicative model was developed using the combined data from both sites. The coefficients of the regression analysis are presented in Table 4.11. Predicted values of modulus using the single model for both sites along with those inferred from variations in moisture contents are plotted against time for both sites in Figure 4.70.

From Figure 4.70, one can see that maximum differences between predicted resilient modulus and those inferred from variations in moisture contents occurred in July of 2004. At this time, the single model under-predicted peak resilient modulus by approximately 6.5 ksi, which is almost 90 percent of measured peak resilient modulus at this time. Therefore, one single equation seems not be able to be used for similar subgrade soils at both sites.

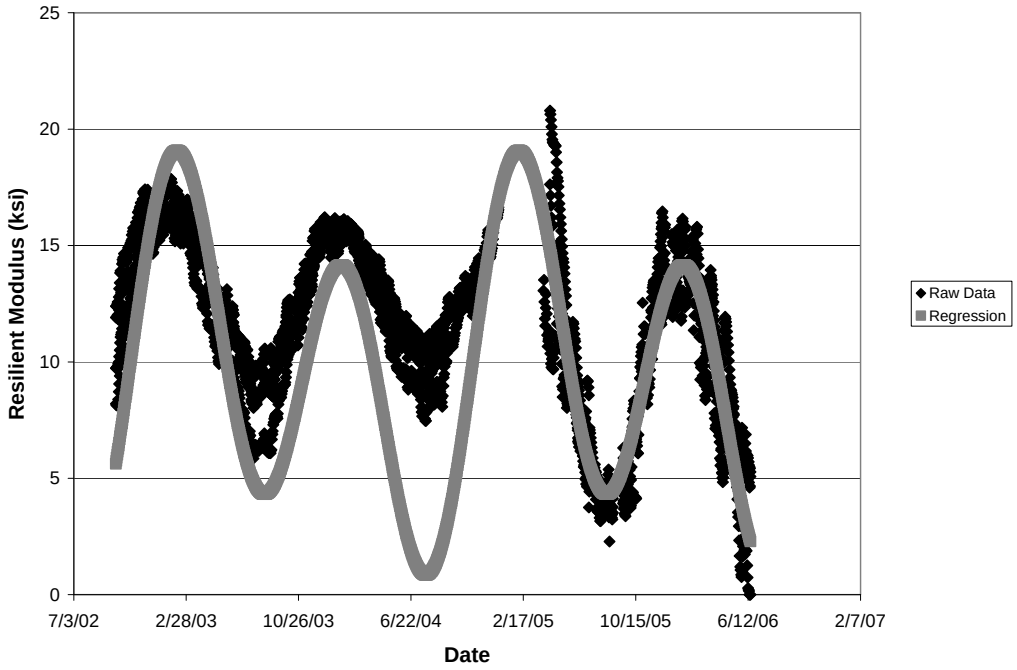

Figure 4.70 Soil resilient modulus vs. time for the subgrade soils at both sites.

Table 4.11 Results of the Analysis on resilient modulus of the subgrade soils at both sites.

	a_0	a_1	b_1	a_2	b_2
Subgrade soil at both sites	9.63	-1.87	-2.36	5.84	3.74

4.10 Discussion and Conclusions

From the raw data presented previously in this chapter and the statistical analyses that were performed, the following summary and conclusions can be drawn:

- Daily average air temperatures at the ERC and the Ft. Smith test site can be predicted using the predicative models presented in Equation 4.1 with model coefficients in Table 4.2. At a 95 percent confidence level, maximum differences of air temperatures between the test sites and nearby NOAA weather stations (the ERC test site and Drake Field Airport, the ERC test site and the Northwest Arkansas Regional Airport, the Ft. Smith test site and Ft. Smith Regional Airport) are within 3.0 degree Celsius. Air temperature obtained from nearby NOAA weather stations can be used in the EICM with adequate accuracy.
- At a 95 percent confidence level, a maximum difference of air temperatures between the Drake Field Airport and Ft. Smith Regional Airport is 5.3 degrees Celsius. Air temperature from the Northwest Arkansas area should not be used in the EICM model for a site in the River Valley or vice versa.
- Seasonal variations of soil temperatures in the pavement system generally decrease with depth in summer, and increase with depth in the winter. Soil temperatures for different depths in the pavement at the Ft. Smith test site can be

predicted using the predicative models presented in Equation 4.1 with model coefficients in Table 4.3.

- At a 95 percent confidence level, maximum differences of precipitation between the test sites and nearby NOAA weather stations could be as much as 1 inch. At a 95 percent of confidence level, a maximum difference between precipitation obtained from the Drake Field Airport and Ft. Smith Regional Airport weather stations could be as much as 1.3 inches.
- From the literature review, researchers have found the groundwater level to have a significant effect on the moisture content in pavement systems when the location of free water surface is relatively shallow. At the both test sites in this study, the highest measured groundwater levels were below the lowest moisture probes in subgrade soils. Changes in groundwater levels seem to follow the same trend as that in moisture contents in the subgrade soils at the ERC. Groundwater levels and moisture contents both have high peak values in summers and low peak values in winters. However, no obvious relationship was found between groundwater level and the moisture content of subgrade soils in the pavement systems at the Ft. Smith test site. This is probably because the measuring period had much lower-than-average annual precipitation at the Ft Smith site. Groundwater levels began to respond to the drought during the measuring period as indicated by a constant decrease in groundwater level during most of the measuring period. However, moisture contents in the subgrade soils had not began to response to this during the measuring period.

- Approximately 53 percent of total precipitation volume ran off from the surface of test pad A at the ERC while only 38 percent ran off from the Ft. Smith test site. Approximately 5.5 percent of total precipitation volume was collected form the edge drain of test pad A at the ERC while 11 percent was collected from the Ft. Smith site.
- Moisture migrated much faster in the horizontal direction than in the vertical direction in base materials. The moisture migration pattern can be illustrated by the line and ellipse in Figure 4.21.
- After a precipitation event, some portion of water that migrated into pavement systems would remain in pavement systems for a relatively long period because base materials are not free-draining materials.
- For a smaller precipitation event, a higher percentage of precipitation would migrate into pavement systems.
- Using the storage model and measured runoff a water balance was generally achieved for test pad A at the ERC.
- Only moisture contents of base materials at the shallow depth (2 inches below the base surface) responded to precipitation events. Moisture content changes in the base materials at deeper depths (deeper than 2 inches) were more likely seasonal and are independent of precipitation events.
- Precipitation had almost no effect on the moisture content in subgrade soils, except for those areas in the vicinity of edge drains. The moisture content in subgrade soils changed with season independently from precipitation events.

- Frost depths in the Northwest Arkansas area and River Valley area were less than 1 foot measured from pavement surfaces.
- Degrees of saturation in the base and subbase materials at the ERC and Ft. Smith test sites generally increased with depth from approximately 55 percent to near 100 percent. Degrees of saturation in the subgrade soils at the ERC and the Ft. Smith test site changed with seasons and can be predicted using the predicative models presented in Equation 4.1 with model coefficients in Tables 4.6 and 4.7. A single prediction model presented in Equation 4.1 with model coefficients in Table 4.8 can be used for both sites.
- Resilient modulus of the A-6 subgrade soils encountered at the ERC and the Ft. Smith test site changed with seasons and could be described with periodic functions. Predicted values ranged from 18 ksi during winters and values of 3 to 6 ksi during summers. Resilient modulus of the A-6 subgrade soils encountered at the ERC and the Ft. Smith test site could be predicted using the predicative models presented in Equation 4.1 with model coefficients in Tables 4.9.and 4.10. A single model can not be used for both sites.

Chapter 5 Evaluation of the EICM in Arkansas

5.1 Introduction

As mentioned in Chapter 2, the Enhanced Integrated Climatic Model (EICM) will be integrated into the future AASHTO Mechanistic-Empirical Pavement Design Guide, MEPDG, (200x design guide, 2004). The EICM has the ability to predict moisture content and temperature profiles in pavement systems based on climatic data obtained from NOAA weather stations and easily obtained material properties of the pavement systems. However, Ahmed and his coworkers (2005) evaluated the EICM using data from two LTPP test sites in New Jersey and a wide discrepancy was observed between predicted and measured temperatures and moisture contents. Therefore, they concluded that the EICM, as presented by Larson and Dempsey (1997, 2001 and 2004) was not suitable for New Jersey. As a result of the work conducted by Ahmed in New Jersey the applicability of the EICM for Arkansas was questioned. The data from this study was used to partially check the validity of the EICM predictions to values actually measured in Northwest Arkansas.

In this chapter, the theoretical background of the EICM is reviewed. The results of sensitivity analyses for input parameters of the EICM are presented. Finally, measured air temperature, precipitation and ground water table data, collected from the ERC and the field test site, supplemented by climatic data obtained from nearby NOAA weather stations, were used as inputs for the EICM. Predicted soil temperatures and moisture contents in the pavement systems were then compared with measured soil temperatures and moisture contents to evaluate the suitability of the EICM in Arkansas. The latest version of the EICM, 3.2 Beta dated September 19, 2006 was used in this study.

5.2 Theoretical Background of the EICM

The original version of the EICM, referred to as simply the Integrated Climatic Model (ICM), was developed for the Federal Highway Administration (FHWA) at the Texas A&M University by Lytton, Pufahl, Liang and Dempsey (1990). The original version was then modified by Larson and Dempsey in 1997 and 1999 as ICM Version 2.0 and 2.1, respectively. Further improvements were made as part of the Design Guide development to further improve the moisture prediction capabilities of ICM version 2.1. This version of the model was called the Enhanced Integrated Climatic Model (EICM) (200x Design Guide, 2004). As discussed in Chapter 2, the EICM consists of three sub-models: the infiltration and drainage model (ID), the climatic-materials-structures model (CMS), and the frost heave and thaw settlement model (CRREL). The ID model was developed at the Texas A&M University by Lytton, Pufahl, Michalak, Liang and Dempsey (1990), the CMS model was developed at the University of Illinois by Dempsey, Herlach and Patel (1985), and the CRREL model was developed at the United States Army Cold Regions Research and Engineering Laboratory (CRREL) by Guymon, Berg and Johnson (1986). Before performing the evaluation of the EICM in Arkansas, this section gives a short review of the theories behind each of the models.

5.2.1 ID Model

The ID model was developed at the Texas A&M University by Lytton, Pufahl, Michalak, Liang and Dempsey in 1990. The Infiltration and Drainage Model (ID) consists of three sub-models. They are the drainage analysis model, pavement evaluation model and infiltration model.

The drainage model uses a numerical technique to compute the degree of drainage (drained area / total area in percent) versus time of an initially saturated granular base course with lateral drainage overlying a permeable or impermeable subgrade. This analysis assumes that the base course is a free draining material (Lytton, Pufahl, Michalak, Liang and Dempsey, 1990).

The Pavement Evaluation module of the ID model uses an empirical procedure to evaluate the relative adequacy of the base course design in terms of the amount of time that is required to reach a critical degree of saturation from an initially 100 percent saturation. The critical degree of saturation was defined in the model as a degree of saturation above which the excess pore water pressures in the base material would be developed under repeated traffic loading. According to Lytton and his coworkers (1990), Haynes and Yoder concluded that the critical degree of saturation was 85 percent and Martin and Toan concluded that it was 80 percent. In the model, a critical degree of saturation of 85 percent was used. The more rapidly the base course can drain from an initially saturated condition to the critical degree of saturation, the more effective it will be as a load carrying member of the pavement structure under wet conditions.

The Infiltration model includes probabilistic analyses of rainfall amounts and patterns derived from the Precipitation Model or from actual rainfall amounts. In the latest version of the EICM, the Precipitation Model has been superseded by directly using precipitation data from nearby NOAA weather stations. Therefore, an introduction to the Precipitation Model is not included here. The infiltration model then conducts a rainfall analysis to calculate the probability of wet and dry days. The infiltration model uses these

analyses to model the infiltration of water through cracks in the pavement and calculates the probability of having a wet or dry pavement profile.

It should be noted that the drainage model assumes that the base course is composed of a free draining material. A permeable base is defined as "an open-graded drainage layer with a typical laboratory hydraulic conductivity value of 0.35 cm/s or greater" in the 200x Design Guide (2004). According to Zhou (1993), Mathis (1989) indicated that the hydraulic conductivity value of free-draining base materials generally ranged from 0.07 cm/s to 1 cm/s. The U.S. Army Corps of Engineers (1983) stated that free-draining base materials should contain two percent or less, by weight, of grains that can pass the No. 200 sieve. However, the base materials at the ERC and Ft. Smith sites were composed of dense-graded aggregates with hydraulic conductivities of 3.1×10^{-3} cm/s and 6×10^{-4} cm/s, respectively. These bases are the typical of the base material used in Arkansas (AHTD Class 7), and would not be considered free draining, using the above mentioned criteria.

5.2.2 CMS Model

The CMS model was developed based on an energy balance analysis at pavement surfaces as illustrated in Equation 5.1.

$$Q_i - Q_r + Q_a - Q_e \pm Q_c \pm Q_h \pm Q_g = 0 \qquad 5.1$$

Where:

Q_i = incoming short wave radiation;

Q_r = reflected short wave radiation;

Q_a = incoming long wave radiation;

Q_e = outgoing long wave radiation;

Q_c = sensible for convective heat transfer (function of air temperature and wind speed);

Q_h = effects of transpiration, condensation, evaporation and sublimation; and

Q_g = energy absorbed by the ground.

Based on Equation 5.1, heat flux at the pavement surfaces can be generated, which is then used to establish the temperature profile through asphalt concrete and Portland cement concrete layers. A one-dimensional, forward difference, heat transfer model is used to determine the temperature distribution in the pavement layers. The temperature data at the bottom of the pavement layer is then given to the CRREL model to predict soil temperatures. The model considers radiation, convection, conduction, and the effect of latent heat. It dose not consider transpiration, condensation, evaporation, or sublimation. Heat fluxes caused by precipitation and moisture infiltration are also neglected (Larson and Dempsey, 1997). The variables in Equation 5.1 are illustrated in Figure 5.1.

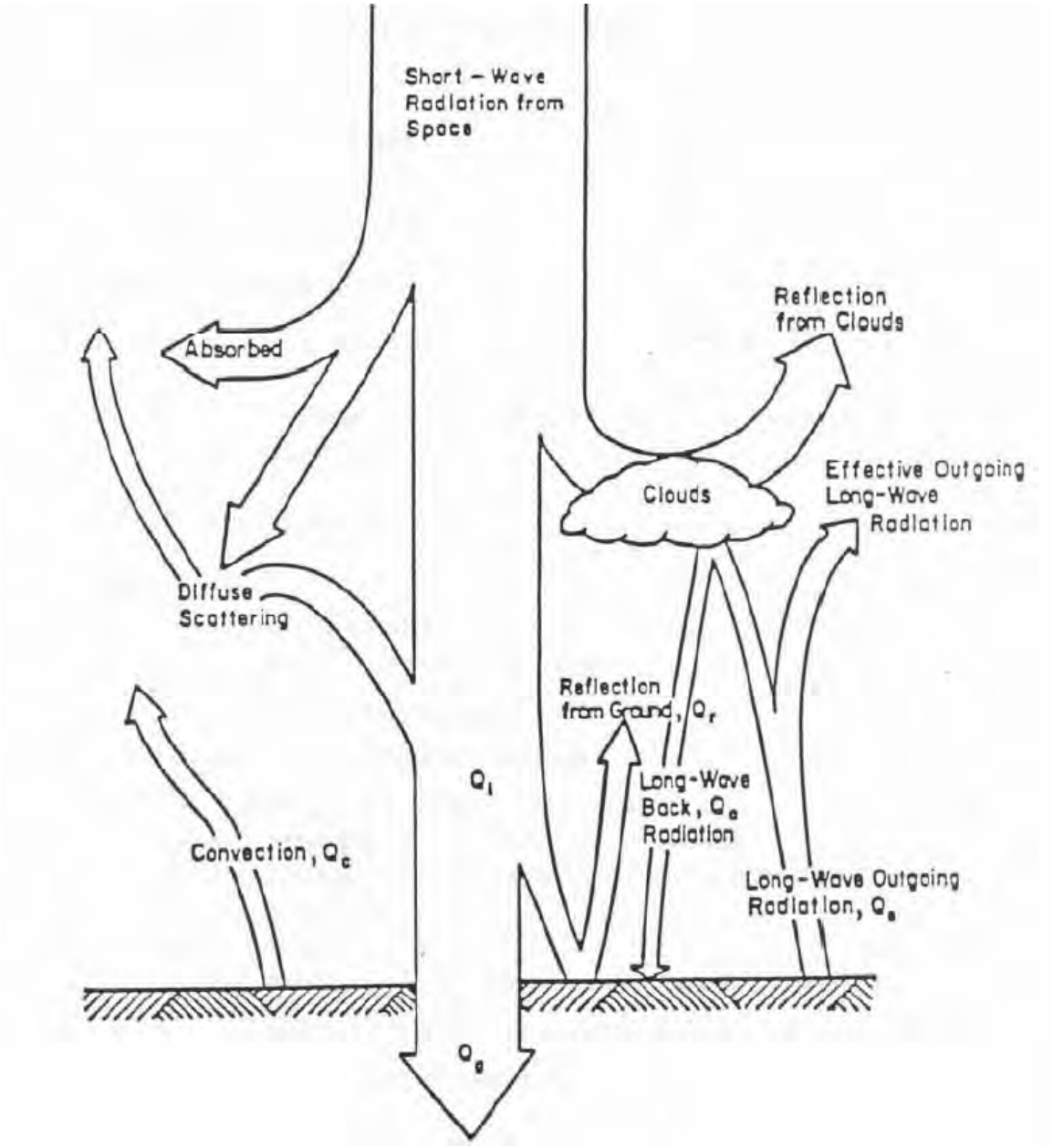

Figure 5.1 Heat transfer between pavement surface and air on a sunny day (Lytton, 1990).

5.2.3 CRREL Model

The CRREL (U.S. Army Cold Regions Research and Engineering Laboratory) model was developed by Guymon, Berg and Johanson (1986). The CRREL model uses

the temperature profiles in a pavement system established by the CMS model as input. Based on a mathematical model that couples heat and moisture flow in soil the volumetric ice content and volumetric unfrozen water content are computed. Then by comparing the sum of the ice and water volumes with the porosity of the soil, the model can compute frost heave or thaw settlement. In the latest version of the EICM, the Fredlund and Xing equations (1997) are used to predict soil suction and relative hydraulic conductivity in the soil as a function of the degree of saturation. These values are computed based on simpler index properties of the soil. These equations replaced the Gardner equations which were used in previous versions to obtain the soil-water characteristic curve (SWCC).

5.3 Sensitivity Analyses

Climatic input data for the EICM consists of air temperature, precipitation, ground water table location, wind speed, sunshine and humidity. Because wind speed, sunshine and humidity were not measured at the test sites, the measured values for air temperature, precipitation and ground water table location were supplemented by wind speed, sunshine and humidity data obtained from nearby national NOAA weather stations. Because all of the input variables to the EICM are typically taken from weather stations in the EICM data base, their values potentially could be different than conditions encountered at the site of interest. This variation was documented in Chapter 4. The following sensitivity analysis attempts to quantify the potential differences in outputs by using a combination of measured and supplemented input variables. Comparisons between measured data and weather station data were used to develop the potential range

in input values for Northwest Arkansas and the western portion of the Arkansas River Valley. At the conclusion of the sensitivity analysis comparisons of output predictions to actual measured values are given.

In Chapter 4, measured air temperatures at the test sites were compared with air temperatures obtained from nearby NOAA weather stations and it was concluded that the difference would be within 3 ^{o}C with a 95 percent confidence. Air temperatures in the Northwest Arkansas area were also compared with those in the River Valley area using air temperature data from the Drake Field Airport and Ft. Smith Regional Airport weather stations. From this analysis it was concluded that the expected difference in temperatures between the two sites would be within 5.3 ^{o}C, with a 95% confidence. To investigate the impact of a variation in air temperature on EICM predicted temperatures in the pavement systems a sensitivity analysis was carried out on air temperature versus asphalt and soil temperatures at various levels in the pavement system. Even though asphalt temperature was not measured at the test sites, a sensitivity analysis was performed to investigate the effect of air temperatures on predicted asphalt temperatures because temperature has much more effect on asphalt's structural properties than on those of base and subgrade materials.

The thermal properties of asphalt, which are inputs for the EICM, were not measured in this study. Thermal properties of asphalt include surface short wave absorptivity, thermal conductivity (K) and heat capacity (Q). While thermal properties of the asphalt will affect predicted temperatures in the entire pavement system, they are especially significant in predicting temperatures in the asphalt layer. Therefore sensitivity

analyses were conducted to ascertain the impact of using values of these properties which are within the typical ranges.

To perform the sensitivity analyses, one input parameter for the EICM was assigned different values within its normal range while the other input parameters were held constant. Predicted soil temperatures and moisture contents in the pavement system corresponding to the different values of the input parameter under investigation were compared. The typical ranges and values for the environmental factors are presented in Table 5.1, the typical ranges and values for asphalt thermal properties are presented in Table 5.2, and measured or typical values of the base and subgrade soils for the Ft. Smith test site are presented in Table 5.3.

Table 5.1 Summary of Environmental Input Factors in the EICM.

Environmental Factor	Typical Range (measured or obtained from the NOAA weather station)	Constant Value used in sensitivity analyses
Air Temperature (^{0}F)	-15 to 115	-15 to 115
Wind Speed (mph)	0 - 30	0
Percent Sunshine (%)	0 - 100	50
Precipitation (inches)	0 - 3.5	0
Humidity (%)	10 - 100	50
Water Table (feet)	4 -11	7

Table 5.2 Summary of Asphalt Material Properties Required in the EICM.

Asphalt Property	Typical Range (200x Design Guide)	Constant Value used in sensitivity analyses
Surface Short Wave Absorptivity	0.8 – 0.98	0.8
Thermal Conductivity (Btu/(ft)(hr)(^{o}F)	0.44 – 0.81	0.67
Heat Capacity Btu/(lb)(^{o}F)	0.22 – 0.4	0.22

Table 5.3 Summary of Material Properties of Base and Subgrade Materials used in the EICM.

Material Properties	Base	Subgrade
Porosity	0.18	0.35
Saturated Hydraulic Conductivity (ft/hr)	0.0708	0.0000118
Dry Unit Weight (pcf)	135.2	112.8
Dry Thermal Conductivity (Btu/(ft)(hr)(^{o}F)	0.27	0.18
Dry Heat Capacity Btu/(lb)(^{o}F)	0.2	0.2
Initial Volumetric Moisture Content	13.4	29.6
PI	16	13
D60 (mm)	9.475	2.432
Passing No. 4 Sieve	46.8	71.8
Passing No. 200 Sieve	16.2	44.1

While conducting the sensitivity analyses, it was discovered that even through all environmental factors were held constant during the analysis, soil temperatures would still change with season. The model predicted higher temperatures in summers and lower temperatures in winters as illustrated in Figure 5.2. Figure 5.2 shows EICM predicted temperatures in the middle of the base layer when using a constant air temperature of 55 ^{o}F and constant values for all other environmental factors. The results shown in Figure 5.2 are apparently not reasonable because the base temperature in the pavement should remain constant if all environment factors are constant. It appears that some internal variables in the EICM change with season in such a way that higher soil temperatures are predicted in summers and lower soil temperatures in winters. As a result a classical sensitivity analysis could not be conducted because the user does not have access to control these internal variables.

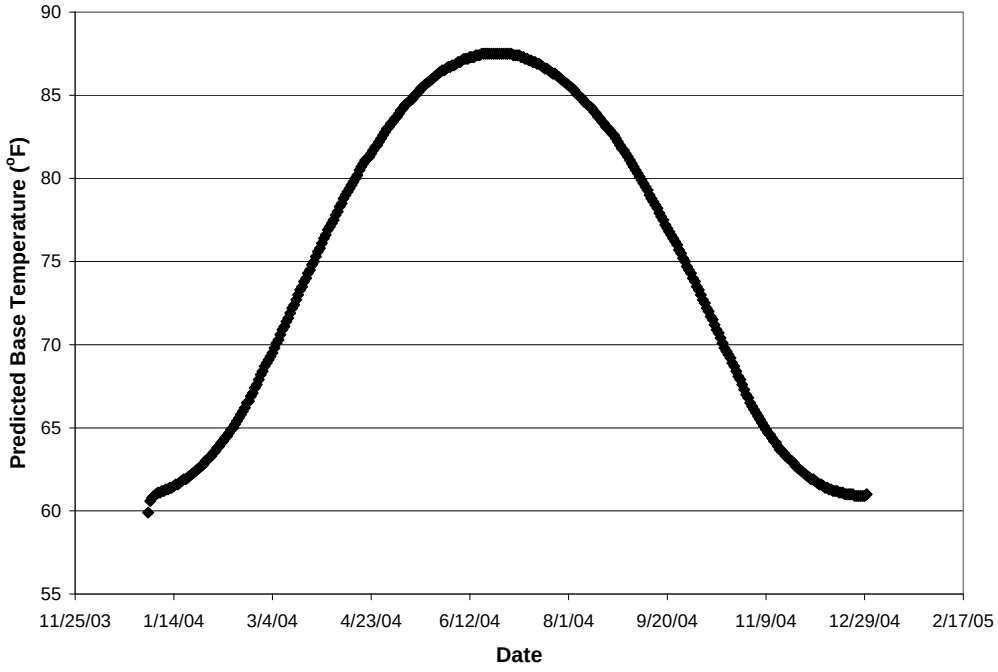

Figure 5.2 Predicted temperatures in the middle of the base layer of the Ft. Smith site using a constant air temperature of 55 ^{o}F and constant values for other environmental factors.

A sensitivity analysis was attempted to determine the effect of wind speed on temperatures throughout the pavement profile. Pavement temperatures at the middle of the asphalt layer, and the middle of the base layer and at depths of 2 inches, 10 inches and 24 inches below the subgrade surface were predicted using the EICM at different combinations of a constant air temperature and variable wind speed. The results of this analysis revealed that predicted temperatures in asphalt, base and subgrade materials were all the same, independent of depth, for a given combination of constant air temperature and wind speed. The results of this analysis are shown in Figure 5.3. Since the predicted temperatures in the pavement system were all the same, independent of depth, Figure 5.3 is illustrative of predicted pavement temperatures for all depths. This obvious discrepancy in temperature prediction is probably due to the EICM's inability to

process a constant air temperature over an entire year. These results from this analysis confirm that it is not possible and meaningless to perform a classical sensitivity analysis using constant values for all of the environmental factors.

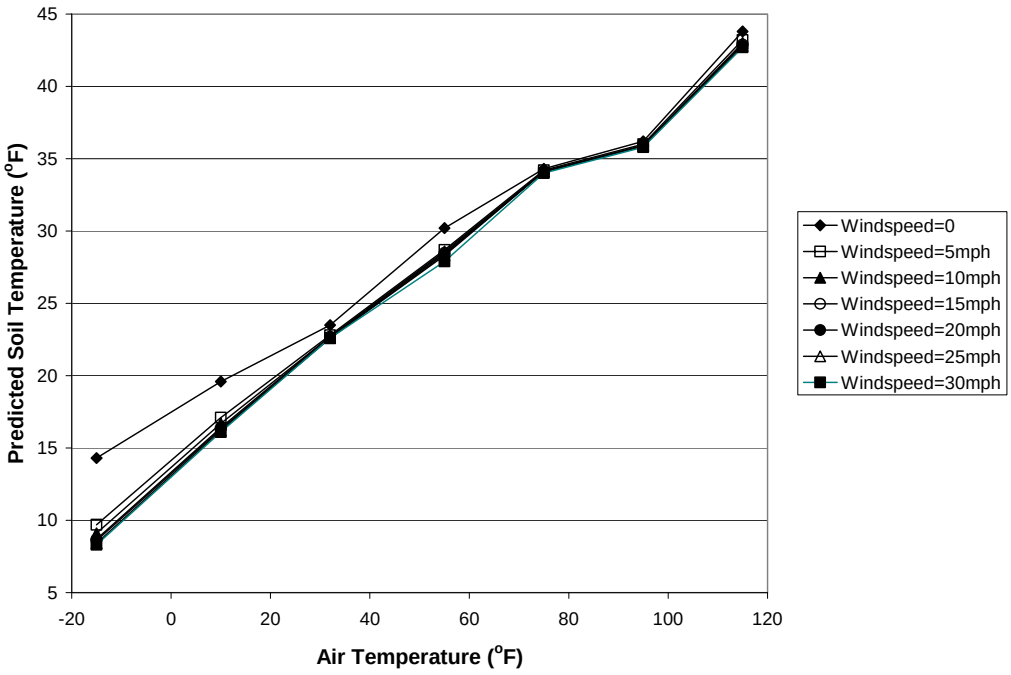

Figure 5.3 Summary of the results for the sensitivity analyses for wind speed on pavement temperatures in the middle of the asphalt layer, middle of the base material, and at depths of 2 inches, 10 inches and 24 inches below the subgrade surface at the Ft. Smith site.

Because a classical sensitivity analysis could not be performed, a "modified" sensitivity analysis was performed to gain insight on how predicted temperature and moisture content in the pavement vary with season. In the modified sensitivity analysis, environmental data obtained from the Ft. Smith Regional Airport weather station were used. To perform the modified sensitivity analyses, one input parameter is assigned different constant values within its normal range while values for the other environmental parameters were those obtained from the weather station instead of the constant values used in the previous classical sensitivity analyses.

5.3.1 Air Temperature

This portion of the modified sensitivity analysis was performed to investigate the effect of air temperatures on asphalt temperatures. As discussed previously, the EICM might have some internal variables that could affect predicted soil temperatures beside the required environmental factors. Therefore, it is meaningless to use constant air temperatures to do a classical sensitivity analysis on air temperature. In this study, air temperature from the Ft Smith Regional Airport weather station was used as an air temperature set for the base input to the model. In Chapter 4, it was concluded that air temperature differences between the Northwest Arkansas area and River Valley area were within 9.5 ˚F (5.3˚C) with a confidence level of 95 percent. Therefore, the sensitivity analysis for air temperatures was performed for air temperatures ranging from minus 10 ˚F to plus 10 ˚F. To accomplish this, new annual air temperature sets were created by subtracting or adding 5 and 10 degrees to the temperatures in the base set. In this manner the model could be run for five temperature sets over a range of 20 degrees Fahrenheit in increments of five degrees. All other input parameters were held constant during the analysis. Then predicted asphalt temperatures using each air temperature set were compared. The purpose of this portion of the analysis was to investigate how predicted asphalt temperatures change with different input air temperature sets. Four locations within the asphalt layer were selected for analysis; the top and bottom of the layer and at intermediate locations at 3 and 6 inches below the asphalt surface.

The results of the analyses indicate plots of predicted asphalt temperature versus time look similar for the four locations with higher predicted temperatures at the asphalt surface. Therefore, only predicted asphalt surface temperatures are presented in Figure

5.4. Predicted asphalt temperatures for the other locations are included in Appendix C. In order to reduce the number of data points in the plots and improve readability, only predicted asphalt temperatures for every fifth day are plotted in Figure 5.4. In comparing the base air temperatures with the predicted asphalt surface temperatures (using the base temperatures denoted as "0" in the legend) in Figure 5.4 one can see that predicted asphalt surface temperatures are as much as 41 ˚F higher than air temperatures in summer. While, in the winter, predicted asphalt surface temperatures are generally less than 15 ˚F higher than air temperatures. From Figure 5.4, it can also be seen that the spread in predicted asphalt surface temperatures over the 20 degree air temperature spread for each day are generally less than 20 degrees. This indicates that a change of one degree in air temperature results in less than one degree in predicted asphalt temperature.

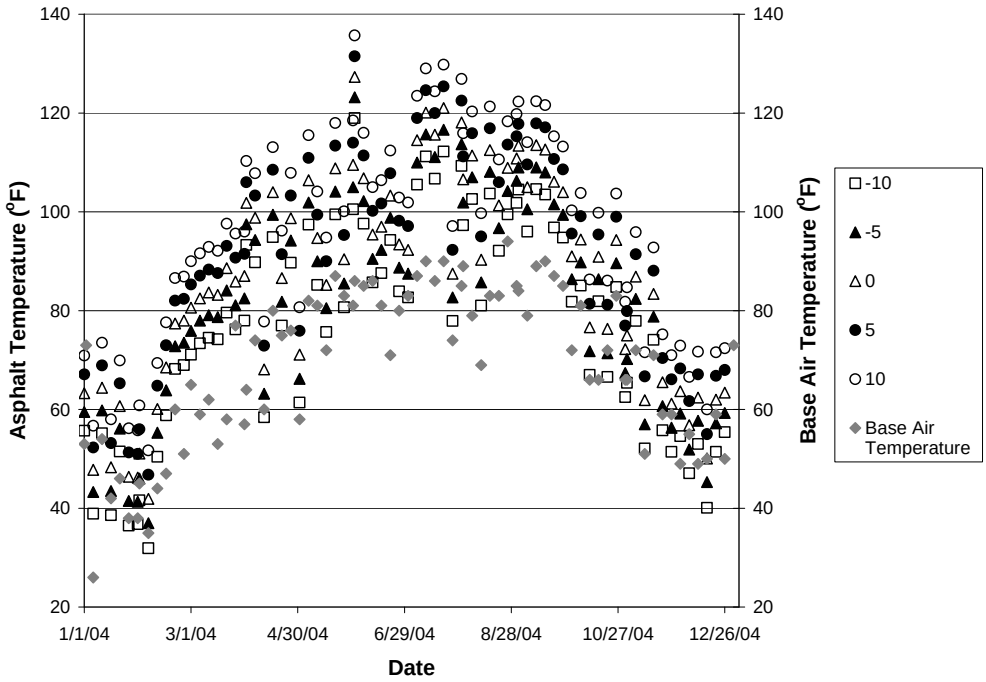

Figure 5.4 Comparison of air temperatures and predicted asphalt surface temperatures for different air temperature sets at the Ft Smith site.

To investigate a change in asphalt temperature on asphalt modulus, a relationship between the asphalt modulus and its temperature proposed by Lukanen (2000) was used. The relationship is illustrated in Equation 5.2

$$M_{r1} = M_{r2} \times 10^{-0.021 \times (t_1 - t_2)} \quad 5.2$$

Where:

M_{r1} = asphalt modulus at temperature t_1, ^{o}C

M_{r2} = asphalt modulus at temperature t_2, ^{o}C

Using Equation 5.2, it can be determined that a 3 ˚C difference in asphalt temperatures would result in an approximately 11 percent change in asphalt modulus. However, a 5.3 ˚C difference in asphalt temperatures would result in an approximately 30 percent change in asphalt modulus. Therefore, one can reasonably conclude that air temperature from nearby NOAA weather stations can be used in the EICM with adequacy accuracy (less than 11 percent effect on predicted asphalt modulus). However, it appears that air temperatures in the Northwest Arkansas area can not be used in the EICM with adequate accuracy for a site in the River Valley area because predicted asphalt modulus could be affected by as much as 30 percent.

5.3.2 Wind Speed

The climatic data obtained from the weather station indicates that wind speeds at the weather station are generally below 30 miles per hour (mph). Therefore, the sensitivity analysis for wind speeds was performed for wind speeds ranging from 0 to 30 mph in increments of 5 mph.

The results of the analyses indicate that the predicted soil temperatures and moisture contents for each layer look similar over the time span analyzed. As a result, only predicted soil temperatures and moisture contents in the middle of the base material are presented in Figures 5.5 and 5.6.

A visual inspection of Figure 5.5, reveals that predicted temperatures in the base material of the pavement system are more sensitive to changes in wind speeds during summer months than winter months and the majority of temperature change in is when wind speeds change from 0 to 5 mph. Predicted temperatures are relatively insensitive to wind speeds above 5 mph for all seasons. From Figure 5.5, one can see that a maximum change in predicted temperatures in the pavement system can be as much as 20 ^{o}F in the summer with wind speeds changing from 0 to 5 mph, while a maximum change in predicted temperatures is only 10 ^{o}F in the summer when wind speeds change from 5 to 30 mph. It appears that weather conditions can be broken into two scenarios windy, (for wind speeds greater than 5 mph) and no wind. Also, From Figure 5.5, it can be seen that predicted temperatures in the base material are much higher than air temperatures in summer when the wind speed is zero and are relatively close to the air temperatures when wind speed is five mph or greater.

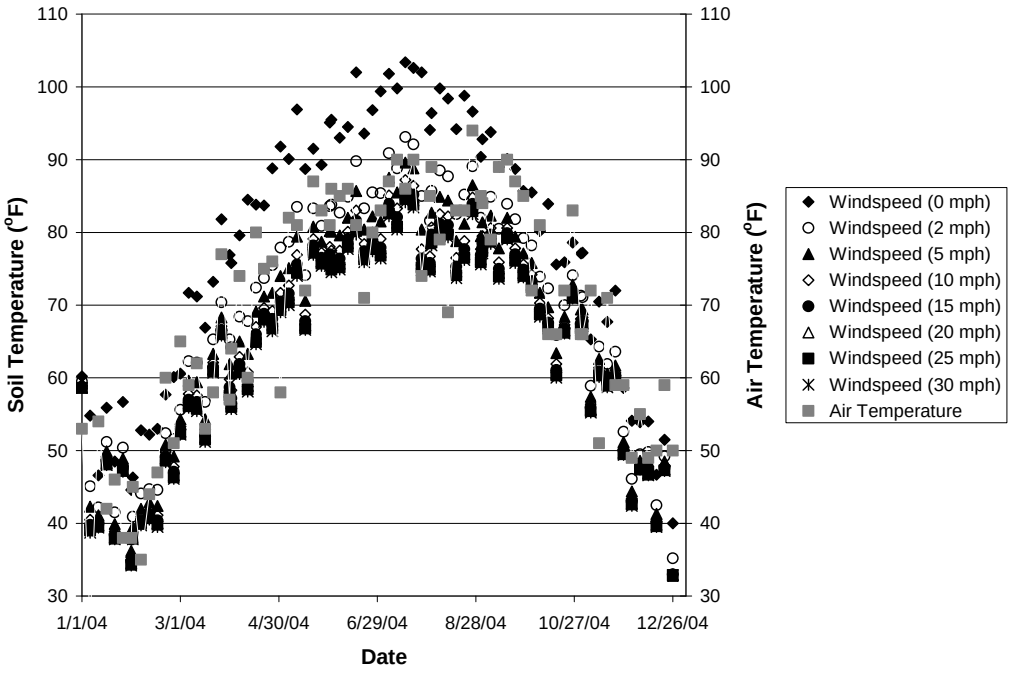

Figure 5.5 Comparison of air temperatures and predicted soil temperatures for a depth of 2 inches below the base surface at the Ft Smith site for different wind speeds.

To determine the wind speed variability between Northwest Arkansas and the River Valley, wind speeds from 2004 for Drake Field and Ft. Smith Regional airports were compared. It was discovered that during approximately 26 percent of the year of 2004, one airport was windy while the other one had no wind, which indicates that using wind speed data from the Drake Field Airport weather station in the EICM could cause significant over- or under-prediction of temperatures in a pavement system in Ft Smith. Unfortunately, wind speeds were not measured at any of the test sites. So, wind speed data from nearby weather stations was used throughout the analyses to get a relative feel for the variation of outputs of the EICM with changing wind speeds that were indicative of the region.

The results presented Figure 5.6 show that the wind speed has no noticeable effect (less than 1 percent) on predicted moisture contents in the pavement system. In Figure

5.6, the predicted moisture contents for different wind speeds overlap each other during most of the analysis period. During December, the base material was partially frozen but to different degrees for different wind speeds, which is indicates that wind speed may have an affect on the predicted depth of frost penetration.

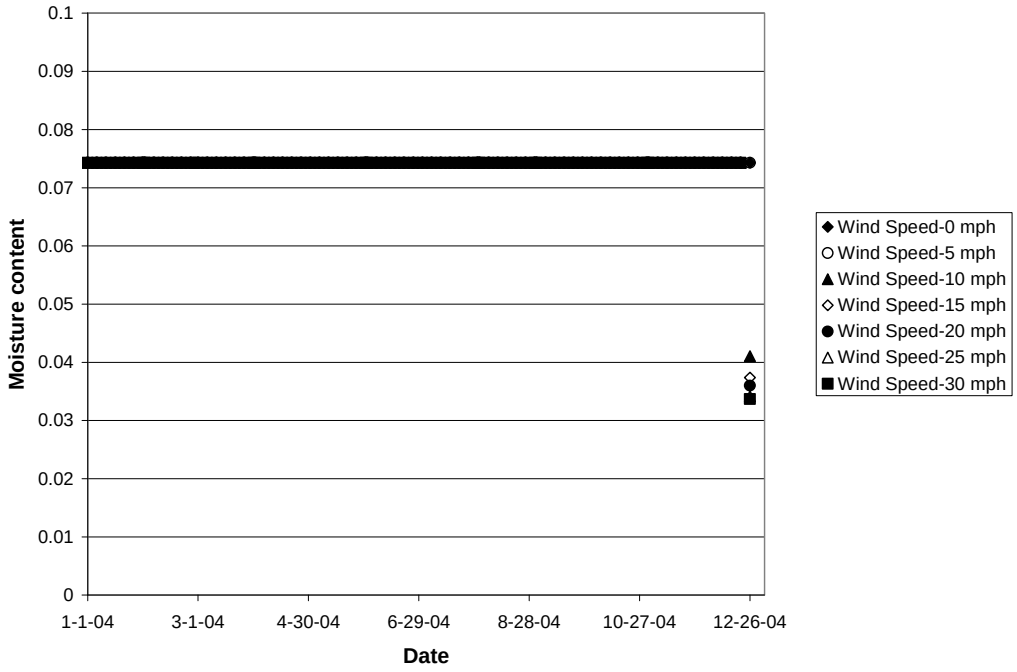

Figure 5.6 Predicted moisture contents for a depth of 2 inches below the base surface at the Ft Smith site for different wind speeds.

5.3.3 Sunshine

The percent sunshine value is a required climatic input for the EICM. Based on the climatic data obtained from the weather stations, percentages of sunshine could vary from 0 to 100 percent. So the sensitivity analysis was performed at percentages of sunshine ranging from 0 to 100 percent in increments of 25 percent. Because only temperature and moisture contents were measured at the field sites, only predicted

moisture contents and temperatures in the base material in the pavement system for different percentages of sunshine are presented in Figures 5.7 and 5.8.

From Figure 5.7, it can be seen that the percent sunshine value has no effect on predicted temperatures in the pavement system (less than 1 percent) in the winter, and only a slightly higher effect (less than 5 percent) on predicted temperatures in the summer. Therefore, from a practical standpoint, it can be reasonably concluded that percent sun shine data from nearby weather stations can be used in the EICM with adequate accuracy. From Figure 5.8, one can see that the percent sun shine has no noticeable effect (less than 1 percent) on predicted moisture contents in the pavement during any season.

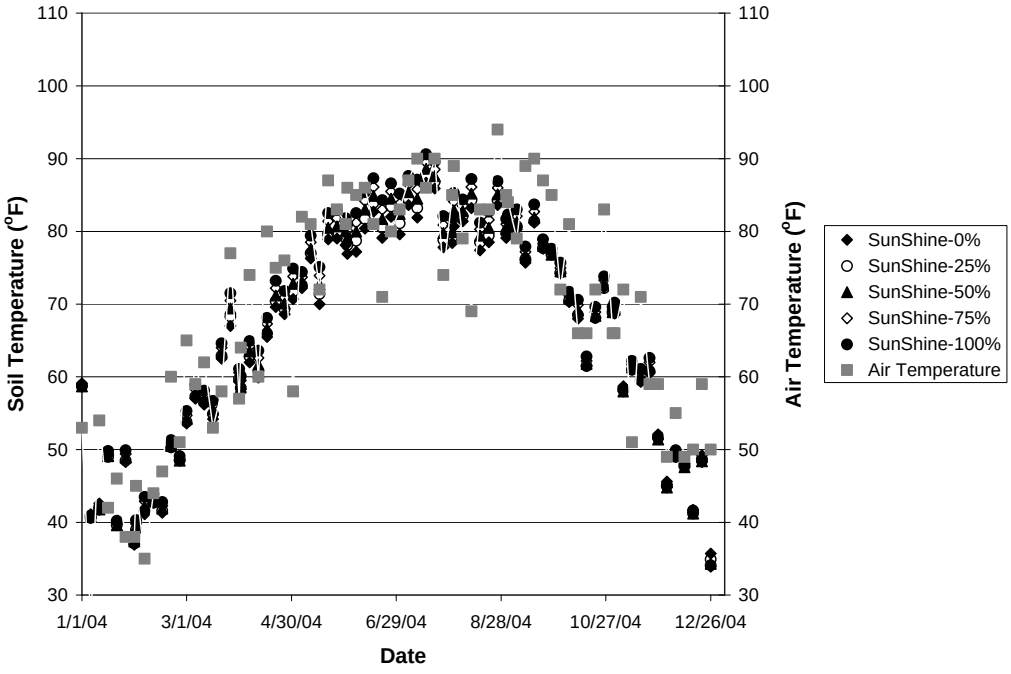

Figure 5.7 Comparison of air temperatures and predicted soil temperatures for a depth of 2 inches below the base surface at the Ft Smith Site for different percentages of sun shine.

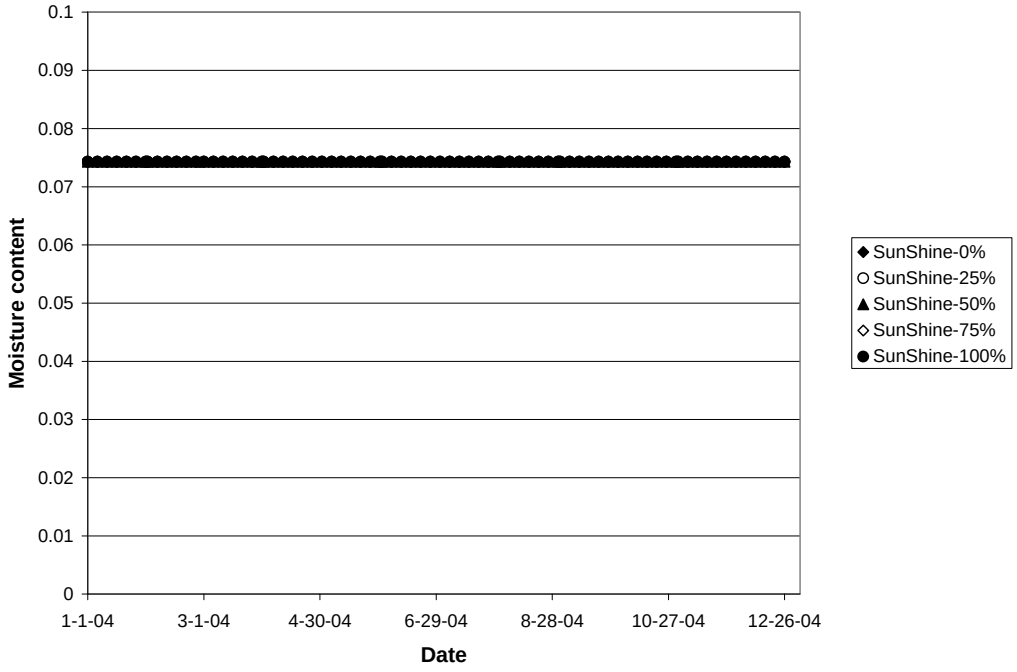

Figure 5.8 Predicted moisture contents for a depth of 2 inches below the base surface at the Ft Smith site for different percentages of sun shine.

5.3.4 Humidity

Humidity is another required input for the EICM. Based on the climatic data obtained from the Ft. Smith weather station, humidity could vary from 10 to 100 percent. Therefore, the sensitivity analysis for humidity was performed for humidity ranging from 10 to 100 percent in increments of 30 percent. From Figures 5.9 and 5.10, it is obvious that the humidity has virtually no effect (much less than 1 percent) on predicted temperatures and moisture contents in the pavement system. Based on this analysis it would appear the humidity is not an important input parameter, however, humidity may affect other outputs of the model that were not investigated in this study.

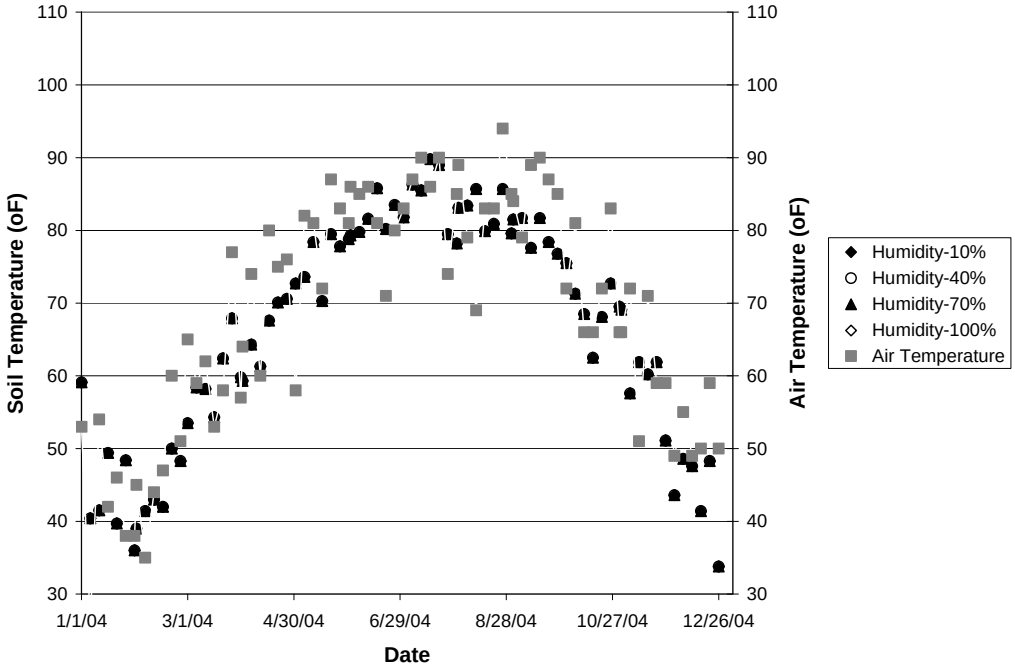

Figure 5.9 Comparison of air temperatures and predicted soil temperatures for a depth of 2 inches below the base surface at the Ft Smith site for different relative humidity.

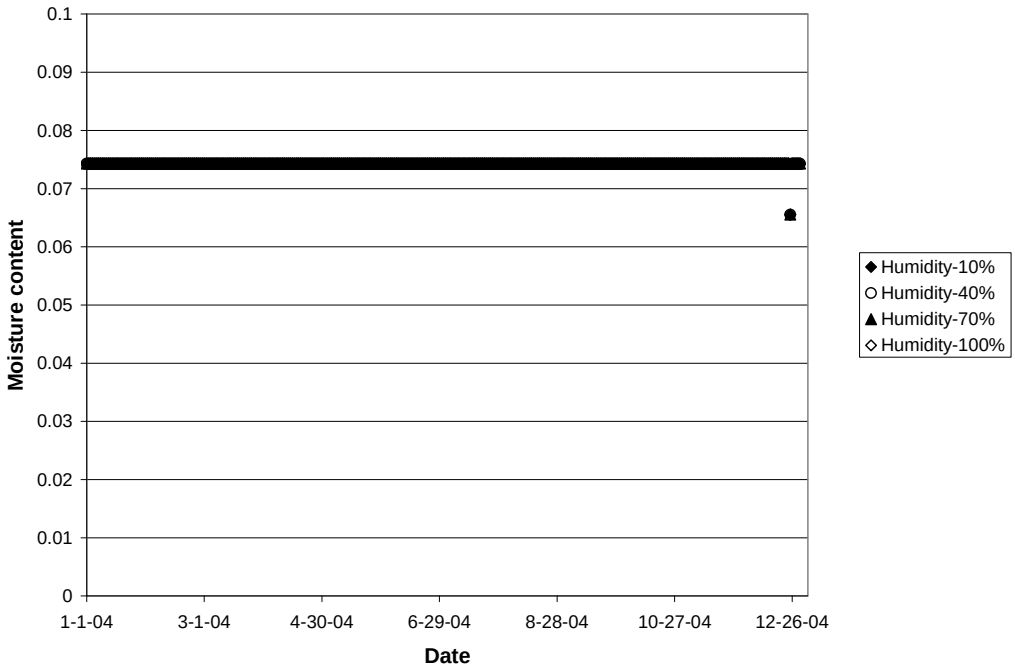

Figure 5.10 Predicted moisture contents for a depth of 2 inches below the base surface at the Ft. Smith site for different relative humidity.

5.3.5 Groundwater Level

The location of the groundwater is a required input for the EICM. Based on the measured data at the Ft. Smith test site, groundwater levels ranged from 4 to 11 feet below the pavement surface. Therefore, the sensitivity analysis for groundwater levels was performed for groundwater levels ranging from 4 to 12 feet in increments of 2 feet. From Figures 5.11 and 5.12, it is obvious that the groundwater level within its measured range has no noticeable effect (much less than 1 percent) on predicted temperatures or moisture contents in the pavement system.

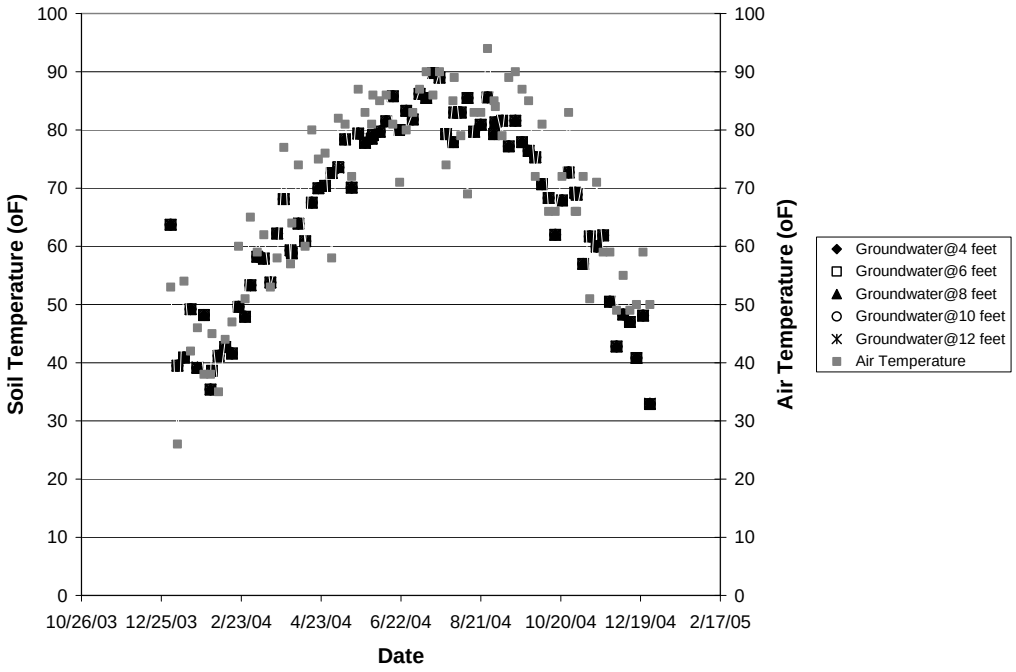

Figure 5.11 Comparison of air temperatures and predicted soil temperatures for a depth of 2 inches below the base surface for different groundwater levels.

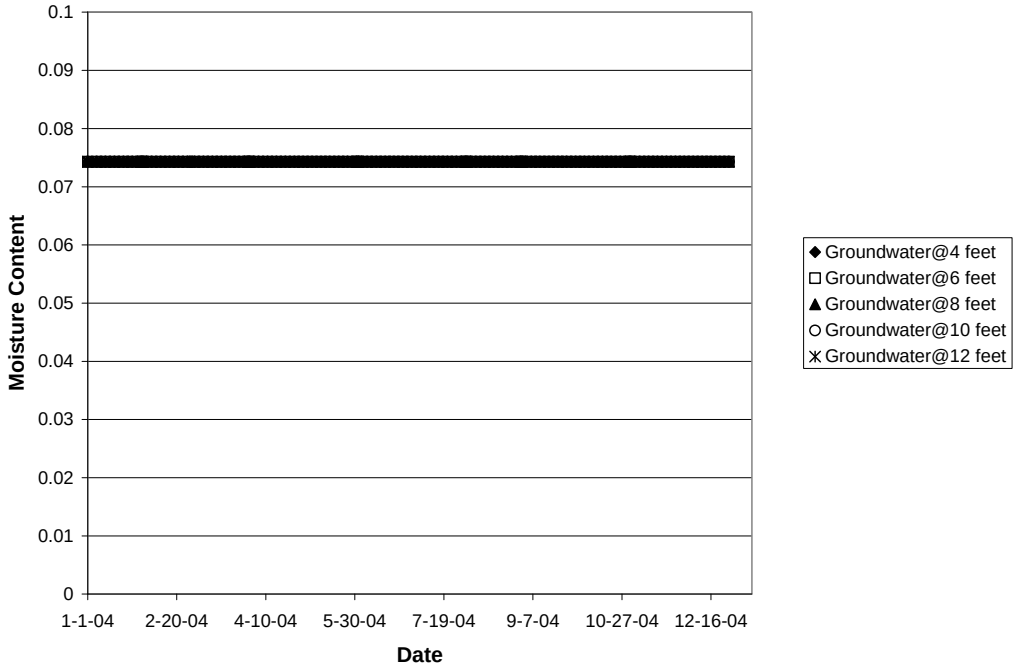

Figure 5.12 Predicted moisture contents for a depth of 2 inches below the base surface for different groundwater levels.

Based on the sensitivity analyses performed for climatic factors, including air temperatures, wind speeds, sunshine, humidity and groundwater levels, it can be concluded that using sunshine and humidity data obtained from a weather station that is close to a target test site will not significantly affect predicted temperatures and moisture contents in the pavement system at the target site. However, using wind speed data from nearby weather stations may cause a relatively significant effect on predicted temperatures in the pavement system, but not on predicted moisture contents in the pavement system. Air temperatures have a significant effect on predicted asphalt temperatures, and a change of one degree in air temperatures will generally result in a change of approximately one degree in the predicted asphalt temperatures. The groundwater level has almost no effect on predicted temperatures and moisture contents in the pavement system when it is relatively shallow.

5.3.6 Surface Short Wave Absorptivity

The surface short wave absorptivity of the asphalt surface layer depends on its composition, color, and texture. This quantity directly correlates with the amount of available solar energy that is absorbed by the pavement surface. Typical values of the surface short wave absorptivity for various asphalt pavement materials range from 0.8 to 0.98 (200X Design Guide). Therefore, the sensitivity analysis for the surface short wave absorptivity was performed for the absorptivities ranging from 0.8 to 0.98 in increments of 0.06 to determine their affect on pavement system temperatures. From Figures 5.13 and 5.14, one can see that short wave absorptivity has more effect on predicted asphalt or soil temperatures in the summer than in the winter and that effect of the surface short wave absorptivity on predicted temperatures in the pavement system generally decrease with depth. From Figure 5.13, one can see that maximum changes in predicted asphalt temperatures at the asphalt surface are generally within 13^{o}F when surface short wave absorptivity values change from 0.8 to 0.98. One can also see that asphalt surface temperatures are generally higher than air temperatures. From Figure 5.14, one can see that surface short wave absorptivity has almost no effect on predicted temperature in the base layer. On this basis, it can be reasonably concluded that values of the surface short wave absorptivity have a relatively significant impact on predicted asphalt temperatures. While, predicted temperatures in the base course and subgrade soil are relatively less sensitive to the surface short wave absorptivity, and using a value in the typical range in the EICM would give a relatively accurate predication on temperatures in the base course and subgrade soil.

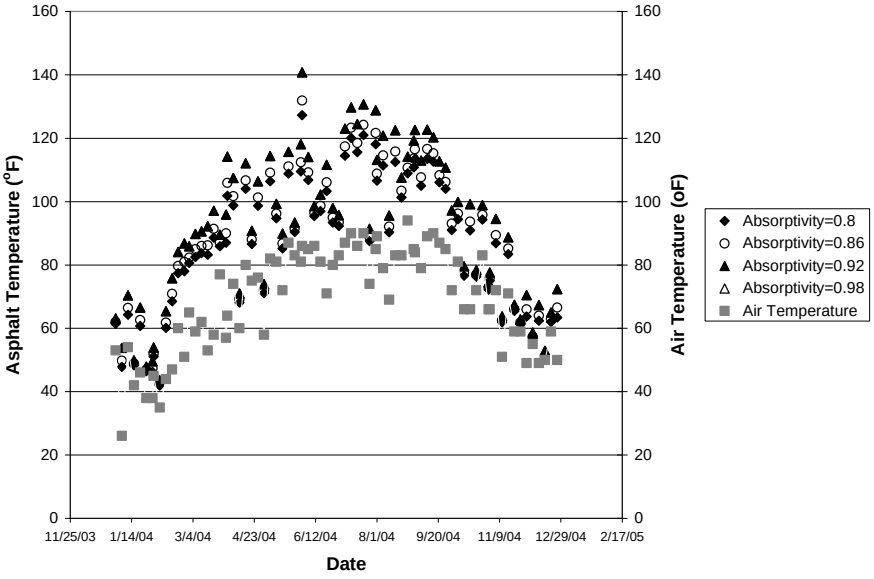

Figure 5.13 Comparison of air temperatures and predicted asphalt temperatures at the asphalt surface at the Ft Smith site for different surface shortwave absorptivity values.

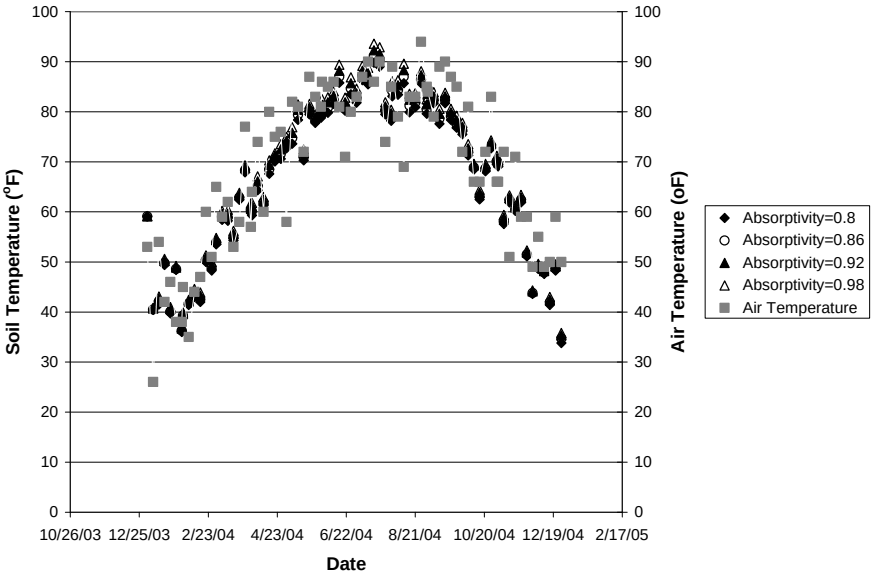

Figure 5.14 Comparison of air temperatures and predicted soil temperatures for a depth of 2 inches below the base surface at the Ft. Smith site for different surface shortwave absorptivity.

5.3.7 Thermal Conductivity

The thermal conductivity (K) of the asphalt layer is the quantity of heat that flows normally across a unit area of asphalt surface per unit of time and per unit of temperature gradient. Typical values of the thermal conductivity of the asphalt layer range from 0.44 to 0.81 Btu/(ft)(hr)(^{o}F) (200X Design Guide). Therefore, the sensitivity analysis for the thermal conductivity was performed for the thermal conductivities ranging from 0.44 to 0.81 in increments of about 0.12. Predicted temperatures for the asphalt surface and the base layer for different thermal conductivity values are presented in Figures 5.15 through 5.16.

From Figures 5.15 and 5.16, one can see that effects of the thermal conductivity on predicted temperatures in the pavement system generally decrease with depth. From Figure 5.15, it can be seen that maximum changes in predicted asphalt temperatures at the asphalt surface are generally within 5 ^{o}F when thermal conductivity values change from 0.44 to 0.81 Btu/(ft)(hr)(^{o}F). From Figure 5.16, it can be seen that thermal conductivity has almost no effect on predicted soil temperature in the base layer. From a practical standpoint, it can be reasonably concluded that predicted temperatures in the pavement system are relatively insensitive to the thermal conductivity, and using a value in the typical range in the EICM would give a relatively accurate predication on temperatures in the pavement system.

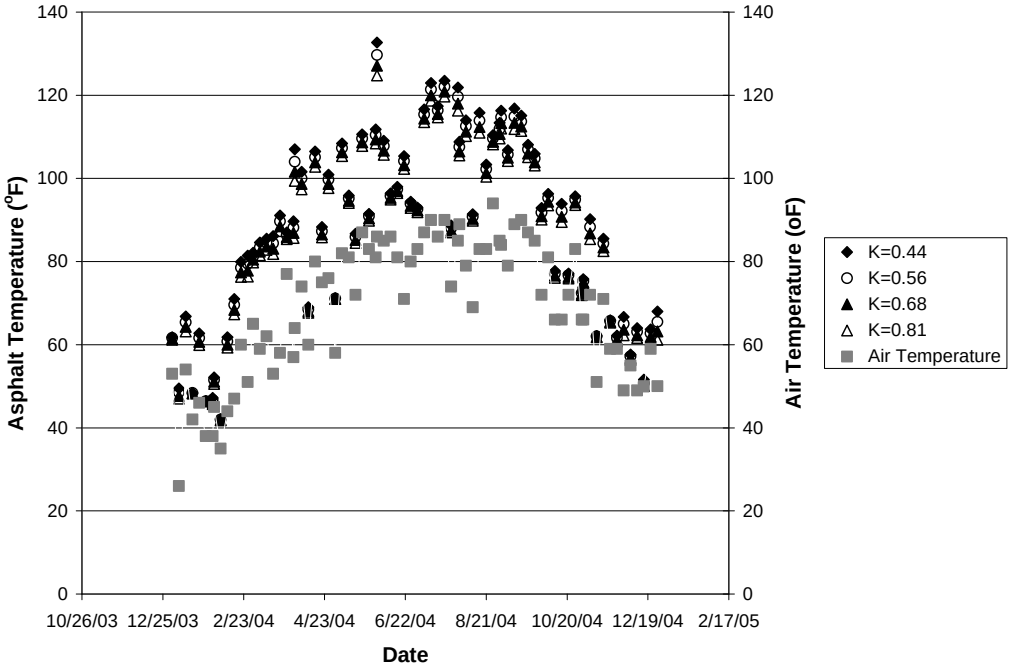

Figure 5.15 Comparison of air temperatures and predicted asphalt temperatures at the asphalt surface at the Ft Smith site for different thermal conductivity.

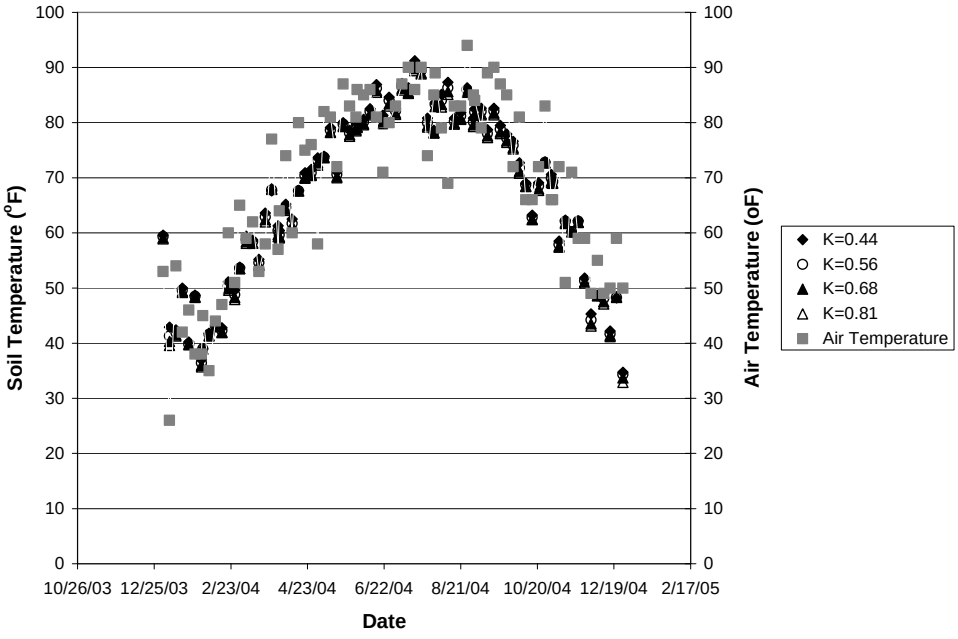

Figure 5.16 Comparison of air temperatures and predicted soil temperatures for a depth of 2 inches below the base surface at the Ft Smith site for different thermal conductivity.

5.3.8 Heat Capacity

The heat capacity (Q) of the asphalt layer is the actual amount of heat energy Q necessary to change the temperature of a unit mass by one degree. Typical values of the heat capacity of the asphalt layer range from 0.22 to 0.4 Btu/(lb)(^{o}F) (200X Design Guide). Therefore, the sensitivity analysis for the heat capacity was performed for the heat capacity ranging from 0.22 to 0.4 Btu/(lb)(^{o}F) in increments of 0.06. Predicted temperatures at the asphalt surface and in the base layer in the pavement system for different heat capacity are presented in Figures 5.17 and 5.18.

From Figure 5.17, one can see that maximum changes in predicted asphalt surface temperatures are generally within 5.5 ^{o}F when heat capacity values change from 0.22 to 0.4 Btu/(lb)(^{o}F), From Figure 5.18, it can seen that heat capacity has almost no effect on predicted soil temperature in the base layer. From a practical standpoint, it can be reasonably concluded that predicted temperatures in the pavement system are relatively insensitive to the heat capacity, and using a value in the typical range in the EICM would give a relatively accurate predication on temperatures in the pavement system.

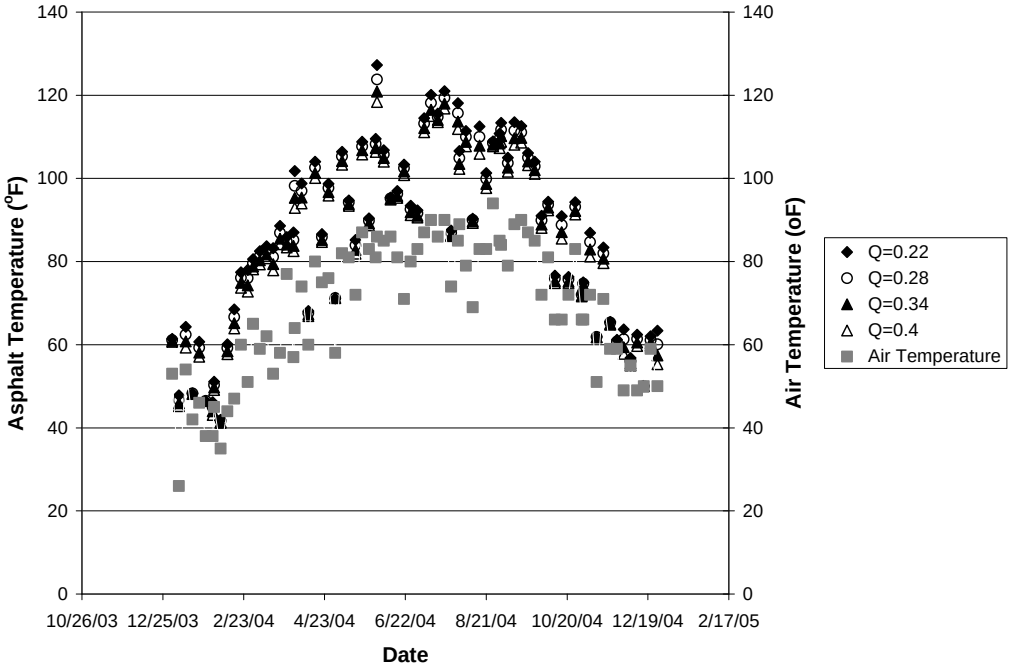

Figure 5.17 Comparison of air temperatures and predicted asphalt temperatures at the asphalt surface at the Ft Smith site for different heat capacity values.

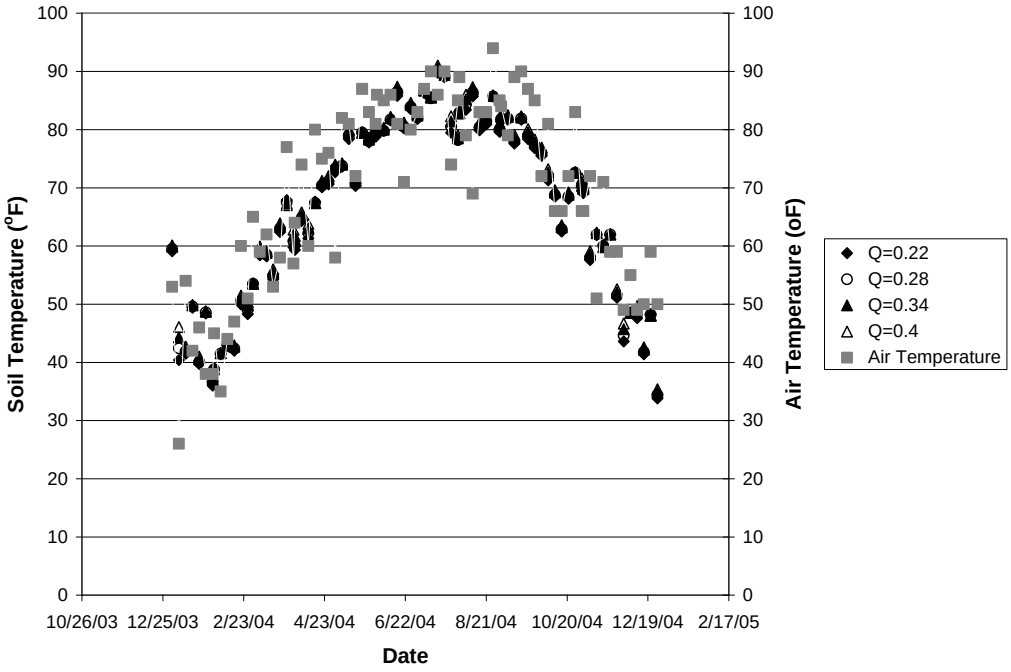

Figure 5.18 Comparison of air temperatures and predicted soil temperatures for a depth of 2 inches below the base surface at the Ft Smith site for different heat capacity values.

5.4 Evaluation of the EICM

In this section, measured moisture contents and soil temperatures were compared with predicted moisture contents and soil temperatures at the Ft. Smith site and the ERC to evaluate the suitability of the EICM in Arkansas.

5.4.1 Field Test Site

The field test site at Ft. Smith consisted of 9 inches of asphalt concrete underlain by 4 inches of the base course over the subgrade soil. Four layers of moisture probes and temperature probes were installed at the field test site. The first layer was installed in the middle of the base course. The remaining three layers were installed in the subgrade soil at depths of 2 inches, 10 inches and 24 inches below the subgrade surface, respectively.

Measured air temperatures, soil temperatures, precipitation intensities, soil moisture, surface and subsurface flow, and groundwater levels were measured at the site. These data were supplemented by wind speeds, percentages of sunshine and humidity obtained from the Fort Smith Regional Airport weather station which is located about 5 miles northeast of the site. The measured and supplemented data were used as climatic inputs for the EICM. Laboratory-measured material properties of the base and subgrade material, including grain-size distributions, maximum dry densities, optimum moisture contents, saturated hydraulic conductivity, specific gravity and Atterberg limits, were used as inputs for material properties required in the EICM.

Thermal properties of pavement systems including surface short wave absorptivity, thermal conductivity and heat capacity were not measured. However, based on the sensitivity analyses performed, it appears that these inputs have no significant

effect on predicted temperatures in the base course and subgrade soil when used in the model within their typical ranges. Therefore, default thermal properties for asphalt concrete and default thermal properties for the base and subgrade material based on AASHTO classifications included in the EICM were adopted for analyses.

Soil temperatures and moisture contents predicted by the EICM were compared with the measured soil temperatures and moisture contents at the same depths. The results of this comparison are illustrated in Figures 5.19 through 5.26. The other outputs of the model, pore water pressure and ice content were not evaluated. It should be noted that the moisture content output of the EICM is volumetric moisture content. While, measured moisture contents at each site are gravimetric moisture contents. To compare predicted volumetric moisture contents with measured gravimetric moisture contents, predicted volumetric moisture contents were converted to gravimetric moisture contents using Equation 5.3.

$$G_w = \frac{\gamma_w}{\gamma_d} V_w \qquad 5.3$$

Where,

G_w = gravimetric moisture content,

γ_w = unit weight of water, 62.4 pcf,

γ_d = dry unit weight of the soil,

V_w = predicted volumetric moisture content;

Inspection of Figures 5.19 to 5.22, reveals that the EICM does a good job of predicting soil temperatures in the winter and spring periods. Only relatively small discrepancies were observed between predicted and measured temperatures during these periods. However, relatively large differences between measured and predicted

temperatures were observed during the summer. A maximum difference of approximately 11 ^{o}F was observed for this period. To statistically quantify the difference between measured and predicted temperatures in the pavement, t tests were performed on differences between measured and predicted temperatures (predicted soil temperatures minus measured soil temperatures). The results of the t tests are presented in Table 5.4. From this analysis it can be seen that the null hypotheses are rejected, which means that means of differences between measured and predicted values are not equal to zero at a confidence level of 95 percent. From this analysis one can be 95 percent sure that the maximum difference between measured and predicted temperatures will be approximately 10 ^{o}F (mean plus 1.98 times standard deviation). Even though asphalt temperature was not measured at the Ft Smith site, it can be reasonable to say that the maximum difference between measured and predicted asphalt temperature would be 10 ^{o}F or greater because Table 5.4 indicates that standard deviation gets bigger as the depth below the pavement surface gets smaller. As discussed previously, a 10 ^{o}F difference in asphalt temperature will cause a 30 percent change in asphalt modulus. Therefore, it can be concluded that the EICM can not predict soil temperature with adequate accuracy.

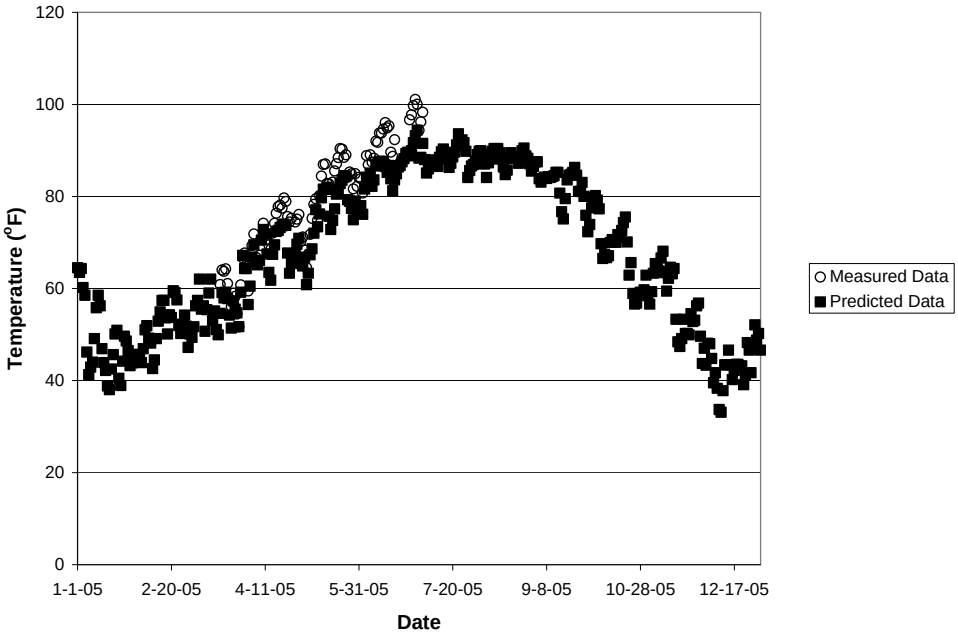

Figure 5.19 Comparison of measured and predicted unbound aggregate temperatures for a depth of 2 inches below the base surface at the Ft. Smith test site.

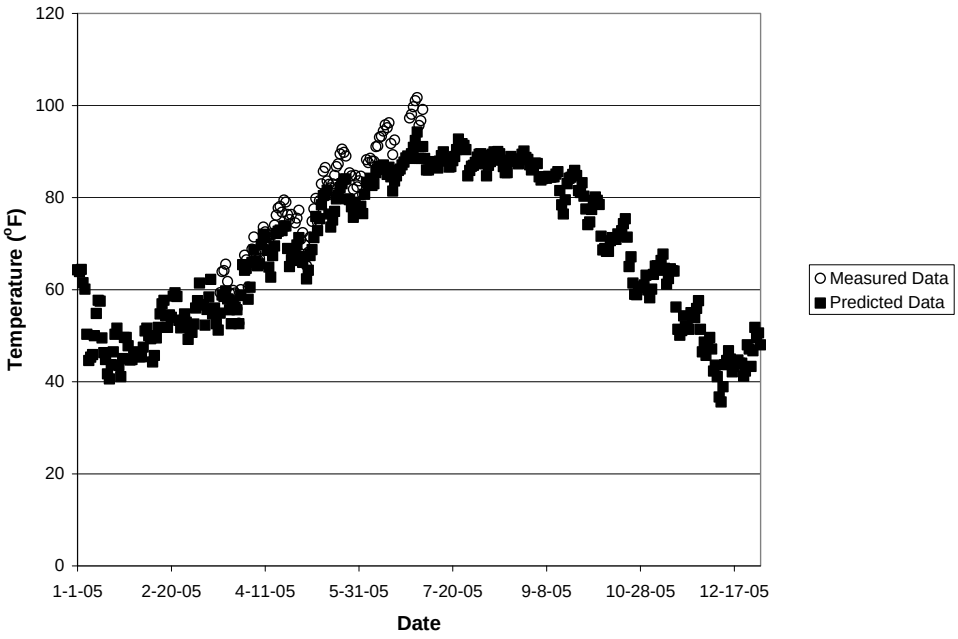

Figure 5.20 Comparison of measured and predicted soil temperatures for a depth of approximately 2 inches below the subgrade surface at the Ft. Smith test site.

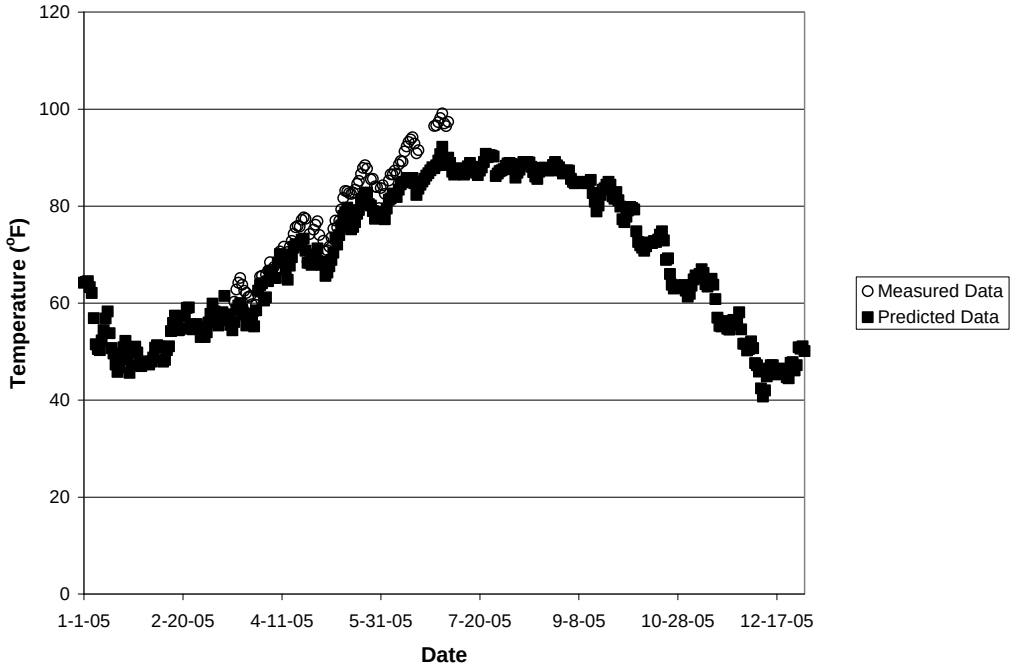

Figure 5.21 Comparison of measured and predicted soil temperatures for a depth of approximately 10 inches below the subgrade surface at the Ft. Smith test site.

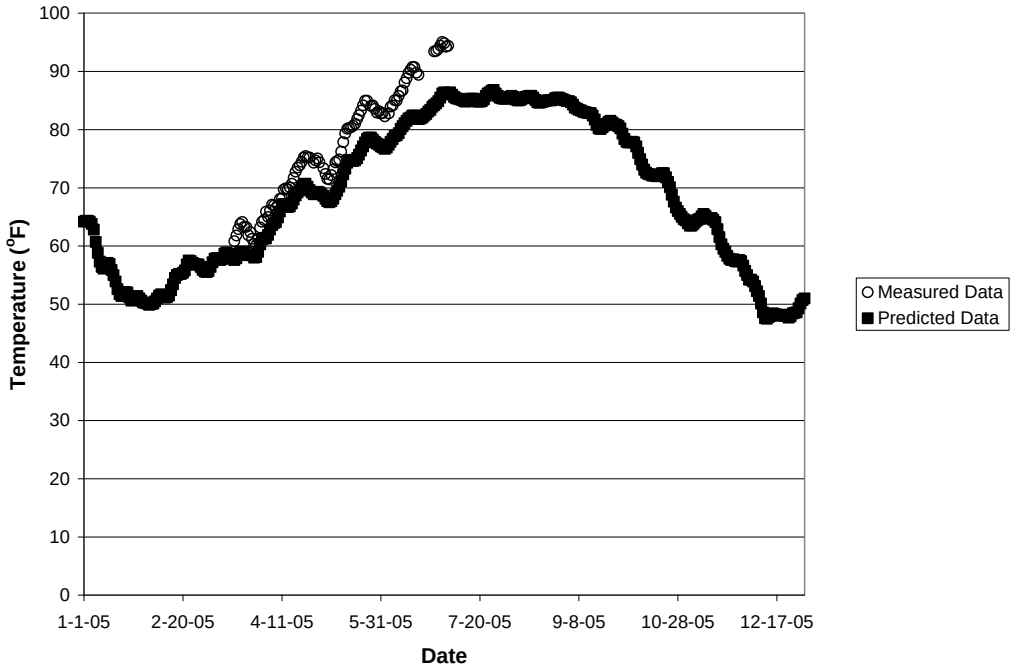

Figure 5.22 Comparison of measured and predicted soil temperatures for a depth of approximately 24 inches below the subgrade surface at the Ft. Smith test site.

Table 5.4 Results of t-tests on differences between measured and predicted temperatures in the pavement at the Ft Smith site.

	Base Layer	Subgrade-2”	Subgrade-10”	Subgrade-24”
Null hypothesis H_0	$\mu_d=0$	$\mu_d=0$	$\mu_d=0$	$\mu_d=0$
Level of significance	0.05	0.05	0.05	0.05
Sample Size	100	99	96	98
Sample mean (mean of sample difference)	-5.09	-5.29	-4.89	-5.30
Sample standard deviation	2.60	2.49	2.11	1.90
t test statistic	-19.55	-21.12	-22.67	-27.61
$t_{0.025,n-1}$	1.98	1.98	1.98	1.98
95% Confidence Interval	5.09±0.52	5.29±0.50	4.89±0.43	5.30±0.38

Figure 5.23 illustrates that the EICM generally over-predicted moisture content in the base material by as much as 3 percent for the Ft. Smith test site. This represents a 60 percent error in predicting the correct moisture content. It can also be seen that predicted moisture contents in the base material at the Ft Smith site are constant over almost the entire year. This is probably because the ID model, which is a sub-model in the EICM, assumes that the base material is a free-draining material. Under this assumption, “free water” would drain out of the base layer at a much faster rate than new water could infiltrate into the pavement system during precipitation events. The moisture content reported by the EICM in the base material is “bound” moisture held by capillary forces in the base material. The effects of this “bound” moisture are considered in the EICM through adjustments to pavement material properties, such as percentage of fines (200X Design Guide). The amount of the “bound” water is related to pavement material properties, which are constant with time. Therefore, predicted moisture contents in the base material are constant over time. A significant drop in predicted moisture contents was observed during December in Figure 5.66. This is because the EICM predicted that the base material was partially frozen at this depth. However, TDR-measured moisture

contents did not show any significant change in moisture, which indicates that no freezing occurred during this period. Therefore, it can be concluded that the EICM over predicts the frozen depth in the pavement system.

From Figures 5.24 through 5.26, it can be seen that the EICM can not predict the periodic nature of moisture change with season. During the summer, predicted moisture contents are generally lower than measured moisture contents with these differences being as much as 50 percent. This would result in significantly over-predicted resilient modulus in the summer. While, in the winter, the EICM generally over-predicted moisture contents in the subgrade soils, which would result in under-predicted resilient modulus values. Therefore, it can be concluded that the EICM is not suitable for predicting moisture content in the pavement system at the Ft. Smith site.

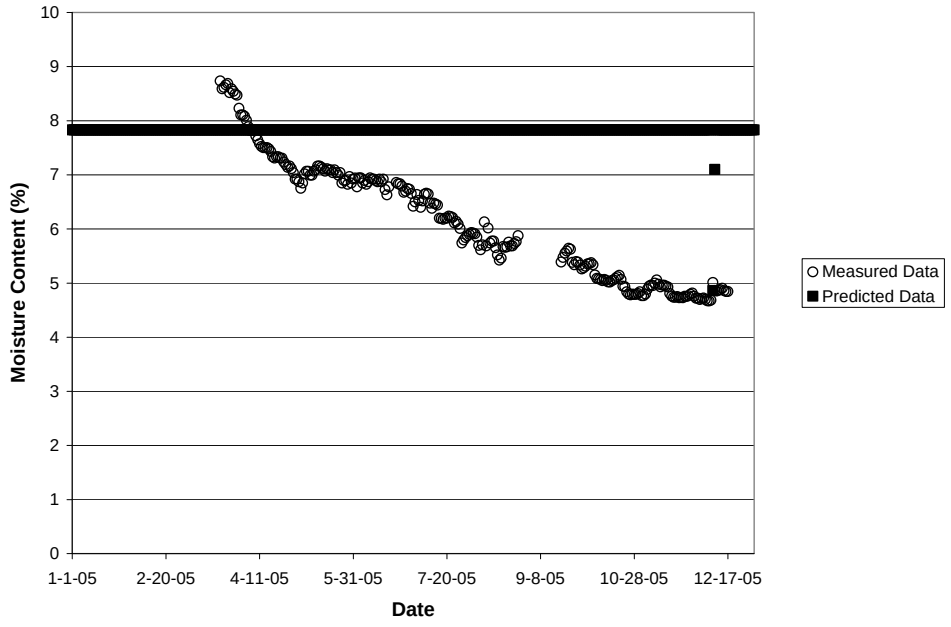

Figure 5.23 Comparison of measured and predicted moisture contents for a depth of approximately 2 inches below the base surface at the Ft. Smith test site.

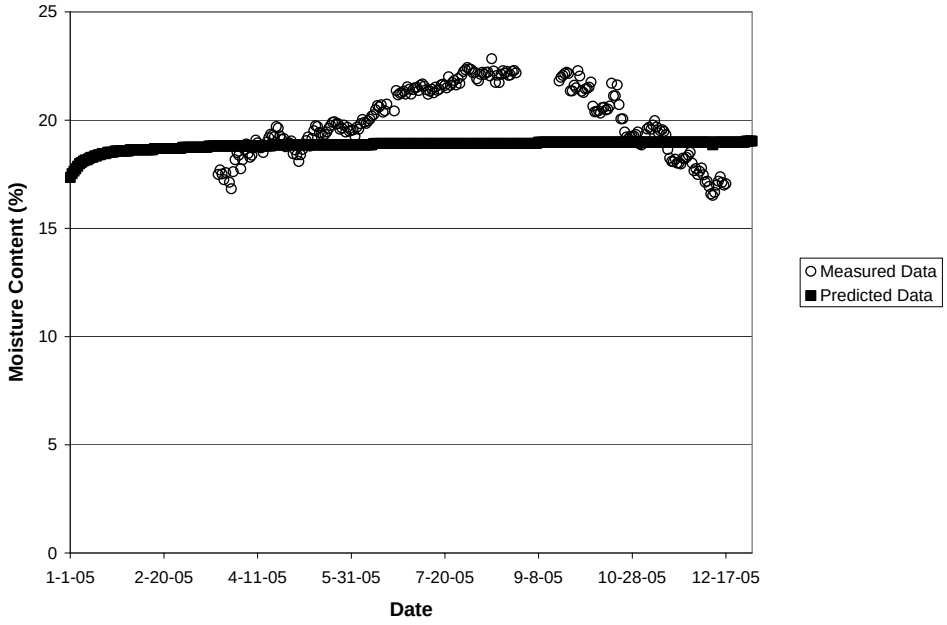

Figure 5.24 Comparison of measured and predicted moisture contents for a depth of approximately 2 inches below the subgrade surface at the Ft. Smith test site.

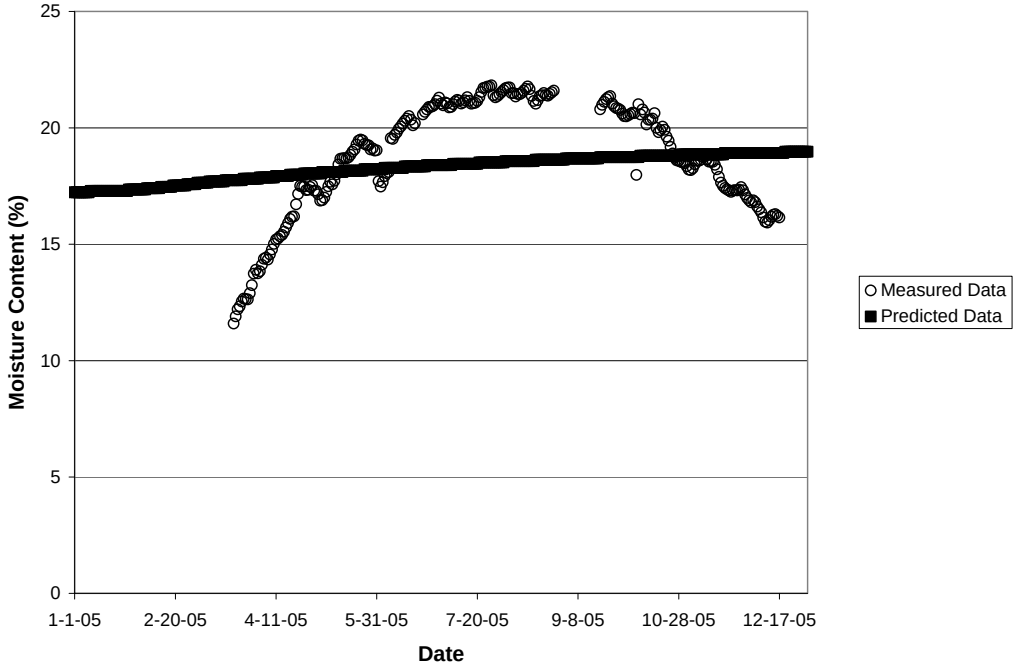

Figure 5.25 Comparison of measured and predicted moisture contents for a depth of approximately 10 inches below the subgrade surface at the Ft. Smith test site.

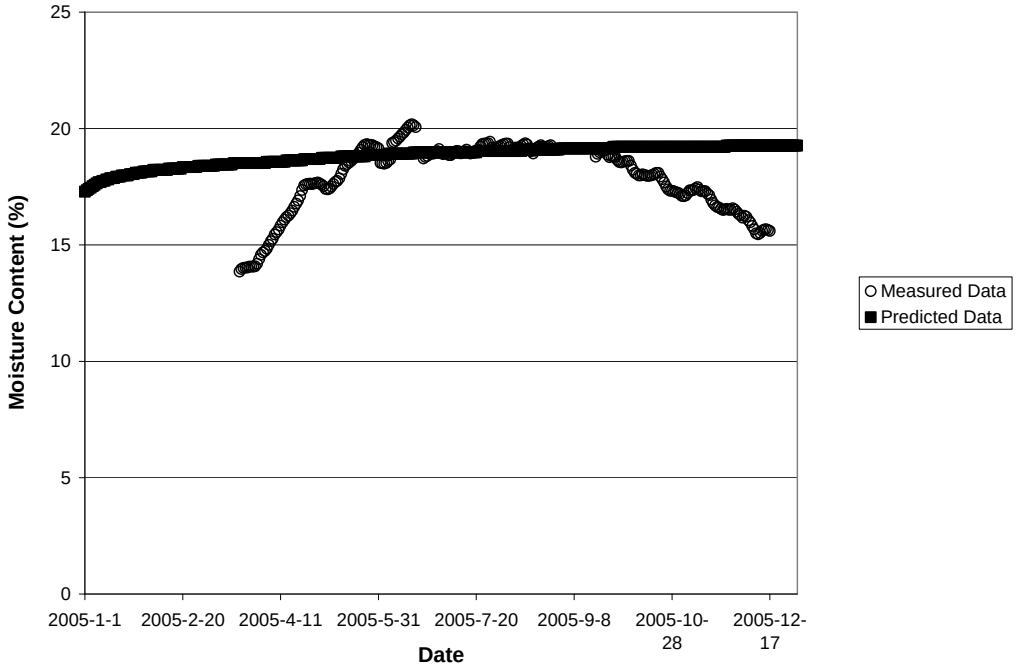

Figure 5.26 Comparison of measured and predicted moisture contents for a depth of approximately 24 inches below the subgrade surface at the Ft. Smith test site.

5.4.2 Test Pads at the ERC

Since the moisture probes installed in test pad B at the ERC were recovered for use at the field test site in August, 2004 and because groundwater level measurements did not start until June, 2004. Only about two months of complete data are available for test pad B. Therefore, evaluation of the EICM was only performed for test pad A at the ERC.

As discussed previously, test pad A at the ERC consists of about 3 inches of asphalt concrete underlain by 7 inches of the base course and 12 inches of the subbase course over the subgrade soil. A total of five layers of moisture probes were installed in test pad A. The first layer was installed at a depth of about 2 inches below the surface of the base course. The second layer was installed at a depth of the interface between the base and subbase material. The third layer was installed about 8 inches below the surface

of the subbase course. The remaining two layers were installed in the subgrade soil at depths of about 2 inches and 10 inches below the surface of the subgrade soil.

Wind speed, sunshine and humidity data obtained from the Drake Field airport weather station in Fayetteville, AR and measured air temperatures, precipitation and groundwater levels at the ERC were used as climatic inputs required for the EICM. The Drake Field airport weather station is located about 3 miles south of the ERC and should give good estimates for the inputs that were not physically measure at the ERC.

Laboratory-measured material properties of the base, subbase and subgrade materials and default thermal properties of pavement materials, as used in the analysis in the Ft. Smith test site, were also used as material property inputs required for the EICM.

Since temperature probes were not installed in test pads at the ERC, only predicted moisture contents using the EICM at depths where moisture probes were installed were compared with measured moisture contents. The results of the comparisons are presented in Figures 5.27 to 5.31.

From Figure 5.27, it can be seen that predicted moisture contents for a depth of approximately 2 inches below the base surface of test pad A at the ERC form a lower bound for the measured moisture contents with an average error of approximately 20 percent and as much as 100 percent error at the peak of measured values. The percent error in this study was defined as ratios of differences between measured and predicted values, and predicted values. The EICM can not predict the effect of precipitation on moisture contents at this depth and the cyclic nature of the rise and fall of measured moisture is a result of response to precipitation events. From Figures 5.28 and 5.29, it can be seen that the EICM generally under-predicted moisture contents at deeper depths in

base and subbase materials. The measured values in this region appeared not to be affected by precipitation events and remained relatively stable during the entire period of measurements. Average differences between predicted and measured moisture contents at the deeper depths in the base and subbase materials are as great as 100 percent with the difference becoming greater with depth. Compared to the Ft Smith test site, the EICM predicts lower moisture contents in the base materials at the ERC than those at the Ft Smith site. This is probably because of the fact that the base material for the Ft Smith site had a larger fine content than that for the ERC. Also, from these figures, one can see that predicted moisture contents in the base and subbase materials are constant during most of the period. During January, February and December, the EICM predicted moisture contents in the base and subbase materials dropped much more significantly than the measured moisture contents. This drop in predicted moisture contents was the result of freezing in this layer, while the measured moisture contents did not show any freezing. This indicates that the EICM over-predicts the depth of frost penetration for this area.

From Figures 5.30 and 5.31, it can be seen the EICM can not predict periodic nature of changes in moisture in the subgrade soils. The EICM under-predicts moisture content of the subgrade soil at a depth of two inches below the subgrade surface at the ERC during most of the year, with maximum errors as much as 33 percent in summers. At a depth of approximately 10 inches below the subgrade surface, the EICM generally over-predicts moisture contents by as much as 10 percent error in winters and under-predicts moisture contents by as much as 8 percent in summers. More significantly at the 2” level in the subgrade the predicted values form a lower bound for the measured values, while at the 10” level the predicted values are more of an average of the measured values.

It appears that the EICM does a better job of predicting moisture as the depth below the pavement surface gets larger, but instantaneous errors can be great in the areas that most affect pavement performance. Therefore, it can be concluded that the EICM is not suitable for predicting moisture content in the pavement system at the ERC. .

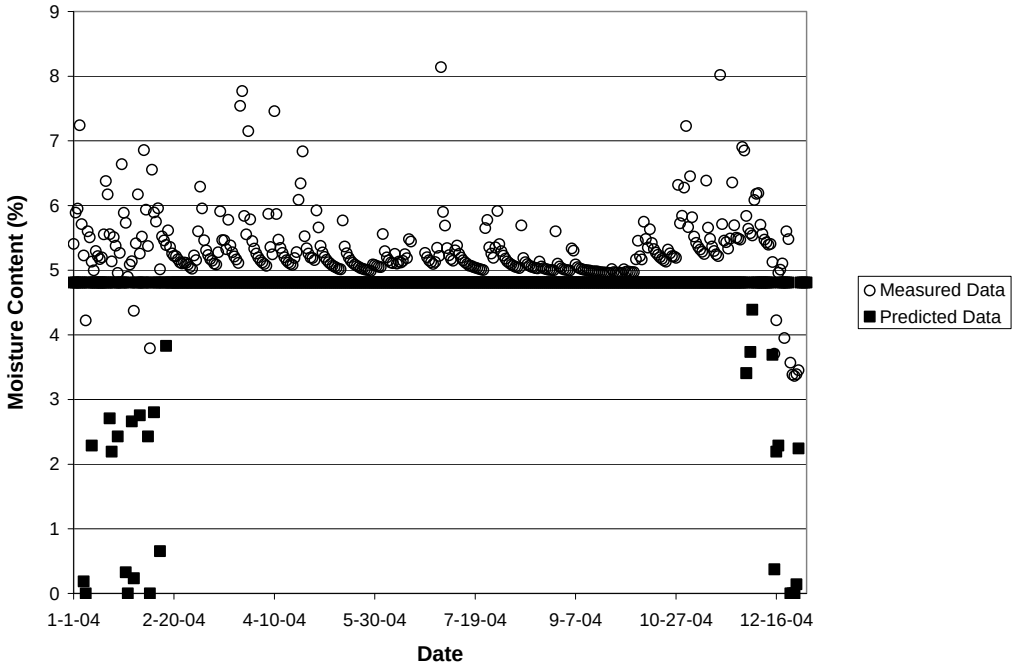

Figure 5.27 Comparison of measured and predicted moisture contents for a depth of approximately 2 inches below the base surface of test pad A at the ERC.

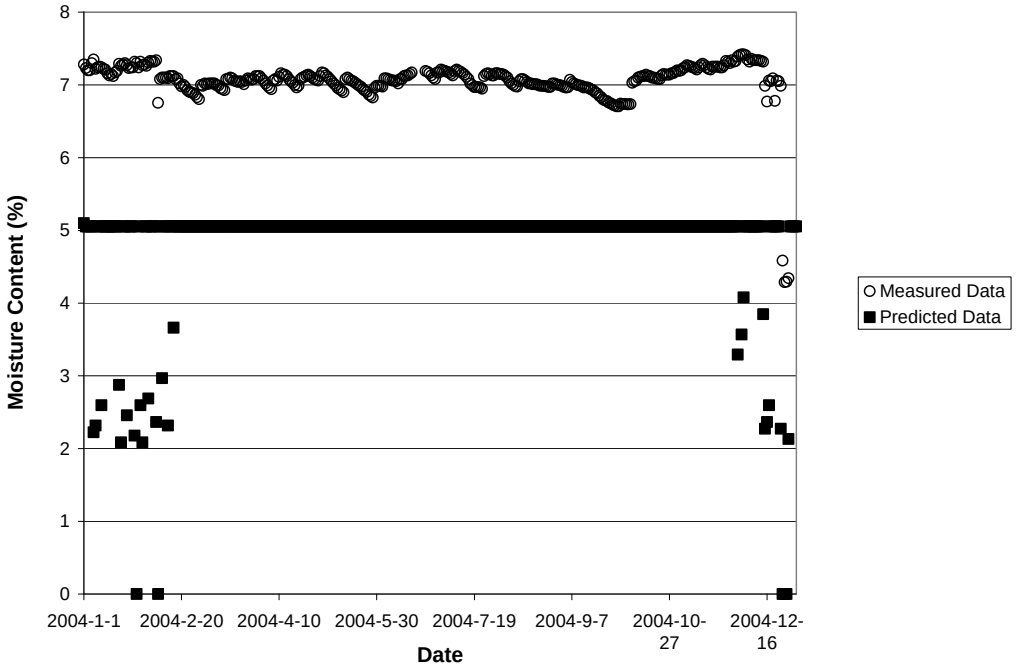

Figure 5.28 Comparison of measured and predicted moisture contents at the interface of the base and subbase materials of test pad A at the ERC.

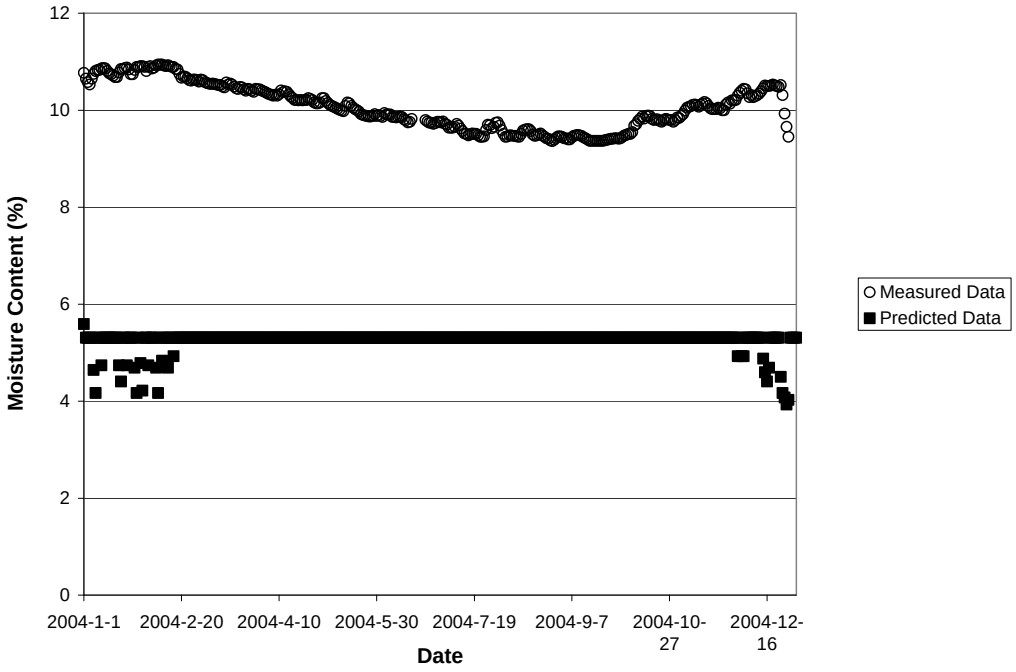

Figure 5.29 Comparison of measured and predicted moisture contents for a depth of approximately 8 inches below the subbase surface of test pad A at the ERC.

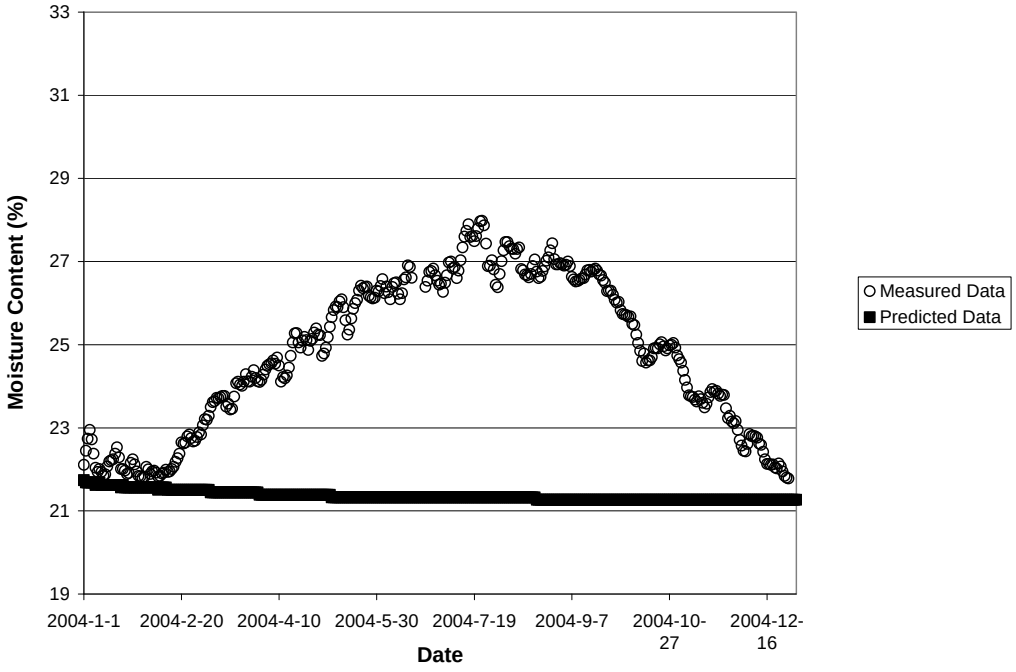

Figure 5.30 Comparison of measured and predicted moisture contents for a depth of approximately 2 inches below the subgrade surface of test pad A at the ERC.

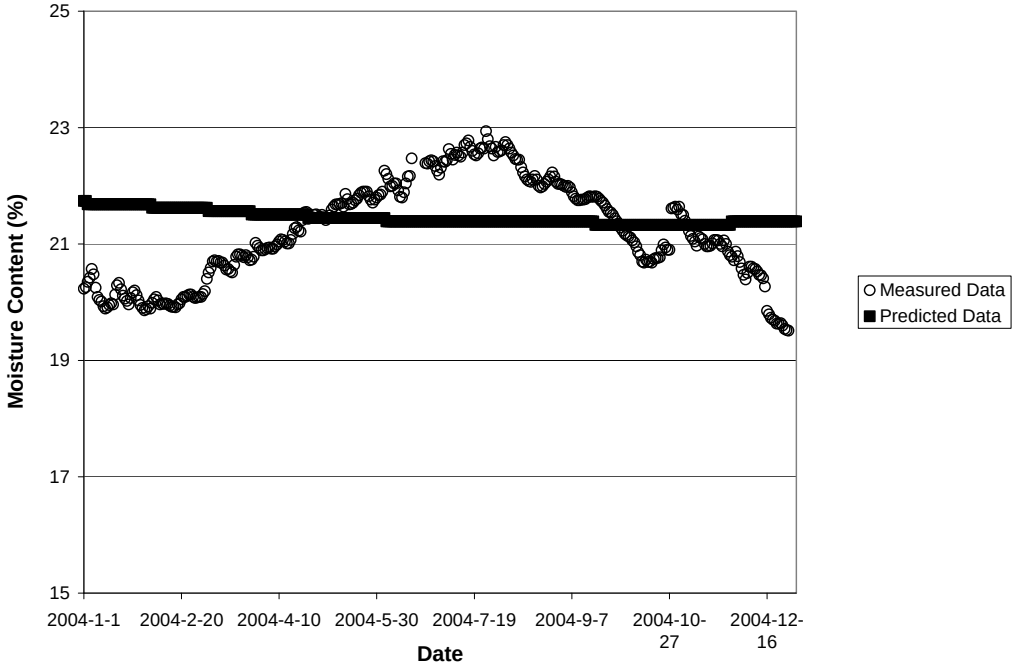

Figure 5.31 Comparison of measured and predicted moisture contents for a depth of approximately 10 inches below the subgrade surface of test pad A at the ERC.

5.5 Discussion and Conclusions

From the sensitivity analyses performed previously in this chapter and comparisons between predicted and measured soil temperatures and moisture contents in the pavement systems at the Ft Smith test site and test pad A at the ERC, the following conclusions can be drawn:

Sensitivity Analysis

- A change of 1 degree in air temperatures will result in a change of 1 degree or less in predicted asphalt temperatures.
- A maximum change in predicted soil temperatures in the pavement system is approximately 20 ^{o}F with wind speeds varying from 0 to 5 mph, while a maximum change in predicted soil temperatures is only 10 ^{o}F when wind speeds change from 5 to 30 mph. It appears that weather conditions of wind (wind speed >5 mph) and no wind (wind speed 0 mph) could make a relatively large difference on predicted temperatures in the pavement system and predicted temperatures are not really sensitive to the magnitude of wind speed when it is windy.
- The wind speed has no noticeable effect on predicted moisture contents in the pavement system.
- Percent sunshine has up to 5 percent effect on predicted soil temperatures and has almost no effect on predicted moisture contents in the pavement system.
- The relative humidity has no noticeable effect on predicted moisture contents and temperatures in the pavement system.

- Among wind speed, sunshine and humidity, wind speed has the biggest effect on predicted temperatures in the pavements especially when wind speed changes from 0 to 5 mph.
- Effects of the surface short wave absorptivity on predicted temperatures in the pavement system generally decrease with depth. Values of the surface short wave absorptivity have a relatively significant impact on predicted asphalt temperatures, especially near the asphalt surface. While, predicted temperatures in the base course and subgrade soil are less sensitive to the surface short wave absorptivity.
- Effects of the thermal conductivity and heat capacity on predicted temperatures in the pavement system generally decrease with depth. Predicted temperatures in the pavement system are relatively insensitive to the thermal conductivity and heat capacity, and using a value in the typical range in the EICM would give a relatively accurate predication on temperatures in the pavement system.

Comparison of Predicted to Measured

- The EICM predicted temperatures in the pavement pretty well during the winter, spring and fall at the test site in Fort Smith, Arkansas. However, a relatively large discrepancy between measured and predicted soil temperature was observed in the summer.
- The EICM did predict seasonal periodical changes in moisture contents in the subgrade soils. Generally, the EICM under-predicted moisture contents in

summers by as much as 50 percent. While, in winters, the EICM generally over-predicted moisture contents by as much as 50 percent.

Chapter 6 Finite Element Modeling

6.1 Introduction

To better understand the pattern of water migration through pavement systems and to theoretically confirm the conclusions obtained from laboratory and field tests, finite element modeling (FEM) was performed. A commercially available finite element program – PlaxFlow, which was developed by Plaxis b.v., Netherlands, was used for the FEM analyses. Because complete moisture data were able to be collected for test pad A at the ERC for a relatively long period, the FEM was performed with material and geometry properties for test pad A at the ERC.

6.2 PlaxFlow

PlaxFlow can be used to perform seepage analyses for both steady and transient groundwater flow. PlaxFlow also provides state-of-art capabilities to incorporate time-dependent boundary conditions. The basic theory of groundwater flow used in PlaxFlow is Darcy's law, which describes flow in a porous medium based on hydraulic gradient and material constitutive properties. The ability to model both saturated and unsaturated flow is included in the software.

Like most other finite element software, the first step in the analysis is to create a geometry model in PlaxFlow. A geometry model can be created using the following geometry features.

- Points and Lines. These are the basic items for the creation of a geometry model.

- Screens. Screen elements are used to model impermeable structural objects within the boundaries of a geometry model. A zero Darcy flux is specified boundary condition over the screen elements.
- Drains. Drain elements are used to model a drainage line within a geometry model where pore water pressures are set to zero.
- Wells. Well elements are used to model points within a geometry model where a specific flux (discharge) is subtracted from or added to the soil.
- Tunnels. Tunnel elements are used to create circular and non-circular tunnel cross-sections. Tunnel elements are permeable objects within the boundaries of a geometry model. Screen elements can be used to add an impermeable screen to the outer tunnel contour.

The material properties required in a PlaxFlow model include vertical and horizontal saturated hydraulic conductivity, void ratio and soil water characteristics curve (SWCC) or SWCC model parameters for each soil stratum in the model. Three levels of material property input options are provided in PlaxFlow. They are “Standard Option”, “Advanced Option” and “Expert Option”. In the “Standard Option”, PlaxFlow allows a simplified selection of properties for the most common soil types. A linear SWCC based on the Approximate Van Genuchten model is used in this option. The “Advanced Option” allows selection of more extended soil types based on different soil classification systems. It also allows both linear and non-linear SWCCs based on the Van Genuchten and Approximate Van Genuchten models. For both the “Standard Option” and “Advanced Option”, no user-defined SWCCs are allowed. The “Expert Option”,

however, allows the use of the Van Genuchten model, the Approximate Van Genuchten model, a user-defined model, and full saturated model.

After creating the geometry model and supplying the required material properties for each stratum in the model, PlaxFlow allows an automatic finite element mesh generation. Five levels of global coarseness are included in the software. They are very coarse, coarse, medium, fine and very fine. Coarseness of the mesh can be adjusted locally by defining a local element size factor.

After generating the mesh, boundary conditions can then be specified. Boundary conditions in PlaxFlow consist of free boundary, groundwater head, closed flow boundary, precipitation (infiltration), inflow, outflow and seepage surfaces. PlaxFlow also supports time-dependent boundary conditions. The time-dependent conditions, such as precipitation, can be defined by a linear or harmonic function or by means of an input table.

Output parameters of PlaxFlow include active pore pressure, groundwater head, degree of saturation and flow field. The output from PlaxFlow can be viewed as shading, contours or flow arrows in figures for each time step and can also be viewed as plots or tables for selected cross sections of the model or for specific points.

6.3 FEM Set-Up and Calibration

6.3.1 Selection of the Precipitation Event

The groundwater level is a required input parameter in the finite element analysis. Groundwater levels were measured from June through November of 2004 for test pads at the ERC. A relatively large precipitation event during the groundwater monitoring

program occurred on October 27, 2004. It lasted from 17:50 on the 27th to 9:25 on October 28, 2004. The precipitation event was relatively large and was broken into several peaks. The peaks included relatively larger and small peaks. Therefore, this event was selected for the finite element analysis. During this event, 1.53 inches of rainfall were measured. The groundwater level was measured to be about 70 inches below the pavement surface at the time of the precipitation event. For the purpose of the analysis, the whole hour before the precipitation event, 17:00 on October 27, 2004 was used as the starting point (time 0) in the analysis and the analysis was performed for a 24-hour period.

6.3.2 Geometry Model and Boundary Conditions

As mentioned earlier, moisture probes were installed in the middle of test pad A at the ERC. A cross-section at the middle of the test pad was used to perform the finite element modeling. Illustrated in Figure 6.1 is the geometry model that was created based on actual dimensions of test pad A. The cross-section was extended 10 feet to the left of the asphalt to model the soil conditions on that side of the test pad. On the right side, the cross-section was extended about 12 feet to provide a reservoir where water could move out of the pavement system. Six types of materials are included in the geometry model. The first one is asphalt, which is the top layer in the middle. The upper two inches of the base material was modeled as a separate material with a higher hydraulic conductivity and lower soil suction than the underlying base on the assumption that some of the fines had been leached from the surface before asphalt was placed on it. The upper base material is shown as the second layer in the middle portion of Figure 6.1. The lower

portion of the base material, subbase and subgrade soils are shown as the third, fourth and fifth layers in the middle portion of the diagram. The material on the left side of the model was modeled given the same properties as the subgrade soil. The geometry also includes a material type for drainage material around the edge drain and reservoir material on the right side of the illustration. Drain elements were specified around the edge drain to simulate the edge drain. The material properties of each portion of the model will be discussed in the next section. After creating the geometry model and entering the required material properties, a finite element mesh was generated using a "very fine" global coarseness. The mesh is shown in Figure 6.2.

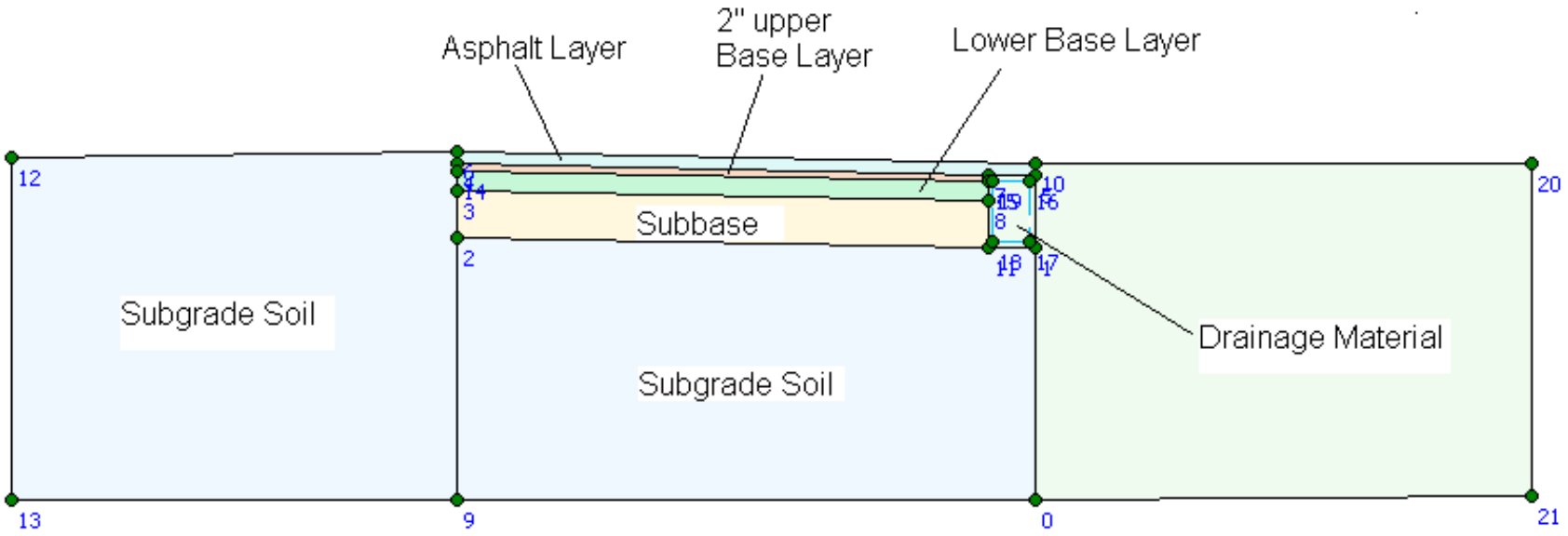

Figure 6.1 Geometry model of the FEM Analysis.

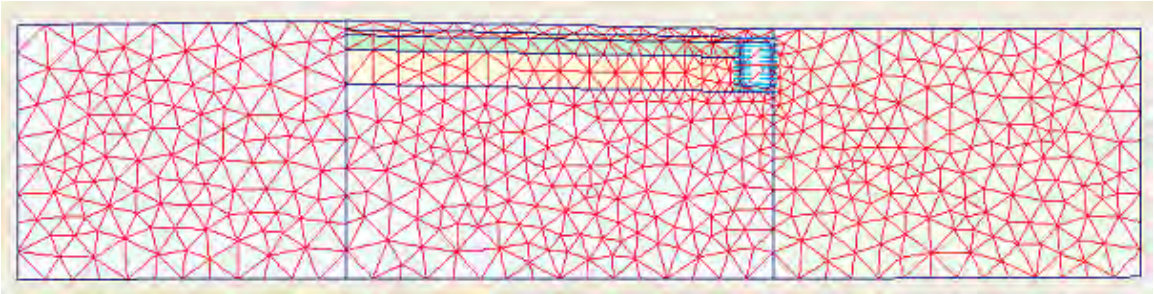

Figure 6.2 Mesh generation.

After the mesh was generated, boundary conditions and the groundwater level were specified. As shown in Figure 6.3, the left and right sides of the model were given closed boundaries. The bottom of the model was given a groundwater head boundary. The top of the model was given a free boundary for the asphalt and subgrade soil on the left, and a closed boundary for the reservoir material on the right.

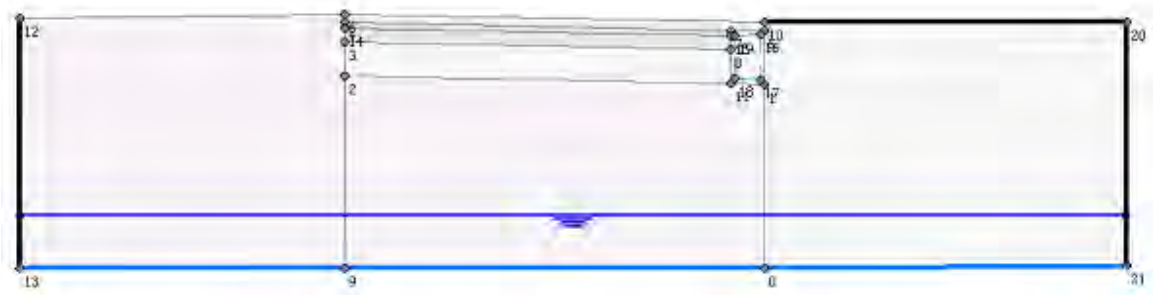

Figure 6.3 Boundary conditions and groundwater level for the initial phase.

After the initial boundary conditions were established, a transient phase was created to simulate water migration during the precipitation event. The transient phase has the same boundary conditions except that a time-dependent precipitation event was specified on the asphalt surface in the middle of the model and the subgrade soil on the left. The time-dependent precipitation event was input using an input table which produced the infiltration function illustrated in Figure 6.4. The boundary conditions for the transient phase are illustrated in Figure 6.5.

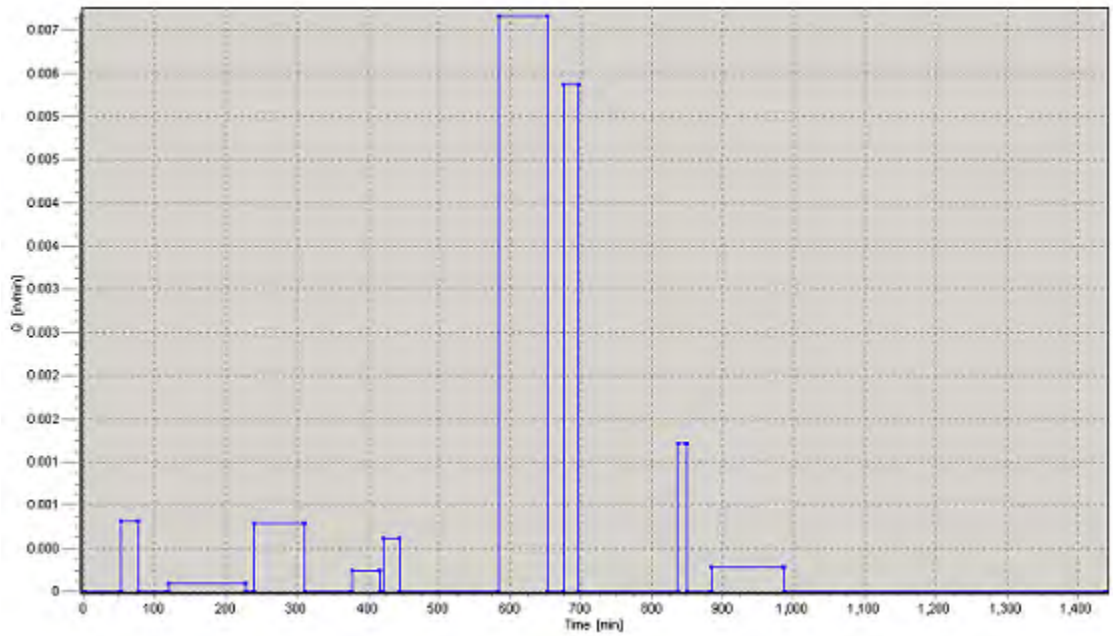

Figure 6.4 Illustration of the precipitation event.

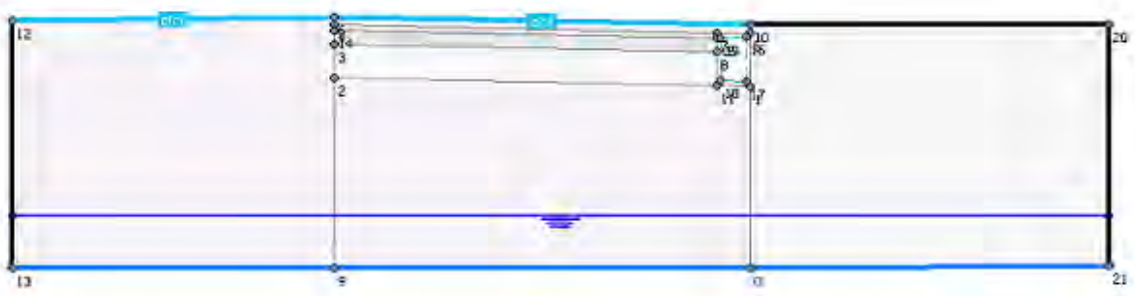

Figure 6.5 Boundary conditions for the transient phase (during the precipitation event).

6.3.3 Material Properties

6.3.3.1 Saturated Hydraulic Conductivity

As discussed in Chapter 3, the hydraulic conductivity of pavement materials and the underlying soils were measured in the laboratory. The hydraulic conductivity of the asphalt concretes at the ERC was also measured in field. The laboratory-measured hydraulic conductivity of base, subbase and subgrade soils was 3.3×10^{-3}, 3.1×10^{-3}. and 3×10^{-8} cm/second, respectively. The laboratory-measured hydraulic conductivity

measured on asphalt cores obtained from test pad A at the ERC varied significantly from 0 to 5.75×10^{-4} cm/second. The hydraulic conductivity measured using field permeameters ranged from 0 to 2.2×10^{-3} cm/second.

No hydraulic conductivity and classification tests were performed on the clear gravel used around the edge drain. Terzaghi (1948) suggested that a hydraulic conductivity value in a range of 10 to 1000 cm/s could be used for clear gravel. For the purpose of the FEM model, a saturated hydraulic conductivity value of 100 cm/s was chosen for clean gravel. Default unsaturated material properties of sand, which represented the coarsest material included in the software, were used to model the clear gravel.

6.3.3.2 Soil Water Characteristic Curve (SWCC)

Because the pavement materials and the underlying subgrade soil are generally not saturated under most conditions, unsaturated material properties have to be used in the FEM. The SWCC is a primary unsaturated material property, which defines the relationship between water content and suction for a given soil. The SWCCs for the pavement materials and the underlying subgrade soil at the ERC were not measured. According to 200X Design Guide (2004), the equations proposed by Fredlund and Xing in 1994 showed a good agreement with an extended database and were recommended for use in the 200X Design Guide. Therefore, the equations proposed by Fredlund and Xing were used to develop the SWCCs for the pavement materials and the underlying subgrade soil in this study. Fredlund and Xing's equations are illustrated in Equations 6.1 and 6.2

$$\theta(h) = C(h) \times \left[\frac{\theta_{sat}}{\left[\ln\left[Exp(1) + \left(\frac{h}{a_f} \right)^{b_f} \right] \right]^{c_f}} \right] \quad 6.1$$

$$C(h) = 1 - \frac{\ln\left(1 + \frac{h}{h_r}\right)}{\ln\left(1 + \frac{145000}{h_r}\right)} \quad 6.2$$

$$\theta_{sat} = 1 - \frac{\gamma_{d\max}}{\gamma_{water} G_s} \quad 6.3$$

Where:

$\theta(h)$ = volumetric water content;

h = metric suction (psi);

a_f, b_f, c_f and h_r = model parameters;

θ_{sat} = saturated volumetric water content;

γ_{dmax} = maximum dry density;

γ_{water} = unit weight of water;

G_s = specific gravity.

The SWCC model parameters can be related to soil index properties according to the AASHTO 200X Design Guide. For cohesive soils, the model parameters can be correlated with the product of P_{200} (decimal) and PI. P_{200} and PI stand for the percentage passing an U.S. No. 200 sieve and plastic index, respectively. For cohesionless soil, the model parameters can be correlated with the D_{60}, which stands for the effective grain size corresponding to 60 percent passing by weight.

For cohesive soils:

$$a_f = \frac{0.00364 \times (P_{200} PI)^{3.35} + 4 \times (P_{200} PI) + 11}{6.895} \; psi \tag{6.4}$$

$$\frac{b_f}{c_f} = -2.313 \times (P_{200} PI)^{0.14} + 5 \tag{6.5}$$

$$c_f = 0.0514 \times (P_{200} PI)^{0.465} + 0.5 \tag{6.6}$$

$$\frac{h_r}{a_f} = 32.44 \times e^{0.0186(P_{200} PI)} \tag{6.7}$$

For cohesionless soils:

$$a_f = \frac{0.8627 \times (D_{60})^{-0.751}}{6.895} \; psi \tag{6.8}$$

$$b_f = 7.5 \tag{6.9}$$

$$c_f = 0.1772 \times \ln(D_{60}) + 0.7734 \tag{6.10}$$

$$\frac{h_r}{a_f} = \frac{1}{D_{60} + 9.7 \times e^{-4}} \tag{6.11}$$

The SWCCs obtained for the base, subbase and subgrade materials at the ERC using the Fredlund and Xing equations and correlations between model parameters and soil index properties are presented in Figures 6.6 through 6.8.

If the SWCC is known, the relative hydraulic conductivity can be calculated using Equation 6.12, which was proposed by Fredlund and his coworkers (1994).

$$k_r(h) = \frac{\int_{\ln(h)}^{\ln(145000)} \frac{\theta(e^y) - \theta(h)}{e^y} \theta'(e^y) dy}{\int_{\ln(a_f)}^{\ln(145000)} \frac{\theta(e^y) - \theta_{sat}}{e^y} \theta'(e^y) dy} \tag{6.12}$$

Where:

$k_r(h)$ = relative coefficient of hydraulic conductivity;

Using Equation 6.12, relationships between metric suction and relative hydraulic conductivity for base, subbase and subgrade materials were calculated and are presented in Figures 6.9 through 6.11.

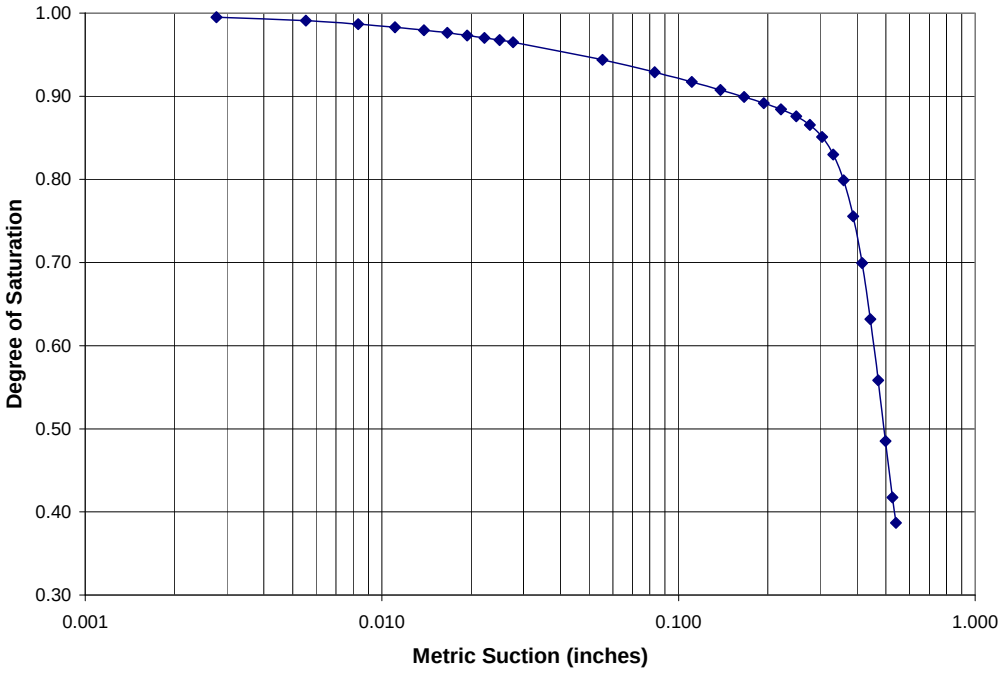

Figure 6.6 Soil water characteristic curve based on Fredlund and Xing's equations for the base material at the ERC.

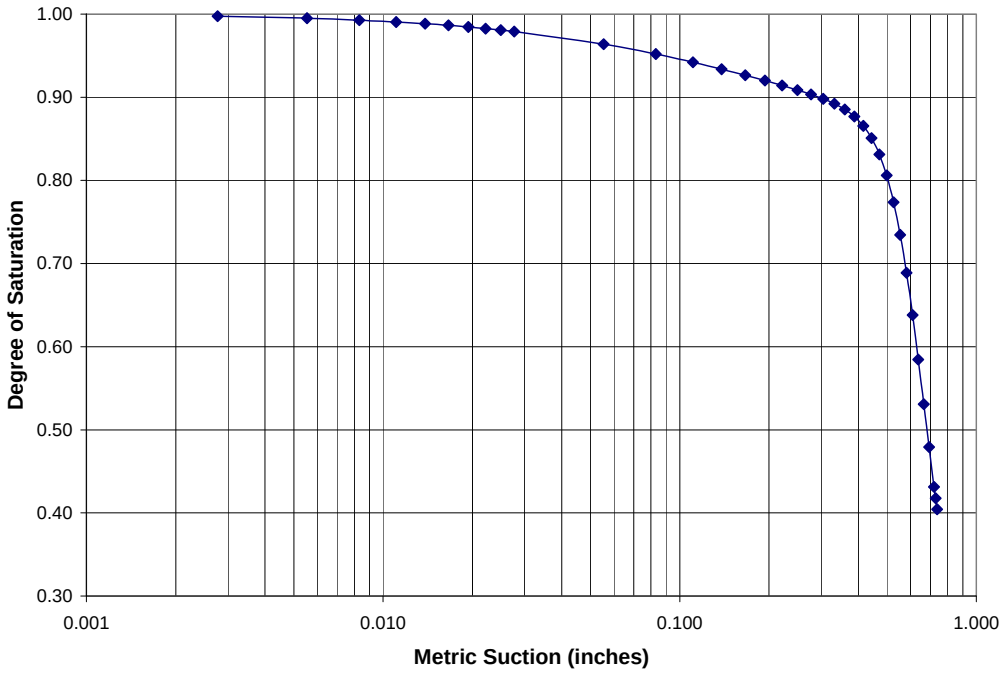

Figure 6.7 Soil water characteristic curve based on Fredlund and Xing's equations for the subbase material at the ERC.

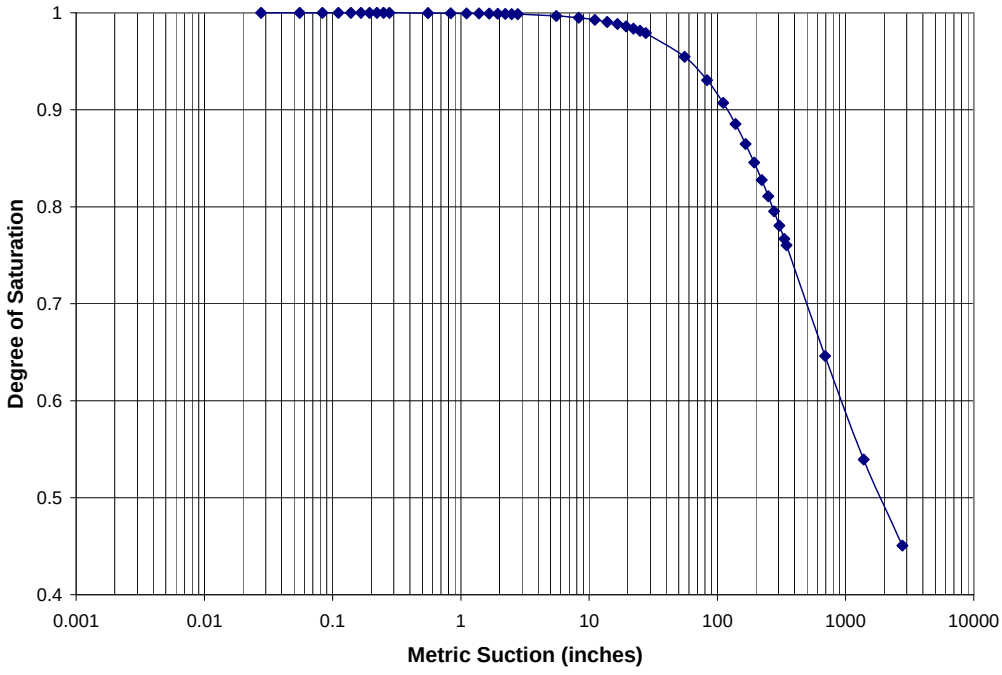

Figure 6.8 Soil water characteristic curve based on Fredlund and Xing's equations for the subgrade soil at the ERC.

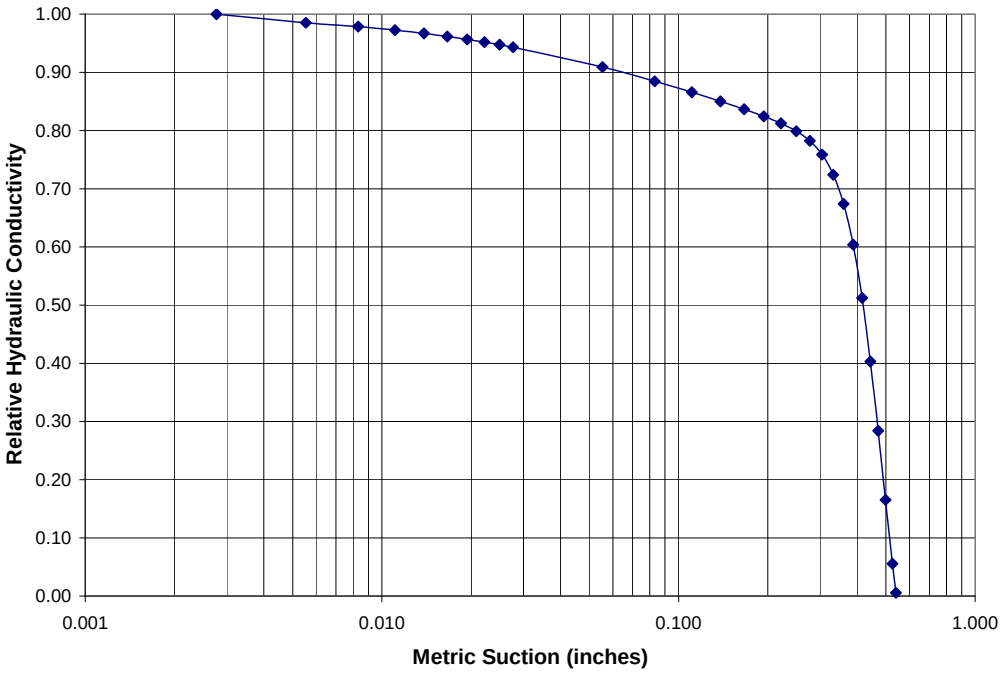

Figure 6.9 Metric suction versus relative hydraulic conductivity for the base material at the ERC.

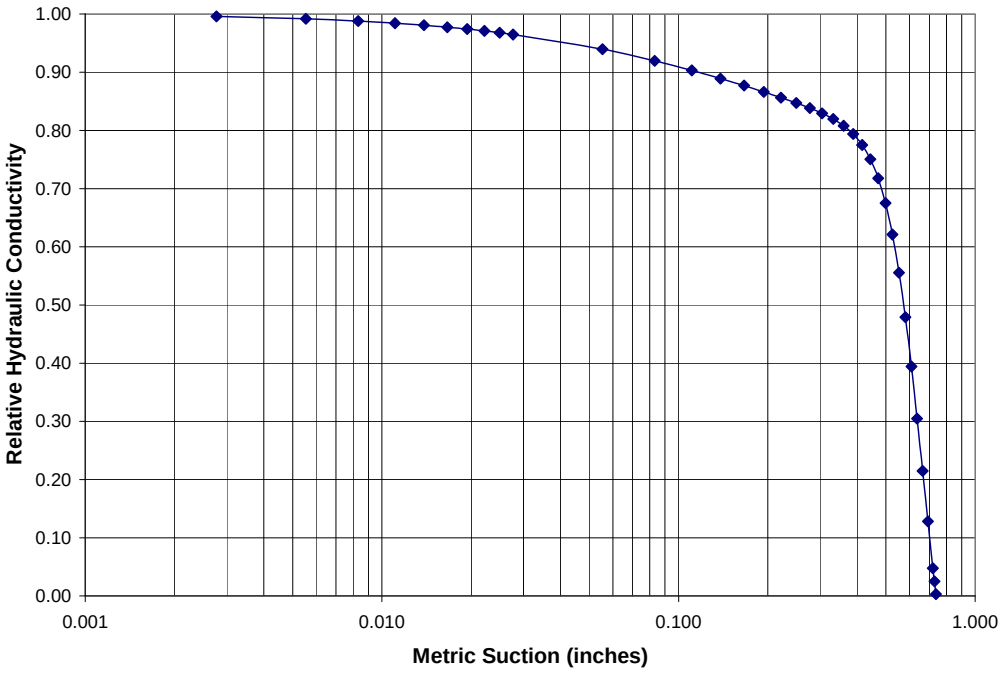

Figure 6.10 Metric suction versus relative hydraulic conductivity for the subbase material at the ERC.

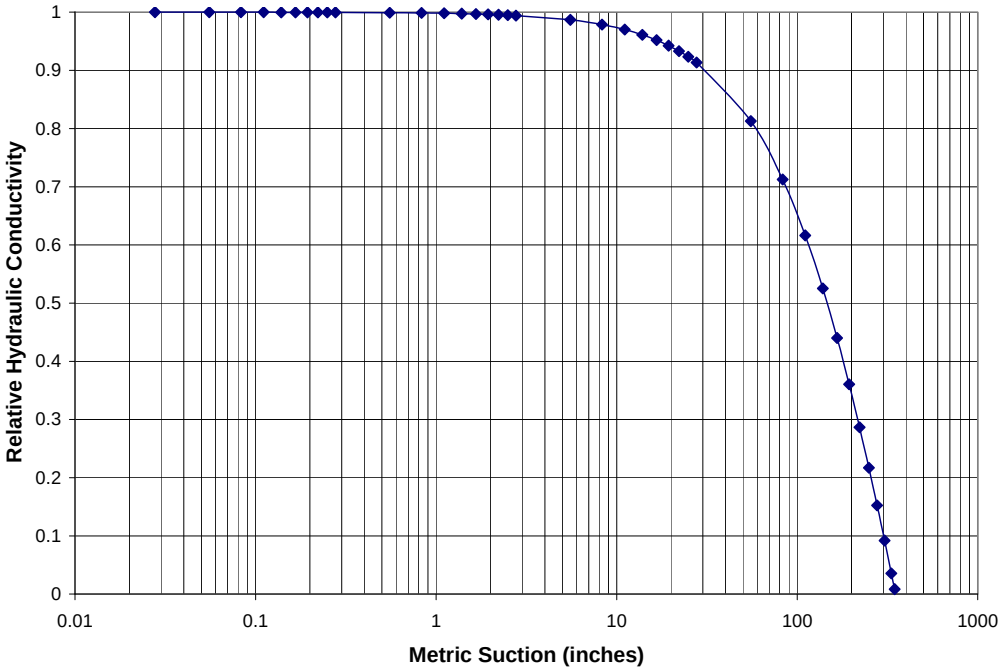

Figure 6.11 Metric suction versus relative hydraulic conductivity for the subgrade soil at the ERC.

6.3.4 Model Calibration

The SWCCs for the pavement materials and the underlying subgrade soil were not actually measured. Fredlund and Xing equations had to be used to obtain the SWCCs for these materials. Because of possible micro- and macro-structure that may develop in the pavement during and after construction, the SWCCs obtained using Fredlund and Xing equations may not truly describe the actual relationship between soil suction and moisture content. In addition, laboratory- and field-measured asphalt hydraulic conductivity change dramatically with location with values ranging from 0 to about 1×10^{-3} cm/s. Because of the uncertainty of these properties, the model was calibrated by changing the SWCCs of the pavement materials and the underlying subgrade soil and hydraulic conductivity of the asphalt layer. The goal of the model calibration was to match predicted degrees of saturation with measured degrees of saturations at the same location.

The SWCC describes the relationship between soil suction and moisture content and hydraulic conductivity is a measure of the capability of a medium to transmit water. By the definition the initial moisture contents in the pavement system before a precipitation event are controlled predominately by the SWCCs of the pavement materials and the underlying subgrade soil and the location of the ground water table. The hydraulic conductivity of the asphalt layer will only affect moisture contents in the pavement system after the precipitation event begins. So the model calibration was performed in two steps. The first step was to match predicted initial moisture contents in the pavement before a precipitation event with the measured initial moisture contents at the same locations. This was accomplished by changing the SWCCs of the pavement materials and underlying subgrade soil. In the second step predicted moisture content changes during a precipitation event are matched to the measured moisture content changes during changing the asphalt hydraulic conductivity within its measured range.

6.3.4.1 Calibration on the SWCCs

The measured degrees of saturation at the moisture probe locations before the precipitation event are presented in Figure 6.12.

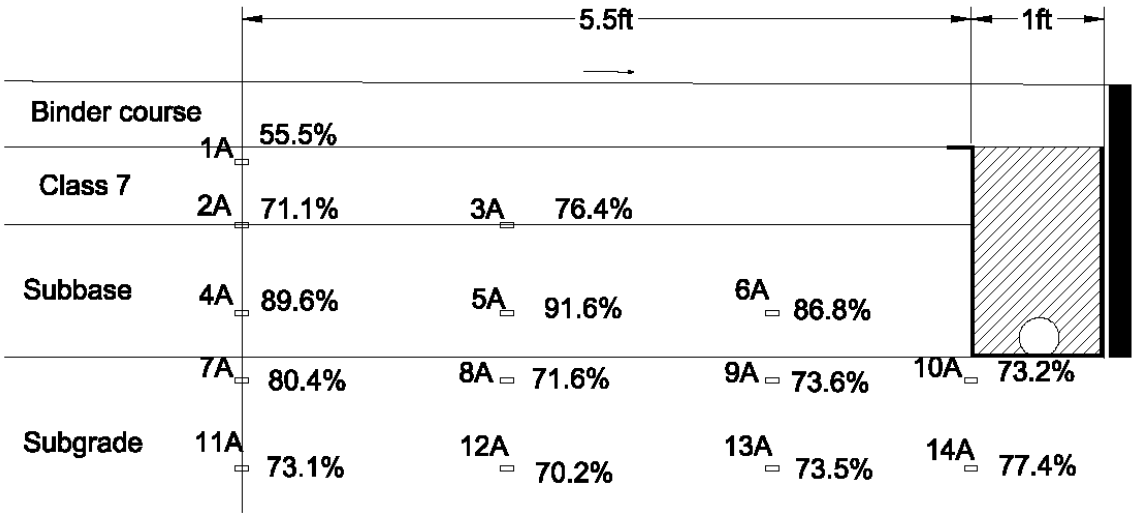

Figure 6.12 Measured initial degrees of saturation before the precipitation event.

The SWCCs created using the Fredlund and Xing equations were used as the initial SWCCs in the analysis. The predicted initial degrees of saturation at the probe locations resulting from this analysis are presented in Figure 6.13. By comparing the predicted initial degrees of saturation shown in Figure 6.13 with the measured initial degrees of saturation shown in Figure 6.12, it can be seen that the predicted degrees of saturation in the base and subbase materials are as much as 42 percent lower than the measured values. On the other hand, the predicted degrees of saturation in the subgrade soil are as much as 27 percent higher than measured values.

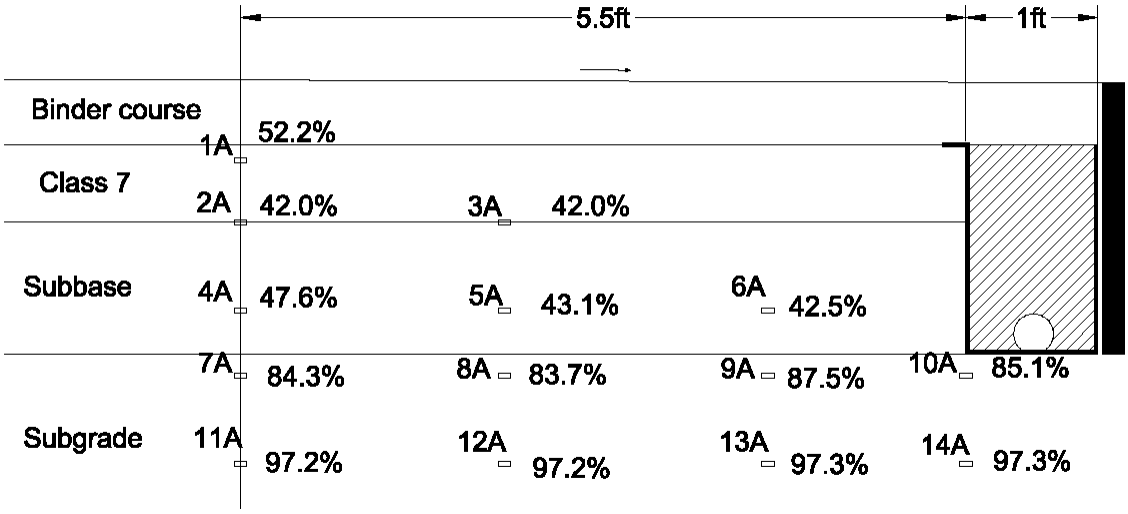

Figure 6.13 Predicted degrees of saturation before the precipitation event using Fredlund and Xing SWCCs.

To adjust the predicted initial degrees of saturation in the base and subbase materials so that they more closely matched the measured values, the SWCCs for these materials were shifted laterally toward the right as shown in Figures 6.5 and 6.6. By doing so, the soil suction was increased for the same degree of saturation. At same time the SWCC for the subgrade soil was shifted laterally toward the left, as shown in Figure 6.7, to decrease predicted degrees of saturation in the subgrade soil. By doing so, the soil suction was decreased for the same degree of saturation. After several trials, the modified Fredlund and Xing SWCCs shown in Figures 6.14 through 6.16 were developed which seemed to give a best agreement between measured and predicted initial degrees of saturation. Predicted initial degrees of saturation using these modified SWCCs are shown in Figure 6.17. By comparing Figure 6.17 with Figure 6.12, it can be seen that predicted initial degrees of saturations are generally within 15 percent of measured degrees of saturation in the base and subbase materials, and generally within 5 percent of measured degrees of saturation in the subgrade soil. Because engineering properties of aggregate

base and subbase materials are less sensitive to moisture content than fine-grained subgrade soils, it is reasonable to say that differences of up to 15 percent between measured and predicted degrees of saturation in the base and subbase materials are acceptable. Therefore, the modified Fredlund and Xing SWCCs as shown in Figures 6.14 through 6.16 were used in the FEM analysis.

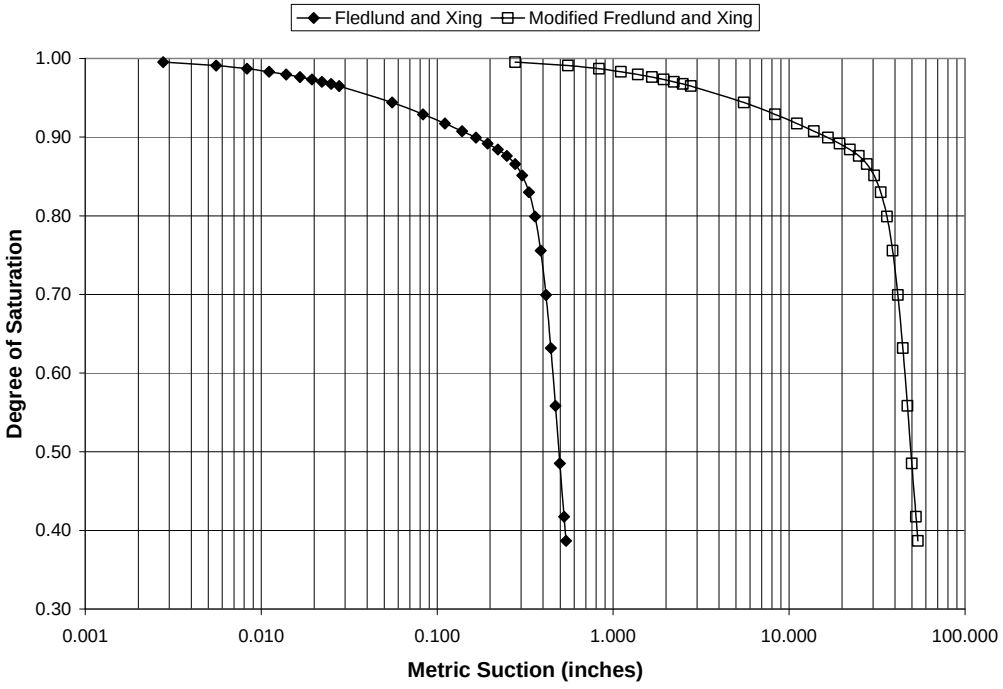

Figure 6.14 Comparison of Fredlund and Xing SWCC and modified Fredlund and Xing SWCC for the base material at the ERC.

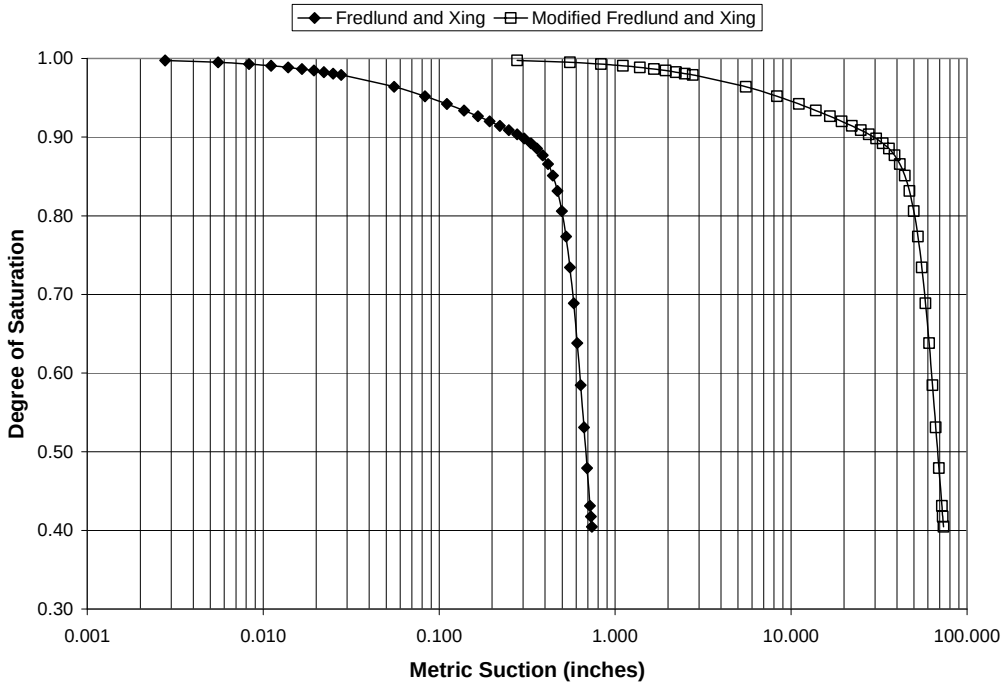

Figure 6.15 Comparison of Fredlund and Xing SWCC and modified Fredlund and Xing SWCC for the subbase material at the ERC.

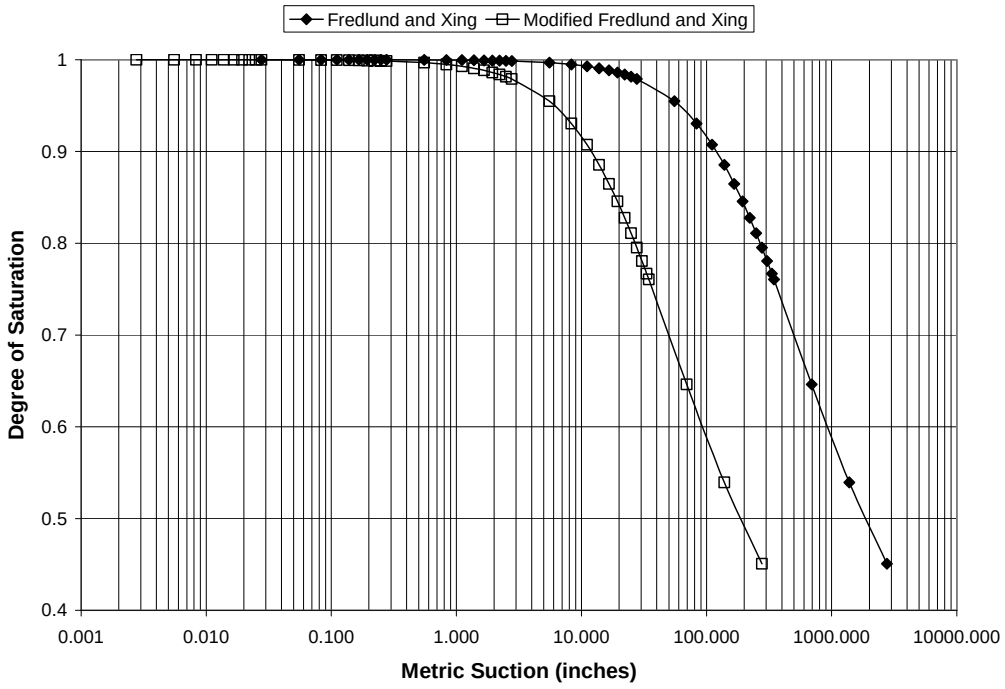

Figure 6.16 Comparison of Fredlund and Xing SWCC and modified Fredlund and Xing SWCC for the subgrade soil at the ERC.

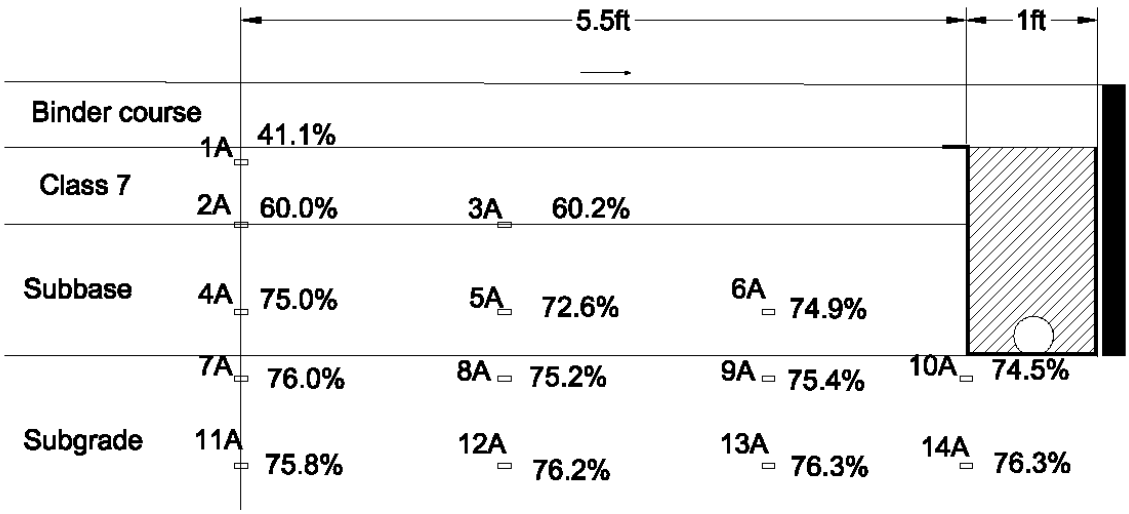

Figure 6.17 Predicted degrees of saturation before the precipitation event using modified Fredlund and Xing SWCCs.

6.3.4.2 Calibration of Asphalt Hydraulic Conductivity

Using the modified SWCCs of the pavement materials and the underlying subgrade soil, the second step of the calibration was performed by changing the asphalt hydraulic conductivity. After multiple trials, a relatively close match was realized between measured and predicted degrees of saturation during the precipitation event by using an asphalt hydraulic conductivity value of 2.1×10^{-5} cm/s. Predicted degrees of saturation at the moisture probe locations were plotted during the 24-hour analysis period in Figures 6.18 through 6.21. For comparison, measured degrees of saturation at the same locations were also plotted in Figures 6.18 through 6.21.

From Figures 6.18 and 6.19, it can be seen that the predicted changes in degrees of saturation in the upper 2 inches of the base material are smaller than measured values. However, predicted changes at deeper depths in the base and subbase materials are larger than measured values. These discrepancies between predicted and measured degrees of saturation may be the result of possible channels at the interface between the asphalt and

base layers. These might also be caused by micro- or macro-structures in the pavement materials developed during and after construction. From Figures 6.18 and 6.19, however, it is obvious that significant changes in both measured and predicted degrees of saturation in the base and subbase materials occurred around 600 minutes. This indicates that an asphalt hydraulic conductivity of 2.1×10^{-5} cm/s is a reasonable value for use in the FEM analysis.

From Figures 6.20 and 6.21, it can be seen that measured and predicted degrees of saturation in the subgrade soil generally have a pretty good agreement. Maximum differences between measured and predicted degrees of saturation are generally within approximately 8 percent. Predicted degrees of saturation are relatively constant independent of the precipitation event. However, one can see that measured degrees of saturation at locations near the edge drain (Probes 10 and 14) increased by as much as 7.5 percent during the precipitation event. This might be caused by micro- or macro-structure developed around the edge drain.

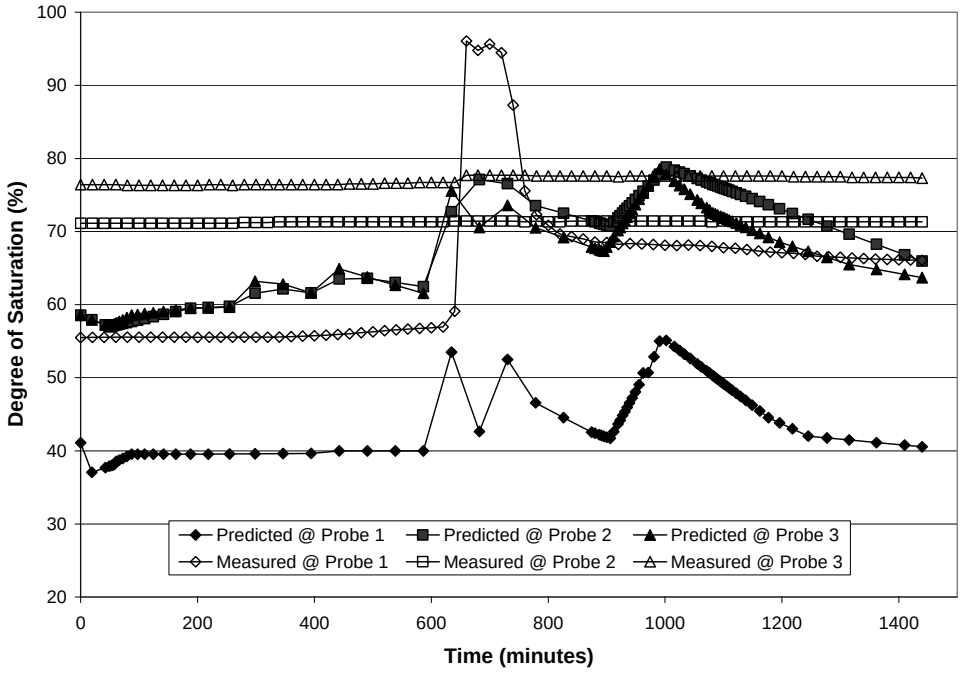

Figure 6.18 Comparison of measured and predicted degrees of saturation at a depth of 2 inches below the base surface (Probe 1) and at the interface of the base and subbase layers (Probes 2 and 3) following a precipitation event.

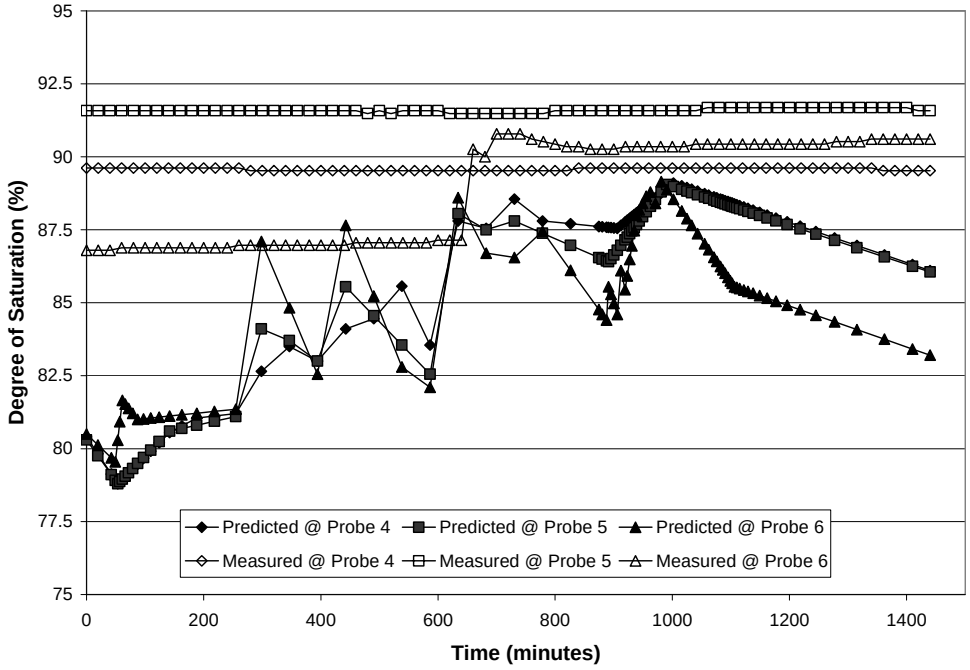

Figure 6.19 Comparison of measured and predicted degrees of saturation at a depth of 10 inches below the subbase surface in the subbase material following a precipitation event.

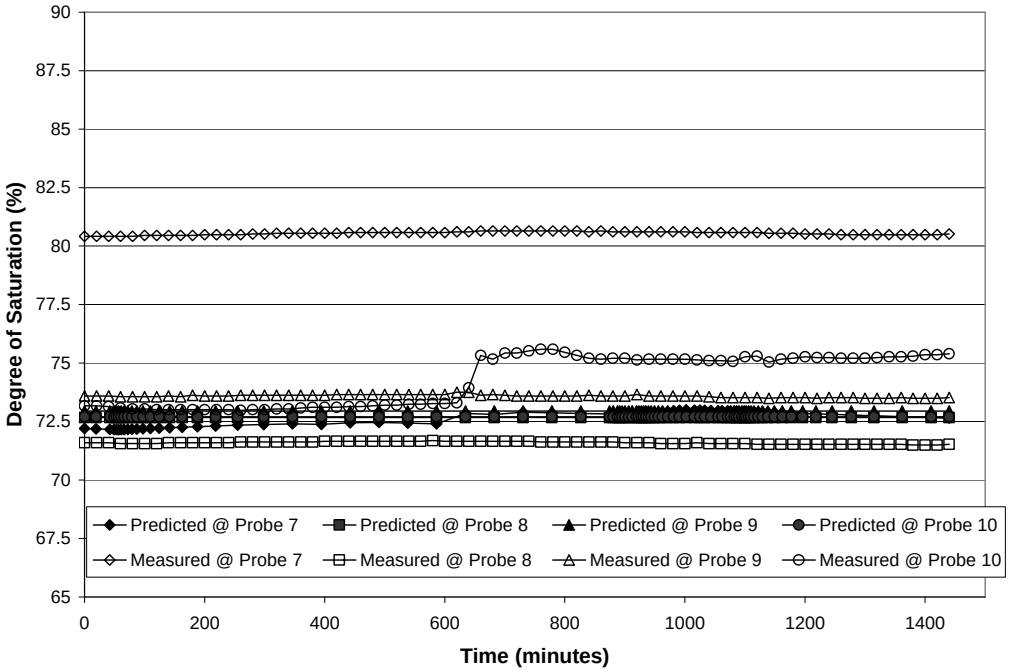

Figure 6.20 Comparison of measured and predicted degrees of saturation at a depth of 2 inches below the subgrade surface following a precipitation event.

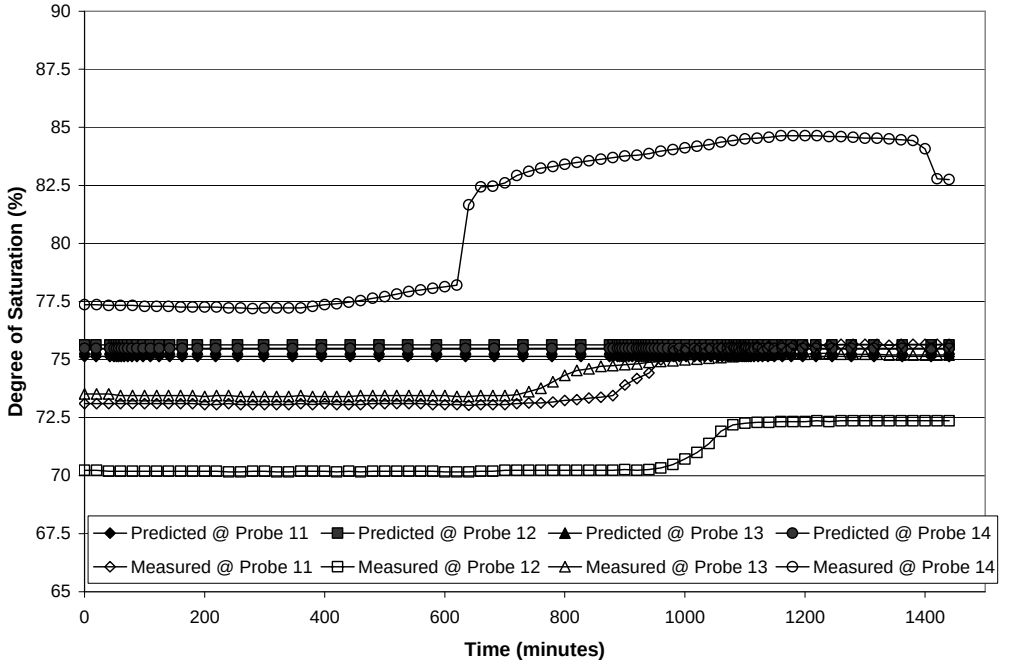

Figure 6.21 Comparison of measured and predicted degrees of saturation at a depth of 10 inches below the subgrade surface following a precipitation event.

As discussed earlier, possible channels might have developed at the interface between the asphalt and base layers. In addition, micro- or macro-structures in the pavement materials might have developed during and after construction. In an effort to model these conditions and to get a better model calibration, hydraulic conductivity of the upper two inches of the base material was increased to account for possible channels at the interface between the asphalt and base layers. Also hydraulic conductivities of the lower portion of base and subbase materials were decreased to account for possible intrusion of fines or some level of anisotropy developing in the base materials. By decreasing the hydraulic conductivity of the lower portion of the base and subbase materials and at the same time increasing the hydraulic conductivity of the upper 2 inches of the base material, changes in predicted degrees of saturation in the upper 2 inches of the base materials would increase, while changes in predicted degrees of saturation in the lower portion of base and subbase materials would decrease. After multiple trials, a better agreement between predicted and measured degrees of saturation was realized by using hydraulic conductivity of 1 cm/s for the upper 2 inches of the base, 1.3×10^{-4} cm/s for the lower portion of the base material, and 3.1×10^{-6} cm/s for the subbase material. Predicted and measured degrees of saturation are presented in Figures 6.22 through 6.25.

From Figures 6.22 through 6.25, one can see that a better agreement was realized. Only predicted degrees of saturation at a depth of 2 inches below the base surface have significant changes, which generally matches the pattern of changes in measured degrees of saturation. From Figure 6.25, it can also be seen that predicted degrees of saturation at a depth of 10 inches below the subgrade surface remain almost constant during the precipitation event, while, measured degrees of saturation at the same layer had

noticeable increases during the same precipitation. As discussed in Chapter 4, these increases in measured degrees of saturation might be the results of water migration through micro- or macro-structures developed in the subgrade soils from the side of the pavement.

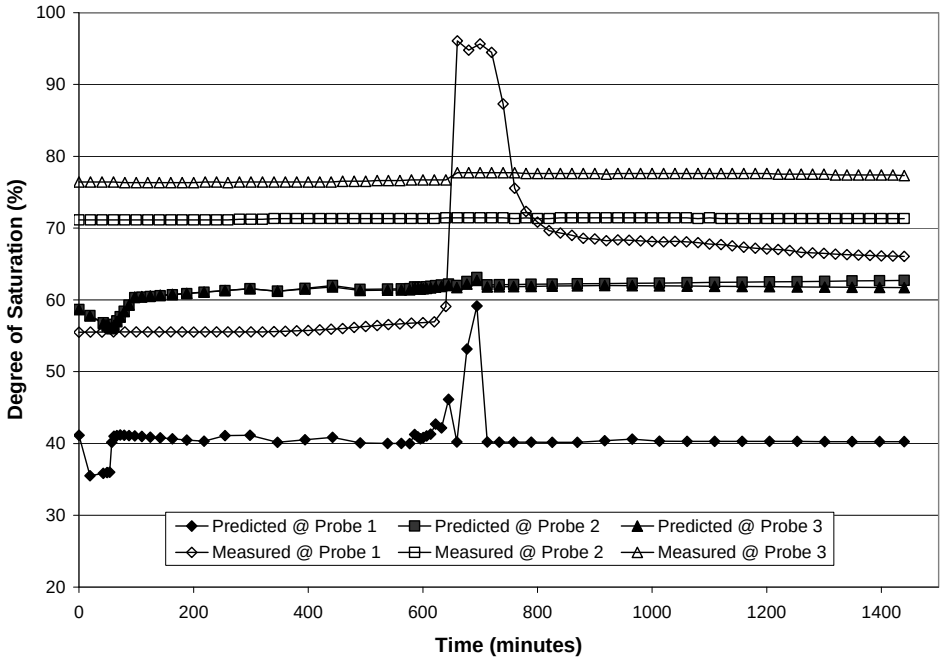

Figure 6.22 Comparison of measured and predicted degrees of saturation at a depth of 2 inches below the base surface and at the interface of the base and subbase layers using modified hydraulic conductivity values following a precipitation event.

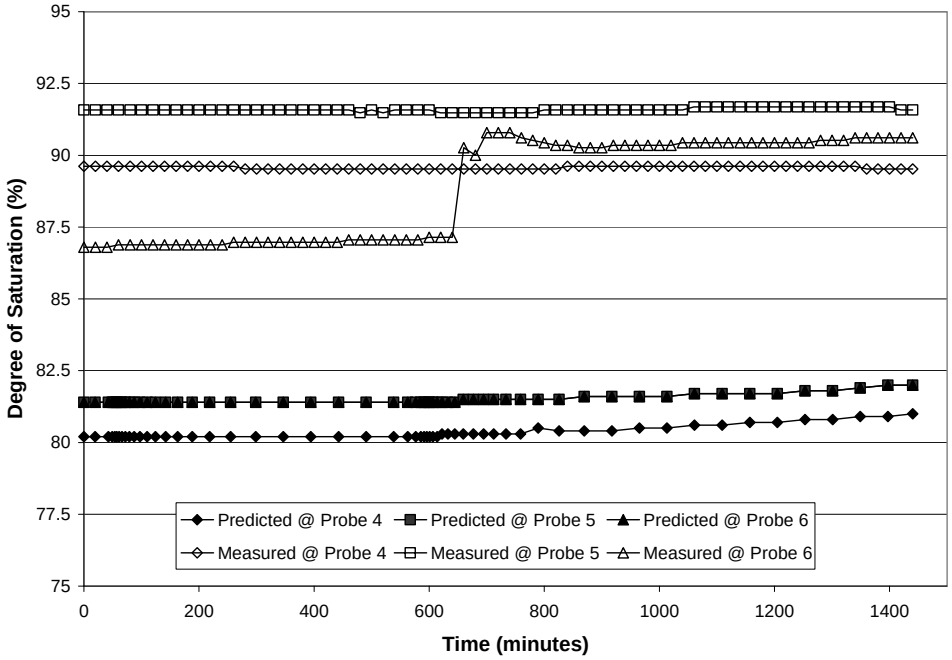

Figure 6.23 Comparison of measured and predicted degrees of saturation at a depth of 10 inches below the subbase surface using modified hydraulic conductivity values following a precipitation event.

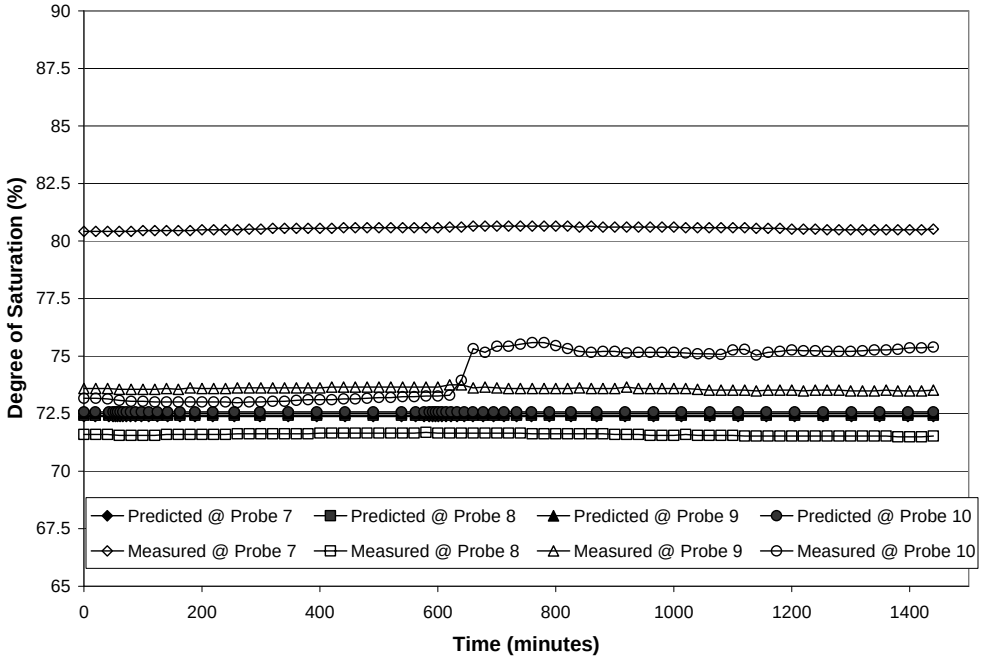

Figure 6.24 Comparison of measured and predicted degrees of saturation at a depth of 2 inches below the subgrade surface using modified hydraulic conductivity values following a precipitation event.

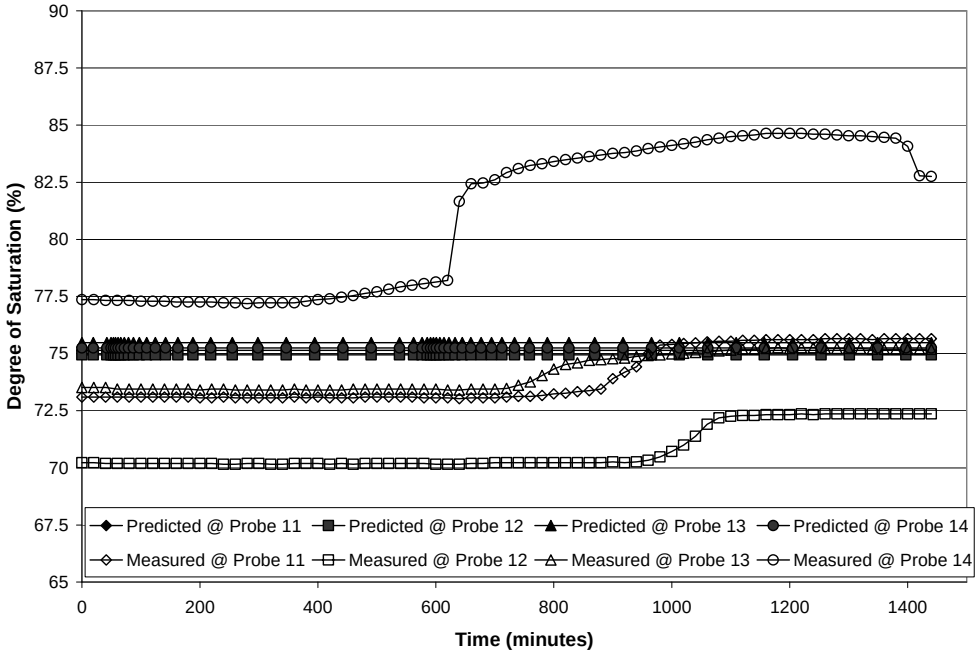

Figure 6.25 Comparison of measured and predicted degrees of saturation at a depth of 10 inches below the subgrade surface using modified hydraulic conductivity values following a precipitation event.

6.4 Results of the FEM

Using the modified SWCCs given in Figures 6.14 through 6.16 and modified hydraulic conductivities for the pavement materials as discussed in the previous section, the finite element analysis was performed. Flow fields in the pavement system at different time steps are presented in Figures 6.26 through 6.32. From these figures, it can be seen that water generally migrates through the asphalt layer vertically and then moves through the upper 2 inches of the base material laterally to the edge drain. The length of the flow vectors in these figures is an indicator of the relative magnitude of flow. Longer arrows represent greater velocity. The flow regime predicted by the FEM analysis is in general agreement with the flow pattern that was indicated by changes in moisture content in Chapter 4. Therefore, it can be concluded that the FEM analysis can be used to

simulate the water migration pattern through pavements with reasonably good accuracy when well calibrated.

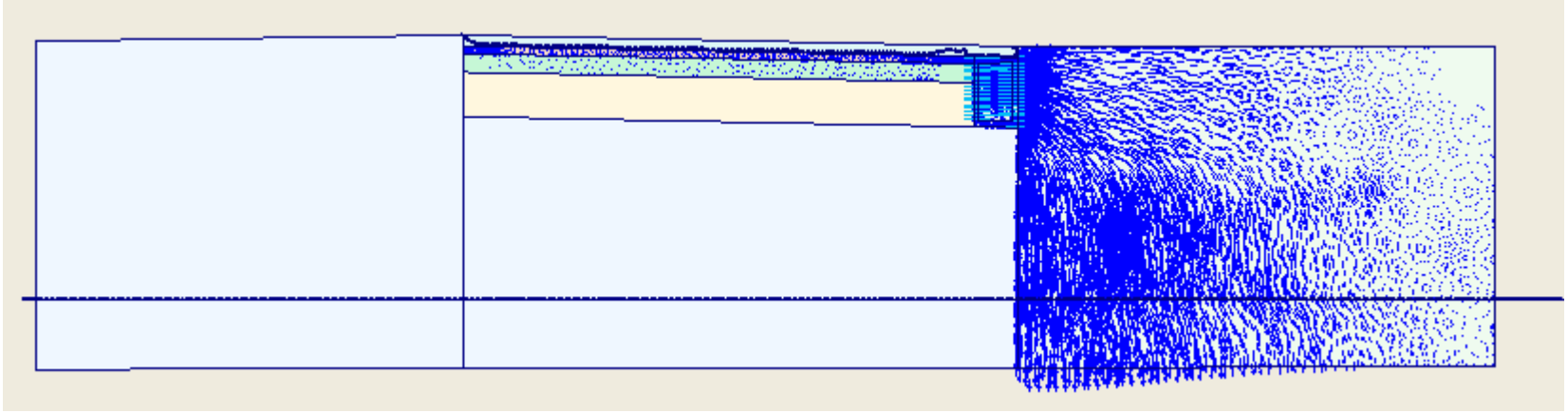

Figure 6.26 Flow field at 71.75 minutes after the precipitation occurred, extreme velocity 18.84×10^{-3} in/min.

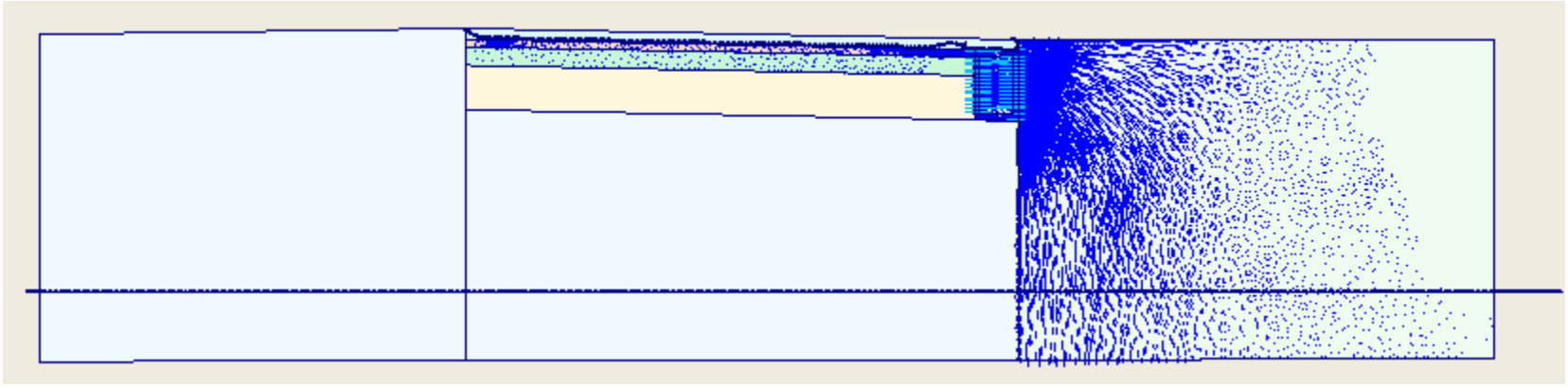

Figure 6.27 Flow field at 141.8 minutes after the precipitation occurred, extreme velocity 9.23×10^{-3} in/min.

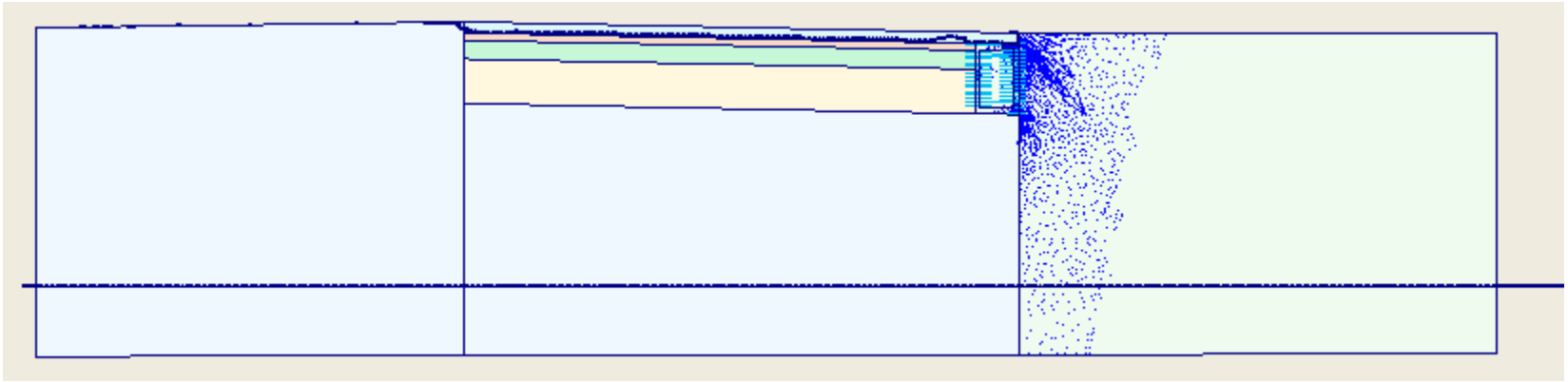

Figure 6.28 Flow field at 298.4 minutes after the precipitation occurred, extreme velocity 5.57 in/min.

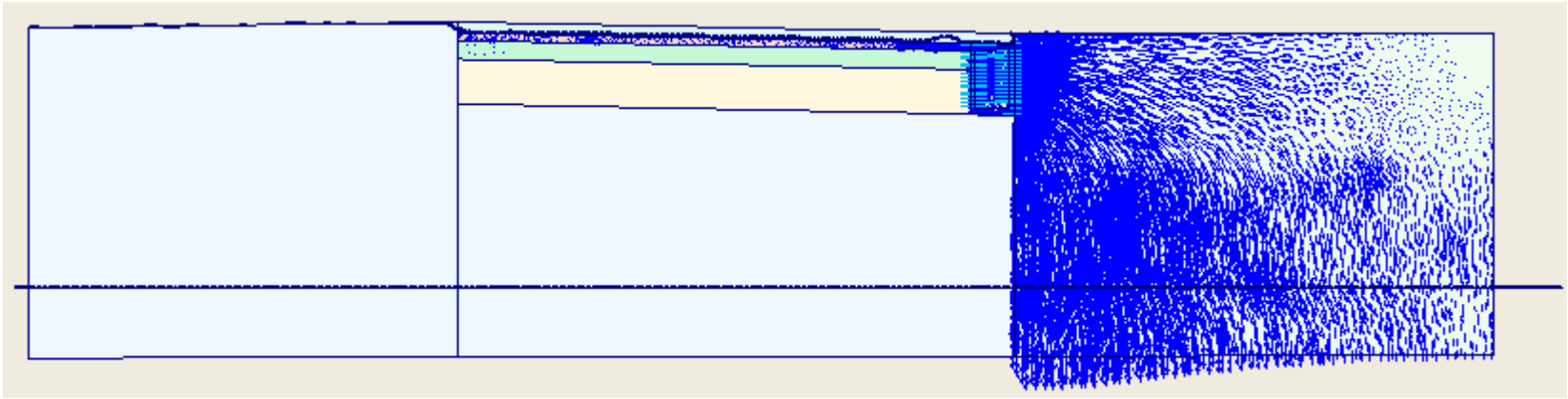

Figure 6.29 Flow field at 394.4 minutes after the precipitation occurred, extreme velocity 9.37×10^{-3} in/min.

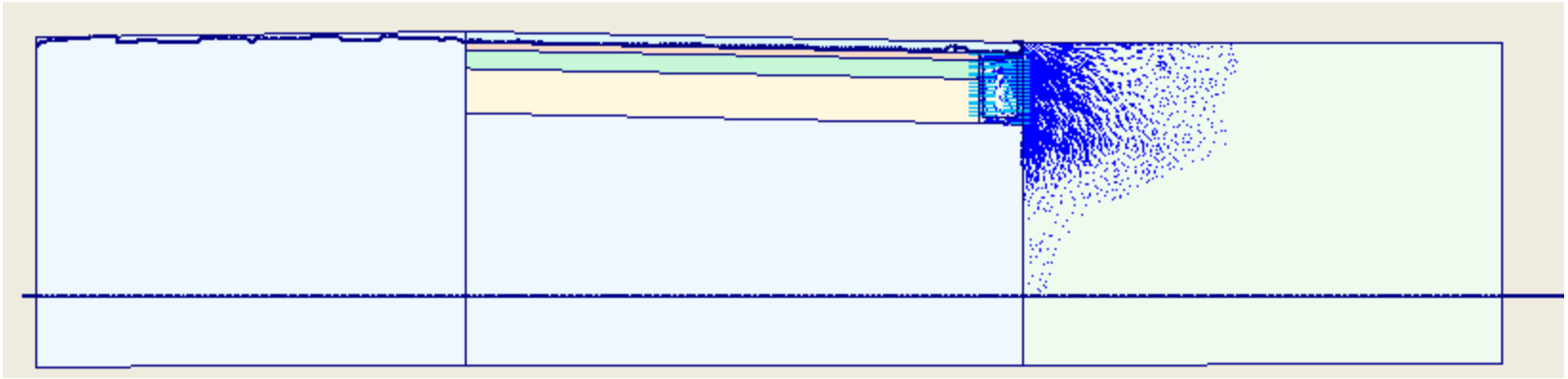

Figure 6.30 Flow field at 591.2 minutes after the precipitation occurred, extreme velocity 1.34 in/min.

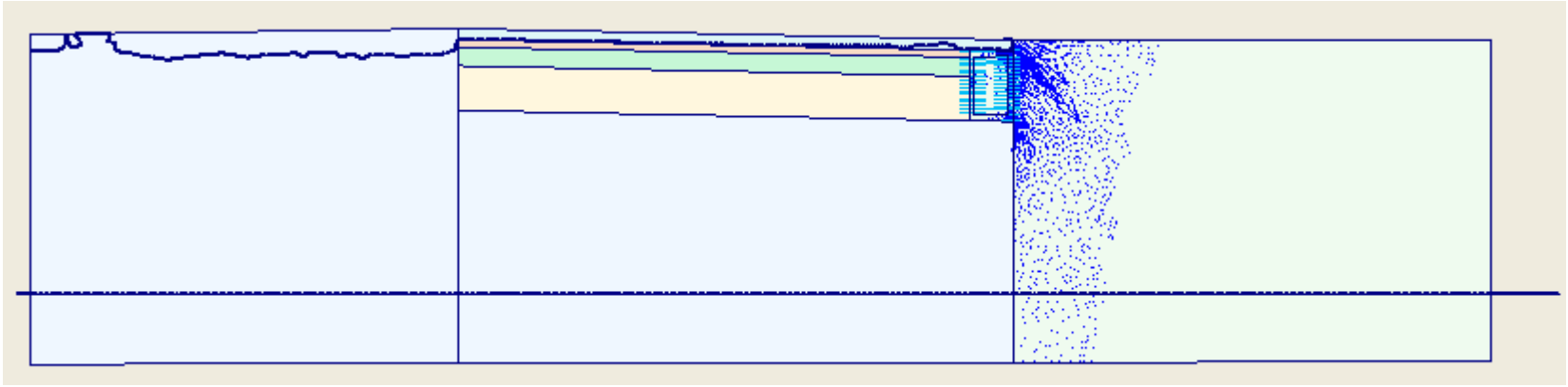

Figure 6.31 Flow field at 965.4 minutes after the precipitation occurred, extreme velocity 5.60 in/min.

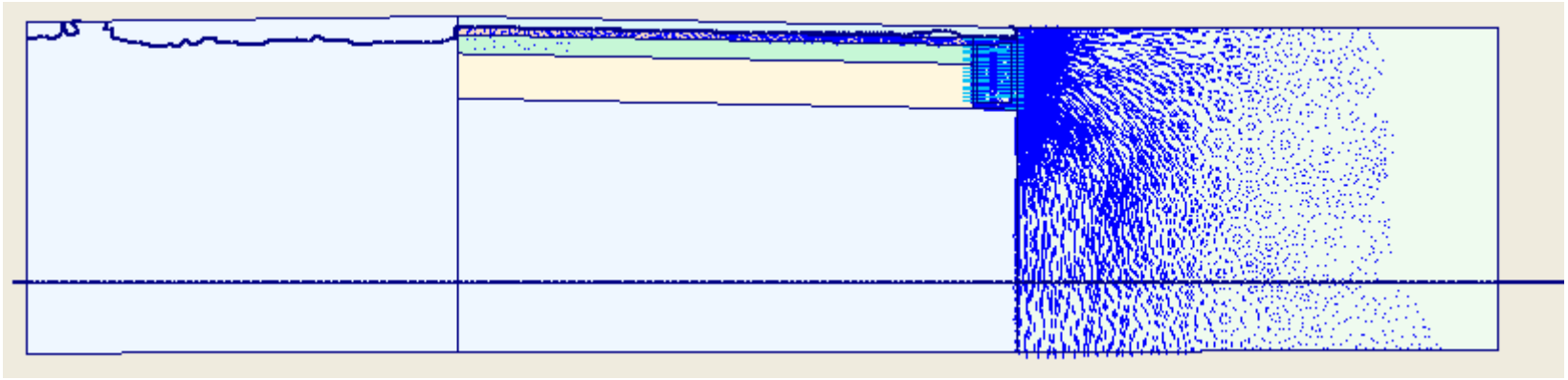

Figure 6.32 Flow field at 1440 minutes after the precipitation occurred, extreme velocity 8.72×10^{-3} in/min.

6.5 Discussion and Conclusions

Based on the calibration of the FEM model and the results of the FEM analysis, the following conclusions can be drawn.

- SWCCs created using Fredlund and Xing equations might have good agreement with laboratory-measured SWCCs. However, in-situ SWCCs might be far different from the SWCCs developed using Fredlund and Xing equations. This is likely due to micro- or macro- structures in soils creating anisotropy, which can not be accounted for in laboratory and Fredlund and Xing equations.
- For the same reason, laboratory-measured hydraulic conductivity of the pavement materials could be significantly different from in-site hydraulic conductivity.
- Laboratory- and field-measured asphalt hydraulic conductivity could change dramatically with location. Based on the calibration of the FEM model an asphalt hydraulic conductivity value of 2.1×10^{-5} cm/s is a reasonable for the asphalt layer of test pad A at the ERC.
- The finite element method appears to be able to predict general trends of moisture migration through the pavement system with good accuracy when well calibrated.

Chapter 7 Conclusions and Recommendations

7.1 Conclusions

A comprehensive literature review was conducted before constructing two test pads at the ERC of the University of Arkansas and developing one field test site in Fort Smith. A comprehensive laboratory testing program was performed to obtain engineering properties of the pavement materials and underlying soils at the ERC and Fort Smith test sites. A comprehensive monitoring and measuring program was also conducted at the ERC and Fort Smith sites to investigate the responses of the pavement systems to various environmental factors. Based on measured data, a water migration pattern through the pavement systems was developed, this pattern was partially validated with a transient FEM seepage model. Additionally, the EICM was evaluated by comparing predicted data with the measured data. Through this research, the following conclusions were drawn.

Material Properties of Pavements

- The hydraulic conductivity of the hot mix asphalt concrete (HMAC) measured with a specific device varies with sample location. Based on the results of field and laboratory tests on the HMAC at the test pads at the ERC, the hydraulic conductivity of the HMAC could vary from near 0 to about 1×10^{-3} cm/s when the test location changed.
- When comparing the results of field hydraulic conductivity tests and laboratory tests, it appears that the results of long-term (at least 2 or 3 days) field testing were in closer agreement to laboratory measured results than the results obtained from short-term (less than 1 hour) field testing. In general, the short term field

tests reported hydraulic conductivities that were at least an order of magnitude higher than the long term field and laboratory tests.

- According to the future AASHTO design guide (2004), SWCCs created using Fredlund and Xing equations might have good agreement with laboratory-measured SWCCs. However, the results of the FEM analyses suggest that in-situ SWCCs might be far different from the SWCCs developed using Fredlund and Xing equations. This is likely due to micro- or macro- structures in soils creating anisotropy, which can not be accounted for in laboratory and Fredlund and Xing equations.
- The results of the FEM analyses suggest that laboratory-measured hydraulic conductivity of the pavement materials could be significantly different from on-site hydraulic conductivity.
- Based on the calibration of the FEM model an asphalt hydraulic conductivity value of 2.1×10^{-5} cm/s is a reasonable for the asphalt layer of test pad A at the ERC.

Moisture Content Changes in Pavements

- Changes in groundwater levels seem to follow seasonal trends. Groundwater levels and moisture contents at the ERC test location had high peak values in summers and low peak values in winters.
- Based on measured responses of moisture to precipitation events in the base materials, moisture migrated much faster in the horizontal direction than in the

vertical direction. The moisture migration pattern appeared to include only the extreme upper region of the base material.

- Only moisture contents of base materials at the shallowest depth (2 inches below the base surface) responded significantly to precipitation events. Moisture content changes in the base materials at deeper depths (deeper than 2 inches) changed according to season not in response to individual precipitation events.
- Precipitation at both sites had almost no effect on the moisture content in subgrade soils, except for those areas in close proximity to the edge drains. The moisture content in subgrade soils changed with season independent of precipitation events.
- After a precipitation event, some portion of water that migrated into pavement systems would remain in pavement systems for a relatively long period because base materials were not free-draining materials.
- Using the storage model and measured runoff a water balance was generally achieved for test pad A at the ERC.
- Frost depths in the Northwest Arkansas area and River Valley area were less than 1 foot measured from pavement surfaces during the period of this study.
- Degrees of saturation in the base and subbase materials at the ERC and Ft. Smith test sites generally increased with depth from approximately 55 percent to near 100 percent. Degrees of saturation in the subgrade soils at the ERC and the Ft. Smith test site changed with seasons and can be predicted using the predicative models developed in this study. A single prediction model could be used for both sites.

- Resilient modulus of the A-6 subgrade soils encountered at the ERC and the Ft. Smith test site changed with seasons and could be described with periodic functions developed in this study. Predicted values ranged from 18 ksi during winters and values of 3 to 6 ksi during summers. A single model could not be used to predict modulus for both sites.

Evaluation of the EICM and FEM Analyses

- Air temperature obtained from nearby NOAA weather stations in this study (less than 5 miles from the sites) can be used in the EICM with adequate accuracy (less than 11 percent effect on predicted asphalt modulus).
- Air temperatures from a weather station located 50 miles from the test site could not be used reliably in the EICM to predict asphalt temperatures. The asphalt modulus could be off by as much as 30 percent by using the distant weather station data.
- The EICM predicted temperatures in the pavement pretty well during the winter, spring and fall at the test site in Fort Smith, Arkansas. However, a relatively large discrepancy between measured and predicted soil temperature was observed in the summer.
- The EICM did not predict moisture content well in the base and subbase materials at either site. The EICM generally under-predicted moisture content in the base and subbase materials by as much as 100 percent.
- The EICM did not predict seasonal changes in moisture content in the subgrade soils at either site. Based on field measurements the EICM under-predicted

moisture contents in the summer by as much as 50 percent. While, in the winter, the EICM over-predicted moisture contents by as much as 50 percent. It appears that the EICM prediction on moisture content got better with depth.

- The finite element method appears to be able to predict general trends of moisture migration through the pavement system with good accuracy when well calibrated.

7.2 Recommendations

- More test sites and monitoring and measuring programs should be conducted in other areas of Arkansas to either verify the observations and conclusions obtained in this study.
- Additional environmental factors, such as wind speed, percent sunshine and humidity that are included in the EICM should be measured at test sites for a better evaluation of the EICM in Arkansas.
- Asphalt temperature should be measured because temperature is more critical to asphalt engineering properties than those of unbound base and subgrade materials.
- A better flow measurement device that is suitable for uncontrolled field conditions should be developed and used for future measurements of runoff and subsurface drainage.
- Consideration should be given to conduct tests on two identical test sites except that one test site has an edge drain and the other one does not. This would result in a better understanding of effectiveness of edge drains.

Bibliography

Siddiqui, S. I., Drnevich, V. P., and Deschamps, R. J., "Time Domain Reflectometry Development for Use in Geotechnical Engineering," Geotechnical Testing Journal, GTJODJ, Vol. 23, No. 1, March 2000, pp. 9-20

Benson, C. H. and Bosscher, P. J., "Time-Domain Reflectometry (TDR) in Geotechnics: A Review," Nondestructive and Automated Testing for Soil and Rock Properties, ASTM STP 1350, W. A. Marr and C. E. Fairhurst, Eds., American Society for Testing and Materials, West Conshohocken, PA, 1999

Jones, S. B., Wraith, J. M. and Or, D., "Time Domain Reflectometry Measurement Principles and Applications," Hydrological Processes, Vol. 16, 2000, pp.141-153

O'Connor, K. M., and Dowding, C. H., "GeoMeasurements by Pulsing TDR Cables and Probes," CRC Press LLC, 1999

Suwansawat, S., "Using Time Domain Reflectometry for Measuring Water Content in Compacted Clays," Master Thesis, University of Wisconsin-Madison, 1997

Dasberg S. and Hopmans, J. W., "Time Domain Reflectometry Calibration for Uniformly and Nonuniformly Wetted Sandy and Clayey Loam Soils," Soil Science Society of America Journal, Vol. 56, No. 5, 1992, pp. 1341-1345

Ferre, P. A., Rudolph, D. L. and Kachanoski, R. G., "Spatial Averaging of Water Content by Time Domain Reflectometry: Implications for Twin Rod Probes with and without Dielectric Coatings," Water Resources Research, Vol. 32, No. 2, February 1996, pp. 271-279

Roth, C. H., Malicki, M. A. and Plagge, R., "Empirical of the Relationship Between Soil Dielectric Constant and Volumetric Water Content as the Basis for Calibrating Soil Moisture Measurements by TDR," Journal of Soil Science, Vol. 43, No. 1, March 1992, pp. 1-13

Dowding, C. H. and Huang, F., "Early Detection of Rock Movement with Time Domain Reflectometry," Journal of Geotechnical Engineering, Vol. 120, No. 8, August 1994, pp. 1413-1427

Ledieu, J., Ridder, P. D., Clerck, P. D. and Dautrebande, S., "A Method of Measuring Soil Moisture by Time-Domain Reflectometry," Journal of Hydrology, Vol. 88, No. ¾, November 1986, pp. 319-328

Hilhorst, M.A. and Dirksen C., "Dielectric Water Content Sensors: Time Domian versus Frequency Domain," Symposium and Workshop on Time Domain Reflectometry in

Environmental, Infrastructure, and Mining Applications, Special Publication SP 19-94 Evanston, Illinois, September 7-9, 1994

Topp, G. C., Davis, J. L. and Annan, A. P., "Electromagnetic Determination of Soil Water Content: Measurements in Coaxial Transmission Lines," Water Resources Research, Vol. 16, No. 3, June 1980, pp. 574-582

Drungil, C. E. C., Abt, K. and Gish, T.J., "Soil Moisture Determination in Gravelly Soils with Time Domain Reflectometry," Transactions of the ASAE, Vol. 32(1), January-February 1989, pp. 177-180

Zegelin, S. J., White, I. and Jenkins, D. R., "Improved Field Probes for Soil Water Content and Electrical Conductivity Measurement Using Time Domain Reflectometry," Water Resources Research, Vol. 25, No. 11, November 1989, pp. 2367-2376

Selig, E. T. and Mansukhani, S., "Relationship of Soil Moisture to the Dielectric Property," Journal of the Geotechnical Engineering Division, August 1975, pp. 755-770

Dirksen, C. and Dasberg, S., "Improved Calibration of Time Domain Reflectometry Soil Water Content Measurements," Soil Science Society of America Journal, Vol. 57, May-June 1993, pp. 660-667

Andrews, J. R., "Time Domain Reflectometry," Symposium and Workshop on Time Domain Reflectometry in Environmental, Infrastructure, and Mining Applications, Special Publication SP 19-94 Evanston, Illinois, September 7-9, 1994, pp.4-13

Nissen, H. H. and Mϕldrup, P., "Theoretical Background for the TDR Methodology," Proceedings of the Symposium: Time-Domain Reflectometry Applications in Soil Science," Research Centre Foulum, September 16, 1994, pp. 9-23

Baran, E., "Use of Time Domain Reflectometry for Monitoring Moisture Changes in Crushed Rock Pavements," Symposium and Workshop on Time Domain Reflectometry in Environmental, Infrastructure, and Mining Applications, Special Publication SP 19-94 Evanston, Illinois, September 7-9, 1994, pp. 349-356

Aimone-Martin, C. T., Oravecz, K. I. and Nytra, T. K., "TDR Calibration for Quantifying Rock Mass Deformation at the WIPP Site, Carlsbad, New Mexico," Symposium and Workshop on Time Domain Reflectometry in Environmental, Infrastructure, and Mining Applications, Special Publication SP 19-94 Evanston, Illinois, September 7-9, 1994, pp.507-517

Dowding, C. H. and Pierce, C. E., "Measurement of Localized Failure Planes in Soil with Time Domain Reflectometry," Symposium and Workshop on Time Domain Reflectometry in Environmental, Infrastructure, and Mining Applications, Special Publication SP 19-94 Evanston, Illinois, September 7-9, 1994, pp. 569-578

Drumm, E. C., Reeves, J. S., Madgett, M. R. and Trolinger, W. D., "Subgrade Resilient Modulus Correction for Saturation Effects," Journal of Geotechnical and Geoenvironmenal Engineering, July 1997, pp. 663-670

Heydinger, A. G., "Evaluation of Seasonal Effects on Subgrade Soils," Transportation Research Record 1821, TRB, National Research Council, Washington, D. C., 2003, pp.47-55

Rainwater, N. R., Yoder, R. E., Drumm, E. C. and Wilson, G. V., "Comprehensive Monitoring Systems for Measuring Subgrade Moisture Condition," Journal of Transportation Engineering, Vol. 125, No. 5, September/October 1999, pp. 439-448

Elliott, R. P. and Thornton, S. I., "Simplification of Subgrade Resilient Modulus Testing," Transportation Research Record 1192, TRB, National Research Council, Washington, D. C., 1988, pp.1-7

Elliott, R. P. and Thornton, S. I., "Resilient Modulus and AASHTO Pavement Design," Transportation Research Record 1196, TRB, National Research Council, Washington, D. C., 1988, pp.116-124

http://cru.cahe.wsu.edu/CEPublications/pnw0475/pnw0475.html

George, B. H., "Comparison of Techniques for Measuring the Water Content of Soil and Other Porous Media," master thesis, University of Sydney, New South Wales, Australia, 1999

Florida Department of Transportation, "Florida Method of Test for Measurement of Water Permeability of Compacted Asphalt Paving Mixtures," September, 2000

ASTM D2216, "Standard Test Method for Laboratory Determination of Water (Moisture) Content of Soil and Rock by Mass," ASTM International

Cooley, L. A., and Brown, E. R., "Selection and Evaluation of Field Permeability Device for Asphalt Pavements," Transportation Research Record 1723, TRB, National Research Council, Washington, D. C., 2000, pp.73-82

Maupin, G. W., "Asphalt Permeability Testing in Virginia," Transportation Research Record 1723, TRB, National Research Council, Washington, D. C., 2000, pp.83-96

Prowell, B. D. and Dudley, M. C., "Evaluation of Measurement Techniques for Asphalt Pavement Density and Permeability," Transportation Research Record 1789, TRB, National Research Council, Washington, D. C., 2002, pp.36-44

Mallick, R. B., Cooley, L. A., Teto, M. and Bradbury, R., "Development of a Simple Test for Evaluation of In-Place Permeability of Asphalt Mixes," International Journal of Pavement Engineering, Vol. 2 (2), 2001, pp. 67-83

Cooley, L. A., “Permeability of Superpave Mixtures: Evaluation of Field Permeameters,” NCAT Report No. 99-1, February 1999

Hichs, R. G., “Moisture Damage in Asphalt Concrete,” National Cooperative Highway Research Program Synthesis of Highway Practice 175, October 1991

Hsaibati, K., Armaghani, J. and Fisher, J., “Effect of Moisture on Modulus Values of Base and Subgrade Materials,” Transportation Research Record 1716, TRB, National Research Council, Washington, D. C., 2000, pp.20-29

Patterson, D. E. and Smith, M.W, “The Measurement of Unfrozen Water Content by Time Domain Reflectometr: Results from Laboratory Tests,” Canadian Geotechnical Journal, Vol. 18, 1981, pp. 131-144

Dalton, F. N. and Van Genuchten, M. Th., “The Time-Domain Reflectometry Method for Measuring Soil Water Content and Salinity,” Geoderma, Vol. 38, 1986, pp. 237-250

Topp, G. C., Davis, J. L., Bailey, W. G. and Zebchuk, W. D., “The Measurement of Soil Water Content Using a Portable TDR Hand Probe,” Can. J. Soil Sci. 64, Aug, 1984, pp. 313-321

Topp, G. C. and Davis, J. L., “Measurement of Soil Water Content Using Time-Domain Reflectometry (TDR): a Field Evaluation,” Soil Sci. Soc. Am. J. 49, 1985, pp. 19-24

Rushton, K. R. and Redshaw, S. C., “Seepage and Groundwater Flow Numerical Analysis by Analog and Digital Methods,” John Wiley & Sons, Ltd. 1979

Zaradny, H, “Groundwater Flow in Saturated and Unsaturated Soil,” A.A.Balkema Publishers, 1993

Hoffman, G. J., Howell, T. A and Solomon, K. H., “Management of Farm Irrigation Systems,” the American Society of Agricultural Engineers, December 1990

Faust, C. R. and Mercer, J. W., “Ground-Water Modeling: Numerical Models,” Ground Water, Vol. 18, No. 4, July-August 1980, pp. 395-409

Huang, Y. H., “Pavement Analysis and Design,” Prentice-Hall, Inc., 1993

Hall, K. D. and Ng, H. G., “Development of Void Pathway Test for Investigating Void Interconnectivity in Compacted Hot-Mix Asphalt Concrete,” Transportation Research Record 1767, TRB, National Research Council, Washington, D. C., 2001, pp.40-47

Cooley, L. A. and Maghsoodloo, S., “Round-Robin Study for Field Permeability Test,” Transportation Research Record 1789, TRB, National Research Council, Washington, D. C., 2002, pp.25-35

Gogula, A., Hossain, M., Romanoschi, S. and Fager, G. A., "Correlation between the Laboratory and Field Permeability Values for the Superpave Pavements," Proceedings of the 2003 Mid-Continent Transportation Research Symposium, Ames, Iowa, August 2003

Mohammad, L. N., Herath, A. and Huang, B., "Evaluation of Permeability of Superpave Asphalt Mixtures," Transportation Research Record 1832, TRB, National Research Council, Washington, D. C., 2003, pp.50-58

Roberson, R. L. and Siekmeier, J., "Using a Multisegment Time Domain Reflectometry Probe to Determine Frost Depth in Pavement Systems," Transportation Research Record 1709, TRB, National Research Council, Washington, D. C., 2000, pp.108-113

Benson, C., Bosscher, P., and Jong, D., "Predicting Seasonal Changes in Pavement Stiffness and Capacity Caused by Freezing and Thawing," Geotechnical Engineering Report 97-9, University of Wisconsin-Madison

Davis, J. L., Baker, T. H. W., Hayhoe, H. N. and Topp, G. C., "Locating the Frozen-Unfrozen Interface in Soils Using Time-Domain Reflectometry," Canadian Geotechnical Journal, Vol. 19, 1982, pp. 511-517

Spaans, E. J. A. and Baker, J. M., "Examining the Use of Time Domain Reflectometry for Measuring Liquid Water Content in Frozen Soil," Water Resources Research, Vol. 31, 1995, pp. 2917-2925

AI-Samahiji, D., Houston, S. L. and Houston, W. N., "Degree and Extend of Wetting Due to Capillary Rise in Soils," Transportation Research Record 1709, TRB, National Research Council, Washington, D. C., 2000, pp.114-120

Bowders, J. J., Neupane, D. and Loehr, J. E., "Sidewall Leakage in Hydraulic Conductivity Testing of Asphalt Concrete Specimens," ASTM Geotechnical Testing Journal, June 2002

Neupane, D., Bowders, J. J., Loehr, J. E., Bouazza, A. and Trautwein, S. J., "Sealed Double Ring Infiltrometers for Estimating Very Low Hydraulic Conductivity," ASTM Geotechnical Testing Journal, 12 December 2003

ASTM D 5093-02, Test Method for Field Measurement of Infiltration Rate Using a Double-Ring Infiltrometer with a Sealed-Inner Ring, 1997

ASTM D 3385-94, Standard Test Method for Infiltration Rate of Soils in Field Using Double-Ring Infiltrometer, 1997

Muhanna, A. S., Rahman, M.S., and Lambe P.C. (1998), "Model for Resilient Modulus and Permanent Strain of Subgrade Soils", Transportation Research Record 1619, National Research Council, Washington, D.C., 1998, pp.85-93

Drumm, E.C., Reeves, J.S., Madgett, M.R., and Trolinger, W.D. (1997), "Subgrade Resilient Modulus Correction for Saturation Effects", Journal of Geotechnical and Geoenvironmental Engineering, Vol.123, No. 7, July 1997, pp.663-670

Santha, B.L., (1994), "Resilient Modulus of Subgrade Soils: Comparison of Two Constitutive Equations", Transportation Research Record 1462, National Research Council, Washington, D.C., 1994, pp.79-90

Jin, M.S., Lee, K.W., and Kovacs, W.D. (1994), "Seasonal Variation of Resilient Modulus of Subgrade Soils", Journal of Transportation Engineering, Vol. 120, No. 4, July/August, 1994, pp. 603-616

Rada, G and Witczak, M.W., (1981), "Comprehensive Evaluation of Laboratory Resilient Moduli Results for Granular Material ", Transportation Research Record 810, National Research Council, Washington, D.C., 1981, pp.23-33

Barksdale, R.D. and Alba, J. (1997), "Laboratory Determination of Resilient Modulus for Flexible Pavement Design", Prepared for National Cooperative Highway Research Program, Project I-28, Transportation Research Board, National Research Council, June 1997

ARA, Inc,, ERES Division (2000), "Resilient Modulus as Function of Soil Moisture – Summary of Predictive Models", Prepared for National Cooperative Highway Research Program, Transportation Research Board, National Research Council, June 2000

Drnevich, V.P., Siddiqui, S.I., Lovell, J. and Yi, Q. (2001), "Water Content and Density of Soil In Situ by the Purdue TDR Method", Second International Symposium and Workshop on Time Domain Reflectometry for Innovative Geotechnical Applications, 2001, pp457 – 469

Baker, J.M. and Lascano, R.J. (1989), "The Spatial Sensitivity of Time-Domain Reflectometry", Soil Science, Volume 147, No. 5, pp378-384

Knight, J.H. (1992), "The Sensitivity of Time Domain Reflectometry Measurements to Lateral Variations in Soil Water Content", Water Resources Research, Volume 28, No. 9, pp 2345-2352

Liu, R., Chen, X., He, R., Ma, W. and Wu, H. (1998), "Establishment of Reliable Methodologies to Determine In-Situ Moisture Content of Base and Subgrade Soils", Final Report Prepared for Texas Department of Transportation, Project No.: TxDOT P7-3935

Westerman, J.R. (1998), "AHTD's Experience with Superpave Pavement Permeability", A Presentation for the Arkansas Superpave Symposium, January 21, 1998 in Little Rock, Arkansas

Hainin, M.R. and Cooley, L.A. (2003),"An Investigation of Factors Influencing Permeability of Superpave Mixes", International Journal of Pavements, Volume 2, Number 1-2, January-May, 2003, pp 41-52

Shackel, B., Ball, J. and Mearing, M. (2003), "Using Permeable Eco-Paving to Achieve Improved Water Quality for Urban Pavements", 7th International Conference on Concrete Block Paving, 12-15 October 2003, Sun City, South Africa

Cristina, C.M. and Sansalone, J.J. (2003), "Kinematic Wave Model of Urban Pavement Rainfall-Runoff Subject to Traffic Loadings", Journal of Environmental Engineering, Vol. 129, No.7, July 2003

Lytton, R.L., Pufahl, D.E., Michalak, C.H., Liang, H.S., and Dempsey, B.J. (1990), "An Integrated Model of the Climatic Effects on Pavement", Texas Transportation Institute, Texas A&M University, Report No. FHWA-RD-90-033, Federal Highway Administration, McLean, VA.

Lukanen, E.O., Stubstad, R., and Briggs, R. (2000), "Temperature Predictions and Adjustment Factors for Asphalt Pavement", Federal Highway Administration Report FHWA-RD-98-085, McLean, VA.

Fredlund, D.G., Xing, A., and Huang, S., (1994), "Predicting the Permeability Function for Unsaturated Soils Using the Soil-Water Characteristic Curve", Canadian Geotechnical Journal, Vol. 3, No. 4, 1994, pp. 533-546

Terzaghi, K. and Peck, R.B. (1948), "Soil Mechanics in Engineering Practice", John Wiley & Sons, New York

Guymon, G. L., R. L. Berg, and T. C. Johnson (1986), "Mathematical Model of Frost Heave and Thaw Settlement in Pavement", Report: U.S. Army Cold Region Research and Engineering Laboratory, Hanover, New Hampshire

Dempsey, B. J., W. A. Herlach, and A. J. Patel (1985), "The Climatic-Material-Structural Pavement Analysis Program", FHWA/RD-84/115, Vol. 3, Final Report, Federal Highway Administration, Washington D.C.

Zhou, H. P., Moore, L., Huddleston, J., and Gower, J. (1993), "Determination of Free-Draining Base Materials Properties", Transportation Research Record 1425, National Research Council, Washington, D.C., 1993, pp.54-63

Department of the Army Corps of Engineers, (1984), "Pavement Criteria for Seasonal Frost Conditions", Engineer Manual, EM 1110-3-138, April 1984